

# Expanding the Reaction Scope of Nucleic Acids *via* Metathesis

By

Lucy A. Arkinstall

Supervisor: Rachel K. O'Reilly



UNIVERSITY OF  
BIRMINGHAM

A thesis submitted to  
The University of Birmingham  
for a degree of  
DOCTOR OF PHILOSOPHY

School of Chemistry  
College of Engineering and Physical Sciences  
University of Birmingham  
November 2020

UNIVERSITY OF  
BIRMINGHAM

**University of Birmingham Research Archive**

**e-theses repository**

This unpublished thesis/dissertation is copyright of the author and/or third parties. The intellectual property rights of the author or third parties in respect of this work are as defined by The Copyright Designs and Patents Act 1988 or as modified by any successor legislation.

Any use made of information contained in this thesis/dissertation must be in accordance with that legislation and must be properly acknowledged. Further distribution or reproduction in any format is prohibited without the permission of the copyright holder.

# Abstract

The sequence-specificity and programmability of DNA has led to an increasing emergence of DNA nanotechnology. However, with this comes a rise in the demand for DNA-compatible chemistries. This thesis explores the use metathesis, a carbon-carbon bond forming reaction, in DNA nanotechnology.

Chapter 1 provides an introduction to DNA nanotechnology including DNA-origami, DNA-polymer conjugates and DNA-templated synthesis. The currently explored DNA-compatible chemistries are discussed, and the history and potential of the metathesis mechanism is covered. In Chapter 2 the compatibility of the metathesis reaction with DNA is explored. The stability of DNA in the presence of Ru-metathesis catalysts is assessed and any interactions between the catalyst and DNA are studied.

Chapters 3 to 5 build upon the knowledge gained in Chapter 2 and focus on utilizing metathesis in DNA-nanotechnology. Chapter 3 covers attempts to prepare DNA bottlebrush polymers *via* the direct graft-through ring-opening metathesis polymerization of DNA macromonomers. Chapter 4 discusses attempts to isolate nucleic acid-functionalized metathesis catalysts with the aim of utilizing them in templating reactions. Finally, Chapter 5 covers an alternative *in situ* approach to DNA-functionalized metathesis catalysts which was explored following challenges with the isolation of catalysts discussed in Chapter 4.

*For Uncle Bernard, in loving memory*

# Acknowledgements

When I reflect upon the past four years, it has certainly been a journey with its fair share of obstacles along the way. However, as the journey comes to an end, I feel eternally grateful to all those who have supported and encouraged me along the way, and without whom I would not be where I am today.

Firstly, I must thank my supervisor, Professor Rachel O'Reilly, for the opportunity to work in such a vibrant group surrounded by world-class research. Your hard-work and commitment to scientific research is truly inspiring and has shaped me into the researcher I am today. I am very grateful for all the support, guidance and encouragement you have provided me. Your kindness and empathy helped me to get through some of the most challenging of times.

I must also thank all the members of the O'Reilly and Dove groups for their friendship, support and for making each day in the lab a pleasure. In particular, I wish to thank Dr Jonathan Husband and Dr Samuel Nuñez-Pertiñez for their friendship and willingness to put up with my constant chatter from day one.

I wish to thank all the past and current members of 'Team DNA' for their scientific discussions and willingness to discuss unforeseen experimental results. In particular, I would like to express my sincerest gratitude to Dr Thomas Wilks and Dr Samuel Nuñez-Pertiñez for the time they devoted to training me in DNA analysis. Furthermore, I must thank Dr Jeffrey Foster for sharing with me his expertise in metathesis, constant encouragement and willingness to participate in scientific discussions.

I also wish to thank all those who gave up their time to proof-read sections of this thesis: Dr Thomas Wilks, Dr Jeffrey Foster, Dr Jennifer Frommer, Dr Jonathan Husband and Dr Kayla Delle Chiaie. Furthermore, I would like to thank all staff in the analytical department for their support; in particular, Dr Chi Tsang and Dr Christopher Williams for their support and help in maintaining the LCMS.

In addition, I would not be here today without the love and support of my family - Mum, Dad, Sophie, Grandma and Adam. You have stood by my side through moments of hardship and joy and constantly encouraged me throughout. Adam I cannot put into words how thankful I am for the love and support you have shown. I truly could not have completed this thesis without you by my side.

# Declarations

This thesis is submitted to The University of Birmingham in support of my application for the degree of Doctor of Philosophy. It has been composed by me and it has not been submitted for any other degree or professional qualification. The work presented herein has been conducted by myself, except for the following:

- Chapter 3 was completed in collaboration with Dr Jeffrey Foster; specifically, **M1**, **M2** and **3.03** were synthesized by Dr Jeffrey Foster and used as received. In addition, Dr Jeffrey Foster developed the macroinitiator approach which was published in 2018 and collected the data plotted in **Figures 3.3** and **3.14**. The synthesis of **M3**, and the preparation and fluorescence study of **P1-ACM** were conducted by Dr Jonathan Husband and Dr Jeffrey Foster, respectively.
- In Chapter 4, the PNA sequences were synthesized by Dr Samuel Nuñez-Pertiñez.
- In Chapter 5, the synthetic pathway to **5.05** was designed in collaboration with Dr Jeffrey Foster. Furthermore, Dr Jeffrey Foster synthesized **5.07** which was used as received and conducted the control study between **5.06** and **5.07**.
- All high-resolution mass spectrometry data was obtained by Analytical Facility Staff at the University of Warwick and the University of Birmingham.

Parts of this thesis have been submitted for publication in the following journals:

- S. Varlas, S. B. Lawrenson, L. A. Arkinstall, R. K. O'Reilly and J. C. Foster, *Progress in Polymer Science*, 2020, **107**, 101278 (Chapter 1 - Section 1.3).
- J. C. Foster, S. Varlas, L. D. Blackman, L. A. Arkinstall and R. K. O'Reilly, *Angew. Chem. Int. Ed.* 2018, **57**, 10672 (Chapter 3 - Section 3.3.1).

# List of Publications

J. C. Foster, S. Varlas, L. D. Blackman, L. A. Arkinstall and R. K. O'Reilly, *Angew. Chem. Int. Ed.* 2018, **57**, 10672.

S. Varlas, J. C. Foster, L. A. Arkinstall, J. R. Jones, R. Keogh, R. T. Mathers and R. K. O'Reilly, *ACS Macro Lett.*, 2019, **8**, 466.

S. Varlas, S. B. Lawrenson, L. A. Arkinstall, R. K. O'Reilly and J. C. Foster, *Prog. Polym. Sci.*, 2020, **107**, 101278

J. C. Foster, M. C. Grocott, L. A. Arkinstall, S. Varlas, M. J. Redding, S. M. Grayson and R. K. O'Reilly, *J. Am. Chem. Soc.*, 2020, **142**, 13878.



# List of Symbols and Abbreviations

$\alpha_o$	Area of the hydrophilic headgroup
<b>A</b>	Adenine
<b>A<sub>  </sub></b>	Light polarised parallel
<b>A<sub>⊥</sub></b>	Light polarised perpendicular
<b>ACMs</b>	Aminochloromaleimides
<b>AGP</b>	Alpha-1-glycoprotein
<b>AM</b>	AquaMet
<b>AOs</b>	Antisense oligonucleotides
<b>ATRP</b>	Atom-transfer radical polymerization
<b>a.u.</b>	Absorbance units
<b>BP</b>	Base pairs
<b>C</b>	Cytosine
<b>CD</b>	Circular dichroism
<b>ctDNA</b>	Calf thymus deoxyribonucleic acid
<b>CuAAC</b>	Copper-catalyzed azide alkyne cycloaddition
<b>CM</b>	Cross-metathesis
<b>Đ</b>	Dispersity
<b>DA<sub>inv</sub></b>	Inverse electron demand Diels-Alder
<b>DECLs</b>	DNA-encoded chemical libraries
<b>DMAP</b>	4-Dimethylaminopyridine
<b>DME</b>	Dimethoxyethane
<b>DMF</b>	<i>N,N</i> -dimethylformamide
<b>DMSO</b>	Dimethyl sulfoxide
<b>DNA</b>	Deoxyribonucleic acid
<b>DIPEA</b>	<i>N,N</i> -Diisopropylethylamine
<b>DLS</b>	Dynamic-light scattering
<b>DP</b>	Degree of polymerization

<b>dsDNA</b>	Double-stranded deoxyribonucleic acid
<b>DTS</b>	DNA-templated synthesis
<b>DPBS</b>	Dulbecco's phosphate buffered saline
<b>EDC-HCl</b>	<i>N</i> -(3-Dimethylaminopropyl)- <i>N'</i> -ethylcarbodiimide hydrochloride
<b>ESAC</b>	Encoded self-assembling combinatorial
<b>Eq.</b>	Molar equivalents
<b>EVE</b>	Ethyl vinyl ether
<b>FRET</b>	Förster-resonance energy transfer
<b>G</b>	Guanine
<b>GCMS</b>	Gas chromatography-mass spectrometry
<b>G1</b>	Grubbs 1 <sup>st</sup> generation catalyst
<b>G2</b>	Grubbs 2 <sup>nd</sup> generation catalyst
<b>G3</b>	Grubbs 3 <sup>rd</sup> generation catalyst
<b>HCR</b>	Hairpin hybridization chain reaction
<b>HG1</b>	Hoveyda-Grubbs 1 <sup>st</sup> generation catalyst
<b>HG2</b>	Hoveyda-Grubbs 2 <sup>nd</sup> generation catalyst
<b>HOBt</b>	Hydroxybenzotriazole
<b>HPLC</b>	High-performance liquid chromatography
<b>IR</b>	Infrared
<b><math>K_a</math></b>	Equilibrium binding constant
<b><math>k_i</math></b>	Initiation rate coefficient
<b><math>k_p</math></b>	Propagation rate coefficient
<b>KHMDS</b>	Potassium bis(trimethylsilyl)amide
<b>KOtBu</b>	Potassium <i>t</i> -butoxide
<b><math>l_c</math></b>	Length of hydrophobic chain
<b>LCMS</b>	Liquid chromatography-mass spectrometry
<b>LCST</b>	Lower-critical solution temperature
<b>LD</b>	Linear dichroism
<b>LD<sup>r</sup></b>	Reduced linear dichroism
<b>mRNA</b>	Messenger ribonucleic acid

<b>MLCT</b>	Metal-to-ligand charge transfer
<b>NHC</b>	<i>N</i> -heterocyclic carbene
<b>NHS</b>	<i>N</i> -hydroxysuccinimide
<b>NMP</b>	<i>N</i> -methyl-2-pyrrolidone
<b>NMR</b>	Nuclear magnetic resonance
<b><i>P</i></b>	Critical packing parameter
<b>PAGE</b>	Polyacrylamide gel electrophoresis
<b>PB2</b>	pH2 phosphate solution
<b>PCL</b>	Poly( $\epsilon$ -caprolactone)
<b>PCR</b>	Polymerase chain reaction
<b>PEG</b>	Poly(ethylene glycol)
<b>PI</b>	Polyisoprene
<b>PLGA</b>	Poly(D,L-lactic-co-glycolic acid)
<b>PNA</b>	Peptide nucleic acid
<b>PNIPAM</b>	Poly( <i>N</i> -isopropylacrylamide)
<b>PPE</b>	Poly( <i>p</i> -phenyleneethynylene)
<b>PPO</b>	Poly(propylene oxide)
<b>PS</b>	Polystyrene
<b>RAFT</b>	Reversible addition-fragmentation chain transfer
<b>RCM</b>	Ring-closing metathesis
<b>RI</b>	Refractive index
<b>RNA</b>	Ribonucleic acid
<b>ROM</b>	Ring-opening metathesis
<b>ROMP</b>	Ring-opening metathesis polymerization
<b>S</b>	Orientation factor
<b>SEC</b>	Size exclusion chromatography
<b>ssDNA</b>	Single-stranded deoxyribonucleic acid
<b>T</b>	Thymine
<b>TAE</b>	Tris-acetate-EDTA
<b>TAMRA</b>	5-Carboxytetramethylrhodamine

<b>TBE</b>	Tris-borate-EDTA
<b>tBuOH</b>	<i>tert</i> -butanol
<b>TEM</b>	Transmission electron microscopy
<b>TEA</b>	Triethylamine
<b>TEAA</b>	Triethyl ammonium acetate
<b>THF</b>	Tetrahydrofuran
<b>TIPS</b>	Triisopropylsilyl
<b>TLC</b>	Thin-layer chromatography
$T_m$	Melting temperature
<b>TMS</b>	Trimethylsilane
<b>UV-Vis</b>	Ultraviolet-visible
<b>v</b>	Volume of the hydrophobic segment

# Contents

List of Figures .....	xvi
List of Schemes .....	xxii
List of Tables .....	xxiv
Chapter 1: Introduction .....	1
1.1 Nucleic acid nanotechnology .....	1
1.1.1 The rise of nanotechnology .....	1
1.1.2 Nucleic acid-based nanotechnology.....	1
1.1.2.1 DNA origami.....	6
1.1.2.2 Molecular machines .....	7
1.1.2.3 Hybrid materials .....	8
1.1.2.4 DNA-encoded chemical libraries for small molecule discovery .....	16
1.2 DNA-compatible chemistries.....	24
1.2.1 What is a DNA-compatible reaction? .....	24
1.2.2 Current DNA-compatible chemistries .....	24
1.3 Olefin Metathesis .....	28
1.3.1 Catalyst development.....	28
1.3.2 Metathesis in aqueous media .....	32
1.3.3 The potential of metathesis in DNA nanotechnology .....	34
1.4 Project aims.....	35
1.5 References .....	37
Chapter 2: Scoping the Potential of Metathesis in DNA Nanotechnology .....	43
2.1 Abstract.....	43
2.2 Background .....	43
2.2.1 Metathesis in the presence of DNA.....	43
2.2.2 DNA-ligand interactions .....	47
2.3 Results & Discussion .....	49
2.3.1 Stability of DNA in the presence of HG2 .....	49
2.3.2 Stability of DNA in the presence of PEG-G3 .....	55
2.3.3 The origins behind the disappearance of SYBR gold fluorescence .....	62
2.3.4 Interaction between dsDNA and PEG-G3.....	67
2.3.4.1 UV-Vis studies to determine the interaction between dsDNA and PEG-G3 .....	67
2.3.4.2 Linear dichroism studies.....	73
2.4 Conclusions .....	77
2.5 Experimental .....	81
2.5.1 Materials.....	81
2.5.2 Instrumentation.....	82
2.5.3 Derivatization of $K_a$ .....	84
2.5.4 Synthesis of G3 .....	86
2.5.5 Synthesis of 2.01.....	87

2.5.6	Synthesis of PEG-G3 .....	89
2.6	References .....	91
<b>Chapter 3: The Graft-Through Polymerization of DNA <i>via</i> ROMP.....</b>		<b>93</b>
3.1	Abstract.....	93
3.2	Background .....	93
3.2.1	Synthesis of DNA-polymer conjugates .....	94
3.3	Results & Discussion .....	98
3.3.1	The macroinitiator approach versus conventional aqueous ROMP approaches.....	98
3.3.2	Synthesis of an oligonucleotide macromonomer .....	102
3.3.3	Stability of DNA under the polymerization conditions .....	111
3.3.4	Optimization of the polymerization conditions .....	115
3.3.5	Polymerization of P1* .....	122
3.3.5.1	Characterization of P1* - Size Exclusion Chromatography .....	129
3.3.5.2	Characterization of P1* - Morphology .....	131
3.3.6	Controlling the morphology of DNA-polymer conjugates .....	134
3.3.6.1	Analysis of P2* .....	135
3.3.6.2	Morphology of P3* .....	138
3.3.7	Hybridization of P3* .....	139
3.4	Conclusions .....	141
3.5	Experimental section .....	143
3.5.1	Materials.....	143
3.5.2	Instrumentation.....	144
3.5.3	Synthesis of 3.01.....	147
3.5.4	Synthesis of 3.02.....	149
3.5.5	Synthesis of 3.03.....	150
3.5.6	Synthesis of M3 .....	152
3.5.7	Synthesis of M4 .....	154
3.5.8	Synthesis of 3i.....	156
3.5.9	Synthesis of 3ii.....	157
3.5.10	Synthesis of 3iii.....	157
3.5.11	Synthesis of 3iv.....	158
3.5.12	Preparation of P0.....	158
3.5.13	Preparation of P2.....	159
3.5.14	Preparation of P1.....	160
3.5.15	Preparation of P3.....	160
3.5.16	DNA-ligation .....	160
3.6	References .....	162
<b>Chapter 4: The Synthesis of Nucleic Acid -Functionalized Metathesis Catalysts .....</b>		<b>164</b>
4.1	Abstract.....	164
4.2	Introduction .....	164
4.3	Results & Discussion .....	169
4.3.1	Synthesis of DNA-functionalized metathesis catalysts using click chemistry .....	169

4.3.1.1	Synthesis of alkyne-functionalized ligands.....	169
4.3.1.2	Conjugation of alkyne-functionalized ligands to metathesis catalysts .....	174
4.3.1.3	Protection of the alkyne group.....	179
4.3.2	Synthesis of DNA-functionalized metathesis catalysts using amide bond formation.....	183
4.3.3	Synthesis of PNA-functionalized metathesis catalysts using amide bond formation.....	194
4.4	Conclusion.....	196
4.5	<b>Experimental section</b> .....	<b>199</b>
4.5.1	Materials.....	199
4.5.2	Instrumentation.....	200
4.5.3	Synthesis of 4.01.....	201
4.5.4	Synthesis of 4.02.....	202
4.5.5	Synthesis of 4.03.....	204
4.5.6	Synthesis of 4.05.....	206
4.5.7	Synthesis of 4.06.....	208
4.5.8	Synthesis of 4.07.....	210
4.5.9	Synthesis of 4.08.....	211
4.5.10	Synthesis of 4.09.....	213
4.5.11	Synthesis of 4.10.....	215
4.5.12	Synthesis of 4.11.....	216
4.5.13	Synthesis of 4.12.....	217
4.5.14	Synthesis of 4.13.....	219
4.5.15	Synthesis of 4.14.....	220
4.5.16	Synthesis of 4.15.....	223
4.5.17	Preparation of C3.....	225
4.5.18	Preparation of C4.....	226
4.5.19	General procedure for the solution-phase coupling to DNA .....	227
4.5.20	General procedure for the solid-phase coupling to DNA.....	228
4.5.21	General procedure for the solution-phase coupling to PNA.....	228
4.6	References .....	229
 <b>Chapter 5: Cross-Metathesis on Enyne-Functionalized DNA: An <i>in situ</i> Method</b> .....		<b>232</b>
5.1	<b>Abstract</b> .....	<b>232</b>
5.2	<b>Introduction</b> .....	<b>232</b>
5.3	<b>Results &amp; Discussion</b> .....	<b>236</b>
5.3.1	Synthesis of DNA-functionalized enyne .....	236
5.3.2	Off-templated DNA cross-metathesis .....	239
5.3.2.1	Proof-of-concept study using PEG-functionalized enyne.....	239
5.3.2.2	Functionalization of DNA via enyne metathesis in H <sub>2</sub> O .....	241
5.3.2.3	Functionalization of DNA via enyne metathesis in H <sub>2</sub> O/organic solvent mixtures.....	250
5.3.3	DNA-templated cross-metathesis .....	262
5.4	<b>Conclusions</b> .....	<b>266</b>
5.5	<b>Experimental Section</b> .....	<b>268</b>
5.5.1	Materials.....	268
5.5.2	Instrumentation.....	269
5.5.3	Synthesis of 5.01.....	272

5.5.4	Synthesis of 5.02.....	273
5.5.5	Synthesis of 5.03.....	274
5.5.6	Synthesis of 5.04.....	276
5.5.7	Synthesis of 5.05.....	278
5.5.8	Synthesis of 5.06.....	280
5.5.9	Synthesis of 5i.....	281
5.5.10	Synthesis of 5viii .....	282
5.5.11	Cross-metathesis small-molecule study.....	283
5.5.12	General protocols for the off-templated Cross-metathesis of 5i.....	283
5.5.12.1	Aquamet in PB2 .....	283
5.5.12.2	Ru-Cat in tBuOH/H <sub>2</sub> O.....	283
5.5.12.3	Ru-Cat in MeOAc/EtOH/H <sub>2</sub> O .....	284
5.5.13	General protocol for the templated cross-metathesis .....	285
5.6	References .....	286
	Conclusions and Future work .....	288



# List of Figures

## Chapter 1: Introduction

<b>Figure 1.1</b> Schematic showing the double helical structure adopted by DNA, the chemical composition of the sugar-phosphate backbone and Watson-Crick base pairs .....	2
<b>Figure 1.2</b> – Schematic showing (a) a DNA four-way junction and (b) a DNA double-crossover structure. ....	4
<b>Figure 1.3</b> A timeline showing the progress in DNA-nanotechnology over the past four decades.....	5
<b>Figure 1.4</b> 2D shapes prepared <i>via</i> DNA-origami.....	7
<b>Figure 1.5</b> Schematic showing the self-assembly of DNA-polymer conjugates in the presence of a cationic species to form polyelectrolyte complex micelles. ....	10
<b>Figure 1.6</b> Solution-phase coupling methods utilized for the conjugation of DNA to hydrophilic polymers.....	11
<b>Figure 1.7</b> Schematic showing the relationship between the critical packing parameter ( $p$ ) calculated from the molecular structure and the resulting particle morphology .....	12
<b>Figure 1.8</b> (a) Common DNA-polymer architectures. (b) Approaches to prepare DNA-polymer conjugates.....	15
<b>Figure 1.9</b> Schematic showing how molecular evolution can be achieved using DECLs .....	16
<b>Figure 1.10</b> Schematic representing the split and pool approach to prepare DECLs. ....	17
<b>Figure 1.11</b> Schematic highlighting DNA-directed approaches towards DNA-encoded chemical libraries. ....	19
<b>Figure 1.12</b> (a) Common DNA architectures employed in DTS. (b) Strand-displacement mechanism .....	21
<b>Figure 1.13</b> Toehold displacement mechanism .....	22
<b>Figure 1.14</b> Autonomous molecular machines for the sequence specific synthesis of oligomers.....	23
<b>Figure 1.15</b> Generally accepted metathesis mechanism .....	29
<b>Figure 1.16</b> Chemical structures of common commercially available metathesis catalysts.....	30
<b>Figure 1.17</b> Examples of water-soluble catalysts recently reported.....	33
<b>Figure 1.18</b> Commonly explored metathesis reactions: Cross-metathesis (CM), ring-closing metathesis (RCM) and ring-opening metathesis polymerization (ROMP).....	35

## Chapter 2: Scoping the Potential of Metathesis in DNA Nanotechnology

<b>Figure 2.1</b> Comparison between the backbone structure of DNA, RNA and PNA.....	44
<b>Figure 2.2</b> Schematic showing the four modes of binding of small molecules to DNA.....	47
<b>Figure 2.3</b> Plot showing the typical spectral changes observed for each of the possible binding modes .....	49

<b>Figure 2.4</b> (a) Structure of HG2. (b) Sequence of S1-NH <sub>2</sub> . (c) 15% native PAGE gel of S1-NH <sub>2</sub> incubated with 1 equivalent of HG2.....	51
<b>Figure 2.5</b> (a) Sequence of C2. (b) 15% native PAGE gel of C2 incubated with 150 equivalents of HG2 .....	52
<b>Figure 2.6</b> HPLC-UV chromatogram at 260 nm of S0-NH <sub>2</sub> following incubation with differing equivalents of HG2 and MgCl <sub>2</sub> .....	54
<b>Figure 2.7</b> <sup>1</sup> H NMR spectra of G3 and PEG-G3 .....	57
<b>Figure 2.8</b> (a) DNA sequences S2-NH <sub>2</sub> and C2. (b) 18% Native PAGE gel of DNA after incubation with PEG-G3.....	58
<b>Figure 2.9</b> 18% Native PAGE gel of C2 analysed after incubation with <b>PEG-G3</b> for 15, 30, 45 and 60 min with and without the addition of 8000 equivalents of MgCl <sub>2</sub> .....	60
<b>Figure 2.10</b> (a) Sequence of S2-NH <sub>2</sub> -FAM. (b) 18% Native PAGE gel of S2-NH <sub>2</sub> -FAM analysed after incubation with PEG-G3 for 15, 30, 45 and 60 minutes with and without the addition of 8000 equivalents of MgCl <sub>2</sub> .....	61
<b>Figure 2.11</b> Fluorescence intensity of SYBR™ Gold stained-C2 at 539 nm after the addition of increasing equivalents of PEG-G3.....	63
<b>Figure 2.12</b> Fluorescence intensity of SYBR™ Gold stained-C2 complex at 539 nm: time-course study .....	64
<b>Figure 2.13</b> Proposed schematic to explain differences in the visualization properties of ssDNA and dsDNA. ....	66
<b>Figure 2.14</b> (a) UV-Vis spectrum of PEG-G3 in the absence and presence of 0.5 equivalents of ctDNA. (b) UV-Vis spectrum of ctDNA upon the addition of PEG-G3. ....	68
<b>Figure 2.15</b> UV-Vis spectroscopy titration series showing the effect of the addition of ctDNA to PEG-G3 .....	69
<b>Figure 2.16</b> Delta absorbance plots.....	70
<b>Figure 2.17</b> Plot to calculate K <sub>a</sub> . ....	71
<b>Figure 2.18</b> (a) UV-vis spectrum of a solution of PEG-G3 in H <sub>2</sub> O: time-course experiment....	73
<b>Figure 2.19</b> Schematic to show the orientation of DNA under flow.....	75
<b>Figure 2.20</b> LD spectroscopy titration series showing the effect of adding PEG-G3 to ctDNA under cuvette flow. ....	76
<b>Figure 2.21</b> Orientation of PEG-G3 with the PEG groups parallel to the flow and the nucleobases perpendicular to the flow.....	77
<b>Figure 2.22</b> Schematic to demonstrate the proposed events taking place when PEG-G3 is mixed with fluorescent DNA.....	80
<b>Figure 2.23</b> <sup>1</sup> H NMR spectrum of G3 .....	87
<b>Figure 2.24</b> <sup>1</sup> H NMR spectrum of 2.01 .....	88
<b>Figure 2.25</b> <sup>1</sup> H NMR spectrum of PEG-G3 .....	90

### Chapter 3: The Graft-through Polymerization of DNA *via* ROMP

<b>Figure 3.1</b> Schematic of DNA polymer architectures and preparation routes .....	94
---	----

<b>Figure 3.2</b> Schematic showing the graft-through polymerization of norbornene-functionalized DNA.....	97
<b>Figure 3.3</b> The macroinitiator approach to prepare DNA-polymer conjugates.....	100
<b>Figure 3.4</b> Schematic for the graft-through polymerization of DNA using a water-soluble metathesis macroinitiator. ....	101
<b>Figure 3.5</b> LCMS-UV chromatogram of the reaction mixture collected following the reaction of S0-NH <sub>2</sub> with <i>cis</i> -5-norbornene- <i>exo</i> -2,3-dicarboxylic anhydride .....	104
<b>Figure 3.6</b> HPLC-UV chromatogram of 3ii .....	106
<b>Figure 3.7</b> <sup>1</sup> H NMR spectrum of methyl 5-norbornene-2-carboxylate (3.01).....	108
<b>Figure 3.8</b> <sup>1</sup> H NMR spectrum of the <i>exo</i> -rich mixture of 5-norbornene carboxylic acid (3.02).....	109
<b>Figure 3.9</b> <sup>1</sup> H NMR spectrum of the <i>exo</i> -5-norbornene carboxylic acid (3.02).....	109
<b>Figure 3.10</b> LCMS-UV chromatogram of 3iii.....	111
<b>Figure 3.11</b> (a) Structure of S1-NH <sub>2</sub> . (b) 18 % Native PAGE gel of S1-NH <sub>2</sub> following incubation under polymerization conditions .....	113
<b>Figure 3.12</b> LCMS-UV chromatogram of 3iii after being incubated under the polymerization conditions .....	115
<b>Figure 3.13</b> (a) Adenine-succinimide interaction (b) Proposed interaction between Guanine and succinimide.....	117
<b>Figure 3.14</b> Normalized SEC RI molar mass distributions of P0 in the presence of nucleobases .....	119
<b>Figure 3.15</b> Structure of S0-NH <sub>2</sub> -TAMRA.....	120
<b>Figure 3.16</b> (a) The polymerization conditions S0-NH <sub>2</sub> -TAMRA was subjected to. (b) LC-MS-UV chromatogram of S0-NH <sub>2</sub> -TAMRA incubated with the macroinitiator. (c) 15% native PAGE of S0-NH <sub>2</sub> -TAMRA incubated with the macroinitiator. (d) 15% denaturing PAGE of S0-NH <sub>2</sub> -TAMRA incubated with the macroinitiator. ....	121
<b>Figure 3.17</b> (a) Structure of C0-Cy5. (b) 15% native PAGE gel of P1 mixed with complementary oligonucleotide.....	125
<b>Figure 3.18</b> (a) Synthesis of 3iv. (b) LC-MS UV Chromatogram of 3iv.....	127
<b>Figure 3.19</b> (a) Polymerization of 3iv to yield P1*. (b) 15% denaturing PAGE of P1* .....	128
<b>Figure 3.20</b> SEC analysis of P0 and P1* .....	130
<b>Figure 3.21</b> Schematic demonstrating the proposed collapse of P1* in an aqueous solution .....	132
<b>Figure 3.22</b> (a) Synthesis of P1-ACM. (b) Fluorescence of M3 at varying percentages of H <sub>2</sub> O. (c) Fluorescence of P1-ACM at varying percentages of H <sub>2</sub> O.....	133
<b>Figure 3.23</b> Schematic showing the entrapment of a DNA-polymer conjugate during the polymerization.....	134
<b>Figure 3.24</b> (a) Structure of P1* and P3*. (b) DMF SEC traces of P1* and P3*. (c) 15% denaturing PAGE of P1* and P3* .....	137

<b>Figure 3.25</b> (a) Schematic for the polymerization of P3-ACM. (b) Fluorescence of M3 at increasing volumes of H <sub>2</sub> O .....	139
<b>Figure 3.26</b> (a) Fluorescence emission spectra of S3-TAMRA-NH <sub>2</sub> in the presence of Ma1 excited at 545 nm. (b) Fluorescence emission at 580 nm of S3-TAMRA-NH <sub>2</sub> in the presence of 200 equivalents Ma1. ....	140
<b>Figure 3.27</b> (a) Fluorescence of S0-NH <sub>2</sub> -TAMRA upon addition of C0-IAbRQ. (b) Fluorescence of P3* upon addition of C0-IAbRQ .....	141
<b>Figure 3.28</b> <sup>1</sup> H NMR spectrum of 3.01 .....	148
<b>Figure 3.29</b> <sup>1</sup> H NMR spectrum of 3.02 .....	150
<b>Figure 3.30</b> <sup>1</sup> H NMR spectrum of 3.03 .....	151
<b>Figure 3.31</b> <sup>13</sup> C NMR spectrum of 3.03 .....	152
<b>Figure 3.32</b> <sup>1</sup> H NMR spectrum of M3 .....	153
<b>Figure 3.33</b> <sup>13</sup> C NMR spectrum of M3 .....	154
<b>Figure 3.34</b> <sup>1</sup> H NMR spectrum of M4 .....	155
<b>Figure 3.35</b> <sup>13</sup> C NMR spectrum of M4 .....	156
<b>Figure 3.36</b> <sup>1</sup> H NMR spectrum of P0 .....	159
<b>Figure 3.37</b> <sup>1</sup> H NMR spectrum of P2 .....	160
<b>Figure 3.38</b> (a) Enzymatic ligation of S0-NH <sub>2</sub> and Ligase_S0.....	161

#### **Chapter 4: The Synthesis of Nucleic Acid-Functionalized Metathesis Catalysts**

<b>Figure 4.1</b> Schematic demonstrating a templated metathesis reaction.....	166
<b>Figure 4.2</b> Ru-based metathesis catalysts developed by the groups of Grubbs and Hoveyda .....	166
<b>Figure 4.3</b> (a) Functionalization locations on HG2 type catalysts.....	167
<b>Figure 4.4</b> The 'release and return' mechanism, used to recycle and recover Ru-based metathesis catalysts .....	168
<b>Figure 4.5</b> <sup>1</sup> H NMR spectrum of 4.03 .....	171
<b>Figure 4.6</b> <sup>1</sup> H NMR spectrum of 4.06 .....	174
<b>Figure 4.7</b> <sup>1</sup> H NMR spectra of the green solid isolated utilizing reaction conditions 1d .....	177
<b>Figure 4.8</b> <sup>1</sup> H NMR spectrum of 4.09 .....	181
<b>Figure 4.9</b> <sup>1</sup> H NMR spectrum of C3 .....	182
<b>Figure 4.10</b> <sup>1</sup> H NMR spectrum of 4.14 .....	184
<b>Figure 4.11</b> (a) S0-NH <sub>2</sub> sequence utilized throughout this study. (b) Conditions attempted for the conjugation of a carboxylic acid functionalized benzylidene ligand to S0-NH <sub>2</sub> . (c) LC-MS-UV chromatogram of the resultant product.....	185
<b>Figure 4.12</b> <sup>1</sup> H NMR spectrum of 4.15 .....	186
<b>Figure 4.13</b> (a) Synthesis of 4i utilizing an activated-ester (4.15). (b) LC-MS-UV chromatogram of 4i.....	187
<b>Figure 4.14</b> (a) Synthesis of C4. (b) <sup>1</sup> H NMR spectra of C4.....	188

<b>Figure 4.15</b> (a) Synthetic scheme for the preparation of 4ii. (b) LCMS-UV chromatogram of the product utilizing 1000 equivalents of C4 and 0 equivalents of MgCl <sub>2</sub> . (c) LCMS-UV chromatogram of the product utilizing 100 equivalents of C4 and 4000 equivalents of MgCl <sub>2</sub> .....	189
<b>Figure 4.16</b> (a) Structure of DEAE Sepharose. (b) Synthesis of 4ii on the solid-phase. (c) LCMS-UV chromatogram of 4ii .....	191
<b>Figure 4.17</b> a) Structure of the linker utilized on the 5' end of S0-iSp-NH <sub>2</sub> . (b) Synthesis of 4ii on the solid-phase. (c) LCMS-UV chromatogram of 4ii .....	193
<b>Figure 4.18</b> (a) Structure and sequence of PS0 and Ac-PS0-Lys. The reaction of PS0/Ac-PS0-Lys with 4.15 to prepare benzylidene functionalized PNA, 4iii.....	195
<b>Figure 4.19</b> – LCMS-UV chromatogram at 260 nm of 4iii. ....	196
<b>Figure 4.20</b> <sup>1</sup> H NMR spectrum of 4.01 .....	202
<b>Figure 4.21</b> <sup>1</sup> H NMR spectrum of 4.02 .....	204
<b>Figure 4.22</b> <sup>1</sup> H NMR spectrum of 4.03 .....	205
<b>Figure 4.23</b> <sup>1</sup> H NMR spectrum of 4.05 .....	207
<b>Figure 4.24</b> <sup>13</sup> C NMR spectrum of 4.05 .....	207
<b>Figure 4.25</b> <sup>1</sup> H NMR spectrum of 4.06 .....	209
<b>Figure 4.26</b> <sup>13</sup> C NMR spectrum of 4.06 .....	210
<b>Figure 4.27</b> <sup>1</sup> H NMR spectrum of 4.07 .....	211
<b>Figure 4.28</b> <sup>1</sup> H NMR spectrum of 4.08 .....	212
<b>Figure 4.29</b> <sup>13</sup> C NMR spectrum of 4.08 .....	213
<b>Figure 4.30</b> <sup>1</sup> H NMR spectrum of 4.09 .....	214
<b>Figure 4.31</b> <sup>13</sup> C NMR spectrum of 4.09 .....	215
<b>Figure 4.32</b> <sup>1</sup> H NMR spectrum of 4.10 .....	216
<b>Figure 4.33</b> <sup>1</sup> H NMR spectrum of 4.11 .....	217
<b>Figure 4.34</b> <sup>1</sup> H NMR spectrum of 4.12 .....	218
<b>Figure 4.35</b> <sup>1</sup> H NMR spectrum of 4.13 .....	220
<b>Figure 4.36</b> <sup>1</sup> H NMR spectrum of 4.14 .....	221
<b>Figure 4.37</b> <sup>13</sup> C NMR spectrum of 4.14 .....	222
<b>Figure 4.38</b> <sup>1</sup> H NMR spectrum of 4.15 .....	224
<b>Figure 4.39</b> <sup>13</sup> C NMR spectrum of 4.15 .....	224
<b>Figure 4.40</b> <sup>1</sup> H NMR spectrum of C3 .....	226
<b>Figure 4.41</b> <sup>1</sup> H NMR spectrum of C4 .....	227

## Chapter 5: Cross-Metathesis on Enyne-Functionalized DNA: An *in situ* Method

<b>Figure 5.1</b> The generic structure of the enyne scaffold .....	235
<b>Figure 5.2</b> <sup>1</sup> H NMR spectrum of 5.05 .....	237
<b>Figure 5.3</b> (a) Sequence of S0-NH <sub>2</sub> ; (b) Synthesis of 5i; (c) LCMS UV Chromatogram of 5i ...	238
<b>Figure 5.4</b> <sup>1</sup> H NMR spectrum of 5.06 .....	240

<b>Figure 5.5</b> DMF SEC traces of 5.08, 5.06 and methoxy PEG: (a) RI Chromatogram; (b) UV Chromatogram at 350 nm .....	241
<b>Figure 5.6</b> (a) Enyne metathesis to prepare a fluorescently labelled oligonucleotide ( <b>5ii</b> ). (b) Reaction conditions explored varying the equivalents of <b>5.07</b> and AM. (c) 15% Native PAGE gels).....	242
<b>Figure 5.7</b> GCMS chromatogram of cross-metathesis mixtures .....	246
<b>Figure 5.8</b> 15% Native PAGE analysis of S0-NH <sub>2</sub> subjected to varying equivalents of AM ....	247
<b>Figure 5.9</b> (a) CM of allyl-alcohol; LCMS-UV chromatogram following the reaction of 5i with (b) 10 mol% AM; and (c) 33 mol% AM. ....	250
<b>Figure 5.10</b> Fluorescence melting profile of S0-NH <sub>2</sub> -TAMRA/CO-Quencher duplex in tris-buffer and tBuOH/H <sub>2</sub> O .....	253
<b>Figure 5.11</b> (a) CM of 5i with allyl alcohol. (b) LCMS-UV chromatogram at 260 nm of product mixture (c) Deconvoluted mass spectrum of the products eluted .....	255
<b>Figure 5.12</b> (a) CM of 5i with <i>cis</i> -2-butene-1,4-diol. (b) LCMS-UV chromatogram of product mixtures (c) Reaction conversions calculated from the peak integrations.....	257
<b>Figure 5.13</b> Fluorescence melting profile of S0-NH <sub>2</sub> -TAMRA/CO-Quencher duplex in tris-buffer, tBuOH/H <sub>2</sub> O and H <sub>2</sub> O/EtOH/MeOAc .....	259
<b>Figure 5.14</b> (a) CM with <i>cis</i> -2-butene-1,4-diol. (b) LCMS-UV chromatogram of product mixtures. (c) Reaction conversions calculated from peak integrations.....	260
<b>Figure 5.15</b> (a) LCMS-UV chromatogram at 260 nm following the reaction of 5i with 3a-3d. (b) Reaction conversions calculated from the peak integrations.....	261
<b>Figure 5.16</b> (a) Synthesis of 5viii. (b) LCMS UV chromatogram of 5viii (c) Deconvoluted mass spectrum of the purified product obtained. ....	263
<b>Figure 5.17</b> (a) Templated metathesis mechanism between 5i and 5viii. (b) 15% denaturing PAGE analysis.....	265
<b>Figure 5.18</b> <sup>1</sup> H NMR spectrum of 5.01 .....	273
<b>Figure 5.19</b> <sup>1</sup> H NMR spectrum of 5.02 .....	274
<b>Figure 5.20</b> <sup>1</sup> H NMR spectrum of 5.03 .....	275
<b>Figure 5.21</b> <sup>13</sup> C NMR spectrum of 5.03 .....	276
<b>Figure 5.22</b> <sup>1</sup> H NMR spectrum of 5.04 .....	277
<b>Figure 5.23</b> <sup>13</sup> C NMR spectrum of 5.04 .....	278
<b>Figure 5.24</b> <sup>1</sup> H NMR spectrum of 5.05 .....	279
<b>Figure 5.25</b> <sup>13</sup> C NMR spectrum of 5.05 .....	280
<b>Figure 5.26</b> <sup>1</sup> H NMR spectrum of 5.06 .....	281
<b>Figure 5.27</b> GCMS chromatogram of reaction mixtures 1a and 1f .....	283

# List of Schemes

## Chapter 2: Scoping the Potential of Metathesis in DNA Nanotechnology

Scheme 2.1 Synthesis of PEG-G3.....	56
Scheme 2.2 The equilibrium formed between free DNA base pairs (BP) and PEG-G3.....	70
Scheme 2.3 Oxidation of G3, resulting in the loss of the MLCT band.....	72

## Chapter 3: The Graft-through Polymerization of DNA *via* ROMP

Scheme 3.1 Accepted ROMP mechanism <i>via</i> a metal alkylidene complex. ....	96
Scheme 3.2 (a) Structure of S0-NH <sub>2</sub> (b) Synthesis of 3i .....	103
Scheme 3.3 Synthesis of 3ii .....	105
Scheme 3.4 Synthesis of sterically pure <i>exo</i> -5-norbornene carboxylic acid (3.02). ....	107
Scheme 3.5 Synthesis of 3iii. ....	110
Scheme 3.6 (a) Polymerization of P0, which is used as the control reaction for further analysis. (b) Polymerization of P1. ....	116
Scheme 3.7 The preparation of a fluorescently tagged DNA-polymer conjugate, P1*, post-polymerization by either DNA ligation (approach 1) or DNA annealing (approach 2). ....	124
Scheme 3.8 Polymerization of P2 and P3*.....	135

## Chapter 4: The Synthesis of Nucleic Acid-Functionalized Metathesis Catalysts

Scheme 4.1 Synthesis of alkyne functionalized N-heterocyclic ligand (4.03).....	171
Scheme 4.2 Proposed two-step synthesis towards an alkyne-functionalized benzylidene ligand. ....	172
Scheme 4.3 The reaction of 3-formyl-4-isopropoxy phenyl boronic acid with propargyl bromide and 1-bromo-4-ethynylbenzene to give intermediates 4.04 and 4.05 respectively .....	173
Scheme 4.4 Synthesis of an alkyne functionalized benzylidene ligand (4.06).....	174
Scheme 4.5 The conjugation of an alkyne-functionalized NHC ligand to HG1. ....	175
Scheme 4.6 Conjugation of 4.06 to G2 in an attempt to prepare an alkyne functionalized catalyst C2.....	178
Scheme 4.7 Synthesis of a TIPS protected alkyne functionalized NHC ligand (4.09).....	180
Scheme 4.8 Conjugation of 4.09 to G1 to yield C3. ....	182
Scheme 4.9 Synthesis of a carboxylic functionalized benzylidene ligand (4.14) .....	183
Scheme 4.10 Synthesis of a benzylidene ligand functionalized with an NHS activated-ester (4.15).....	186

## Chapter 5: Cross-Metathesis on Enyne-Functionalized DNA: An *in situ* Method

Scheme 5.1 Tandem ROM/RCM of a monomer containing two typically unreactive functional groups.....	233
---	-----

<b>Scheme 5.2</b> The synthesis of a functionalized metathesis catalyst using enynes .....	233
<b>Scheme 5.3</b> The use of enyne metathesis to prepare (a) well-defined heterotelechelic polymers; or (b) polymer-polymer coupling. ....	234
<b>Scheme 5.4</b> The potential of utilizing enyne functionalized DNA to prepare an <i>in situ</i> DNA-Ru catalyst which could subsequently go on to react with alkenes in both a templated and non-templated manner.....	236
<b>Scheme 5.5</b> The synthesis of 5.05 .....	237
<b>Scheme 5.6</b> Synthesis of 5.06.....	239
<b>Scheme 5.7</b> Enyne-metathesis reaction between 5.06 and 5.07 to prepare a fluorescently labelled PEG-polymer 5.08. ....	240
<b>Scheme 5.8</b> Possible reaction products formed following the reaction of G3 with allyl alcohol in the presence of 5i. ....	252



# List of Tables

## Chapter 1: Introduction

<b>Table 1.1</b> DNA compatible chemistries reported in the literature. ....	25
<b>Table 1.2</b> Summary of the key features of the commercially available catalysts.....	31

## Chapter 2: Scoping the Potential of Metathesis in DNA Nanotechnology

<b>Table 2.1</b> Summary of the examples of 'on-DNA' metathesis reported including the mechanism of metathesis studied, the solvent, and any additional additives/conditions required for the success of the reaction. ....	45
<b>Table 2.2</b> Conditions tested for the stability of DNA in the presence of 150 equivalents of PEG-G3.....	58

## Chapter 3: The Graft-through Polymerization of DNA *via* ROMP

<b>Table 3.1</b> Reaction conditions tested and the conversions for the synthesis of <b>3i</b> .....	104
<b>Table 3.2</b> Solvent ratios tested for the stability and solubility study conducted with S1-NH <sub>2</sub> . .....	112

## Chapter 4: The Synthesis of Nucleic Acid-Functionalized Metathesis Catalysts

<b>Table 4.1</b> A summary of the reaction conditions trialled for the synthesis of <b>C1</b> from <b>4.03</b> and HG1. ....	176
<b>Table 4.2</b> A summary of the reaction conditions attempted for the formation of <b>4iii</b> . ....	194

## Chapter 5: Cross-Metathesis on Enyne-Functionalized DNA: An *in situ* Method

<b>Table 5.1</b> Screening the CM of allyl-alcohol.....	245
<b>Table 5.2</b> Screening the CM of acrylate-esters. ....	249

# Chapter 1: Introduction

## 1.1 Nucleic acid nanotechnology

### 1.1.1 The rise of nanotechnology

Nanotechnology has often been described as one of the most promising technologies of the 21<sup>st</sup> century with applications ranging from drug delivery systems to food safety.<sup>1</sup> The concept of nanotechnology was first introduced in 1959 during the annual meeting of the American Physical Society, when Nobel Prize laureate Richard Feynman presented a lecture entitled “There’s plenty of Room at the Bottom.” During the lecture he outlined a vision of arranging atoms one by one, a vision later named nanotechnology.<sup>2</sup>

Norio Taniguchi was the first to coin the term nanotechnology in 1974 to describe semiconductor processes that occurred on the order of a nanometer.<sup>3</sup> The beginning of the 21<sup>st</sup> century has since seen a rapid increase in nanotechnology and today nanotechnology impacts our everyday lives from the pharmaceutical industry<sup>4</sup> to the food<sup>5</sup> and cosmetic<sup>6</sup> industries.

### 1.1.2 Nucleic acid-based nanotechnology

Nucleic acids possess a number of attractive features for use in nanotechnology including their nanometer size and molecular recognition properties based on the Watson-Crick base pairs. Indeed, nature has utilized nucleic acid nanotechnology for billions of years to reliably store genetic information and in biological nanomachines such as the ribosome. Inspired by nature and with the development of solid-phase phosphoramidite chemistry for oligonucleotide

synthesis<sup>7</sup>, researchers have extensively explored the use of deoxyribonucleic acid (DNA) in nanotechnology over the last four decades.<sup>8</sup>

DNA is a linear polymer made up of four different bases: adenine (A), thymine (T), guanine (G) and cytosine (C). The backbone of the polymer is made from sugar-phosphates which at physiological pH exist as anions. DNA adopts a double-helical structure, held together by hydrogen bonds between individual bases on opposite strands (Watson-Crick base pairs). Adenine always pairs with thymine and guanine always pairs with cytosine; therefore, only complementary sequences will pair together in an antiparallel fashion to form a double helix.<sup>9</sup> The most prominent form of double helical DNA found in nature is B-DNA: a right-handed double helix, shown in Figure 1.1.<sup>10</sup>

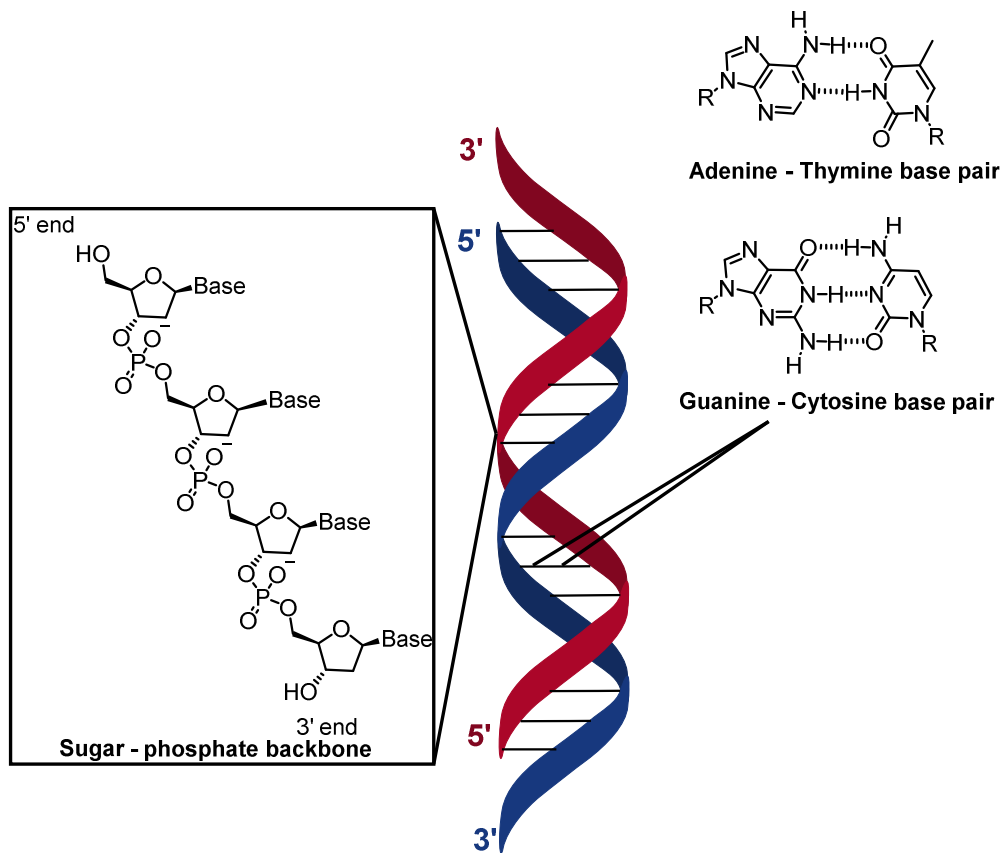


**Figure 1.1** Schematic showing the double helical structure adopted by DNA, the chemical composition of the sugar-phosphate backbone and Watson-Crick base pairs formed between A and T; and G and C.

One of the most attractive features of DNA for nanotechnology is the predictable, sequence-specific binding of oligonucleotides to form duplexes.<sup>11</sup> The stability of the resultant duplexes is dependent upon inter-strand hydrogen bonding and base stacking interactions which are mainly hydrophobic and electrostatic in nature. Base-stacking interactions increase in increasing salt concentrations as the salt screens the repulsive negative charges between the phosphate backbone.<sup>9, 12</sup> The temperature at which the 50% of the DNA transitions from a duplex to randomly coiled ssDNA is the melting temperature ( $T_m$ ). Significantly, biology is now no longer the only branch of science exploiting this self-assembly behavior of DNA and thus DNA has become increasingly prevalent in the materials world.<sup>11, 13, 14</sup>

DNA can self-assemble into a number of structures far more complex than a double helix which are vital for key biological processes. For example, branched DNA junctions, such as the Holliday junction, are vital for genetic recombination.<sup>15</sup> However, for many years the isolation of such structures proved to be exceptionally difficult due to the transient nature of the junction, limiting their use outside of living organisms. A major breakthrough occurred in 1983 when Nadrian Seeman isolated the first synthetic DNA branched junction.<sup>16</sup> This was followed by the discovery of rigid and stable double-crossover molecules in 1993 which really opened up the potential of using DNA to build extended structures (Figure 1.2).<sup>17, 18</sup>

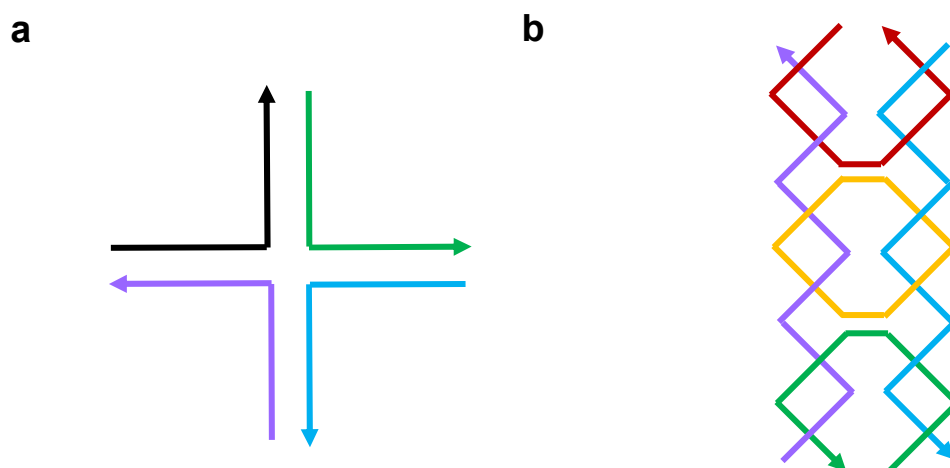


**Figure 1.2** – Schematic showing (a) a DNA four-way junction and (b) a DNA double-crossover structure.

Since these key discoveries a vast number of studies utilizing DNA in materials science commenced. An extensive amount of research focused on the use of DNA to build 3D nanostructures and dynamic molecular machines with a high level of precision.<sup>19</sup> Furthermore, DNA was utilized for the programmed assembly of large chemical libraries used in materials discovery and for the formation of novel biohybrid materials.<sup>20, 21</sup> Figure 1.3 summarizes key landmarks in these areas which are discussed in greater depth below.

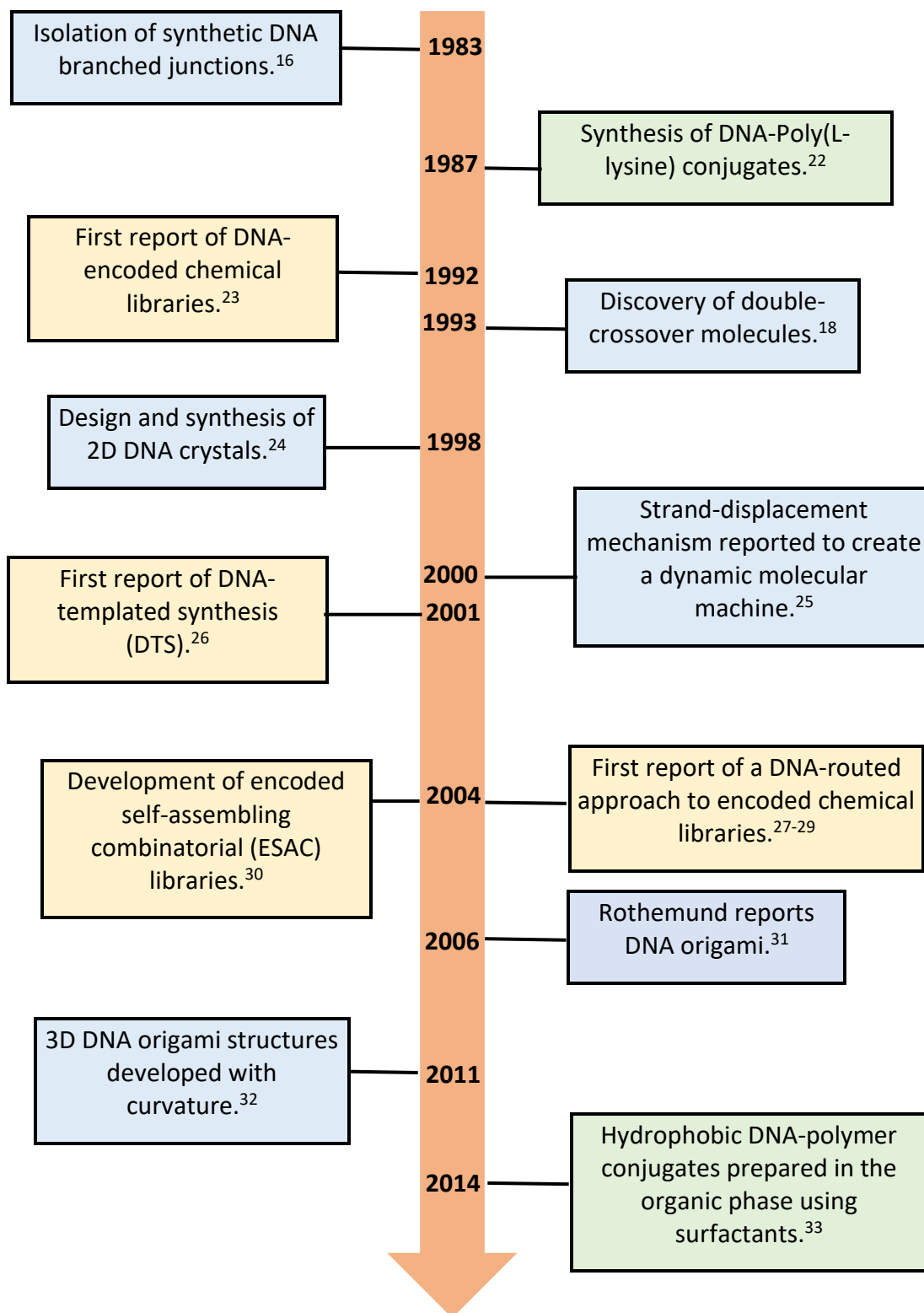


**Figure 1.3** A timeline showing the progress in DNA-nanotechnology over the past four decades.

### 1.1.2.1 DNA origami

Owing to the pioneering work of Seeman and others, discussed above, the first higher order 2D DNA crystal was prepared in 1998,<sup>24</sup> which was subsequently extended into periodic DNA structures.<sup>34</sup> These studies fundamentally paved the way for the first report of DNA origami in 2006 by Paul Rothemund.<sup>31</sup> Origami refers to the art or process of folding paper into representational shapes; thus, DNA-origami refers to the folding of DNA into structural shapes.

The DNA origami process involves folding long single-stranded DNA (ssDNA), known as the scaffold, into the desired shape using short oligonucleotides designed to be complementary to different parts of the scaffold. These short strands crosslink spatially distant segments of the scaffold holding the structure together and thus are described as the staples. Rothemund demonstrated the use of DNA origami to prepare an array of 2D shapes from squares and stars to smiley faces (Figure 1.4).

In 2009, the folding of such 2D planar origami sheets led to development of hollow 3D tetrahedrons,<sup>35</sup> cubes<sup>36, 37</sup> and prisms<sup>38</sup>. Furthermore, in 2011 3D structures were prepared by adjusting the cross-over points so that the DNA helices do not pack into a single plane, leading to curved surfaces. This led to the development of a number of complex 3D shapes including spherical shapes, ellipsoidal shells and nanoflasks.<sup>32</sup> Finally, the introduction of multi-arm junctions led to further more complex wire-frame structures.<sup>39, 40</sup>

The scaling up of DNA origami structures by using individual DNA origami tiles has led to the development of complex structures with high precision that have been extensively exploited in the development of molecular machines which will be discussed in greater depth below.

Furthermore, the programmability of DNA means DNA origami nanostructures are one of the most promising drug delivery carriers and they have been extensively studied for the delivery of anti-cancer drugs<sup>41</sup> and antibodies.<sup>42</sup>

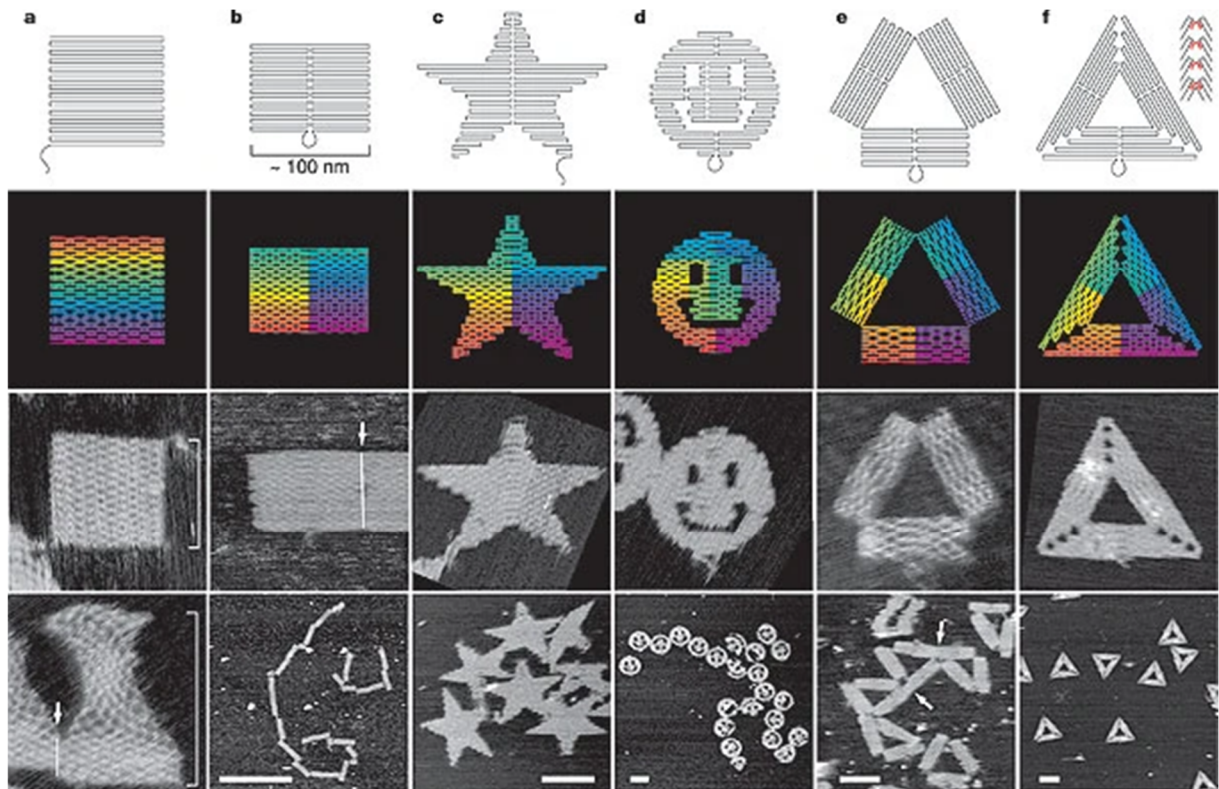


**Figure 1.4** 2D shapes prepared via DNA-origami. Top row: folding paths. Second row: diagrams showing the bend of helices. Third and Fourth rows are AFM images. Scale bars for lower AFM images: b - 1  $\mu$ M, c-f - 100 nm. Figure taken with permission from: Nature, Folding DNA to create nanoscale shapes and patterns, P. Rothmund, 2006.<sup>31</sup>

### 1.1.2.2 Molecular machines

Natural biomolecular machines including the ribosome and ATPases are pivotal to roles such as protein synthesis and energy production; however, these machines are built with an extreme level of precision and complexity beyond the current capabilities of synthetic chemistry. Nonetheless, the synthesis of artificial molecular machines has been the source of much effort over the last three decades and the use of DNA nanotechnology to prepare such machines offers much promise in this area.<sup>43</sup> As discussed above, the development of DNA



origami allows for the production of complex 3D nanostructures and these have since been utilized for the development of DNA machines.

The combination of rigid DNA nanostructures with a dynamic mechanism leads to the formation of a dynamic molecular machine. Two main approaches to create motion have been explored. Firstly, a strand-displacement mechanism can be adopted, where the moving body is complementary to two competing DNA sequences. One of the sequences has a larger stretch of complementary base sequences and hence displaces the moving sequence from the complementary shorter strand.<sup>25</sup> In 2010, Seeman and co-workers utilized such an approach to prepare a DNA walker composed of three parts: A DNA origami tile that provides the track, two-state DNA machines attached to the tile and containing the cargo, and a DNA walker that can move along the track to collect the cargo.<sup>44</sup> In this design all movements were processed through strand displacement reactions. However, motion can also be created through the use of enzymes, and in 2010 Stojanovic and co-workers demonstrated that a so-called molecular spider comprising of a streptavidin molecule as an inert body and three catalytic DNAzyme legs can undergo directional movement along a DNA-origami track. The track contained a series of staple strands complementary to the DNAzyme legs; thus, the spider was capable of walking through the track and catalytically degrading it through DNA cleavage.<sup>45, 46</sup>

#### 1.1.2.3 Hybrid materials

Thus far, it has been shown that the programmability of DNA is by far one of the most attractive features as it offers the possibility of synthesizing nanomaterials with a level of precision not typically attainable using standard synthetic chemistry. However, whilst the control and selectivity of biopolymers such as DNA are far superior to synthetic polymers, they

do not contain the breadth of chemical design and thus the stability and synthetic accessibility. In contrast, over the years, polymer chemists have built up a large repertoire of monomers which can be polymerized *via* many different mechanisms to prepare polymer structures whose properties such as self-assembly and stability can be easily tuned to reach a versatile range of applications. It is thus not surprising that researchers have become increasingly interested in hybrid materials combining the robustness and tunability of synthetic polymers with the specificity and programmability of DNA.<sup>21, 47, 48</sup>

The first example of a DNA-polymer conjugate dates back to the 1980's when DNA was grafted on to poly(L-lysine) to promote antiviral activity.<sup>22,49</sup> Since then DNA has been conjugated to a number of water soluble polymers such as poly(ethylene glycol) (PEG),<sup>50-55</sup> poly(D,L-lactic-co-glycolic acid) (PLGA)<sup>56</sup>, poly(*N*-isopropylacrylamide) (PNIPAM)<sup>57, 58</sup> and poly(*p*-phenyleneethynylene) (PPE)<sup>59</sup>. Much of the early work surrounding DNA-polymer conjugates was focused on attempts to improve the stability and cellular uptake of antisense oligonucleotides (AOs). AOs are short sequences of ssDNA or ribonucleic acid (RNA) complementary to a target sequence on messenger RNA (mRNA) and have proven to be effective against a number of diseases through the disruption of gene expression.<sup>60</sup> However, AOs are susceptible to enzymatic degradation by nucleases and display poor cellular uptake.<sup>61</sup> Park and others demonstrated that the conjugation of AOs to PEG forms a diblock copolymer which, in the presence of a cationic complex, self-assembles to form a polyelectrolyte complex micelle (Figure 1.5). The neutral DNA-complex is in the core of the micelle and hence protected from nucleases whilst the hydrophilic shell improves cellular uptake.<sup>50-54</sup>

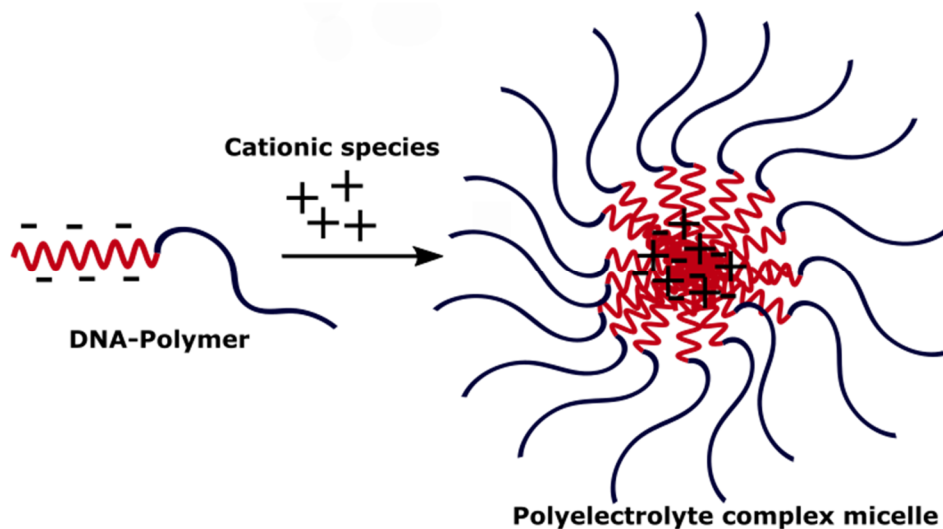


**Figure 1.5** Self-assembly of DNA-polymer conjugates in the presence of a cationic species to form polyelectrolyte complex micelles that protect the AOs from nucleases and enhance cellular uptake. Red lines – DNA; blue lines – polymer.

Further applications of water-soluble DNA polymer conjugates exist beyond those used for therapeutic delivery. For example, the thermoresponsive behavior of PNIPAM has been used for affinity separation due to the precipitation of the respective DNA-polymer conjugates above the lower-critical solution temperature (LCST) of PNIPAM.<sup>57, 58, 62, 63</sup> Furthermore, the conjugation of DNA to a conjugated polymer such as PPE was utilized for the label-free detection of DNA.<sup>59</sup> Such water-soluble DNA polymer conjugates are often prepared *via* a solution-phase coupling methodology utilizing activated-ester chemistry,<sup>50-52, 56</sup> Michael addition<sup>53, 54</sup> or disulfide bond formation (Figure 1.6).<sup>55</sup>

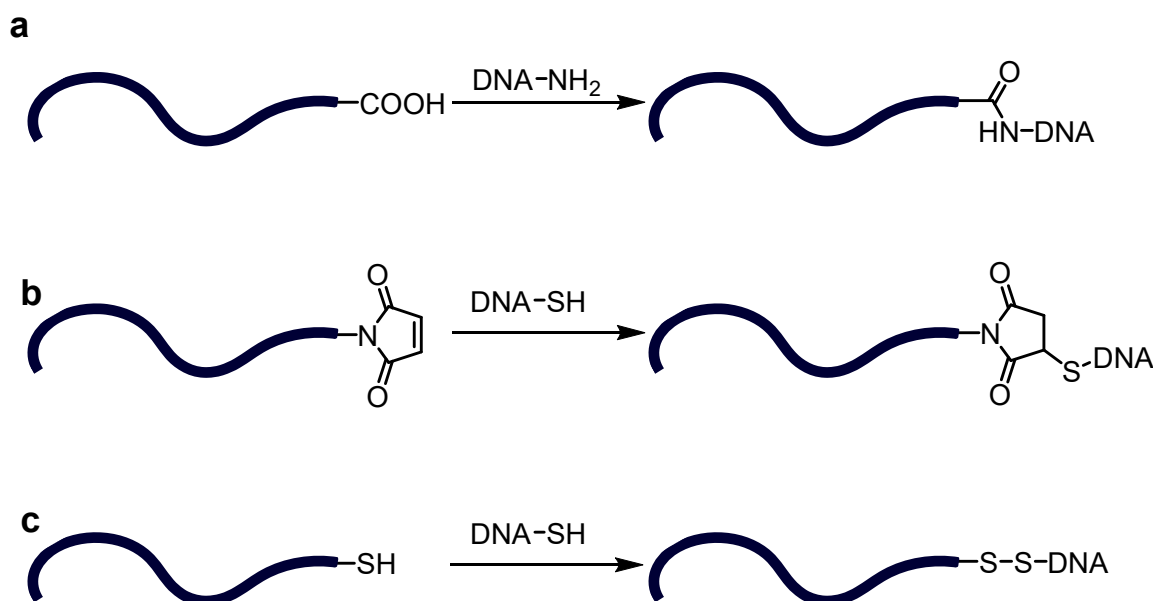


**Figure 1.6** Solution-phase coupling methods utilized for the conjugation of DNA to hydrophilic polymers (blue lines). (a) Activated-ester chemistry; (b) Michael addition; (c) disulfide bond formation.

Recently, the conjugation of oligonucleotides to hydrophobic polymers has been conducted to prepare amphiphilic molecules capable of undergoing self-assembly. The self-assembly behavior of such amphiphilic molecules is typically governed by hydrophobic, electrostatic and other intermolecular interactions and results in a variety of morphologies including spheres, cylinders and vesicles.<sup>21</sup> The morphology is usually dictated by the critical packing parameter ( $p$ ). The critical packing parameter is related to the volume of the hydrophobic segment ( $v$ ), the area of the hydrophilic headgroup ( $a_0$ ) and the length of the hydrophobic chain ( $l_c$ ), such that  $p = v/a_0l_c$ . For structures at equilibrium the morphology can be predicted from  $p$  as follows:  $p < 1/3$ , spherical micelles with a high interfacial curvature are favoured, cylinders are favoured when  $p$  ranges from  $1/3$  to  $1/2$  and vesicles are formed if  $p$  ranges from  $1/2$  to  $1$  (Figure 1.7).<sup>64</sup> However, the uniqueness of DNA-polymer conjugates is that they are capable of further self-assembly into higher-order structures through DNA hybridization as will be illustrated in a latter example.

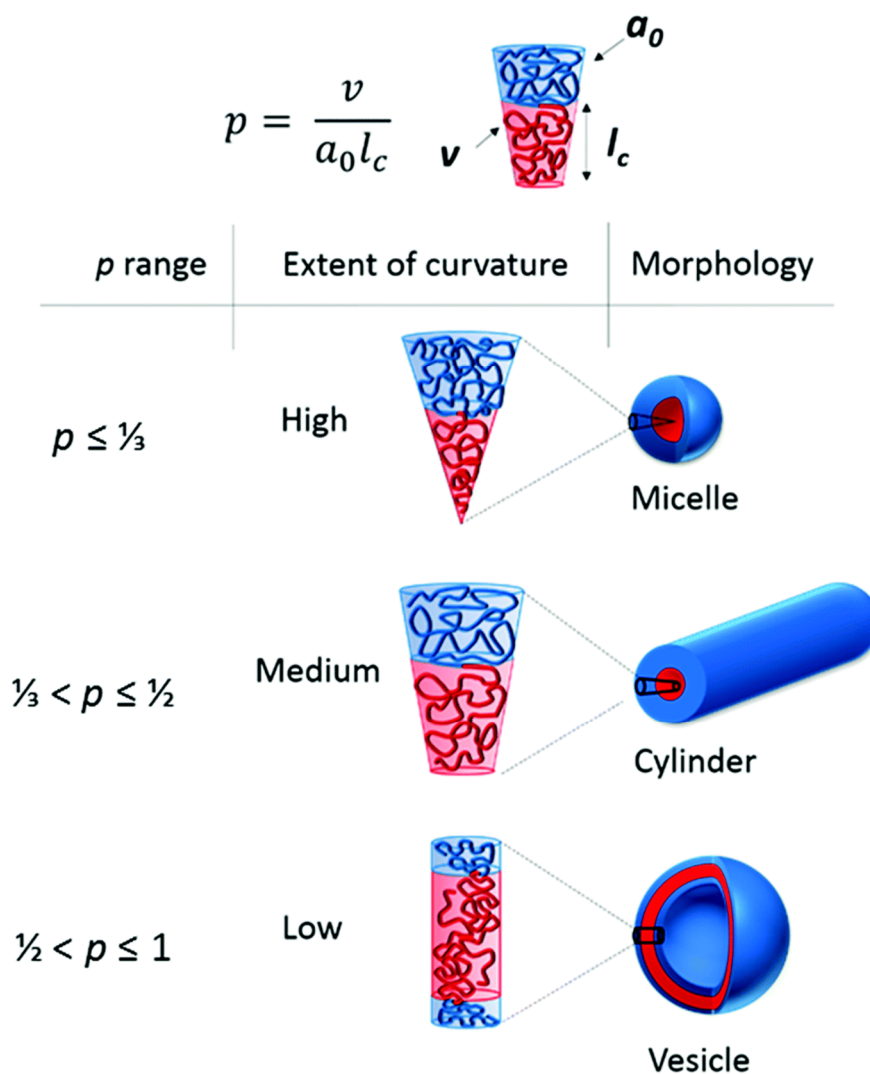


**Figure 1.7** Schematic showing the relationship between the critical packing parameter ( $p$ ) calculated from the molecular structure and the resulting particle morphology. Figure taken with permission from Doncom *et al.* - Published by The Royal Society of Chemistry.<sup>64</sup>

The conjugation of oligonucleotides to hydrophobic polymers is more challenging than to hydrophilic polymers due to the contrasting solubility properties of DNA to the hydrophobic polymer. As a consequence of this, the solution-phase conjugation of oligonucleotides to polymers is particularly low yielding. In 2016, Wilks *et al.* screened a number of coupling chemistries in organic solvents capable of solubilising more hydrophobic polymers.<sup>65</sup> In this work, three coupling chemistries were studied: amide coupling chemistry, the thiol-ene reaction and the inverse electron demand Diels-Alder ( $DA_{inv}$ ) reaction. The conjugation of DNA

to PNIPAM was attempted in a range of organic solvents and despite the success of the amide coupling chemistry and thiol-ene reaction under aqueous conditions, in organic solvents both chemistries yielded no product. In contrast, the  $DA_{inv}$  reaction yielded DNA-polymer conjugates in up to 40% yield in *N,N*-dimethylformamide (DMF), *N,N*-dimethylacetamide and *N*-methyl-2-pyrrolidone. Whilst this study illustrated the limitations with solution-phase coupling in organic solvents, the same authors did successfully couple DNA to PNIPAM and polystyrene (PS) using copper-catalyzed azide alkyne cycloaddition (CuAAC) achieving yields up to 90%.<sup>66</sup> Furthermore, the DNA on the PNIPAM conjugate was capable of self-assembling into a DNA-tetrahedron and then the resulting conjugate further assembled into large well-defined nanoparticles near the LCST of PNIPAM. This study thus demonstrates how the DNA and polymer properties can be utilized to form well-defined higher order structures. More recently, a copper-free azide-alkyne click reaction was used to couple DNA to poly( $\epsilon$ -caprolactone) (PCL) in a (9:1 v/v) dimethyl sulfoxide (DMSO): water mixture, achieving up to 85% yields.<sup>67</sup>

One way of overcoming the solubility issues when using hydrophobic polymers is to couple the polymer whilst the DNA remains on the solid support. Whilst on the solid support many of the protecting groups including those on the phosphate backbone remain and therefore the DNA is completely organosoluble. This methodology has been successfully utilized to couple a range of hydrophobic polymers to DNA using amide coupling chemistry<sup>68</sup> and CuAAC<sup>69, 70</sup>. However, this approach not only requires access to an automated solid-phase synthesizer, but the coupling chemistry must also remain stable under the highly basic conditions used to cleave the DNA from the resin. Therefore, Herrmann and co-workers demonstrated that DNA can be transferred to the organic phase through use of a surfactant

omitting the need for a solid-phase synthesizer.<sup>33</sup> In this approach, the counterions which are present along the DNA-phosphate backbone are replaced with quaternary ammonium surfactants, this provided a hydrophobic coating around the DNA and thus facilitated the solution phase coupling of DNA to PS, poly(propylene oxide) (PPO) and polyisoprene (PI).

All examples discussed thus far involved the coupling of DNA post-polymerization and this coupling was completed either in solution or on the solid phase. This 'graft-to' approach has received the most attention over the last three decades due to the vast array of known coupling chemistries available and the ability to access a number of polymer architectures including linear<sup>66</sup>, brush<sup>71</sup> and hyperbranched<sup>72</sup> polymers.<sup>21</sup> However, despite its success, the limited conjugation yields obtained can lead to difficulties during the purification of the sample and make it difficult to control the grafting density. As a result, in recent years there has been an increasing interest in 'graft-through' and 'graft-from' approaches to prepare DNA-polymer conjugates (Figure 1.8). However, thus far only a handful of examples are present in the literature.

The 'graft-from' approach involves the growing of a polymer chain from the DNA. Thus far, this approach has only been utilized to prepare linear conjugates *via* either reversible addition-fragmentation chain transfer (RAFT) polymerization<sup>73-75</sup> or atom-transfer radical polymerization (ATRP).<sup>76, 77</sup> In contrast, the 'graft-through' approach involves the direct polymerization of a DNA macromonomer and examples so far are limited to those based on the ring-opening metathesis polymerization (ROMP) of DNA-monomers.<sup>33, 78</sup> It should be noted that the previously discussed solubility issue still remains for the 'graft-to' and 'graft-through' polymerizations of amphiphilic DNA-polymer conjugates. Therefore, the use of either

solid-phase chemistry or protecting groups are often required. However, a breakthrough has been made over the last couple of years to allow for the solution-phase ‘graft-from’ polymerization of DNA-polymer conjugates.<sup>75, 79</sup>

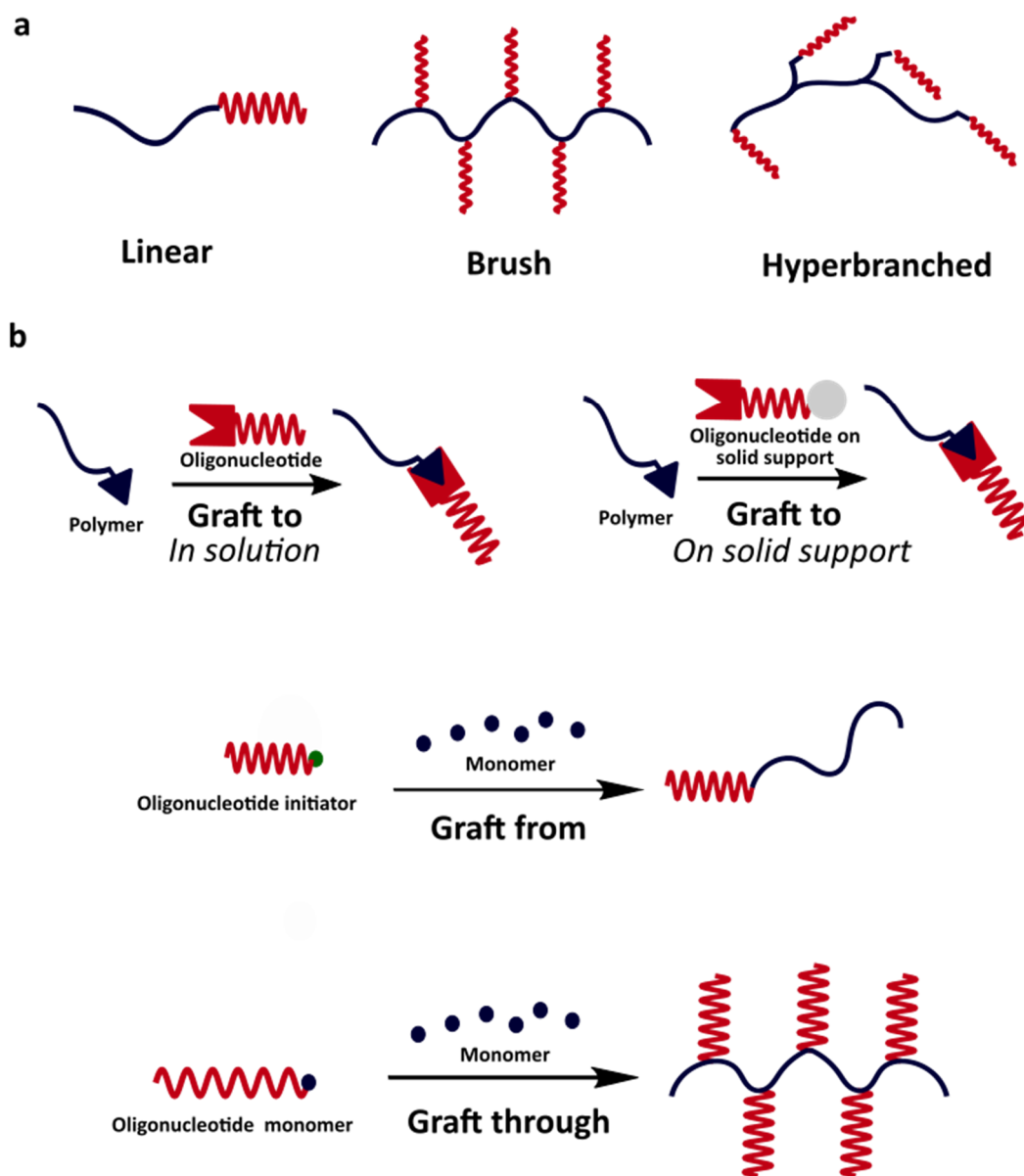


**Figure 1.8** (a) Common DNA-polymer architectures. (b) Approaches to prepare DNA-polymer conjugates. Red lines – DNA; blue lines – polymer; blue spheres – monomers; green spheres – initiator and grey spheres – solid support.



#### 1.1.2.4 DNA-encoded chemical libraries for small molecule discovery

Alongside hybrid materials DNA can further support synthetic chemistry in the form of DNA-encoded chemical libraries (DECLs). The discovery of bioactive molecules capable of binding targets of interest is a continuous effort in the pharmaceutical industry and a vast amount of money is spent on it each year. A selection-based approach in which a large library of compounds are synthesized and then tested for the desired interaction in one-pot could substantially reduce the cost and time taken to screen libraries. One approach showing great potential is DECLs.<sup>80</sup> DNA is particularly attractive for screening because a DNA 'tag' can act as a barcode which can be amplified *via* polymerase chain reaction (PCR) and then 'read-back' through advancements in DNA sequencing. Furthermore, if the DNA directs the chemistry then the DNA can go through multiple rounds of mutation and translation to facilitate molecular evolution (Figure 1.9).

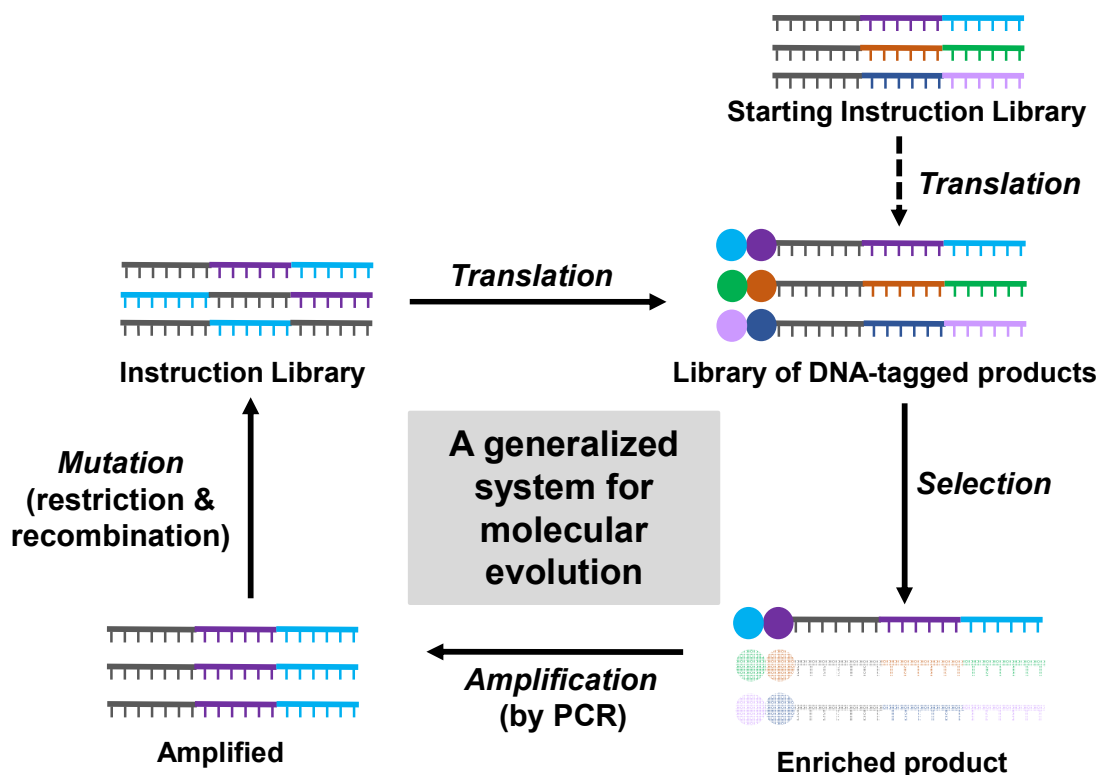


**Figure 1.9** Schematic showing how molecular evolution can be achieved using DECLs. Figure adapted from Wilks et al.<sup>20</sup>

The first DECL was reported by Brenner and Lerner in 1992.<sup>23</sup> Since then a huge number of strategies have been developed and they can broadly be split into two types: DNA-recorded synthesis and DNA-directed synthesis.

#### 1.1.2.4.1 DNA-recorded synthesis

The most common approach for DNA-recorded synthesis relies upon a split and pool approach. Here, chemical compounds are synthesized *via* multiple steps and at each step a DNA 'tag' is added. The initial building blocks are coupled to DNA and then pooled and split into different vessels for the reaction of the next compound. After each subsequent reaction the oligonucleotide is ligated to add the next barcode. The alternation between chemistry steps followed by ligation is continued until the desired library is prepared (Figure 1.10).<sup>81, 82</sup>

The advantage of this approach is its simplicity and it has been utilized to prepare libraries containing up to 800 million members.<sup>83</sup> However, the small-molecule library is not generated from a library of DNA and thus the library cannot be subjected to the multiple rounds of translation, selection, amplification and mutation required for molecular evolution.

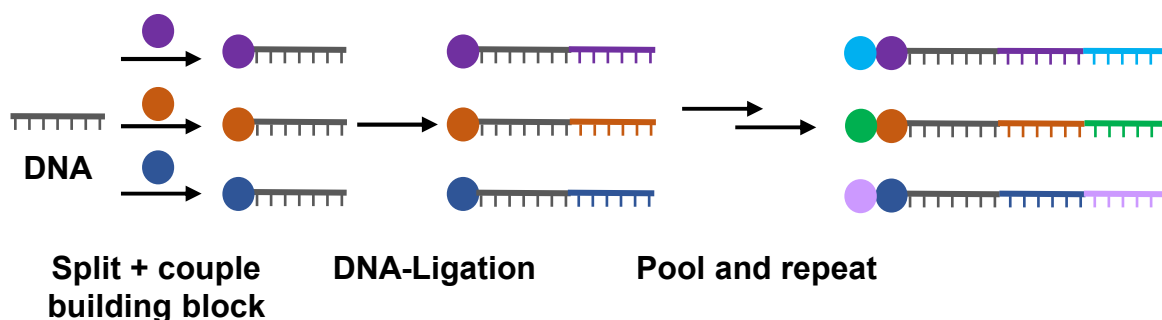


*Figure 1.10 Schematic representing the split and pool approach to prepare DECLs.*

#### 1.1.2.4.2 DNA-directed synthesis

A number of DNA-directed methods have also been developed. In this approach the DNA not only acts as a barcode to 'tag' the chemistry, but it also directs the chemical modification. The

most common approach utilizes DNA-templated synthesis (DTS) and was first demonstrated by Liu and Gartner in 2001 (Figure 1.11a).<sup>26</sup> In DTS, the Watson-Crick base pairing recruits a complementary oligonucleotide which then promotes a reaction between the DNA-linked reagents. This approach therefore allows for the one-pot synthesis of a small molecule library conjugated to their template which are unique to each small molecule. The DNA tags can then be subsequently used for *in vitro* selection, PCR amplification and DNA sequencing to reveal the identity of the synthetic molecule. In 2008, Liu and co-workers developed a library containing 13824 small molecule macrocycles demonstrating the potential of this approach.<sup>84</sup> However, one limitation of this approach is the requirement to synthesize a large number of modified oligonucleotides prior to performing DTS. Therefore, in 2004 Halpin and Harbury developed an alternative DNA-directing approach known as DNA routing which circumvented this issue (Figure 1.11b).<sup>27-29</sup>

In the DNA routing approach, the DNA is immobilized on the solid phase which allows for the chemistry to be conducted in the organic phase. The immobilized DNA contains a number of coding regions which route the DNA templates into physically partitioned subpools which subsequently undergo a reaction. This approach was utilized to prepare a library of  $10^6$  non-natural peptides.<sup>28</sup>

The final DNA-directed approach, named encoded self-assembling combinatorial (ESAC) libraries, was reported by Neri and co-workers in 2004.<sup>30</sup> This approach, labeled a dual-pharmacophore chemical library, has two molecules attached to the adjoining extremities of complementary DNA strands (Figure 1.11c). DNA hybridization brings together two independent DNA libraries to form a possible fragment pair for synergistically binding to a

target protein. This approach was utilized for the identification of synergistic binders to alpha-1-glycoprotein (AGP).<sup>85</sup> However, following the identification of a synergistic binding pair a linker is required to create a discrete organic molecule. To minimize the number of linkers that need to be synthesized *via* traditional organic chemistry, several bidentate ligands were first synthesized and screened on-DNA using fluorescent polarization. This minimized the quantities of scaffolds used and allowed for affinity measurements to be conducted in solution.<sup>86</sup>

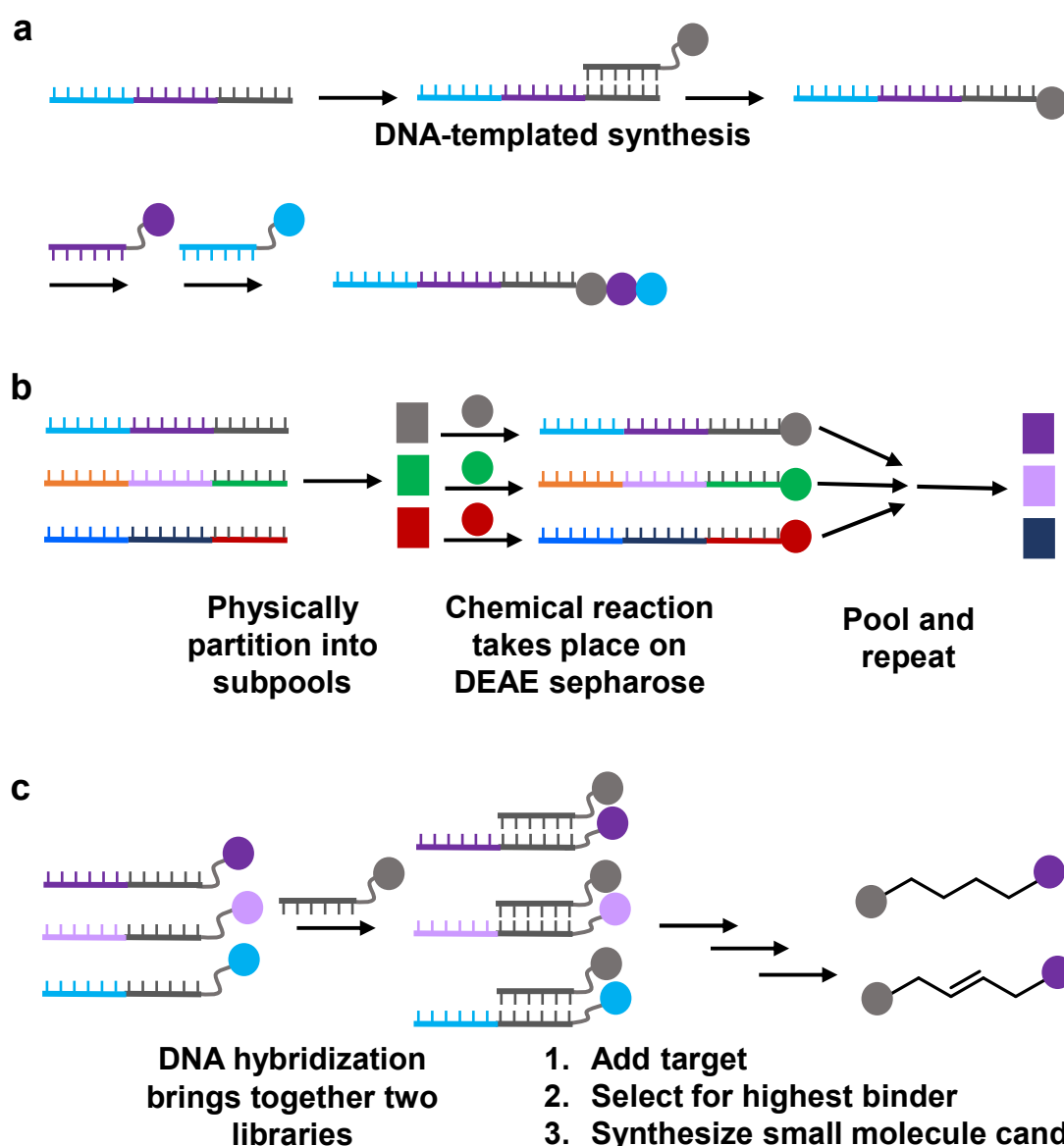


**Figure 1.11** Schematic highlighting DNA-directed approaches towards DECLS. (a) DTS; (b) DNA-routing; and (c) ESAC libraries.

#### 1.1.2.4.2.1 Expanding DTS for sequence-controlled polymer synthesis

In the last decade there has been a push to prepare libraries of longer oligomers which will not only provide access to more complex libraries but can also lead to the preparation of sequence-controlled polymers.<sup>20</sup> Despite huge progress in controlled polymerizations over recent years, the ability to prepare sequence controlled polymers akin to those produced by the ribosome remains a challenge.

Whilst preparing DECLs, Liu and co-workers reported a three-step DTS to prepare a library of macrocycles.<sup>84</sup> Since this report a number of researchers have attempted to exploit multistep DTS to prepare oligomers of significant length. When designing the DTS method, three DNA architectures are commonly utilized to bring reactants together: end-of-helix, cross-nick and junction-based designs (Figure 1.12a).

Initial designs by O'Reilly and co-workers were based on a strand-displacement method, which utilized a toehold domain to remove the active strand once the reaction was complete, facilitating subsequent strand addition (Figure 1.12b).<sup>87</sup> This design aided the synthesis of decamers, the longest sequence specific oligomers prepared to-date.<sup>88</sup> However, in this simple design the oligomer sequence was determined by the order of addition of the reactive monomers and not the template. Therefore, a more sophisticated cross-nick design was developed which allowed for all the reactive monomers to be present in one pot; however, the addition of sequential instruction strands was still required to determine the oligomer sequence and thus the template strand did not retain all the product encoding information.<sup>89</sup> Around the same time, Liu and co-workers proposed an alternative toehold displacement method (Figure 1.13). In contrast to the strand exchange method, this method retained all

product-encoding information on the template strand so the sequence could be ‘read-back’. However, the movement of the reactive center away from the template severely limited the oligomer length that could be achieved.<sup>90</sup>

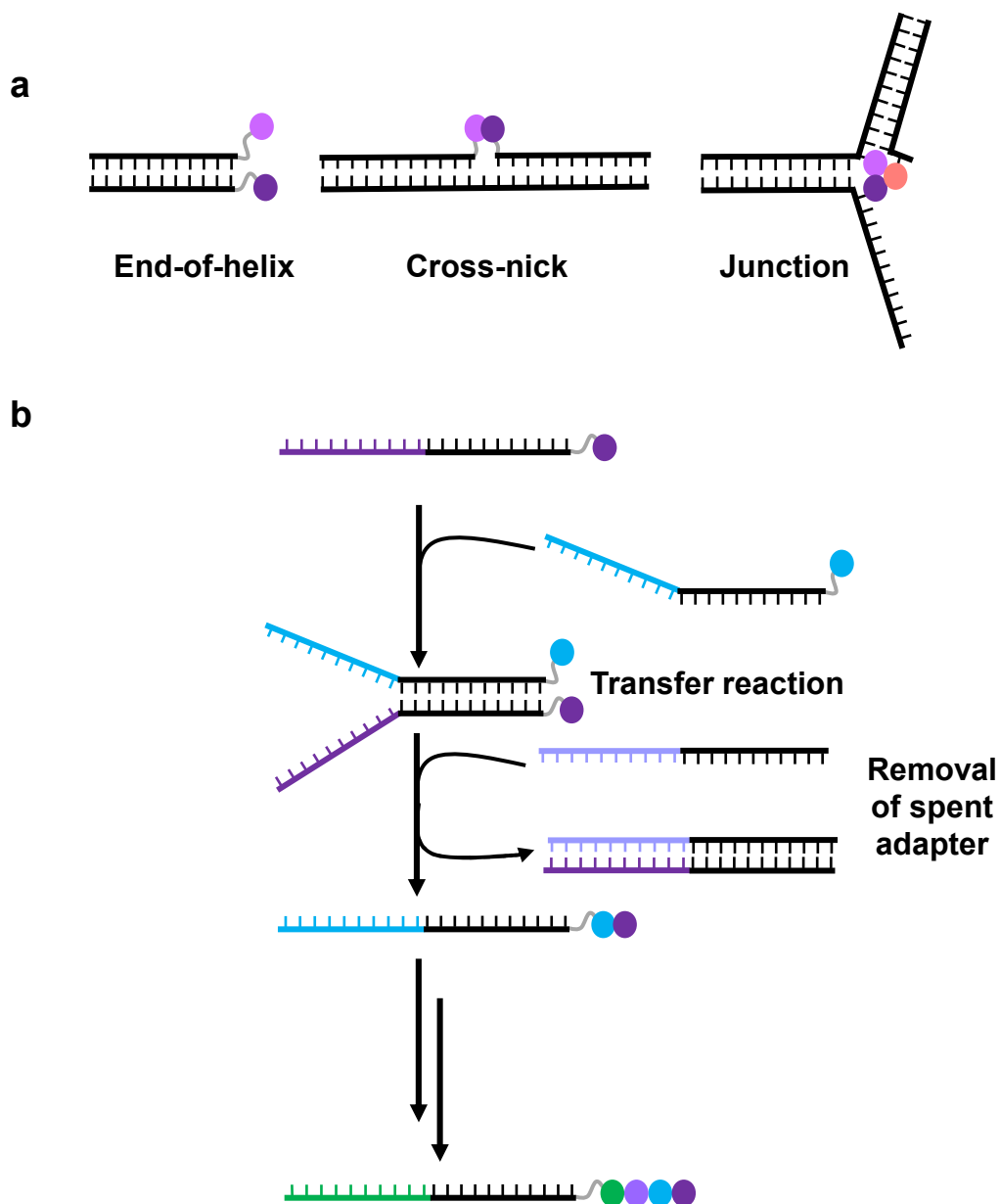


**Figure 1.12** (a) Common DNA architectures employed in DTS. (b) Strand-displacement method by O'Reilly and co-workers used to synthesize sequence specific oligomers through successive Wittig olefination reactions.<sup>87</sup>

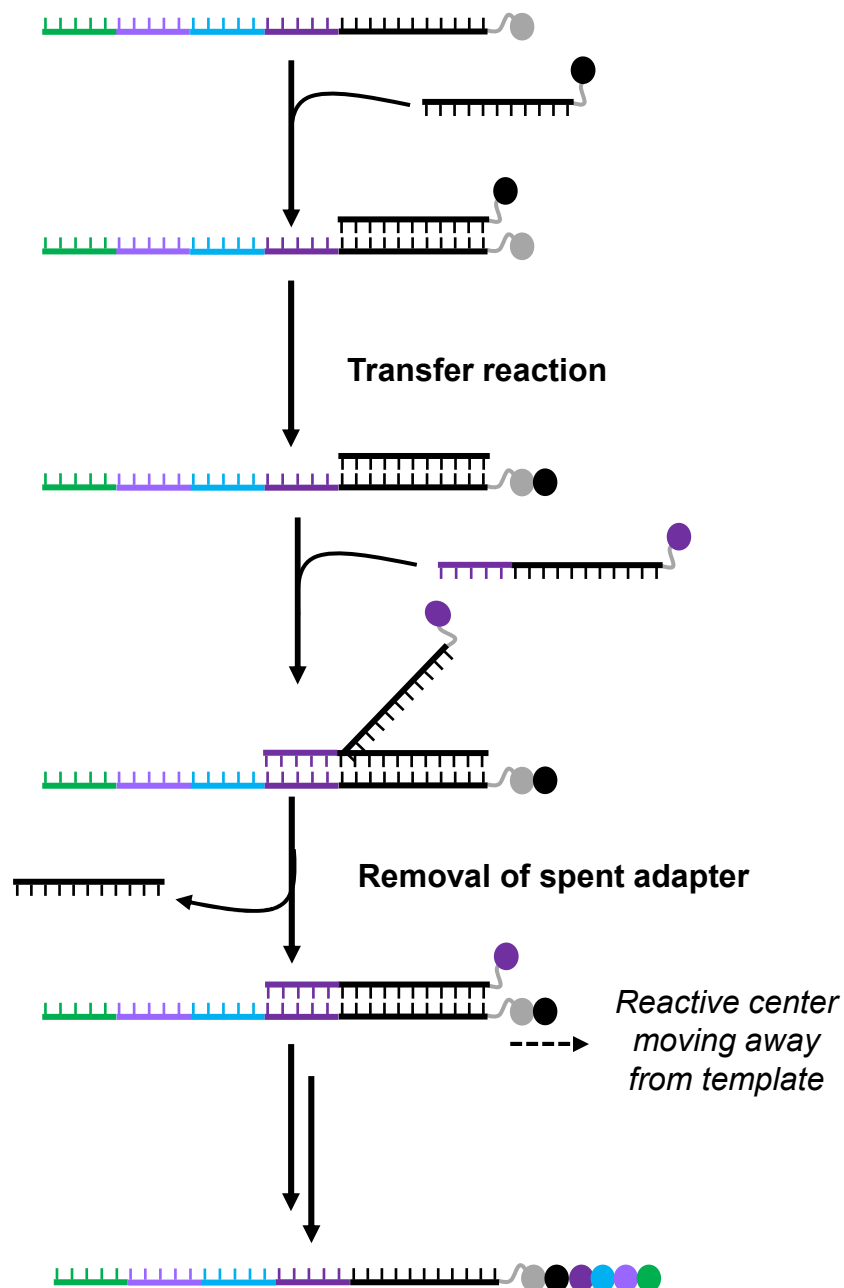


**Figure 1.13** Toehold displacement method used to synthesize sequence specific oligomers through successive amine acylation reactions by Liu and co-workers.<sup>90</sup>

Whilst the above discussed methods significantly improved the maximum attainable length of oligomers by multistep DTS. The biggest development for materials discovery came with the development of two autonomous designs the DNA walker<sup>91</sup> and a hairpin hybridization chain reaction (HCR) method<sup>92</sup> (Figure 1.14). Both methods proceed without any externally supplied stimuli and a record of each sequence is produced for 'read-back'.

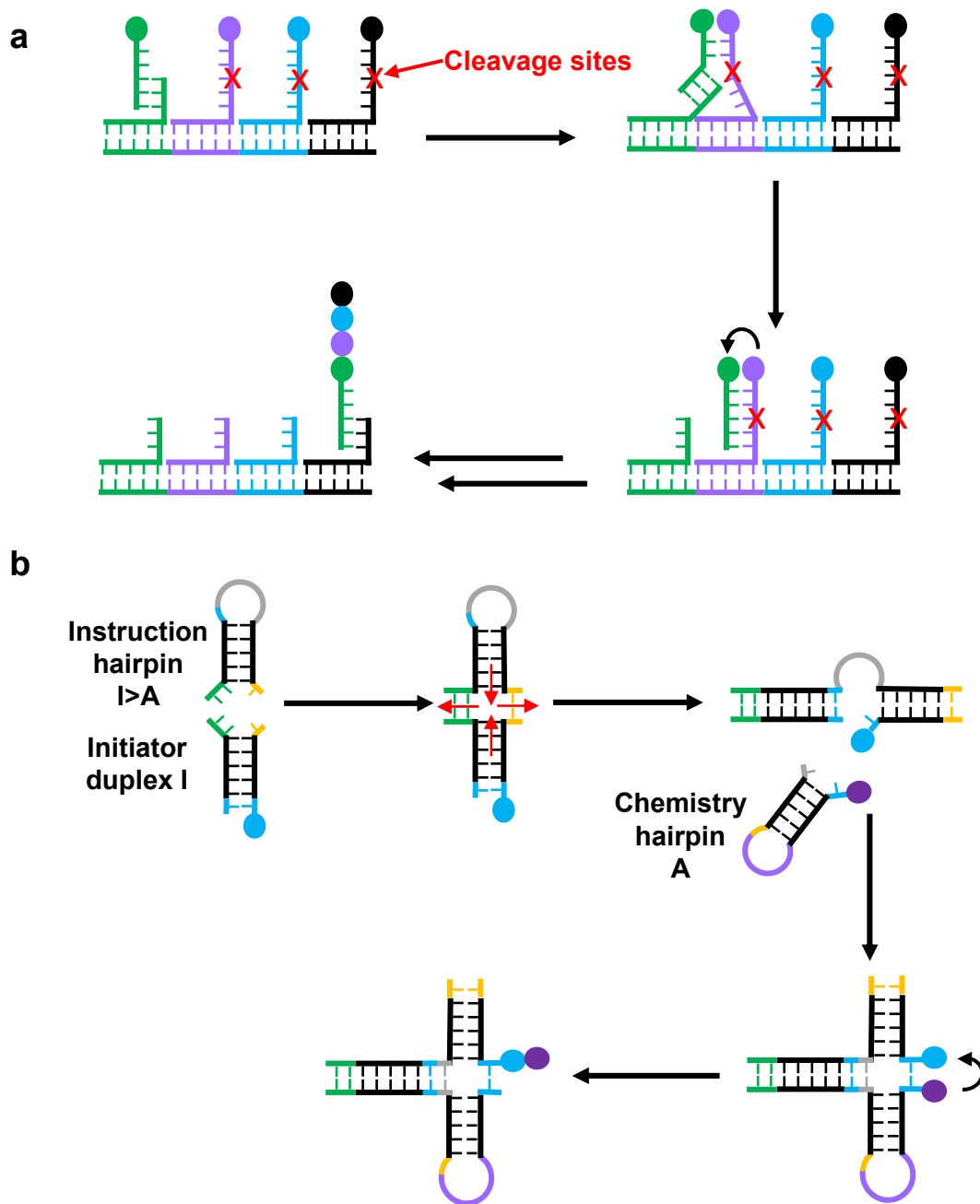


**Figure 1.14** Autonomous molecular machines for the sequence specific synthesis of oligomers. (a) DNA-walker designed by Liu and co-workers used to generate oligomers through amine acylation<sup>91</sup> (b) HCR mechanism designed by Tuberfield and co-workers used to generate oligomers through amine acylation or Wittig olefination.<sup>92</sup>



## 1.2 DNA-compatible chemistries

### 1.2.1 What is a DNA-compatible reaction?

With the presence of several international suppliers of custom-made oligonucleotides, DNA is now more accessible than ever and as such the growth of DNA nanotechnology is likely to continue. However, the success of DNA-nanotechnology relies heavily on the presence of DNA-compatible chemistries. Indeed, the success of a DECL is solely dependent on the structural diversity of the resulting small molecules. However, despite the vast portfolio of chemical reactions available to synthetic chemists, very few of these reactions have thus far been proven to be DNA-compatible.

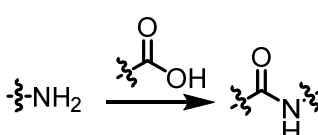
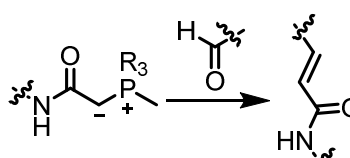
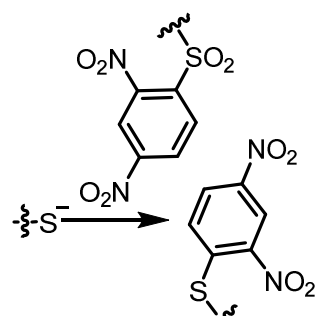
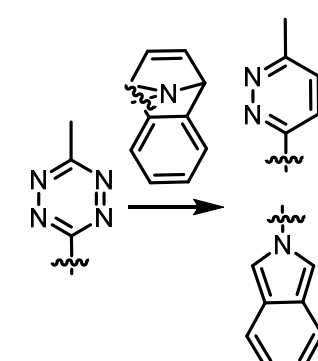
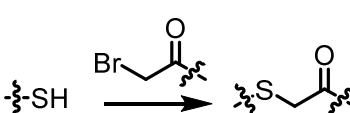
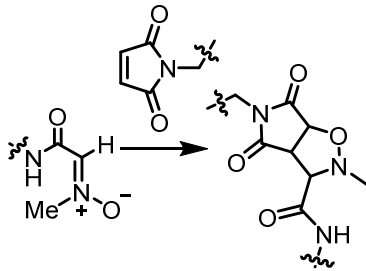
In order for a chemical reaction to be classified as DNA-compatible it must be conducted under conditions that solubilize the DNA substrate and do not modify or destroy the information encoded therein.<sup>93</sup> As such DNA compatible chemistries are typically required to be robust and work in the presence of protic solvents.

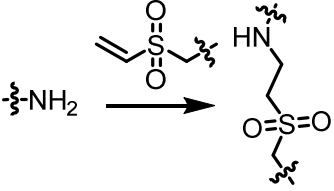
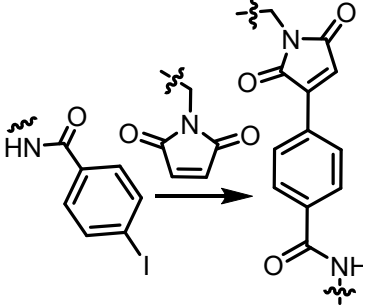
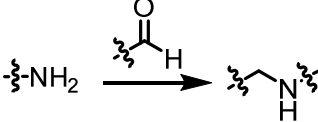
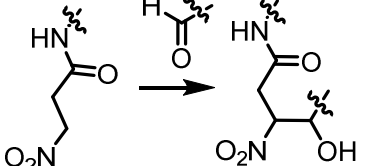
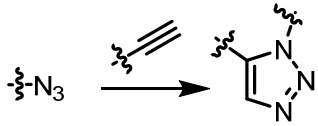
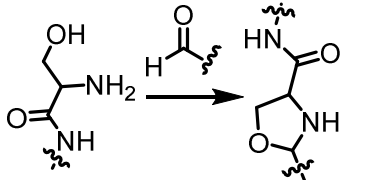
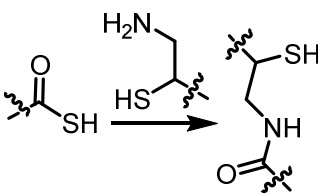
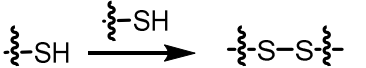
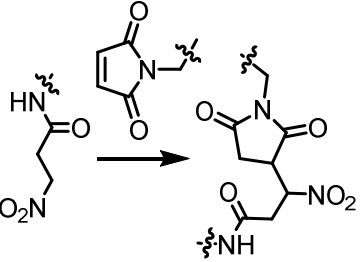
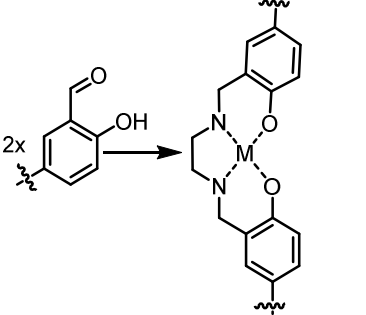
### 1.2.2 Current DNA-compatible chemistries

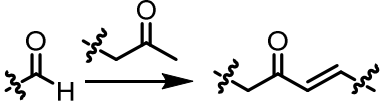
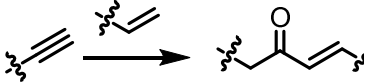
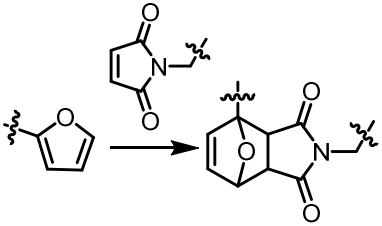
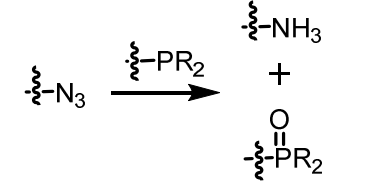
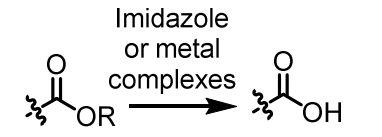
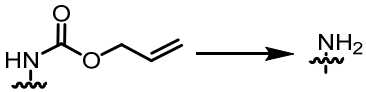
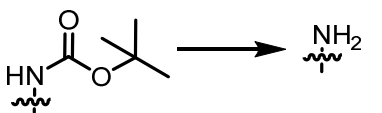
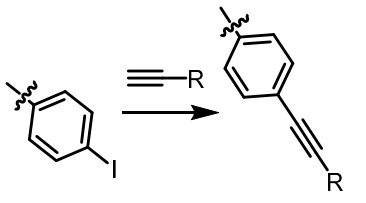
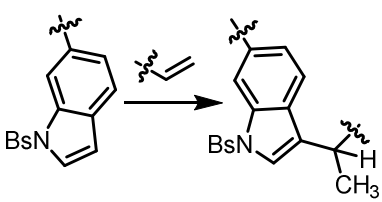
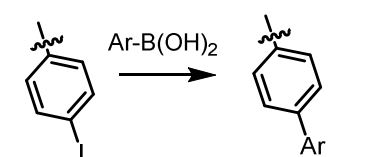
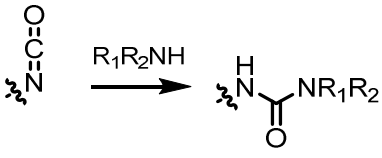
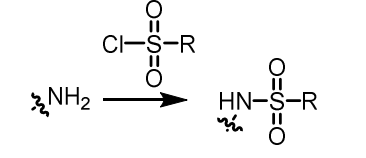
Since the rise in DECLs in early 2000's, studies to identify DNA-compatible chemistries, particularly those unrelated to the nucleic acid backbone of DNA have commenced. Table 1.1 introduces many of the DNA-compatible chemistries studied so far which, despite the rising interest in this area, is still a very limited list. Entries 1 – 20 cover reactions that are not only DNA-compatible but have also been exploited in DNA-templated reactions; entries 21-30 cover some additional chemistries found to be DNA-compatible but not yet reported on DNA-templates. The vast majority of reactions are coupling reactions utilized to ligate two DNA strands together, or for the coupling of DNA to synthetic materials. However, as discussed

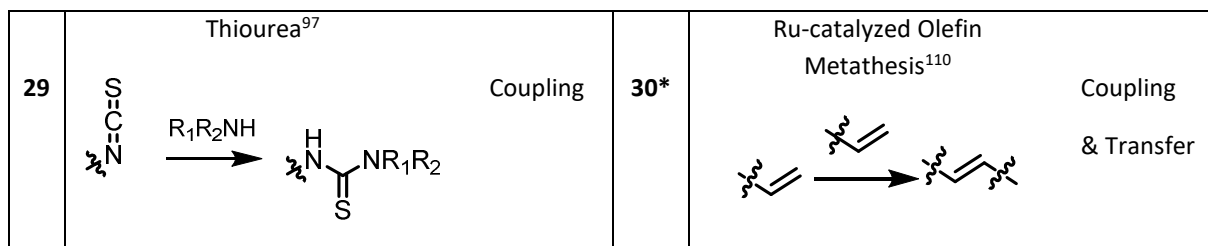
above, multistep DTS requires a transfer chemistry of which they are currently only four tested chemistries (entries 1-4). It is therefore evident that whilst significant advancements have been made in improving the number of DNA-compatible chemistries further research in this area is required to fully exploit the full potential of DNA-nanotechnology.

**Table 1.1** DNA compatible chemistries reported in the literature. <sup>†</sup>Templated reaction conducted in an organic solvent mixture. <sup>\*</sup>First reported after this work commenced.

	Chemistry	Reaction Type		Chemistry	Reaction Type
1	Amine Acylation <sup>94</sup> 	Coupling & Transfer	2	Wittig Olefination <sup>87-89, 94</sup> 	Coupling & Transfer
3	Nucleophilic aromatic substitution <sup>95</sup> 	Transfer	4	Tetrazine transfer <sup>96</sup> 	Transfer
5	Nucleophilic substitution <sup>26</sup> 	Coupling	6	1,3-nitron cycloaddition <sup>94</sup> 	Coupling

7	<p>Conjugate addition<sup>26</sup></p>  <p>Coupling</p>	8	<p>Heck coupling<sup>94</sup></p>  <p>Coupling</p>
9	<p>Reductive amination<sup>94, 97</sup></p>  <p>Coupling</p>	10	<p>Nitro-aldol reaction<sup>94</sup></p>  <p>Coupling</p>
11	<p>Huisgen cycloaddition<sup>98</sup></p>  <p>Coupling</p>	12	<p>Oxazolidine Formation<sup>99</sup></p>  <p>Coupling</p>
13	<p>Native chemical ligation<sup>100</sup></p>  <p>Coupling</p>	14	<p>Disulfide bond formation<sup>100</sup></p>  <p>Coupling</p>
15	<p>Nitro-Michael reaction<sup>94</sup></p>  <p>Coupling</p>	16	<p>Metallosalen Formation<sup>101</sup></p>  <p>Coupling</p>

17	<p>Aldol condensation<sup>102</sup></p> <p>Coupling<sup>†</sup></p> 	18	<p>Pd-Cross coupling<sup>103</sup></p> <p>Coupling</p> 
19	<p>Diels-Alder cycloaddition<sup>104</sup></p> <p>Coupling</p> 	20	<p>Staudinger reaction<sup>105</sup></p> <p>Functional group inter-conversion</p> 
21	<p>Ester hydrolysis<sup>106, 107</sup></p> <p>Imidazole or metal complexes</p> <p>Functional group inter-conversion</p> 	22	<p>Alloc deprotection<sup>97</sup></p> <p>Functional group inter-conversion</p> 
23	<p>Boc deprotection<sup>97</sup></p> <p>Functional group inter-conversion</p> 	24	<p>Sonogashira<sup>97</sup></p> <p>Coupling</p> 
25	<p>Hydroarylation<sup>108</sup></p> <p>Coupling</p> 	26	<p>Suzuki coupling<sup>109</sup></p> <p>Coupling</p> 
27	<p>Carbamylation with isocyanates<sup>97</sup></p> <p>Coupling</p> 	28	<p>Sulfonamides<sup>97</sup></p> <p>Coupling</p> 



## 1.3 Olefin Metathesis

One very significant chemical transformation that is difficult to achieve using the current chemical portfolio (Table 1.1) is carbon-carbon bond formation. Forming the backbone to most organic molecules, carbon-carbon bonds are essential and thus have received a lot of attention in the synthetic chemistry community.<sup>111</sup> One chemistry capable of achieving such transformation is the Nobel Prize winning olefin metathesis reaction first reported in 1967 by Calderon and co-workers.<sup>112</sup>

### 1.3.1 Catalyst development

The capability of metathesis to prepare a notoriously difficult carbon-carbon bond has fueled several decades of extensive research into the catalytic mechanism. This knowledge and understanding has since been utilized to prepare a large catalyst portfolio. The mechanism by which metathesis proceeds was first reported in 1971 by Hérrison and Chauvin, Figure 1.15.<sup>113</sup> Initially the olefin coordinates to a metal alkylidene catalyst and then a [2+2] cycloaddition leads to a metallocyclobutane intermediate. A [2+2] cycloreversion of the metallocyclobutane intermediate releases the olefin product and a catalytically active alkylidene.

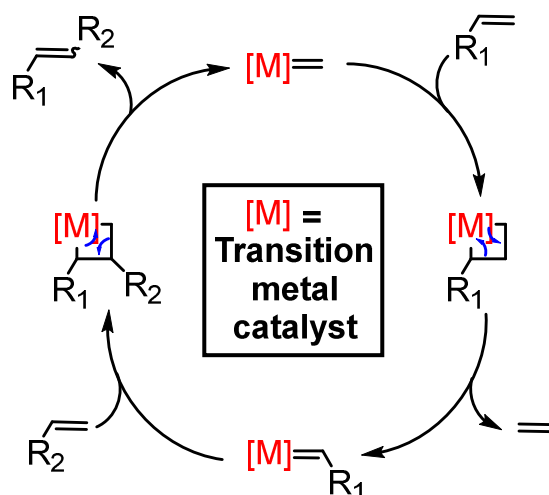


**Figure 1.15** The generally accepted olefin metathesis mechanism catalyzed by a metal alkylidene proceeds via a metallocyclobutane.

Initial catalysts utilized for metathesis were based on early transition metals such as tungsten or molybdenum grafted on to silica or combined with co-catalysts.<sup>114</sup> In the mid-1970s, the first single component metathesis catalysts were developed based on tantalum and tungsten.<sup>115, 116</sup> However, the first commercially available catalyst did not appear until 1990 in the form of Schrock catalyst.<sup>117</sup> The molybdenum-based catalyst was the first catalyst to exhibit exceptionally high activity and thus led to the routine use of metathesis. However, the biggest limitation of Schrock catalyst was the poor functional group tolerance and oxophilic behavior of the catalyst which resulted in all reactions requiring air-free conditions. A series of ruthenium catalysts developed from the mid-1990's by Grubbs and others became the first functional group tolerant catalysts which possess much greater stability to moisture and air and are thus widely used in the chemistry community (Figure 1.16).<sup>118-121</sup> Table 1.2 summarizes the key properties of the most popular commercially available catalysts.

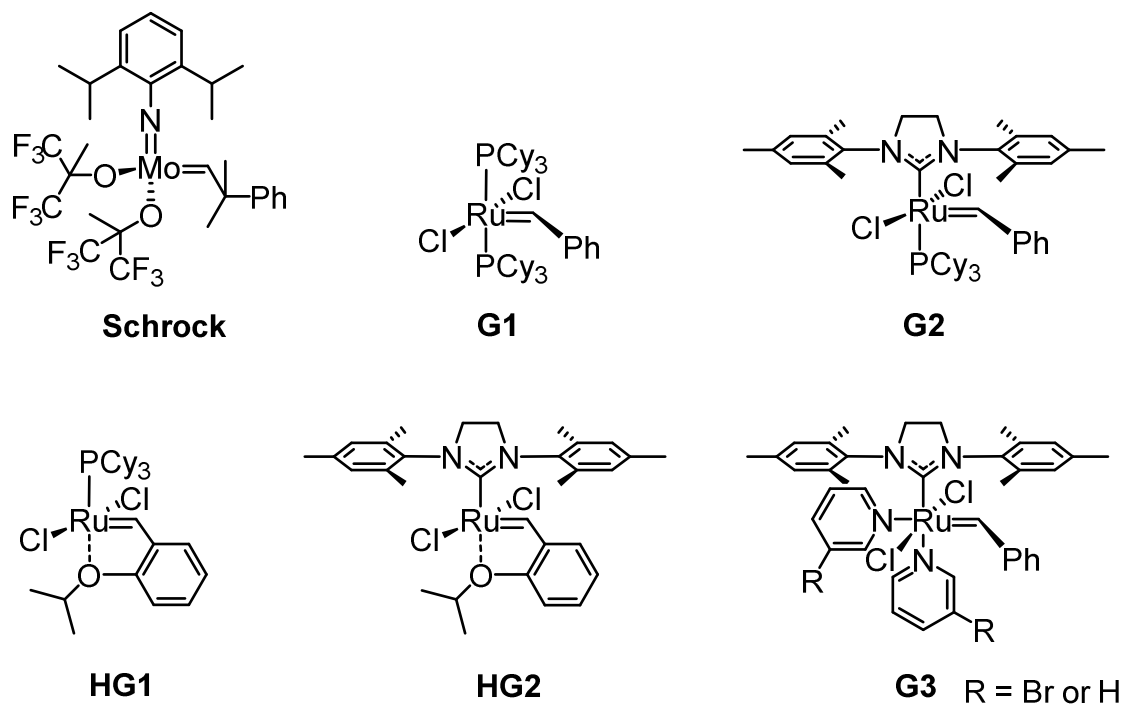


**Figure 1.16** Chemical structures of common commercially available metathesis catalysts.

Whilst the first-generation Ru-catalyst (G1) exhibited excellent functional group tolerance and improved stability compared to Schrock catalyst, the catalyst did possess limited activity compared to the highly active Schrock catalyst. Mechanistic studies revealed that G1 proceeded *via* a dissociative mechanism; therefore, the 16-electron species G1 undergoes a reversible phosphine dissociation to yield the active 14-electron species which can either rebind phosphine or coordinate to the olefin.<sup>122</sup> Replacing one of the phosphine ligands in G1 with an *N*-heterocyclic ligand (NHC) led to the development of a second-generation Ru-catalyst (G2) which was found to possess improved binding to olefins in the presence of free phosphine.<sup>123, 124</sup>

**Table 1.2** Summary of the key features of the commercially available catalysts introduced in Figure 1.15. Table previously reported by Varlas et al.<sup>125</sup>

Catalyst	Year	Metal Center	Advantages	Limitations	Ref.
Schrock	1990	Mo	<ul style="list-style-type: none"> <li>Extremely high reactivity</li> </ul>	<ul style="list-style-type: none"> <li>Must be handled under inert conditions</li> <li>Limited functional group tolerance</li> </ul>	Schrock and co-workers <sup>117</sup>
G1	1995	Ru	<ul style="list-style-type: none"> <li>Enhanced stability in air</li> <li>High functional group tolerance</li> </ul>	<ul style="list-style-type: none"> <li>Reduced reactivity compared to Mo compounds</li> </ul>	Grubbs and co-workers <sup>118, 126</sup>
G2	1999	Ru	<ul style="list-style-type: none"> <li>Greater activity than G1</li> <li>Enhanced stability compared with G1 and HG1</li> </ul>	<ul style="list-style-type: none"> <li>Lower reactivity compared to Mo compounds</li> <li>Poor polymerization control due to slow initiation compared to propagation</li> </ul>	Nolan, <sup>127, 128</sup> Herrmann, <sup>129, 130</sup> Grubbs and co-workers <sup>131-133</sup>
HG1	2000	Ru	<ul style="list-style-type: none"> <li>Greater stability in air than G1</li> <li>Catalyst can be recovered and recycled in some cases</li> </ul>	<ul style="list-style-type: none"> <li>Slower initiation than G1 and G2</li> </ul>	Hoveyda and co-workers <sup>120</sup>
HG2	2000	Ru	<ul style="list-style-type: none"> <li>Greater stability in air than all other catalysts</li> <li>Catalyst can be recovered and recycled in some cases</li> <li>Workhorse catalyst in CM and RCM reactions</li> </ul>	<ul style="list-style-type: none"> <li>Slower initiation than G1 and G2</li> </ul>	Hoveyda, <sup>121</sup> Blechert and co-workers <sup>134</sup>
G3	2002	Ru	<ul style="list-style-type: none"> <li>Superior initiation rates-catalyzes living ROMP of norbornenes</li> </ul>	<ul style="list-style-type: none"> <li>Limited benchtop stability</li> </ul>	Grubbs and co-workers <sup>135</sup>

Phosphine free catalysts have since been reported in the form of Hoveyda-Grubbs 2<sup>nd</sup> generation catalyst (HG2) and Grubbs 3<sup>rd</sup> generation catalyst (G3). HG2 reported simultaneously by the groups of Hoveyda<sup>121</sup> and Blechert<sup>134</sup> replaces the phosphine ligand



with bidentate styrene ligand and shows a unique level of reactivity especially towards electron deficient alkenes and increased stability. The combination of these properties mean it is often the catalyst of choice for cross-metathesis (CM) and ring-closing metathesis (RCM) transformations. In contrast, G3 which is formed through the replacement of the phosphine ligands in G2 with pyridine ligands possess limited benchtop stability but is extremely fast initiating and thus is often the catalyst of choice for ROMP.<sup>135</sup>

### 1.3.2 Metathesis in aqueous media

Thus far all catalysts introduced possess excellent activity in organic solvents but are insoluble under aqueous conditions. Aqueous solubility would be essential for DNA technology, and indeed other biological applications such as protein modification, to fully exploit the metathesis reaction.<sup>136</sup> Fortunately, the inexpensive, non-flammable and non-toxic nature of water has resulted in considerable efforts towards the development of water-soluble metathesis catalysts and a number of variations are now reported.<sup>137</sup>

The greater stability of Ru-based metathesis catalysts compared to molybdenum catalysts makes these complexes promising candidates for aqueous ROMP and as such attempts to prepare water soluble catalysts have focused on these scaffolds. Water solubilizing groups including both ionic and neutral polar groups may be added to the catalysts on the phosphine, NHC, benzylidene or pyridine ligands to render the catalysts water soluble and this approach has been studied extensively (Figure 1.17). Initial work focused on the addition of cationic ligands to the phosphine groups on G1-type scaffolds and such catalysts promoted the ROMP of water soluble oxanorbornene monomers but not without the addition of Brønsted acids. However, due to the greater stability of HG2, more recently work has focused on the

functionalization of this scaffold with water solubilizing groups. Grela and co-workers found that whilst the addition of one cationic group led to water solubility (typically ca. 1 mg mL<sup>-1</sup>), the addition of a cationic group to the NHC and benzylidene ligand led to a catalyst highly soluble in aqueous media (35 mg mL<sup>-1</sup>). This catalyst was successfully used for the CM and RCM of a range of water-soluble substrates in neat water.<sup>138</sup>

As an alternative to the use of ionic ligands a number of studies have focused on the addition of neutral polar groups, most commonly PEG to render the catalyst water soluble. One of the most successful catalysts developed by Grubbs and co-workers included the addition of PEG on to the backbone of the unsaturated NHC ligand. The catalyst was found to be highly water-soluble and active performing ROMP, RCM and CM in aqueous media.<sup>139</sup> However, the slow initiation of G2-type catalysts limits the capability of living-ROMP. Therefore, the addition of PEG to the pyridine ligands of G3 was studied resulting in a faster initiating water-soluble catalyst.<sup>140</sup>

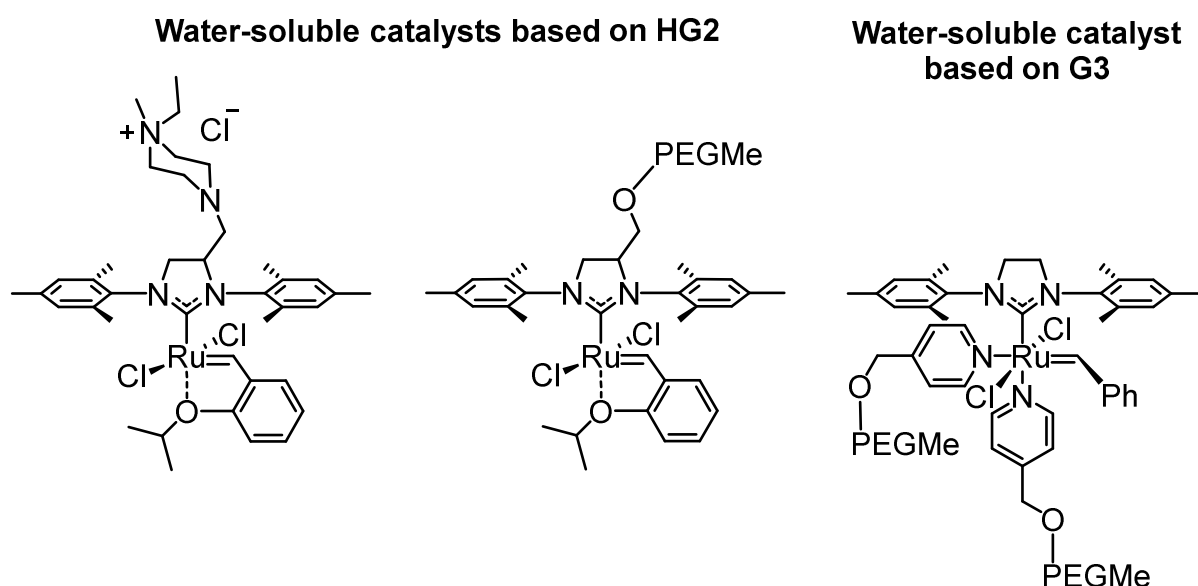


**Figure 1.17** Examples of water-soluble catalysts recently reported.<sup>138-140</sup>

In order to avoid challenging multistep syntheses of water-soluble catalysts, alternative studies have attempted to use the commercially available Grubbs-type catalysts in water/organic solvent mixtures. Across a number of independent studies, a range of water miscible organic solvents have been tested including methanol, DMF, tetrahydrofuran (THF), 1,4-dioxane and dimethoxyethane (DME). However, often unless a high organic content is utilized fully homogenous systems are not achieved and the reaction is slow.<sup>141, 142</sup> Whilst metathesis in aqueous media is yet to be as efficient as that in organic solvents it has opened the possibility of performing metathesis on biomolecules.<sup>136</sup>

### 1.3.3 The potential of metathesis in DNA nanotechnology

Several metathesis reactions have been reported which are of interest to the DNA community, these include CM, RCM and ROMP (Figure 1.18). These transformations were identified to be valuable to the DNA community in a number of ways. Firstly, CM leads to a transfer reaction which until now has not been explored as a reaction compatible with DTS. However, such chemistry could not only overcome the stability issues with the current chemistry, but it could also lead to the development of sequence-defined polymers with a unique non-natural polymer backbone. Secondly, RCM is widely used in the pharmaceutical industry for the synthesis of large macrocyclic ring; therefore, the development of 'on-DNA' RCM could further the structural diversity of DECLs allowing for a greater area of chemical space to be screened. Whilst this is not an area covered within this thesis, a number of other groups have been exploring this area in recent years.<sup>110, 143</sup> Finally, the fast polymerization kinetics of ROMP and resulting well-spaced backbone make metathesis particularly well-suited to the 'graft-through' polymerization of DNA macromonomers towards DNA-polymer conjugates. However, prior to this work few publications existed in this area.<sup>33</sup>

---

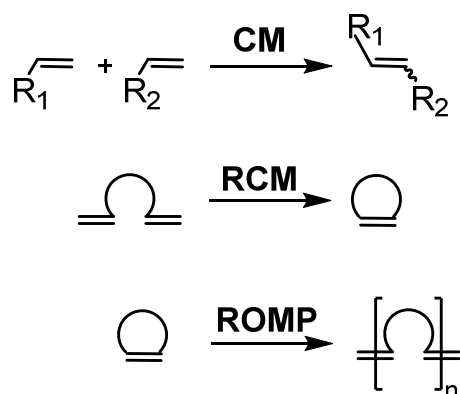


**Figure 1.18** Commonly explored metathesis reactions: Cross-metathesis (CM), ring-closing metathesis (RCM) and ring-opening metathesis polymerization (ROMP).

## 1.4 Project aims

It is clear that the continued success of DNA nanotechnology is reliant upon the expansion of DNA-compatible chemistries. One particular chemistry of interest is the Ru-catalyzed olefin metathesis reaction, capable of yielding macrocyclic rings, facilitating transfer reactions and preparing polymers through a ring-opening mechanism. Previous DNA-templated transfer reactions studied in the O'Reilly group, such as Wittig olefination and amine acylation, suffered from poor stability in the aqueous environment required for DTS; thus, the study of new chemistries is paramount in order to identify chemistries which can overcome this limitation.

To this end, the first aim of this project was to study the compatibility of metathesis with DNA, in particular unprotected DNA. At the beginning of this project there were no previous reports of metathesis in the presence of unprotected DNA and thus a greater understanding of the interactions between the catalyst and DNA was required.

The second aim was to prepare DNA-polymer conjugates *via* the ring-opening metathesis polymerization of a DNA-macromonomer. It was hoped that this would provide a simple

methodology to prepare DNA-polymer conjugates *via* the graft-through polymerization of native DNA.

Finally, in an attempt to add this chemistry to the repertoire of chemistries available for DTS; the preparation of a DNA-functionalized metathesis catalyst was attempted.

## 1.5 References

1. S. Bayda, M. Adeel, T. Tuccinardi, M. Cordani and F. Rizzolio, *Molecules*, 2020, **25**, 15.
2. R. P. Feynman, *Caltech Eng. Sci.*, 1960, **23**, 22-36.
3. N. Taniguchi, *Proceeding of the ICPE*, Tokyo, 1974.
4. C. Kinnear, T. L. Moore, L. Rodriguez-Lorenzo, B. Rothen-Rutishauser and A. Petri-Fink, *Chem. Rev.*, 2017, **117**, 11476-11521.
5. T. Singh, S. Shukla, P. Kumar, V. Wahla, V. K. Bajpai and I. A. Rather, *Frontiers in Microbiology*, 2017, **8**, 1501.
6. L. M. Katz, K. Dewan and R. L. Bronaugh, *Food Chem. Toxicol.*, 2015, **85**, 127-137.
7. L. J. McBride and M. H. Caruthers, *Tetrahedron Lett.*, 1983, **24**, 245-248.
8. N. Michelotti, A. Johnson-Buck, A. J. Manzo and N. G. Walter, *WIREs Nanomed. and Nanobiotechnol.*, 2012, **4**, 139-152.
9. T. Brown and T. Brown (Jnr), *Nucleic Acids Book*, ATDBio Ltd, <https://www.atdbio.com/nucleic-acids-book> (accessed 10.11.2020).
10. J. D. Watson and F. H. C. Crick, *Nature*, 1953, **171**, 737-738.
11. N. C. Seeman, *Annu. Rev. Biochem.*, 2010, **79**, 65-87.
12. P. Yakovchuk, E. Protozanova and M. D. Frank-Kamenetskii, *Nucleic Acids Res.*, 2006, **34**, 564-574.
13. N. C. Seeman, *Nature*, 2003, **421**, 427-431.
14. Y.-W. Kwon, C. H. Lee, D.-H. Choi and J.-I. Jin, *J. Mater. Chem.*, 2009, **19**, 1353-1380.
15. R. Holliday, *Genetical Research*, 1964, **5**, 282-304.
16. N. R. Kallenbach, R.-I. Ma and N. C. Seeman, *Nature*, 1983, **305**, 829-831.
17. T. H. LaBean, H. Yan, J. Kopatsch, F. Liu, E. Winfree, J. H. Reif and N. C. Seeman, *J. Am. Chem. Soc.*, 2000, **122**, 1848-1860.
18. T. J. Fu and N. C. Seeman, *Biochemistry*, 1993, **32**, 3211-3220.
19. F. Hong, F. Zhang, Y. Liu and H. Yan, *Chem. Rev.*, 2017, **117**, 12584-12640.
20. R. K. O'Reilly, A. J. Turberfield and T. R. Wilks, *Acc. Chem. Res.*, 2017, **50**, 2496-2509.
21. H. Sun, L. Yang, M. P. Thompson, S. Schara, W. Cao, W. Choi, Z. Hu, N. Zang, W. Tan and N. C. Gianneschi, *Bioconjugate Chem.*, 2019, **30**, 1889-1904.
22. M. Lemaitre, C. Bisbal, B. Bayard and B. Lebleu, *Nucleosides & Nucleotides*, 1987, **6**, 311-315.
23. S. Brenner and R. A. Lerner, *Proc. Natl. Acad. Sci.*, 1992, **89**, 5381-5383.
24. E. Winfree, F. Liu, L. A. Wenzler and N. C. Seeman, *Nature*, 1998, **394**, 539-544.
25. B. Yurke, A. J. Turberfield, A. P. Mills, F. C. Simmel and J. L. Neumann, *Nature*, 2000, **406**, 605-608.
26. Z. J. Gartner and D. R. Liu, *J. Am. Chem. Soc.*, 2001, **123**, 6961-6963.
27. D. R. Halpin and P. B. Harbury, *PLOS Biology*, 2004, **2**, 1015-1021.
28. D. R. Halpin and P. B. Harbury, *PLOS Biology*, 2004, **2**, 1022-1030.
29. D. R. Halpin, J. A. Lee, S. J. Wrenn and P. B. Harbury, *PLOS Biology*, 2004, **2**, 1031-1038.
30. S. Melkko, J. Scheuermann, C. E. Dumelin and D. Neri, *Nat. Biotechnol.*, 2004, **22**, 568-574.
31. P. W. K. Rothmund, *Nature*, 2006, **440**, 297-302.
32. D. Han, S. Pal, J. Nangreave, Z. Deng, Y. Liu and H. Yan, *Science*, 2011, **332**, 342-346.

33. K. Liu, L. F. Zheng, Q. Liu, J. W. de Vries, J. Y. Gerasimov and A. Herrmann, *J. Am. Chem. Soc.*, 2014, **136**, 14255-14262.
34. C. Lin, Y. Liu, S. Rinker and H. Yan, *ChemPhysChem*, 2006, **7**, 1641-1647.
35. Y. Ke, J. Sharma, M. Liu, K. Jahn, Y. Liu and H. Yan, *Nano Lett.*, 2009, **9**, 2445-2447.
36. E. S. Andersen, M. Dong, M. M. Nielsen, K. Jahn, R. Subramani, W. Mamdouh, M. M. Golas, B. Sander, H. Stark, C. L. P. Oliveira, J. S. Pedersen, V. Birkedal, F. Besenbacher, K. V. Gothelf and J. Kjems, *Nature*, 2009, **459**, 73-76.
37. A. Kuzuya and M. Komiyama, *Chem. Commun.*, 2009, 4182-4184.
38. M. Endo, K. Hidaka, T. Kato, K. Namba and H. Sugiyama, *J. Am. Chem. Soc.*, 2009, **131**, 15570-15571.
39. F. Zhang, S. Jiang, S. Wu, Y. Li, C. Mao, Y. Liu and H. Yan, *Nature Nanotechnology*, 2015, **10**, 779-784.
40. D. Han, S. Pal, Y. Yang, S. Jiang, J. Nangreave, Y. Liu and H. Yan, *Science*, 2013, **339**, 1412-1415.
41. Q. Jiang, C. Song, J. Nangreave, X. Liu, L. Lin, D. Qiu, Z.-G. Wang, G. Zou, X. Liang, H. Yan and B. Ding, *J. Am. Chem. Soc.*, 2012, **134**, 13396-13403.
42. S. M. Douglas, I. Bachelet and G. M. Church, *Science*, 2012, **335**, 831-834.
43. H. Ramezani and H. Dietz, *Nat. Rev. Genet.*, 2020, **21**, 5-26.
44. H. Gu, J. Chao, S.-J. Xiao and N. C. Seeman, *Nature*, 2010, **465**, 202-205.
45. K. Lund, A. J. Manzo, N. Dabby, N. Michelotti, A. Johnson-Buck, J. Nangreave, S. Taylor, R. Pei, M. N. Stojanovic, N. G. Walter, E. Winfree and H. Yan, *Nature*, 2010, **465**, 206-210.
46. R. Pei, S. K. Taylor, D. Stefanovic, S. Rudchenko, T. E. Mitchell and M. N. Stojanovic, *J. Am. Chem. Soc.*, 2006, **128**, 12693-12699.
47. M. Kwak and A. Herrmann, *Angew. Chem. Int. Ed.*, 2010, **49**, 8574-8587.
48. F. Jia, H. Li, R. Chen and K. Zhang, *Bioconjugate Chem.*, 2019, **30**, 1880-1888.
49. M. Lemaitre, B. Bayard and B. Lebleu, *Proc. Natl. Acad. Sci.*, 1987, **84**, 648-652.
50. J. H. Jeong, S. W. Kim and T. G. Park, *J. Controlled Release*, 2003, **93**, 183-191.
51. J. H. Jeong, S. W. Kim and T. G. Park, *Bioconjugate Chem.*, 2003, **14**, 473-479.
52. J. H. Jeong, S. H. Kim, S. W. Kim and T. G. Park, *Bioconjugate Chem.*, 2005, **16**, 1034-1037.
53. M. Oishi, S. Sasaki, Y. Nagasaki and K. Kataoka, *Biomacromolecules*, 2003, **4**, 1426-1432.
54. M. Oishi, F. Nagatsugi, S. Sasaki, Y. Nagasaki and K. Kataoka, *ChemBioChem*, 2005, **6**, 718-725.
55. M. Oishi, T. Hayama, Y. Akiyama, S. Takae, A. Harada, Y. Yamasaki, F. Nagatsugi, S. Sasaki, Y. Nagasaki and K. Kataoka, *Biomacromolecules*, 2005, **6**, 2449-2454.
56. J. H. Jeong and T. G. Park, *Bioconjugate Chem.*, 2001, **12**, 917-923.
57. R. B. Fong, Z. Ding, C. J. Long, A. S. Hoffman and P. S. Stayton, *Bioconjugate Chem.*, 1999, **10**, 720-725.
58. M. D. Costioli, I. Fisch, F. Garret-Flaudy, F. Hilbrig and R. Freitag, *Biotechnol. Bioeng.*, 2003, **81**, 535-545.
59. K. Lee, L. K. Povlich and J. Kim, *Adv. Funct. Mater.*, 2007, **17**, 2580-2587.
60. A. M. Quemener, L. Bachelot, A. Forestier, E. Donnou-Fournet, D. Gilot and M.-D. Galibert, *WIREs RNA*, 2020, **11**, e1594.

61. R. W. Wagner, *Nature*, 1994, **372**, 333-335.
62. M. Maeda, C. Nishimura, A. Inenaga and M. Takagi, *Reactive Polymers*, 1993, **21**, 27-35.
63. D. Umeno and M. Maeda, *Anal. Sci.*, 1997, **13**, 553-556.
64. K. E. B. Doncom, L. D. Blackman, D. B. Wright, M. I. Gibson and R. K. O'Reilly, *Chem. Soc. Rev.*, 2017, **46**, 4119-4134.
65. T. R. Wilks and R. K. O'Reilly, *Sci. Rep.*, 2016, **6**, 39192.
66. T. R. Wilks, J. Bath, J. W. de Vries, J. E. Raymond, A. Herrmann, A. J. Turberfield and R. K. O'Reilly, *ACS Nano*, 2013, **7**, 8561-8572.
67. D. Wang, X. Lu, F. Jia, X. Tan, X. Sun, X. Cao, F. Wai, C. Zhang and K. Zhang, *Chem. Mater.*, 2017, **29**, 9882-9886.
68. M. P. Chien, A. M. Rush, M. P. Thompson and N. C. Gianneschi, *Angew. Chem. Int. Ed.*, 2010, **49**, 5076-5080.
69. S. K. Albert, H. V. P. Thelu, M. Golla, N. Krishnan, S. Chaudhary and R. Varghese, *Angew. Chem. Int. Ed.*, 2014, **53**, 8352-8357.
70. F. Jia, X. Lu, X. Tan and K. Zhang, *Chem. Commun.*, 2015, **51**, 7843-7846.
71. F. Jia, X. Lu, X. Tan, D. Wang, X. Cao and K. Zhang, *Angew. Chem. Int. Ed.*, 2017, **56**, 1239-1243.
72. L. Yang, H. Sun, Y. Liu, W. Hou, Y. Yang, R. Cai, C. Cui, P. Zhang, X. Pan, X. Li, L. Li, B. S. Sumerlin and W. Tan, *Angew. Chem. Int. Ed.*, 2018, **57**, 17048-17052.
73. P. He and L. He, *Biomacromolecules*, 2009, **10**, 1804-1809.
74. T. Lueckerath, K. Koynov, S. Loescher, C. J. Whitfield, L. Nuhn, A. Walther, C. Barner-Kowollik, D. Y. W. Ng and T. Weil, *Angew. Chem. Int. Ed.*, 2020, **59**, 15474-15479.
75. T. Lueckerath, T. Strauch, K. Koynov, C. Barner-Kowollik, D. Y. W. Ng and T. Weil, *Biomacromolecules*, 2019, **20**, 212-221.
76. Y. Tokura, Y. Jiang, A. Welle, M. H. Stenzel, K. M. Krzemien, J. Michaelis, R. Berger, C. Barner-Kowollik, Y. Wu and T. Weil, *Angew. Chem. Int. Ed.*, 2016, **55**, 5692-5697.
77. S. E. Averick, S. K. Dey, D. Grahacharya, K. Matyjaszewski and S. R. Das, *Angew. Chem. Int. Ed.*, 2014, **53**, 2739-2744.
78. X. Tan, H. Lu, Y. Sun, X. Chen, D. Wang, F. Jia and K. Zhang, *Chem*, 2019, **5**, 1584-1596.
79. T. Lueckerath, K. Koynov, S. Loescher, C. J. Whitfield, L. Nuhn, A. Walther, C. Barner-Kowollik, D. Y. W. Ng and T. Weil, *Angew. Chem. Int. Ed.*, 2020, **59**, 15474-15479.
80. R. E. Kleiner, C. E. Dumelin and D. R. Liu, *Chem. Soc. Rev.*, 2011, **40**, 5707-5717.
81. F. Buller, L. Mannocci, Y. Zhang, C. E. Dumelin, J. Scheuermann and D. Neri, *Bioorg. Med. Chem. Lett.*, 2008, **18**, 5926-5931.
82. L. Mannocci, Y. Zhang, J. Scheuermann, M. Leimbacher, G. De Bellis, E. Rizzi, C. Dumelin, S. Melkko and D. Neri, *Proc. Natl. Acad. Sci.*, 2008, **105**, 17670-17675.
83. M. A. Clark, R. A. Acharya, C. C. Arico-Muendel, S. L. Belyanskaya, D. R. Benjamin, N. R. Carlson, P. A. Centrella, C. H. Chiu, S. P. Creaser, J. W. Cuzzo, C. P. Davie, Y. Ding, G. J. Franklin, K. D. Franzen, M. L. Geffter, S. P. Hale, N. J. V. Hansen, D. I. Israel, J. Jiang, M. J. Kavarana, M. S. Kelley, C. S. Kollmann, F. Li, K. Lind, S. Mataruse, P. F. Medeiros, J. A. Messer, P. Myers, H. O'Keefe, M. C. Oliff, C. E. Rise, A. L. Satz, S. R. Skinner, J. L. Svendsen, L. Tang, K. van Vloten, R. W. Wagner, G. Yao, B. Zhao and B. A. Morgan, *Nat. Chem. Biol.*, 2009, **5**, 647-654.



84. B. N. Tse, T. M. Snyder, Y. Shen and D. R. Liu, *J. Am. Chem. Soc.*, 2008, **130**, 15611-15626.
85. M. Wichert, N. Krall, W. Decurtins, R. M. Franzini, F. Pretto, P. Schneider, D. Neri and J. Scheuermann, *Nat. Chem.*, 2015, **7**, 241-249.
86. M. Bigatti, A. Dal Corso, S. Vanetti, S. Cazzamalli, U. Rieder, J. Scheuermann, D. Neri and F. Sladojevich, *ChemMedChem*, 2017, **12**, 1748-1752.
87. M. L. McKee, P. J. Milnes, J. Bath, E. Stulz, A. J. Turberfield and R. K. O'Reilly, *Angew. Chem. Int. Ed.*, 2010, **49**, 7948-7951.
88. P. J. Milnes, M. L. McKee, J. Bath, L. J. Song, E. Stulz, A. J. Turberfield and R. K. O'Reilly, *Chem. Commun.*, 2012, **48**, 5614-5616.
89. M. L. McKee, P. J. Milnes, J. Bath, E. Stulz, R. K. O'Reilly and A. J. Turberfield, *J. Am. Chem. Soc.*, 2012, **134**, 1446-1449.
90. Y. He and D. R. Liu, *J. Am. Chem. Soc.*, 2011, **133**, 9972-9975.
91. Y. He and D. R. Liu, *Nat. Nanotechnol.*, 2010, **5**, 778-782.
92. W. J. Meng, R. A. Muscat, M. L. McKee, P. J. Milnes, A. H. El-Sagheer, J. Bath, B. G. Davis, T. Brown, R. K. O'Reilly and A. J. Turberfield, *Nat. Chem.*, 2016, **8**, 542-548.
93. M. L. Malone and B. M. Paegel, *ACS Comb. Sci.*, 2016, **18**, 182-187.
94. Z. J. Gartner, M. W. Kanan and D. R. Liu, *Angew. Chem. Int. Ed.*, 2002, **41**, 1796-+.
95. A. Shibata, H. Abe, M. Ito, Y. Kondo, S. Shimizu, K. Aikawa and Y. Ito, *Chem. Commun.*, 2009, 6586-6588.
96. H. Wu, B. T. Cisneros, C. M. Cole and N. K. Devaraj, *J. Am. Chem. Soc.*, 2014, **136**, 17942-17945.
97. A. L. Satz, J. Cai, Y. Chen, R. Goodnow, F. Gruber, A. Kowalczyk, A. Petersen, G. Naderi-Oboodi, L. Orzechowski and Q. Strebel, *Bioconjugate Chem.*, 2015, **26**, 1623-1632.
98. Z. J. Gartner, R. Grubina, C. T. Calderone and D. R. Liu, *Angew. Chem. Int. Ed.*, 2003, **42**, 1370-1375.
99. X. Y. Li, Z. J. Gartner, B. N. Tse and D. R. Liu, *J. Am. Chem. Soc.*, 2004, **126**, 5090-5092.
100. D. Li, X. Wang, F. Shi, R. Sha, N. C. Seeman and J. W. Canary, *Org. Biomol. Chem.*, 2014, **12**, 8823-8827.
101. J. L. Czapinski and T. L. Sheppard, *J. Am. Chem. Soc.*, 2001, **123**, 8618-8619.
102. M. M. Rozenman and D. R. Liu, *Chembiochem*, 2006, **7**, 253-256.
103. M. W. Kanan, M. M. Rozenman, K. Sakurai, T. M. Snyder and D. R. Liu, *Nature*, 2004, **431**, 545-549.
104. A. H. El-Sagheer, V. V. Cheong and T. Brown, *Org. Biomol. Chem.*, 2011, **9**, 232-235.
105. K. Sakurai, T. M. Snyder and D. R. Liu, *J. Am. Chem. Soc.*, 2005, **127**, 1660-1661.
106. J. Brunner, A. Mokhir and R. Kraemer, *J. Am. Chem. Soc.*, 2003, **125**, 12410-12411.
107. Z. Ma and J.-S. Taylor, *Proc. Natl. Acad. Sci.*, 2000, **97**, 11159-11163.
108. M. M. Rozenman, M. W. Kanan and D. R. Liu, *J. Am. Chem. Soc.*, 2007, **129**, 14933-14938.
109. Y. Ding and M. A. Clark, *ACS Comb. Sci.*, 2015, **17**, 1-4.
110. X. J. Lu, L. J. Fan, C. B. Phelps, C. P. Davie and C. P. Donahue, *Bioconjugate Chem.*, 2017, **28**, 1625-1629.
111. M. Rueping and I. Atodiresei, in *Comprehensive Chirality*, ed. E. M. Carreira and H. Yamamoto, Elsevier, Amsterdam, 2012, vol.6, pp. 345-373.
112. C. Nissam, H. Y. Chen and K. W. Scott, *Tetrahedron Lett.*, 1967, **8**, 3327-3329.

113. P. Jean-Louis Hérisson and Y. Chauvin, *Die Makromolekulare Chemie*, 1971, **141**, 161-176.
114. P. H. Deshmukh and S. Blechert, *Dalton Trans.*, 2007, 2479-2491.
115. R. R. Schrock, *J. Am. Chem. Soc.*, 1975, **97**, 6577-6578.
116. J. Kress, M. Wesolek and J. A. Osborn, *J. Chem. Soc., Chem. Commun.*, 1982, 514-516.
117. R. R. Schrock, J. S. Murdzek, G. C. Bazan, J. Robbins, M. DiMare and M. O'Regan, *J. Am. Chem. Soc.*, 1990, **112**, 3875-3886.
118. P. Schwab, M. B. France, J. W. Ziller and R. H. Grubbs, *Angew. Chem. Int. Ed.*, 1995, **34**, 2039-2041.
119. P. Schwab, R. H. Grubbs and J. W. Ziller, *J. Am. Chem. Soc.*, 1996, **118**, 100-110.
120. J. S. Kingsbury, J. P. A. Harrity, P. J. Bonitatebus and A. H. Hoveyda, *J. Am. Chem. Soc.*, 1999, **121**, 791-799.
121. S. B. Garber, J. S. Kingsbury, B. L. Gray and A. H. Hoveyda, *J. Am. Chem. Soc.*, 2000, **122**, 8168-8179.
122. E. L. Dias, S. T. Nguyen and R. H. Grubbs, *J. Am. Chem. Soc.*, 1997, **119**, 3887-3897.
123. M. S. Sanford, J. A. Love and R. H. Grubbs, *J. Am. Chem. Soc.*, 2001, **123**, 6543-6554.
124. M. S. Sanford, M. Ulman and R. H. Grubbs, *J. Am. Chem. Soc.*, 2001, **123**, 749-750.
125. S. Varlas, S. B. Lawrenson, L. A. Arkinstall, R. K. O'Reilly and J. C. Foster, *Prog. Polym. Sci.*, 2020, **107**, 101278.
126. P. Schwab, R. H. Grubbs and J. W. Ziller, *J. Am. Chem. Soc.*, 1996, **118**, 100-110.
127. J. Huang, H.-J. Schanz, E. D. Stevens and S. P. Nolan, *Organometallics*, 1999, **18**, 5375-5380.
128. J. Huang, E. D. Stevens, S. P. Nolan and J. L. Petersen, *J. Am. Chem. Soc.*, 1999, **121**, 2674-2678.
129. L. Ackermann, A. Fürstner, T. Weskamp, F. J. Kohl and W. A. Herrmann, *Tetrahedron Lett.*, 1999, **40**, 4787-4790.
130. T. Weskamp, F. J. Kohl and W. A. Herrmann, *J. Organomet. Chem.*, 1999, **582**, 362-365.
131. A. K. Chatterjee and R. H. Grubbs, *Org. Lett.*, 1999, **1**, 1751-1753.
132. M. Scholl, T. M. Trnka, J. P. Morgan and R. H. Grubbs, *Tetrahedron Lett.*, 1999, **40**, 2247-2250.
133. M. Scholl, S. Ding, C. W. Lee and R. H. Grubbs, *Org. Lett.*, 1999, **1**, 953-956.
134. S. Gessler, S. Randl and S. Blechert, *Tetrahedron Lett.*, 2000, **41**, 9973-9976.
135. J. A. Love, J. P. Morgan, T. M. Trnka and R. H. Grubbs, *Angew. Chem. Int. Ed.*, 2002, **41**, 4035-4037.
136. S. A. Isarov and J. K. Pokorski, *Acs Macro Lett.*, 2015, **4**, 969-973.
137. J. Tomasek and J. Schatz, *Green Chem.*, 2013, **15**, 2317-2338.
138. K. Skowerski, G. Szczepaniak, C. Wierzbicka, Ł. Gułajski, M. Bieniek and K. Grela, *Catalysis Science & Technology*, 2012, **2**, 2424-2427.
139. S. H. Hong and R. H. Grubbs, *J. Am. Chem. Soc.*, 2006, **128**, 3508-3509.
140. K. Breitenkamp and T. Emrick, *J. Polym. Sci., Part A: Polym. Chem.*, 2005, **43**, 5715-5721.
141. J. B. Binder, J. J. Blank and R. T. Raines, *Org. Lett.*, 2007, **9**, 4885-4888.
142. S. J. Connon, M. Rivard, M. Zaja and S. Blechert, *Adv. Synth. Catal.*, 2003, **345**, 572-575.

143. O. B. C. Monty, P. Nyshadham, K. M. Bohren, M. Palaniappan, M. M. Matzuk, D. W. Young and N. Simmons, *ACS Comb. Sci.*, 2020, **22**, 80-88.

# Chapter 2: Scoping the Potential of Metathesis in DNA Nanotechnology

## 2.1 Abstract

The stability of short oligonucleotides in the presence of Ru-metathesis catalysts was explored by polyacrylamide gel electrophoresis (PAGE). In the presence of equimolar Ru-metathesis catalyst DNA remained stable for several days; however, as the equivalents of catalyst increased  $\text{MgCl}_2$  was required to maintain DNA stability.  $\text{MgCl}_2$  was believed to minimize an electrostatic interaction between DNA and the Ru-catalyst. Furthermore, the fluorescence quenching of common nucleic acid stains in the presence of Ru-metathesis catalysts was observed and this will likely prove an important discovery for future analysis of DNA-metathesis work.

## 2.2 Background

### 2.2.1 Metathesis in the presence of DNA

As explored in Chapter 1, the rapid expansion of DNA nanotechnology has resulted in an increasing demand for more DNA compatible chemistries; particularly in the areas of DNA encoded chemical libraries (DECLs) and DNA-templated synthesis (DTS). Whilst many pharmaceutical companies have begun to utilise DECLs as a rapid and cost-effective way of screening a large number of compounds for biological targets, the research area is currently disadvantaged by the limited number of DNA-compatible, solution-phase chemistries available.<sup>1-3</sup> There are several requirements for a reaction to be classified as 'DNA-compatible'

but most importantly the reaction must take place under conditions which solubilise the DNA and the conditions must not modify or destroy the DNA.<sup>4</sup>

To circumvent the solubility and stability issues of DNA, which severely limits the chemistries available, peptide nucleic acids (PNAs) are of growing interest for the preparation of encoded libraries.<sup>5</sup> PNA is an artificially synthesized oligonucleotide in which the sugar-phosphate backbone has been replaced by a pseudo-peptide skeleton, nucleobases are linked to the skeleton and thus, PNA binds with DNA and RNA with high specificity and selectivity (Figure 2.1).<sup>6</sup> However, in contrast to DNA and RNA, the absence of the sugar-phosphate renders PNA soluble in a range of organic solvents such as DMF, DMSO and *N*-methyl-2-pyrrolidone (NMP).<sup>7</sup> Furthermore, PNA duplexes are thermally more stable than DNA and are not degraded by nucleases or proteases.<sup>6</sup> These properties increase the scope of chemistries that are compatible with PNA and our group has recently demonstrated the stability of dsPNA in up to 95 vol% organic solvent.<sup>8</sup> The stability of dsPNA is far superior to dsDNA which vastly increases the number of compatible chemistries.<sup>9</sup> However, despite these advantages there is a significant limitation with using PNA as it cannot be recognised by enzymes and therefore amplified by PCR. This greatly increases the complexity of analysis of PNA-encoded chemical libraries.<sup>1</sup> As a result of this major limitation of PNA, the search for DNA-compatible chemistries is still of profound interest.

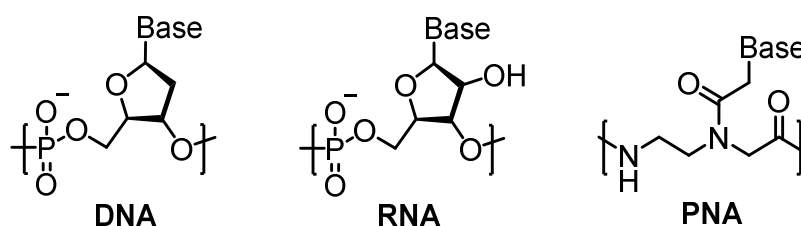


**Figure 2.1** Comparison between the backbone structure of DNA, RNA and PNA.

In particular, olefin metathesis is of great interest due to its ability to form carbon-carbon bonds, a fundamental, yet usually challenging reaction in organic synthesis.<sup>10</sup> Considering the importance of this chemical transformation it is not surprising that over the last six years attempts to perform metathesis in the presence of DNA have been undertaken. However, thus far, only handful of attempts have been completed with varied and often limited success, summarised in Table 2.1 and discussed in greater depth herein.

**Table 2.1** Summary of the examples of 'on-DNA' metathesis reported including the mechanism of metathesis studied, the solvent, and any additional additives/conditions required for the success of the reaction.

Publication / Year	Metathesis class	Solvent	Additives/conditions to note
Liu <i>et al</i> (2014) <sup>11</sup>	ROMP	THF	Cationic surfactant : didodecyldimethylammonium bromide
Lu <i>et al</i> (2017) <sup>12</sup>	RCM/CM	3:2 H <sub>2</sub> O:t-BuOH	MgCl <sub>2</sub>
Tan <i>et al</i> (2019) <sup>13</sup>	ROMP	CH <sub>2</sub> Cl <sub>2</sub>	Phosphotriester- and exocyclic-amine protected DNA
Monty <i>et al</i> (2020) <sup>14</sup>	RCM/CM	5:4:1 H <sub>2</sub> O:EtOH:MeOAc	2,2'-biphenyldiamine, MgCl <sub>2</sub> , NH <sub>4</sub> Cl

The first report of metathesis 'on-DNA' dates back to 2014. Here, Liu *et al* addressed the limited number of chemistries compatible with DNA by exchanging the counterions, which are present along the DNA phosphate backbone, with a surfactant to yield the DNA organosoluble.<sup>11</sup> The authors were able to demonstrate the success of this methodology to couple hydrophobic moieties to DNA, in addition to the polymerization of norbornene functionalized DNA by ROMP. This was the first report of metathesis on protected DNA. Of

significant interest was a study conducted by a separate research group at the same time as the former, where the 'graft through polymerization' of PNA monomers was completed.<sup>15</sup> In this publication, the authors stated that subsequent attempts to polymerize DNA monomers had been unsuccessful, emphasising the chemical versatility offered by PNA in contrast to DNA. Furthermore, this highlighted the significance of Liu *et al* using protected DNA and suggests that either the use of an organic solvent, the protection of the backbone, or indeed both are essential for the success of metathesis in the presence of DNA. Finally, further emphasis on the importance of protecting the DNA phosphate backbone was reported in 2019 by Tan *et al*.<sup>13</sup> Here, the authors reported the second successful ROMP of DNA monomers. However, once again the approach relied upon the use of protecting groups along the phosphate backbone, to transfer the DNA into an organic phase.

Despite the increasing interest in the ROMP of DNA monomers, little explanation for the benefits and indeed necessity of using protected DNA was reported. This raised questions over the feasibility of metathesis in the presence of unprotected, native DNA which would be essential if this chemistry was to be exploited in DECLs and DTS.

These questions were answered, in-part, in 2016 when scientists at GlaxoSmithKline reported the preparation of a DNA-encoded macrocycle library *via* the on-DNA RCM.<sup>12</sup> Whilst optimized conditions were reported to achieve 85% conversion; the authors noted that several of the Ru-catalysts, induced DNA decomposition. However, the authors did not conduct any further studies into such decomposition and instead utilized a large excess (>4000 equiv.) of MgCl<sub>2</sub> to prevent decomposition. MgCl<sub>2</sub> has previously been utilized in the CM modification of proteins

and RCM stapling of unprotected peptides, and is believed to act as a mild Lewis acid masking coordinating functional groups.<sup>16, 17</sup>

Poor understanding regarding the incompatibility of the typical metathesis conditions with DNA was likely to explain the sparse number of reports utilizing metathesis in DECLs since 2016, which was currently limited to just one publication by Monty *et al.*, in 2020.<sup>14</sup> Whilst in this publication a diverse range of metathesis partners were utilized to prepare DECLs, the conditions still relied heavily on the addition of  $MgCl_2$  and an additional acidic buffer  $NH_4Cl$ , with little understanding over the role of these additives.<sup>14</sup> It was therefore apparent that progression in this area was severely limited by a poor understanding of the interactions between the typical Ru-catalysts utilized for metathesis and DNA.

### 2.2.2 DNA-ligand interactions

There are four main modes of binding for small molecules to double-stranded DNA (dsDNA): (1) major groove binding; (2) minor groove binding; (3) external binding; (4) intercalation (Figure 2.2).<sup>18</sup>

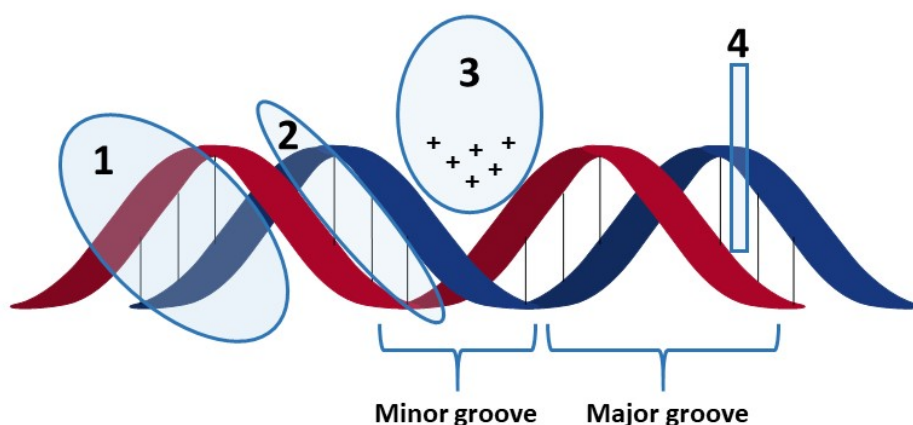


**Figure 2.2** Schematic showing the four modes of binding of small molecules to DNA: (1) major groove binding (2) minor groove binding (3) external binding and (4) intercalation.



The interactions of small-molecules with dsDNA is of particular interest to the medicinal chemistry community due to the therapeutic applications of many small-molecule DNA binders. For example, intercalators which are often large planar aromatic molecules such as acridines are one of the most promising small-molecule anticancer targets.<sup>19</sup> Furthermore, minor groove binders are also of increasing interest due to their antitumor and antibacterial activity with improved specificity over intercalators.<sup>18, 20</sup>

Binding that does not involve intercalation or binding at the groove is a more ambiguous concept which is often known as external binding. The main example of external binding is the electrostatic binding of positively charged species to the negatively charged phosphate backbone. However, additional factors such as Van der Waals forces or dipole-dipole forces can increase the external binding of small molecules to DNA.

Many spectroscopic techniques have been identified to assess the mode of DNA binding and they are often used collectively to predict a binding mode. Some of the most utilized techniques include circular dichroism (CD) spectroscopy, linear dichroism (LD) spectroscopy and ultraviolet-visible (UV-Vis) spectroscopy.<sup>18</sup> Figure 2.3 summarises the typical spectroscopic changes observed for each binding mode, and also highlights the importance of utilizing multiple spectroscopic techniques in order to accurately predict the binding mode. However, it is important to highlight that the binding mode is an ambiguous concept and many small molecules can bind *via* more than one mode at any one time. Furthermore, the binding mode may also be sequence dependent.

The aim of this chapter was to gain a greater understanding of the interactions taking place between DNA and the typical Ru-metathesis catalysts. Further knowledge in this area was

seen as essential, in order to be able to rationalise the conditions required to perform metathesis 'on-DNA' and to expand the utilization of metathesis in DNA nanotechnology.

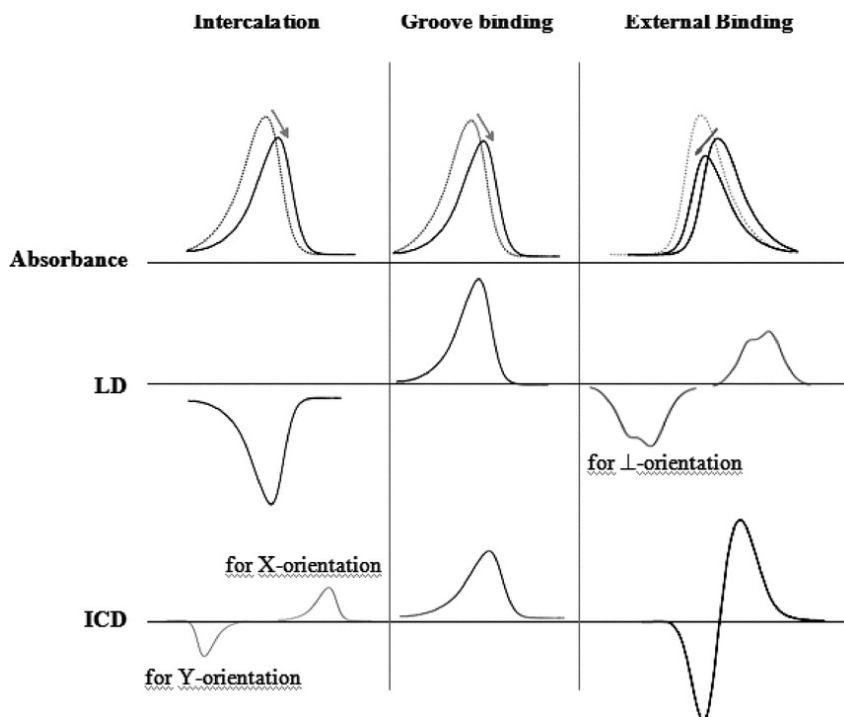


**Figure 2.3** Plots showing the typical spectral changes observed for each of the possible binding modes. Note in this case external binding covers porphyrins which are external stacking molecules. Figure taken with permission from *Applied Spectroscopy Reviews, Use of UV-Vis Spectrometry to Gain Information on the Mode of Binding of Small Molecules to DNAs and RNAs*, T. Biver, 2012.<sup>18</sup>

## 2.3 Results & Discussion

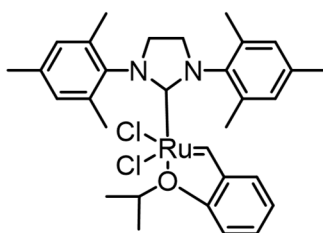
### 2.3.1 Stability of DNA in the presence of HG2

Initially, the stability of DNA in the presence of an Ru-metathesis catalyst was investigated following the suggestion by Lu *et al* that Ru-induced DNA degradation could occur.<sup>12</sup> Gel electrophoresis is a commonly used method to study DNA degradation as it separates molecules based on their size and charge. Therefore, fragmented DNA was expected to appear as a ladder or smear down the gel due to cleavage of the backbone. For this study

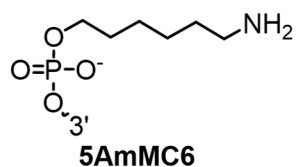
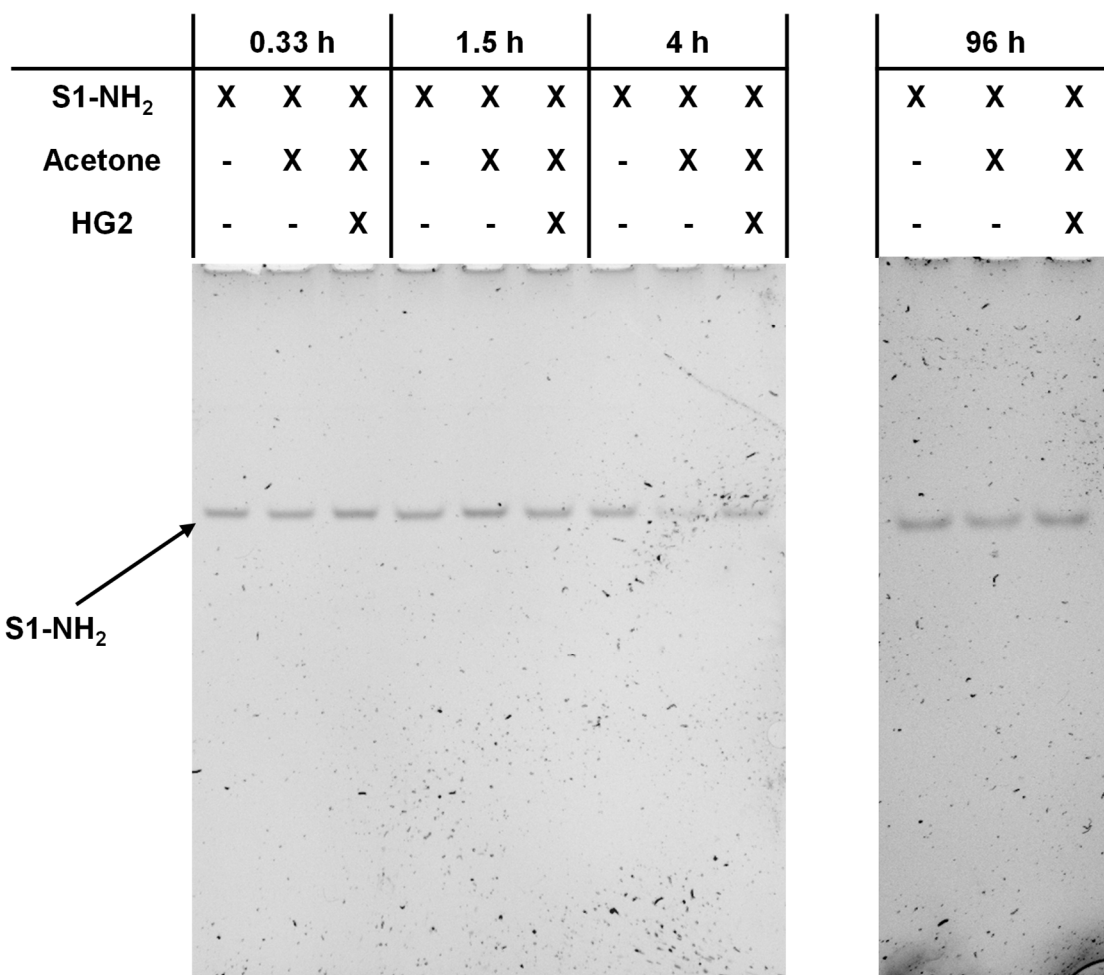
polyacrylamide gel electrophoresis (PAGE) was utilized as it can successfully separate short oligonucleotides.<sup>21</sup>

Initial studies were conducted using the commercially available catalyst, HG2 (Figure 2.4a). HG2 is not soluble in H<sub>2</sub>O; therefore, a 1 mg mL<sup>-1</sup> stock solution was prepared in acetone, 1.25 μL of this solution was diluted to 100 μL using a 20 μM aqueous solution of ssDNA. The initial oligonucleotide studied contained 30 bases and was modified with an amine on the 5' end, S1-NH<sub>2</sub> (Figure 2.4b). S1-NH<sub>2</sub> was incubated with HG2 at room temperature for 96 h, aliquots were taken at several time points for analysis by 15% native PAGE. A control experiment was also conducted with an equal volume of acetone to ensure that any observations made were due to the presence of HG2 and not the solvent.

As mentioned above the fragmentation of DNA was expected to yield a smear or ladder like appearance down the gel. Figure 2.4c shows that throughout the gel only one band was present at all time points, equal to that of S1-NH<sub>2</sub>. This would suggest that the DNA remained intact throughout the entirety of the experiment. However, one should note that on this occasion an equimolar amount of HG2 to S1-NH<sub>2</sub> was utilized and this was in contrast to the work conducted by Lu *et al* where a large excess of Ru-catalyst (at least 150 equivalents) was used.<sup>12</sup> It is probable that degradation may become more significant at higher catalyst loadings.

**a****HG2****b**

S1-NH<sub>2</sub> = 5'-/5AmMC6/AGG GAT TGT CTT AGT GTG CGA ATA GGT AAC-3'

**5AmMC6****c**

**Figure 2.4** (a) Structure of HG2. (b) Sequence of S1-NH<sub>2</sub>. (c) 15% native PAGE gel, after SYBR™ Gold staining, visualized under UV light. Aliquots of S1-NH<sub>2</sub> in (1) acetone; or (2) acetone and HG2 (1 equivalent) were compared to S1-NH<sub>2</sub> in H<sub>2</sub>O at the same time intervals. Only one band was observed in each lane suggesting DNA stability throughout the entirety of the experiment.

To test the stability of DNA in the presence of higher catalyst loadings, the above experiment was repeated using 150 equivalents of HG2. An alternative 30 base oligonucleotide was utilized for this study due to availability, C2 (Figure 2.5a), and 45 vol% acetone was added to each mixture to aid with the solubility of the larger mass of HG2. The samples were incubated at room-temperature for up to 1 h and aliquots were taken every 15 minutes and immediately frozen in liquid nitrogen for storage prior to native PAGE analysis. Samples with and without the addition of 2625 equivalents of MgCl<sub>2</sub> were compared, Figure 2.5b.

**a**

C2 = 5'-AGG GAT TGT CTT AGT GTG CGT TCA TAC CAG - 3'

**b**

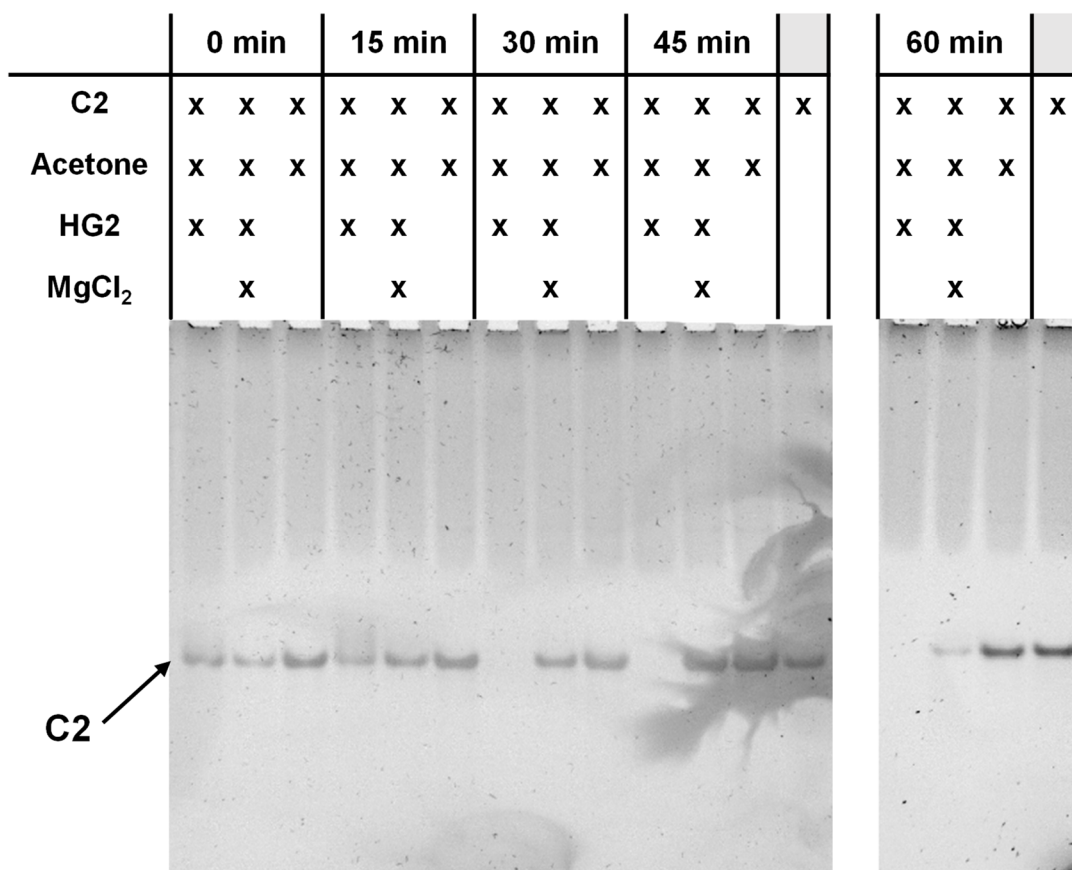


**Figure 2.5** (a) Sequence of C2. (b) 15% native PAGE gel after SYBR™ Gold staining, visualized under UV light. Aliquots of C2 in (1) acetone; or (2) acetone and HG2; or (3) acetone, HG2 (150 equivalents) and MgCl<sub>2</sub> (2625 equivalents) at 15 minute intervals were compared to C2 in H<sub>2</sub>O.

The results highlighted a clear difference between the samples incubated with HG2 with and without MgCl<sub>2</sub>. The samples incubated with HG2 and MgCl<sub>2</sub> remained intact throughout the entirety of the experiment as indicated by the presence of a single band at each timepoint. However, no band was observed in the samples incubated with HG2 without MgCl<sub>2</sub> after the first 15-minute time point.

During the design set-up it was originally assumed that degraded DNA would appear as a ladder of bands down the PAGE gel, owing to the cleavage of the phosphate backbone. Therefore, the absence of fragmented DNA in Figure 2.5b would suggest that cleavage of the phosphate backbone is not taking place. However, the absence of bands in the samples incubated without MgCl<sub>2</sub> still required an explanation.

As discussed, the initial set-up assumed DNA degradation *via* the cleavage of the phosphate backbone leading to the formation of shorter oligomers. However, if the DNA is rapidly degraded to very short oligomers (1-2 bases) these may not be sufficiently stained with SYBR™ Gold and thus, their bands may not be visible. Furthermore, alternative DNA degradation pathways have also been reported such as loss of nitrogenous bases due to hydrolysis. Most commonly this is the purine bases and known as depurination.<sup>22</sup> Depurination is the hydrolysis of the bond between the purine and the deoxyribose sugar of DNA which is particularly prevalent under acidic conditions. As depurination cleaves the purine bases, the SYBR™ Gold may again be unable to stain the bases, leading to an empty lane such as those seen in Figure 2.5b.

Previously it has been reported that the depurination of DNA is suppressed in the presence of salts and thus, one hypothesis is that HG2 could be causing DNA depurination in the absence

of salts such as  $\text{MgCl}_2$ . This would not be the first time depurination has been accelerated in the presence of transition metals, as previous cases have been reported in the presence of platinum, palladium and copper.<sup>23, 24</sup>

Finally, the stability of a 17-base oligonucleotide ( $\text{S0-NH}_2$ ) was analysed by high-performance liquid chromatography (HPLC) under differing equivalents of catalyst and  $\text{MgCl}_2$ . In particular, the presence of the peak at 5.6 minutes, associated with the intact  $\text{S0-NH}_2$  was studied. The results in Figure 2.6 show that in the presence of 1000 equivalents of HG2 with no  $\text{MgCl}_2$  (red trace) the peak associated with  $\text{S0-NH}_2$  is absent; however, a small peak can be detected in a sample incubated with 4000 equivalents of  $\text{MgCl}_2$  (black trace) and this peak is even larger in a sample incubated with the same equivalents of  $\text{MgCl}_2$  but lower equivalents of HG2 (blue trace).

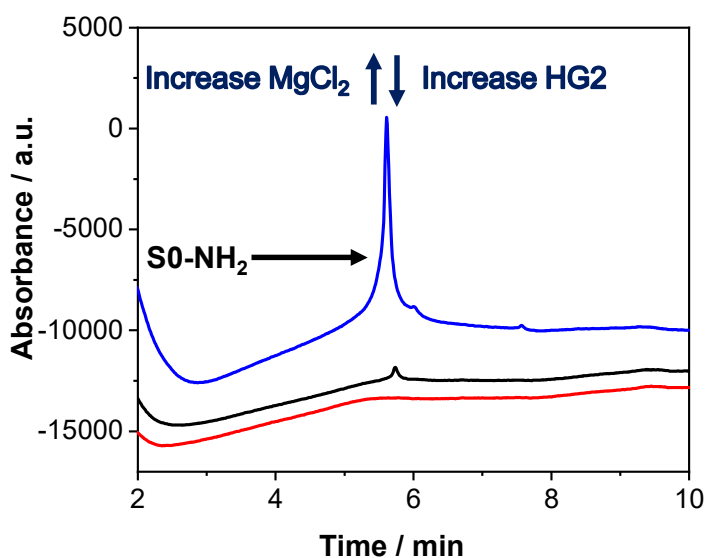


**Figure 2.6** HPLC-UV chromatogram at 260 nm of  $\text{S0-NH}_2$  following incubation with differing equivalents of HG2 and  $\text{MgCl}_2$  for 2 h. Red trace = 1000 eq. HG2 and 0 eq.  $\text{MgCl}_2$ ; black trace = 1000 eq. HG2 and 4000 eq.  $\text{MgCl}_2$ ; blue trace = 100 eq. HG2 and 4000 eq.  $\text{MgCl}_2$ . Equivalents calculated with respect to  $\text{S0-NH}_2$ . Products eluted with a gradient of buffer A, 0.1 M triethylammonium acetate (TEAA), in a 95:5 mixture of  $\text{H}_2\text{O}$  and acetonitrile and buffer B, 0.1 M TEAA, in a 30:70 mixture of  $\text{H}_2\text{O}$  and acetonitrile.

The HPLC results (Figure 2.6) appear to corroborate with the PAGE results (Figures 2.4 and 2.5) and suggest that in order to retain oligonucleotide integrity lower catalyst loadings are required and/or the addition of MgCl<sub>2</sub>. For example, DNA appeared stable in the presence of 1 equivalent of HG2 without any MgCl<sub>2</sub>; however, in the presence of 1000 equivalents of HG2, a large excess of MgCl<sub>2</sub> was required in order to retain the integrity of DNA. Further interpretation of the PAGE results was difficult due to the visualization method utilized, which is reliant upon the binding of a nucleic acid gel stain, SYBR™ Gold, to DNA. Unfortunately, as the stain is a proprietary dye from Invitrogen™ the exact structure and mode of binding to DNA is not disclosed. Therefore, the effect of DNA degradation on the binding and thus fluorescence properties is unknown. However, the disappearance of the DNA band over time would strongly indicate a change in the integrity of the DNA and this is supported by the HPLC results.

### 2.3.2 Stability of DNA in the presence of PEG-G3

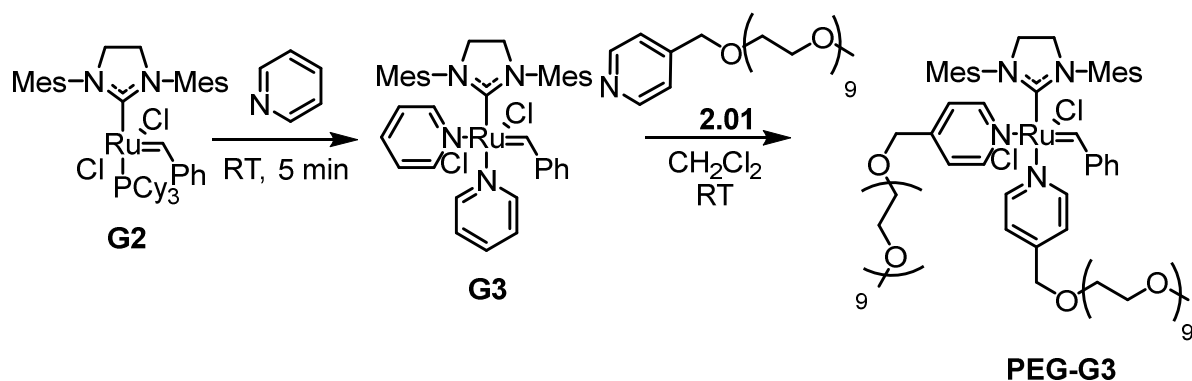
Following the analysis of HG2, further studies were conducted with a water-soluble metathesis catalyst. The use of a water-soluble metathesis catalyst would avoid the need for additional organic solvents which are often not compatible with DECLs and DTS due to the disruption of hydrogen-bonding in the duplex lowering the  $T_m$ . The water-soluble catalyst chosen for this study was a PEGylated Grubbs third generation catalyst (**PEG-G3**), previously used by Pokorski and co-workers in the ROMP of proteins.<sup>25</sup> The catalyst was synthesized from the commercially available G2 catalyst in a two-step process (Scheme 2.1). Firstly, **G3** was prepared from G2 by the addition of pyridine and subsequent precipitation into a non-polar solvent such as hexane. Addition of PEG-substituted pyridine (**2.01**) then led to the desired product, **PEG-G3** which was utilized without further purification (Figure 2.7).



Following the preparation of **PEG-G3**, the stability of both ssDNA and dsDNA was assessed in a 100% aqueous environment. The analysis was once again completed *via* native PAGE and the study utilized S2-NH<sub>2</sub> with the complementary sequence C2. Annealing of the two aforementioned oligonucleotides was conducted isothermally at room-temperature.

The ssDNA and dsDNA was then subjected to 150 equivalents of **PEG-G3** with and without the addition of 8000 equivalents of MgCl<sub>2</sub> (Table 2.2). Aliquots were taken every 15 minutes for 1 h and immediately frozen in liquid nitrogen prior to native PAGE analysis. Note that the 0 minute time point corresponds to a sample taken immediately after the addition of **PEG-G3**.

Two significant observations were made from the resulting gel (Figure 2.8): (1) no ssDNA was detected with or without MgCl<sub>2</sub> (lanes **a**, **c** and **e**) with the exception of sample **1c** at 60 minutes; and (2) when dsDNA was studied a broad high molar mass band, reminiscent of that observed for a DNA-polymer conjugate, was identified in all lanes (lanes **b** and **d**).



**Scheme 2.1** Synthesis of **PEG-G3**.

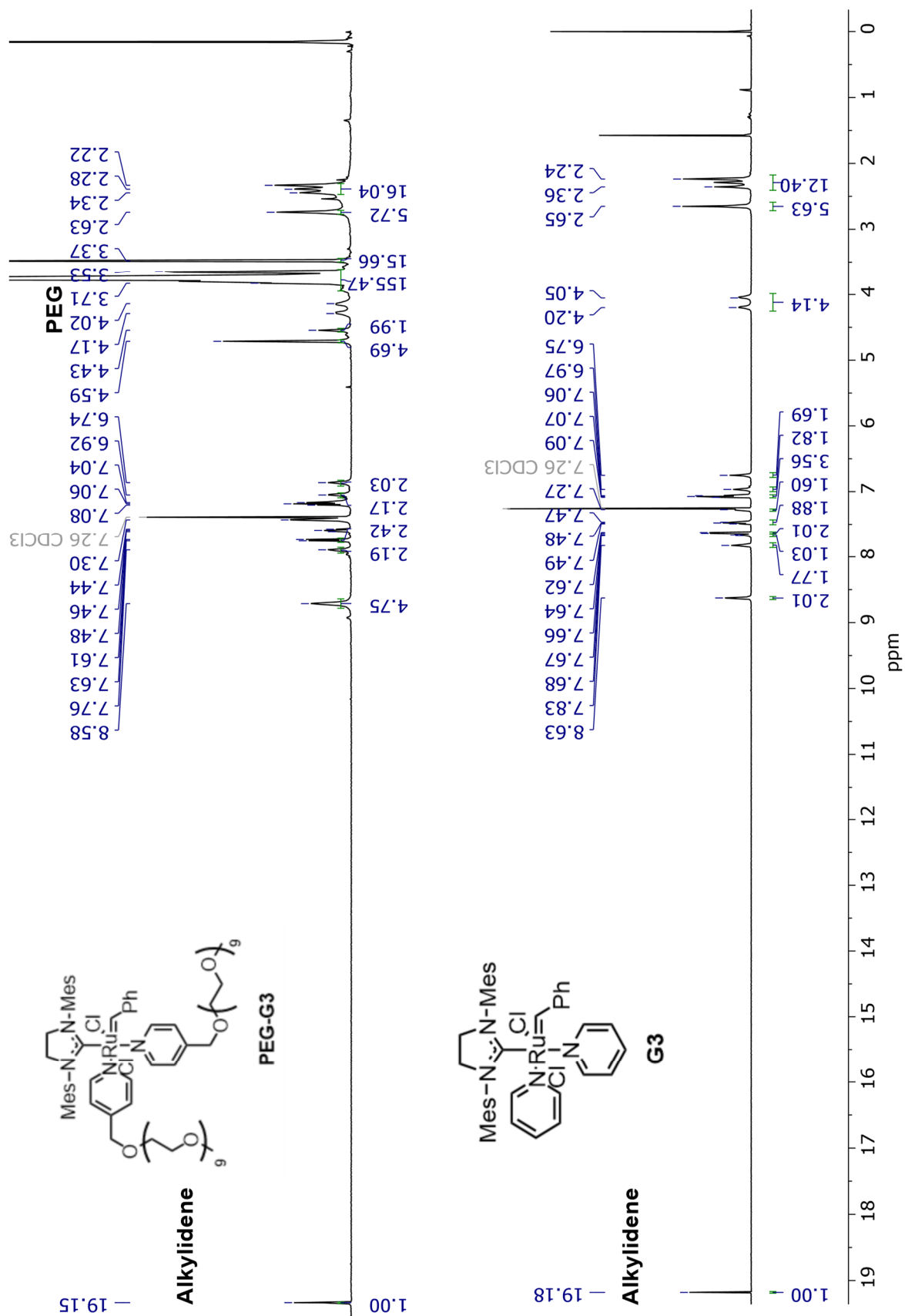
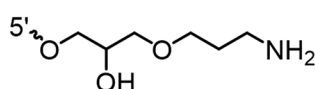


Figure 2.7  $^1\text{H}$  NMR spectra of **PEG-G3** (top) and **G3** (bottom) in  $\text{CDCl}_3$  (500 MHz, 298K).

**Table 2.2** Conditions tested for the stability of DNA in the presence of 150 equivalents of **PEG-G3**.  
<sup>†</sup>Equivalents reported with respect to oligonucleotide.

Reaction #	DNA Sequence	Equivalents of MgCl <sub>2</sub> <sup>†</sup>
<b>1a</b>	S2-NH <sub>2</sub> (ssDNA)	0
<b>1b</b>	S2-NH <sub>2</sub> + C2 (dsDNA)	0
<b>1c</b>	S2-NH <sub>2</sub> (ssDNA)	8000
<b>1d</b>	S2-NH <sub>2</sub> + C2 (dsDNA)	8000
<b>1e</b>	C2 (ssDNA)	0

**a**  
 S2-NH<sub>2</sub> = 5'-CTG GTA TGA ACG CAC ACT AAG ACA ATC CCT / 3AmMO/-3'  
 C2 = 5'-AGG GAT TGT CTT AGT GTG CGT TCA TAC CAG-3'



**3AmMO**

**b**

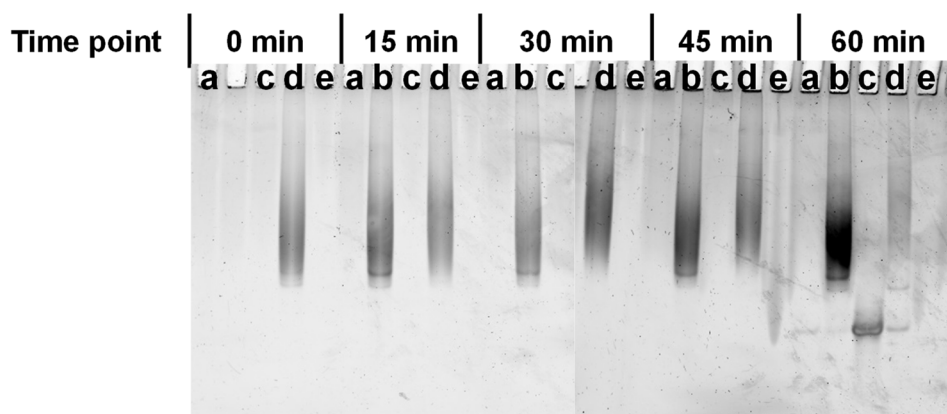


**Figure 2.8** (a) DNA sequences utilized in this study: S2-NH<sub>2</sub> and C2. (b) 18% Native PAGE gel of reaction mixtures **1a** – **1e** analysed after incubation with **PEG-G3** for 0, 15, 30, 45 and 60 min respectively. Stained with SYBR™ Gold and visualized under UV light.

The absence of any bands representative of ssDNA was especially interesting, particularly as those bands at the 0 minute time point were absent. Similar experiments were repeated and

the absence of any bands representing ssDNA was a consistent observation. It was deemed highly unlikely that the DNA degradation mechanisms discussed above for HG2 (Section 2.3.1) could be occurring at such a rate to account for this observation. Furthermore, such explanation would not be consistent with the reappearance of the band from sample **1c** at 60 minutes. Thus, it was hypothesized that a differing factor must be causing these observations.

As the gel stain, SYBR™ Gold, is a cyanine based dye with a low intrinsic fluorescence until bound to DNA.<sup>26</sup> It was hypothesized that the absence of any bands in the gel could be as a result of **PEG-G3** disrupting the mode of action of SYBR™ Gold and thus, a separate study was conducted to look further into this, Section 2.3.3.

Furthermore, the presence of broad bands in all lanes containing samples **1b** and **1e** provided strong evidence that **PEG-G3** was binding to dsDNA and thus studies into the mode of this binding were conducted, Section 2.3.4.

Unfortunately, due to the absence of bands corresponding to ssDNA and the presence of broad high molar mass bands in the lanes containing dsDNA, the PAGE gel (Figure 2.8b) could not be utilized to confirm the stability of DNA in the presence of **PEG-G3**. Therefore, several attempts were made to repeat the degradation studies whilst avoiding any interactions between **PEG-G3** and DNA. Firstly, ethyl vinyl ether (EVE) was added following the removal of aliquots for PAGE analysis. EVE is commonly used to quench ROMP reactions as it forms a non-reactive Fischer carbene complex.<sup>27</sup> Therefore, it was anticipated that if the interaction or mechanism of quenching was occurring through the alkylidene on **PEG-G3** the addition of EVE would break this interaction, sequestering **PEG-G3**. However, following the addition of EVE to aliquots of C2 incubated with **PEG-G3**, no bands were observed in the gel following native

PAGE analysis (Figure 2.9). This result suggested that the interaction or mechanism of quenching was not occurring through the alkylidene.

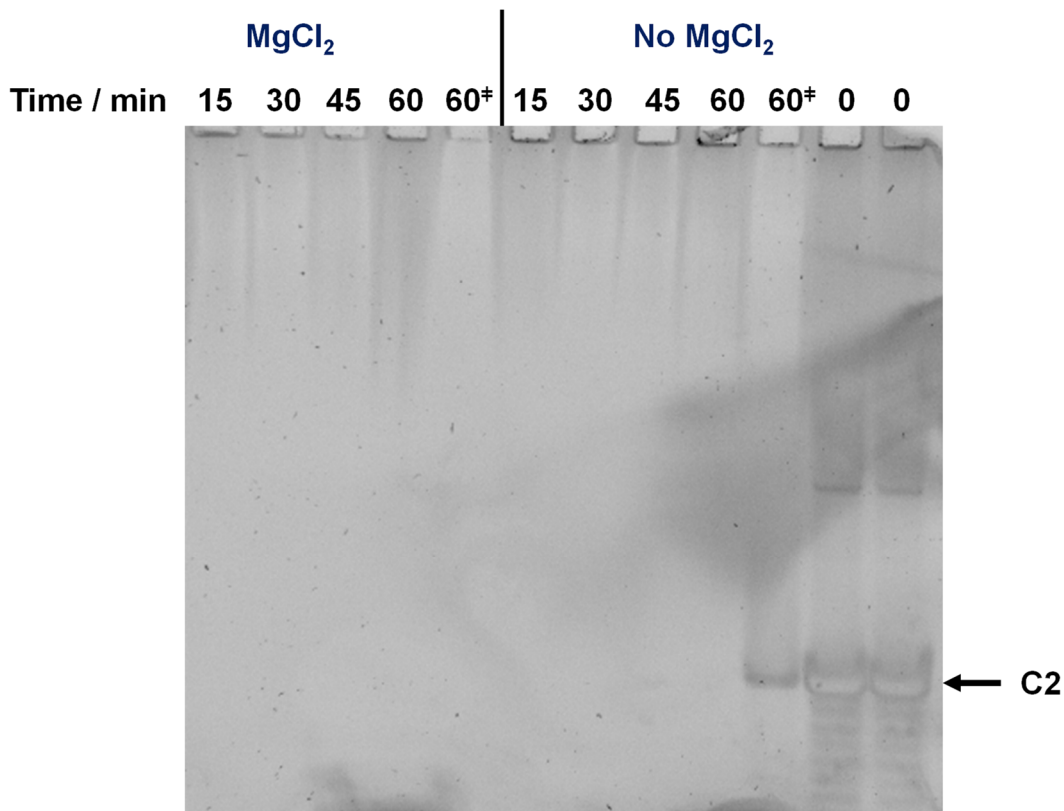
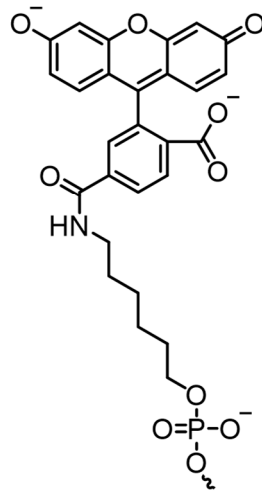


**Figure 2.9** 18% Native PAGE gel of C2 analysed after incubation with **PEG-G3** for 15, 30, 45 and 60 min respectively with and without the addition of 8000 equivalents of MgCl<sub>2</sub>. 2  $\mu$ L of EVE was added to each aliquot prior to native PAGE analysis and the results were compared to the two control lanes containing C2 and C2 with 2  $\mu$ L EVE. Stained with SYBR<sup>TM</sup> Gold and visualized under UV light. <sup>#</sup>5  $\mu$ L EVE was added to these samples.

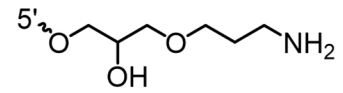
Finally, a fluorescently labelled oligonucleotide functionalised with fluorescein on the 5' end, S2-NH<sub>2</sub>-FAM was utilized to avoid the need for SYBR<sup>TM</sup> gold staining. In contrast to SYBR<sup>TM</sup> gold, the fluorescence of fluorescein is expected to be detectable whether it is conjugated to the DNA or free in solution. As a consequence of this, the appearance of fluorescent bands would be expected irrespective of the integrity of the oligonucleotide. Typically, any free fluorophore would migrate to the bottom of the gel; however, following the incubation of S2-NH<sub>2</sub>-FAM with **PEG-G3** no fluorescent bands were observed in the native PAGE gel (Figure 2.10).

**a**

S2-NH<sub>2</sub>-FAM = 5'-/56-FAM/CTG GTA TGA ACG CAC ACT AAG ACA ATC CCT/3AmMO/-3'



**56-FAM**



**3AmMO**

**b**

		15 min		30 min		45 min		60 min	
S2-NH <sub>2</sub> -FAM	X	X	X	X	X	X	X	X	X
PEG-G3	-	X	X	X	X	X	X	X	X
MgCl <sub>2</sub>	-	X	-	X	-	X	-	X	-

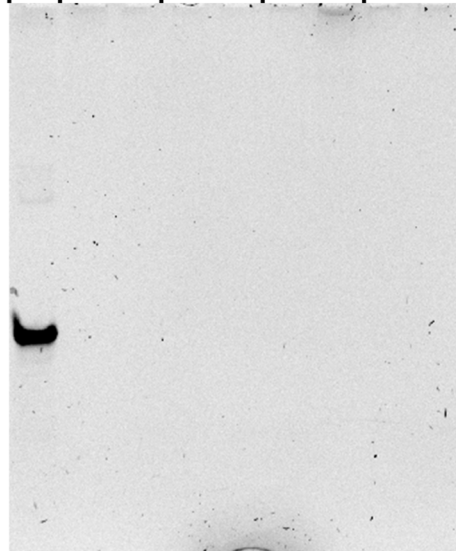


**Figure 2.10** (a) Sequence of S2-NH<sub>2</sub>-FAM. (b) 18% Native PAGE gel of S2-NH<sub>2</sub>-FAM analysed after incubation with PEG-G3 for 15, 30, 45 and 60 minutes respectively with and without the addition of 8000 equivalents of MgCl<sub>2</sub>. Visualized under UV light.

This result was significant as it supported the hypothesis of fluorescence quenching rather than DNA degradation. The result also highlighted the significance of understanding the interactions between Ru-metathesis catalysts and fluorophores.

In contrast to the studies conducted with HG2, analysis of oligonucleotides in the presence of **PEG-G3** was not possible *via* HPLC as the PEG groups dominated the chromatogram. Therefore, it was not possible to comment on the stability of oligonucleotides in the presence of the water-soluble catalyst **PEG-G3**. However, one may expect similar trends to HG2 which highlighted the importance of the addition of MgCl<sub>2</sub> and keeping the catalyst loading as low as possible.

### 2.3.3 The origins behind the disappearance of SYBR gold fluorescence

As alluded to earlier in this chapter SYBR™ Gold is a proprietary dye from Invitrogen™ and thus the exact structure and mode of binding to DNA is not disclosed. However, as the dye can stain ssDNA, and dsDNA under highly denaturing conditions, it is expected to bind to the phosphate backbone.<sup>28</sup> The absence of fluorescence bands in the presence of **PEG-G3** was hypothesized to be as a result of either: (1) **PEG-G3** degrading DNA preventing the staining of SYBR™ Gold; or (2) **PEG-G3** degrading SYBR™ Gold; or (3) **PEG-G3** quenching the fluorescence of DNA-stained SYBR™ Gold; or (4) the SYBR™ Gold binding to ssDNA being blocked by the presence of **PEG-G3** and thus no fluorescence.

Initially, the fluorescence of SYBR™ Gold stained-C2 was analyzed in the presence of increasing equivalents of **PEG-G3**. The fluorescence of SYBR Gold™ at 539 nm was found to decrease rapidly in the presence of increasing amounts of **PEG-G3** (Figure 2.11). This result supported

the hypothesis that the absence of bands in the PAGE gel (Figure 2.8) was most likely as a result of **PEG-G3** disrupting the function of the fluorescence stain.

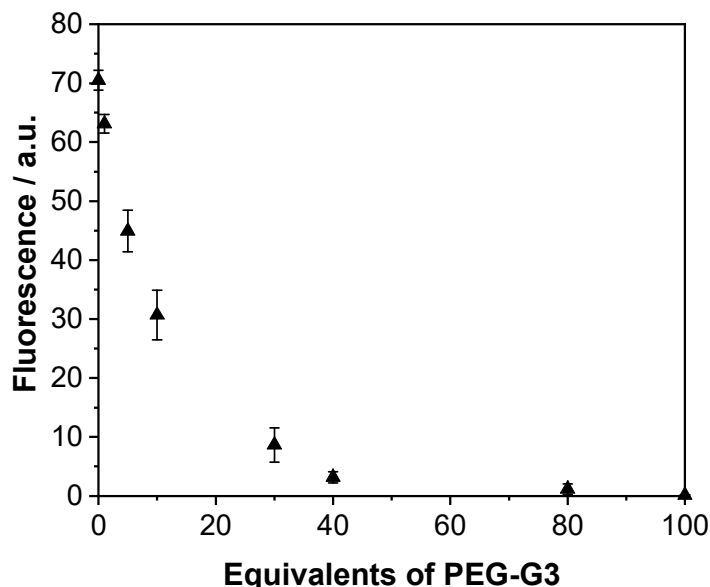


**Figure 2.11** Fluorescence intensity of SYBR™ Gold stained-C2 at 539 nm after the addition of increasing equivalents of **PEG-G3**. Equivalents are calculated with respect to C2. Error bars are based on the standard error across three measurements. Excitation  $\lambda = 498$  nm.

In addition, the fluorescence of SYBR™ Gold stained-C2 was monitored over time in the presence of 1, 5 and 10 equivalents of **PEG-G3**. Figure 2.12 shows that the fluorescence of 5  $\mu$ M SYBR™ Gold stained-C2 initially dropped very rapidly but then plateaued after approximately 8 minutes. The drop was found to be dependent upon the equivalents of **PEG-G3** added with a higher number of equivalents leading to a larger fluorescence decrease. The rapid decrease followed by a plateau was not consistent with the degradation of DNA or SYBR™ Gold, where a continuous decrease would be expected. Therefore, the cause of fluorescence quenching was hypothesized to be as a result of the latter two possibilities: either the quenching of SYBR™ Gold stained-C2 fluorescence or the blocking of the binding of SYBR™ Gold to C2.



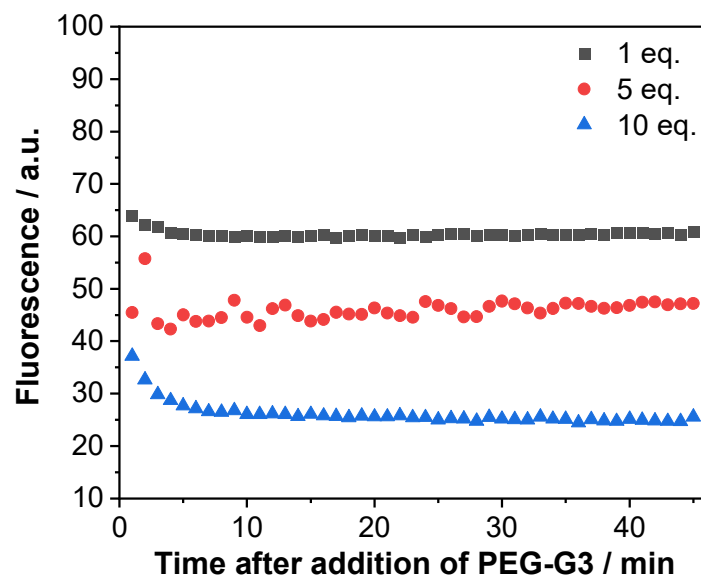


**Figure 2.12** Fluorescence intensity of SYBR™ Gold stained-C2 complex at 539 nm over time with varying equivalents of **PEG-G3**: (black square) 1 equivalent of **PEG-G3** relative to DNA; (red circle) 5 equivalents of **PEG-G3** relative to DNA; (blue triangle) 10 equivalents of **PEG-G3** relative to DNA. Excitation  $\lambda = 498$  nm.

A number of quenching mechanisms are possible to explain the reduction in fluorescence, including collisional quenching, static quenching and energy transfer to name a few. Of note, there are numerous reports of fluorescently labelled oligonucleotides being quenched through a photoinduced electron transfer mechanism.<sup>29, 30</sup> In particular, the fluorescence quenching of an ethidium bromide-DNA complex with a six-coordinated Ru(II) complex was believed to be due to the DNA-mediated electron transfer from the excited ethidium to the Ru(II) complex.<sup>31</sup>

However, of interest in this particular study, was the previous observation that SYBR™ Gold stained-dsDNA could be visualized following the addition of **PEG-G3** (Figure 2.8) and thus, it was hypothesized that the difference in visualization may be as a result of the different binding modes of **PEG-G3** and SYBR™ Gold to dsDNA and ssDNA. Therefore, an experiment was conducted to identify if SYBR™ Gold displaced **PEG-G3** upon the addition of a complementary strand as depicted in Figure 2.13a. The fluorescence of S2-NH<sub>2</sub> in Tris annealing buffer (3.33

$\mu\text{M}$ ) was analysed at 539 nm following the excitation of light at 498 nm (Figure 2.13b). Originally, the fluorescence of S2-NH<sub>2</sub> alone was low, due the low intrinsic fluorescence of DNA. However, upon the addition of SYBR™ Gold the fluorescence rapidly increased.

Following the addition of **PEG-G3** the fluorescence rapidly decreased initially, before adopting a slower decrease. It was hypothesized that these two stages may represent two separate events: (1) a rapid decrease due to the fluorescence quenching of SYBR™ Gold; and (2) a slow decrease as a result of DNA degradation. Upon the addition of a complementary strand, C2, the original fluorescence was not restored; however, it did plateau suggesting the termination of DNA degradation. This could be due to either improved stability of dsDNA or the degradation of the catalysts.

Overall, the differences in the binding modes of dsDNA and ssDNA with SYBR™ Gold and **PEG-G3** do not appear to account for the difference in the visualization abilities of stained dsDNA and ssDNA observed in Figure 2.8 as the initial fluorescence is not restored. Based on the fluorescent data obtained, it was hypothesized that the fluorescence quenching was likely as a result of **PEG-G3** quenching the fluorescence of SYBR™ Gold stained-DNA, and based on previous literature the most likely explanation for this is *via* a DNA mediated photo-induced electron-transfer mechanism. Furthermore, it was suggested that the visualisation of dsDNA by PAGE analysis was a result of the larger concentration of DNA present which minimised the quenching effect allowing for visualization. Finally, the suggestion of photoinduced charge transfer being the cause of the fluorescence quenching provides further evidence for a DNA-**PEG-G3** interaction.

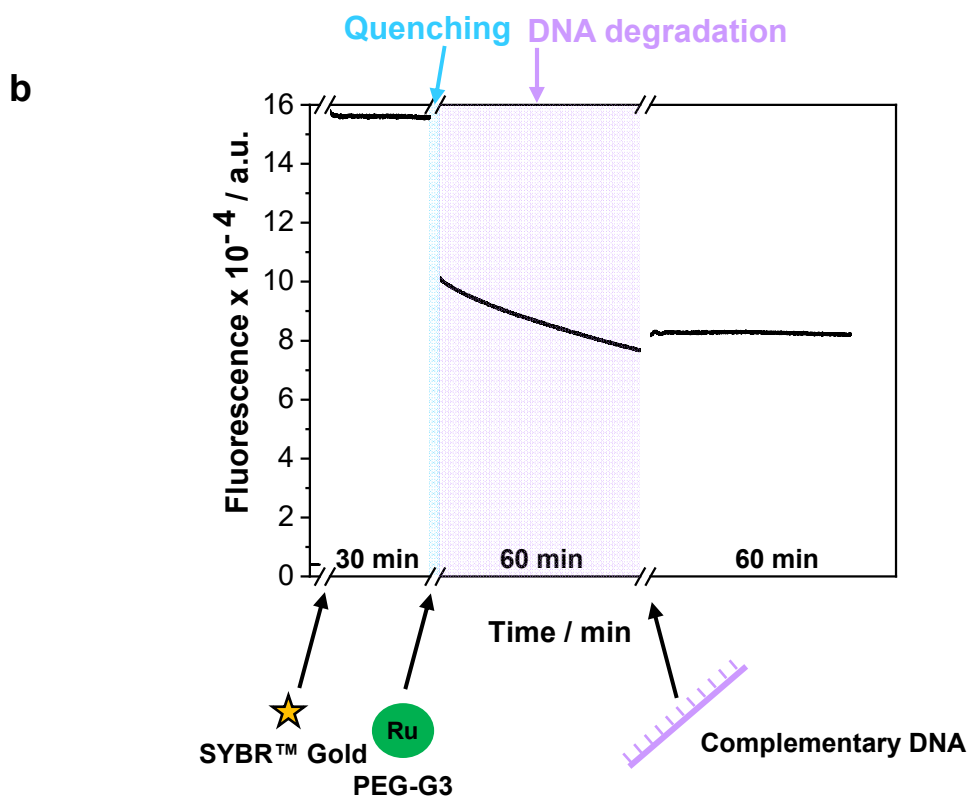
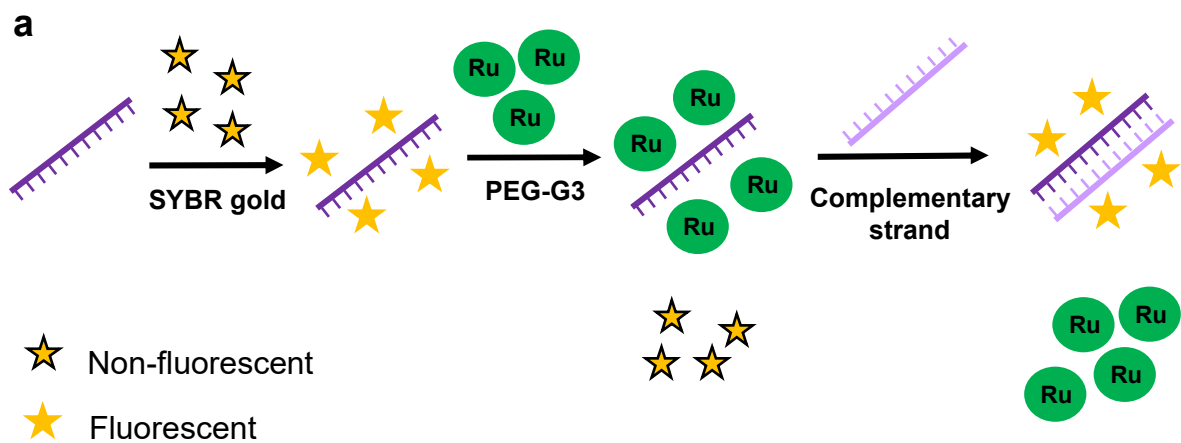


**Figure 2.13** (a) Proposed schematic to explain differences in the visualization properties of ssDNA and dsDNA. (b) Fluorescence at 539 nm of S2-NH<sub>2</sub> upon the addition SYBR™ Gold, PEG-G3 and then a complementary DNA sequence (C2).  $\lambda = 498$  nm.

### 2.3.4 Interaction between dsDNA and PEG-G3

A second set of experiments were conducted to identify the mode of binding between dsDNA and **PEG-G3**. As introduced in Section 2.2.2 the mode of binding may be classified as either: (1) intercalation; (2) major groove binding; (3) minor groove binding; or (4) external binding.

#### 2.3.4.1 UV-Vis studies to determine the interaction between dsDNA and PEG-G3

UV-Vis spectroscopy has been heavily utilized to identify DNA-small molecule interactions due to shifts occurring in the absorption spectrum.<sup>18, 32</sup> When a small molecule is added to a solution of DNA, if it does not bind to DNA then the UV-Vis spectrum will simply be the sum of both spectra; however, upon binding there are characteristic changes in the spectra.<sup>33</sup> For this study, DNA isolated from calf thymus (ctDNA) was used as it is commercially available and well-studied, mainly owing to its resemblance to mammalian DNA and ease of extraction from the thymus gland of a calf.<sup>34</sup>

In an initial study the absorbance of ctDNA at 260 nm, where the nucleobases are known to strongly absorb, was monitored upon the addition of **PEG-G3**. However, as shown in Figure 2.14a, **PEG-G3** also absorbs strongly in this region and therefore the data was corrected to remove the intrinsic absorbance of **PEG-G3** at 260 nm. Following this correction, a very slight hypochromic and bathochromic shift was observed at 260 nm following the addition 0 to 2 equivalents of **PEG-G3** (Figure 2.14b).

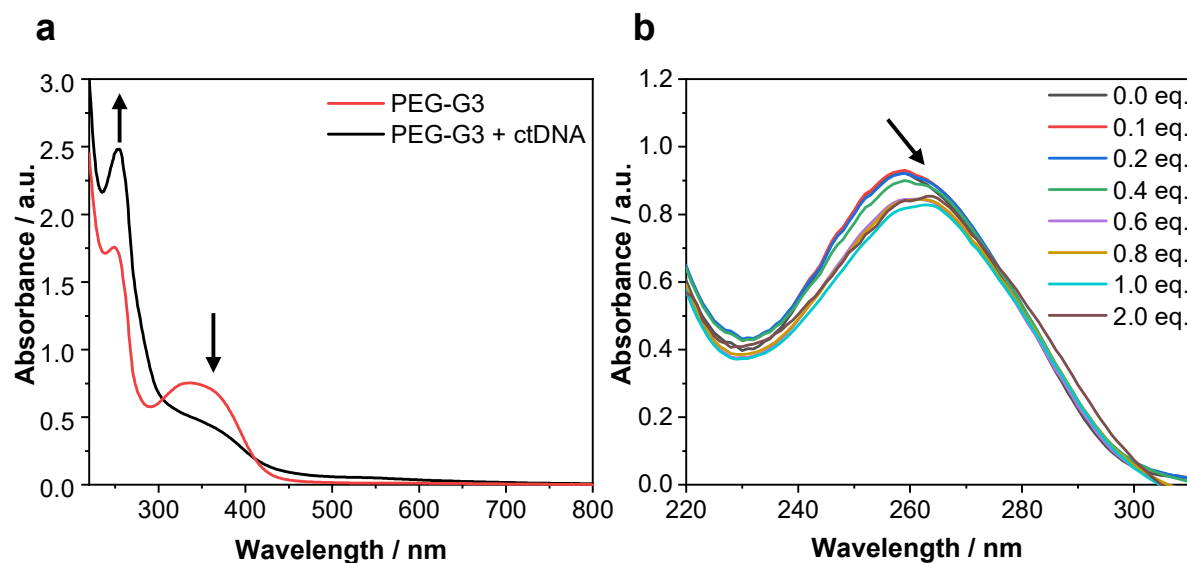


**Figure 2.14** (a) UV-Vis spectrum of **PEG-G3** (red trace) in the absence and presence of 0.5 equivalents of ctDNA (black trace). Equivalents of base pairs calculated with respect to **PEG-G3**. The arrows indicate an increase in absorbance at 260 nm due to the cumulative absorbance of **PEG-G3** and ctDNA at 260 nm, and a decrease in absorbance at 350 nm in the presence of ctDNA. (b) UV-Vis spectrum of ctDNA upon the addition of **PEG-G3**. The data was corrected to take into the account the intrinsic absorbance of **PEG-G3** and the total volume change was kept low <0.4%. The arrow indicates a very slight hypochromic and bathochromic shift. Equivalents of **PEG-G3** calculated with respect to DNA base pairs.

In general, hypochromism and bathochromism are associated with the stabilization of the DNA-duplex and tightening of the duplex.<sup>35</sup> After the first titration series, it was noted that **PEG-G3** has a characteristic absorbance peak at 350 nm associated with the metal-to-ligand charge transfer (MLCT) peak. In the presence of ctDNA the aforementioned absorbance peak appeared to dramatically decrease (Figure 2.14a). Therefore, a second titration series was conducted monitoring the absorption of **PEG-G3** at 350 nm following subsequent additions of ctDNA (Figure 2.15).

Figure 2.15 once again shows a hypochromic shift of the MLCT band upon the addition of ctDNA. In total, 29 aliquots of ctDNA were titrated into the solution, resulting in a 0.42:1 ratio of DNA base pairs (BP) : **PEG-G3**, the spectra was corrected to take into account the volume

change upon each addition. A hypochromic shift in the small molecule absorbance is typically associated with intercalative binding, due to  $\pi$ - $\pi$  stacking.<sup>36</sup>

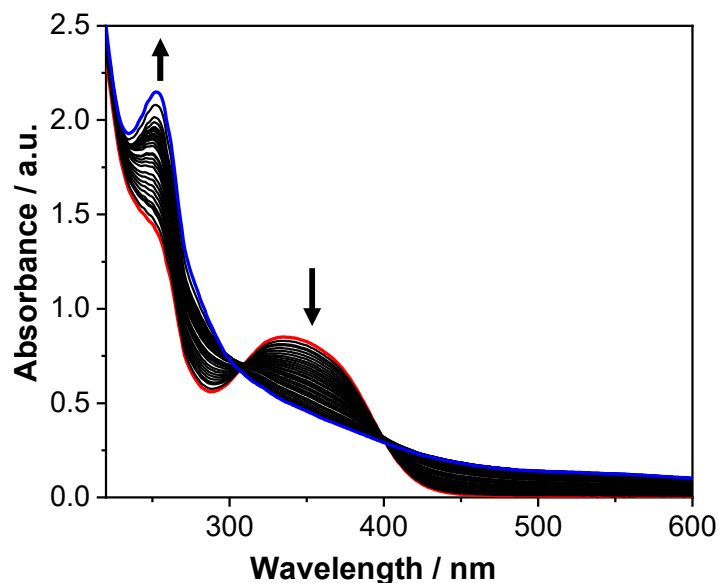


**Figure 2.15** UV-Vis spectroscopy titration series showing the effect of the addition of ctDNA to **PEG-G3**. 29, 2  $\mu$ M additions of 1.44 Mm ctDNA were added to a maximum equivalents of 0.42 base pairs. The absorbance was corrected to take into account the additional volume. The arrows indicate an increase in absorbance at 260 nm and a decrease of absorbance at 350 nm. Red trace = 0 eq. of ctDNA BP; Blue trace = 0.42 eq. ctDNA BP.

The change in absorbance can be utilized to extract an equilibrium binding constant,  $K_a$  using the Benesi-Hildebrand method.<sup>37</sup> Firstly, a difference absorbance plot or delta plot was prepared by subtracting the corrected UV spectrum at each point in the titration series from that of **PEG-G3** (Figure 2.16).<sup>38</sup> The delta plots allow for identification of the wavelength at which the maximum change in absorbance occurs, and this wavelength was identified to be 352 nm.

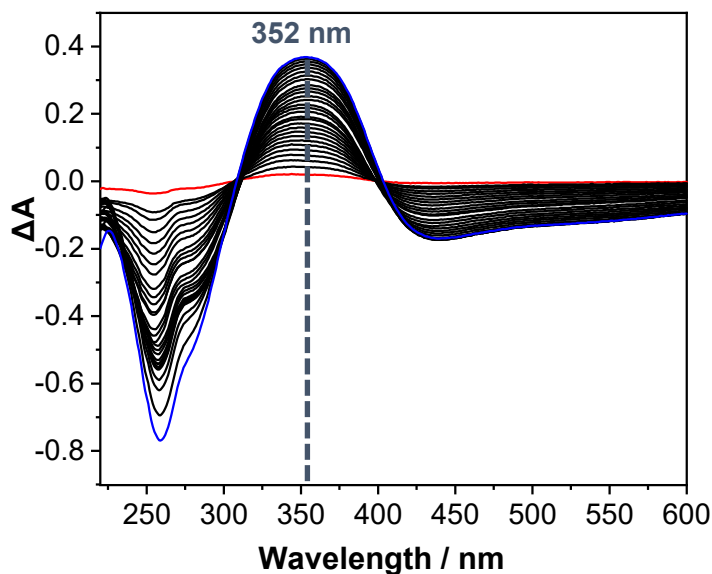
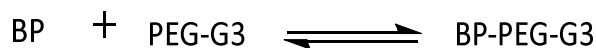


**Figure 2.16** Delta plots obtained by subtracting the corrected UV-Vis spectrum at each point in the titration from that of **PEG-G3**. Red trace = 0 eq. of ctDNA base pairs; Blue trace = 0.42 eq. ctDNA base pairs.

The derivatization of the binding constant can then be calculated based on the equilibrium between **PEG-G3** and free DNA base pairs (BP) as shown in Scheme 2.2.



**Scheme 2.2** The equilibrium formed between free DNA base pairs (BP) and **PEG-G3**.

The relationship between the change in absorbance and  $K_a$  is shown in Equation 2.1, the derivation of this equation is shown in Section 2.5.3 and taken from a report by Wilks *et al.*<sup>39</sup>

$$\Delta A = \frac{\Delta A_{\text{max}} K_a [\text{BP}]}{(1 + K_a [\text{BP}])}$$

**Equation 2.1** Relationship between the change in absorbance and concentration of base pairs used to calculate the equilibrium binding constant,  $K_a$ .

The change in absorbance at 352 nm was plotted against the concentration of base pairs and then a non-linear least squares fit was applied to the data using Equation 2.1.  $\Delta A_{\text{max}}$  which is the maximum change in absorbance at 352 nm was iterated manually to give the best fit,

whilst setting the upper bound limit to 0.818 which is the absorbance at 352 nm of **PEG-G3** alone. When  $\Delta A_{\max}$  was 0.794,  $K_a$  was calculated to be  $19000 \pm 2000 \text{ M}^{-1}$  (Figure 2.17).

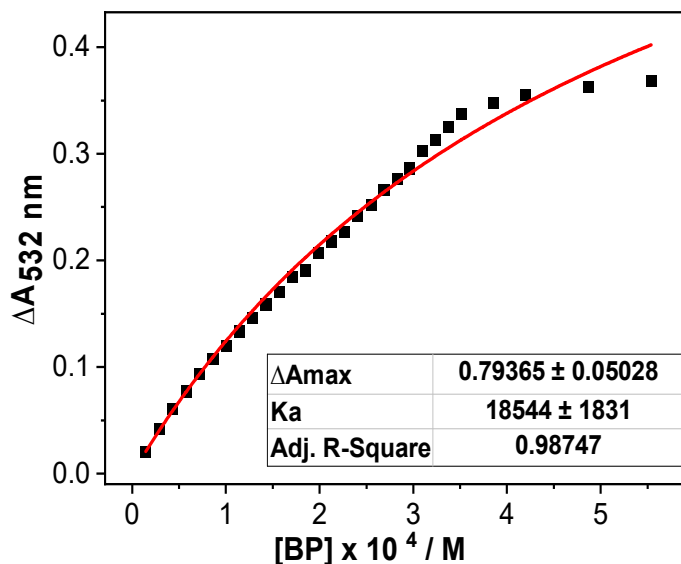
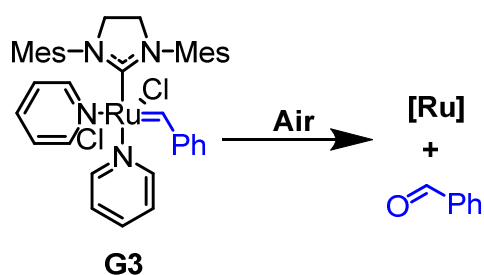


**Figure 2.17** Plot BP concentration against the change in absorbance at 352 nm. A non-linear least squares fit was applied to the data (red line) to calculate  $K_a$ .

The  $K_a$  value calculated was based on a number of assumptions; firstly, there is no cooperativity between the binding of **PEG-G3** to adjacent base pairs, and secondly the concentration of **PEG-G3** remains constant throughout the experiment. The latter assumption is incorrect due to the volume increase during the experiment; however, the data was corrected to take this into account. Finally, the biggest limitation of this method is the assumption that the concentration of free BP in solution is mathematically equivalent to the total concentration of BP.<sup>40</sup> This is an assumption that is never fully valid even when a high excess of BP is used; however, in this scenario where the  $[\text{BP}] < [\text{PEG-G3}]$  the assumption is likely to be grossly inaccurate reducing the accuracy of the calculated value; thus the value calculated can only be used as an estimation.



The strong absorbance of **PEG-G3** around 350 nm used to calculate  $K_a$  is likely due to MLCT into the  $\pi^*$  orbital of the benzylidene ligand.<sup>41, 42</sup> Previous studies completed by Forcina *et al.*, demonstrated that upon the deliberate oxidation of **G3** the formation of benzaldehyde was observed by <sup>1</sup>H NMR spectroscopy (Scheme 2.3) and thus, the loss of the MLCT band.<sup>41</sup> A similar decrease in the MLCT band of a Hoveyda-Grubbs type water-soluble catalyst was observed over a 16 h period under N<sub>2</sub>.<sup>43</sup> Any decrease in the 350 nm absorption due to oxidation would have an effect on the  $K_a$  value previously calculated. Therefore, the UV-Vis spectrum of **PEG-G3** in H<sub>2</sub>O was monitored over time, and analogous to previous reports a reduction in the MLCT band was observed (Figure 2.18a).



**Scheme 2.3** Oxidation of **G3**, resulting in the loss of the MLCT band as postulated by Forcina *et al.*<sup>41</sup>

The intrinsic reduction of the MLCT band in H<sub>2</sub>O, was then compared to the reduction observed in the presence of ctDNA (0.37 equiv). The absorbance spectra of **PEG-G3** was recorded immediately before and after the addition of a concentrated solution of ctDNA in H<sub>2</sub>O and this result was compared to a control experiment using pure water, with no added ctDNA (Figure 2.18b). The addition of ctDNA resulted in a 0.12 absorbance unit (a.u) decrease in the MLCT band, compared to a 0.05 a.u decrease upon the addition of pure H<sub>2</sub>O. Furthermore, a 10 nm hypsochromic in  $\lambda_{max}$  was observed upon the addition of ctDNA; however, no shift in  $\lambda_{max}$  occurred upon the addition of H<sub>2</sub>O.

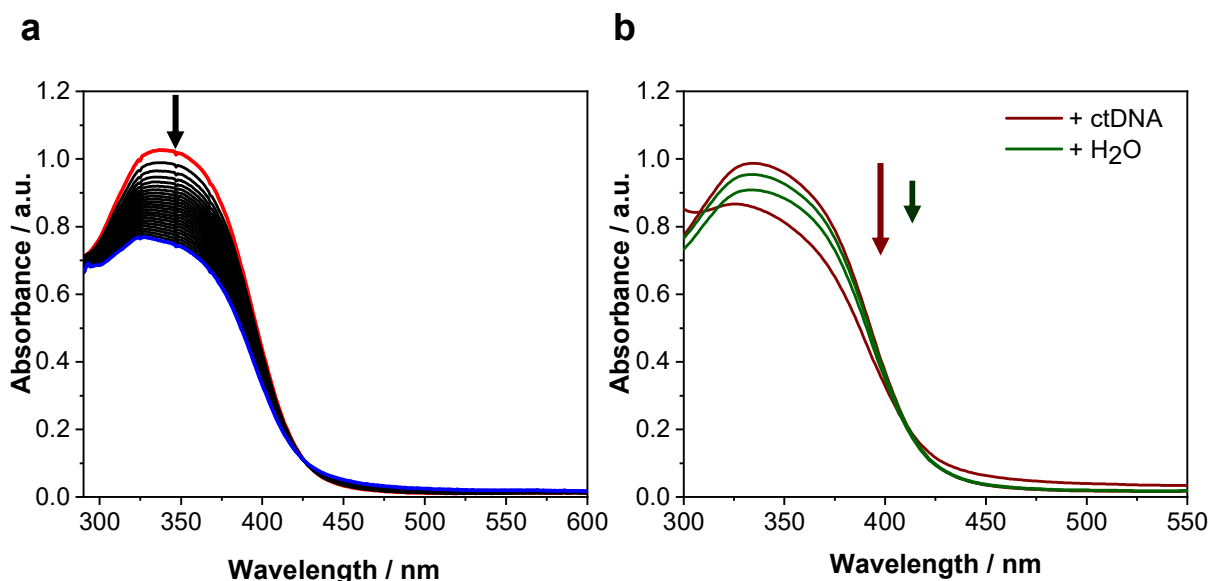


**Figure 2.18** (a) UV-vis spectrum of a solution of **PEG-G3** (0.14 M) in  $H_2O$ , monitored every 5 min for 115 min. Red trace = 0 min; blue trace = 115 min. (b) UV-vis spectrum of a solution of **PEG-G3** (0.14 M) in  $H_2O$ : upon the addition of 70  $\mu$ l ctDNA (1.5 M) in  $H_2O$  (red trace); and upon the addition of 70  $\mu$ L  $H_2O$  (green trace).

The results suggest that the hypochromic shift observed in Figure 2.15 is likely due to two simultaneous effects: (1) the oxidation of **PEG-G3** in  $H_2O$ ; and (2) the addition of ctDNA. Whilst the greater drop in absorbance upon the addition of ctDNA could be due to ctDNA accelerating the degradation of the catalyst. The hypsochromic shift observed in the MLCT peak would suggest an interaction is occurring between ctDNA and **PEG-G3** and corroborates with the shifts observed in the UV-Vis spectra of ctDNA (Figure 2.14b). As a consequence of the two simultaneous effects impacting  $\Delta A$ , the  $K_a$  value reported is likely to be an over-estimate.

#### 2.3.4.2 Linear dichroism studies

Following the UV-Vis spectroscopy studies which were suggestive of an interaction between DNA and **PEG-G3**, further studies were conducted in an attempt to determine the binding mode between **PEG-G3** and DNA. Linear dichroism was introduced in Section 2.2.2 as a useful analytical technique to determine the mode of binding of small molecules to DNA.

LD is defined as the differential absorption of light polarised parallel and perpendicular to a reference,  $x$ , at a given wavelength (Equation 2.2).<sup>44</sup>

$$LD = A_{\parallel} - A_{\perp}$$

**Equation 2.2** *Linear dichroism is defined as the differential absorption of light polarised parallel ( $A_{\parallel}$ ) and perpendicular ( $A_{\perp}$ ) to a reference.*

LD therefore requires the orientation of the molecule either intrinsically or during the experiment. If DNA is dissolved in a solvent and then flowed past a stationary phase the DNA will align with the long axis in the direction of the flow; therefore, making it suitable for LD measurements.

In a randomly oriented sample, the  $LD = 0$ ; thus, as the degree of orientation increases the intensity of the LD signal increases and is proportional to the magnitude of the absorbance of the sample. The LD spectrum of DNA contains characteristic peaks in the ultraviolet region, 180 - 300 nm, which can be monitored upon the addition of small molecules. If a small molecule binds to DNA in a particular orientation an LD signal will be induced and thus, the direction of this signal can provide information on the orientation of the small molecule with respect to the flow.<sup>45</sup>

B-DNA aligns under flow with the phosphate backbone parallel to the flow and the bases perpendicular (Figure 2.19). The LD spectrum of native DNA is therefore the same shape as the absorption spectrum but with a negative peak at 260 nm as the bases which are absorbing are perpendicular to the flow. Small molecules that bind to DNA in a specific orientation will also exhibit an LD response in the regions they absorb UV light and the direction of this signal (positive or negative) can provide information on the binding mode.<sup>44, 46</sup> For example, a positive LD response implies that the small molecule is aligned parallel to the axis and is

therefore consistent with groove binding. In contrast, a negative response implies that the small molecule is aligned perpendicular to the axis and is therefore more consistent with intercalation. Molecules that do not bind to DNA or bind to DNA in a non-specific orientation do not exhibit an LD response.

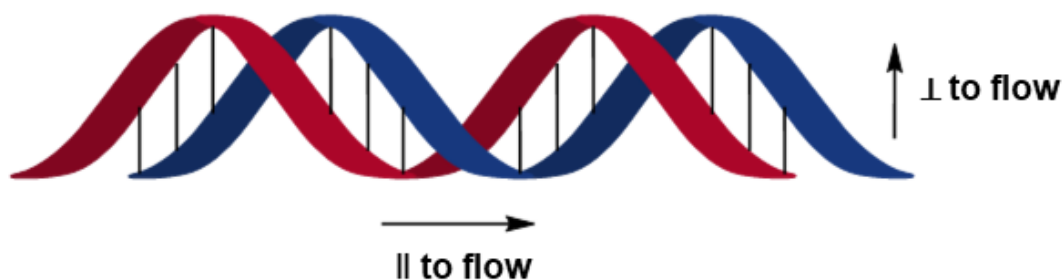


**Figure 2.19** Schematic to show the orientation of DNA under flow. The phosphate backbone aligns parallel to the flow whilst the bases align perpendicular to the flow.

To complete this study the LD spectrum of ctDNA was recorded and then monitored following the addition of **PEG-G3** (Figure 2.20). In particular, the region around 350 nm where the MLCT band of **PEG-G3** appears was studied closely for the appearance of an LD-response. However, no response was observed around 350 nm suggesting that either: the orientation of the Ru is non-directional and thus, most consistent with an external binding interaction; or the catalyst is degrading too quickly and thus no longer absorbing in that region.

Of interest was the LD response of ctDNA at 260 nm which appeared to be decreasing upon the addition of catalyst. The magnitude of the LD signal is related to the degree of orientation, which is described by an orientation parameter  $S$ , Equation 2.3.<sup>44, 46</sup>

$$LD^r = \frac{LD}{A_{iso}} = 3S \left( \frac{1}{2} (3 \cos^2 \alpha - 1) \right)$$

**Equation 2.3** The reduced linear dichroism ( $LD^r$ ) is the ratio of the linear dichroism signal and the absorbance of the isotropic sample. This is related to an orientation factor,  $S$  and the angle,  $\alpha$  between the helix and the light-absorbing transition dipole.

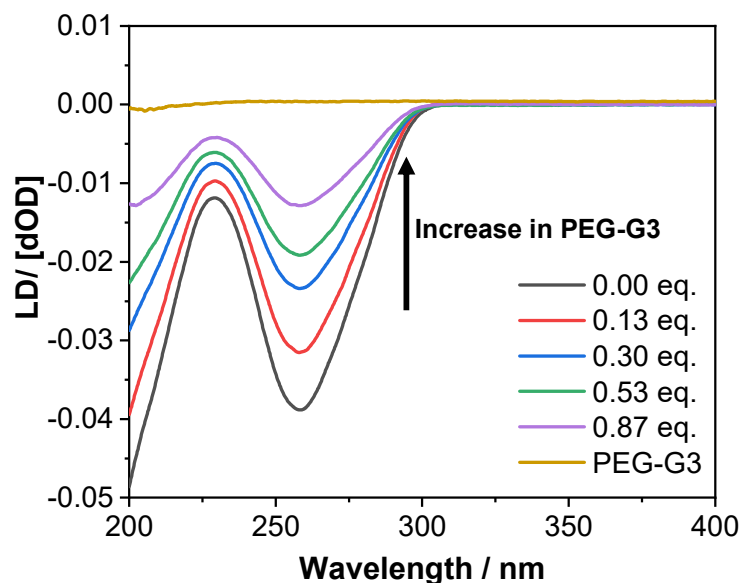


**Figure 2.20** LD spectroscopy titration series showing the effect of adding 0 to 0.87 equiv. **PEG-G3** to ctDNA under cuvette flow.

The orientation parameter,  $S$ , can be used to provide information about the length and flexibility of DNA. For example, as the helix becomes stiffer and longer, the magnitude of  $S$  increases and thus, the magnitude of the linear dichroism response increases. Similarly, a reduction in the linear dichroism response is indicative of bending.

The decrease in the linear dichroism response observed in Figure 2.20 upon the addition of **PEG-G3** could provide evidence for the **PEG-G3** induced DNA bending. The induction of DNA bending has previously been reported in the presence of small, mobile multivalent cations.<sup>47</sup> However, the interpretation of this result is complicated by the absorbance of **PEG-G3** in this region as initially shown in Figure 2.14a. The absorbance of **PEG-G3** at 260 nm is expected to be due to the presence of the PEGylated pyridine ligands and thus, the decrease in the linear dichroism response could reflect the orientation of these groups parallel to the double helix as depicted in Figure 2.21. As the nucleobases absorbing in the same region are perpendicular to the flow, the two groups would cancel each other out reducing the magnitude of the

response. Note that in solution the mono-pyridine species is expected to be the dominant product due to loss of one of the weakly associated pyridine ligand.<sup>48</sup>

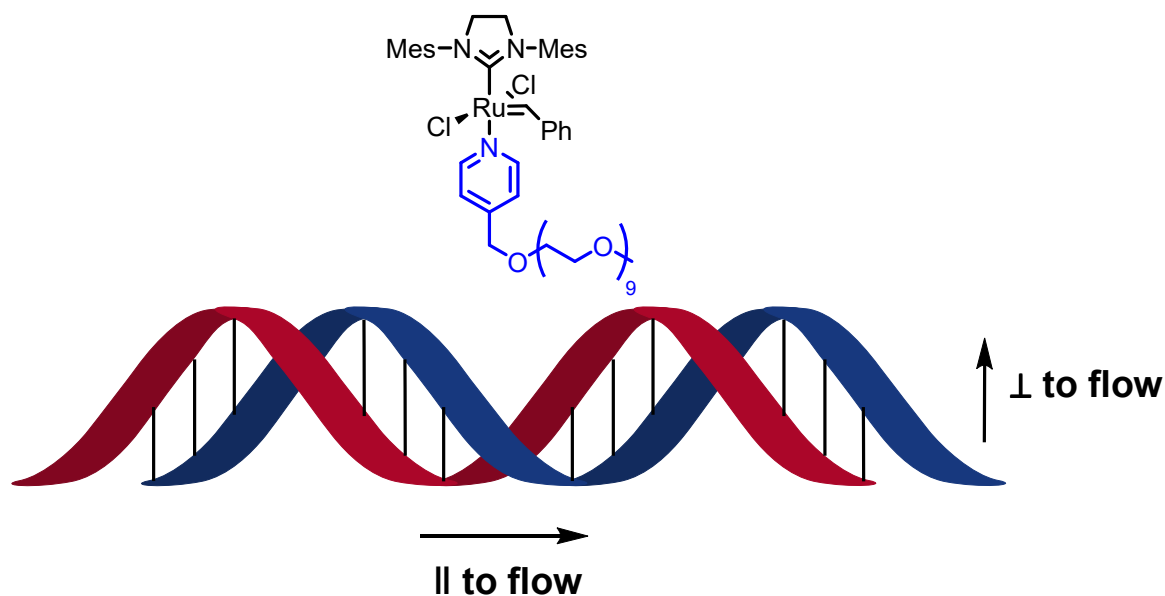


**Figure 2.21** Orientation of **PEG-G3** with the PEG groups (highlighted) parallel to the flow and the nucleobases perpendicular to the flow.

## 2.4 Conclusions

The purpose of this chapter was to explore the compatibility of metathesis catalysts with DNA. Whilst several publications have begun to explore the use of metathesis in DECLs, studies into the interactions between the catalyst and DNA have not been conducted until now.

The initial aim was to explore the stability of DNA in the presence of Ru metathesis catalysts, HG2 and a water-soluble variant, **PEG-G3**. ssDNA appeared stable in the presence of 1 equivalent of HG2 for a significant amount of time (at least 96 h). However, in the presence of 150 equivalents of HG2 a significant difference between those samples incubated with and without MgCl<sub>2</sub> was observed in agreement with the work conducted by Lu *et al.*<sup>12</sup> In the samples incubated without MgCl<sub>2</sub> a loss of any bands in the PAGE gel was noted after 15

minutes. This was hypothesized to be due to depurination, rather than the cleavage of the phosphate backbone; however, due to limited data on the binding mode of the nucleic acid gel stain utilized a definite conclusion on the mode of degradation could not be reached. Instead, it was concluded that in order to retain the integrity of DNA the minimum catalyst loading should be utilized alongside a large excess of  $MgCl_2$ .

Similar stability studies conducted in the presence of a water-soluble catalyst, **PEG-G3**, were problematic due to the absence of fluorescence when using both a SYBR Gold™ stain and fluorescently labelled oligonucleotide. Following further studies this was attributed to fluorescence quenching by a photoinduced electron transfer mechanism in the presence of Ru bound to DNA and a time course study revealed a rapid drop in fluorescence due to SYBR™ Gold quenching, followed by a steady fluorescence decrease due to DNA degradation.

The latter section of this study focussed on confirming the binding between DNA and **PEG-G3**. Native PAGE results indicated the presence of an interaction between dsDNA and **PEG-G3** due to the appearance of a broad band in the gel, typical of a DNA-polymer conjugate. Furthermore, UV-Vis spectroscopy studies identified shifts in the MLCT band upon the addition of ctDNA which could not be explained by catalyst degradation alone and thus, provided further evidence of an interaction. Finally, linear dichroism was utilized in an attempt to identify the mode of this binding. Whilst no LD response was recorded for the MLCT band, the LD response associated with the absorbance of the nucleobases decreased over time providing further evidence for an interaction.

It was proposed that the binding is most likely due to an electrostatic interaction between the negatively charged phosphate backbone and positively charged Ru-catalyst, further

strengthened and orientated by dipole-dipole interactions between PEG and DNA. This result explains why fluorescence quenching by electron transfer was more problematic with **PEG-G3** than HG2 as the former is likely to be bind more strongly to DNA. Furthermore, the addition of Lewis acids such as  $Mg^{2+}$  are likely to block this DNA-Ru interaction improving the stability of DNA.

Overall, our studies have identified four simultaneous effects taking place when fluorescent DNA is mixed with **PEG-G3**. (1) DNA-degradation particularly prevalent at high catalyst concentrations but found to be prevented in the presence of  $Mg^{2+}$ ; (2) Fluorescence quenching which has been found to hinder DNA analysis; (3) DNA-catalyst binding; and (4) catalyst degradation, these effects are highlighted in Figure 2.22. Due to the complexity of this system and multitude of effects taking place simultaneously, a number of questions still remain including the effect of catalyst degradation on the DNA stability, binding and fluorescence. To answer this question, a comprehensive understanding of catalyst degradation is required, and isolation of such degraded products will be needed. These studies are still very much in their infancy but will prove invaluable for the future understanding of the impact of Ru metathesis catalysts on DNA.



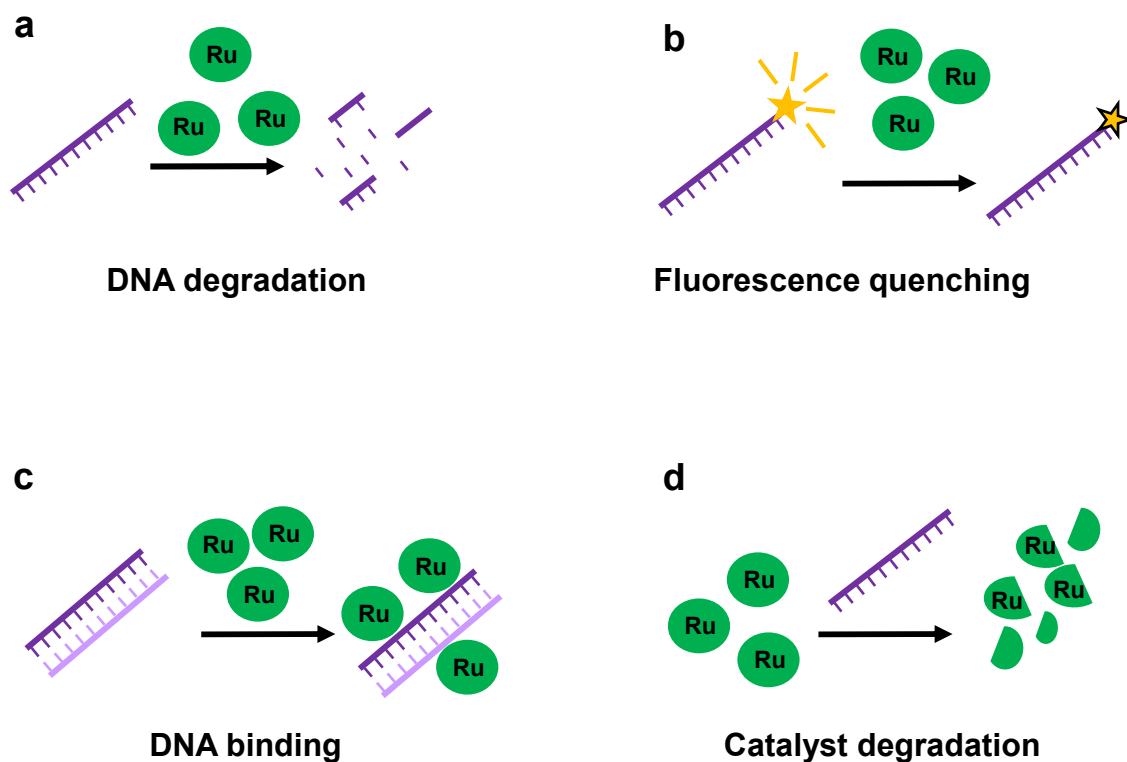


**Figure 2.22** Schematic to demonstrate the proposed events taking place when **PEG-G3** is mixed with fluorescent DNA. (a) DNA degradation; (b) Fluorescence quenching; (c) Ru-DNA binding and (d) catalyst degradation.

Despite the complexity of the results obtained, the results suggest that the feasibility of metathesis ‘on-DNA’ is plausible under carefully selected conditions which can minimize the interactions between the metathesis catalyst and DNA namely a minimal catalyst loading and the addition of Lewis acids such as  $\text{MgCl}_2$ . Throughout the remainder of this thesis we will utilize this knowledge in an attempt to demonstrate the capabilities of metathesis in DNA nanotechnology.

## 2.5 Experimental

### 2.5.1 Materials

Oligonucleotides were purchased from Integrated DNA technologies, Inc. and resuspended in 18MΩ H<sub>2</sub>O to a concentration of 200 μM before use. Concentrations were calculated from the absorbance values at 260 nm using the reported extinction coefficients.

Name	Sequence (5'→3')	Extinction coefficient/ L/(mole·cm)
S0-NH <sub>2</sub>	5AmMC6/CGA GAC TCA ACG ACA TG	169,300
S1-NH <sub>2</sub>	5AmMC6/AGG GAT TGT CTT AGT GTG CGA ATA GGT AAC	303,700
S2-NH <sub>2</sub>	CTG GTA TGA ACG CAC ACT AAG ACA ATC CCT/3AmMo	290,400
S2-NH <sub>2</sub> -FAM	56-FAM/CTG GTA TGA ACG CAC ACT AAG ACA ATC CCT/3AmMo	311,360
C2	AGG GAT TGT CTT AGT GTG CGT TCA TAC CAG	291,600

Deoxyribonucleic acid sodium salt from calf thymus (ctDNA) was purchased from Sigma-Aldrich and dissolved in 18 mΩ H<sub>2</sub>O by gently inverting at 0 °C. The concentration of base pairs was calculated using the absorbance value at 260 nm and based upon the average molar mass reported to be 650 g mol<sup>-1</sup>.

Grubbs second generation catalyst, Hoveyda-Grubbs second generation catalyst, Poly(ethylene glycol) monomethyl ether and sodium hydride in mineral oil were purchased from Sigma-Aldrich and used as received. SYBR™ Gold Nucleic acid gel stain (10,000X concentrate in DMSO) was purchased from ThermoFisher. Dry solvents were purified over

Innovative Technology SPS alumina solvent columns and degassed using a standard freeze-pump thaw technique.

Dulbecco's phosphate buffered saline (DPBS) without calcium chloride, pH 7.5 was purchased from Sigma-Aldrich and made up using 18 MΩ H<sub>2</sub>O - the pH was adjusted to 6.5 with HCl. 10 x Tris-acetate-EDTA (TAE) buffer was purchased from Sigma-Aldrich and contains 0.4 M Tris acetate and 0.01 M EDTA. Tris annealing buffer contained 100 mM Tris, 50 mM NaCl and 1 mM EDTA in 18MΩ H<sub>2</sub>O adjusted to pH 8.

### 2.5.2 Instrumentation

*NMR Spectroscopy.* <sup>1</sup>H and <sup>13</sup>C nuclear magnetic resonance (NMR) spectra were recorded on a Bruker Advance III HD400 spectrometer or a Bruker Advance III AV600 in the solvents indicated at 298 K. Chemical shifts are reported on the δ scale in parts-per-million (ppm) and are referenced to the residual non-deuterated and deuterated solvent resonances respectively. (CDCl<sub>3</sub> <sup>1</sup>H: δ = 7.26 ppm; <sup>13</sup>C: δ = 77.2 ppm).

*High Performance Liquid Chromatography.* High Performance Liquid Chromatography (HPLC) analysis of oligonucleotides was performed on a modular Shimadzu instrument with the following modules: CBM-20A system controller, LC-20AD solvent deliver module, SIL-20AC HT autosampler, CTO-20AC column oven, SPD-M20A photodiode array UV-Vis detector, RF-20A spectrofluorometric detector and a FRC-10 fraction collector. Chromatography was performed on a Waters XBridge™ OST C18 2.5 μM column heated to 60 °C. Flow rate was set at 0.8 mL min<sup>-1</sup> and a linear gradient of buffers A and B: buffer A, 0.1 M TEAA, in a 95:5 mixture of H<sub>2</sub>O and acetonitrile; buffer B, 0.1 M TEAA, 30:70 mixture of H<sub>2</sub>O and acetonitrile.

*Gel Electrophoresis.* Native polyacrylamide gels were run at 2 °C in 1 TAE buffer at 180V – 200V using a vertical nucleic acid electrophoresis cell connected to a PowerPack basic power supply (BioRad). Samples were combined with 20% loading buffer (0.05% bromophenol blue, 25% glycerol in 1 x TAE) prior to running. Non-fluorescent DNA was stained using a 1:1000 aqueous SYBR® Gold nucleic acid gel stain (ThermoFisher) and visualized using either a Uvitec Cambridge transilluminator or a BioRad ChemiDoc™ MP Imaging system. The images were processed using BioRad ImageLab software v 6.0.1.

*Fluorescence Spectroscopy.* Fluorescence data was obtained using an Edinburgh Instruments FS5 spectrofluorometer or an Agilent Cary Eclipse Fluorescence spectrophotometer equipped with a photomultiplier tube (PMT) detector. To a 5 µM solution of C2 was added 0.2 µL SYBR™ Gold (10,000x in DMSO), a 0.04 M solution of **PEG-G3** in DPBS (pH 6.5) was titrated into the solution and the fluorescence was recorded after each addition (excitation at 498 nm, emission 539 nm).

*UV-Vis spectroscopy.* UV-Vis spectroscopy was recorded on an Evolution 350 UV-Vis spectrophotometer equipped with Xenon Flash Lamp light source and Dual Matched Silicon Photodiodes detector. 6.9 µL of **PEG-G3** in DPBS (pH 6.5, 0.04 M) was diluted to 2 mL with 18 MΩ H<sub>2</sub>O and the absorbance was recorded 2 minutes after the addition of ctDNA in 18 MΩ H<sub>2</sub>O (1.44 mM). Alternatively, the absorbance of 69 µM ctDNA in 18 MΩ H<sub>2</sub>O was recorded following the addition of **PEG-G3** in DPBS (pH 6.5, 0.04 M).

*LD spectroscopy.* LD spectroscopy was recorded on a J-720 CD spectrometer at University of Warwick. To a 50 µM solution of ctDNA in 18 MΩ H<sub>2</sub>O was added the appropriate volume of **PEG-G3** in DPBS (pH 6.5, 0.04M) and the LD was recorded.

### 2.5.3 Derivatization of $K_a$

The derivation of the equation used to calculate the equilibrium binding constant,  $K_a$ , has previously been reported by T. Wilks.<sup>39</sup>

The total concentrations of BP and **PEG-G3** in solution ( $[BP]_0$  and  $[PEG-G3]_0$ ) are related to the concentrations of free BP, free **PEG-G3** and the BP-**PEG-G3** complex.

$$[BP]_0 = [BP] + [BP-PEG-G3]$$

$$[PEG-G3]_0 = [PEG-G3] + [BP-PEG-G3]$$

**Equation 2. 4** *The total concentration of BP and PEG-G3.*

The mole fraction of BP-**PEG-G3**,  $f_{BP-PEG-G3}$  can then be defined as follows:

$$f_{BP-PEG-G3} = \frac{[BP-PEG-G3]}{[PEG-G3] + [BP-PEG-G3]} = \frac{[BP-PEG-G3]}{[PEG-G3]_0}$$

**Equation 2.5** *Definition of the mole fraction of  $f_{BP-PEG-G3}$  present in solution.*

Based on the equilibrium stated in Scheme 2.2, the equilibrium binding constant can be defined as follows:

$$K_a = \frac{[BP-PEG-G3]}{[BP][PEG-G3]}$$

**Equation 2.6** *Definition of the equilibrium binding constant,  $K_a$ .*

Substituting Equation 2.6 into Equation 2.5 the mole fraction of BP-**PEG-G3** can be re-written in terms of the equilibrium binding constant,  $K_a$ .

$$f_{BP-PEG-G3} = \frac{K_a[BP]}{1 + K_a[BP]}$$

**Equation 2. 7** *Definition of the mole fraction of BP-PEG-G3 in terms of the equilibrium binding constant,  $K_a$ .*

The concentration of BP-PEG-G3 can be written in terms of the mole fraction of BP-PEG-G3 and the total concentration of PEG-G3.

$$[\text{BP-PEG-G3}] = f_{\text{BP-PEG-G3}}[\text{PEG-G3}]_0$$

**Equation 2.8** Definition of the concentration of BP-PEG-G3 in terms of the mole fraction of BP-PEG-G3 and the total concentration of PEG-G3.

Substituting Equation 2.7 into Equation 2.8 defines the concentration of BP-PEG-G3 in terms of  $K_a$ .

$$[\text{BP-PEG-G3}] = \frac{K_a[\text{BP}][\text{PEG-G3}]_0}{1 + K_a[\text{BP}]}$$

**Equation 2.9** Concentration of [BP-PEG-G3] in terms of  $K_a$ .

The change in the absorbance of PEG-G3 noted upon DNA-binding can be defined as stated in Equation 2.10, where  $\epsilon_{\Delta\text{BP-PEG-G3}}$  is the difference in extinction coefficients between free and bound PEG-G3 (delta extinction coefficient).

$$\Delta A = \epsilon_{\Delta\text{BP-PEG-G3}}[\text{BP-PEG-G3}]$$

**Equation 2.10** Definition of the change in absorbance ( $\Delta A$ ) in terms of the concentration of the base pair-acridine complex and the delta extinction coefficient.

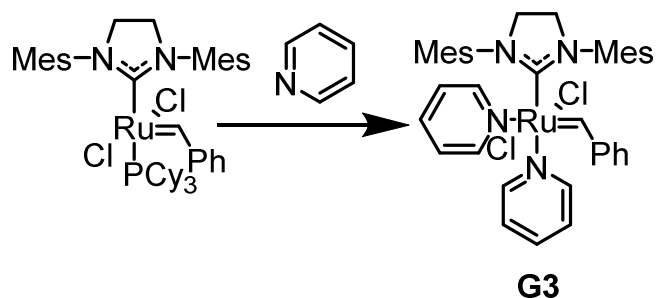
Substitution of Equation 2.9 into Equation 2.10 relates the change in absorbance ( $\Delta A$ ) to  $K_a$ .

Noting that the delta extinction coefficient multiplied by the initial concentration of PEG-G3 is equal to the maximum change in absorbance ( $\Delta A_{\text{Max}}$ ), Equation 2.11 can be obtained.

$$\Delta A = \frac{K_a[\text{BP}]\epsilon_{\Delta\text{BP-PEG-G3}}[\text{PEG-G3}]_0}{1 + K_a[\text{BP}]} = \frac{K_a[\text{BP}]\Delta A_{\text{max}}}{1 + K_a[\text{BP}]}$$

**Equation 2.11** Relationship between the change in absorbance and  $K_a$  and [BP].

#### 2.5.4 Synthesis of G3



G2 was converted to **G3** according to a previously reported procedure.<sup>25</sup> To a 20 mL scintillation vial equipped with a magnetic stir bar was added G2 (100 mg, 0.12 mmol) and 1 mL pyridine. The mixture was stirred for 5 minutes at 25 °C until the red color disappeared to yield a clear, dark green solution. 10 mL of cold hexane was added and the solution was stirred for a further 5 minutes. The green precipitate that formed was isolated *via* filtration and washed with 20 mL of cold hexane to yield a green solid (0.0267 g, 31%). <sup>1</sup>H NMR (600 MHz; 298 K; CDCl<sub>3</sub>) δ =19.18 (s, 1H, H-alkylidene), 8.63 (s, 2H, Arom-*H*), 7.83 (s, 2H, Arom-*H*), 7.67 (t, 1H, Arom-*H*), 7.63 (d, 2H, Arom-*H*), 7.48 (t, 2H, Arom-*H*), 7.27 (m, 2H, Arom-*H*), 7.06-7.09 (m, 4H, Arom-*H*), 6.97 (s, 2H, Arom-*H*), 6.75 (s, 2H, Arom-*H*), 4.12 (br d, 4H, NCH<sub>2</sub>CH<sub>2</sub>N), 2.65 (s, 6H, Ar-CH<sub>3</sub>), 2.24-2.36 (m, 12H, Ar-CH<sub>3</sub>). Characterization matches that reported in the literature.<sup>25</sup>

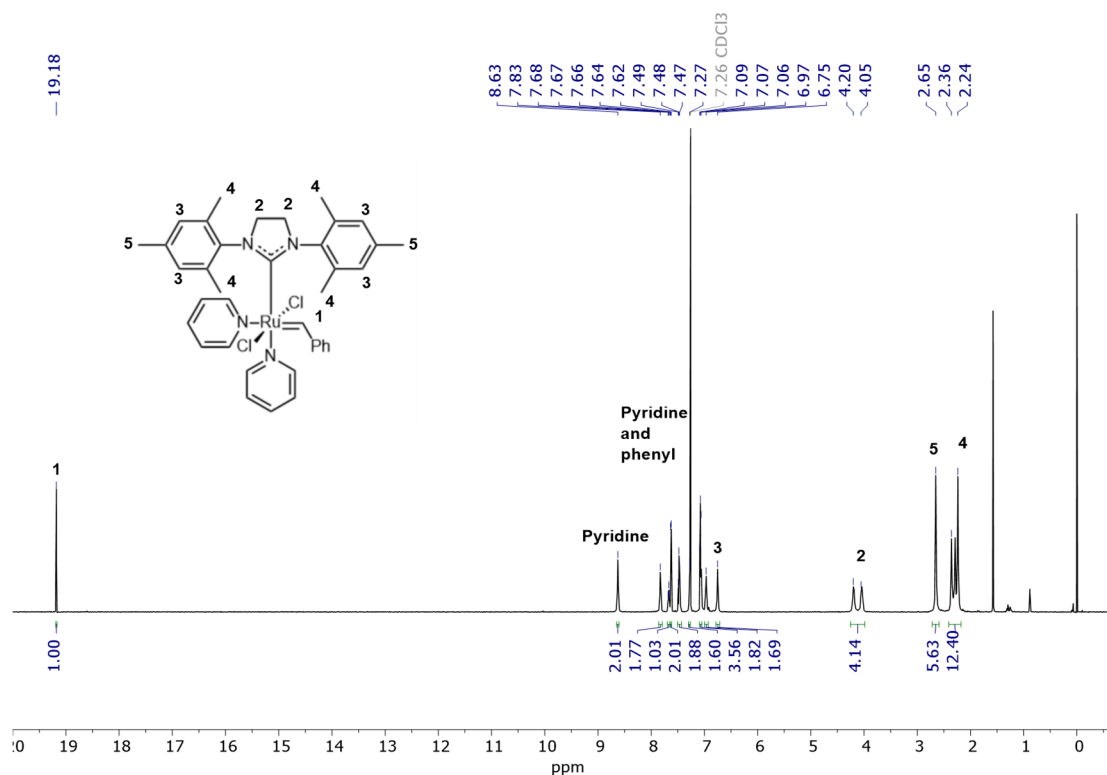
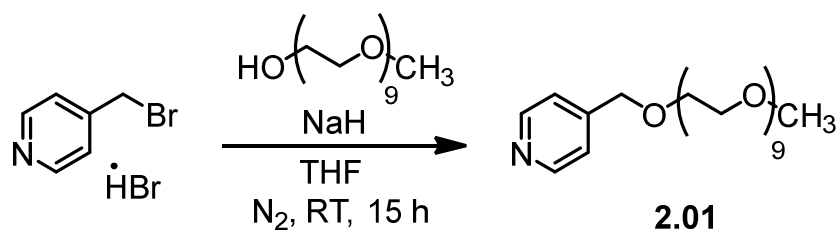


**Figure 2.23** <sup>1</sup>H NMR spectrum of **G3** in CDCl<sub>3</sub> (600 MHz, CDCl<sub>3</sub>).

### 2.5.5 Synthesis of 2.01



The ligand was prepared based on a modified version of a previously reported protocol.<sup>25</sup> Poly(ethylene glycol) monomethyl ether ( $M_n \sim 350$ , 1.05 g, 3.0 mmol) was added dropwise to a slurry of sodium hydride (120 mg, 3.0 mmol) in 15 mL dry THF and stirred for 30 minutes under N<sub>2</sub> at 25 °C. 4-(bromomethyl)pyridine hydrobromide (1.14g, 4.5 mmol) was then added, followed immediately by another portion of sodium hydride (120 mg, 3.0 mmol). The slurry was allowed to stir vigorously under N<sub>2</sub> for 14.5 h at 25 °C. The reaction was quenched by the



addition of a few drops of isopropanol, ethanol and then 1.5 mL of water over ice. The resulting mixture was then filtered, and the filtrate concentrated under reduced pressure. The crude product was then extracted into CH<sub>2</sub>Cl<sub>2</sub> and concentrated prior to purification by silica column chromatography in 5:95 (v/v) methanol:CH<sub>2</sub>Cl<sub>2</sub> with 0.1% TEA to yield a pale yellow oil (0.238 g, 18 %). <sup>1</sup>H NMR (400MHz; 298K; CDCl<sub>3</sub>) δ = 8.49 (d, 2H, *J*<sub>H-H</sub> = 5.2 Hz, 2 x Arom-*H*), 7.21 (d, 2H, *J*<sub>H-H</sub> = 5.6 Hz, 2 x Arom-*H*), 4.52 (s, 2H, Ar-CH<sub>2</sub>O), 3.66-3.47 (m, PEG methylene), 3.30 (s, 3H, PEG methyl). <sup>13</sup>C NMR (100 MHz; CDCl<sub>3</sub>; 298K) 149.8, 121.7 (Arom-C), 71.9, 71.5, 70.5, 70.2 (Arom-C, 3 x CH<sub>2</sub>) 59.0 (CH<sub>3</sub>). Characterization matches that reported in the literature but contains residual poly(ethylene glycol) monomethyl ether which was not deemed to be an issue further on.<sup>25</sup>

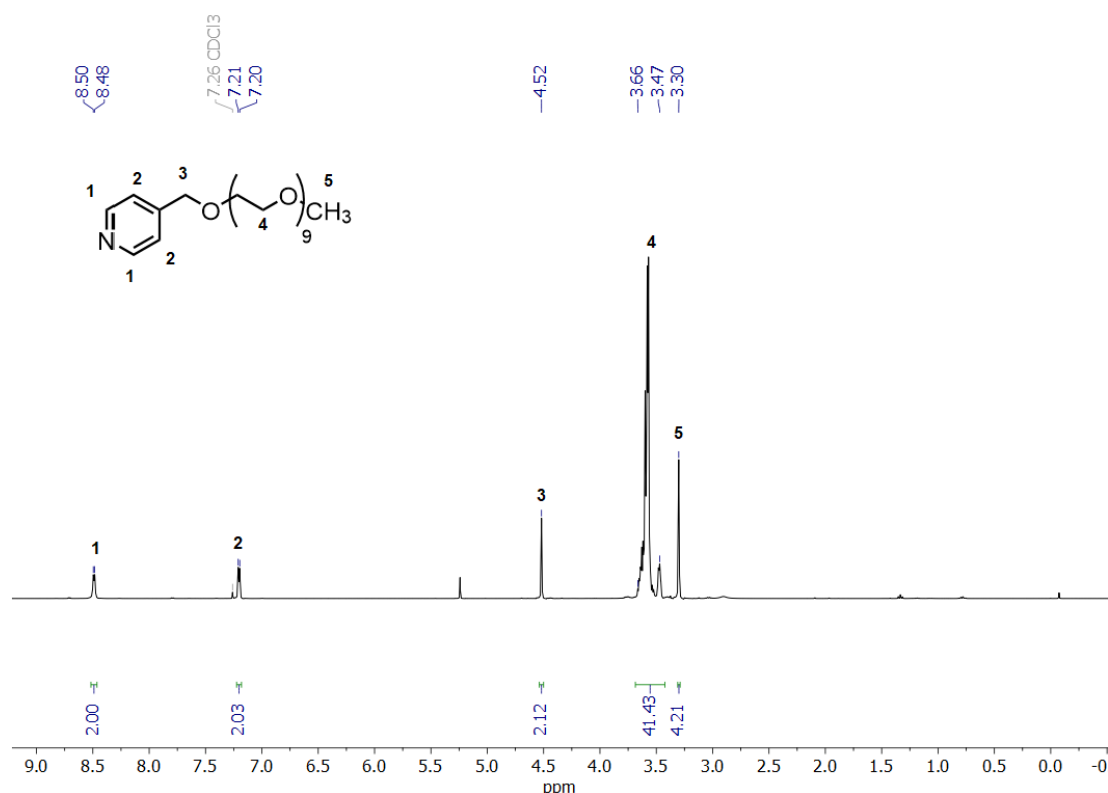
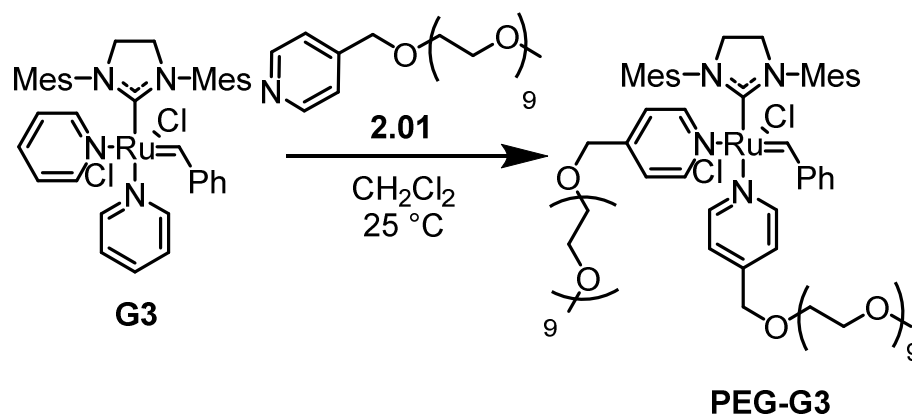


**Figure 2.24** <sup>1</sup>H NMR spectrum of **2.01** in CDCl<sub>3</sub> (400 MHz, 298K).

### 2.5.6 Synthesis of PEG-G3



The water soluble catalyst was prepared from **G3** according to a previously reported procedure.<sup>25</sup> A 25 mL round-bottom flask equipped with a magnetic stir bar was charged with *p*-poly(ethylene glycol)-substituted pyridine (20 mg, 45 μmol) dissolved in 0.35 mL dry CH<sub>2</sub>Cl<sub>2</sub> and stirred for 5 min. **G3** (10 mg, 14 μmol) dissolved in 0.35 mL dry CH<sub>2</sub>Cl<sub>2</sub> was then added dropwise *via* syringe, the flask was purged with N<sub>2</sub>, and wrapped in aluminium foil to keep out the light. The following steps were then completed, Step 1: The solution was allowed to stir at 25 °C for 30 minutes in the dark. Step 2: Nitrogen inlet and outlet lines were then attached to the flask and the CH<sub>2</sub>Cl<sub>2</sub> was allowed to slowly evaporate under a weak nitrogen stream over another 30 minutes. Step 3: The contents were then concentrated further under high vacuum for 5 minutes to yield a green-yellow oily residue. The residue was then re-dissolved in 0.35 mL dry CH<sub>2</sub>Cl<sub>2</sub>, and steps 1 – 3 were repeated 5 more times to yield a dark green solution which was used directly in the next step. <sup>1</sup>H NMR (400MHz; 298K; CDCl<sub>3</sub>) δ = 19.15 (s, 1H, H-alkylidene) 8.58 (s, 4H, Arom-*H*), 7.76 (s, 2H, Arom-*H*), 7.62 (d, 2H, Arom-*H*), 7.46 (t, 1H, Arom-*H*), 7.30 (s, 4H, Arom-*H*), 7.06 (t, 4H, Arom-*H*), 4.59 (s, 4H, Ar-CH<sub>2</sub>O), 4.10 (br d, 4H, (NCH<sub>2</sub>CH<sub>2</sub>N), 3.53-3.72 (m, PEG methylene), 3.37 (s, PEG methyl), 2.63 (s, 6H, Ar-CH<sub>3</sub>), 2.22-2.34 (m, 12H, Ar-CH<sub>3</sub>). Characterization matches that reported in the literature.<sup>25</sup>

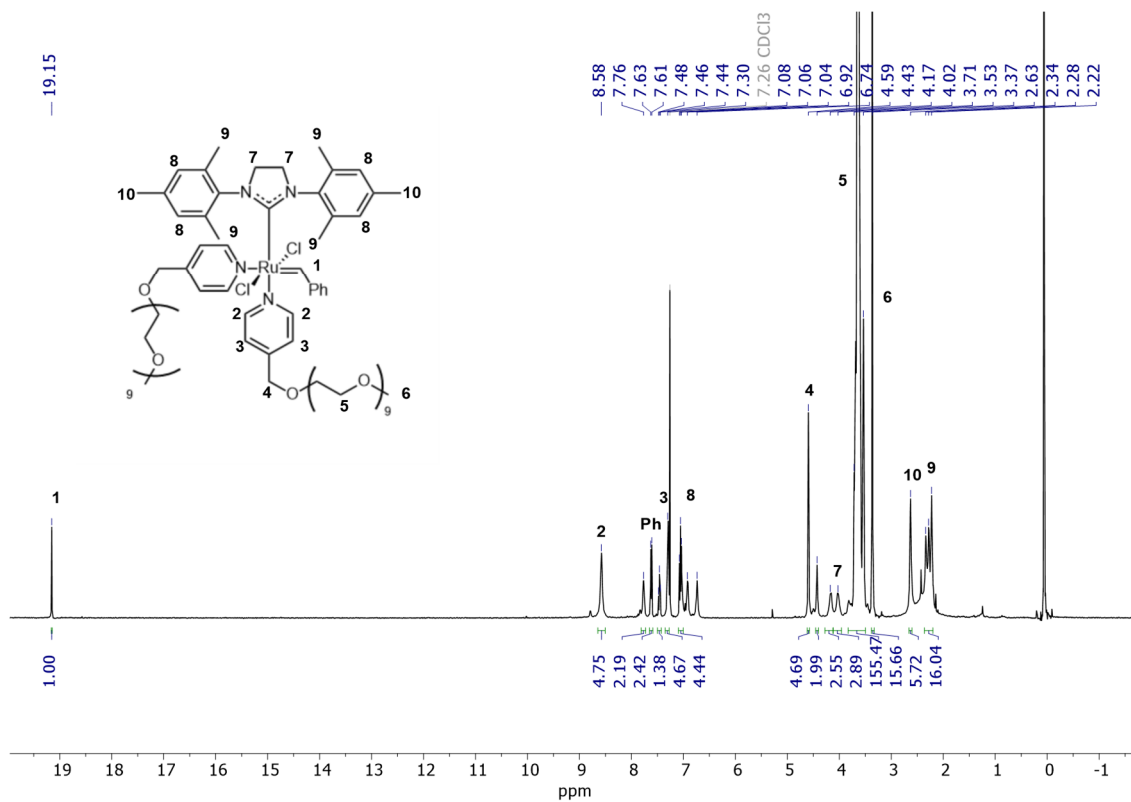


Figure 2.25  $^1\text{H}$  NMR spectrum of PEG-G3 in  $\text{CDCl}_3$  (400 MHz, 298K).

## 2.6 References

1. N. Favalli, G. Bassi, J. Scheuermann and D. Neri, *FEBS Letters*, 2018, **592**, 2168-2180.
2. L. Mannocci, M. Leimbacher, M. Wichert, J. Scheuermann and D. Neri, *Chem. Commun.*, 2011, **47**, 12747-12753.
3. G. Zimmermann and D. Neri, *Drug Discovery Today*, 2016, **21**, 1828-1834.
4. M. L. Malone and B. M. Paegel, *ACS Comb. Sci.*, 2016, **18**, 182-187.
5. C. Zambaldo, S. Barluenga and N. Winssinger, *Curr. Opin. Chem. Biol.*, 2015, **26**, 8-15.
6. F. Pellestor and P. Paulasova, *Eur. J. Hum. Genet.*, 2004, **12**, 694-700.
7. A. Singhal, V. Bagnacani, R. Corradini and P. E. Nielsen, *ACS Chem. Biol.*, 2014, **9**, 2612-2620.
8. S. Núñez-Pertíñez, T. R. Wilks and R. K. O'Reilly, *Org. Biomol. Chem.*, 2019, **17**, 7874-7877.
9. S. Kumar, A. Pearse, Y. Liu and R. E. Taylor, *Nat. Commun.*, 2020, **11**, 2960.
10. M. Schuster and S. Blechert, *Angew. Chem. Int. Ed.*, 1997, **36**, 2036-2056.
11. K. Liu, L. F. Zheng, Q. Liu, J. W. de Vries, J. Y. Gerasimov and A. Herrmann, *J. Am. Chem. Soc.*, 2014, **136**, 14255-14262.
12. X. J. Lu, L. J. Fan, C. B. Phelps, C. P. Davie and C. P. Donahue, *Bioconjugate Chem.*, 2017, **28**, 1625-1629.
13. X. Tan, H. Lu, Y. Sun, X. Chen, D. Wang, F. Jia and K. Zhang, *Chem*, 2019, **5**, 1584-1596.
14. O. B. C. Monty, P. Nyshadham, K. M. Bohren, M. Palaniappan, M. M. Matzuk, D. W. Young and N. Simmons, *ACS Comb. Sci.*, 2020, **22**, 80-88.
15. C. R. James, A. M. Rush, T. Insley, L. Vuković, L. Adamiak, P. Král and N. C. Gianneschi, *J. Am. Chem. Soc.*, 2014, **136**, 11216-11219.
16. S. Masuda, S. Tsuda and T. Yoshiya, *Org. Biomol. Chem.*, 2018, **16**, 9364-9367.
17. Y. A. Lin, J. M. Chalker and B. G. Davis, *ChemBioChem*, 2009, **10**, 959-969.
18. T. Biver, *Applied Spectroscopy Reviews*, 2012, **47**, 272-325.
19. B. C. Baguley, L. P. Wakelin, J. D. Jacintho and P. Kovacic, *Curr. Med. Chem.*, 2003, **10**, 2643-2649.
20. X. Cai, P. J. Gray and D. D. Von Hoff, *Cancer Treat. Rev.*, 2009, **35**, 437-450.
21. M. L. McKee, P. J. Milnes, J. Bath, E. Stulz, A. J. Turberfield and R. K. O'Reilly, *Angew. Chem. Int. Ed.*, 2010, **49**, 7948-7951.
22. S. Chakarov, R. Petkova, G. C. Russev and N. Zhelev, *BioDiscovery*, 2014, **11**, e8957.
23. N. Farah, H. S. Dresner, K. J. Searles, R. Winiarsky, M. Moosikasuwana, A. Cajigas, S. Hahm and J. J. Steinberg, *Cancer Invest.*, 2000, **18**, 314-326.
24. J. Barton, in *Bioinorganic Chemistry*, ed. I. Bertini, H.B. Gray, S. Lippard and J. Valentine, University Science Books, USA, 1994, ch.8, pp. 455-503.
25. S. A. Isarov and J. K. Pokorski, *Acs Macro Lett.*, 2015, **4**, 969-973.
26. R. S. Tuma, M. P. Beaudet, X. Jin, L. J. Jones, C.-Y. Cheung, S. Yue and V. L. Singer, *Anal. Biochem.*, 1999, **268**, 278-288.
27. M. S. Sanford, J. A. Love and R. H. Grubbs, *J. Am. Chem. Soc.*, 2001, **123**, 6543-6554.
28. D. Guillen, M. Schievelbein, K. Patel, D. Jose and J. Ouellet, *PLOS ONE*, 2020, **15**, e0229527.
29. T. Heinlein, J.-P. Knemeyer, O. Piestert and M. Sauer, *J. Phys. Chem. B*, 2003, **107**, 7957-7964.

30. M. Torimura, S. Kurata, K. Yamada, T. Yokomaku, Y. Kamagata, T. Kanagawa and R. Kurane, *Anal. Sci.*, 2001, **17**, 155-160.
31. J. Hong, G.-S. Yang, C.-Y. Duan, Z.-J. Guo and L.-G. Zhu, *Inorg. Chem. Commun.*, 2005, **8**, 988-991.
32. M. Sirajuddin, S. Ali and A. Badshah, *J. Photochem. Photobiol., B*, 2013, **124**, 1-19.
33. A. Rodger, in *Encyclopedia of Biophysics*, ed. G. C. K. Roberts, Springer Berlin Heidelberg, Berlin, Heidelberg, 2013, pp. 31-33.
34. M. A. Halim, F. Bertorelle, T. Doussineau and R. Antoine, *Rapid Commun. Mass Spectrom.*, 2019, **33**, 35-39.
35. X.-L. Li, Y.-J. Hu, H. Wang, B.-Q. Yu and H.-L. Yue, *Biomacromolecules*, 2012, **13**, 873-880.
36. D. Bera, L. Verdonck, M. Glassner, A. Madder and R. Hoogenboom, *Macromol. Rapid Commun.*, 2019, **40**, 1800900.
37. H. A. Benesi and J. H. Hildebrand, *J. Am. Chem. Soc.*, 1949, **71**, 2703-2707.
38. M. B. Lyles and I. L. Cameron, *Biophys. Chem.*, 2002, **96**, 53-76.
39. T. R. Wilks, PhD Thesis, University of Warwick, 2013.
40. A. E. Hargrove, Z. Zhong, J. L. Sessler and E. V. Anslyn, *New J. Chem.*, 2010, **34**, 348-354.
41. V. Forcina, A. García-Domínguez and G. C. Lloyd-Jones, *Faraday Discuss.*, 2019, **220**, 179-195.
42. V. Thiel, M. Hendann, K.-J. Wannowius and H. Plenio, *J. Am. Chem. Soc.*, 2012, **134**, 1104-1114.
43. T. Matsuo, T. Yoshida, A. Fujii, K. Kawahara and S. Hirota, *Organometallics*, 2013, **32**, 5313-5319.
44. B. Nordén and T. Kurucsev, *J. Mol. Recognit.*, 1994, **7**, 141-155.
45. A. Rodger, G. Dorrington and D. L. Ang, *Analyst*, 2016, **141**, 6490-6498.
46. A. Rodger, in *Encyclopedia of Biophysics*, ed. G. C. K. Roberts, Springer Berlin Heidelberg, Berlin, Heidelberg, 2013, pp. 1761-1763.
47. I. Rouzina and V. A. Bloomfield, *Biophys. J.*, 1998, **74**, 3152-3164.
48. D. J. Walsh, S. Hong Lau, M. G. Hyatt, and D. Guironnet, *J. Am. Chem. Soc.*, 2017, **139**, 13644-13647.

# Chapter 3: The Graft-Through Polymerization of DNA *via* ROMP

## 3.1 Abstract

With a fruitful number of applications, DNA-polymer conjugates are highly sought after. However, thus far the preparation of conjugates relies upon a 'grafting-to' approach which often limits the grafting density and reproducibility of the polymers. Here, aqueous ROMP was used to prepare a DNA-polymer conjugates *via* a 'grafting-through' approach. A number of optimization studies were conducted to find conditions under which the DNA was stable and the polymerization proceeded. Two DNA-PEG bottlebrush polymers were prepared varying the PEG sidechain length and a unique solution-phase behavior was observed.

## 3.2 Background

The combination of biomacromolecules such as nucleic acids and peptides with synthetic polymers has long been studied, as it combines the robustness and versatility of synthetic polymers with the programmability and recognition properties of biomolecules. Whilst the synthesis of peptide-polymer conjugates is well established, the synthesis of DNA-polymer conjugates has only become prevalent in the last couple of decades.<sup>2</sup> There are now a vast array of applications for DNA-polymers conjugates: in drug delivery, synthetic polymers can protect AOs from nucleases whilst enhancing their cellular uptake;<sup>3</sup> in DNA-detection, owing to the ease of functionalization of synthetic polymers;<sup>4</sup> and in nanoscience, as DNA-polymer conjugates can self-assemble into a vast array of DNA-nanoparticle morphologies.<sup>5</sup>

### 3.2.1 Synthesis of DNA-polymer conjugates

In Chapter 1, the various architectures of DNA-polymer conjugates were introduced, alongside some brief examples of the three main methodologies to prepare such conjugates: 'grafting to', 'grafting from' and 'grafting through' (Figure 3.1). The ability to access a variety of polymer topologies is of interest because polymers of different topology can vary dramatically in their material properties.<sup>6</sup>

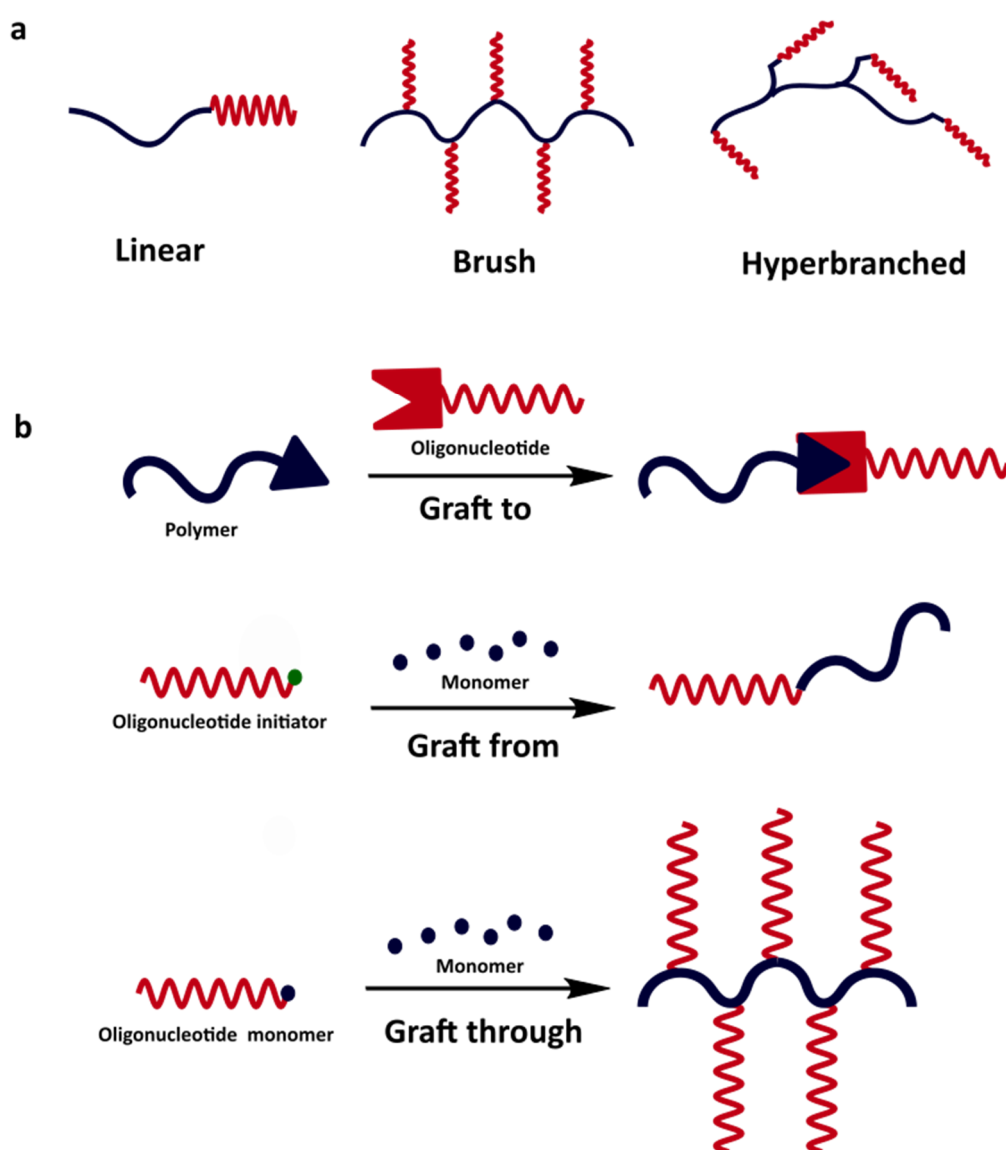


**Figure 3.1** (a) Schematic of DNA polymer architectures. (b) Routes towards DNA-polymer conjugates: 'grafting to', 'grafting from' and 'grafting through'.

The 'grafting to' approach involves the coupling of an oligonucleotide to a synthetic polymer post-polymerization and has been well utilized to access all three DNA-polymer architectures. The success of this approach resides heavily on the efficiency of the azide-alkyne cycloaddition reaction in the presence of DNA.<sup>7</sup> However, a recent study conducted in the O'Reilly group demonstrated that the coupling of DNA to hydrophobic polymers is not straightforward and the number of chemistries available for such transformations are limited in both number and efficiency.<sup>8</sup> This limited coupling efficiency is particularly detrimental when preparing brush-like polymers as it leads to a limited grafting density and poor reproducibility; thus, in recent years there has been a push to develop 'grafting from' and 'grafting through' approaches.

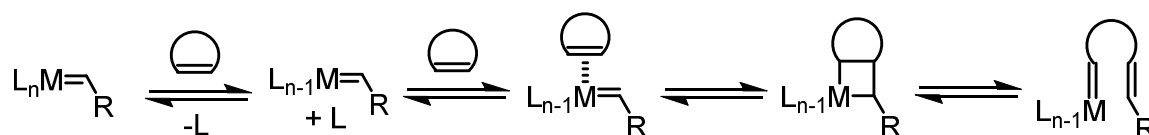
'Grafting from' involves the polymerization of a synthetic polymer from an oligonucleotide macroinitiator and approaches have been developed using RAFT polymerization<sup>9, 10</sup> and ATRP.<sup>11-14</sup> However, in all cases thus far, the architecture has been limited to linear polymers. In contrast, the 'grafting through' method leads to brush-like architectures with excellent control over grafting density and thus is a highly desirable approach to prepare DNA-polymer brushes. The approach utilizes an oligonucleotide macromonomer which is incorporated into the polymer during the polymerization. This is often highly efficient and yields densely grafted polymers. Several groups have studied the 'grafting through' approach to prepare DNA polymer conjugates and thus far, all examples have utilized ROMP.

ROMP operates according to a chain-growth mechanism and is composed of three main steps: initiation, propagation and termination (Scheme 3.1).<sup>15</sup> The initiation stage involves a [2+2] cycloaddition between the metal alkylidene and olefin to form a metallocyclobutane intermediate which then undergoes a cycloreversion reaction to yield a new metal alkylidene.

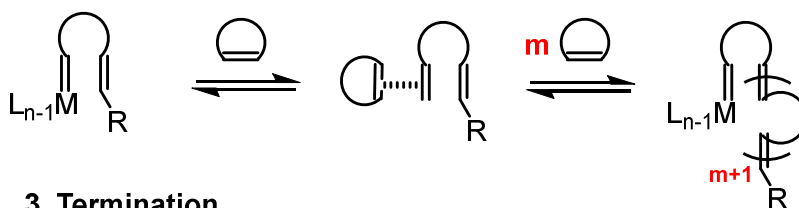


During the propagation stage the resulting metal alkylidene continues to react with cyclic olefins to grow the polymer from the metal center. The propagation stage continues until (1) all monomer has been consumed; (2) an equilibrium has been reached due to the thermodynamic considerations; or (3) the reaction has been terminated by deactivation of the catalyst. The most common reagents utilized for quenching the reaction are vinyl ethers which lead to the formation of non-reactive Fischer carbenes.<sup>16</sup> In some circumstances chain-transfer can also occur through inter- and intramolecular cross-metathesis reactions.

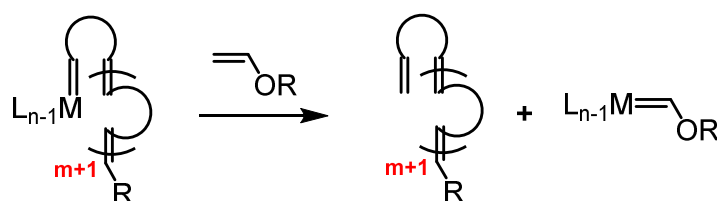
### 1. Initiation



### 2. Propagation



### 3. Termination



**Scheme 3.1** Accepted ROMP mechanism catalyzed by metal alkylidene complexes.

The most commonly utilized catalyst for ROMP is the extremely fast initiating G3 catalyst first introduced in Chapter 1.<sup>17</sup> The combination of this catalyst with a suitably strained cycloolefin can lead to ROMP occurring in a living fashion, yielding low dispersity polymers with controllable molar mass. Typically, norbornene monomers are utilized due to the high ring strain ( $27.2 \text{ kcal mol}^{-1} / 113.8 \text{ kJ mol}^{-1}$ )<sup>18</sup> resulting in fast propagation kinetics. Furthermore, the steric hindrance around the resulting polynorbornene backbone suppresses any

secondary metathesis reactions.<sup>19</sup> The fast polymerization kinetics and resulting well-spaced backbone makes ROMP an ideal polymerization technique for the preparation of bottlebrush polymers.

In 2014, the Gianneschi group first explored the ROMP of nucleic acid macromonomers using G3.<sup>20</sup> However, whilst they were successful in polymerizing norbornene-functionalized PNAs (an organosoluble nucleic acid analogue), the polymerization of DNA was unsuccessful, reportedly due to the polyanionic phosphate backbone of DNA and the poor solubility of the commercially available metathesis catalysts in aqueous media. In the same year, Herrmann and co-workers developed a strategy to overcome the previous shortcomings by protecting the polyanionic phosphate backbone with a surfactant, rendering the DNA organosoluble and protecting the catalyst from potential co-ordination with the phosphate backbone (Figure 3.2).<sup>21</sup> This led to the successful preparation of DNA bottlebrush polymers; however, this approach requires a number of steps including the difficult step of removing the surfactant following the polymerization.

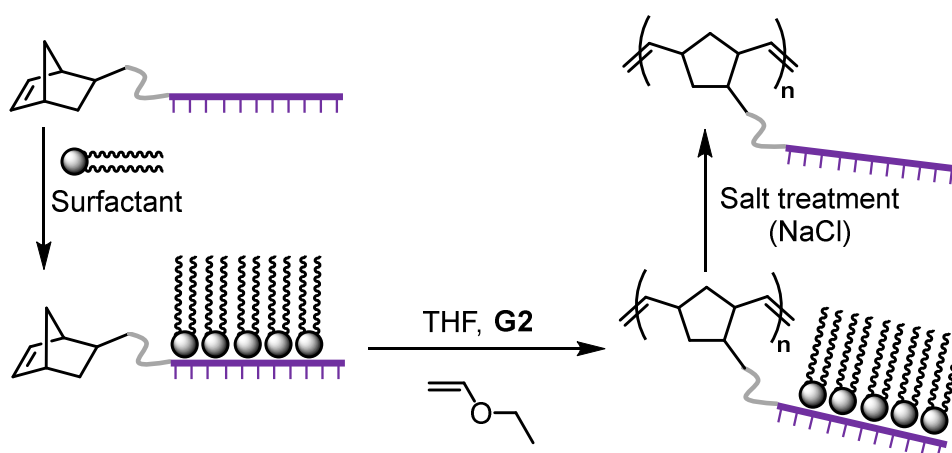


**Figure 3.2** The graft-through polymerization of norbornene-functionalized DNA. Here, Herrmann and co-workers protected the backbone with a surfactant so the polymerization could be conducted in organic solvents.<sup>21</sup>

Recently, Zhang and co-workers addressed some of these shortcomings by identifying a new approach to prepare a protected oligonucleotide.<sup>22</sup> In this approach, the ester bond, which typically tethers the oligonucleotide to the solid support during the solid-phase synthesis of DNA, was replaced with a disulfide linkage. The advantage of the disulfide linkage was that it can be cleaved under much milder conditions than the ester linkage and thus, the release of the oligonucleotide from the solid support could be achieved, whilst keeping the phosphotriester and exocyclic amine protecting groups intact.<sup>22</sup> This resulted in a protected oligonucleotide which was fully organosoluble. Following the functionalization of the protected oligonucleotide with a norbornene monomer, the polymerization was conducted using G3 in dichloromethane, to yield high molar mass DNA-graft polymers. Whilst, this approach is a step forward in the graft-through preparation of DNA-polymer conjugates, it still requires additional protection and deprotection steps, and is limited to those with the expertise and facilities to perform DNA solid-phase synthesis.

The work described herein sought to address the current limiting requirement of a protected DNA backbone, with the aim of developing a straightforward approach to the preparation of DNA-bottlebrush polymers. The focus of the Chapter was to utilize aqueous metathesis in an effort to demonstrate the potential of expanding the reaction scope of native DNA to new chemistries such as metathesis.

### 3.3 Results & Discussion

#### 3.3.1 The macroinitiator approach versus conventional aqueous ROMP approaches

The ability of olefin metathesis to perform otherwise challenging C-C bond forming reactions has led to a push to optimize the reaction conditions to be effective in aqueous media.<sup>23</sup> Water

is a highly attractive solvent due to its low cost and safety as it is neither flammable, toxic nor carcinogenic. Furthermore, as many biologically relevant molecules are water-soluble there is an increasing requirement for synthetic methodologies that can be conducted in aqueous media.<sup>23</sup> The most common solution to this problem has been the preparation of water-soluble catalysts, with water-solubilising ligands, such as those described in Chapter 1 - Section 1.3.2. The development of water-soluble catalysts has been successfully utilized in the preparation of protein-polymer conjugates;<sup>24</sup> however, many limitations were identified when relying on such catalysts, including synthetically challenging preparations and poor polymerization control (poor molar mass control and high dispersities). The cause of these limitations was hypothesized to result from the slow initiation of the catalyst; therefore, our group set out to design an improved aqueous metathesis methodology.

To circumvent the issue of slow initiation, a commercially available catalyst was initiated in a water-miscible organic solvent with a hydrophilic monomer to prepare a hydrophilic macroinitiator, which was subsequently transferred into an aqueous solution. The catalyst chosen for this study was **G3**, which is the superior catalyst for ROMP, owing to the fast dissociation of the pyridine ligands and thus, fast initiation rate. A pH2 phosphate solution (PB2) was utilized for the subsequent polymerization in aqueous *milieu*, this was believed to promote ligand dissociation and protect the catalyst from decomposition. However, recent studies in our group have also shown that the catalyst is increasingly stable in PB2 due to the presence of excess Cl<sup>-</sup> ions which prevent the formation of the metathesis inactive and unstable Ru-(OH)<sub>n</sub> complexes.<sup>25</sup> This macroinitiator approach, first published in 2018, is shown in Figure 3.3.<sup>1, 26</sup>

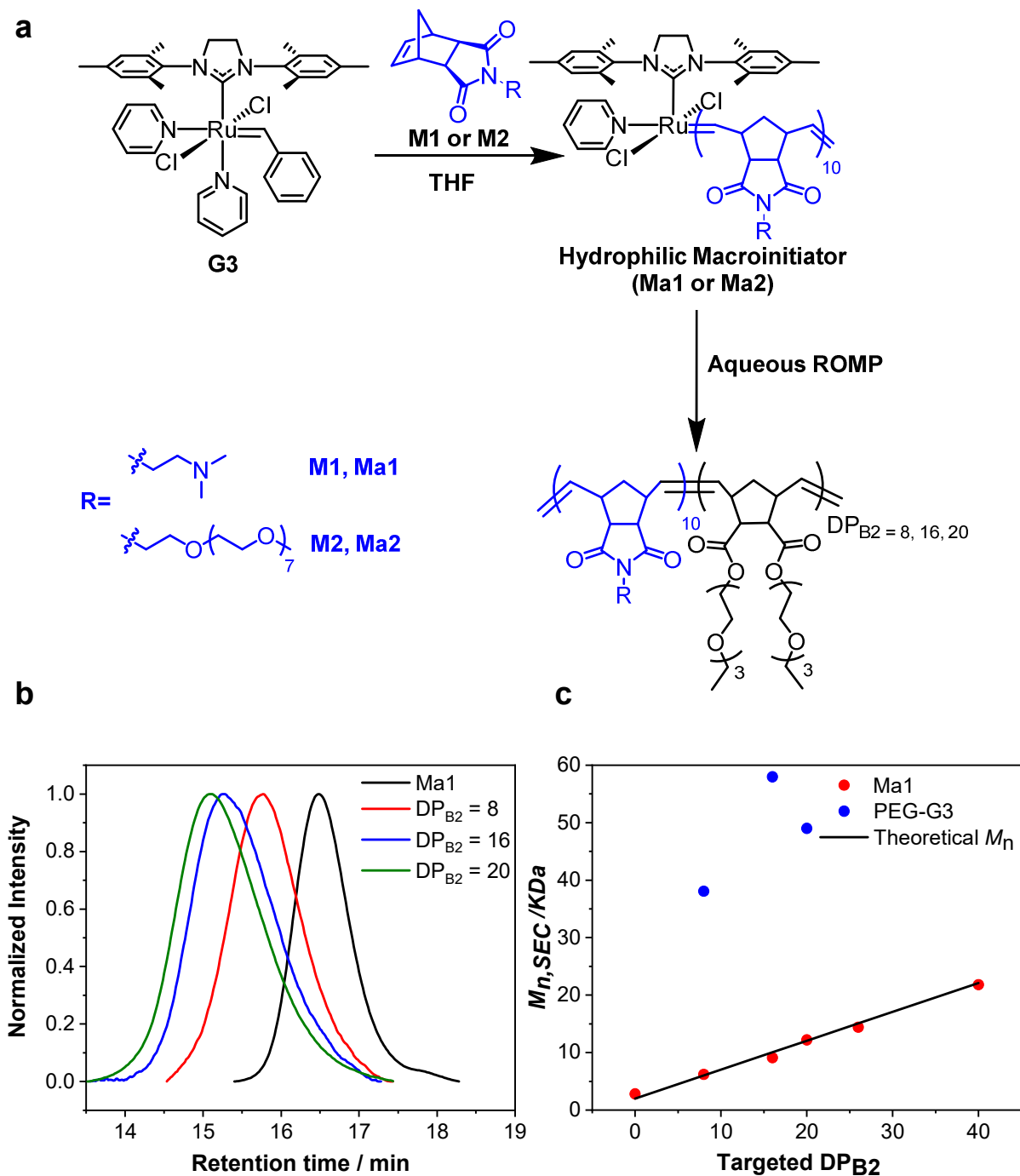


**Figure 3.3** (a) The macroinitiator approach to prepare DNA-polymer conjugates as reported by Foster et al.<sup>1</sup> (b) Normalized SEC traces of the macroinitiator **Ma1** and the resulting polymers of various targeted DP's, polymers were obtained with narrow molar mass distributions ( $\mathcal{D}_M = 1.3$ ). (c)  $M_n$  as a function of targeted DP using a conventional approach with a water-soluble catalyst, **PEG-G3** (blue dots) and the macroinitiator approach (red dots). The blackline represents expected MW values for both routes. All polymerizations were conducted at 1 wt% solids under air at rt for 5 min. Data published by Foster et al.<sup>1</sup>

The monomers utilized in the first block contain either: a pendant tertiary amine (**M1**), which

upon ionization in the acidic buffer, results in a water-soluble macroinitiator (**Ma1**); or a short PEG unit (**M2**) which results in a water-soluble macroinitiator (**Ma2**). A model polymerization utilizing the macroinitiator approach was compared to the same polymerization utilizing **PEG-G3** (introduced in Chapter 2) and the results showed a marked improvement in the molar mass distribution and excellent control over the degree of polymerization (DP) (Figure 3.3 - red dots).<sup>1</sup>

Due to the success of this approach, the macroinitiator approach was employed in subsequent studies to prepare DNA-polymer conjugates. The PEG macromonomer (**M2**) was chosen to prepare **Ma2**. The advantage of this monomer was that it was not positively charged in PB2 and therefore would be less likely to interact with the negatively-charged phosphate backbone of DNA. Herein, attempts to utilize the macroinitiator approach to prepare DNA-polymer bioconjugates, as depicted in Figure 3.4, will be discussed.

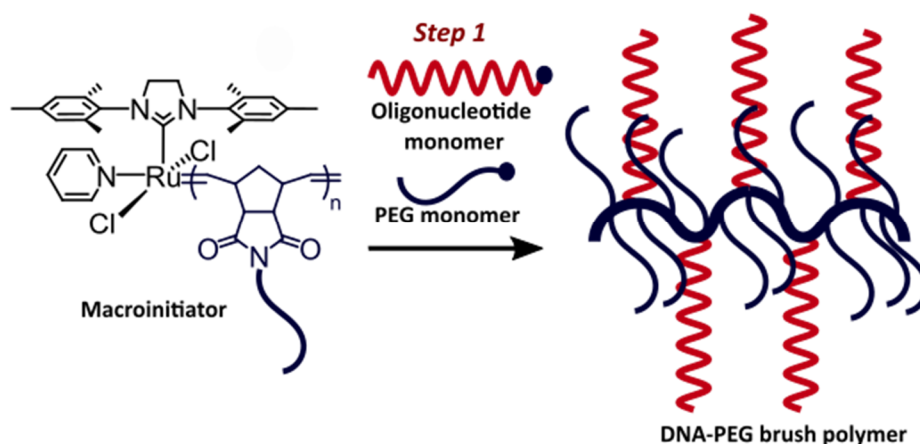


**Figure 3.4** Schematic for the graft-through polymerization of DNA using a water-soluble metathesis macroinitiator.

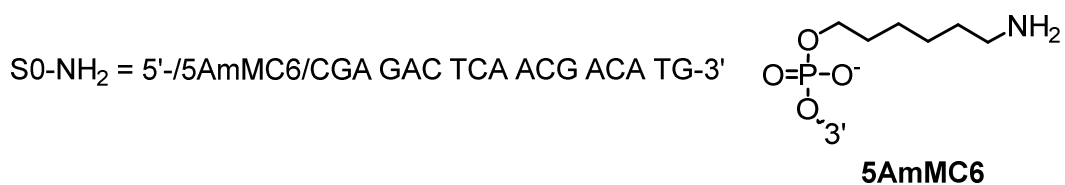
### 3.3.2 Synthesis of an oligonucleotide macromonomer

To facilitate the 'graft-through' ROMP of DNA, a suitable oligonucleotide macromonomer capable of undergoing ROMP was required. ROMP operates *via* the ring-opening of cyclic olefins. However, not all cyclic olefins can be polymerized; the main factor determining their suitability is the presence of large ring strain ( $>5 \text{ kcal mol}^{-1} / 21 \text{ kJ mol}^{-1}$ ).<sup>27</sup> Furthermore, if the polymerization was to be conducted in a living manner (rate of initiation ( $k_i$ )  $\gg$  rate of propagation ( $k_p$ )) a number of other factors, including the steric environment surrounding the olefin, the electronic nature of the olefin itself, and the relative reactivity of the product olefins in the polymer backbone (as they can be involved in back-biting reactions) had to be considered.<sup>15</sup>

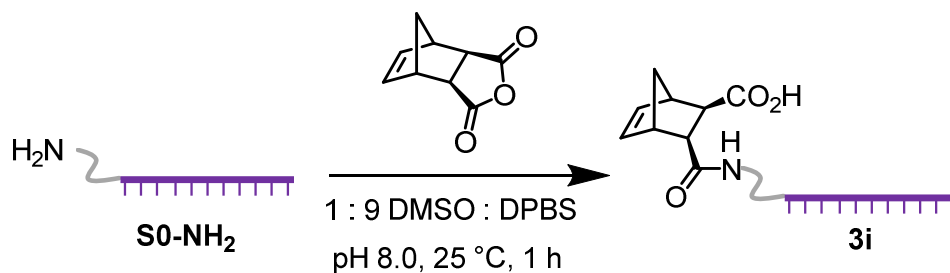
The most utilized class of ROMP monomers are based on norbornenes; their popularity arises from their ease of synthesis and functionalization, high ring-strain ( $27.2 \text{ kcal mol}^{-1} / 113.8 \text{ kJ mol}^{-1}$ )<sup>18</sup> and living-polymerization capabilities. The functionalization of DNA with a norbornene unit was therefore attempted in an effort to prepare an appropriate oligonucleotide macromonomer. The preparation of norbornene-functionalized DNA was attempted using a solution phase coupling method, removing the need for a DNA synthesizer.<sup>8</sup>

Initial conjugation attempts utilized commercially available amino DNA ( $\text{SO-NH}_2$ ) functionalized with an amine group at the 5' end through a hexyl linker. Inspired by the work of Pokorski and co-workers, who prepared lysozyme-functionalized norbornene monomers;<sup>24</sup>  $\text{SO-NH}_2$  was reacted with *cis*-5-norbornene *exo*-2,3-dicarboxylic anhydride (Scheme 3.2).

**a**



**b**



**Scheme 3.2** (a) Structure of S0-NH<sub>2</sub> (b) Synthesis of **3i** adapted from work published by Isarov et al.<sup>24</sup>

The reaction was analyzed by liquid chromatography-mass spectrometry (LCMS). Nucleic acids absorb strongly at 260 nm due to the heterocyclic rings of the nucleotides and thus a UV chromatogram monitoring the absorbance at 260 nm over time can be used to assess the presence of DNA-containing species. As shown in Figure 3.5, several peaks are present in the UV chromatogram of the crude reaction mixture at 260 nm, implying low conversion. However, a small amount of the desired product, **3i**, could be identified and the reaction conversion was estimated to be around 10%. Several other coupling conditions were attempted, varying either the equivalents of *cis*-5-norbornene-*exo*-2,3-dicarboxylic anhydride, the reaction time or the solvent ratio. The results of these optimization experiments are shown in, Table 3.1.



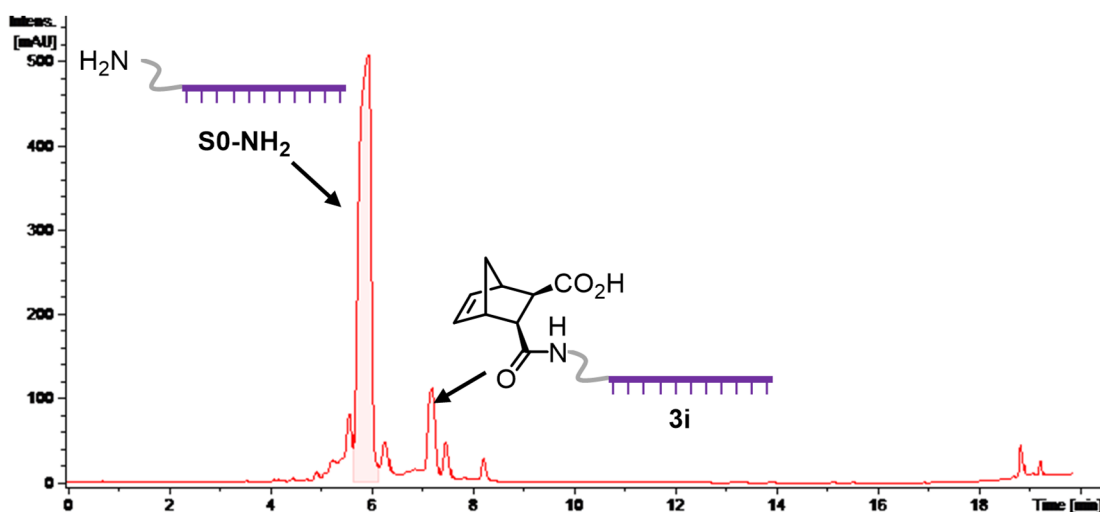


**Figure 3.5** LCMS-UV chromatogram at 260 nm of the reaction mixture collected following the reaction of S0-NH<sub>2</sub> with *cis*-5-norbornene-*exo*-2,3-dicarboxylic anhydride (Scheme 3.2). Products eluted with a gradient of buffer A: 5 vol% MeOH, 10 mM ammonium acetate and buffer B: 70 vol% MeOH, 10 mM ammonium acetate. Peaks assigned via mass spectrometry.

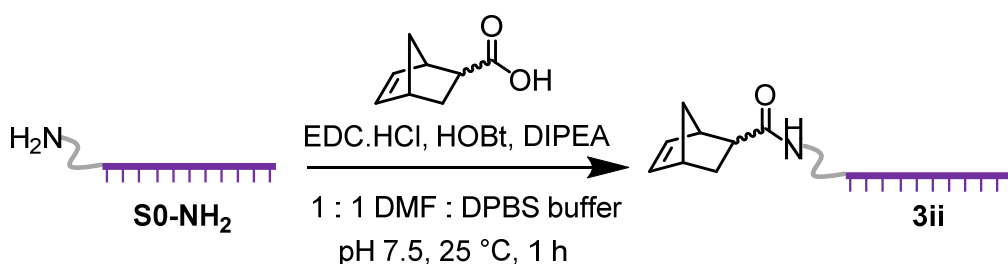
**Table 3.1** Reaction conditions tested and the conversions for the synthesis of **3i**. <sup>†</sup>Equivalents of norbornene calculated relative to DNA. \*Calculated from the peak integrations in the LCMS UV chromatogram.

Reaction #	Eq. norbornene <sup>†</sup>	Reaction time / h	Solvent ratio (DMSO:DPBS)	Conversion* / %
<b>1a</b>	500	1	1:9	10
<b>1b</b>	1000	7	1:9	13
<b>1c</b>	1000	7	1:3	18
<b>1d</b>	1000	7	1:1	49
<b>1e</b>	1000	18	1:1	66

Reactions **1b** and **1c** were heterogenous, as *cis*-5-norbornene-*exo*-2,3-dicarboxylic anhydride was not fully soluble in a 1:9 or 1:3 (v/v) DMSO/ DPBS solvent mixture. However, in 50 vol% DMSO all reagents were fully soluble and a large increase in conversion was achieved. A

further moderate increase was observed when extending the reaction time from 7 h to 18 h, to obtain a maximum conversion of 66%.

Simultaneously, an alternative route to prepare norbornene functionalized DNA was studied based on a protocol by T. Wilks *et al*, who demonstrated that the activated carboxylic acid route (Scheme 3.3) led to near quantitative conversions.<sup>8</sup> S0-NH<sub>2</sub> was therefore reacted with 5-norbornene-carboxylic acid which was activated with the coupling reagents: *N*-(3-Dimethylaminopropyl)-*N'*-ethylcarbodiimide hydrochloride (EDC.HCl) and hydroxybenzotriazole (HOBT).



**Scheme 3.3** Synthesis of **3ii** taken from a protocol by Wilks *et al*.<sup>8</sup>

The reaction proceeded, as stated in the literature, to near 100% conversion and the *exo*- and *endo*- isomer could be separated by HPLC (Figure 3.6a). The pure *exo*-isomer was also prepared and analyzed by HPLC to distinguish between the two isomers (Figure 3.6b). The use of one pure isomer is crucial for ROMP, as the polymerization rates of the two isomers differ significantly, with that of the *exo*-isomer being much greater.<sup>28-30</sup>

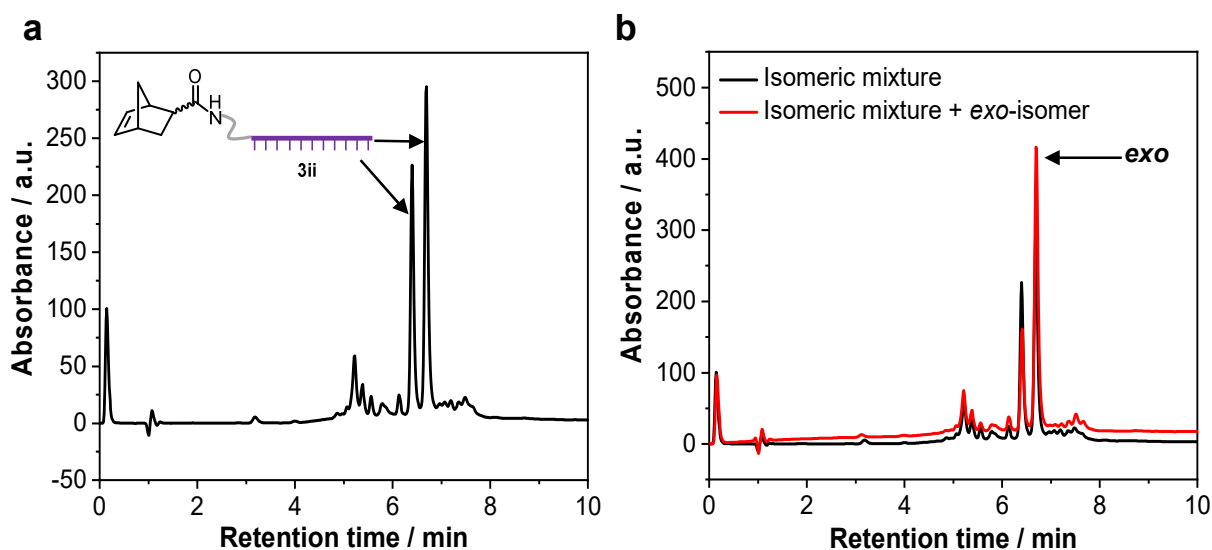
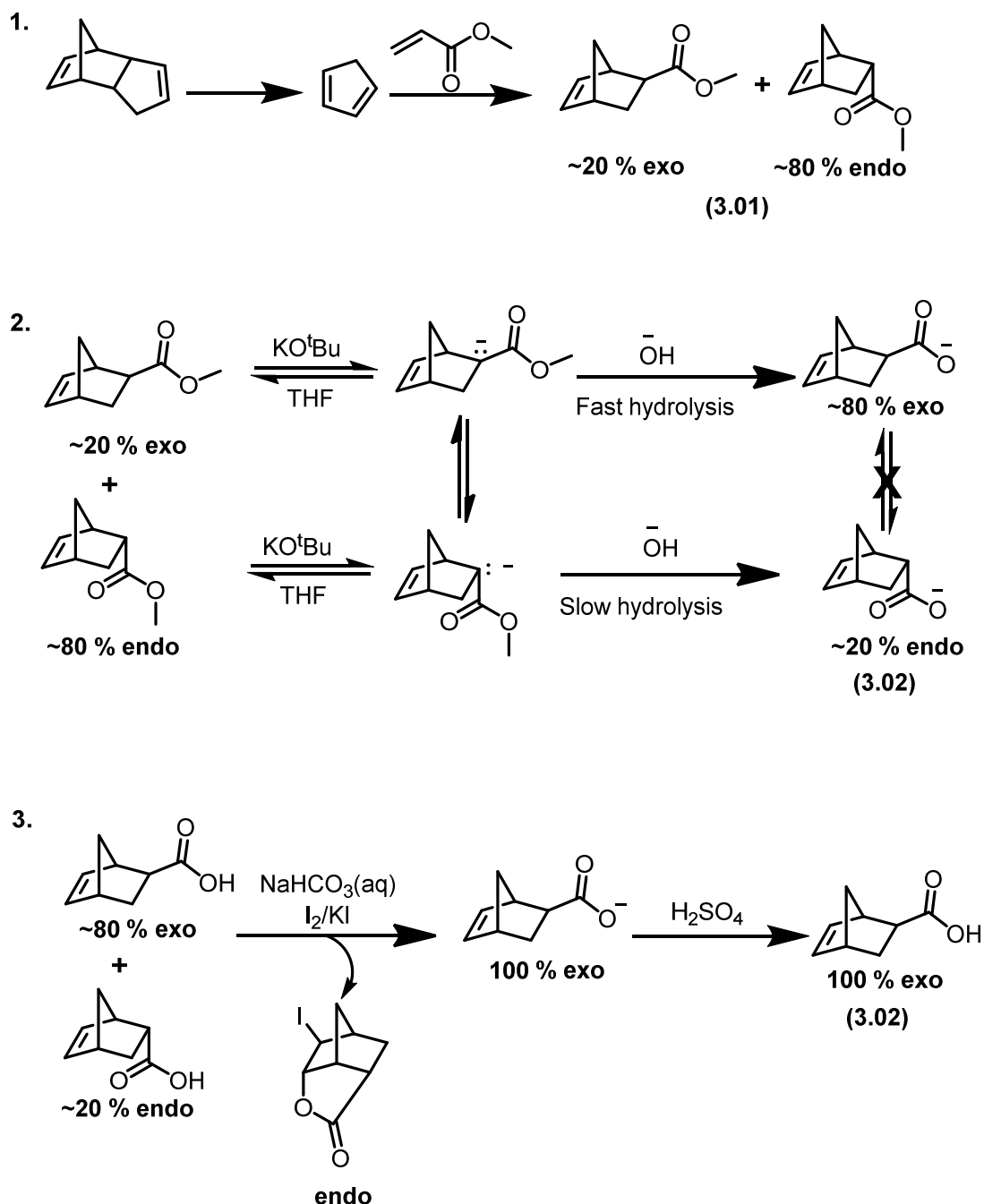


**Figure 3.6** (a) HPLC-UV Chromatogram at 260 nm of **3ii** synthesized using the conditions stated in Scheme 3.3. (b) HPLC-UV chromatogram at 260 nm of **3ii** (black trace) overlaid with **3ii** doped with the sterically pure *exo*-isomer (red trace). The *endo*-isomer was found to elute first followed by the *exo*-isomer. Products eluted with a gradient of buffer A, 0.1 M TEAA, in a 95:5 mixture of H<sub>2</sub>O and acetonitrile and buffer B, 0.1 M TEAA, in a 30:70 mixture of H<sub>2</sub>O and acetonitrile.

The cause for the faster polymerization rate of the *exo*-isomer compared with the *endo*-isomer has been the subject of many studies and was found to be the result of two main factors: (1) in the *endo*-form, the ring-opened monomer has excess steric-crowding around the catalyst center which hinders the approach of the incoming monomer; and (2) the *endo*-isomer is capable of chelating to the Ru through the carbonyl oxygen.<sup>31</sup> The formation of a six-membered chelate was confirmed in a recent study by Hyatt *et al.*<sup>31</sup>

Therefore, the preparation of a DNA macromonomer with *exo*-norbornene was essential for efficient polymerization. Whilst *exo*-5-norbornene carboxylic acid is commercially available, due to the high cost, the monomer was prepared in-house. This synthesis (Scheme 3.4) has been well-studied and proceeds *via* a Diels-Alder reaction between cyclopentadiene (synthesized 'in-situ' from the cracking of dicyclopentadiene) and methyl acrylate.<sup>32</sup> Following the '*endo* rule' the Diels-Alder reaction proceeds to form an *endo*-rich (ca. 80 %) mixture of

methyl 5-norbornene-2-carboxylate (**3.01**, Figure 3.7). The preference for the *endo*-product is best explained by favourable secondary-orbital interactions between the diene and dienophile during cycloaddition.<sup>33</sup>



**Scheme 3.4** Synthesis of sterically pure *exo*-5-norbornene carboxylic acid (**3.02**).

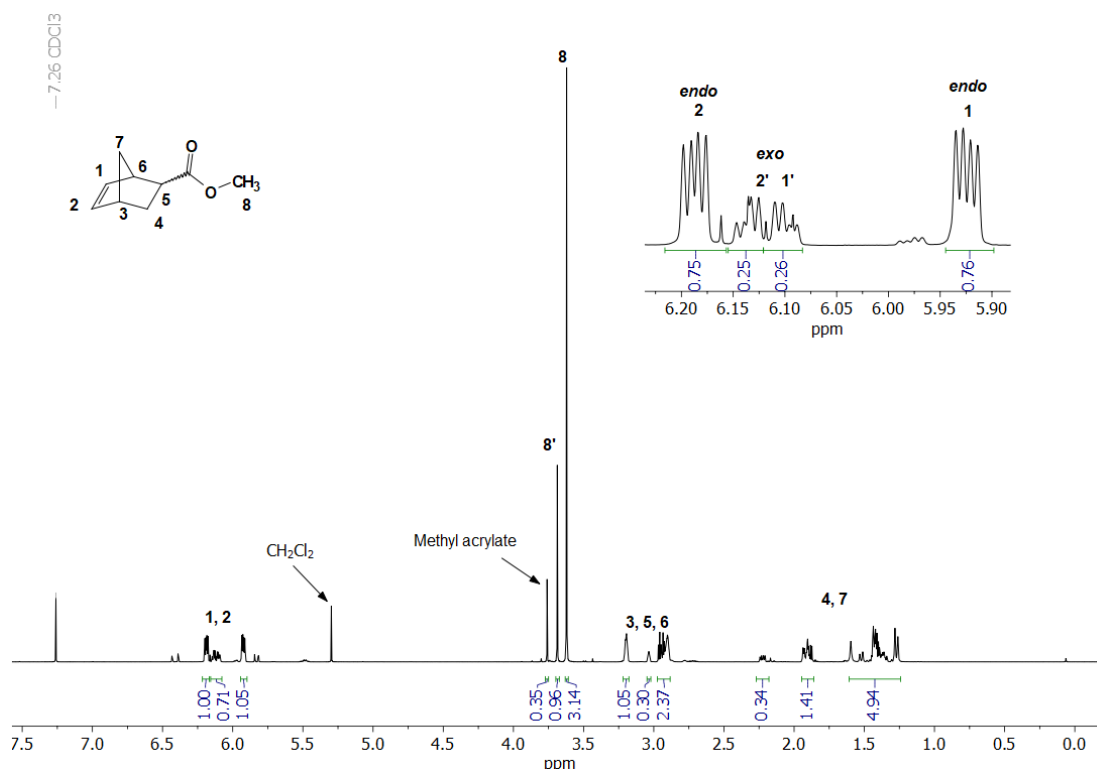


**Figure 3.7**  $^1\text{H}$  NMR spectrum of methyl 5-norbornene-2-carboxylate (**3.01**), in  $\text{CDCl}_3$ , obtained after the Diels-Alder reaction (400 MHz, 298 K).

To obtain the pure *exo*-isomer, its percentage in the mixture was enriched *via* isomerization, which was carried out in the presence of a strong base to form the corresponding carbanion. The carbanion has a  $\text{sp}^3$ -type trigonal pyramid structure with a low activation barrier for inversion. The difference in the rate of hydrolysis of the *endo*- and *exo*- esters can then be utilized to obtain the *exo*-rich carboxylate anion as first demonstrated by Niwayama *et al.*<sup>34</sup> Once hydrolysis has proceeded the resulting product no longer undergoes isomerization as the required dianion is highly disfavoured. The *exo*-selective hydrolysis accompanied by the rapid isomerization led to approximately 85% of the *exo*-product (**3.02**, Figure 3.8).<sup>35</sup> The residual *endo*-product was then removed by iodolactonization to yield *exo*-5-norbornene-2-carboxylic acid (**3.02**) (Figure 3.9).

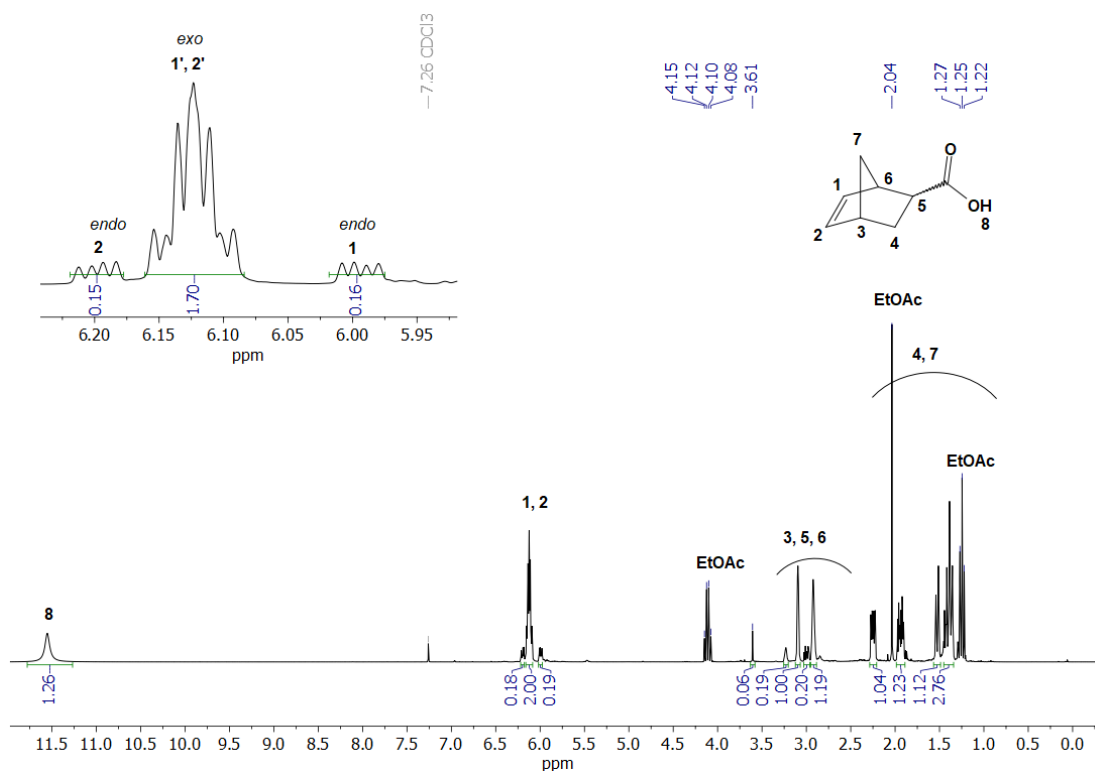


**Figure 3.8**  $^1\text{H}$  NMR spectrum of the exo-rich mixture of 5-norbornene carboxylic acid (**3.02**), in  $\text{CDCl}_3$ , following isomerization (300 MHz, 298K).

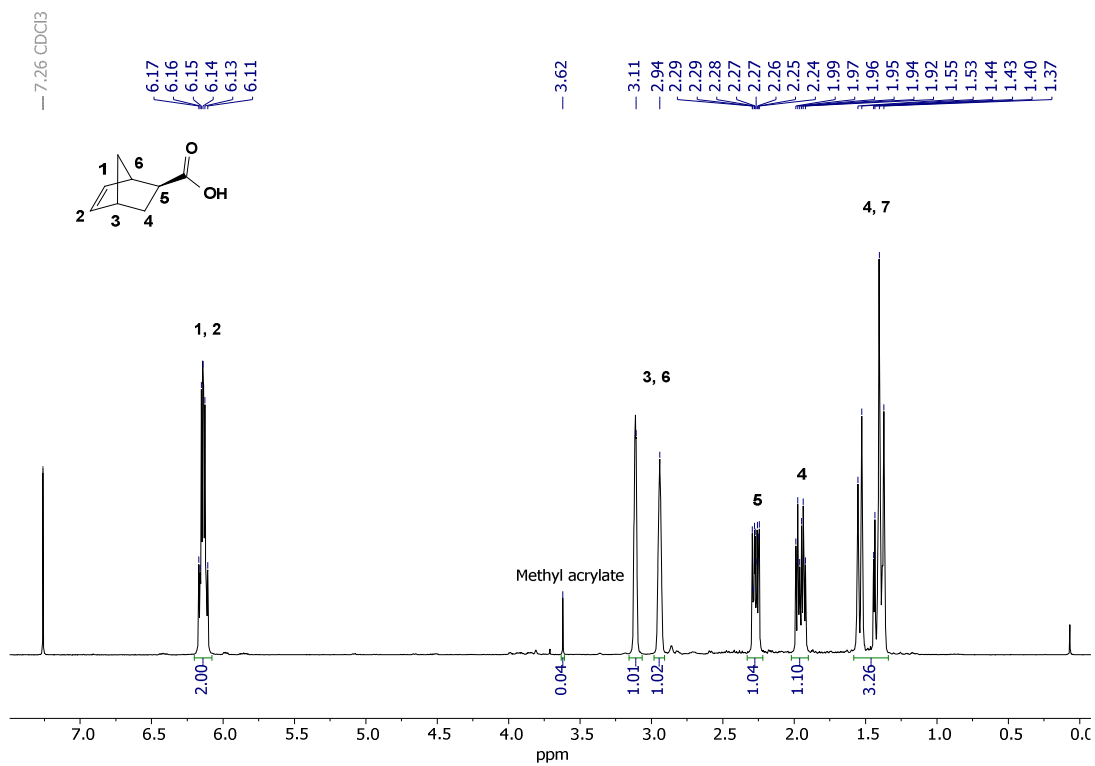
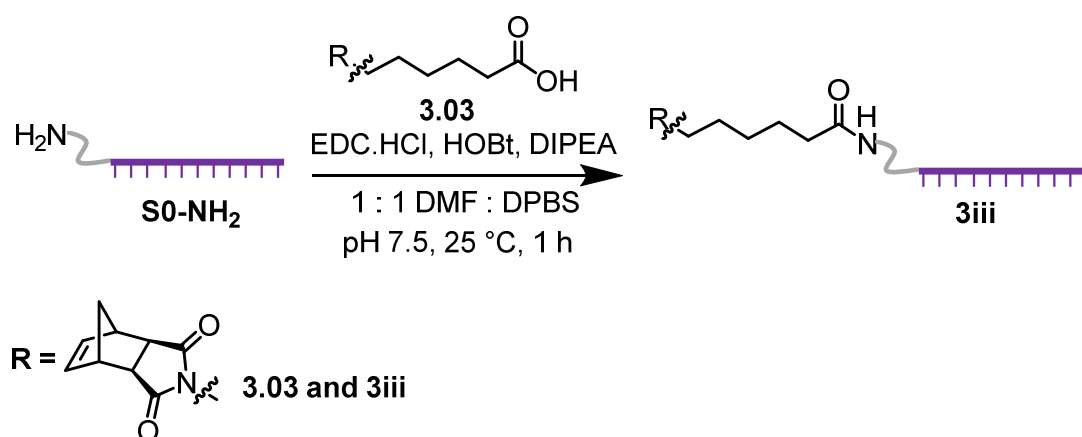


**Figure 3.9**  $^1\text{H}$  NMR spectrum of the exo-5-norbornene carboxylic acid (**3.02**), in  $\text{CDCl}_3$ , following purification (300 MHz, 298K).

Despite the efficient synthesis to prepare **3ii** another oligonucleotide macromonomer was also prepared using the same EDC/HOBt coupling method (**3iii**, Scheme 3.5). The main advantage of **3iii** over **3ii** was the addition of an extra hexyl unit between the norbornene moiety and the oligonucleotide. It was hypothesized that increasing the distance between the oligonucleotide and polymerizable olefin would minimise some of the electrostatic interactions between the Ru-catalyst and DNA identified in Chapter 2. Therefore, monomer **3iii** was synthesized from a carboxylic acid functionalized norbornene monomer (**3.03**). **3.03** had been previously synthesized in the group from aminohexanoic acid and *cis*-5-Norbornene-*exo*-2,3-dicarboxylic anhydride and upon reaction with S0-NH<sub>2</sub> near quantitative conversions were achieved (Figure 3.10).



**Scheme 3.5** Synthesis of **3iii**.

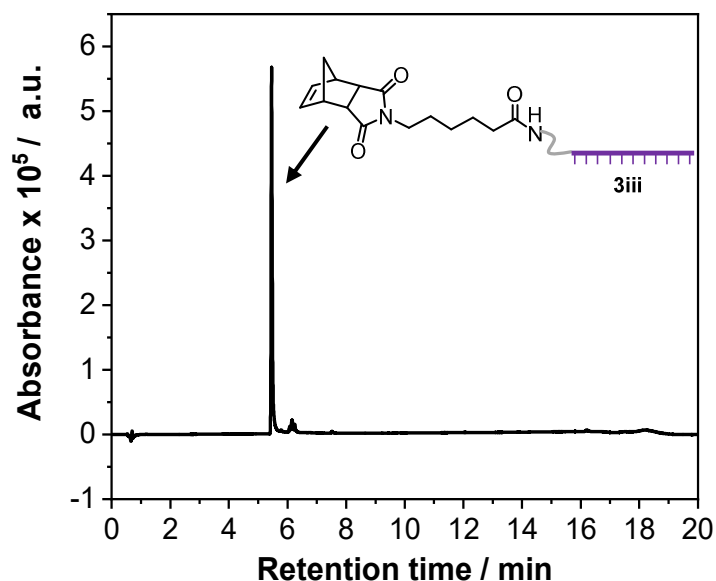


**Figure 3.10** LCMS-UV Chromatogram at 260 nm of **3iii** eluted with a gradient of buffer A: 75 mM TEAA in H<sub>2</sub>O and buffer B: 75 mM TEAA in acetonitrile. Peaks assigned via mass spectrometry.

### 3.3.3 Stability of DNA under the polymerization conditions

In order to utilize the oligonucleotide macromonomer for aqueous ROMP, it was necessary to scope out the solubility and stability of the oligonucleotide under the macroinitiator polymerization conditions, introduced in section 3.3.1. As discussed in Section 3.3.1, the macroinitiator approach was optimized to work under acidic conditions with at least 10 vol% of a water-miscible organic solvent to polymerize the first block. Thus, testing the stability of DNA was particularly important, as under highly acidic conditions, DNA has previously been reported to undergo depurination which is the hydrolysis of the bond between the purine base and its deoxyribose moiety.<sup>36</sup>

Firstly, the solubility and stability of an oligonucleotide (S1-NH<sub>2</sub>) (Figure 3.11a) was studied in two water-miscible solvents: THF and DMF. The two solvents were chosen as they both solubilise **G3** and are miscible with H<sub>2</sub>O. Three different H<sub>2</sub>O/organic solvent ratios were investigated: 10%, 25% and 50% v/v H<sub>2</sub>O (Table 3.2, **2a-2f**) Initially, the samples were



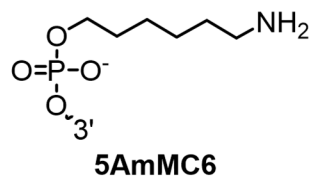
incubated at room temperature for 1 h prior to analysis by native PAGE. Gel electrophoresis is a commonly used analytical technique for oligonucleotides as it separates biomolecules based on their size and charge; thus, the presence of degraded DNA would appear either as a series of bands down the lane due to fragmented oligonucleotides or result in the loss of the DNA band. Following the separation by gel electrophoresis, the DNA samples were stained with SYBR™ Gold, an unsymmetrical cyanine dye which, upon binding to DNA, undergoes a significant fluorescence enhancement that can be visualised using UV light.<sup>37</sup> A single DNA band appeared in all lanes suggesting that the DNA remained stable under all conditions (Figure 3.11b). Solubility was assessed by eye for each set of conditions and all samples appeared to remain soluble.

**Table 3.2** Solvent ratios tested for the stability and solubility study conducted with S1-NH<sub>2</sub>.

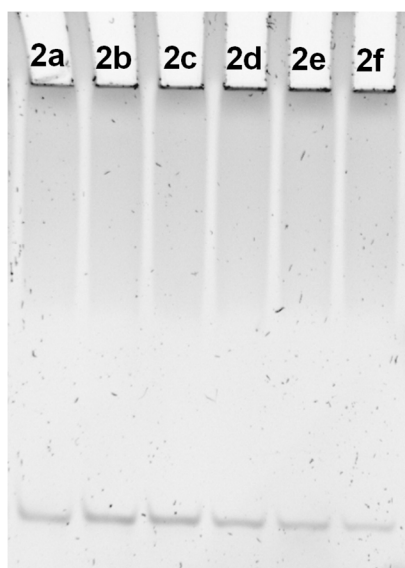
Reaction #	2a	2b	2c	2d	2e	2f	2a'	2b'	2c'	2d'	2e'	2f'
H <sub>2</sub> O (v/v %)	10	25	50	10	25	50	1	2.5	5	1	2.5	5
PB2 (v/v %)	0	0	0	0	0	0	81	81	81	81	81	81
DMF (v/v %)	90	75	50	0	0	0	18	16.5	14	0	0	0
THF (v/v %)	0	0	0	90	75	50	0	0	0	18	16.5	14

**a**

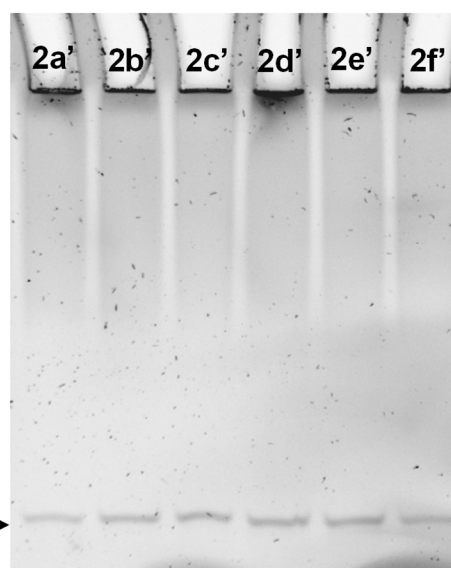
S1-NH<sub>2</sub> = 5'-/5AmMC6/AGG GAT TGT CTT AGT GTG CGA ATA GGT AAC-3'



**b**



**c**



S1-NH<sub>2</sub>

**Figure 3.11** (a) Structure of S1-NH<sub>2</sub>. (b) 18 % Native polyacrylamide gel of 2a-2f. (c) 18% Native polyacrylamide gel of 2a'-2f'. Visualized under UV light after SYBR™ Gold staining.

Each of the previously prepared organic solvents mixtures (**2a-2f**) were then diluted 10-fold with a solution of PB2 containing an added 10 vol% DMF or THF respectively (**2a'-2f'**). Once again all samples appeared soluble by eye and after a further 1 h incubation at room temperature they were analyzed by gel electrophoresis (Figure 3.11c). The presence of a single band in all lanes once again confirmed the stability of the DNA even under the highly acidic conditions.

From this point forward, THF was used in all further studies, as this solvent had previously been successfully utilized for the macroinitiator approach.<sup>1, 26</sup> However, it should be noted

that previous studies identified that the presence of impurities in the commercially purchased THF had a detrimental effect on the catalyst, quenching polymerizations prematurely; therefore, the THF was freshly filtered through basic alumina before each reaction.<sup>1</sup>

Following confirmation of the stability of the commercially purchased amino-DNA, the next step was to ascertain the stability of the oligonucleotide macromonomer (**3iii**); in particular, checking for any hydrolysis of the amide bond. Similar conditions to those stated in **2f** and **2f'** were utilized.

Firstly, **3iii** was incubated in a 1:1 (v/v) mixture of THF/PB2 at room temperature for 30 minutes prior to diluting the sample with PB2 to create a THF:PB2 ratio of 1:9 (v/v). The sample was incubated at room temperature for a further 1 h, prior to the removal of THF under a gentle flow of air. The sample was then desalted through a Bio-spin® 6 column (Biorad) previously equilibrated with ammonium formate before LCMS analysis. One peak was observed in the UV-chromatogram following LCMS analysis (Figure 3.12) and the mass matched that expected (mass expected = 5624.1 Da, mass found = 5624.2 Da), confirming the stability of the DNA macromonomer under the tested conditions.

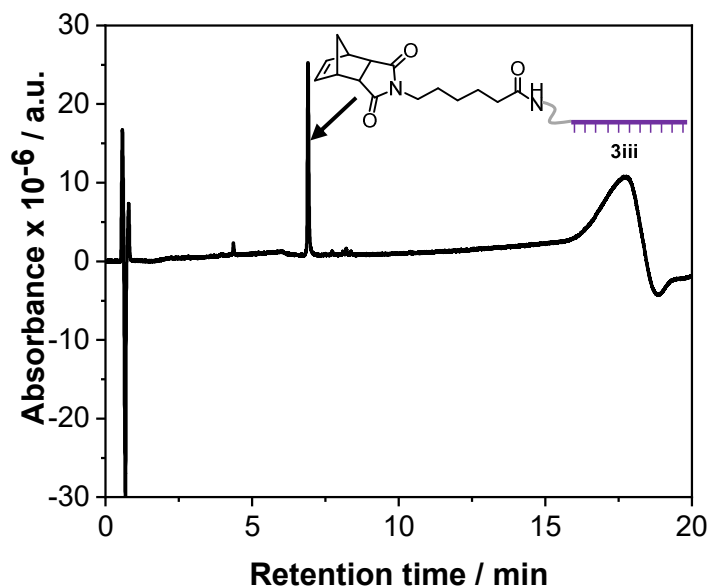


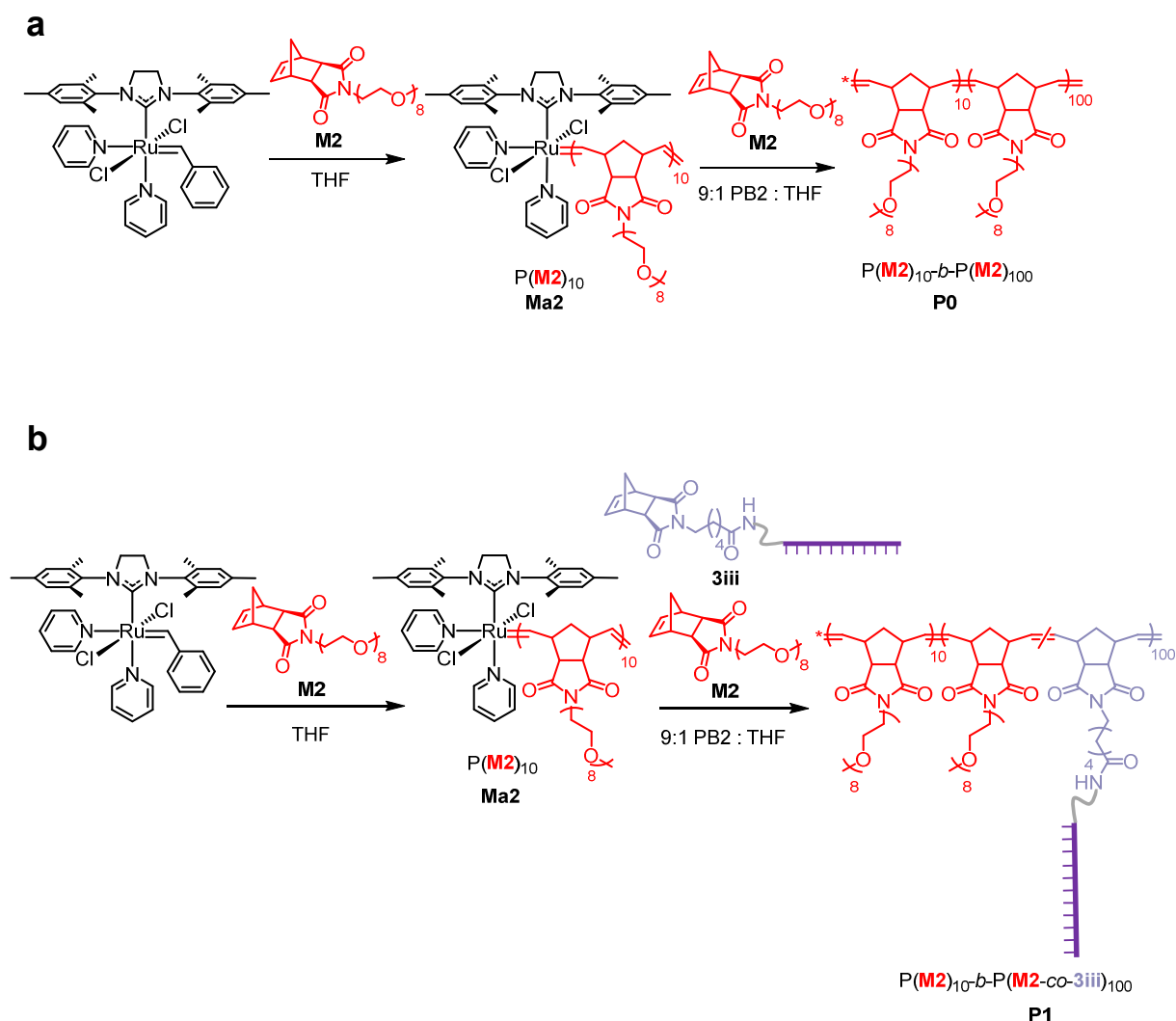
**Figure 3.12** LCMS-UV chromatogram at 260 nm of **3iii** after being incubated under the polymerization conditions eluted with a gradient of buffer A: 75mM TEAA in H<sub>2</sub>O and buffer B: 75 mM TEAA in acetonitrile.

### 3.3.4 Optimization of the polymerization conditions

In Section 3.3.3, the stability of **3iii** in 1:9 (v/v) THF:PB2 for 1 h at room-temperature was confirmed. The solvent ratio and conditions matched those originally reported by Foster *et al.*, and thus made for a good starting point to assess the initial graft-through polymerization of **3iii**.<sup>1</sup> In Chapter 2, an interaction between **PEG-G3** and DNA was identified and thus, it may be anticipated that some of the previously considered additives such as Mg<sup>2+</sup> might be required during the polymerization to minimize unwanted interactions. However, it should be noted that, in contrast to in Chapter 2, the highly acidic conditions (pH2) were expected to push the equilibrium towards the protonation of the phosphate backbone, minimizing electrostatic interactions. Furthermore, the equivalents of catalyst used were low, compared to those studied in Chapter 2, and therefore DNA degradation was expected to be minimized.

Due to limitations on the scale of **3iii** that could be obtained, mainly attributed to the cost of amino-functionalized DNA, **3iii** was copolymerized in the second block with more **M2**. The

polymerization was conducted at a 10 mg mL<sup>-1</sup> scale, with the second block utilizing approximately 10 equivalents of **Ma2** to **3iii**; therefore, approximately 10% of the resultant polymer would be functionalized with DNA. The conditions utilized in the first attempt are shown in Scheme 3.6b and the polymerization was compared to a control reaction with no oligonucleotide (Scheme 3.6a).



**Scheme 3.6** (a) Polymerization of **P0**, which is used as the control reaction for further analysis. (b) Polymerization of **P1**.

As described in work published by Varlas *et al*, the reaction commenced by the polymerization of **M2** with **G3** to prepare P(**M2**)<sub>10</sub>, (**Ma2**).<sup>26</sup> **Ma2** was then transferred to a second solution

containing **M2** and **3iii** in PB2 to target a DNA-polymer conjugate,  $P(\mathbf{M2})_{10}\text{-}b\text{-}P(\mathbf{M2}\text{-}co\text{-}\mathbf{3iii})_{100}$  (**P1**), with a final overall DP of 110 (Scheme 3.6b). After 1 h the polymerizations were quenched with EVE which rapidly forms a non-reactive Fischer carbene complex, terminating the polymerization.<sup>38</sup>

To determine the success of the polymerizations **P0** and **P1** were analyzed by <sup>1</sup>H NMR spectroscopy and the conversion was determined by the integration of the norbornene peaks at 6.2 ppm. The conversion of **P1** was found to be much lower than expected (around 30%) compared to the quantitative conversion observed for the control polymer, **P0**. The results suggested that the presence of **3iii** was inhibiting the polymerization. Based on the observations made in Chapter 2 that DNA interacts with **PEG-G3**, and previous ROMP studies conducted in the presence of adenine functionalized monomers, this result was perhaps not unexpected.<sup>39</sup> Sleiman and co-workers had previously demonstrated the successful addition of succinimide to act as a nucleobase protecting group and prevent unwanted interactions during the ROMP of adenine functionalized norbornene monomers (Figure 3.13a).<sup>39</sup>

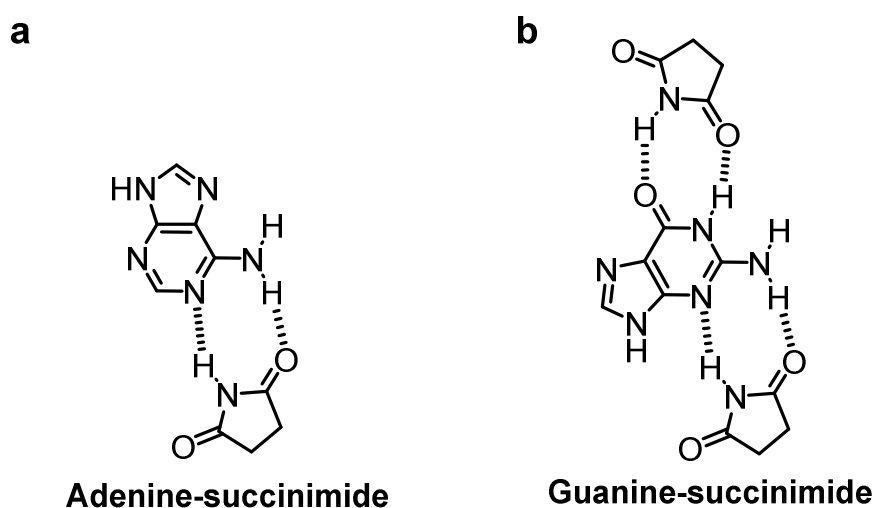


**Figure 3.13** (a) Adenine-succinimide interaction proposed by Sleiman and co-workers.<sup>39</sup> (b) Proposed interaction between guanine and succinimide.

To investigate whether the addition of succinimide would have a similar positive effect in this study, the polymerization of **P0** was initially conducted in the presence of 100 nmol of each of the four nucleobases: A, T, C and G. The polymerizations were analyzed by size exclusion chromatography (SEC) and  $^1\text{H}$ NMR spectroscopy. Those conducted in the presence of A, T and C led to well-controlled polymerizations and near quantitative conversions. However, the presence of G was identified to hinder the polymerization as identified by the lower conversion (67%) and broader molar mass distribution (Figure 3.14a). Sequences rich in guanine are known to self-assemble into tetrameric or ribbon structures which may have hindered the polymerization.<sup>40</sup> Inspired by the work of Sleiman and co-workers, the addition a small amount of succinimide during the polymerization was explored.<sup>39</sup> It was hypothesized that in a similar manner to the adenine-succinimide interaction a guanine-succinimide interaction could also occur and two possible interaction sites were identified (Figure 3.13b). The polymerization to prepare **P0** was repeated in the presence of G + succinimide and complete conversion was achieved ( $\bar{M}_n = 1.28$ ) (Figure 3.14b).

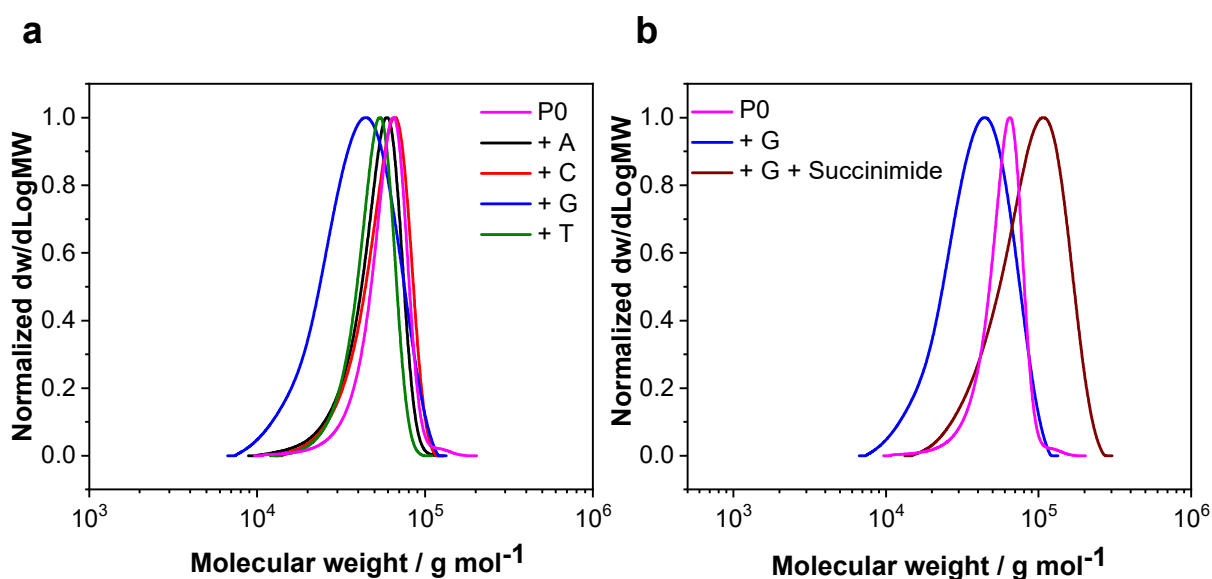


**Figure 3.14** (a) Normalized SEC RI molar mass distribution of **P0** in the absence (pink trace) and presence of 100 nmol **A** (black trace), **C** (red trace), **G** (blue trace) and **T** (green trace). (b) Normalized SEC RI molar mass distribution of **P0** in the absence (pink trace) and presence of **G** (100 nmol) (blue trace) and **G** + succinimide (brown trace). Eluent: DMF + 5 mM  $\text{NH}_4\text{BF}_4$ , PMMA standards.

Conditions leading to the controlled polymerization of **M2** in the presence of **3iii** were therefore identified; however, the stability of the oligonucleotide under these conditions remained to be determined. In Chapter 2, fluorescence quenching of the commonly used DNA stain, SYBR™ Gold, was observed in the presence of Ru-catalysts; therefore, in order visualize the oligonucleotide in the presence of the catalyst an alternative fluorophore was required. Many other commonly utilized DNA stains, such as ethidium bromide, intercalate with DNA, hence are known carcinogens posing several health risks to researchers and thus are undesirable to use in the laboratory. However, DNA appended with a variety of fluorophores at either the 5' or 3' end is commercially available, and this was therefore the strategy pursued.

The aforementioned oligonucleotide **S0-NH<sub>2</sub>** was purchased with an additional 5-carboxytetramethylrhodamine (TAMRA) fluorophore on the 5' end (Figure 3.15). TAMRA is an



orange, fluorescent dye that emits light around 580 nm and thus can be visualized under UV light. The oligonucleotide was subjected to 10 equivalents **Ma2** and 2.5 equivalents of succinimide in 9:1 (v/v) PB2:THF as discussed previously and incubated for 1 h at room temperature prior to analysis by LCMS and native PAGE (Figure 3.16).

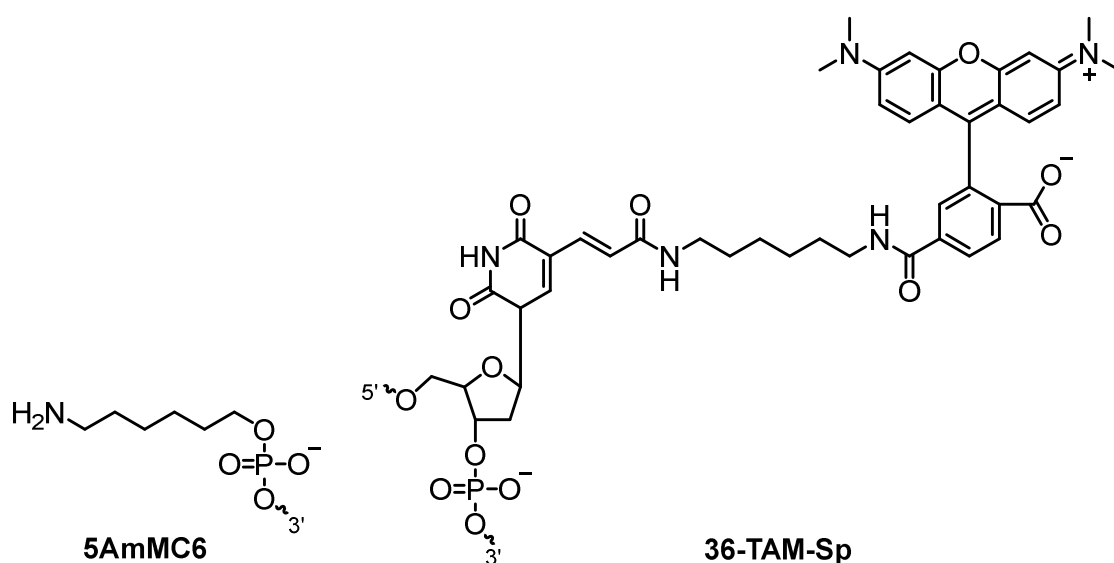


**Figure 3.15** Structure of  $S0-NH_2-TAMRA$ .

A single peak was observed in the 260 nm UV chromatogram following LCMS analysis (Figure 3.16b) and the mass found corroborated strongly with the expected mass (mass found = 6373.1 Da, mass calculated = 6373.1 Da), again signifying the stability of the DNA under the tested conditions. Following native PAGE, the gel was visualized under UV light and excited using green epi-illumination (520-545 nm) (Figure 3.16c). The DNA subjected to the polymerization conditions at two different concentrations (lanes 2 and 3) was compared to the commercially purchased  $S0-NH_2-TAMRA$ , analyzed as received (lane 1). A broad band was observed in lane 3 which is typically seen for DNA-polymer conjugates.<sup>7, 8</sup> This observation

provided strong evidence that the oligonucleotide S0-NH<sub>2</sub>-TAMRA was interacting with the PEG groups on the macroinitiator, as previously seen in Chapter 2.

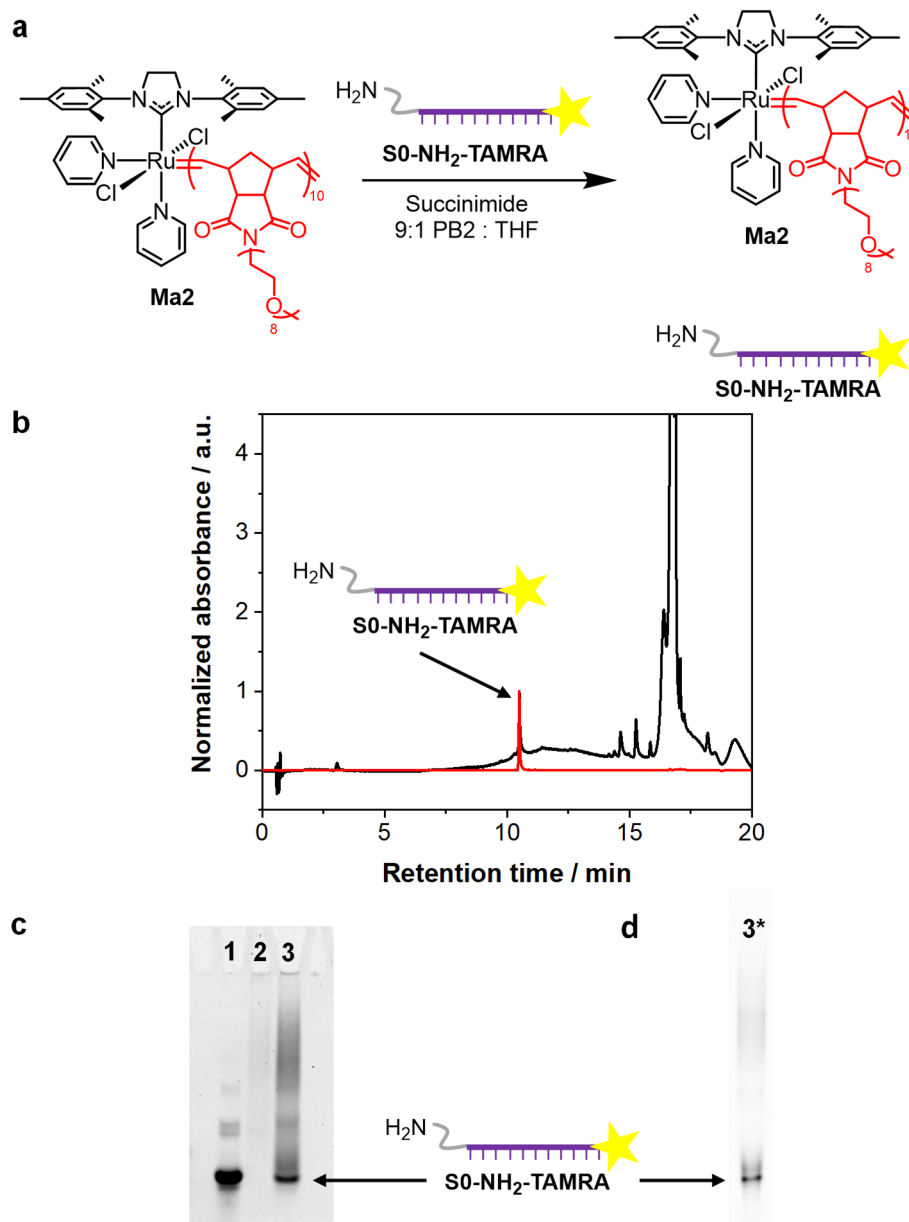


**Figure 3.16** (a) The polymerization conditions S0-NH<sub>2</sub>TAMRA was subjected to. (b) LC-MS-UV chromatogram at 260 nm of S0-NH<sub>2</sub>-TAMRA incubated with the macroinitiator eluted with a gradient of buffer A: 75mM TEAA in H<sub>2</sub>O and buffer B: 75 mM TEAA in acetonitrile. (c) 15% native PAGE of S0-NH<sub>2</sub>-TAMRA (lane 1) and S0-NH<sub>2</sub>-TAMRA incubated with the macroinitiator (lanes 2 & 3) visualized under UV light, exciting TAMRA fluorescence. (d) 15% denaturing PAGE (lane 3\*) S0-NH<sub>2</sub>-TAMRA incubated with the macroinitiator, visualized under UV light, exciting TAMRA fluorescence.

The interaction between DNA and PEG is a phenomenon well reported and most likely occurs through hydrogen bonding and other weak non-covalent interactions.<sup>41, 42</sup> Note that lane 2 contained a diluted sample below the detection limit of the instrument.

PAGE under denaturing conditions has been well-studied in order to disrupt the hydrogen bonding between complementary DNA base pairs and typical conditions include the addition of hydrogen-bond disruptors such as urea or formamide in addition to high temperatures. Inspired by this, PAGE was therefore repeated in the presence of 25 vol% formamide and the samples were heated to 70 °C prior to loading the gel (lane 3\*). Denaturing conditions successfully prevented the DNA-PEG interaction as noted by the disappearance of a broad band in the gel (Figure 3.16d); furthermore, the presence of a single DNA band suggests no DNA degradation was taking place.

### 3.3.5 Polymerization of P1\*

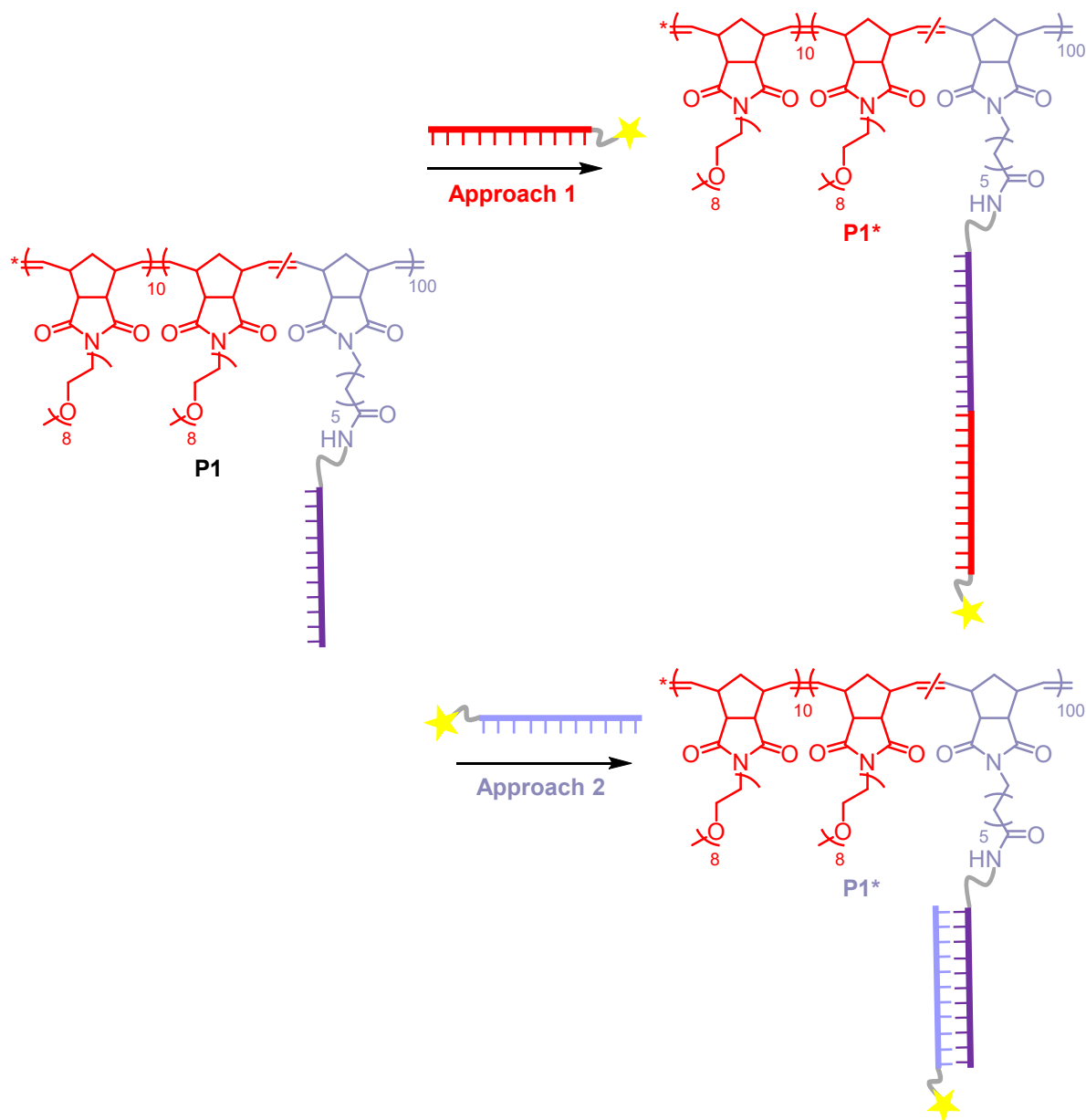
In the previous section, the polymerization conditions were optimized to achieve a controlled polymerization in the presence of oligonucleotides and the stability of the oligonucleotide was confirmed under these conditions. Whilst the success of the bulk polymerization can be determined using conventional methods, namely <sup>1</sup>H NMR spectroscopy to determine the conversion and size-exclusion chromatography to analyze the dispersity of the polymer; due to the nature of our set-up, the incorporation of the oligonucleotides into the polymer could not be confirmed using these techniques. This limitation is as a result of the low concentration of **3iii** utilized in this experiment. To overcome this limitation, DNA-polymer conjugates are often analyzed by techniques such as gel electrophoresis.<sup>7, 8, 22</sup> Due to the high molar mass of

DNA-polymer conjugates they travel noticeably slower through the gels, compared to the unreacted oligonucleotides and thus, can be easily identified.

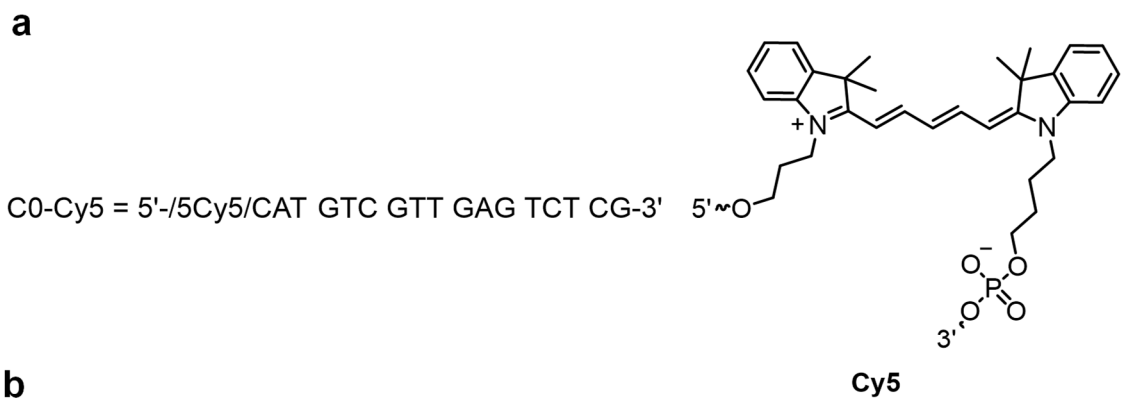
Herein, our predominant analysis technique was therefore gel electrophoresis. For the reasons aforementioned, the use of SYBR™ Gold was avoided and thus, the use of a fluorescently tagged oligonucleotide was required. Due to concerns over the effectiveness of the activated-ester coupling reaction (Scheme 3.5) in the presence of a fluorophore, the addition of the fluorophore post-polymerization was targeted to prepare a fluorescently tagged polymer conjugate, **P1\***. Two approaches were identified (Scheme 3.7): (1) the enzymatically catalyzed ligation reaction or (2) the annealing of a complementary oligonucleotide. Initial proof-of-principle studies for approach 1, the DNA ligation, were conducted using S0-NH<sub>2</sub> and appeared successful (Experimental, Section 3.5.17). However, due to the complexity of this approach, no further work was conducted and attempts continued with approach 2, DNA annealing.

Post-polymerization, **P1** was mixed with a complementary oligonucleotide with a fluorescent cyanine dye, cy5, on the 5' end (C0-Cy5), Figure 3.17. Annealing, was conducted isothermally at room temperature to avoid heating above the LCST of PEG. A pH 8 Tris annealing buffer was utilized (100 mM Tris, 50 mM NaCl and 1mM EDTA) and a control experiment, analyzed by native PAGE, confirmed the successful annealing of free S0-NH<sub>2</sub> and C0-Cy5 under these conditions (Figure 3.17, lane 3). However, upon analysis of **P1** mixed with C0-Cy5 (Figure 3.17, lane 7), the main band identified was a single-stranded C0-Cy5 band suggesting a large amount of DNA did not anneal. A small band was also present at the top of the gel in lane 7, which may represent a large DNA-polymer conjugate; however, this band was present in the two

control lanes **P0** + C0-Cy5 and **P0** + C0-Cy5 + S0-NH<sub>2</sub>, lanes 5 and 6 respectively. Thus, the band is likely a result of the non-covalent, hydrogen-bonding, interaction between the PEG and DNA.



**Scheme 3.7** The preparation of a fluorescently tagged DNA-polymer conjugate, **P1\***, post-polymerization by either DNA ligation (approach 1) or DNA annealing (approach 2).



**b**

S0-NH <sub>2</sub>	X	X	X	X		
C0-Cy5		X	X	X	X	X
P0			X	X	X	
P1						X

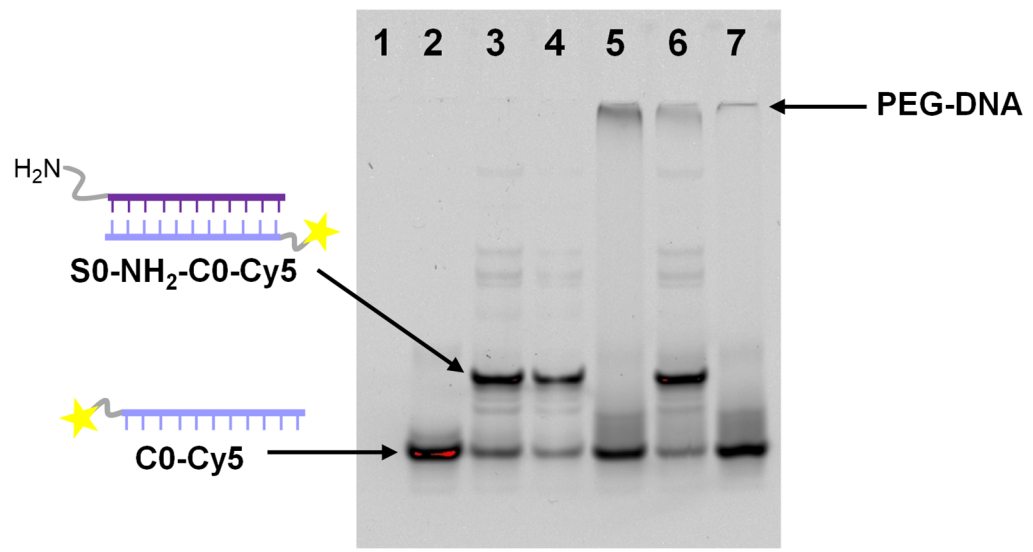


**Figure 3.17** (a) Structure of C0-Cy5. (b) 15% native PAGE gel of P1 mixed with complementary oligonucleotide, visualized under UV-light. †Samples annealed at room temperature overnight prior to analysis.

This result highlighted a number of shortcomings in our current analysis set-up; firstly, it was clear that denaturing PAGE conditions needed to be used to avoid the PEG-DNA interaction as discussed earlier. Unfortunately, the DNA annealing approach did not accommodate these conditions, as it relies on the formation of hydrogen-bonds between the two complementary oligonucleotides. Secondly, the DNA-annealing approach relied on the assumption that the DNA-polymer conjugate can anneal to the complementary oligonucleotide under the same conditions as free DNA. However, of significance is a recent report suggesting that the kinetics of DNA annealing are retarded in the presence of sterically crowded PEG brush and thus, this assumption may not hold true.<sup>43</sup> The combination of these shortcomings prompted a new design set-up to prepare **P1\***.

Despite initial concerns, the functionalization of a fluorescently labelled oligonucleotide with a norbornene moiety was attempted. The addition of the fluorophore pre-polymerization would overcome the two previously discussed limitations with the annealing approach and thus, simplify the analysis. The aforementioned oligonucleotide, S0-NH<sub>2</sub>-TAMRA (Figure 3.15) was utilized and the functionalization was originally attempted using the activated-ester coupling method (Scheme 3.5). In contrast to the preparation of **3iii**, conversion was found to be low (approximately 65%) after shaking at room-temperature for 1 h; therefore, the reaction time was increased to 2 h and almost quantitative conversion to **3iv** was achieved (Figure 3.18).

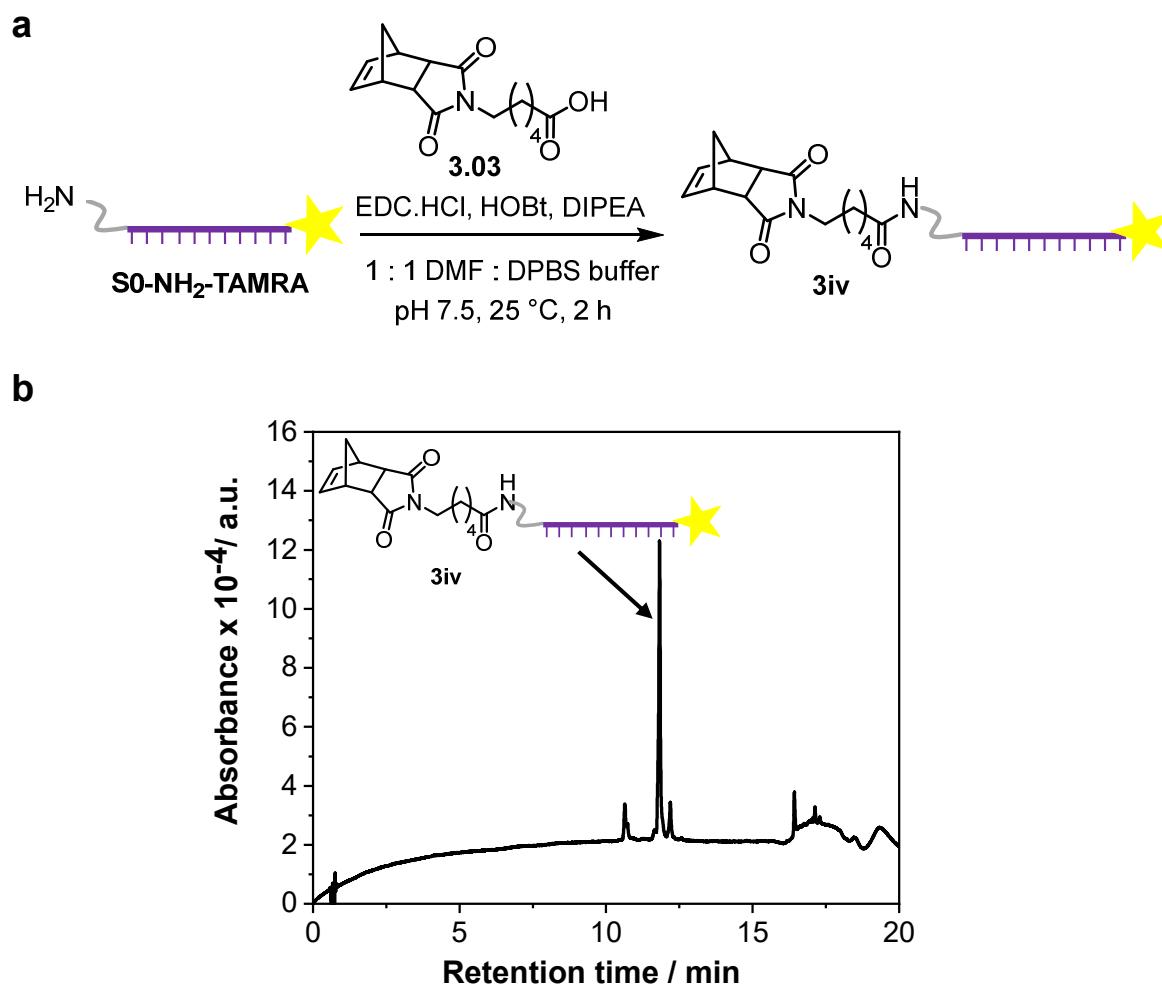


**Figure 3.18** (a) Synthesis of **3iv**. (b) LC-MS UV Chromatogram of **3iv** eluted with a gradient of buffer A: 75 mM TEAA in H<sub>2</sub>O and buffer B: 75 mM TEAA in acetonitrile. Peaks assigned via mass spectrometry.

The polymerization was repeated replacing **3iii** with **3iv** to yield a fluorescently labelled polymer P(**M2**)<sub>10-b</sub>-P(**M2-co-3iv**)<sub>100</sub> (**P1\***), which was analyzed by PAGE (Figure 3.19a). The denaturing conditions discussed previously were utilized, to prevent the DNA-PEG interaction which had previously hindered interpretation of the results. Furthermore, several control lanes were included: **P0** and S0-NH<sub>2</sub>-TAMRA were physically mixed to confirm the denaturing conditions were breaking any hydrogen-bonding interactions (Figure 3.19b, lane 3); and the polymerization was repeated in the presence of S0-NH<sub>2</sub>-TAMRA to ensure any apparent polymerization was occurring through ring-opening of the norbornene functionality (Figure 3.19b, lane 4). The gel was visualized under UV light, exciting the TAMRA moiety, stained with



SYBR™ Gold and then visualized again. As discussed previously the SYBR™ Gold fluorescence was weak due to quenching by Ru. Figure 3.19b shows the two gels overlaid, before (blue stain) and after (black stain) SYBR™ Gold staining.

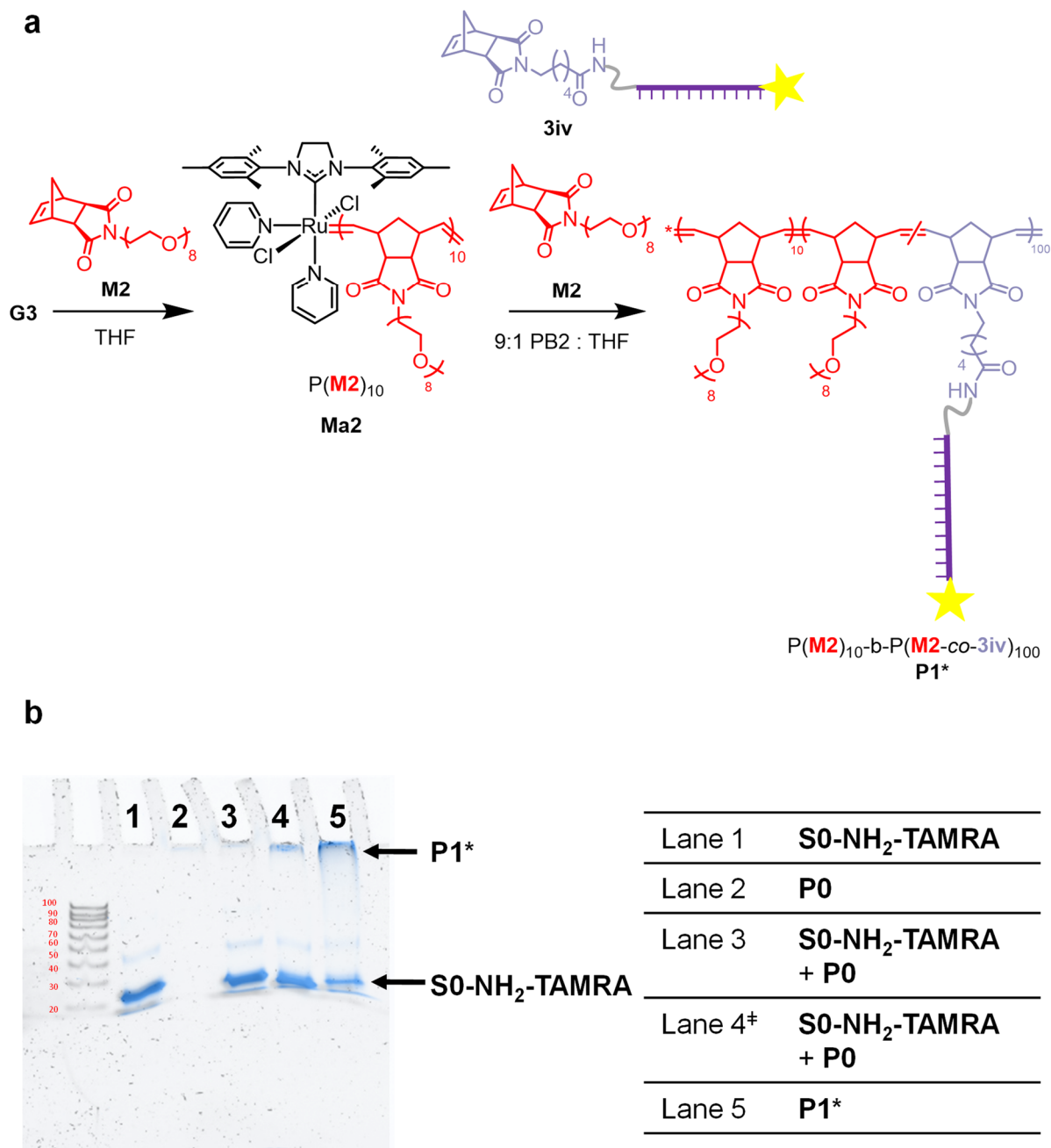


**Figure 3.19** (a) Polymerization of **3iv** to yield **P1\***. (b) 15% denaturing PAGE of **P1\*** analyzed under UV light before (blue stain) and after (black stain) SYBR™ Gold staining.

A band appeared at the top of the lane loaded with **P1\*** (Figure 3.19b, lane 5) as expected for a high molar mass polymer that is too large to travel through the heavily cross-linked gel (15 wt% acrylamide content). Attempts to lower the acrylamide content to 10 wt% were conducted; however, the polymer remained at the top of the well. Therefore, all future work was conducted with a 15% denaturing PAGE gel.

Lane 3 contains only 1 band, representing SO-NH<sub>2</sub>-TAMRA and thus the denaturing conditions appeared to be successful in disrupting hydrogen bonding between PEG and DNA. However, lane 4 was comparable to lane 5 and shows a band (although comparably weaker) at the top of the well alongside a band representing SO-NH<sub>2</sub>-TAMRA. This result, whilst initially surprising, suggested another interaction was taking place between the oligonucleotide and PEG during polymerization, which required further investigation.

#### 3.3.5.1 Characterization of **P1\*** - Size Exclusion Chromatography

The resulting polymer **P1\*** was further characterized in an attempt to explain how the oligonucleotide was interacting with the PEG polymer during the polymerization. Firstly, **P1\*** was analyzed by SEC. Of significant interest was the UV chromatograms at 260 nm, where nucleic acids are strongly absorbing and 559 nm, where the TAMRA unit is strongly absorbing. Thus, a 10 mg mL<sup>-1</sup> sample of **P1\*** in DMF was injected onto the column in an attempt to see these peaks.

Unfortunately, upon analysis it appeared that the PEG polymer alone (**P0**) was strongly absorbing at these wavelengths, most likely due to the presence of residual Ru-catalyst. Therefore, the conjugation of DNA could not be confirmed *via* this characterization technique. However, of significance was a strongly absorbing high molar mass peak in the 260 nm and

559 nm chromatograms of **P1\*** which was not present when **P0** was analyzed at the same concentration (Figures 3.20a & b). Despite the significance of this peak in the UV chromatograms, the refractive index (RI) signal for this high molar mass species was only small (Figure 3.20c), representing approximately 10% of the total species present.

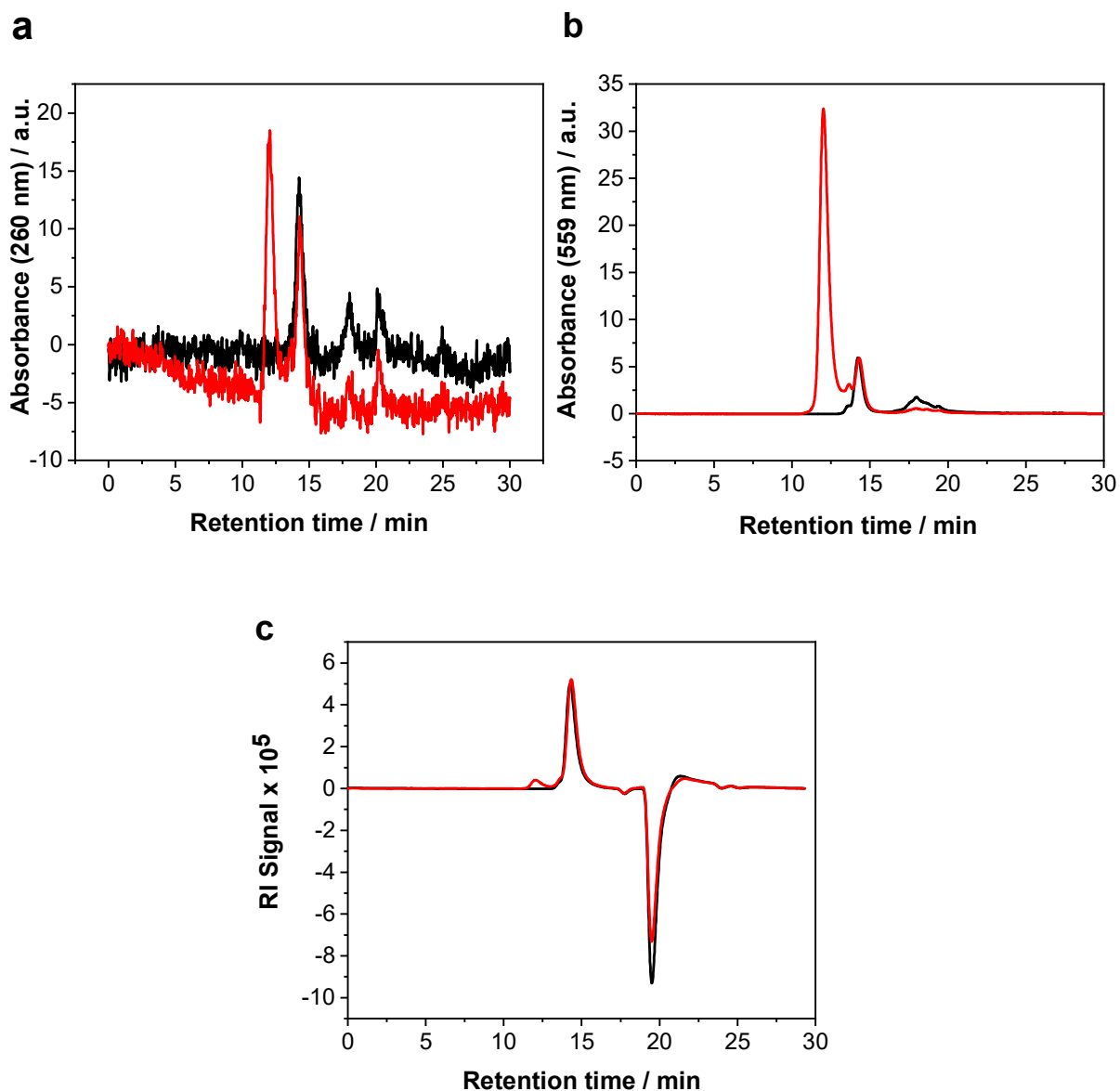


**Figure 3.20** SEC analysis of **P0** (black trace) and **P1\*** (red trace). (a) UV chromatogram recorded at 260 nm. (b) UV chromatogram recorded at 559 nm. (c) RI chromatogram. Eluent: DMF + 5 mM  $\text{NH}_4\text{BF}_4$ , PMMA standards.

Whilst SEC provided no further information as to the mode of binding between the oligonucleotide and PEG, it did provide further indirect evidence that it was indeed binding. Furthermore, the cause of the high molar mass peak was suspected to be due to DNA-induced aggregation.

### 3.3.5.2 Characterization of P1\* - Morphology

A series of studies were also conducted in order to assess the solution behavior of **P1\***. The conformation of bottlebrush polymers is typically driven by the high grafting density, which leads to significant side-chain interactions and thus the entropically unfavourable extension of the polymer backbone.<sup>44-46</sup> However, this scenario is only valid if the solvent quality is good. In a poor quality solvent, the collapse of polymer brushes has been well reported.<sup>47, 48</sup> As previously discussed, the polyethylene glycol sides chains utilized in our study are thermoresponsive and thus, their solubility in water depends upon the temperature. Typically, the LCST of PEG polymers is high (above 100 °C); however, upon copolymerization with hydrophobic moieties the temperature decreases significantly. Furthermore, the LCST increases as the number of ethylene oxide units increases.<sup>49</sup> For our system the PEG unit used is short at just 8 ethylene glycol units and the backbone of bottlebrush polymers prepared *via* ROMP are inherently hydrophobic. The collapse of the system in an aqueous environment was thus a realistic possibility (Figure 3.21).

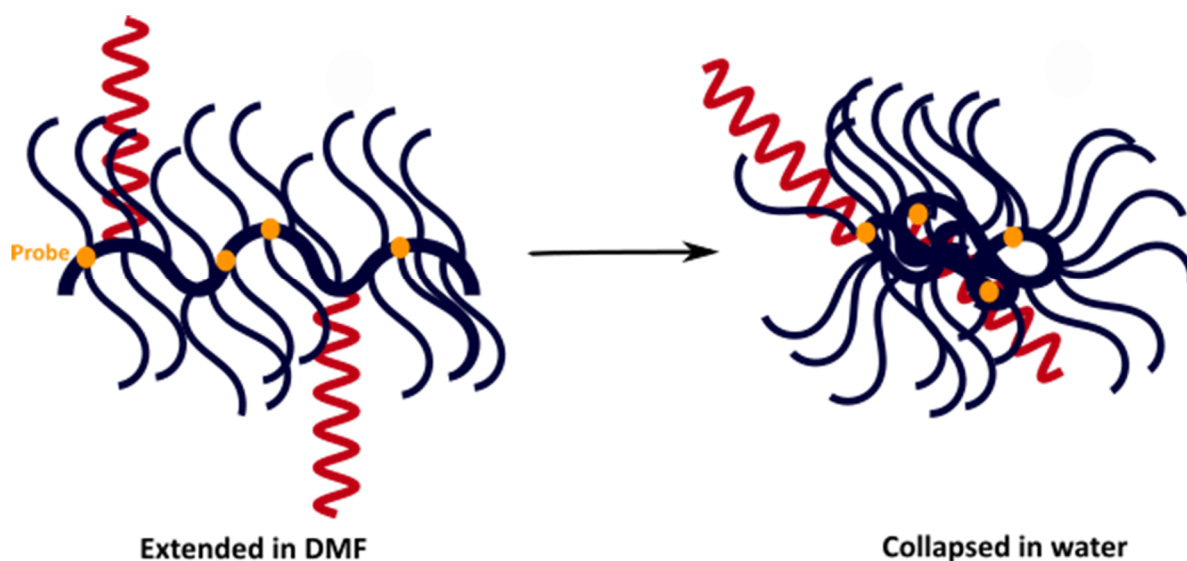


**Figure 3.21** Schematic demonstrating the proposed collapse of  $P1^*$  in an aqueous solution

A solvachromatic dye was used to observe the expected chain collapse (Figure 3.21). Aminochloromaleimides (ACMs) are a class of well-studied small-molecule dyes which are highly emissive in non-polar organic solvents but their fluorescence is rapidly quenched in the presence of protic solvents such as water.<sup>50</sup> A norbornene functionalized ACM, **M3**, was prepared and incorporated into the backbone of DNA-Polymer bioconjugate to prepare  $P(M2)_{10}\text{-}b\text{-}P(M2\text{-}co\text{-}3iii\text{-}co\text{-}M3)_{100}$  (**P1-ACM**) (Figure 3.22a). Note that **3iii** was used to avoid any unwanted interactions between and ACM and TAMRA.

The fluorescence of the **P1-ACM**, at 504 nm, was then studied in DMF and following the titration of increasing volumes of  $H_2O$  (Figure 3.22c). An initial decrease in fluorescence was observed as expected when the dye was exposed to an increasingly protic environment. However, as the amount of water was increased beyond 60% the fluorescence began to increase, indicating that the ACM was once again protected from the protic environment. This result differs to that observed for the free ACM dye (Figure 3.22b) and would be consistent

with the collapse of the bottlebrush polymer in aqueous solutions containing greater than 60 vol% H<sub>2</sub>O.

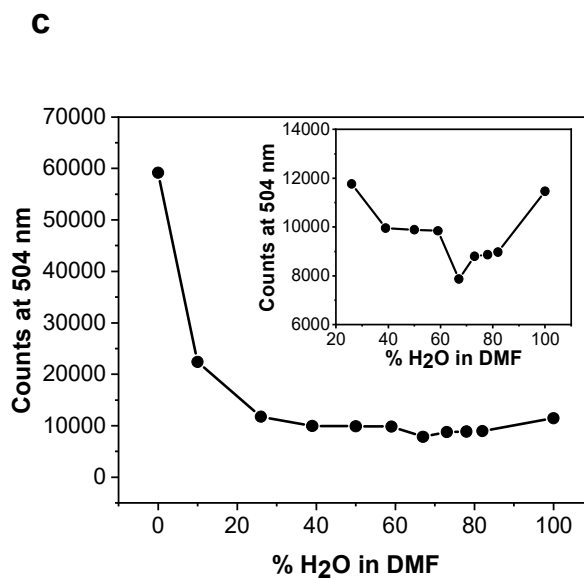
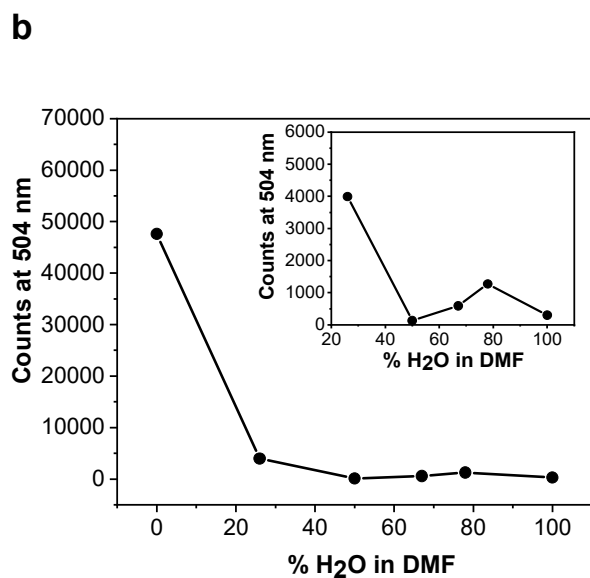
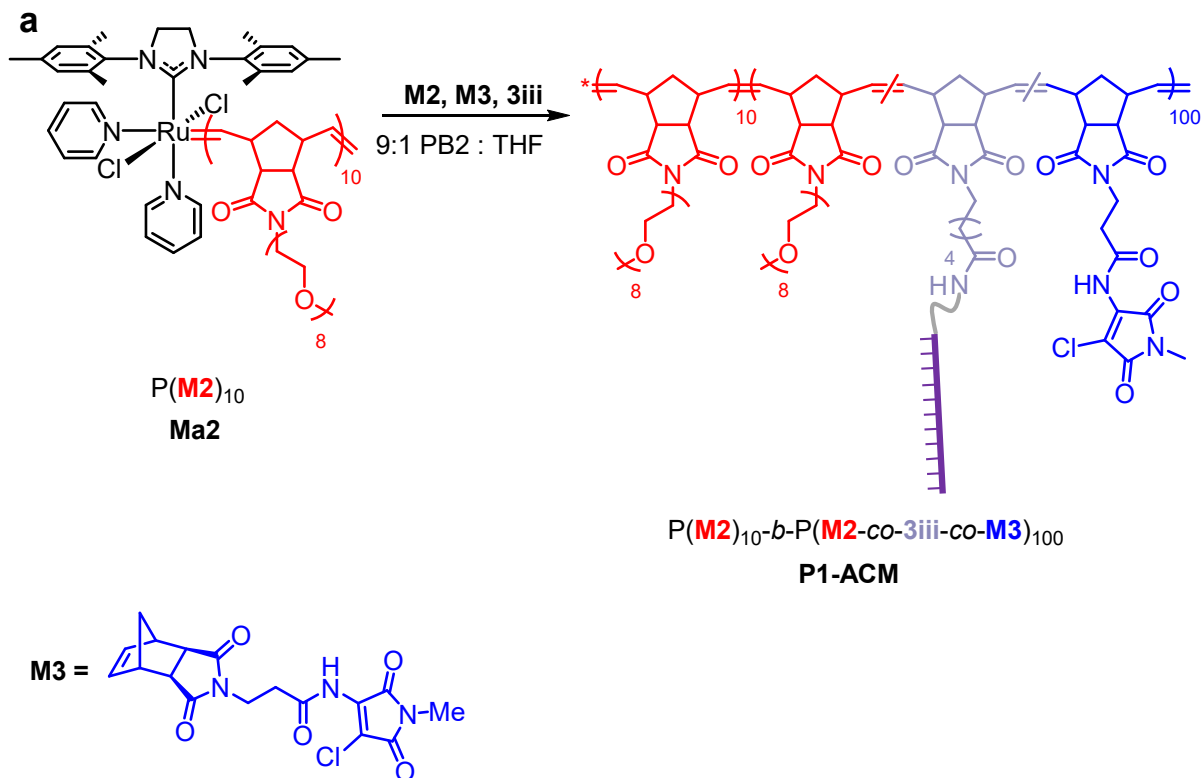


**Figure 3.22** (a) Synthesis of **P1-ACM**. (b) Fluorescence of **M3** at varying percentages of H<sub>2</sub>O. (c) Fluorescence of **P1-ACM** at varying percentages of H<sub>2</sub>O.

Attempts were made to visualize **P1\*** by transmission electron microscopy (TEM). However, due to the small size of the particles (<10 nm, estimated *via* dynamic light scattering) they

could not be distinguished from artefacts arising from the staining process. Nevertheless, identifying the collapsed behavior of **P1\*** was significant and aided in explaining the interaction observed when 50-NH<sub>2</sub>-TAMRA was present during the polymerization of **P0**. It was hypothesized that as the polymerization progressed, the polymer collapsed around the oligonucleotide, physically trapping it. (Figure 3.23).

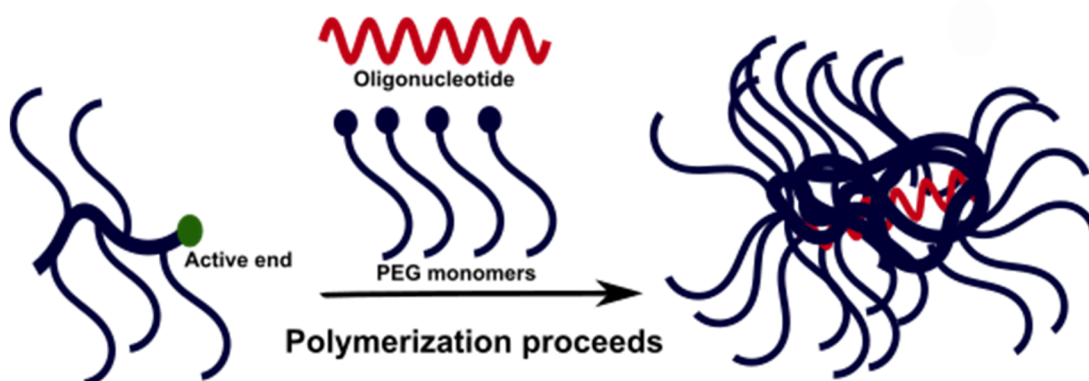


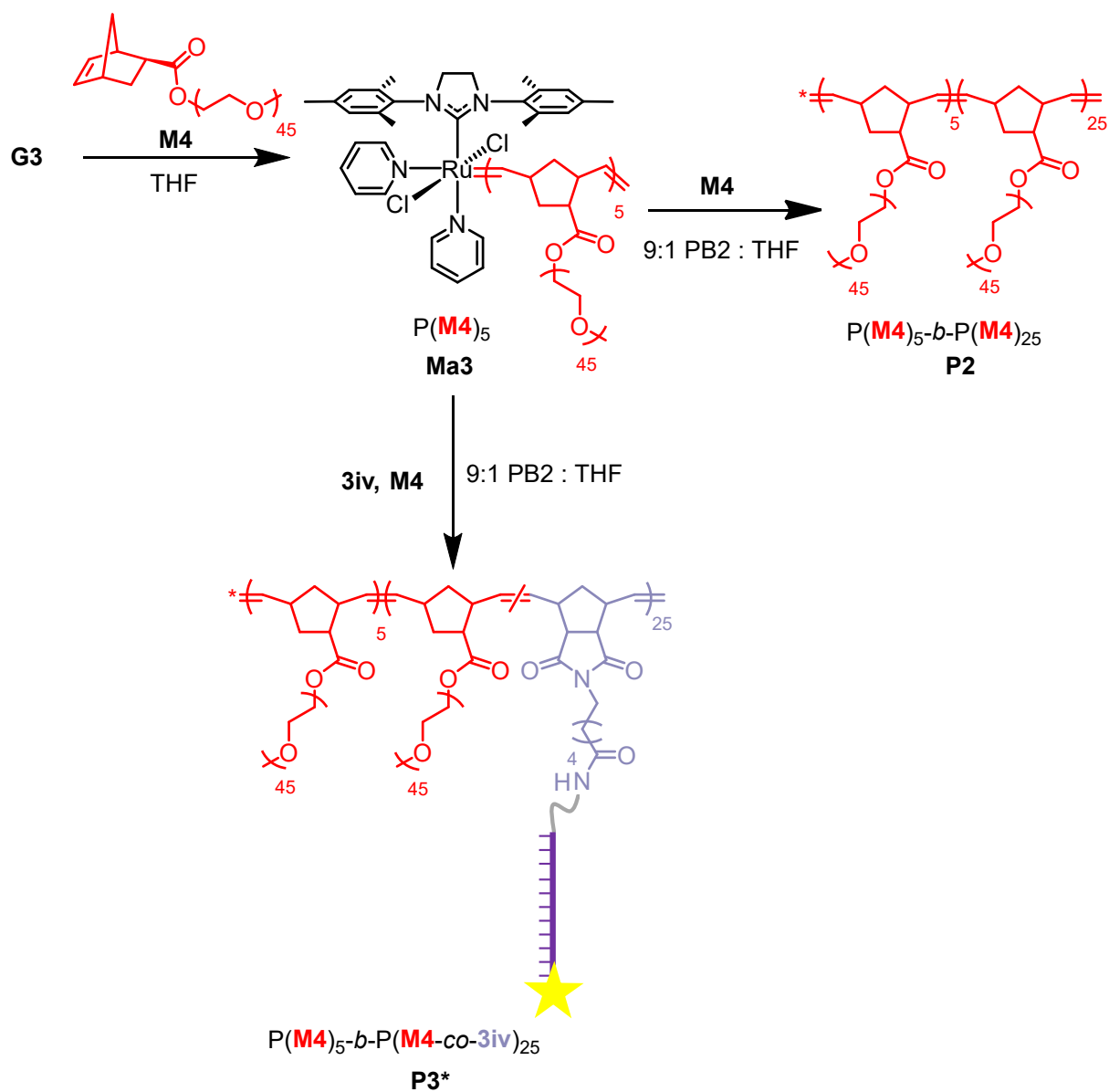
**Figure 3.23** Schematic showing the entrapment of a DNA-polymer conjugate during the polymerization.

### 3.3.6 Controlling the morphology of DNA-polymer conjugates

Previously, the morphology of bottlebrush polymers has been controlled by altering the backbone length or side-chain length.<sup>51</sup> We therefore set out to adjust these parameters in order to prevent the collapse of the DNA-polymer conjugate. The advantages of this were two-fold: firstly, by preventing the collapse of the polymer around the oligonucleotide we hoped that we could gain undisputed proof that the polymerization of our oligonucleotide macromonomer (**3iv**) was occurring covalently. Secondly, accessing DNA-polymer conjugates of a variety of morphologies will be of particular interest for therapeutic delivery.

In order to achieve this, a norbornene monomer with a longer PEG side-chain (**M4**) was synthesized and replaced **M2** in the polymerization. The polymerization was attempted; however, due to the steric hindrance of the longer PEG side-chain a shorter DP of 30 was

targeted to prepare  $P(\mathbf{M4})_5\text{-}b\text{-}P(\mathbf{M4}\text{-}co\text{-}\mathbf{3iv})_{25}$  ( $\mathbf{P3}^*$ ) in the presence of the oligonucleotide macromonomer and a control polymer with no oligonucleotide,  $(\mathbf{M4})_5\text{-}b\text{-}P(\mathbf{M4})_{25}$  ( $\mathbf{P2}$ ) (Scheme 3.8).



**Scheme 3.8** Polymerization of  $\mathbf{P2}$  and  $\mathbf{P3}^*$ .

### 3.3.6.1 Analysis of $\mathbf{P2}^*$

Following the polymerization of  $\mathbf{P3}^*$ , the polymer was analyzed by SEC and denaturing PAGE, and the results were compared to those obtained for  $\mathbf{P1}^*$  (Figure 3.24). Analysis by DMF SEC



resulted in similar traces to those obtained for **P1\*** (Figure 3.24b). Specifically, the UV chromatogram at 559 nm shows a high molar mass peak for **P3\*** which was not present in the control polymer **P2** indicating that the oligonucleotide is present on the polymer and altering the separation within the SEC column.

Furthermore, similarly to **P1\***, the 15% denaturing PAGE analysis of **P3\*** showed a band at the top of the gel in lane 5 as would be expected for a large DNA-polymer conjugate (Figure 3.24c). However, in contrast to **P1\***, no band at the top of the gel was present in the control lane, lane 4. This indicated that the longer PEG side chains and shorter polynorbornene backbone was preventing the collapse of the polymer around the oligonucleotide. Furthermore, the PAGE gel analysis of **P3\*** suggested that the band observed at the top of lane 5 must be due to the ring-opening of the oligonucleotide macromonomer and thus, our initial project aim to perform the 'graft through' ring-opening metathesis polymerization of native DNA had been achieved.

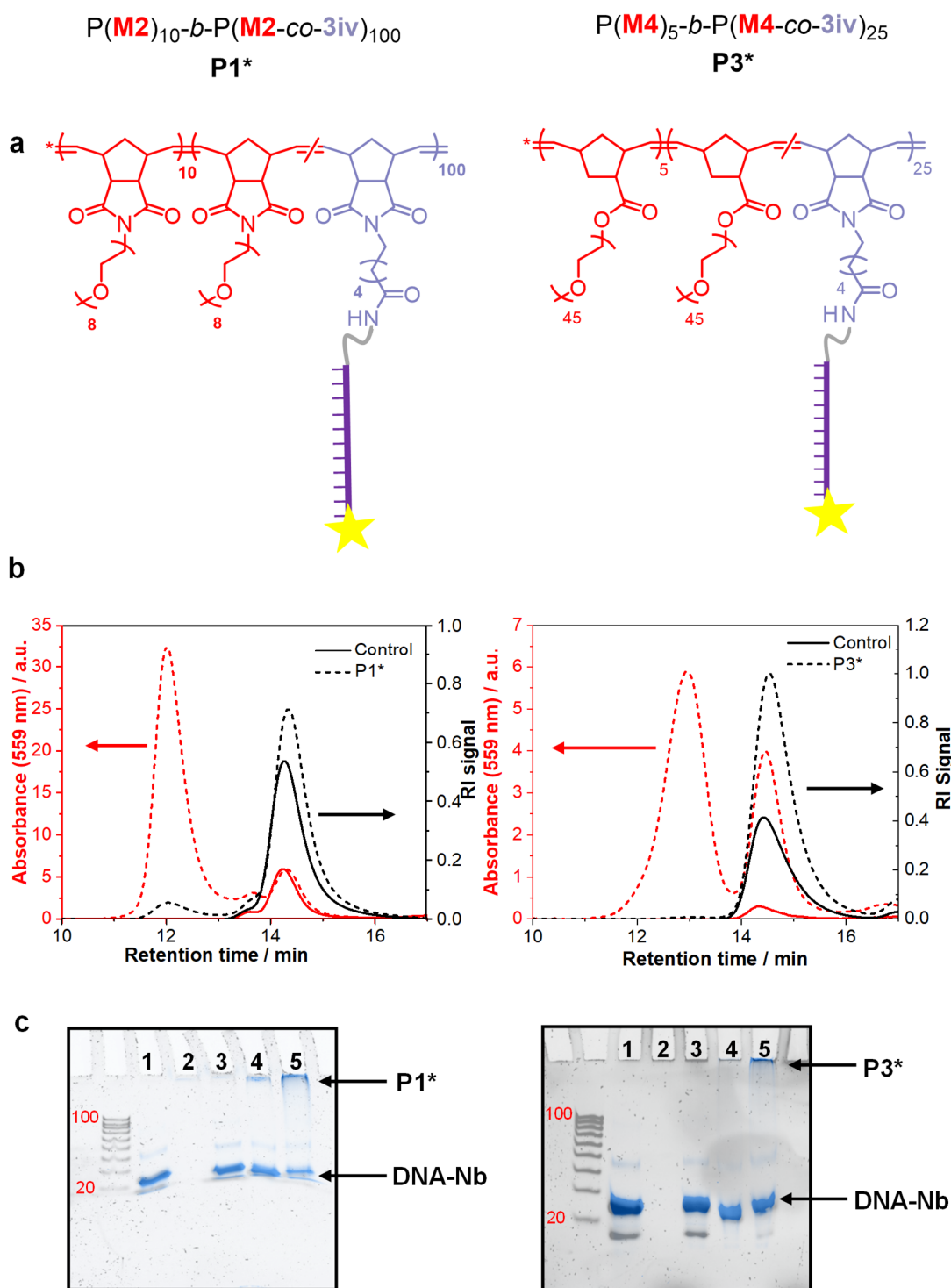


**Figure 3.24** (a) Structure of **P1\*** and **P3\***. (b) DMF SEC traces of **P1\*** and **P3\*** (dash) compared to **P0** and **P2** (line) respectively. Red trace is the UV chromatogram at 559 nm and black track is the RI chromatogram. (c) 15% denaturing PAGE of **P1\*** and **P3\***: Lane 1 – S0-NH<sub>2</sub>-TAMRA; Lane 2 – **P0/P2**; Lane 3 – S0-NH<sub>2</sub>-TAMRA + **P0/P2** (mixed after polymerization); Lane 4 – S0-NH<sub>2</sub>-TAMRA + **P0/P2** (mixed during polymerization); Lane 5 – **P1\*/P3\*** visualized under UV light before (blue bands) and after (black bands) SYBR™ Gold staining.

### 3.3.6.2 Morphology of P3\*

Finally, to support the hypothesis that **P3\*** was not collapsed in aqueous *milieu*, the same fluorescence study using **M3**, was repeated for **P3\***. **M4** and **3iii** were copolymerized with the ACM monomer, **M3**, to yield  $P(\mathbf{M4})_5\text{-}b\text{-}P(\mathbf{M4}\text{-}co\text{-}\mathbf{3iii}\text{-}co\text{-}\mathbf{M3})_{25}$  (**P3-ACM**). The fluorescence was recorded at differing volumes of H<sub>2</sub>O and similarly to the monomer, **M3**, the fluorescence decreased with increasing volumes of H<sub>2</sub>O. However, in contrast to **P1\***, no recovery in fluorescence was detected above a threshold level of H<sub>2</sub>O (Figure 3.25). This result is consistent with the hypothesis that no collapse was occurring and thus, the ACM along the polymer backbone remains exposed to the ever-increasing hydrophilic environment.

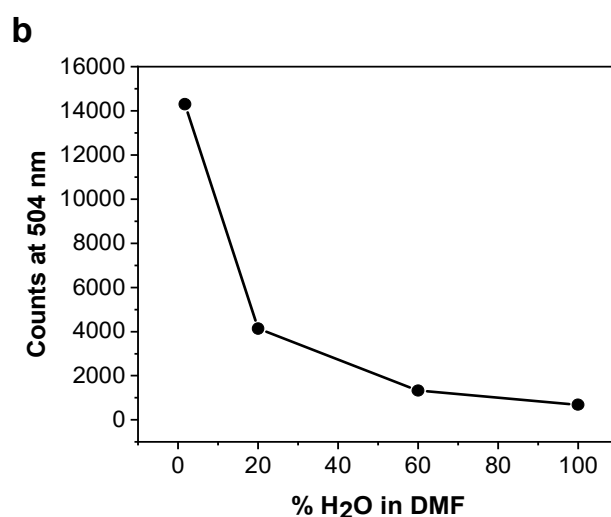
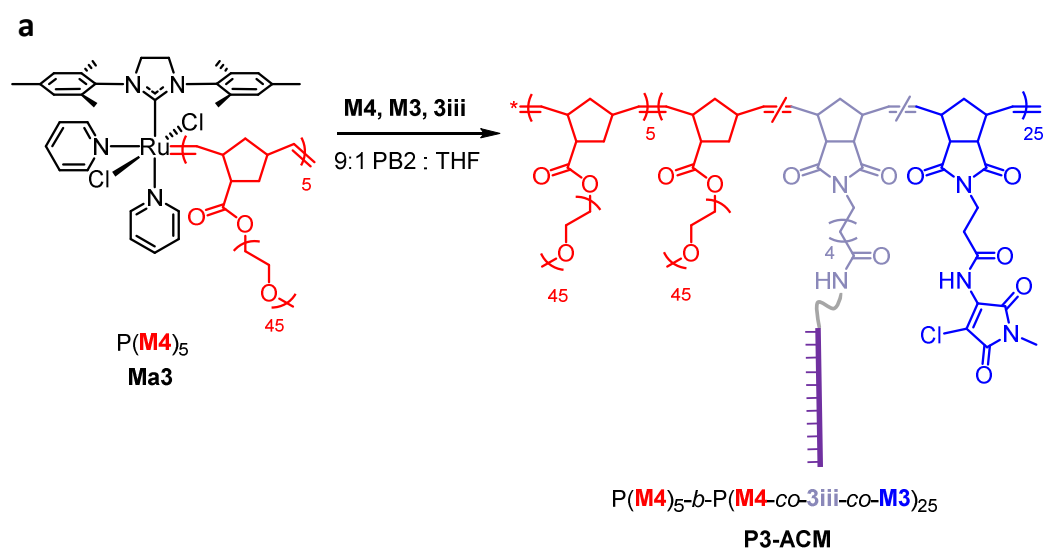


**Figure 3.25** (a) Schematic for the polymerization of **P3-ACM**. (b) Fluorescence of **P3-ACM** at increasing volumes of  $\text{H}_2\text{O}$ .

### 3.3.7 Hybridization of **P3\***

Following the successful ‘graft-through’ polymerization of **3iv** as confirmed by PAGE analysis of **P3\***, the properties of the oligonucleotide conjugated to the polymer were assessed. Previously, Jia *et al.* had studied the hybridization thermodynamics of DNA-PEG conjugates of a variety of different architectures, including brush polymers. Two counteracting effects were observed: (1) The excluded volume effect of the PEG increases the effective concentration of the oligonucleotide leading to more favourable binding; and (2) a PEG-DNA chemical

interaction can destabilize the duplex. For PEG brush polymers the latter effect was found to dominate. However, protein interactions are significantly reduced for brush polymers, yielding them more stable for therapeutic purposes.<sup>43</sup>

In order to assess the hybridization properties of **P3\***, the polymer was first purified by preparative SEC. The purification attempt was to remove unreacted SO-NH<sub>2</sub>-TAMRA and the residual ruthenium catalyst as the fluorescence of TAMRA was found to decrease in the presence of **Ma1** (Figure 3.26). The Ru-induced quenching mechanism is suspected to be similar to that of SYBR™ Gold discussed in Chapter 2, Section 2.3.3.

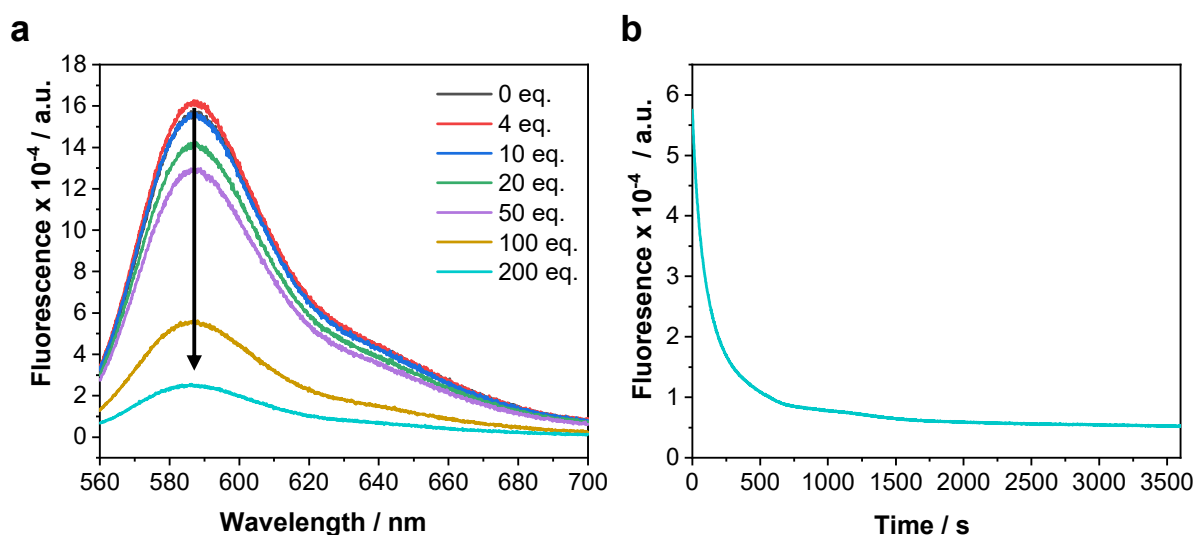


**Figure 3.26** (a) Fluorescence emission spectra of S3-TAMRA-NH<sub>2</sub> in the presence of **Ma1** excited at 545 nm. (b) Fluorescence emission at 580 nm of S3-TAMRA-NH<sub>2</sub> in the presence of 200 equivalents **Ma1**.

Purified **P3\*** collected by preparative SEC, was dialysed through a 3 kDa cellulose membrane into 18 MΩ H<sub>2</sub>O and then approximately 1 equivalent of the complementary oligonucleotide, modified with an Iowa Black RQ dark quencher on the 5' end (CO-IAbRQ), was added. Upon hybridization, the quencher was brought into close contact with TAMRA on the 3' end of the conjugate and thus, a rapid drop in fluorescence was expected. The hybridization of **P3\*** was

compared to free amino-DNA (S0-NH<sub>2</sub>-TAMRA), and whilst a rapid drop in fluorescence upon the addition of the complementary oligonucleotide (C0-IAbRQ) was observed for S0-NH<sub>2</sub>-TAMRA no fluorescence decrease was observed for **P3\*** (Figure 3.27).

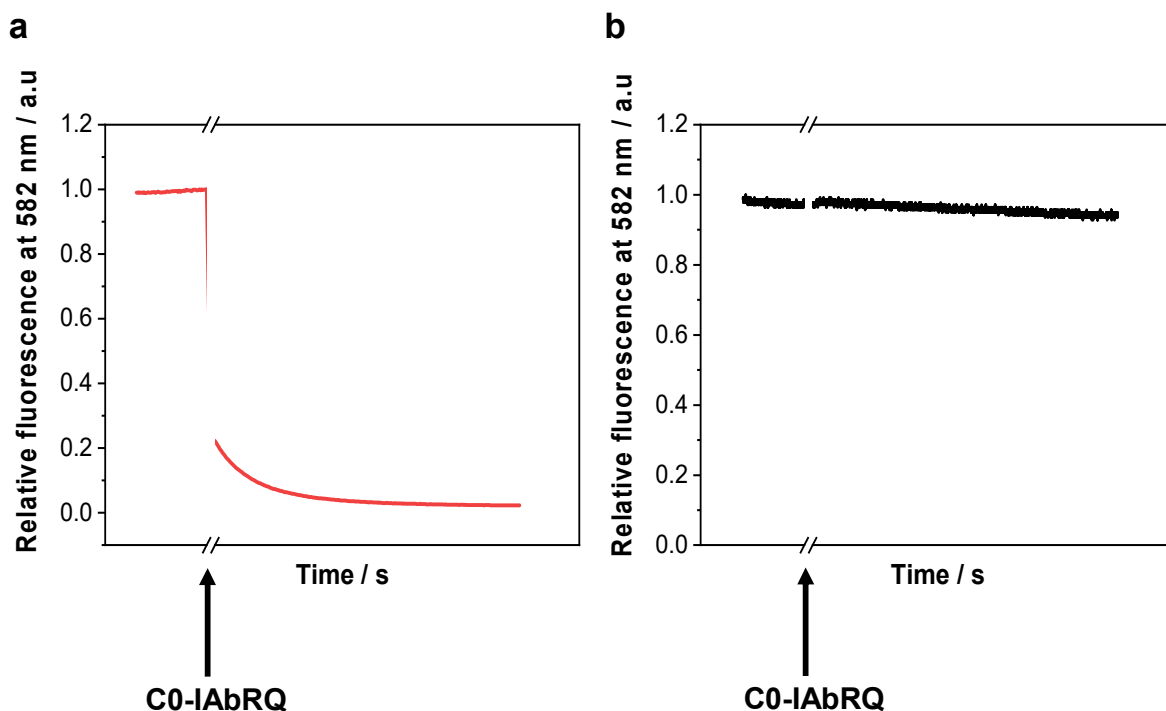


**Figure 3.27** (a) Relative fluorescence intensity of S0-NH<sub>2</sub>-TAMRA upon addition of C0-IAbRQ. (b) Relative fluorescence intensity of **P3\*** upon addition of C0-IAbRQ

The results suggest that no hybridization occurred at room-temperature over the time course of this experiment and thus, the oligonucleotide may be occupying a highly protected environment. Such a protected oligonucleotide would be of interest for therapeutic purposes and is therefore an area of interest for future studies.

### 3.4 Conclusions

In this chapter the graft-through polymerization of native-DNA by aqueous ROMP was explored. A macroinitiator approach was identified to yield controlled polymerizations under aqueous conditions and was the focus of our attempts. Several oligonucleotide

macromonomers were synthesized in near quantitative conversions using a simple one-step solution phase coupling approach. The stability of these macromonomers under the polymerization conditions was confirmed; however, an unexpected non-covalent PEG-DNA interaction was observed. Denaturing PAGE conditions were optimized to prevent the non-covalent interaction, *via* the disruption of hydrogen-bonding, and this allowed for PAGE to be our primary analysis technique.

Two bottlebrush polymers with differing side-chain lengths were explored and our results indicated that differences in the morphology of the polymers, under aqueous conditions, led to differing interactions between the oligonucleotide and polymer. Specifically, a bottlebrush polymer with a shorter PEG sidechain length (**P1\***) appeared to collapse during the polymerization, due to its amphiphilic nature, physically trapping the oligonucleotide inside the particle. In contrast, such behavior was not observed in a bottlebrush polymer containing longer PEG sidechains (**P3\***) and thus, it was concluded that any observed conjugation was as a result of the polymerization of the DNA macromonomer.

Finally, initial hybridization data suggested that **P3\*** was unable to anneal isothermally at room temperature, most probably owing to the steric hindrance of the PEG groups. However, this could prove advantageous for therapeutic purposes, as it is anticipated that such steric hindrance would reduce the accessibility of nucleases to the oligonucleotides and thus prolong the half-life of oligonucleotides *in-vivo*.

## 3.5 Experimental section

### 3.5.1 Materials

Oligonucleotides were purchased from Integrated DNA technologies, Inc. and resuspended in 18MΩ H<sub>2</sub>O to a concentration of 200 μM before use. Concentrations were calculated from the absorbance values at 260 nm using the reported extinction coefficients.

Name	Sequence (5' → 3')	Extinction coefficient/ L/(mole·cm)
S0-NH <sub>2</sub>	5AmMC6/CGA GAC TCA ACG ACA TG	169,300
S0-NH <sub>2</sub> -TAMRA	5AmMC6/CGA GAC TCA ACG ACA TG/36-TAMSp	209,780
S1-NH <sub>2</sub>	5AmMC6/AGG GAT TGT CTT AGT GTG CGA ATA GGT AAC	303,700
C0-Cy5	5Cy5/CAT GTC GTT GAG TCT CG	167,600
C0-IAbRQ	5IAbRQ/ CAT GTC GTT GAG TCT CG	208,057
Ligase_S0	5Phos/CGC CAG CCG CTG CTT GC/36-FAM	162,200
Ligase_C0	GTT GAG TGG AGC AAG CAG CGG CTG GCG CAT GTC GTT GAG TCT CG	416,400
Ligase_C1	CGA GAC TCA ACG ACA TGC GCC AGC CGC TGC TTG CTC CAA TCA AC	404,000

*Cis*-5-norbornene-*exo*-2,3-dicarboxylic anhydride (97%), dicyclopentadiene (90+%) and methyl acrylate (99%) were purchased from Alfa Aesar. 4-Dimethylamino pyridine (DMAP, ≥98 %), methoxy PEG (MW 2000 Da), *exo*-norbornene carboxylic acid (97%), 6-aminohexanoic acid (≥98.5 %), N-(3-Dimethylaminopropyl)-N'-ethylcarbodiimide hydrochloride (EDC.HCl, BioXtra grade), HOBt hydrate (97%), Grubbs 2<sup>nd</sup> generation catalyst and DMF (Biological grade



≥99 %) were purchased from Sigma-Aldrich. THF (HPLC grade) was purchased from VWR Chemicals and was purified *via* passage through a column of basic alumina prior to use. **M1** and **M2** were synthesized as described by Foster *et al.*<sup>1</sup> and Varlas *et al.*<sup>26</sup> respectively. **M3.1** was synthesized as described by Jimaja *et al.*<sup>52</sup> **G3** was synthesized as described in Chapter 2 – Section 2.5.4.

DPBS buffer was prepared by dissolving 9.6 g of DPBS from Sigma-Aldrich into 1 L 18MΩ H<sub>2</sub>O. Phosphate solution, pH = 2 (PB2) was prepared using 100 mM sodium phosphate monobasic dihydrate (NaH<sub>2</sub>PO<sub>4</sub> · 2H<sub>2</sub>O) in 18MΩ H<sub>2</sub>O adjusted to pH = 2 with HCl. 10 x Tris-acetate EDTA (TAE) buffer was purchased from Sigma-Aldrich and contains 0.4 M Tris acetate and 0.01 M EDTA. 10 x Tris-Borate EDTA (TBE) TBE buffer was purchased from Sigma-Aldrich and contains 0.89 M Tris and 0.02 M EDTA adjusted to pH 8.3 with boric acid.

Micro Bio-spin™ 6 columns were purchased from Bio-Rad laboratories. Amicon® Ultra-0.5 mL centrifugal filters (3000 MWCO) were purchased from Millipore. Illustra™ NAP™-5 columns were purchased from GE healthcare. SnakeSkin™ dialysis tubing (MWCO 3 kDa) was purchased from Fisher Scientific.

### 3.5.2 Instrumentation

*NMR Spectroscopy.* <sup>1</sup>H and <sup>13</sup>C nuclear magnetic resonance (NMR) spectra were recorded on a Bruker AVIII-300 spectrometer, Bruker AVIII-400 or Bruker Advance III AV600 in the solvents indicated at 298 K. Chemical shifts are reported on the δ scale in parts-per-million (ppm) and are referenced to the residual non-deuterated and deuterated solvent resonances respectively. (CDCl<sub>3</sub> <sup>1</sup>H: δ = 7.26 ppm; <sup>13</sup>C: δ = 77.2 ppm).

*High-Resolution Mass Spectrometry.* HRMS spectra were recorded by the MS Analytical Facility Service at the University of Birmingham on a Waters Xevo G2-XS QToF Quadrupole Time-of-Flight mass spectrometer.

*High-Performance Liquid Chromatography.* High-Performance Liquid Chromatography (HPLC) analysis of oligonucleotides was performed on a Varian 9250 with autosampler or a modular Shimadzu instrument with the following modules: CBM-20A system controller, LC-20AD solvent deliver module, SIL-20AC HT autosampler, CTO-20AC column oven, SPD-M20A photodiode array UV-Vis detector, RF-20A spectrofluorometric detector and a FRC-10 fraction collector. Chromatography was performed on a Waters XBridge™ OST C18 2.5 μM column heated to 60 °C. Flow rate was set at 0.8 mL/min and a linear gradient of buffers A and B: buffer A, 0.1 M TEAA, in a 95:5 mixture of H<sub>2</sub>O and acetonitrile; buffer B, 0.1 M TEAA, in a 30:70 mixture of H<sub>2</sub>O and acetonitrile.

*Liquid Chromatography-Mass Spectrometry.* Liquid chromatography-mass spectrometry (LCMS) analysis of oligonucleotides was performed on an Agilent 1200 HPLC system coupled to a Bruker AmazonX high resolution ion trap, in negative ion mode. The desalted oligonucleotide samples were eluted through a XBridge oligonucleotide BEH C18 column (130 Å, 2.5 μm, 4.6 x 50 mm) using a 5 vol% MeOH, 10 mM ammonium acetate (buffer A) and a 70 vol% MeOH, 10 mM ammonium acetate (buffer B) solvent system at 0.8 mL/min flow. The data was processed using Compass Data Analysis (Bruker) v.4.1 software, and the MaxEnt integrated deconvolution algorithm. Alternatively, LCMS analysis was performed on a Waters ACQUITY UPLC system coupled to a Xevo GS2-XS qToF mass spectrometer in negative ion mode. The oligonucleotides were eluted through an ACQUITY UPLC oligonucleotide BEH C18

column (130Å, 1.7 µm, 2.1 x 50 mm) using a 75 mM triethylammonium acetate (TEAA, pH 7.0) solution in H<sub>2</sub>O (buffer A) and a 75 mM TEAA solution in MeCN (buffer B) at 60 °C and a 0.2 mL/min flow. The data was processed using ProMass HR software.

*Gel Electrophoresis.* Native polyacrylamide gels were run at 2 °C in 1 x TAE buffer at 180V – 200V using a vertical nucleic acid electrophoresis cell connected to a PowerPack basic power supply (BioRad). Samples were combined with 20% loading buffer (0.05% bromophenol blue, 25% glycerol, 1x TAE) prior to running. Non-fluorescent DNA was stained using a 1:1000 aqueous SYBR<sup>®</sup> Gold nucleic acid gel stain (ThermoFisher) and visualized using a BioRad ChemiDoc™ MP Imaging system. The images were processed using ImageLab software. Denaturing polyacrylamide gels (15% acrylamide, 25% formamide) were run at room temperature in 1 x TBE buffer at 14 amps using a vertical nucleic acid electrophoresis cell connected to a PowerPack basic power supply (BioRad). The samples were diluted 1:1 v/v with formamide solution (90 % formamide) and heated at 70 °C for 10 min prior to running. Non-fluorescent DNA was stained using a 1:1000 aqueous SYBR<sup>®</sup> Gold nucleic acid gel stain (ThermoFisher) and visualized using a BioRad ChemiDoc™ MP Imaging system. The images were processed using ImageLab software.

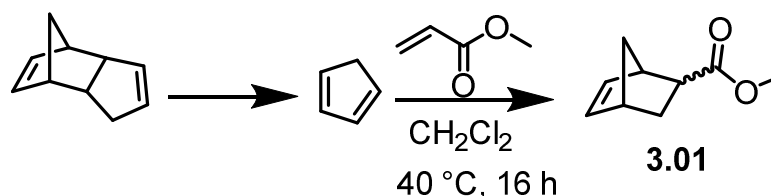
*Size Exclusion Chromatography.* Size exclusion chromatography (SEC) in DMF was performed on an Agilent 1260 Infinity II LC system equipped with a Wyatt DAWN HELEOS II multi-angle laser light scattering (MALLS) detector, a Wyatt Optilab T-rEX differential refractive index detector, an Agilent 1260 Infinity II WR diode array detector, an Agilent guard column (PLGel 5 µM, 50 × 7.5 mm) and two Agilent Mixed-C columns (PLGel 5 µM, 300 × 7.5 mm). The mobile phase was DMF (HPLC grade) containing 5 mM NH<sub>4</sub>BF<sub>4</sub> at 50 °C at flow rate of 1.0 mL min<sup>-1</sup>.

Number average molar mass ( $M_n$ ), mass average molar mass ( $M_w$ ) and dispersities ( $D_M = M_w/M_n$ ) were determined using Wyatt ASTRA v7.1.3 software against poly(methyl methacrylate) (PMMA) standards.

*Fluorescence Spectroscopy.* Fluorescence spectral data was determined using an Edinburgh Instruments FS5 spectrofluorometer. The fluorescence of **P1-ACM** and **P3-ACM** was recorded in differing volumes of H<sub>2</sub>O/DMF recording the full emission spectra recorded following excitation at 380 nm. The fluorescence hybridization studies were conducted by recording the emission at 580 nm of **P3\*** excited at 545 nm in Tris buffer (10 mM Tris, 100 mM NaCl, 20 mM MgCl<sub>2</sub> and 1 mM EDTA).

*Flash Chromatography.* Flash chromatography was performed on a Teledyne ISCO CombiFlash Rf+ Lumen. Samples were purified using RediSep RF normal phase columns.

### 3.5.3 Synthesis of 3.01



The synthesis was adapted from a literature method.<sup>32</sup> Freshly prepared cyclopentadiene (34 mL, 0.40 mol) generated by the pyrolysis of dicyclopentadiene was added to methyl acrylate (40 mL, 0.44 mol) and dichloromethane (40 mL). The mixture was refluxed for 16 h prior to concentration *in vacuo* to yield 3.01 (ca. 20% *exo*) as a colourless oil (54.8 g, 90%).

*Endo* (major):  $^1\text{H NMR}$  (400 MHz; 298K;  $\text{CDCl}_3$ )  $\delta$  = 6.19 (dd, 1H,  $^3J_{\text{H-H}} = 5.7, 3.0$  Hz, *CHCH*), 5.92 (dd, 1H,  $^3J_{\text{H-H}} = 5.7, 3.0$  Hz, *CHCH*), 3.62 (s, 3H,  $\text{CH}_3$ ), 3.22-3.18 (m, 1H, *CH*), 2.95 (dt, 1H,  $^3J_{\text{H-H}} = 9.3, 3.9$  Hz, *CH*), 2.90 (s, 1H, *CH*), 1.95-1.86 (m, 1H,  $\text{CH}_2$ ), 1.55-1.24 (m, 3H, 2 x  $\text{CH}_2$ ).

*Exo* (minor):  $^1\text{H NMR}$  (400 MHz; 298K;  $\text{CDCl}_3$ )  $\delta$  = 6.16-6.08 (m, 2H, *CHCH*), 3.69 (s, 3H,  $\text{CH}_3$ ), 3.04 (s, 1H, *CH*), 2.88 – 2.92 (m, 1H, *CH*), 2.26-2.20 (m, 1H,  $\text{CH}_3$ ), 1.95-1.86 (m, 1H,  $\text{CH}_2$ ), 1.55-1.24 (m, 3H, 2x  $\text{CH}_2$ ).

Characterization matches that reported in the literature.<sup>53</sup>

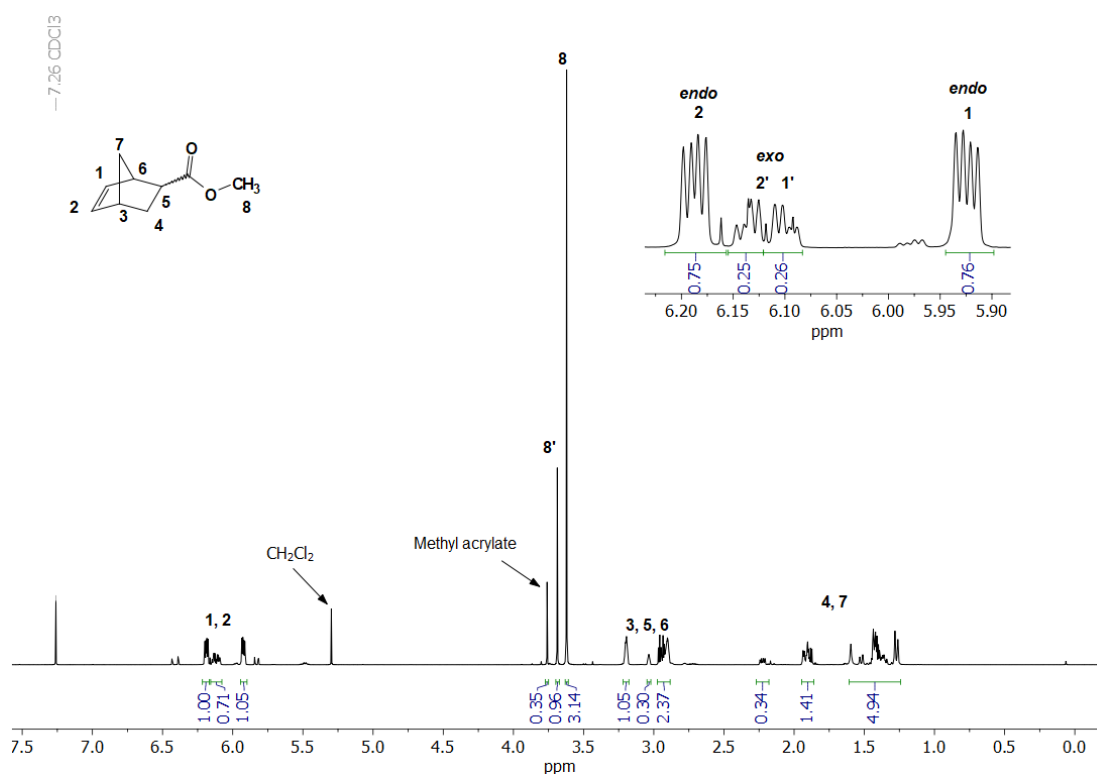
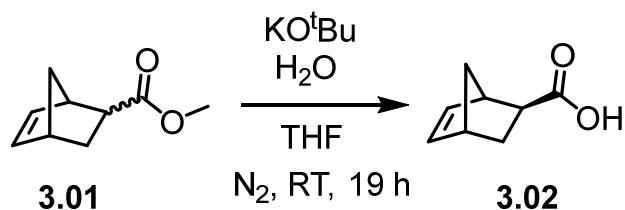


**Figure 3.28**  $^1\text{H NMR}$  spectrum of 3.01 in  $\text{CDCl}_3$  (400 MHz, 298K).

### 3.5.4 Synthesis of 3.02



The synthesis was adapted from a literature method.<sup>35</sup> Potassium t-Butoxide (80.8 g, 0.72 mol) and THF (720 mL) were added to a 2L 3-necked flask purged with N<sub>2</sub>. **3.01** (54.7 g, 0.36 mol) was added to the flask and stirred at room temperature for 1 h. H<sub>2</sub>O (6.5 mL, 0.36 mol) was added to the flask and stirred at room temperature for 1 h. H<sub>2</sub>O (6.5 mL, 0.36 mol) was diluted with THF (338 mL) and added dropwise to the reaction mixture over 18 h. Excess H<sub>2</sub>O (≈ 80 mL) was added to complete the reaction and the reaction mixture was stirred for a further 1 h. The reaction mixture was concentrated to remove THF, diluted with water and then adjusted to pH 2 by the addition of concentrated HCl. The aqueous solution was then extracted with EtOAc (2 x 200 mL) and the organic layers were dried over MgSO<sub>4</sub> and then concentrated. Following rotary evaporation **3.02** (ca. 85% *exo*) was obtained (40.3 g, 81%).

Removal of the *endo*-isomer was carried out using a previously described protocol.<sup>54</sup> **3.02** (85% *exo*) (40 g, 0.29 mol) was dissolved in an aqueous solution of NaHCO<sub>3</sub> (26.76 g, 0.32 mol in 400 mL H<sub>2</sub>O). NaHCO<sub>3</sub> was added until the reaction mixture was around pH 10. In a separate flask, I<sub>2</sub> (49.2 g, 0.19 mol) and KI (52.8 gm 0.32 mol) were dissolved in H<sub>2</sub>O (800 mL). The I<sub>2</sub>/KI solution was added slowly to the flask containing the *endo/exo* norbornene acid until the solution retained a dark brown color. The reaction mixture was then filtered and transferred to a separatory funnel. The aqueous solution was washed with Et<sub>2</sub>O (5 x 500 mL) to remove the iodolactone formed by the *endo* isomer. The aqueous layer was decolorized using solid Na<sub>2</sub>SO<sub>3</sub> and acidified to pH 2 with conc. H<sub>2</sub>SO<sub>4</sub>. The product was extracted with Et<sub>2</sub>O (4 x 500

mL) and the combined organic layers were dried over Na<sub>2</sub>SO<sub>4</sub> and concentrated *in vacuo* to yield **3.02** (100% *exo*) as a pale yellow solid (20.2 g, 51%). <sup>1</sup>H NMR (CDCl<sub>3</sub>; 298K; 300 MHz) δ = 6.20-6.08 (m, 2H, CHCH), 3.11 (s, 1H, CH), 2.94 (s, 1H, CH), 2.29-2.24 (m, 1H, CH), 1.99-1.87 (m, 1H, CH<sub>2</sub>), 1.58-1.34 (m, 3H, CH<sub>2</sub>). Characterization matches that reported in the literature.<sup>54</sup>

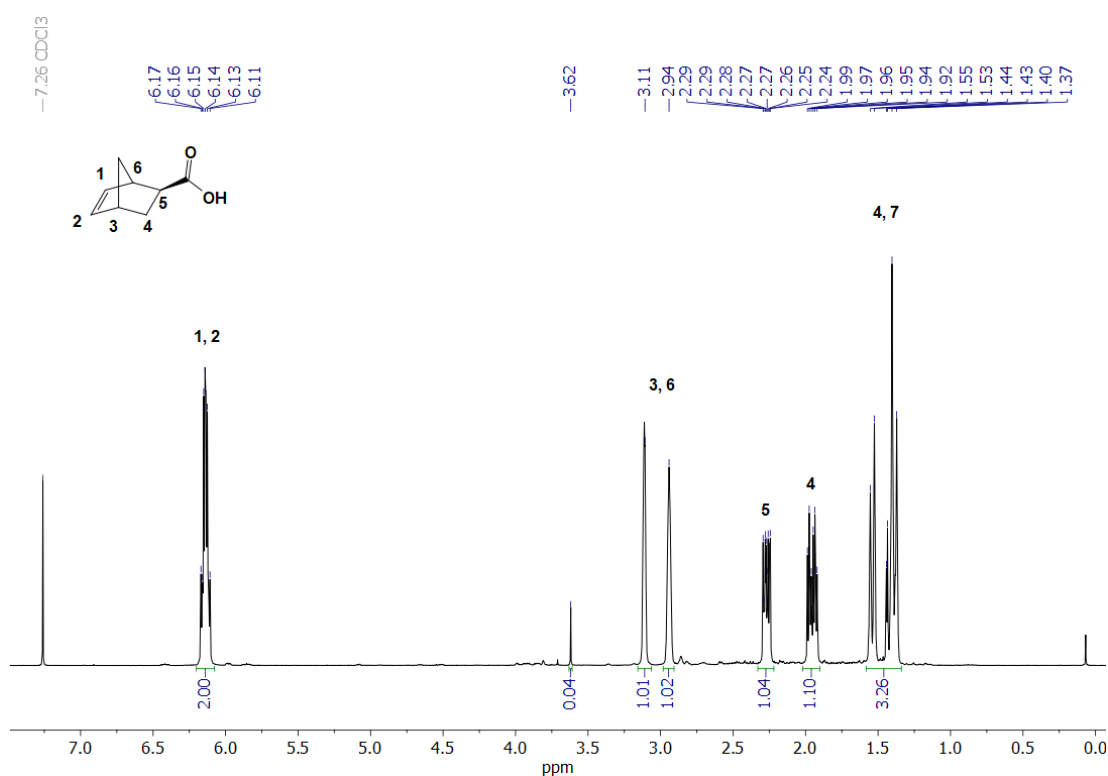
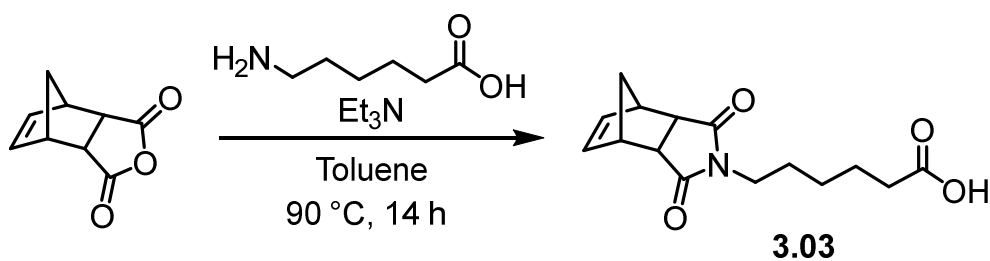


**Figure 3.29** <sup>1</sup>H NMR spectrum of **3.02** in CDCl<sub>3</sub>. (300 MHz, 298K).

### 3.5.5 Synthesis of 3.03



The synthesis of **3.03** was conducted by Dr Jeffrey Foster. A round bottom flask was charged with *cis*-5-Norbornene-*exo*-2,3-dicarboxylic anhydride, aminohexanoic acid, triethylamine, and toluene. The flask was fitted with a condenser, and the reaction mixture was heated at reflux for 14 h. The reaction mixture was then cooled to room temperature and concentrated under reduced pressure. The resulting residue was re-dissolved in EtOAc, and the organic solution was washed with 1N HCl (2x) and brine, dried over MgSO<sub>4</sub>, and concentrated under reduced pressure to yield the pure product as an off-white solid. <sup>1</sup>H NMR (CDCl<sub>3</sub>; 298K; 400 MHz) δ = 6.28 (s, 2H, CH), 3.51 – 3.43 (m, 2H, CH), 3.27 (s, 2H, CH), 2.67 (m, 2H, CH<sub>2</sub>), 2.34 (t, <sup>3</sup>J<sub>H-H</sub> = 7.4 Hz, 2H, CH<sub>2</sub>), 1.71 – 1.47 (m, 5H, CH<sub>2</sub>), 1.35 (m, 2H, CH<sub>2</sub>), 1.21 (d, <sup>3</sup>J<sub>H-H</sub> = 9.8 Hz, 1H, CH<sub>2</sub>). <sup>13</sup>C NMR (CDCl<sub>3</sub>; 298K; 100 MHz) 137.86, 47.82, 47.82, 45.18, 42.74, 38.43, 33.58, 27.43, 26.35, 24.15. HR-MS [M+H]<sup>+</sup> m/z calculated 276.1236, found 276.1239.

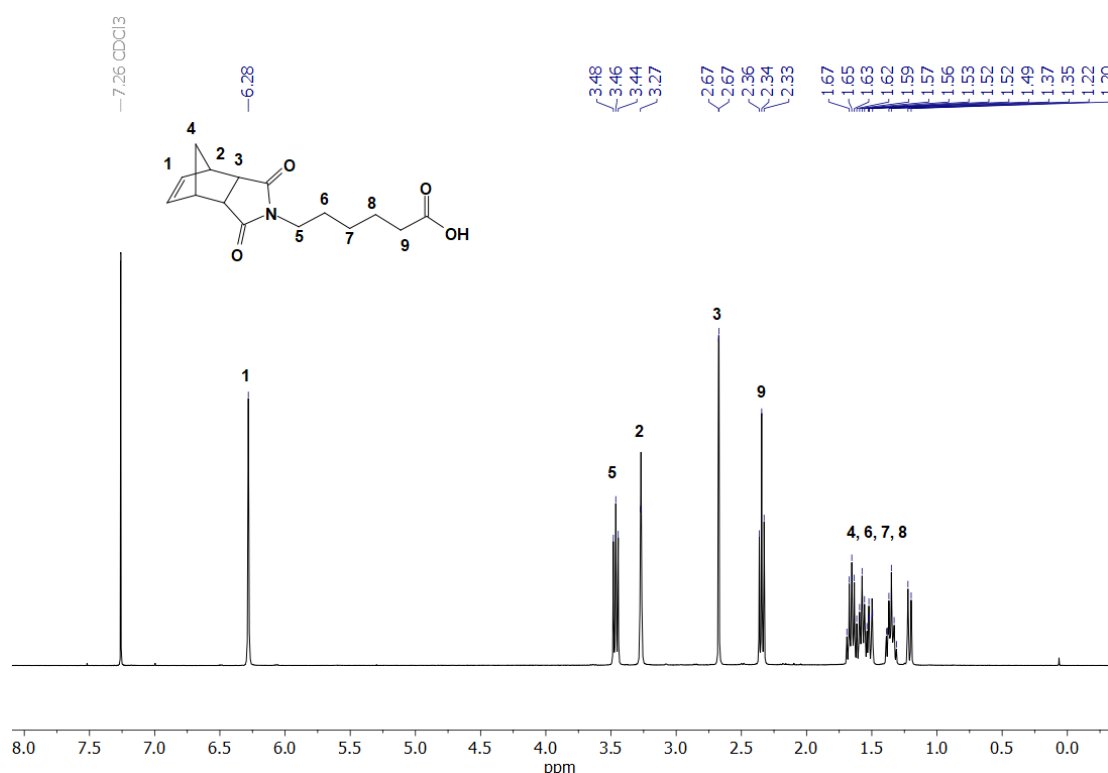


**Figure 3.30** <sup>1</sup>H NMR spectrum of **3.03** in CDCl<sub>3</sub> (400 MHz, 298K).



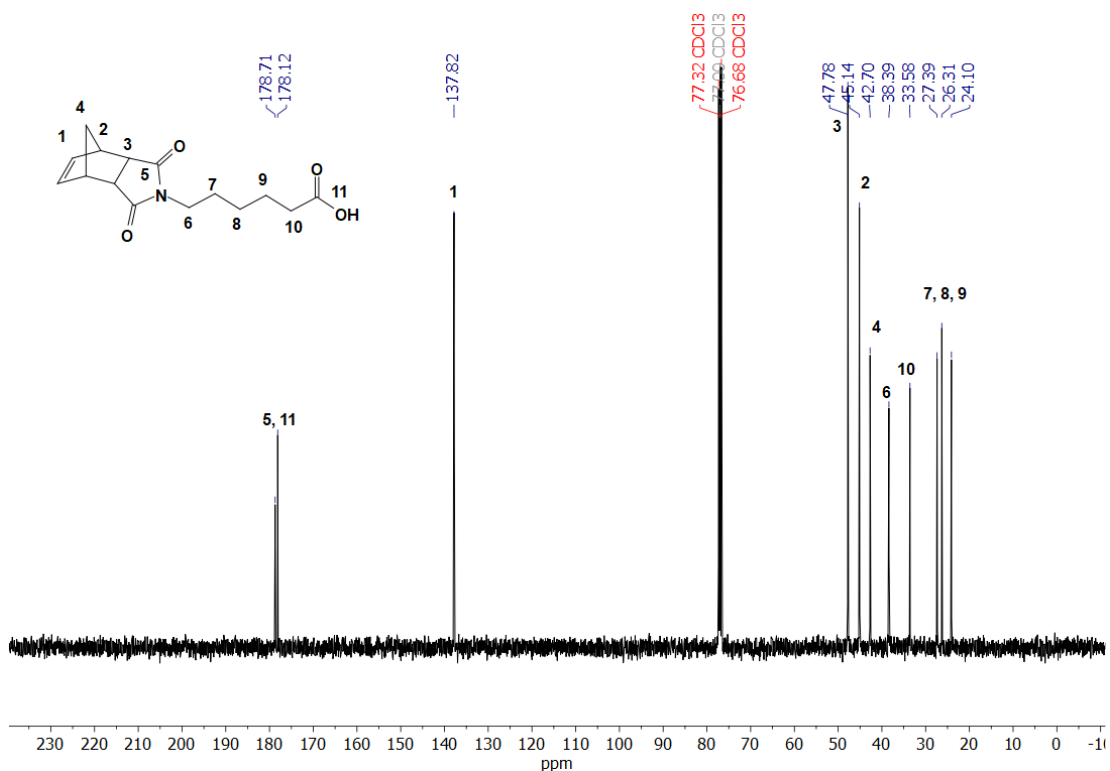
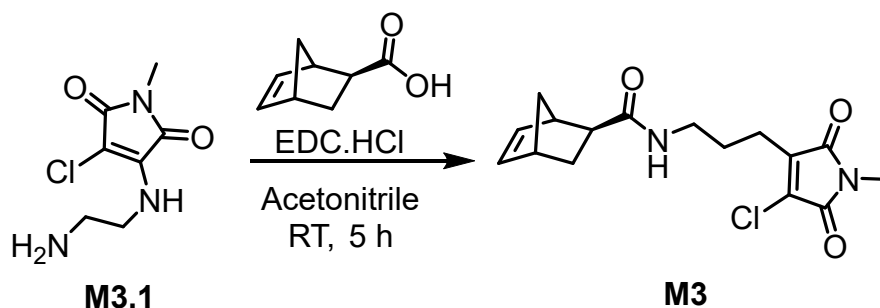


**Figure 3.31**  $^{13}\text{C}$  NMR spectrum of **3.03** in  $\text{CDCl}_3$  (100 MHz, 298K).

### 3.5.6 Synthesis of M3



The synthesis of **M3** was conducted by Dr Jonathan Husband. A round-bottom flask was charged with *exo*-norbornene carboxylic acid (85 mg, 0.41 mmol), 20 mL of acetonitrile and a magnetic stirrer bar. EDC (130 mg, 0.62 mmol) was added, followed by ethylamine-ACM **M3.1** (100 mg, 0.41 mmol). The reaction mixture was stirred for 5 h at which point the solution was dried and purified *via* silica flash column chromatography and eluted with a methanol (0-5%) in  $\text{CH}_2\text{Cl}_2$  gradient, to yield solid **ACM<sub>Nb</sub>** (73 mg, 49%).  $^1\text{H}$  NMR ( $\text{CDCl}_3$ ; 298K; 300 MHz)  $\delta$  = 6.08

(dd,  $^3J_{\text{H-H}} = 5.7, 2.9$  Hz, 1H, CH), 6.02 (dd,  $^3J_{\text{H-H}} = 5.7, 3.0$  Hz, 1H, CH), 5.90 (s, 1H, NH), 5.82 (s, 1H, NH), 3.71 (q,  $^3J_{\text{H-H}} = 5.9$  Hz, 2H, CH<sub>2</sub>), 3.54 (q,  $^3J_{\text{H-H}} = 5.9$  Hz, 2H, CH<sub>2</sub>), 2.99 (s, 3H, CH<sub>3</sub>), 2.93 (m, 2H, CH), 1.99 – 1.89 (m, 1H, CH), 1.89 – 1.79 (m, 1H, CH), 1.65 – 1.55 (m, 1H, CH<sub>2</sub>), 1.36 – 1.16 (m, 3H, CH<sub>2</sub>). <sup>13</sup>C NMR (CDCl<sub>3</sub>; 298K; 100 MHz) 177.1 (CO), 167.8 (CO), 165.5 (CO), 140.8 (CN), 138.4 (CH), 135.8 (CH), 89.8, 47.3 (CH), 46.3 (CH<sub>2</sub>), 44.7 (CH), 43.8 (CH<sub>2</sub>), 41.6 (CH<sub>2</sub>), 40.0 (CH), 30.6 (CH<sub>2</sub>), 24.2 (CH<sub>3</sub>). HR-MS [M+H]<sup>+</sup> m/z calculated 346.0934, found 346.0932.

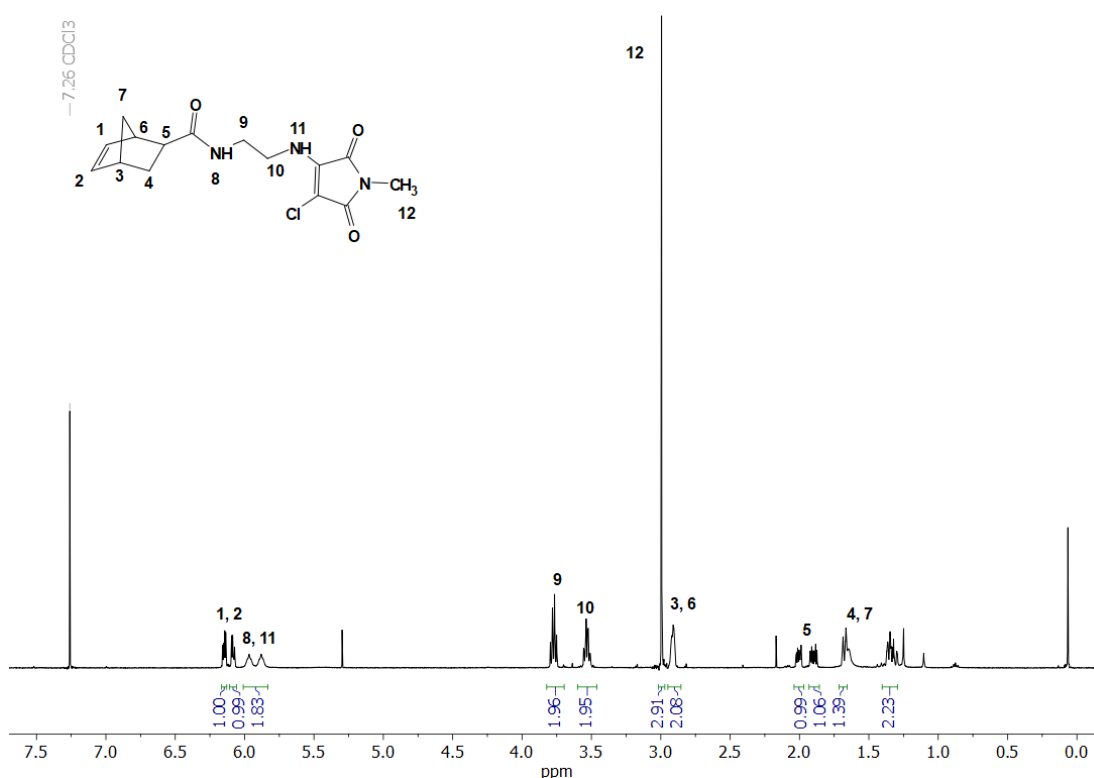


**Figure 3.32** <sup>1</sup>H NMR spectrum of **M3** in CDCl<sub>3</sub> (300 MHz, 298K).

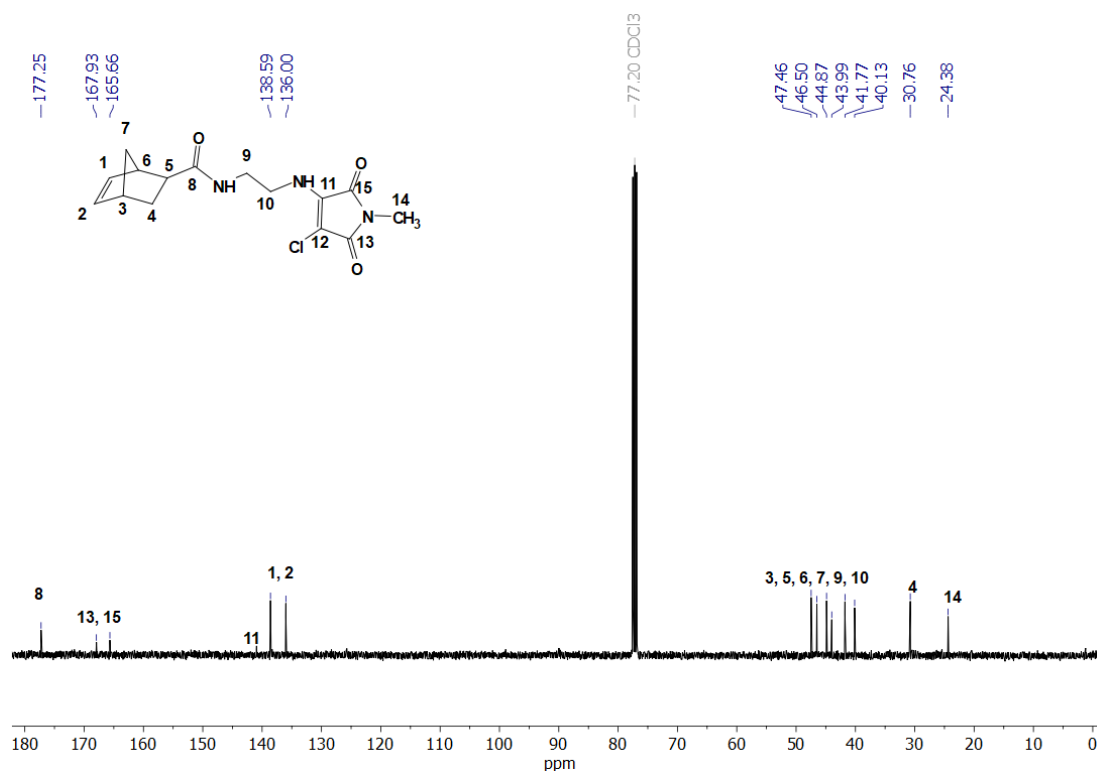
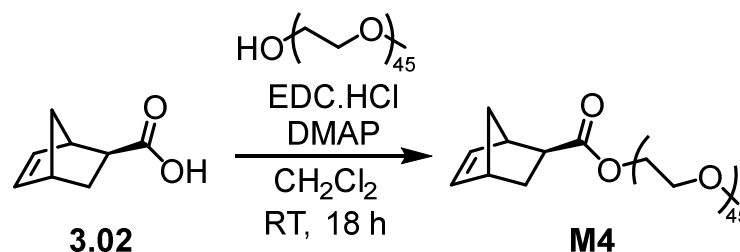


**Figure 3.33**  $^{13}\text{C}$  NMR spectrum of **M3** in  $\text{CDCl}_3$  (100 MHz, 298K).

### 3.5.7 Synthesis of M4



**3.02** (2 g, 14.5 mmol), EDC.HCl (2.78 g, 14.5 mmol), 4-dimethylamino pyridine (0.17 g, 1.4 mmol) and methoxy polyethylene glycol (mw 2000 Da) were solubilised in dichloromethane (50 mL) and stirred at room temperature for 18 h. The solution was washed with 1M HCl solution followed by  $\text{H}_2\text{O}$  and Sat.  $\text{NaHCO}_3$  and finally brine prior to drying over  $\text{MgSO}_4$  and concentrating *in vacuo*. The crude solid was precipitated from dichloromethane into diethyl ether, twice, to yield a white solid (3.18 g, 53%).  $^1\text{H}$  NMR ( $\text{CDCl}_3$ ; 298K; 300 MHz)  $\delta$  = 6.14-6.07 (m, 2H, CHCH), 4.28-4.15 (m, 2H,  $\text{COOCH}_2$ ), 3.86-3.36 (m, 207H,  $\text{OCH}_2$ ), 3.36 (s, 3H,  $\text{OCH}_3$ ), 2.95

(d, 2H, CHCH), 2.31-2.19 (m, 1H, CH<sub>2</sub>CH), 1.91 (dt, 1H, CH<sub>2</sub>), 1.59-1.45 (m, 1H, CH<sub>2</sub>), 1.34 (m, 2H, CH<sub>2</sub>). <sup>13</sup>C NMR (CDCl<sub>3</sub>; 298K; 100 MHz) 138.2 (CO), 135.89 (CH), 70.92 (CH<sub>2</sub>), 46.82 (CH<sub>3</sub>), 46.44 (CH), 43.18 (CH<sub>2</sub>), 41.78 (CH), 30.49 (CH<sub>2</sub>).

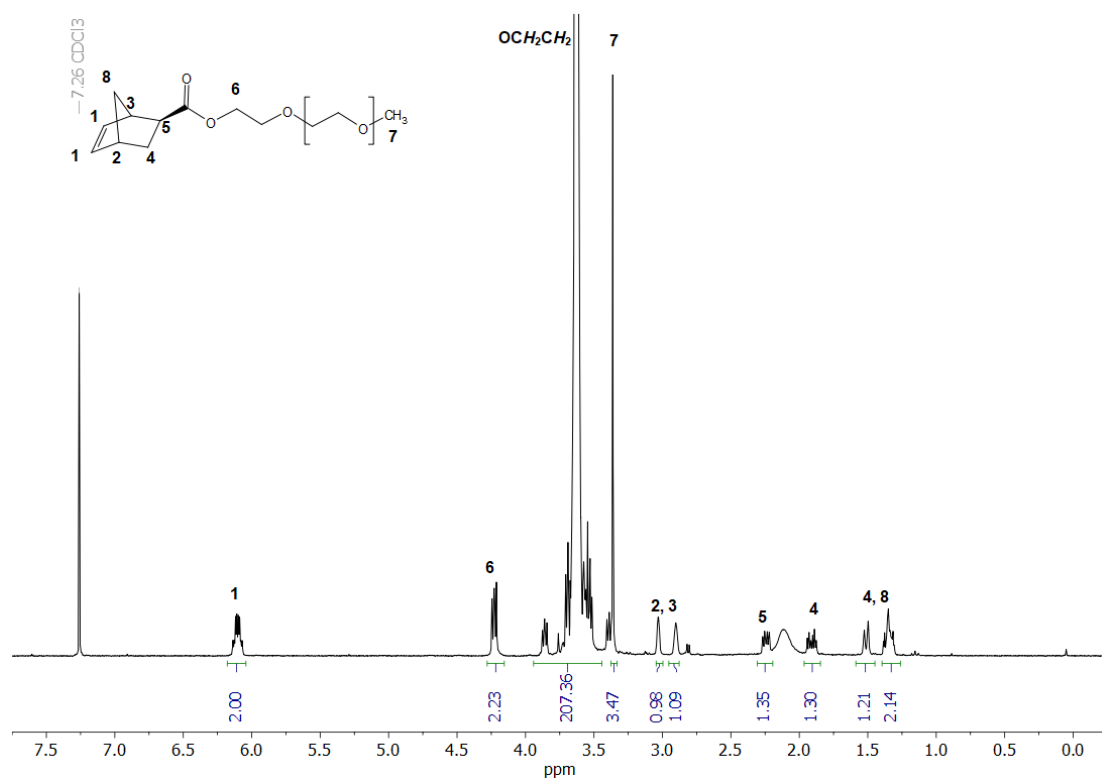


**Figure 3.34** <sup>1</sup>H NMR spectrum of **M4** in CDCl<sub>3</sub> (300 MHz, 298K).

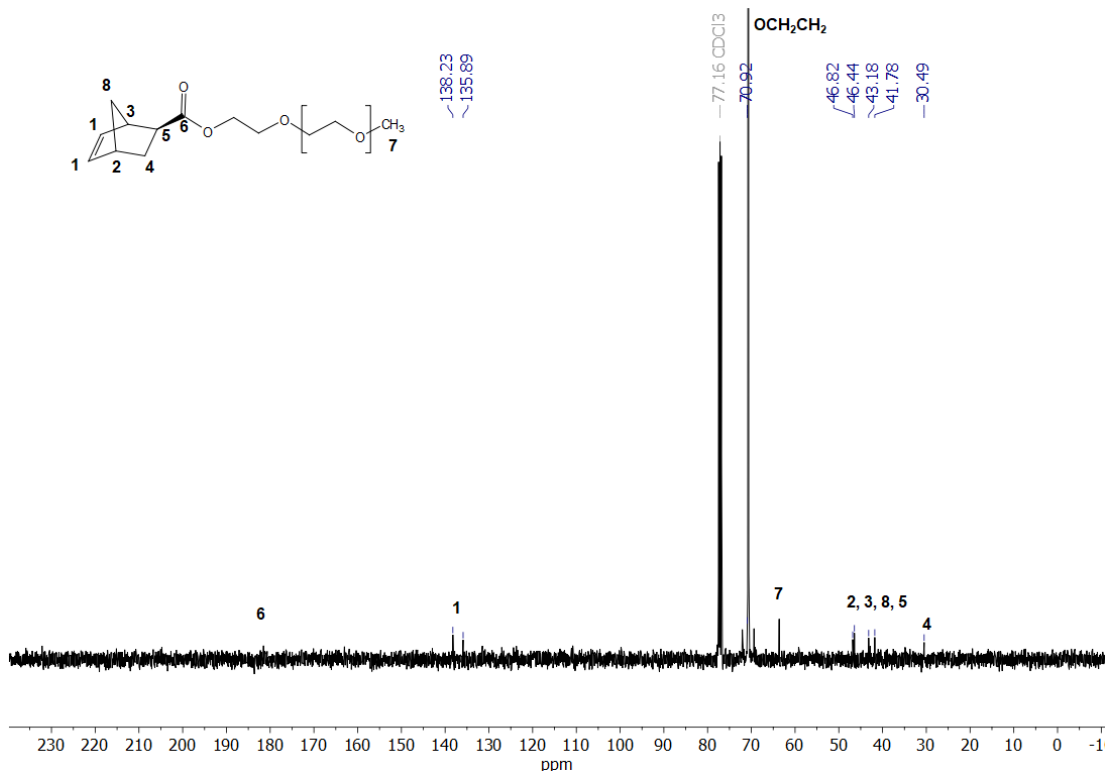
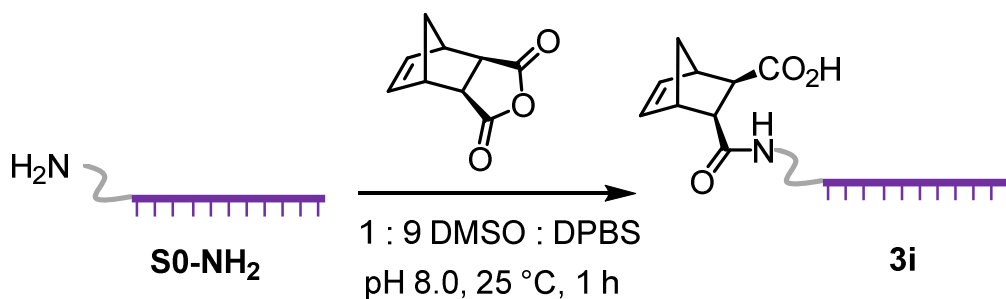


**Figure 3.35**  $^{13}\text{C}$  NMR spectrum of **M4** in  $\text{CDCl}_3$  (100 MHz, 298K)

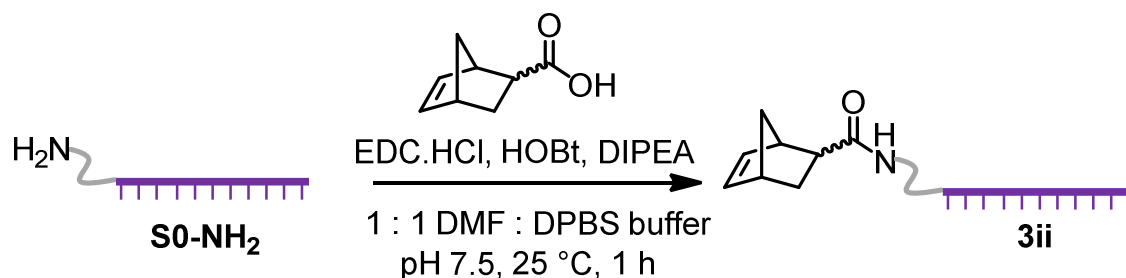
### 3.5.8 Synthesis of **3i**



S0-NH<sub>2</sub> in 18 mΩ H<sub>2</sub>O (1mM, 20 μL, 20 nmol) was diluted with DPBS buffer (adjusted to pH 8 using 0.2 M NaOH). *cis*-5-Norbornene-*exo*-2,3-dicarboxylic anhydride was dissolved in DMSO and added to the oligonucleotide solution (final concentration of S0-NH<sub>2</sub> is 67 μM). After addition was completed, the solution was shaken at room temperature for the desired length of time. Free norbornene was removed *via* elution through a NAP™-5 column equilibrated with 18 mΩ H<sub>2</sub>O and the samples were desalted prior to LCMS analysis through Micro Bio-

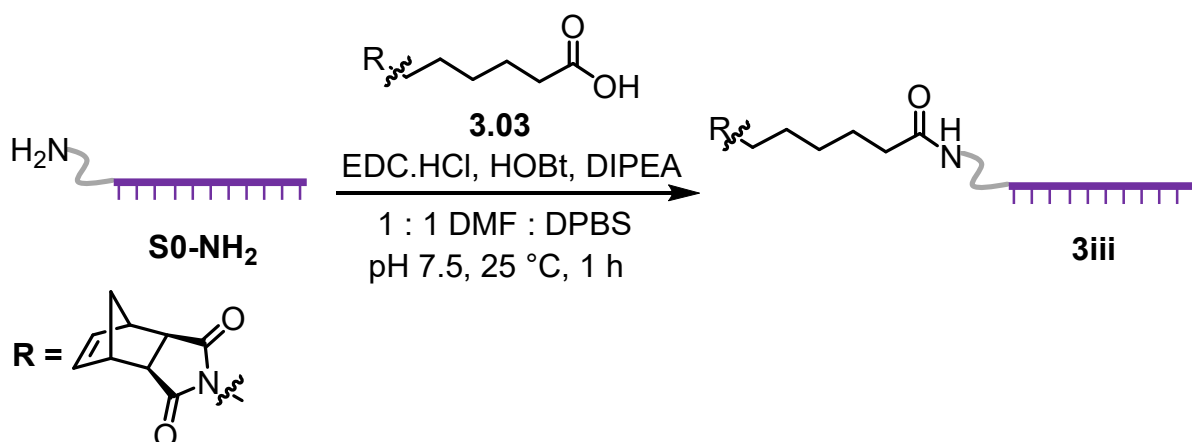
spin™ 6 columns equilibrated with ammonium formate. LC-MS (ESI-)  $m/z$  calculated 5529.0 found 5529.1.

### 3.5.9 Synthesis of 3ii



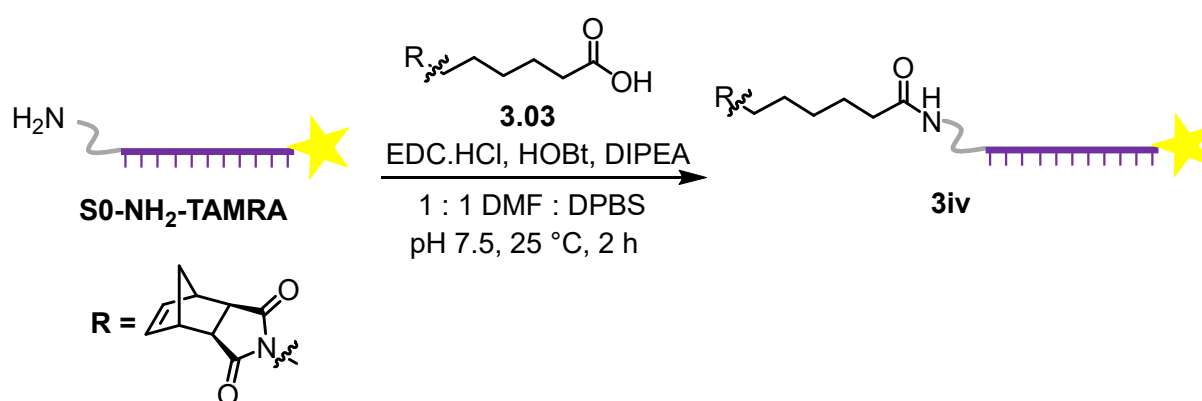
The synthesis was adapted from a literature method.<sup>8</sup> EDC.HCl (100  $\mu\text{L}$ , 300 mM in DMF) was mixed with HOBT (100  $\mu\text{L}$ , 300 mM in DMF), 5-norbornene-2-carboxylic acid (100  $\mu\text{L}$ , 300 mM in DMF) and DPBS (150  $\mu\text{L}$ ) and thoroughly mixed. 300  $\mu\text{L}$  of this solution was mixed with S0-NH<sub>2</sub> in 18 m $\Omega$  H<sub>2</sub>O (100  $\mu\text{L}$ , 200  $\mu\text{M}$ ) and *N,N*-Diisopropylethylamine (DIPEA, 3.6  $\mu\text{L}$ ). After 1 h shaking the flask at room temperature the mixture was filtered through a NAP™-5 column equilibrated with 18 m $\Omega$  H<sub>2</sub>O and then concentrated using an Amicon® Ultra centrifugal filter (3000 Da MWCO). LC-MS (ESI-)  $m/z$  calculated 5487.1, found 5486.5.

### 3.5.10 Synthesis of 3iii



EDC.HCl (100  $\mu$ L, 300 mM in DMF) was mixed with HOBT (100  $\mu$ L, 300 mM in DMF), **3.03** (100  $\mu$ L, 300 mM in DMF) and DPBS (150  $\mu$ L) and thoroughly mixed. 300  $\mu$ L of this solution was mixed with S0-NH<sub>2</sub> in 18 m $\Omega$  H<sub>2</sub>O (100  $\mu$ L, 200  $\mu$ M) and DIPEA (3.6  $\mu$ L). After 1 h shaking the flask at room temperature the mixture was filtered through a NAP™-5 column equilibrated with 18 m $\Omega$  H<sub>2</sub>O and then concentrated using an Amicon® Ultra centrifugal filter (3000 Da MWCO). LC-MS (ESI-) m/z calculated 5624.1, found 5624.1.

### 3.5.11 Synthesis of 3iv



EDC.HCl (100  $\mu$ L, 300 mM in DMF) was mixed with HOBT (100  $\mu$ L, 300 mM in DMF), **3.03** (100  $\mu$ L, 300 mM in DMF) and DPBS (150  $\mu$ L) and thoroughly mixed. 300  $\mu$ L of this solution was mixed with S0-NH<sub>2</sub>-TAMRA in 18 m $\Omega$  H<sub>2</sub>O (100  $\mu$ L, 200  $\mu$ M) and DIPEA (3.6  $\mu$ L). After 2 h shaking the flask at room temperature the mixture was filtered through a NAP™-5 column equilibrated with 18 m $\Omega$  H<sub>2</sub>O and then concentrated using an Amicon® Ultra centrifugal filter (3000 Da MWCO). LC-MS (ESI-) m/z calculated 6633.2, found 6633.2

### 3.5.12 Preparation of P0

A vial was charged with **M2** (10 mg) and 0.9 mL THF (freshly filtered through basic alumina). To the vial was added 100  $\mu$ L of a 15 mg/mL solution of **G3** in THF. The reaction mixture was

stirred for 30 s at room temperature and then 100  $\mu\text{L}$  of this solution was transferred to a vial containing **M2** (10 mg) in 0.9 mL PB2. After 1 h stirring, the polymerization was quenched by the addition of 1 drop of EVE and neutralized with Sat.  $\text{NaHCO}_3$  prior to analysis.

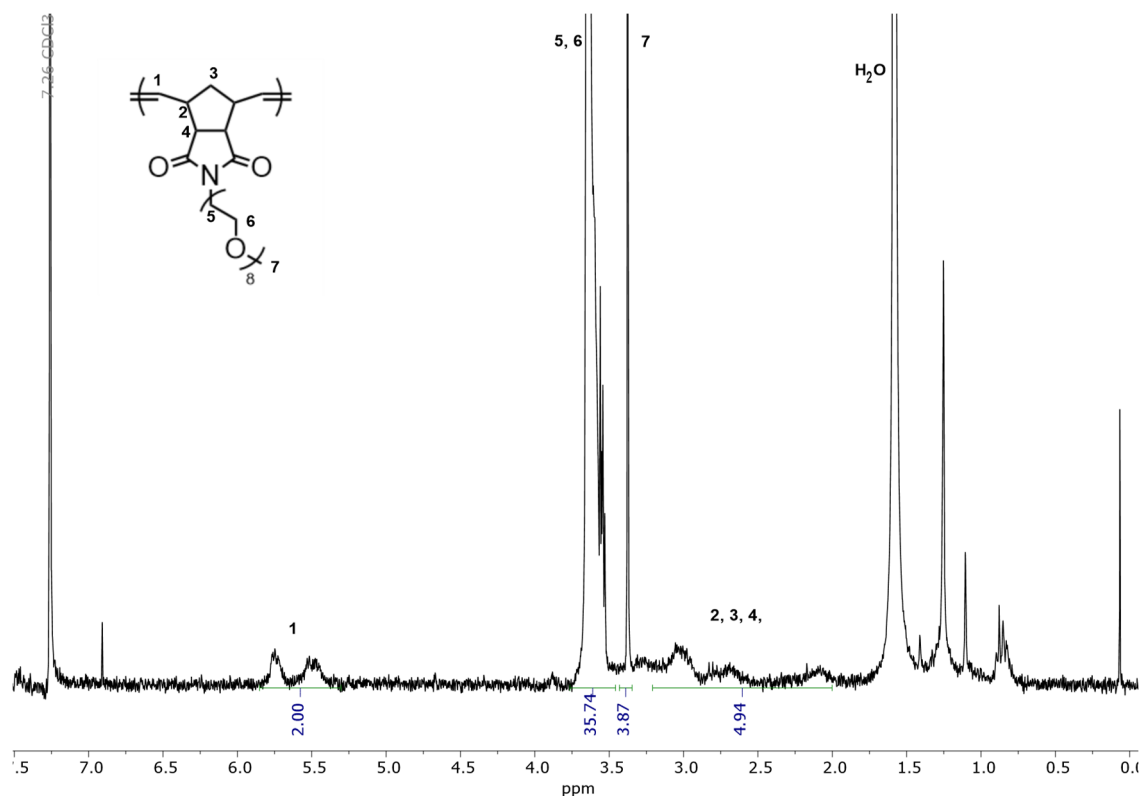


**Figure 3.36**  $^1\text{H}$  NMR spectrum of **P0**. Complete conversion was determined by the disappearance of the norbornene protons expected at 6.2 ppm (300 MHz,  $\text{CDCl}_3$ ).

### 3.5.13 Preparation of P2

A vial was charged with **M4** (20 mg) and 0.9 mL THF (freshly filtered through basic alumina). To the vial was added 100  $\mu\text{L}$  of a 15 mg/mL solution of **G3** in THF. The reaction mixture was stirred for 30 s at room temperature and then 100  $\mu\text{L}$  of this solution was transferred to a vial containing **M4** (10 mg) in 0.9 mL PB2. After 1 h stirring, the polymerization was quenched by the addition of 1 drop of EVE and neutralized with Sat.  $\text{NaHCO}_3$  prior to analysis.



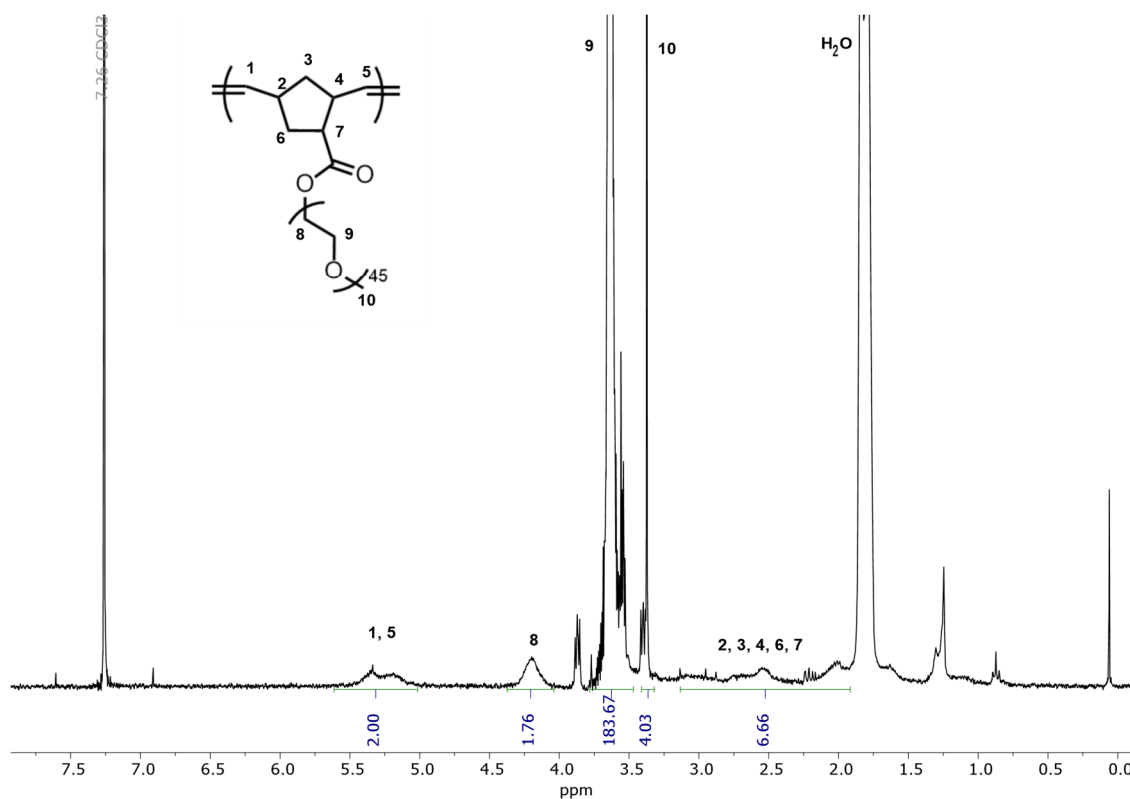


**Figure 3.37**  $^1\text{H}$  NMR spectrum of **P2**. Complete conversion was determined by the disappearance of the norbornene protons expected at 6.2 ppm (300 MHz,  $\text{CDCl}_3$ ).

### 3.5.14 Preparation of P1

The polymerization was conducted as for **P0** except for the addition of **3iii** or **3iv** (ca. 20 nmol) and 10  $\mu\text{L}$  of a 0.05 mg/mL solution of succinimide to the second vial.

### 3.5.15 Preparation of P3

The polymerization was conducted as for **P0** except for the addition of **3iii** or **3iv** (ca. 20 nmol) and 10  $\mu\text{L}$  of a 0.05 mg/mL solution of succinimide to the second vial.

### 3.5.16 DNA-ligation

DNA strands S0-NH<sub>2</sub>, Ligase\_S0 and Ligase\_CO (1  $\mu\text{L}$  of each, 10  $\mu\text{M}$  in 18 m $\Omega$  H<sub>2</sub>O) were mixed with 18 m $\Omega$  H<sub>2</sub>O (87  $\mu\text{L}$ ) and 10  $\times$  T4 DNA ligase buffer (10  $\mu\text{L}$ ) and annealed thermally by heating to 95  $^\circ\text{C}$  and cooling slowly to 15  $^\circ\text{C}$  at 5  $^\circ\text{C min}^{-1}$ . 5  $\mu\text{L}$  sample was removed for PAGE

analysis. To the remaining sample 5  $\mu\text{L}$  (T4 DNA ligase, 400 000 cohesive end units  $\text{mL}^{-1}$ ) was added and the mixture was incubated at room temperature for 1 h. The temperature was then increased to 65°C for 10 minutes to deactivate the enzyme. 50  $\mu\text{L}$  of the sample was removed for PAGE analysis. To the remaining 50  $\mu\text{L}$  of ligase product was added 1  $\mu\text{L}$ , 5  $\mu\text{M}$  Ligase\_C1 and the sample was annealed thermally, as detailed above, prior to analysis by 15% native PAGE.

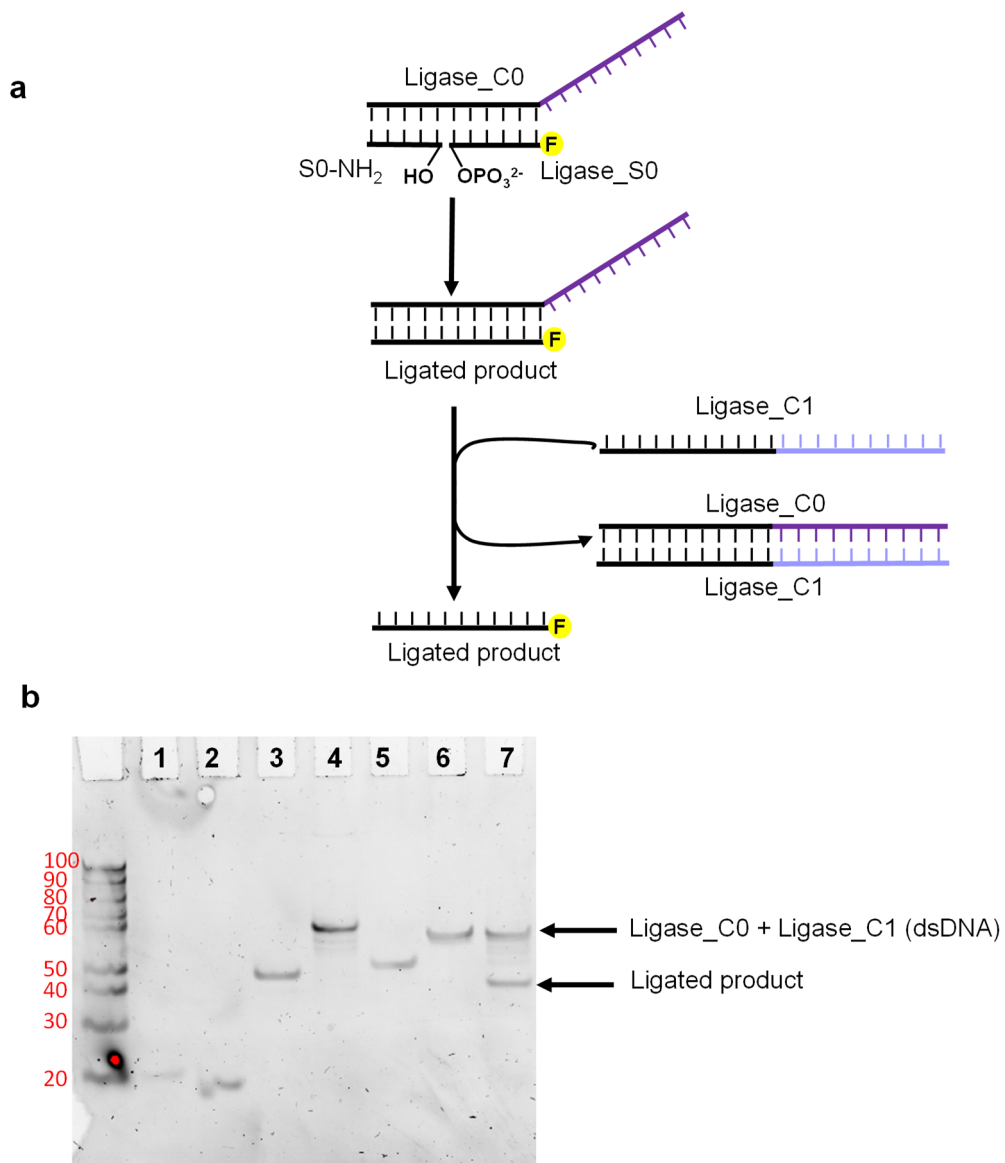


**Figure 3.38** (a) Enzymatic ligation of S0-NH<sub>2</sub> and Ligase\_S0. (b) 15% Native PAGE analysis of S0-NH<sub>2</sub> (lane 1); Ligase\_S0 (Lane 2); Ligase\_CO (Lane 3); Ligase\_S0 + S0-NH<sub>2</sub> + Ligase\_CO (Lane 4); Ligase C1 (Lane 5); Ligase\_C1 + Ligase\_CO (Lane 6). Ligated product after the addition of Ligase\_C1 (Lane 7). The gel was visualized under UV light following SYBR™ Gold staining.

### 3.6 References

1. J. C. Foster, S. Varlas, L. D. Blackman, L. A. Arkinstall and R. K. O'Reilly, *Angew. Chem. Int. Ed.*, 2018, **57**, 10672-10676.
2. J. C. M. van Hest, *Polym. Rev.*, 2007, **47**, 63-92.
3. X. Lu, T.-H. Tran, F. Jia, X. Tan, S. Davis, S. Krishnan, M. M. Amiji and K. Zhang, *J. Am. Chem. Soc.*, 2015, **137**, 12466-12469.
4. M. P. Chien, M. P. Thompson and N. C. Gianneschi, *Chem. Commun.*, 2011, **47**, 167-169.
5. F. Jia, H. Li, R. Chen and K. Zhang, *Bioconjugate Chem.*, 2019, **30**, 1880-1888.
6. K. Matyjaszewski, *Science*, 2011, **333**, 1104.
7. T. R. Wilks, J. Bath, J. W. de Vries, J. E. Raymond, A. Herrmann, A. J. Turberfield and R. K. O'Reilly, *ACS Nano*, 2013, **7**, 8561-8572.
8. T. R. Wilks and R. K. O'Reilly, *Sci. Rep.*, 2016, **6**, 39192.
9. P. He and L. He, *Biomacromolecules*, 2009, **10**, 1804-1809.
10. T. Luckerath, K. Koynov, S. Loescher, C. J. Whitfield, L. Nuhn, A. Walther, C. Barner-Kowollik, D. Y. W. Ng and T. Weil, *Angew. Chem. Int. Ed.*, 2020, **59**, 15474-15479.
11. Y. Tokura, Y. Jiang, A. Welle, M. H. Stenzel, K. M. Krzemien, J. Michaelis, R. Berger, C. Barner-Kowollik, Y. Wu and T. Weil, *Angew. Chem. Int. Ed.*, 2016, **55**, 5692-5697.
12. X. Pan, S. Lathwal, S. Mack, J. Yan, S. R. Das and K. Matyjaszewski, *Angew. Chem. Int. Ed.*, 2017, **56**, 2740-2743.
13. S. Averick, E. Paredes, W. W. Li, K. Matyjaszewski and S. R. Das, *Bioconjugate Chem.*, 2011, **22**, 2030-2037.
14. S. E. Averick, E. Paredes, S. K. Dey, K. M. Snyder, N. Tapinos, K. Matyjaszewski and S. R. Das, *J. Am. Chem. Soc.*, 2013, **135**, 12508-12511.
15. C. W. Bielawski and R. H. Grubbs, *Prog. Polym. Sci.*, 2007, **32**, 1-29.
16. W. Liu, P. J. Nichols and N. Smith, *Tetrahedron Lett.*, 2009, **50**, 6103-6105.
17. J. A. Love, J. P. Morgan, T. M. Trnka and R. H. Grubbs, *Angew. Chem. Int. Ed.*, 2002, **41**, 4035-4037.
18. P. v. R. Schleyer, J. E. Williams and K. R. Blanchard, *J. Am. Chem. Soc.*, 1970, **92**, 2377-2386.
19. T.-L. Choi and R. H. Grubbs, *Angew. Chem. Int. Ed.*, 2003, **42**, 1743-1746.
20. C. R. James, A. M. Rush, T. Insley, L. Vuković, L. Adamiak, P. Král and N. C. Gianneschi, *J. Am. Chem. Soc.*, 2014, **136**, 11216-11219.
21. K. Liu, L. F. Zheng, Q. Liu, J. W. de Vries, J. Y. Gerasimov and A. Herrmann, *J. Am. Chem. Soc.*, 2014, **136**, 14255-14262.
22. X. Tan, H. Lu, Y. Sun, X. Chen, D. Wang, F. Jia and K. Zhang, *Chem*, 2019, **5**, 1584-1596.
23. J. Tomasek and J. Schatz, *Green Chem.*, 2013, **15**, 2317-2338.
24. S. A. Isarov and J. K. Pokorski, *Acs Macro Lett.*, 2015, **4**, 969-973.
25. J. C. Foster, M. C. Grocott, L. A. Arkinstall, S. Varlas, M. J. Redding, S. M. Grayson and R. K. O'Reilly, *J. Am. Chem. Soc.*, 2020, **142**, 13878-13885.
26. S. Varlas, J. C. Foster, L. A. Arkinstall, J. R. Jones, R. Keogh, R. T. Mathers and R. K. O'Reilly, *ACS Macro Lett.*, 2019, **8**, 466-472.
27. S. Sutthasupa, M. Shiotsuki and F. Sanda, *Polym. J.*, 2010, **42**, 905.

28. A. B. Chang, T.-P. Lin, N. B. Thompson, S.-X. Luo, A. L. Liberman-Martin, H.-Y. Chen, B. Lee and R. H. Grubbs, *J. Am. Chem. Soc.*, 2017, **139**, 17683-17693.
29. N. Seehof, S. Grutke and W. Risse, *Macromolecules*, 1993, **26**, 695-700.
30. J. D. Rule and J. S. Moore, *Macromolecules*, 2002, **35**, 7878-7882.
31. M. G. Hyatt, D. J. Walsh, R. L. Lord, J. G. Andino Martinez and D. Guironnet, *J. Am. Chem. Soc.*, 2019, **141**, 17918-17925.
32. M. Kanao, A. Otake, K. Tsuchiya and K. Ogino, *J. Photopolym. Sci. Technol.*, 2009, **22**, 365-370.
33. R. Hoffmann and R. B. Woodward, *J. Am. Chem. Soc.*, 1965, **87**, 4388-4389.
34. S. Niwayama and Y. Hiraga, *Tetrahedron Lett.*, 2003, **44**, 8567-8570.
35. M. Kanao, A. Otake, K. Tsuchiya and K. Ogino, *Int. J. Org. Chem.*, 2012, **2**, 26-30.
36. T. Suzuki, S. Ohsumi and K. Makino, *Nucleic Acids Res.*, 1994, **22**, 4997-5003.
37. R. S. Tuma, M. P. Beaudet, X. Jin, L. J. Jones, C.-Y. Cheung, S. Yue and V. L. Singer, *Anal. Biochem.*, 1999, **268**, 278-288.
38. M. S. Sanford, J. A. Love and R. H. Grubbs, *J. Am. Chem. Soc.*, 2001, **123**, 6543-6554.
39. H. S. Bazzi and H. F. Sleiman, *Macromolecules*, 2002, **35**, 9617-9620.
40. G. Paragi and C. Fonseca Guerra, *Chem. - Eur. J.*, 2017, **23**, 3042-3050.
41. H. Tateishi-Karimata, T. Ohyama, T. Muraoka, P. Podbevsek, A. M. Wawro, S. Tanaka, S.-i. Nakano, K. Kinbara, J. Plavec and N. Sugimoto, *Nucleic Acids Res.*, 2017, **45**, 7021-7030.
42. D. B. Knowles, A. S. LaCroix, N. F. Deines, I. Shkel and M. T. Record, *Proc. Natl. Acad. Sci.*, 2011, **108**, 12699.
43. F. Jia, X. Lu, X. Tan, D. Wang, X. Cao and K. Zhang, *Angew. Chem. Int. Ed.*, 2017, **56**, 1239-1243.
44. S. S. Sheiko, B. S. Sumerlin and K. Matyjaszewski, *Prog. Polym. Sci.*, 2008, **33**, 759-785.
45. C. Feng, Y. Li, D. Yang, J. Hu, X. Zhang and X. Huang, *Chem. Soc. Rev.*, 2011, **40**, 1282-1295.
46. J. Pietrasik, B. S. Sumerlin, R. Y. Lee and K. Matyjaszewski, *Macromol. Chem. Phys.*, 2007, **208**, 30-36.
47. P. E. Theodorakis, W. Paul and K. Binder, *EPL*, 2009, **88**, 63002.
48. C. Li, N. Gunari, K. Fischer, A. Janshoff and M. Schmidt, *Angew. Chem. Int. Ed.*, 2004, **43**, 1101-1104.
49. J.-F. Lutz, *J. Polym. Sci., Part A: Polym. Chem.*, 2008, **46**, 3459-3470.
50. Y. Xie, J. T. Husband, M. Torrent-Sucarrat, H. Yang, W. Liu and R. K. O'Reilly, *Chem. Commun.*, 2018, **54**, 3339-3342.
51. S. Dutta, M. A. Wade, D. J. Walsh, D. Guironnet, S. A. Rogers and C. E. Sing, *Soft Matter*, 2019, **15**, 2928-2941.
52. S. Jimaja, Y. Xie, J. C. Foster, D. Taton, A. P. Dove and R. K. O'Reilly, *Polym. Chem.*, 2020, DOI: 10.1039/D0PY00791A.
53. T.-S. Kim, S.-Y. Seo and D. Shin, *Synlett*, 2015, **26**, 1243-1247.
54. S. C. Radzinski, J. C. Foster and J. B. Matson, *Macromol. Rapid Commun.*, 2016, **37**, 616-621.

# Chapter 4: The Synthesis of Nucleic Acid-Functionalized Metathesis Catalysts

## 4.1 Abstract

Despite an increasing number of reports of multistep DTS over the last decade, the field is still heavily reliant on just two transfer chemistries and thus the identification of new chemistries is a research priority. With an aim to utilize a metathesis transfer reaction, a DNA-functionalized metathesis catalyst was sought. To this end, a range of coupling chemistries were investigated to conjugate Ru-metathesis catalysts to DNA; however, the limited stability of DNA in the presence of the Ru-metathesis catalyst hindered any success. Preliminary studies in the field of PNA-functionalized metathesis catalysts were conducted and may be an indication of the future direction.

## 4.2 Introduction

In Chapter 1 the potential of DTS to template multiple reactions, selectively in one-pot was explored. Furthermore, it was shown how transfer reactions can facilitate autonomous, multistep DTS to afford sequence-defined oligomers in a single solution. This approach is particularly attractive as it avoids the need to manually perform multiple coupling steps which is both costly and time-consuming.

Over the last decade, the O'Reilly and Turberfield Groups, in collaboration, have demonstrated the potential of DTS to prepare sequence controlled-oligomers using acyl transfer<sup>1, 2</sup> or Wittig olefination<sup>1, 3-5</sup> reactions. However, both chemistries displayed limited stability in aqueous media; this severely limited the maximum oligomer length obtained to a

10-mer.<sup>5</sup> Furthermore, each step obtained an average yield of 85% per step, this resulted in very low final yields around 30%.<sup>5</sup> Despite these limitations, investigations into alternative chemistries has so far been limited and is thus, regarded as a priority in order to fully exploit the potential of multistep DTS.

The Nobel Prize winning carbon-carbon double bond forming reaction, olefin cross-metathesis, is a transfer chemistry of high interest, owing to its mild reaction conditions, atom efficiency and tolerance to a wide array of functional groups.<sup>6,7</sup> Furthermore, the widespread utilization of metathesis chemistry has driven the demand for an ever-growing catalogue of metathesis catalysts which can offer improved stability, greater functional-group tolerance, differential solubility and improved catalyst turn-over numbers. Over the last couple of decades the vast majority of reported catalysts are based on the transition metals molybdenum and ruthenium.<sup>8-13</sup> Whilst, molybdenum catalysts can offer extraordinarily fast initiation rates; the inherent instability of these catalysts to air or moisture has somewhat limited their applications. In contrast, ruthenium catalysts offer greater stability, allowing for reactions to be conducted in air and aqueous media, and will therefore be the focus of this chapter.<sup>14</sup>

It was anticipated that the conjugation of ssDNA to a Ru-metathesis catalyst could ultimately lead to the templated transfer of a chemical group from one DNA sequence to the complementary sequence (Figure 4.1). This could ultimately facilitate multistep DTS; however, to date, the exploitation of metathesis in DTS has not yet been explored, and the ability to isolate a DNA-functionalized metathesis catalyst unreported.

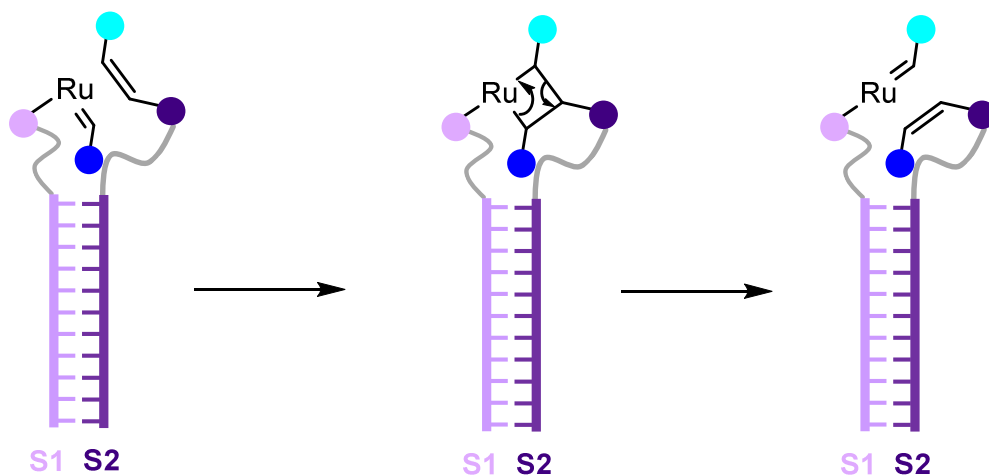


**Figure 4.1** Schematic demonstrating how a templated metathesis reaction can lead to the transfer of chemical groups from one DNA strand (S1) to another (S2) via a metallocyclobutane intermediate.

Four of the most commonly used Ru-based metathesis catalysts were introduced in Chapter 1 and are shown in Figure 4.2. The catalysts, first developed in the late 1990's by the groups of Grubbs and Hoveyda, have often been used as the scaffolds for further functionalization to achieve a large portfolio of catalysts. Catalysts have been designed to support immobilization,<sup>15, 16</sup> aqueous stability,<sup>17, 18</sup> or thermo-switchable behavior.<sup>19</sup>

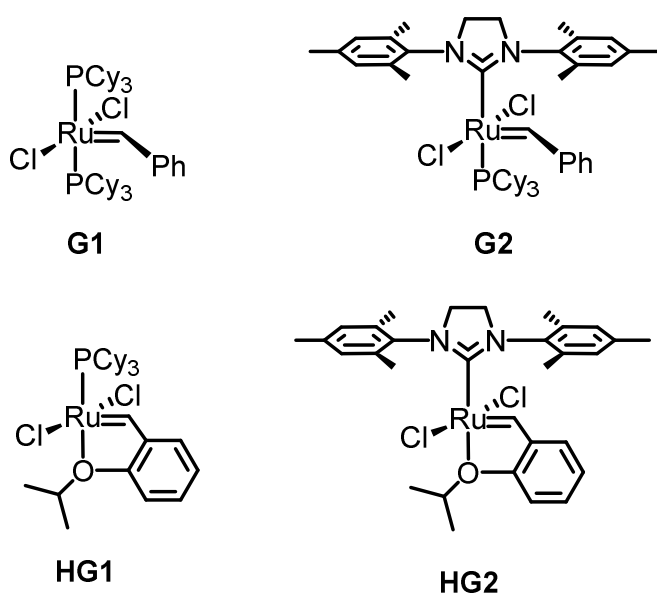


**Figure 4.2** Ru-based metathesis catalysts developed by the groups of Grubbs and Hoveyda.<sup>9, 12, 13, 20-23</sup>

Functionalization of Ru-based metathesis catalysts has been demonstrated through the (1) phosphane ligand, (2) NHC ligand, or (3) benzylidene ligand.<sup>24</sup> However, as phosphine-free catalysts exhibit greater stability from air and moisture, this project will focus on the latter two positions, Figure 4.3.<sup>25</sup> The properties of the catalysts functionalized at the two differing locations varies significantly and can be explained by taking a closer look at the metathesis mechanism.

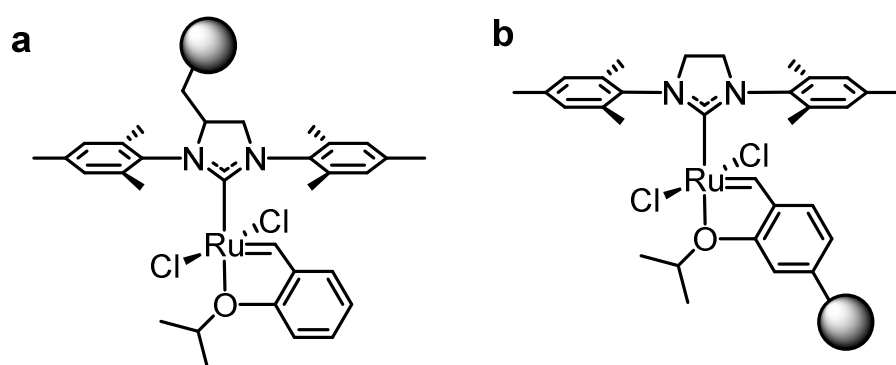


**Figure 4.3** Functionalization locations on HG2 type catalysts (a) through the NHC ligand (b) through the benzylidene ligand.

Functionalization through the alkylidene ligand leads to a ‘boomerang’ or ‘release and return’ mechanism as shown in Figure 4.4.<sup>26</sup> During the initiation step the catalyst becomes detached from the functionalized alkylidene ligand and will thus go on to react with the substrate in a homogenous manner until all the substrate is consumed. Upon consumption, the catalyst may return to the alkylidene, leading to catalyst recyclability and recovery. Indeed, Blechert and co-workers demonstrated this approach through the immobilisation of the Ru-catalysts on to oxanorbornene ROMP polymers, this allowed for the metathesis to be carried out in a homogenous manner and then the recovery of the catalyst in high yields *via* precipitation, once all substrate had been consumed.<sup>27</sup>



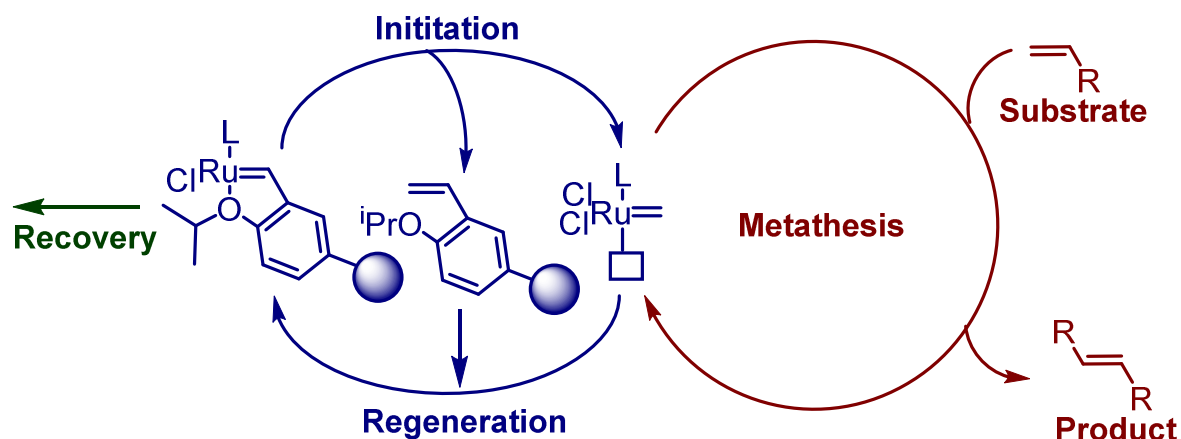


**Figure 4.4** The 'release and return' mechanism, used to recycle and recover Ru-based metathesis catalysts. Figure adapted from Bates *et al.*<sup>26</sup>

In contrast, the NHC ligand forms a strong  $\sigma$ -donor bond with Ru and hence the ligand remains complexed throughout the entire metathesis cycle. As a consequence of this, any functionalization also remains permanently attached to the catalyst throughout. This approach has therefore been heavily exploited to perform metathesis on solid supports.<sup>15, 28</sup> Furthermore, as discussed in chapter 1 - section 1.3.2, functionalization of the NHC ligand with water solubilizing groups such as PEG<sup>29</sup> or cationic groups<sup>30</sup> can render the catalysts water soluble.

Recently, the functionalization of metathesis catalysts has expanded to biomolecules. In 2011, Mayer *et al.* conjugated HG2 through the NHC ligand to a small heat shock protein from *Methanocaldococcus Jannaschii*, in an attempt to prepare an artificial metalloenzyme.<sup>31</sup> Several other artificial metalloenzymes for olefin metathesis have been reported using a range of different anchoring chemistries including supramolecular,<sup>32</sup> dative<sup>33</sup> or covalent bonding<sup>34</sup>. The hybridization of a catalytically active transition metal complex with proteins is believed to bring together the benefits of both individual components; explicitly they, combine the broad catalytic scope of transition metal complexes with the high activity and selectivity offered by

enzymes.<sup>35</sup> It was therefore hypothesized that the covalent conjugation of DNA to Ru-metathesis catalysts could be achieved in a similar manner to that of proteins, forming the focus of this chapter.

## 4.3 Results & Discussion

### 4.3.1 Synthesis of DNA-functionalized metathesis catalysts using click chemistry

Initially, the preparations of two DNA-functionalized metathesis catalysts were targeted: (1) functionalization *via* the benzylidene ligand; and (2) functionalization *via* the NHC ligand. In both cases, a mild yet efficient chemistry was required that would allow for the coupling of a hydrophobic Ru-catalyst to hydrophilic DNA. The coupling of DNA to hydrophobic moieties is particularly challenging and usually relies on the use of a solid-support and thus the availability of a DNA synthesizer. However, cleavage from the solid support following solid-phase synthesis usually requires harsh conditions (i.e. highly basic), which are known to promote the degradation of metathesis catalysts; therefore, an efficient solution-phase coupling chemistry was sought.

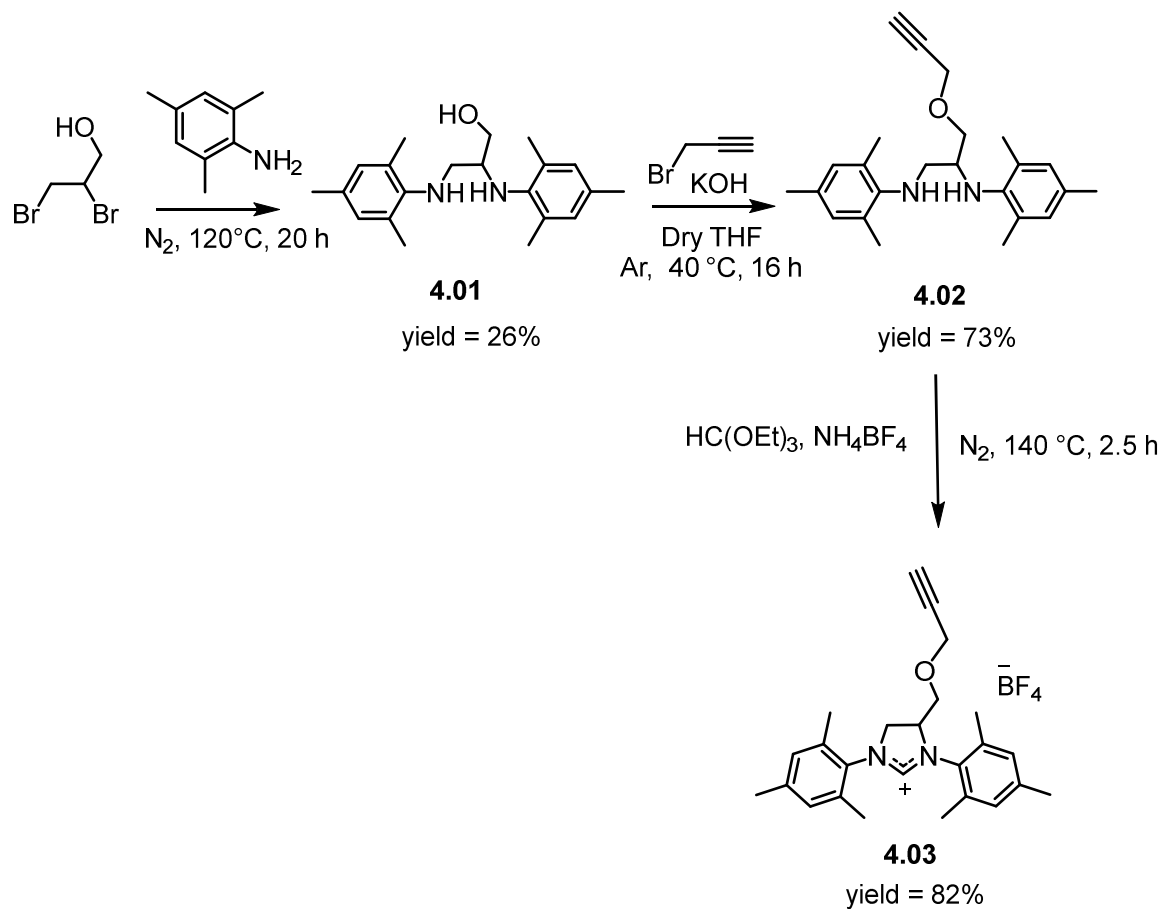
Previously, the group had successfully demonstrated the efficient coupling of hydrophobic polymers to DNA using a CuAAC reaction.<sup>36</sup> This chemistry was particularly appealing due to the commercial availability of azide and alkyne functionalized DNA and thus formed the initial focus of our study.

#### 4.3.1.1 Synthesis of alkyne-functionalized ligands

Initially the preparation of alkyne functionalized benzylidene and NHC ligands were targeted. Whilst metathesis catalysts bearing a variety of functional groups on the NHC ligand have been

prepared, to the best of our knowledge, this would be the first preparation of a catalyst bearing an alkyne group on the NHC ligand; thus, it was anticipated to prove valuable for the coupling of a wide array of moieties to the catalyst including but not limited to DNA. Whilst the use of alkyne functionalized NHC ligands had not been explored in the metathesis community, due to the biological relevance of the imidazolium salt precursors and applications in organic synthesis, functionalization of such derivatives has been well studied.<sup>37</sup> Of significance is a report by Deraedt *et al.*, demonstrating the preparation of alkyne functionalized imidazolium salt (**4.03**) which was derivatized using the CuAAC reaction to prepare dendrimers for Pd nanoparticle stabilization.<sup>38</sup>

In order to prepare an alkyne functionalized NHC ligand for DNA conjugation, the synthesis of **4.03** was conducted as reported by Deraedt *et al.*, in a three-step process from commercially available 2,4,6-trimethylaniline and 2,3-dibromopropanol (Scheme 4.1, Figure 4.5). Comparable yields to those reported in the literature were obtained.<sup>38</sup>



**Scheme 4.1** Synthesis of alkyne functionalized N-heterocyclic ligand (**4.03**) based on a protocol reported by Deraedt et al.<sup>38</sup>

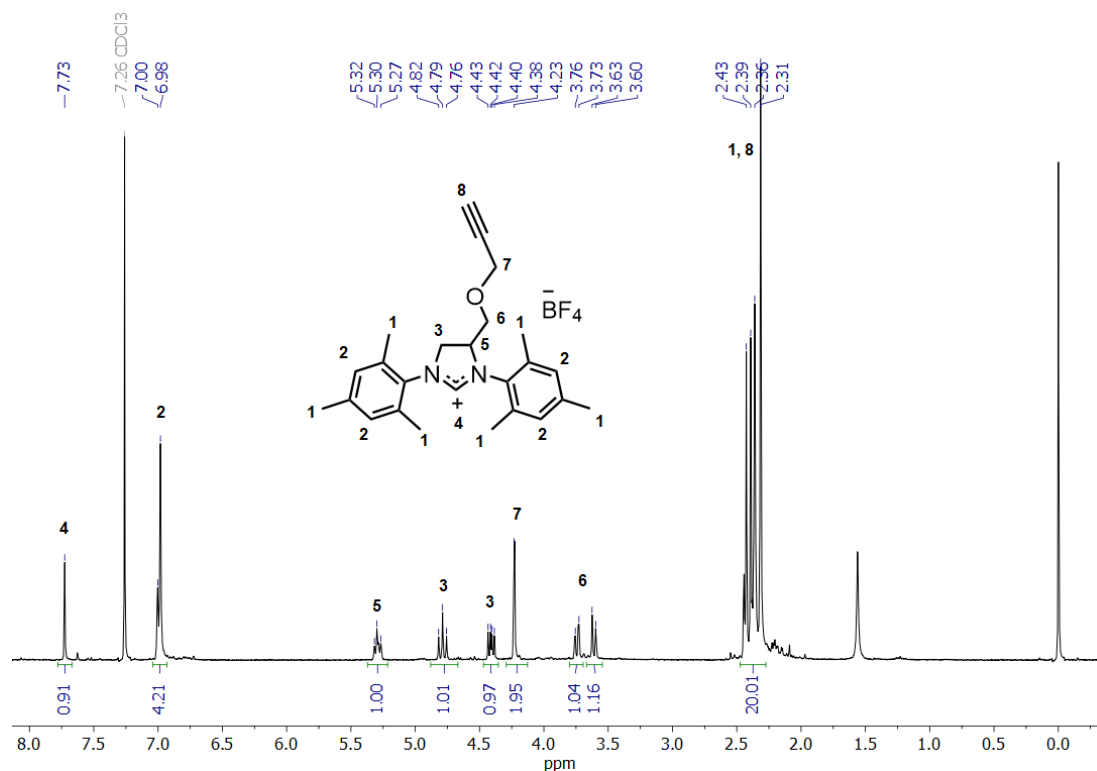
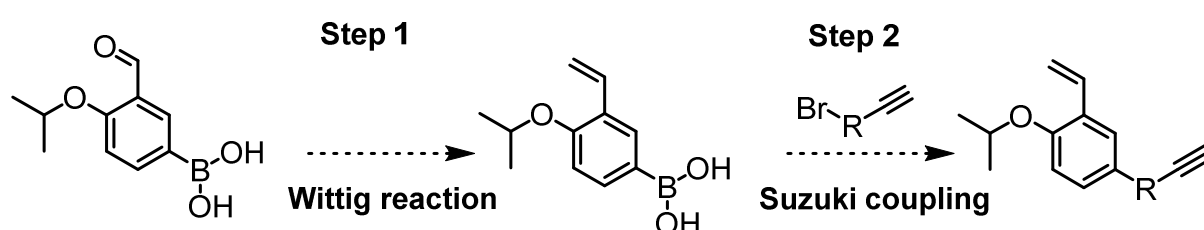


**Figure 4.5** <sup>1</sup>H NMR spectrum of **4.03** in CDCl<sub>3</sub> (400 MHz, 298K).

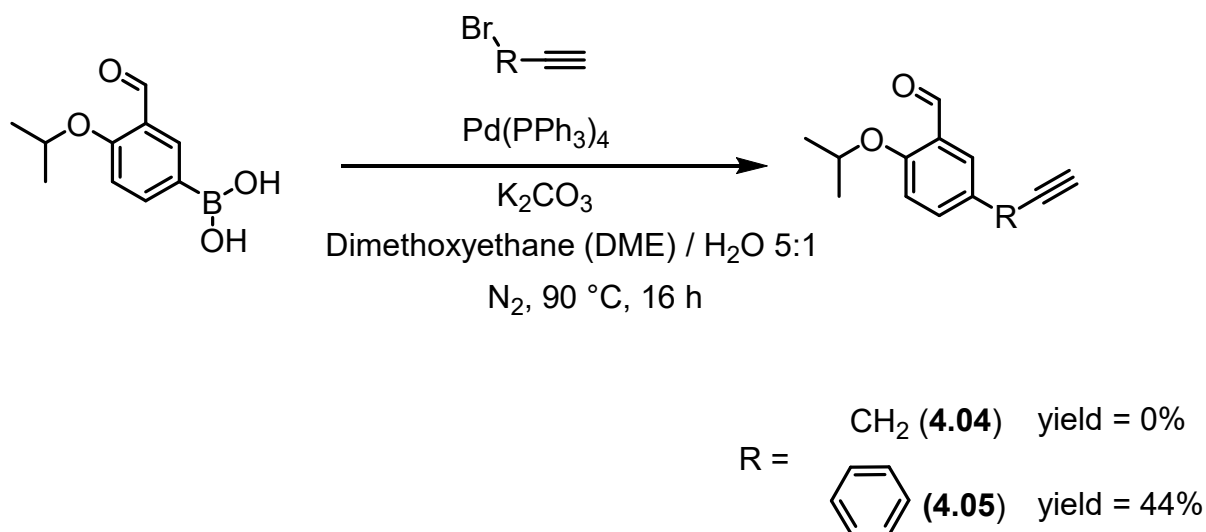
Furthermore, the preparation of metathesis catalysts with an alkyne appended through the benzylidene ligand has been previously reported and well utilized for the immobilization of Grubbs catalysts on to a solid support for heterogeneous catalysis.<sup>39-41</sup> However, the synthesis to prepare an alkyne functionalized benzylidene ligand is usually a five-step process starting from 2,5-dihydroxybenzaldehyde.<sup>39</sup> In this study, a novel two-step synthesis (Scheme 4.2) starting from 3-formyl-4-isopropoxy phenyl boronic acid was designed and attempted.



**Scheme 4.2** Proposed two-step synthesis towards an alkyne-functionalized benzylidene ligand.

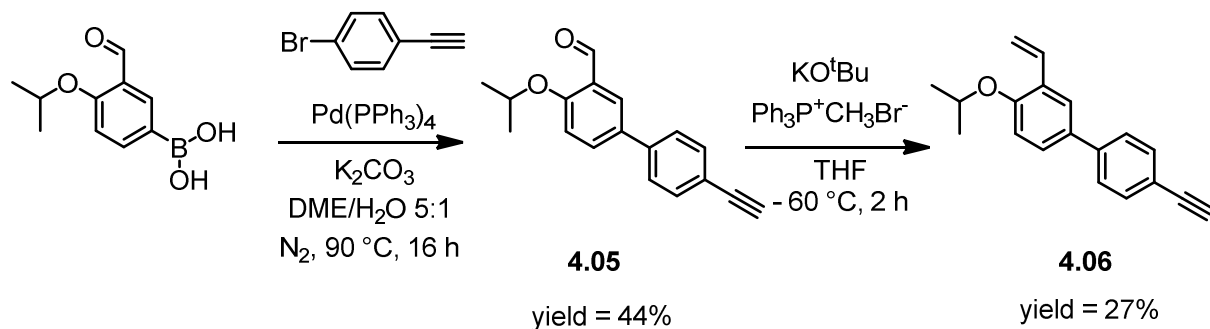
Initially, the Wittig reaction on 3-formyl-4-isopropoxy phenyl boronic acid was attempted using typical Wittig conditions, methyltriphenylphosphonium bromide and a strong base such as potassium *t*-butoxide (KOtBu). However, the reaction yielded a mixture of products which was suspected to be due to the boronic acid forming oligomeric anhydrides.<sup>42</sup> Therefore, the reaction steps were switched to undertake the Suzuki coupling prior to the Wittig reaction.

The palladium-catalysed cross coupling between organoboronic acid and halides developed by Miyaura and Suzuki in 1986 has been expanded over the years to cover a range of alkyl halides in addition to the originally reported aryl halides.<sup>43</sup> However, of concern was a report that under certain conditions the Suzuki coupling reaction can lead to the simultaneous reduction of aldehydes.<sup>44</sup> Therefore, conditions previously utilized to couple halides to 3-formyl-4-isopropoxy phenyl boronic acid were utilized (Scheme 4.3).<sup>45</sup>



**Scheme 4.3** The reaction of 3-formyl-4-isopropoxy phenyl boronic acid with propargyl bromide and 1-bromo-4-ethynylbenzene to give intermediates **4.04** and **4.05** respectively. Reaction with propargyl bromide yielded no desired product.

Initial attempts utilized propargyl bromide; however,  $^1\text{H}$  NMR analysis and IR spectroscopy suggested that no conversion to **4.04** was achieved. This was hypothesized to be the result of several factors. Firstly, propargyl bromide is typically only available in solution with non-polar solvents such as toluene, which are immiscible under the reaction conditions. Secondly, under these conditions, propargyl bromide is prone to hydrolysis *via* the nucleophilic substitution of hydroxide ions, leading to elimination of  $\text{Br}^-$ . As a result of this, the halide was exchanged for a more stable aryl halide, 1-bromo-4-ethynylbenzene, and the reaction repeated to yield the desired product **4.05** following purification. Following the reaction of **4.05** with methyltriphenylphosphonium bromide and  $\text{KOTu}$ , the desired alkyne functionalized benzylidene ligand (**4.06**) was prepared in just two synthetic steps (Scheme 4.4, Figure 4.6).



**Scheme 4.4** Synthesis of an alkyne functionalized benzylidene ligand (4.06).

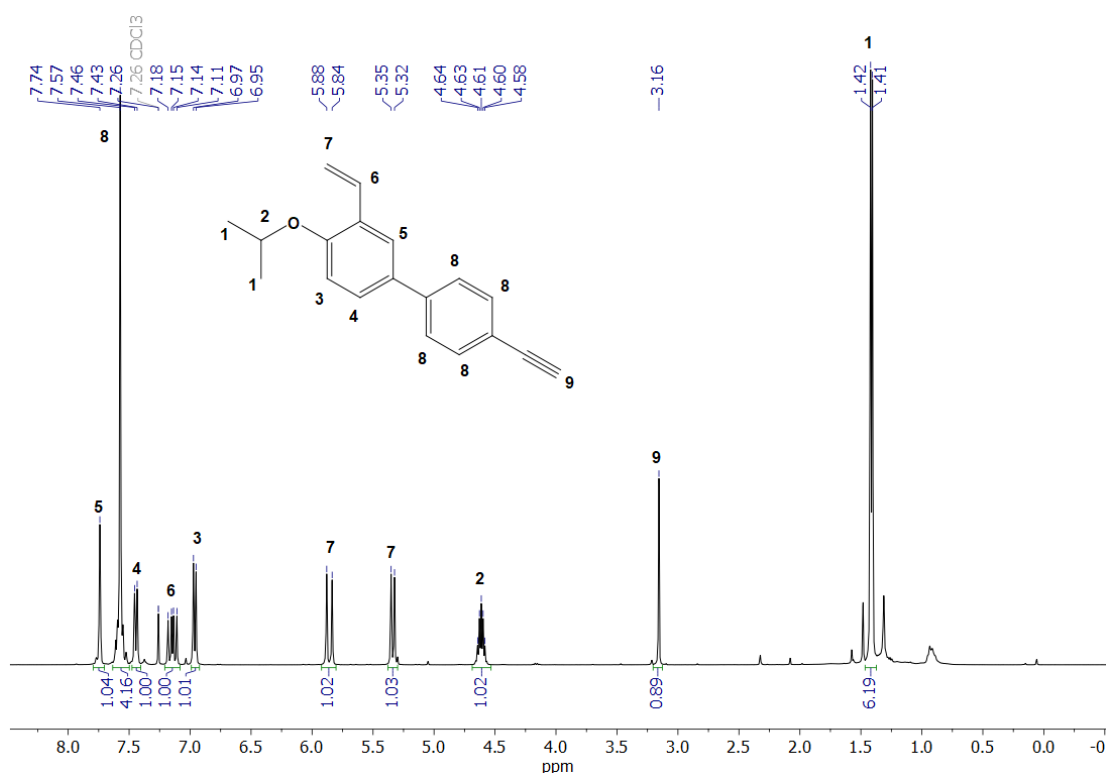
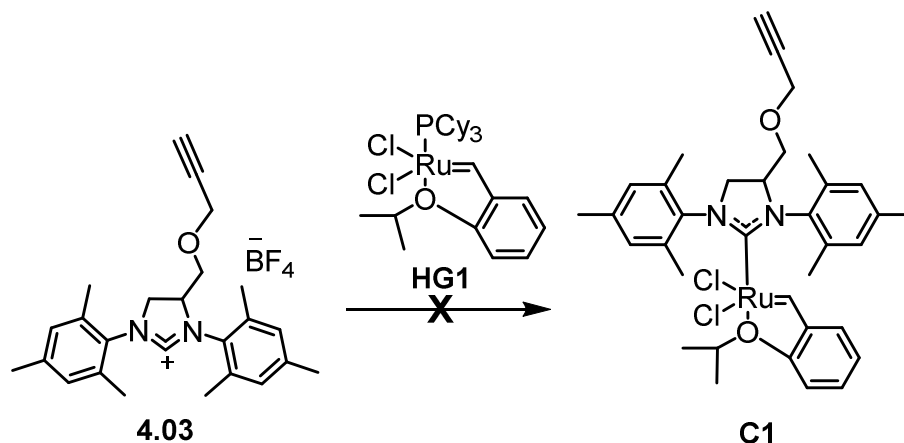


**Figure 4.6**  $^1\text{H}$  NMR spectrum of 4.06 in  $\text{CDCl}_3$  (400 MHz, 298K).

#### 4.3.1.2 Conjugation of alkyne-functionalized ligands to metathesis catalysts

Following the successful synthesis of two alkyne functionalized ligands **4.03** and **4.06**, attempts to conjugate the ligands to Ru-catalysts commenced in order to prepare the final metathesis catalysts with a functional handle. As discussed in Chapter 1, HG2 type catalysts are the most stable, owing to the combination of a chelating group and NHC ligand. Therefore,

attempts to conjugate **4.03** to HG1 proceeded to form an alkyne functionalized HG2 type catalyst, **C1** (Scheme 4.5).



**Scheme 4.5** The conjugation of an alkyne-functionalized NHC ligand (**4.03**) to HG1. Several conditions were tested as stated in Table 4.1.

The conjugation of functionalized NHC ligands to HG1 has been previously well reported by the groups of Bazzi<sup>46</sup> and Grubbs<sup>29</sup>. Typically, a strong base such as potassium bis(trimethylsilyl)amide (KHMDs) is utilized to deprotonate the imidazolium salt to prepare the free carbene, which binds to the Ru-catalyst through strong  $\sigma$ -donation, displacing the phosphine ligand. Due to the high reactivity of free carbenes, the synthesis was conducted under a strictly inert atmosphere. Several reaction conditions were attempted to conjugate **4.03** to HG1 and these are summarized in Table 4.1.

Despite numerous attempts to conjugate **4.03** to HG1, <sup>1</sup>H NMR analysis revealed the presence of mainly starting materials. Initially, it was believed this was due to the insolubility of **4.03** in the reaction solvent, toluene. Therefore, the reaction solvent was changed to 1:1 (v/v) Toluene:THF and homogenous conditions were achieved (Reaction **1d**). Following the reaction, a large amount of HG1 was observed by thin-layer chromatography (TLC); however, a small amount (17 mg, 36%) of a green solid was isolated following silica-gel column



chromatography. The green-product was analyzed by  $^1\text{H}$  NMR spectroscopy (Figure 4.7) and several alkylidene protons were identified, appearing downfield in the  $^1\text{H}$  NMR spectra. This suggested the appearance of numerous Ru-carbene products. Furthermore, an aldehyde peak around 10.5 ppm was observed which was believed to be due to the formation of benzaldehyde as a result of oxidative cleavage of the benzylidene ligand.<sup>47</sup>

**Table 4.1** A summary of the reaction conditions trialled for the synthesis of **C1** from **4.03** and HG1. <sup>†</sup>Equivalentents reported with respect to HG1.

	Solvent	Base	Reaction time / h	Reaction temp/ °C	Eq. <sup>†</sup> Base	Eq. <sup>†</sup> 4.03	Comments
<b>1a</b>	Toluene	KHMDS	3	80	1.2	0.9	<b>4.03</b> limited solubility in toluene. Mainly HG1 observed.
<b>1b</b>	Toluene	KHMDS	16	80	1.5	1.2	<b>4.03</b> limited solubility in toluene. Mainly HG1 observed.
<b>1c</b>	Toluene	KHMDS	24	80	1.5	1.5	<b>4.03</b> limited solubility in toluene. Mainly HG1 observed.
<b>1d</b>	1:1 THF : Toluene	KHMDS	17	80	1.5	1.5	<b>4.03</b> fully soluble in THF/toluene. Many side products identified.

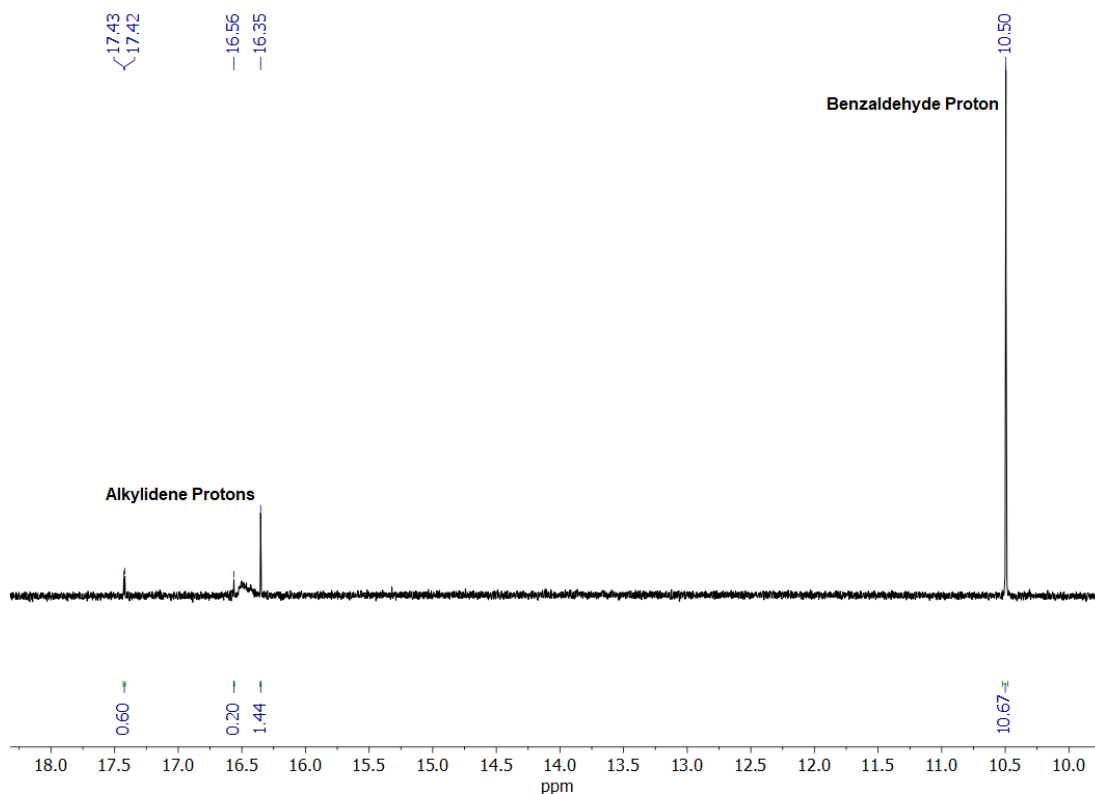
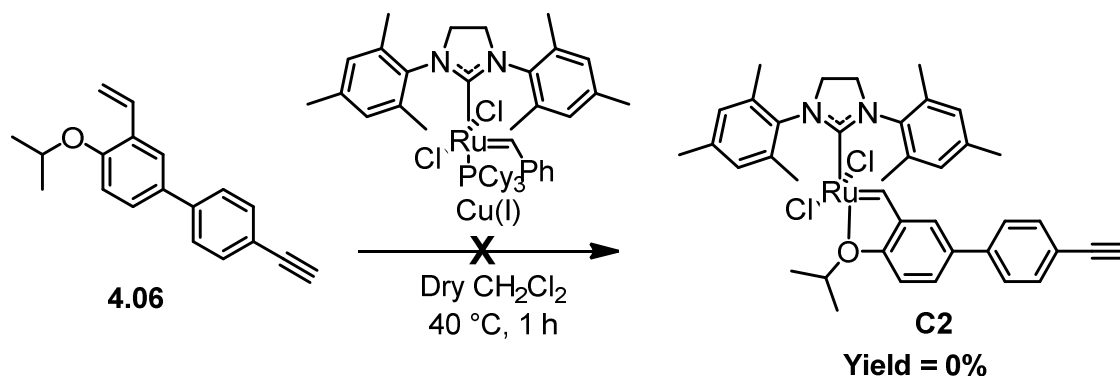


**Figure 4.7**  $^1\text{H}$  NMR spectra of the green solid isolated utilizing reaction conditions **1d** in  $\text{CDCl}_3$ . Multiple peaks downfield and the appearance of a benzaldehyde peak suggests the formation of several side products (600 MHz; 298K).

The lack of reactivity of HG1 with **4.03**, was hypothesized to be due to the deprotonation of the alkyne moiety ( $\text{pK}_a \approx 25$ ) under the highly basic reaction conditions ( $\text{pK}_a \approx 26$ ). The resulting anion is a strong nucleophile which could lead to several unwanted side reactions with the Ru metal.<sup>48</sup>

Finally, attempts to conjugate **4.06** to G2 were conducted in order to prepare a HG2 type catalyst with the alkyne functionalized through the benzylidene ligand, **C2** (Scheme 4.6). Once again, the conditions have been well optimized in the literature, utilizing  $\text{CuCl}$  to act as a phosphine scavenger and encourage the displacement of the phosphine ligand with the benzylidene ligand.<sup>12</sup> A small amount of green product was isolated following column

chromatography; however, analysis of the green product by  $^1\text{H}$  NMR revealed the absence of an alkyne proton suggesting the unsuccessful isolation of **C2**.



**Scheme 4.6** Conjugation of **4.06** to **G2** in an attempt to prepare an alkyne functionalized catalyst **C2**.

In conclusion, the conjugation of both previously synthesized alkyne functionalized ligands, **4.03** and **4.06**, to commercially available Ru-catalysts was unsuccessful. Despite the vast amount of literature in this area, it was noted that all previous reports utilizing an alkyne-functionalized benzylidene ligand, performed the CuAAC reaction prior to the conjugation to the Ru-catalyst. This was significant as the metathesis of alkyne bonds by Ru-metathesis catalysts has previously been reported and it was therefore hypothesized that the issues encountered were due to the presence of the alkyne functionality leading to unwanted side-reactions.<sup>49</sup> Further evidence for this was provided in a report on ROMP of acetylene functionalized norbornene monomers by Binder *et al.* The authors of this study reported high dispersities in their resulting polymers due to the unprotected alkynes cross-linking.<sup>50</sup>

In contrast to the previous reports, performing the CuAAC reaction with DNA prior to the addition of Ru was not seen as a feasible route. This is due to the instability and hydrophilicity of DNA, which would not tolerate the conditions required to couple the ligands to Ru. Namely,

the dry conditions would not solubilise DNA and the strong bases used are likely to lead to DNA degradation.

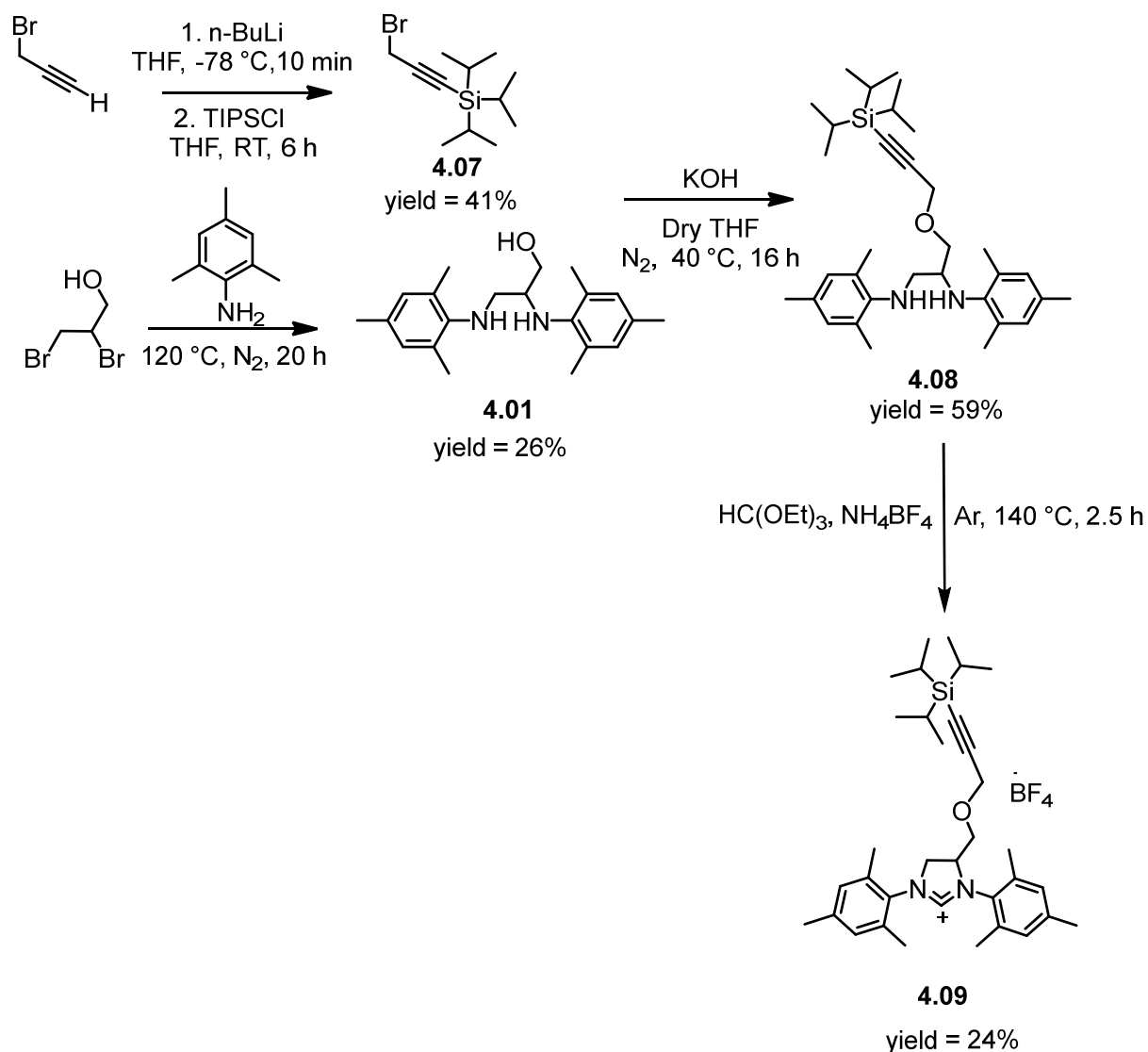
As a consequence of this, two alternative routes were explored and are discussed herein. Firstly, a number of groups have reported the protection of alkyne monomers against metathesis. Such protecting groups investigated include a dicobalt hexacarbonyl complex,<sup>51</sup> and silyl ether protecting groups such as trimethylsilane (TMS).<sup>52, 53</sup> Alternatively, a new functional handle could be utilized. In particular, due to the success of utilizing amide bond formation for the preparation of DNA macromonomers in Chapter 3, this chemistry was explored.

#### 4.3.1.3 Protection of the alkyne group

Initially, the use of an appropriate alkyne protecting group was studied for the preparation of a catalyst functionalized through the NHC ligand. As the deprotonation of the imidazolium salt requires highly basic conditions, TMS would not be appropriate as it is reportedly base labile.<sup>54</sup> In contrast, the bulkier triisopropylsilyl (TIPS) protection group is 100,000 times more stable to basic conditions than TMS and thus was the protection group of choice.<sup>54</sup>

Initially, propargyl bromide was protected with the TIPS protecting group and then the synthesis of the protected-alkyne functionalized NHC ligand (**4.09**) was carried out *via* the previously discussed synthetic pathway (Scheme 4.7). Grela and co-workers reported that the presence of inorganic materials or excess solvent on the NHC ligand has a detrimental effect on the next reaction step, preventing the reaction of the ligand with Grubbs catalysts going to completion.<sup>55</sup> Therefore, care was taken to ensure that **4.09** was isolated as a high purity salt,

via multiple recrystallizations in ethanol, yielding **4.09** as a white crystalline solid in a 4 % overall yield (Figure 4.8).



**Scheme 4.7** Synthesis of a TIPS protected alkyne functionalized NHC ligand (**4.09**). Following the protection of propargyl bromide to **4.07**, conditions previously reported by Deraedt et al. were utilized.<sup>38</sup>

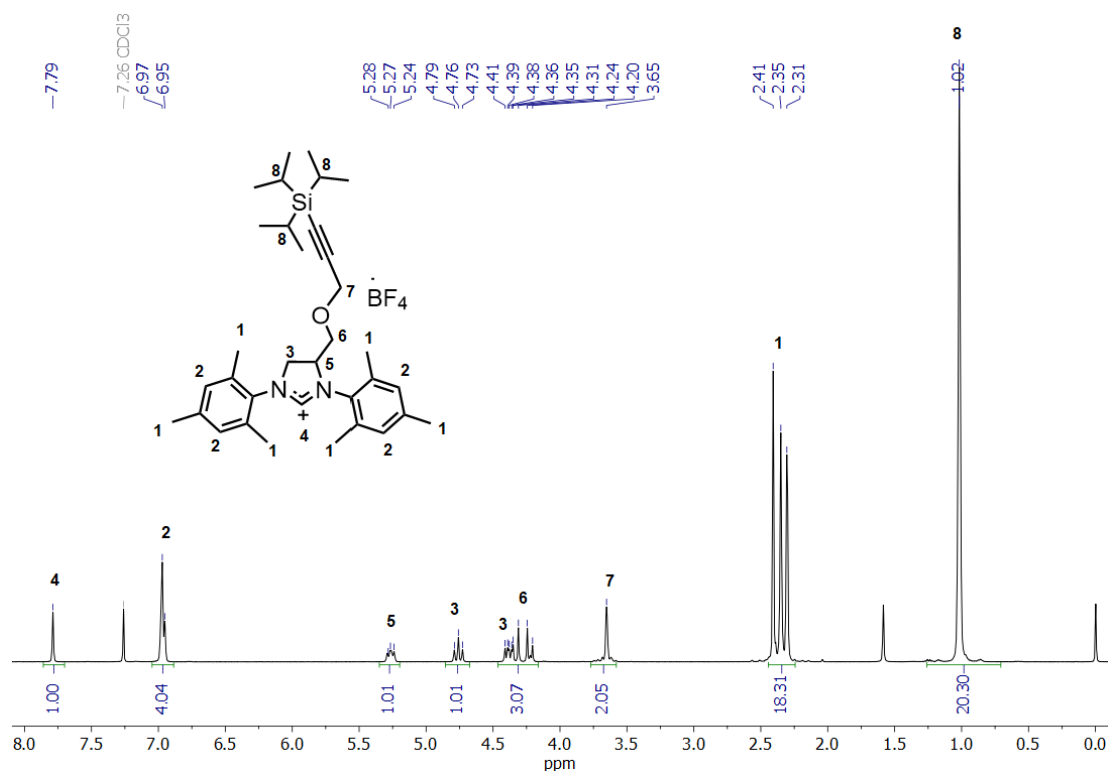
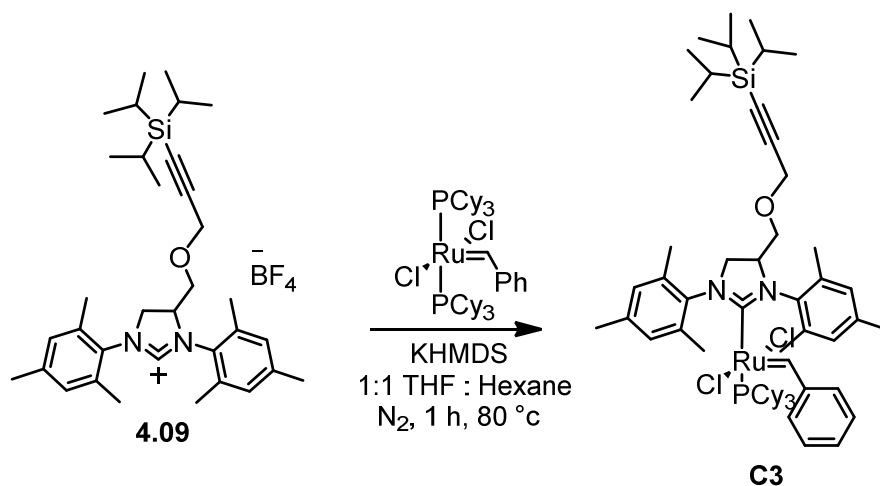
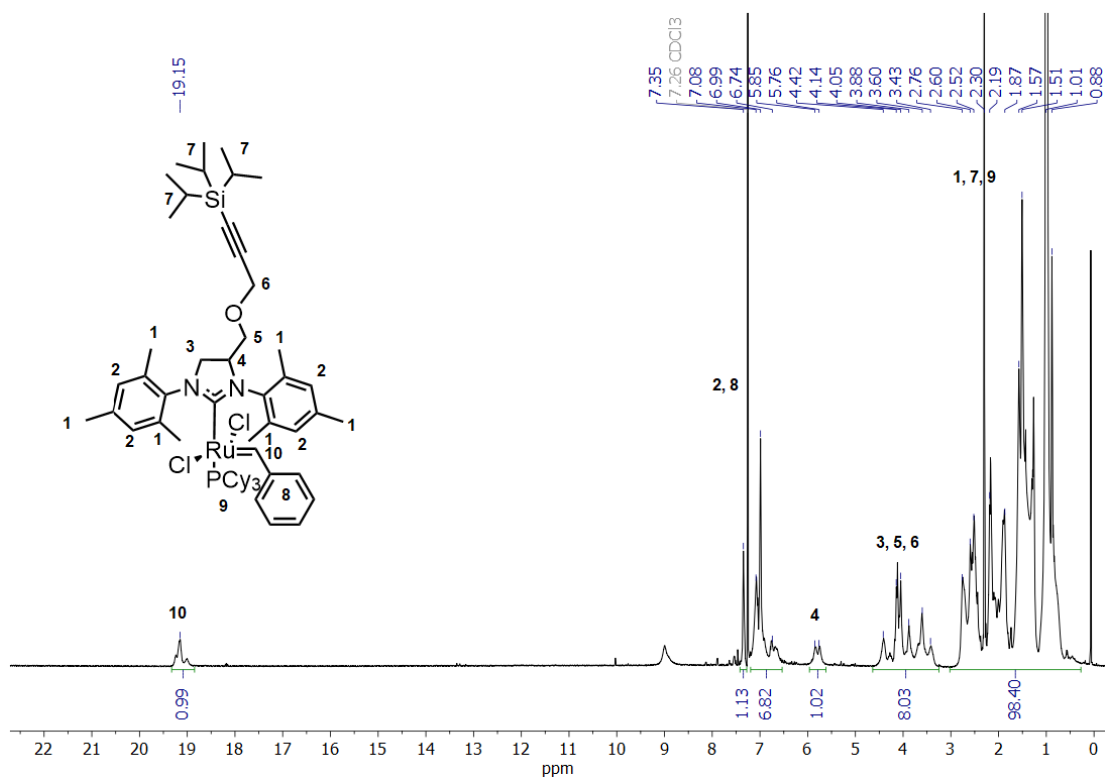


**Figure 4.8**  $^1\text{H}$  NMR spectrum of **4.09** in  $\text{CDCl}_3$  (400 MHz, 298K).

Following the successful synthesis of **4.09**, attempts to conjugate the ligand to a Ru-metathesis catalyst commenced. Initial attempts were conducted with G1 as previous studies had demonstrated that G1 cannot catalyze the metathesis of silyl protected alkynes.<sup>53</sup> Similar conditions to those previously studied (Table 4.1) were utilized: a strong base (KHMDs) and 1:1 (v/v) THF:hexane, which resulted in homogenous conditions (Scheme 4.8).  $^1\text{H}$  NMR spectroscopy of the resulting product did appear to indicate the successful formation of **C3** due to a ppm shift in the alkylidene proton from 20 ppm, typical for G1, to 19 ppm typical for G2 type catalysts (Figure 4.9). The peak at 19 ppm was observed as a multiplet and this was hypothesized to be due to the transient behavior of the labile phosphine ligand.



**Scheme 4.8** Conjugation of **4.09** to **G1** to yield **C3**.

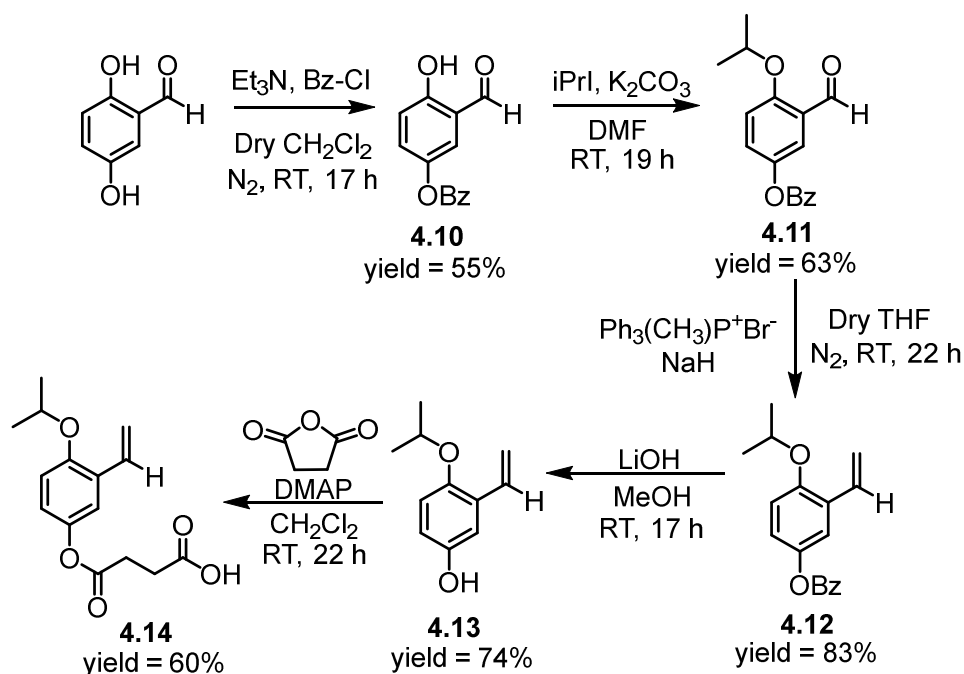


Despite this encouraging result, due to time restraints no further work was conducted with **C3** and instead attempts were focussed towards the functionalization of the catalysts through the benzylidene ligand, discussed below.

### 4.3.2 Synthesis of DNA-functionalized metathesis catalysts using amide bond formation

The conjugation of amino-modified DNA to carboxylic acid functionalized small molecules has been successfully reported for the preparation of norbornene-functionalized DNA (Chapter 3 – Section 3.3.2). Thus, it was anticipated that this chemistry could also be successful for the conjugation of a benzylidene ligand to DNA.

The synthesis of a hydroxyl-functionalized benzylidene ligand (**4.13**) was conducted based on previously reported protocols.<sup>56</sup> The reaction of **4.13** with succinimide leads to the desired carboxylic acid functionalized benzylidene ligand, **4.14** in a 13% overall yield (Scheme 4.9, Figure 4.10). Due to the high cost of the Ru-catalysts, optimization studies for the conjugation to DNA was completed with the benzylidene ligand alone (**4.14**).



**Scheme 4.9** Synthesis of a carboxylic acid functionalized benzylidene ligand (**4.14**). The synthesis of **4.13** was conducted based on previously reported protocols.<sup>56, 57</sup>



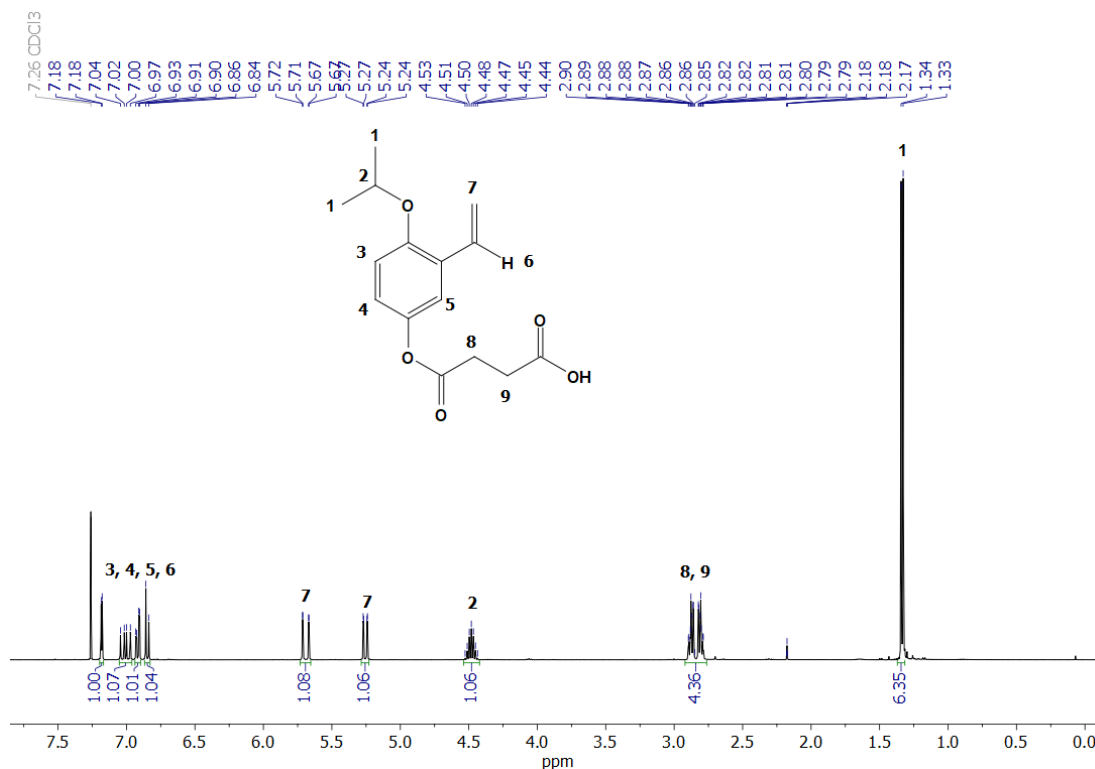


**Figure 4.10**  $^1\text{H}$  NMR spectrum of **4.14** in  $\text{CDCl}_3$  (400 MHz, 298K).

A short oligonucleotide functionalized with an amino-group on the 5' end (5'-NH<sub>2</sub>) was utilized (Figure 4.11a) and conditions identical to those stated in Chapter 3 were tested (Figure 4.11b). The product was analyzed by LCMS which revealed the hydrolysis of the phenyl ester (mass of hydrolyzed product calculated = 5465.0 Da, mass found = 5464.8 Da) under the reaction conditions (Figure 4.11c). The hydrolysis was believed to be accelerated by the presence of a base, DIPEA.

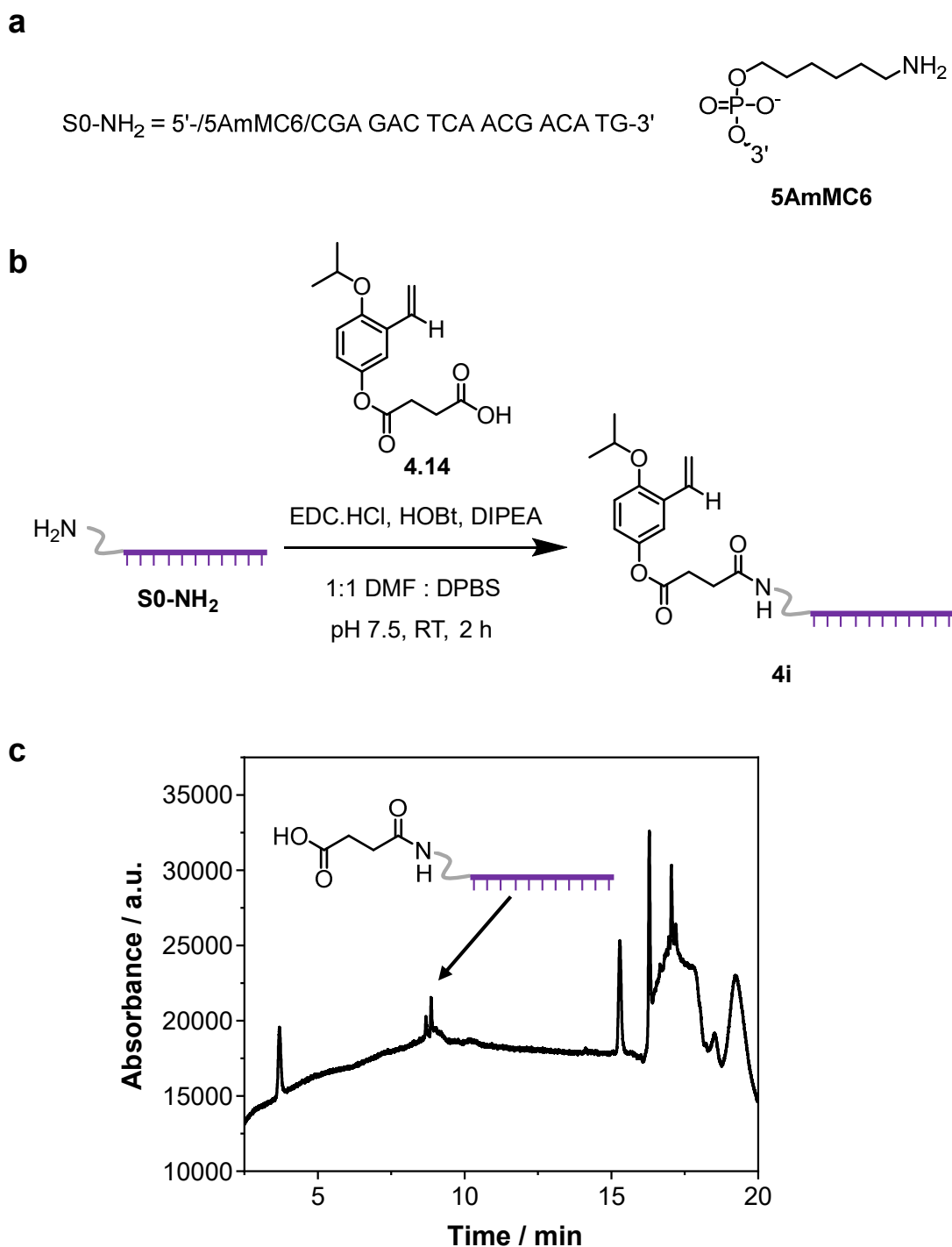
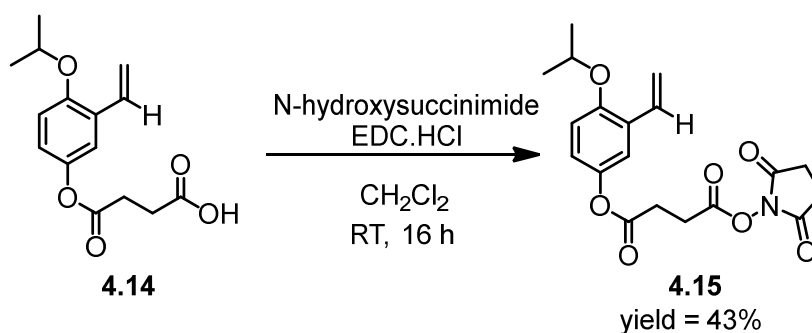


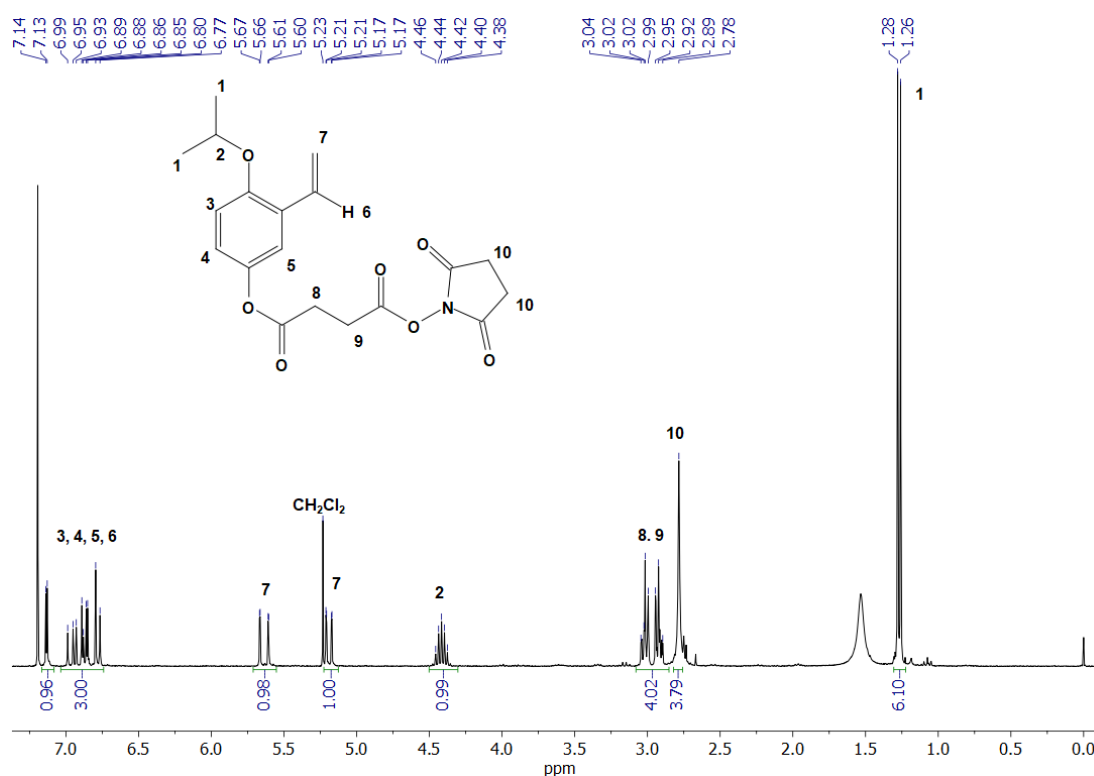
**Figure 4.11** (a) S0-NH<sub>2</sub> sequence utilized throughout this study. (b) Conditions attempted for the conjugation of a carboxylic acid functionalized benzylidene ligand to S0-NH<sub>2</sub>. (c) LC-MS-UV chromatogram at 260 nm of the resultant product eluted with a gradient of buffer A: 75 mM TEAA in H<sub>2</sub>O and buffer B: 75 mM TEAA in acetonitrile, revealing hydrolysis of **4i**. Peaks assigned via mass spectrometry.

The amide bond coupling was therefore split into two separate steps. Firstly, **4.14** was reacted with *N*-hydroxysuccinimide (NHS) to form an activated-ester, **4.15** (Scheme 4.10, Figure 4.12).

The activated-ester **4.15** was then reacted with  $S_0\text{-NH}_2$  under much milder conditions to those previously stated in Figure 4.11b. The reaction was conducted in 8:2 (v/v) DMF:DPBS adjusted to pH 8 for 2 h at room temperature, these conditions were identified to successfully minimize the unwanted hydrolysis of the phenyl ester, whilst also encouraging approximately 80% conversion to the desired product **4i** (mass calculated = 5625.1 Da, mass found = 5625.2 Da) (Figure 4.13).



**Scheme 4.10** Synthesis of a benzylidene ligand functionalized with an NHS activated-ester, **4.15**.



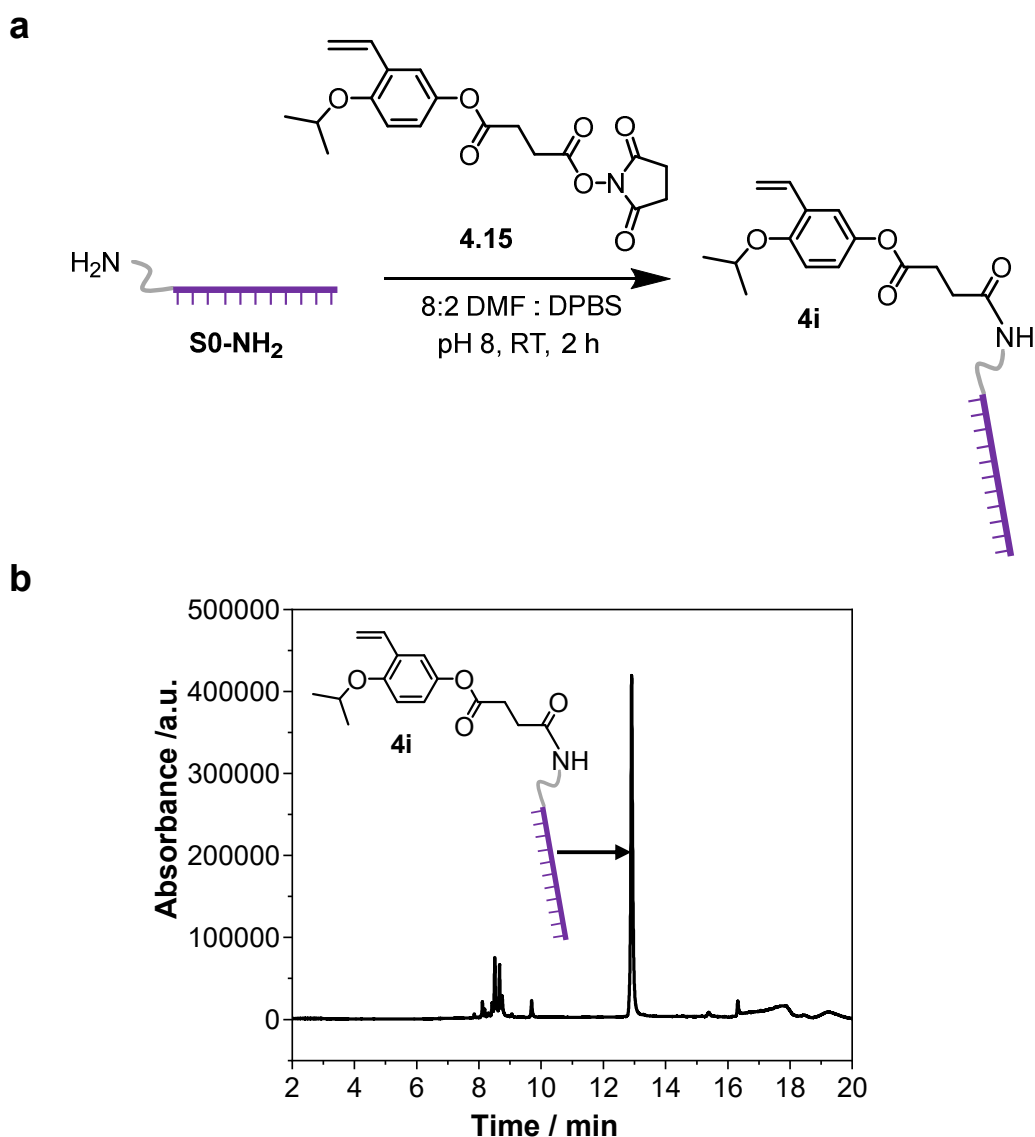


**Figure 4.13** (a) Synthesis of **4i** utilizing an activated-ester (**4.15**). (b) LC-MS-UV chromatogram at 260 nm eluted with a gradient of buffer A: 75 mM TEAA in H<sub>2</sub>O and buffer B: 75 mM TEAA in acetonitrile showing the successful conversion to **4i**. Peaks assigned via mass spectrometry.

Following the successful identification of the conditions required to couple **4.15** to DNA (Figure 4.13a), the benzylidene ligand was first reacted with G2 in the presence of the phosphine scavenger CuCl, to prepare a HG2 type catalyst with an NHS functional handle, **C4**, isolated as a green solid (Figure 4.14).

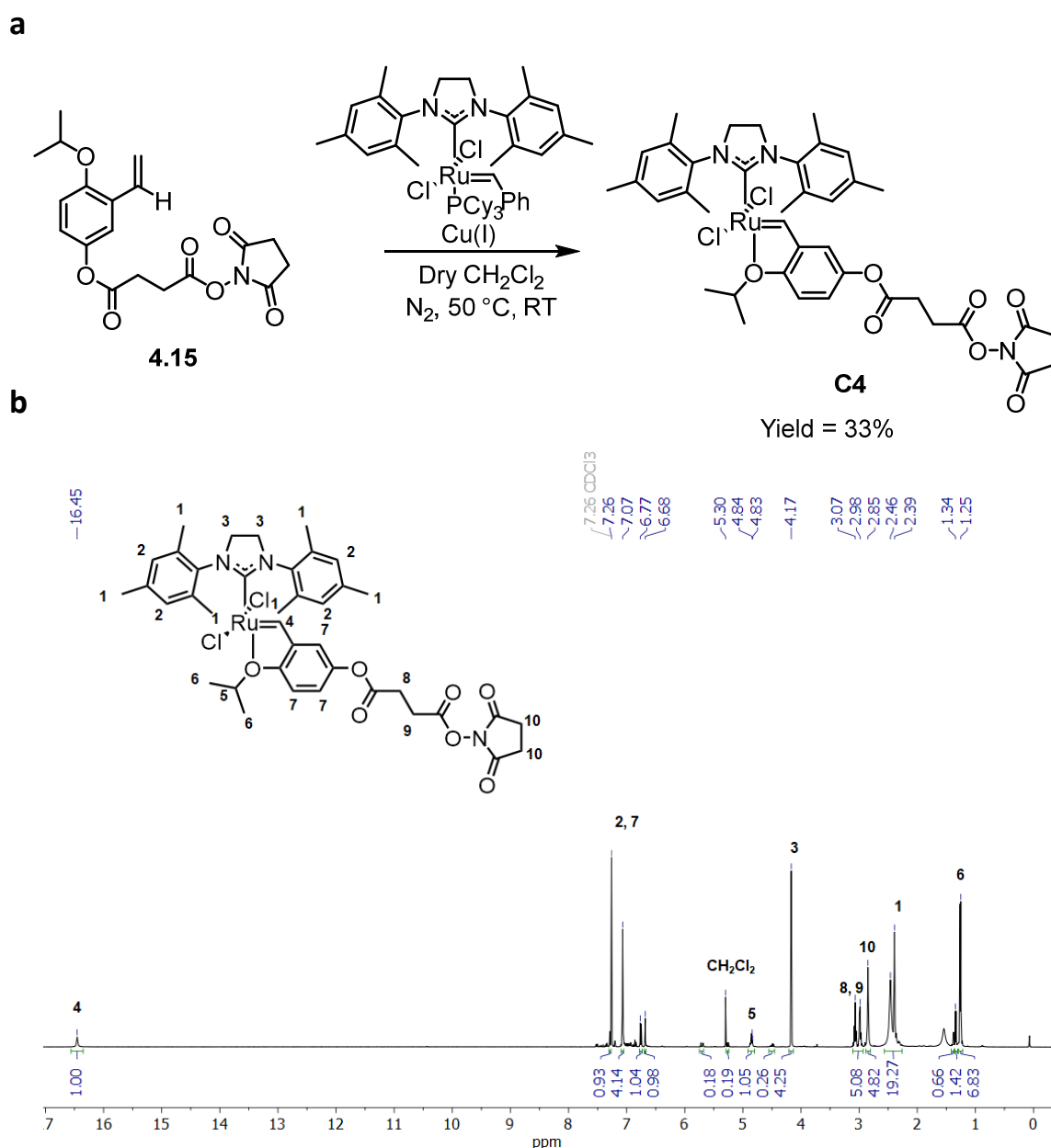


**Figure 4.14** (a) Synthesis of **C4**. (b)  $^1\text{H}$  NMR spectra of **C4** in  $\text{CDCl}_3$  (500 MHz, 298K).

Using the aforementioned conditions, **C4** was then reacted with S0-NH<sub>2</sub> and analyzed by HPLC. Upon HPLC analysis no DNA was detected; although as identified in Chapter 2, this was likely due to the large excess of Ru-catalyst used (1000 equiv.) which induces DNA degradation (Figure 4.15a). It was previously demonstrated that lowering the catalyst concentration and adding a Lewis acidic catalyst, such as MgCl<sub>2</sub>, prevents DNA degradation. Therefore, the

reaction was repeated with 100 equivalents **C4** and in the presence of 4000 equivalents  $\text{MgCl}_2$ . LCMS analysis revealed the presence of unreacted amino-DNA ( $\text{S0-NH}_2$ ) and approximately 3%, of the hydrolyzed benzylidene functionalized DNA, Figure 4.15b.

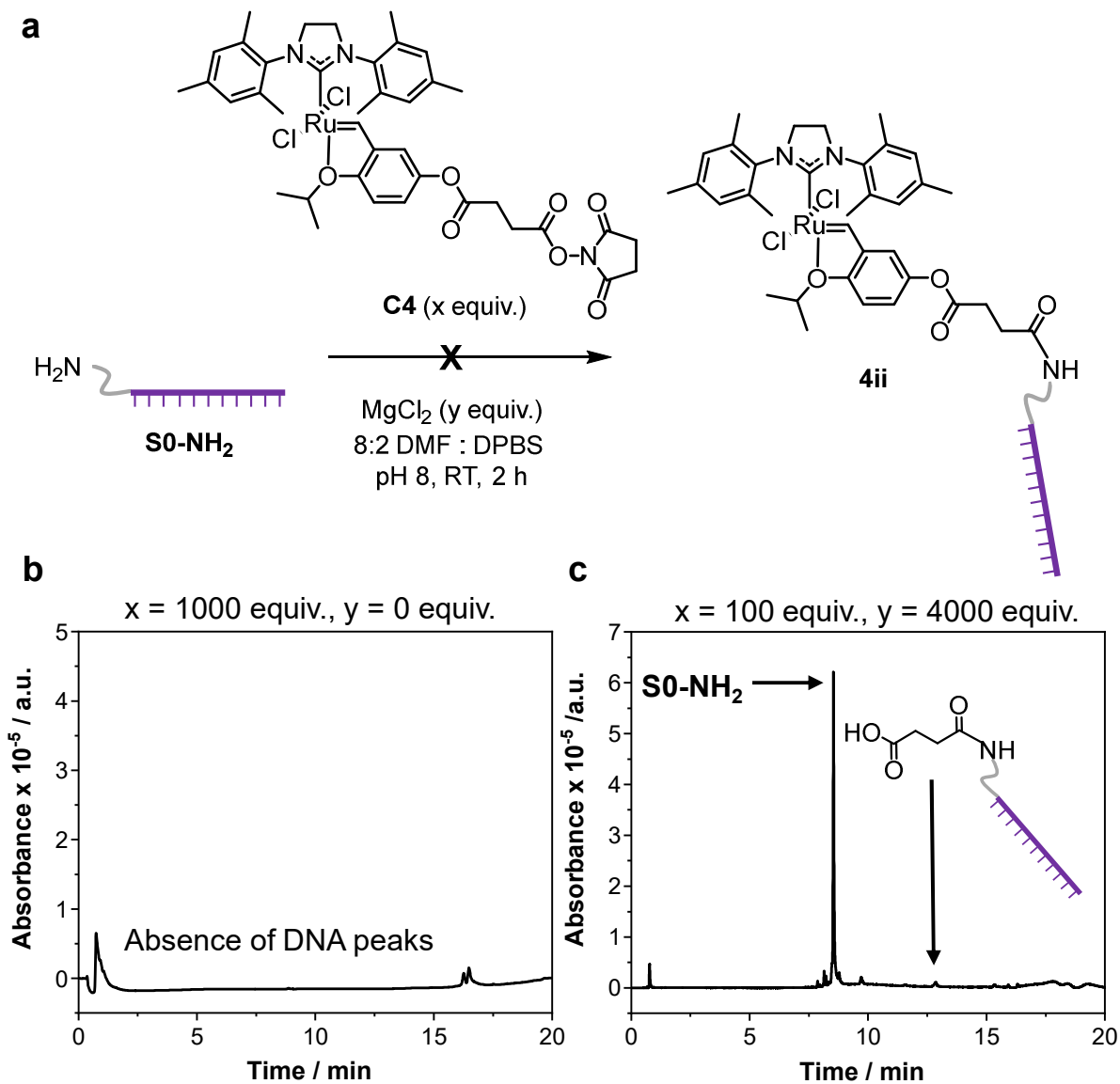


**Figure 4.15** (a) Synthetic scheme for the preparation of **4ii**, the conditions are based on the optimized conditions reported in Figure 4.13. (b) LCMS-UV chromatogram at 260 nm of the product utilizing 1000 equivalents of **C4** and 0 equivalents of  $\text{MgCl}_2$ . (c) LCMS-UV chromatogram at 260 nm of the product utilizing 100 equivalents of **C4** and 4000 equivalents of  $\text{MgCl}_2$  in an attempt to prevent DNA degradation. Equivalents are reported with respect to  $\text{S0-NH}_2$ . Products eluted with a gradient of buffer A: 75 mM TEAA in  $\text{H}_2\text{O}$  and buffer B: 75 mM TEAA in methanol. Peaks assigned via mass spectrometry.

Whilst this report is the first attempt to conjugate Ru metathesis catalysts to DNA; the Barton group has conjugated a vast array of other Ru-complexes to DNA due to their interesting electron-transfer processes. However, the syntheses are predominantly conducted on the solid phase.<sup>58</sup> As discussed above, the Ru metathesis catalysts are unlikely to survive the typical cleavage conditions utilized in DNA solid-phase synthesis (highly basic) due to catalyst degradation.<sup>48</sup> Therefore, the immobilization of unprotected DNA was studied.

In 2004, Harbury and co-workers reported a tertiary amine anion exchange resin, DEAE Sepharose, capable of reversibly binding unprotected DNA. The authors demonstrated the use of this catalyst to prepare DNA-peptide conjugates.<sup>59</sup> Furthermore, Flood *et al* expanded this approach by studying a range of resins to which DNA is able to reversibly adsorb.<sup>60</sup> The main advantage of this approach is that the reaction can be conducted on the solid phase in organic solvents, expanding the reaction scope of DNA compatible studies. However, it was anticipated that the immobilization of DNA may provide additional protection to prevent the unfavorable DNA-Ru interactions believed to be limiting the success of this reaction. Initially, SO-NH<sub>2</sub> was immobilized on DEAE Sepharose (Figure 4.16a) and the conjugation was attempted on the solid phase in DMF (Figure 4.16b).

Following the reaction, the product was eluted from the resin and small molecules removed *via* spin filtration through a molar mass cut-off resin, prior to analysis by LCMS. The results suggested the presence of only DNA starting material SO-NH<sub>2</sub> (Figure 4.16c). However, when comparing this work to that completed by Harbury and coworkers, it was noted that the DNA sequences used in their study contained linkers at least 12 carbon units long.<sup>59</sup> In comparison, this study utilized a much shorter 6 carbon linker. This raised concerns over the ability of the

positively charged Ru-catalyst to access the amine group, which would be held in close proximity to the positively charged DEAE Sepharose.

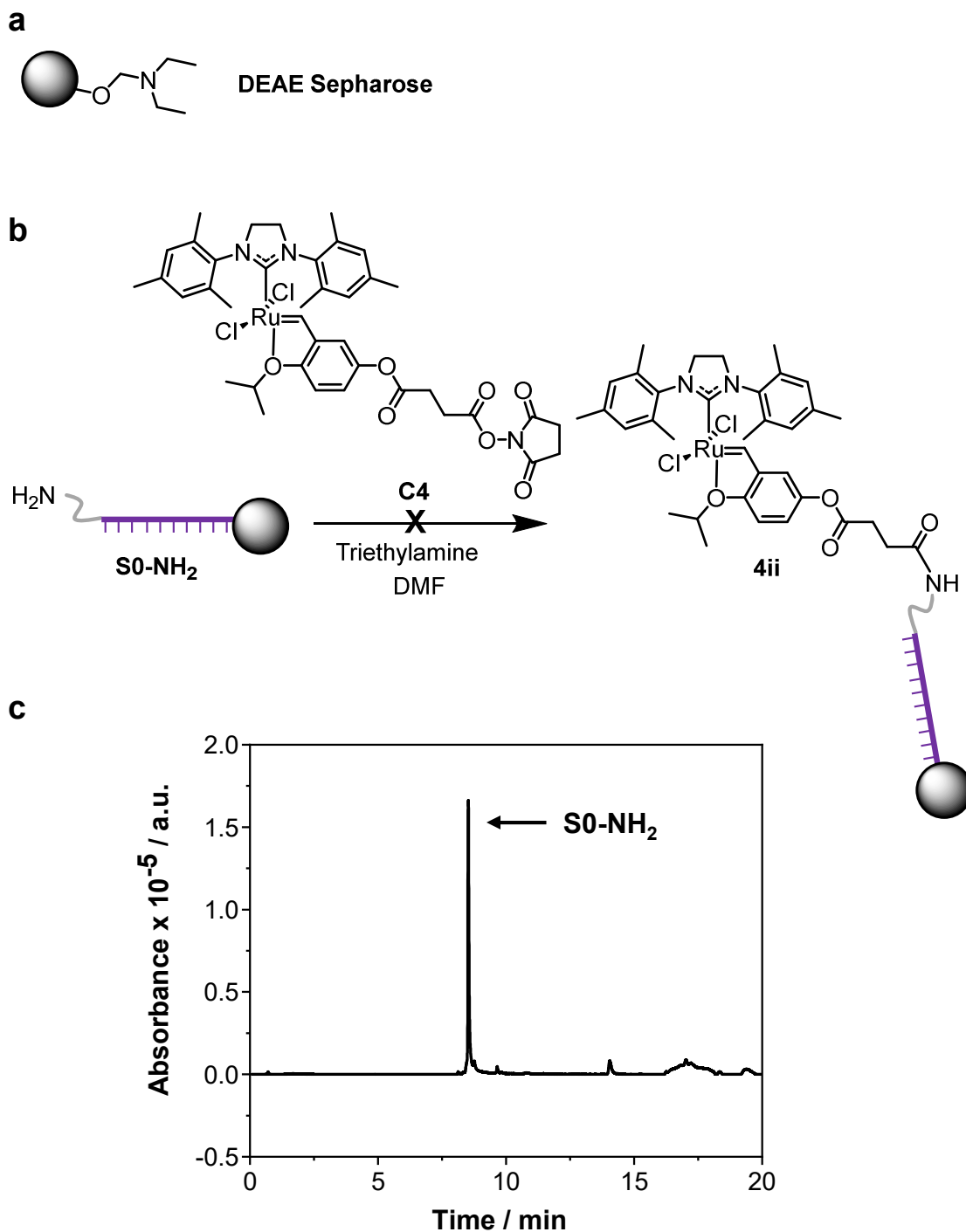


**Figure 4.16** (a) Structure of DEAE Sepharose. (b) Synthesis of **4ii** on the solid-phase. (c) LCMS-UV chromatogram at 260 nm of **4ii** eluted with a gradient of buffer A: 75 mM TEAA in H<sub>2</sub>O and buffer B: 75 mM TEAA in methanol. Peaks assigned via mass spectrometry.



A new DNA sequence, S0-iSp-NH<sub>2</sub> was utilized which contained an internal spacer (iSp18) and a 12-carbon linker (AmMC12) (Figure 4.17a). The reaction was conducted as stated previously (Figure 4.17b) and then analyzed by LCMS; however, once again, only amino-DNA (S0-iSp-NH<sub>2</sub>) was identified (Figure 4.17c). This result would suggest that the chosen resin is not compatible with this chemistry, most likely due to the electrostatic repulsion between the resin and Ru-catalyst.

The unsuccessful attempts to isolate a DNA-conjugated Ru-catalyst were attributed to many of the challenges and limitations identified in Chapter 2. Namely, there appears to be an unwanted interaction between the DNA and Ru-catalysts, leading to DNA degradation unless, as identified in Chapter 2, a low catalyst loading and additives such as MgCl<sub>2</sub> are used. However, the latter conditions do not appear to be compatible with the amide bond forming reaction. This is hypothesized to be due to two factors: firstly, the solution-phase coupling reactions are typically conducted using  $\mu\text{M}$  concentrations of DNA; therefore, a large excess of reagents are usually required to increase the rate of reaction. However, this contradicts the necessity to lower the equivalents of Ru-catalyst for DNA stability. Secondly, the catalyst is insoluble in the aqueous solutions required to solubilize DNA and MgCl<sub>2</sub>. Therefore, achieving homogenous conditions was not possible.

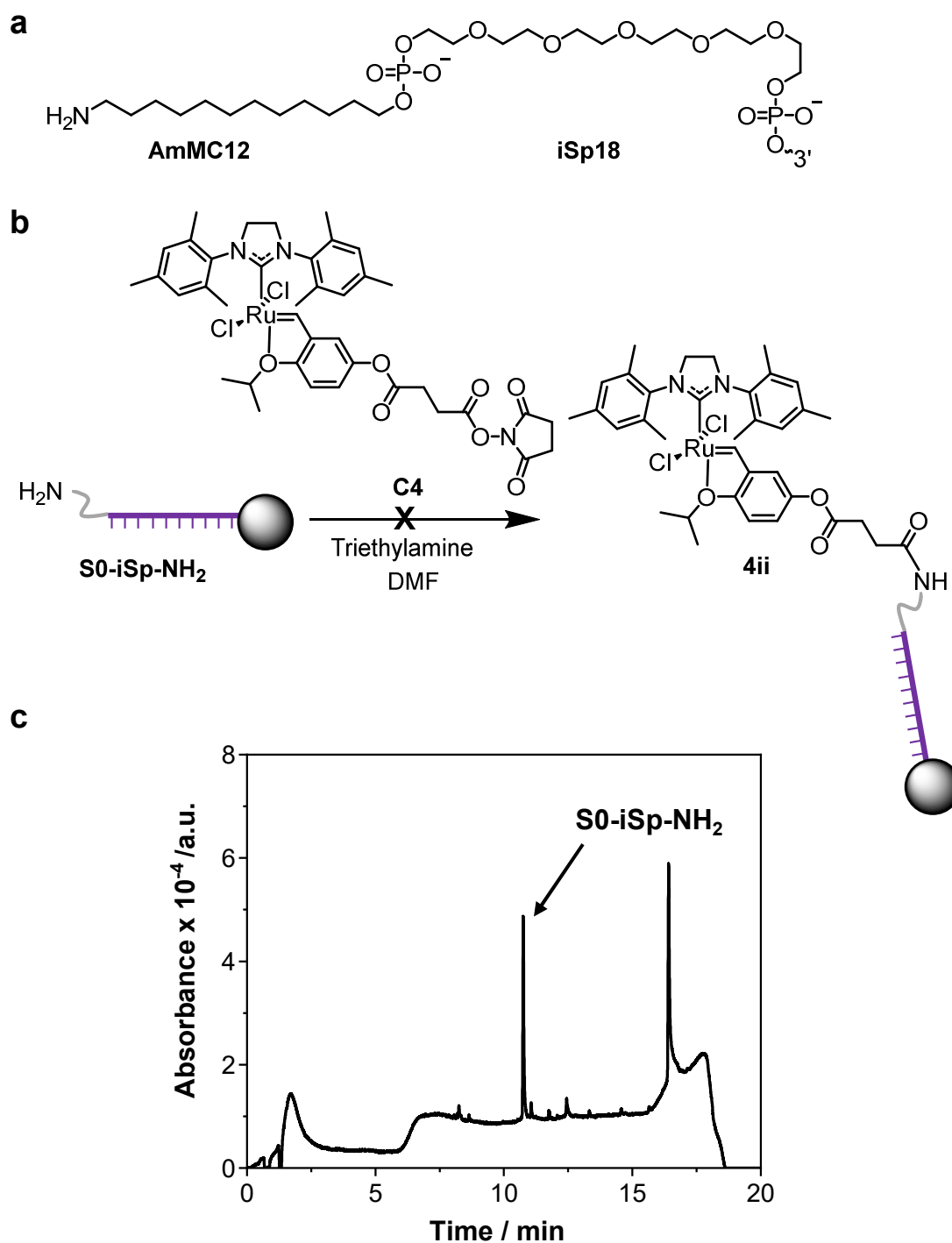


**Figure 4.17** a) Structure of the linker utilized on the 5' end of S0-iSp-NH<sub>2</sub>. (b) Synthesis of **4ii** on the solid-phase. (c) LCMS-UV chromatogram at 260 nm of **4ii**. Products eluted with a gradient of buffer A: 75 mM TEAA in H<sub>2</sub>O and buffer B: 75 mM TEAA in methanol. Peaks assigned via mass spectrometry.

### 4.3.3 Synthesis of PNA-functionalized metathesis catalysts using amide bond formation

Whilst the difficulties to isolate DNA-functionalized metathesis catalysts were disappointing, attempts commenced with its organosoluble counterpart PNA. PNA, unlike DNA, is neutral and thus should not result in an electrostatic interaction with DNA. Furthermore, PNA possess good solubility in common organic solvents such as DMF, DMSO and NMP which also solubilize **C4**.<sup>61</sup>

A short 10-mer PNA sequence was studied, **PS0** and reactions were attempted through both the N and C termini. Reaction of **PS0** through the C-terminus first required the acetylation of the N-terminus and the addition of a Lys residue to the C-terminus to give a free amine, **Ac-PS0-Lys** (Figure 4.18a). As both **C4** and the PNA possess good solubility in DMF this was the solvent of choice for the coupling. Initially, the coupling of **4.15** to PNA was screened under a variety of conditions (Figure 4.18b, Table 4.2).

**Table 4.2** A summary of the reaction conditions attempted for the formation of **4iii**. All reactions were conducted in the presence of 500 equivalents<sup>‡</sup> of **4.15**.<sup>‡</sup>Equivalents reported with respect to PNA (**PS0** or **Ac-PS0-Lys**). \*Conversions reported from the peak integrations of **PS0** to **4iii**.

	Sequence	Solvent	Equiv. <sup>‡</sup> of TEA	Reaction time / h	Temperature / °C	Conversion to <b>4iii</b> *	Observations
<b>2a</b>	Ac-PS0- Lys	DMF	500	2	25	0	Hydrolysis
<b>2b</b>	Ac-PS0- Lys	DMF	0	2	18	0	-
<b>2c</b>	PS0	DMF	2	4	18	18%	-
<b>2d</b>	PS0	DMF	2	19	16	29%	-

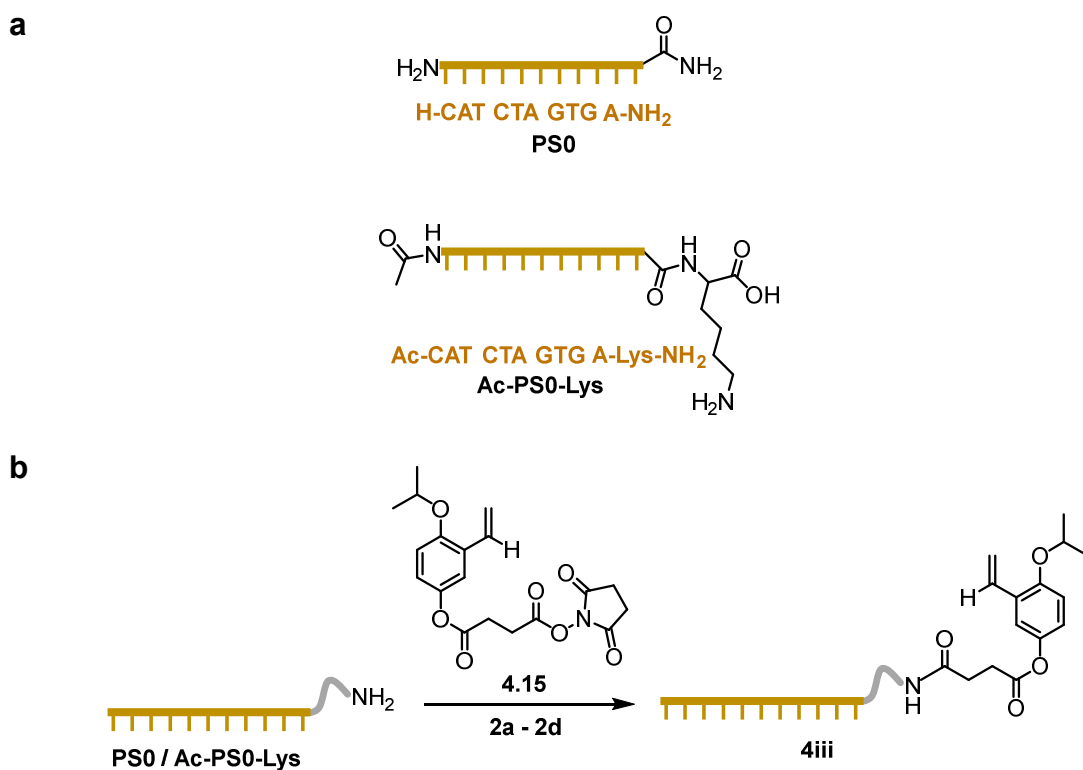


**Figure 4.18** (a) Structure and sequence of *PS0* and *Ac-PS0-Lys*. The reaction of *PS0/Ac-PS0-Lys* with **4.15** to prepare benzylidene functionalized PNA, **4iii**. A number of reaction conditions were screened (**2a – 2d**) as described in **Table 2**.

Similarly, to the coupling of **4.15** to DNA, in the presence of a large excess of triethylamine (TEA) hydrolysis of the phenyl ester was observed and no desired product was yielded (Reaction conditions **2a**). The best results were obtained when a small excess of TEA was utilized (Reaction conditions **2c** and **2d**) and approximately 29% conversion to the desired product was observed (Figure 4.19).

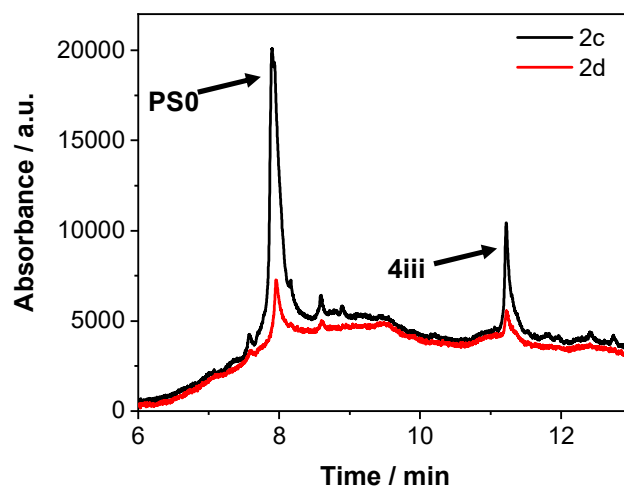


**Figure 4.19** – LCMS-UV Chromatogram at 260 nm of reaction mixtures **2c** and **2d** eluted with a gradient of buffer A: 75 mM TEAA in H<sub>2</sub>O and buffer B: 75 mM TEAA in methanol. Peaks assigned via mass spectrometry.

However, repeating reaction **2d** and replacing **4.15** with **C4** did not yield the desired PNA functionalized catalyst and this was partially attributed to the difficulty separating unreacted catalyst (**C4**) from the PNA. More time would therefore be required to optimize the work-up conditions and ideally the design of **4.15** should be adjusted to remove the troublesome ester functionality so the reaction can be pushed to higher conversions.

#### 4.4 Conclusion

The purpose of this study was to prepare a DNA-functionalized metathesis catalyst with the aim of exploiting such catalyst in DTS. Whilst the preparation of protein-functionalized metathesis catalysts has been reported, the functionalization of metathesis catalyst with DNA has not been explored. The aim was to prepare a Ru-metathesis catalyst with a functional handle that could be coupled to an oligonucleotide in solution.

Original designs were focused on the preparation of an alkyne functionalized catalyst that could be coupled to DNA using CuAAC. To this end, two alkyne functionalized ligands were

prepared but neither ligand could be cleanly added to the Ru-catalyst and this was attributed to the propensity of the alkyne to act as a metathesizable substrate. Protection of the alkyne with a bulky silyl protecting group, TIPS minimized any unwanted side reactions and yielded the desired Ru-metathesis catalyst with a protected alkyne group. Whilst no further work was conducted on this catalyst, this novel catalyst may prove to be a valuable scaffold for the conjugation of a range of substrates to a metathesis catalyst using CuAAC.

The remainder of the chapter focused on the use of activated-ester chemistry to conjugate DNA to the Ru-catalyst. A novel NHS-ester functionalized benzylidene ligand was successfully prepared and conjugated to HG1 to yield the desired catalyst (**C4**). Conditions under which the NHS-ester ligand could be coupled to DNA were studied and mild conditions were identified which facilitated the conjugation without leading to the hydrolysis of the ester functionality in the benzylidene ligand (**4.15**). Unfortunately, these conditions were not successfully translated to the coupling of the catalyst (**C4**) to DNA and this was attributed to the Ru-induced degradation of DNA observed at high catalyst loadings and an electrostatic interaction between the DNA and Ru-catalyst, both identified and discussed in depth in Chapter 2. Immobilization of the catalyst on a solid-phase using an anion exchange resin prevented the Ru-induced degradation of DNA but also prevented any reaction taking place. These studies therefore highlight that the conjugation of an Ru-catalyst to DNA in solution is not a trivial problem and as acknowledged in Chapter 2 would benefit from a greater understanding of the mode of degradation of DNA in the presence of Ru-catalysts.

Whilst the preparation of DNA-functionalized metathesis catalysts were unsuccessful, PNA offers an alternative nucleic-acid substrate capable of templating reactions. It was

hypothesized that PNA may avoid the aforementioned difficulties discussed with DNA as it has a neutral peptide backbone and is therefore unlikely to be complicated by electrostatic interactions. To investigate this, a preliminary study was conducted attempting to couple amino-functionalized PNA to the NHS ester functionalized-catalyst (**C4**); however, due to time constraints successful conditions were not identified. Nevertheless, it is believed that PNA could be coupled to the Ru-metathesis catalyst under successfully identified conditions and this would be an interesting future research area.

## 4.5 Experimental section

### 4.5.1 Materials

Oligonucleotides were purchased from Integrated DNA technologies, Inc. and resuspended in 18MΩ H<sub>2</sub>O to a concentration of 200 μM before use. Concentrations were calculated from the absorbance values at 260 nm using the reported extinction coefficients.

Name	Sequence (5' → 3')	Extinction coefficient/ L/(mole·cm)
S0-NH <sub>2</sub>	5AmMC6/CGA GAC TCA ACG ACA TG	169,300
S0-iSp-NH <sub>2</sub>	5AmMC12//iSp18/CGA GAC TCA ACG ACA TG	169,300

PNA sequences were kindly donated by Samuel Nuñez Pertiñez.<sup>62</sup>

Name	Sequence (N → C)
PS0	H-CAT CTA GTG A-NH <sub>2</sub>
Ac-PS0-Lys	Ac-CAT CTA GTG A-Lys-NH <sub>2</sub>

Reagents were purchased from Sigma-aldrich or other commercial suppliers and used as received. Dry solvents were purified over Innovative Technology SPS alumina solvent columns and degassed using a standard freeze-pump thaw technique.

DPBS buffer was prepared by dissolving 9.6 g of DPBS from Sigma-Aldrich into 1 L 18MΩ H<sub>2</sub>O.



Micro Bio-spin™ 6 columns were purchased from Bio-Rad laboratories. Amicon® Ultra-0.5 mL centrifugal filters (3000 MWCO) were purchased from Millipore. Illustra™ NAP™-5 columns were purchased from GE healthcare.

#### 4.5.2 Instrumentation

*NMR Spectroscopy.* <sup>1</sup>H and <sup>13</sup>C nuclear magnetic resonance (NMR) spectra were recorded on a Bruker Advance III HD400 spectrometer, a Bruker Advance III AV600 spectrometer, Bruker AVIII-300 spectrometer or a Bruker Avance NEO 500 spectrometer in the solvents indicated at 298 K. Chemical shifts are reported on the  $\delta$  scale in parts-per-million (ppm) and are referenced to the residual non-deuterated and deuterated solvent resonances respectively. (CDCl<sub>3</sub> <sup>1</sup>H:  $\delta$  = 7.26 ppm; <sup>13</sup>C:  $\delta$  = 77.2 ppm).

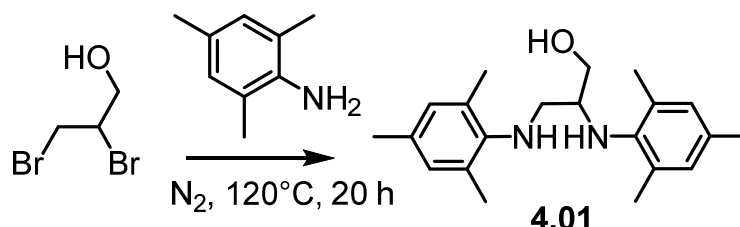
*High-Resolution Mass Spectrometry.* HRMS spectra were recorded by the MS Analytical Facility Service at the University of Warwick or the University of Birmingham on a Bruker UHR-Q-ToF MaXis™ spectrometer with electrospray ionization or a Waters Xevo G2-XS QToF Quadrupole Time-of-Flight mass spectrometer respectively.

*Infrared Spectroscopy.* Infrared (IR) spectroscopy was completed on a PerkinElmer Spectrum 100 FTIR instrument or on an Agilent Technologies Cary 630 FTIR spectrometer.

*Liquid Chromatography-Mass Spectrometry.* Liquid chromatography-mass spectrometry (LCMS) analysis was performed on a Waters ACQUITY UPLC system coupled to a Xevo GS2-XS qToF mass spectrometer in negative ion mode. The oligonucleotides were eluted through an ACQUITY UPLC oligonucleotide BEH C18 column (130Å, 1.7  $\mu$ m, 2.1 x 50 mm) using a 75 mM triethylammonium acetate (TEAA, pH 7.0) solution in H<sub>2</sub>O (buffer A) and a 75 mM TEAA

solution in MeCN (buffer B) at 60 °C and a 0.2 mL/min flow. The data was processed using Promass HR software.

#### 4.5.3 Synthesis of 4.01



The small molecule was prepared based on modified versions of two previously reported protocols.<sup>38, 63</sup> 2,3-Dibromopropanol (2.4 mL, 22.9 mmol) and 2,4,6-trimethylaniline (24.9 mL, 118 mmol) were introduced into a Schlenk tube and degassed. The reaction medium was then stirred at 120 °C for 20 h under N<sub>2</sub>. The temperature was decreased to room temperature and an aqueous solution of NaOH (100 mL, 15 wt%) was added, followed by CH<sub>2</sub>Cl<sub>2</sub> (200 mL) and the mixture was stirred/sonicated until the crude product was solubilized. The organic phase was collected and washed with water (2 x 200 mL) before drying over Na<sub>2</sub>SO<sub>4</sub> and concentrating *in vacuo*. The crude product was purified by column chromatography eluting with a 50:50 mixture of diethyl ether:petroleum ether to yield a white solid (5.8 g, 26%). <sup>1</sup>H NMR (400 MHz; 298K; CDCl<sub>3</sub>) δ = 6.82 (s, 2H Arom-*H*), 6.80 (s, 2H Arom-*H*), 3.97 (dd, 1H, <sup>2</sup>J<sub>H-H</sub> = 11.2 Hz, <sup>3</sup>J<sub>H-H</sub> = 2.6 Hz, CH<sub>A</sub>H<sub>B</sub>OH), 3.85 (dd, 1H, <sup>2</sup>J<sub>H-H</sub> = 11.2 Hz, <sup>3</sup>J<sub>H-H</sub> = 3.8 Hz, CH<sub>A</sub>H<sub>B</sub>OH), 3.4-3.8 (Sb, 2H, 2 x NH), 3.39 (m, 1H, CH), 3.22 (dd, 1H, <sup>2</sup>J<sub>H-H</sub> = 11.8 Hz, <sup>3</sup>J<sub>H-H</sub> = 4.8 Hz, CH<sub>A</sub>H<sub>B</sub>CH), 2.99 (dd, 1H, <sup>2</sup>J<sub>H-H</sub> = 11.8 Hz, <sup>3</sup>J<sub>H-H</sub> = 3.8 Hz, CH<sub>A</sub>H<sub>B</sub>CH), 2.1-2.3 (m, 19H, CH<sub>3</sub>, OH). <sup>13</sup>C NMR (100 MHz; 298K; CDCl<sub>3</sub>) 142.2, 141.7, 132.7, 131.0, 130.6, 129.8, 129.6, 128.8 (Arom-C), 66.1 (CH<sub>2</sub>OH), 56.9 (CH), 52.3 (CH<sub>2</sub>), 20.6, 20.5, 18.9, 17.8 (CH<sub>3</sub>). IR (ν<sub>max</sub> / cm<sup>-1</sup>) 3416s (N-H), 3352m (N-H), 3195b (O-H), 1482s (C=C of Arom). Characterization matches that reported in the

literature,<sup>63</sup> however, approximately 3 wt% 2,4,6-trimethylaniline remains which was deemed not to be an issue moving forward.

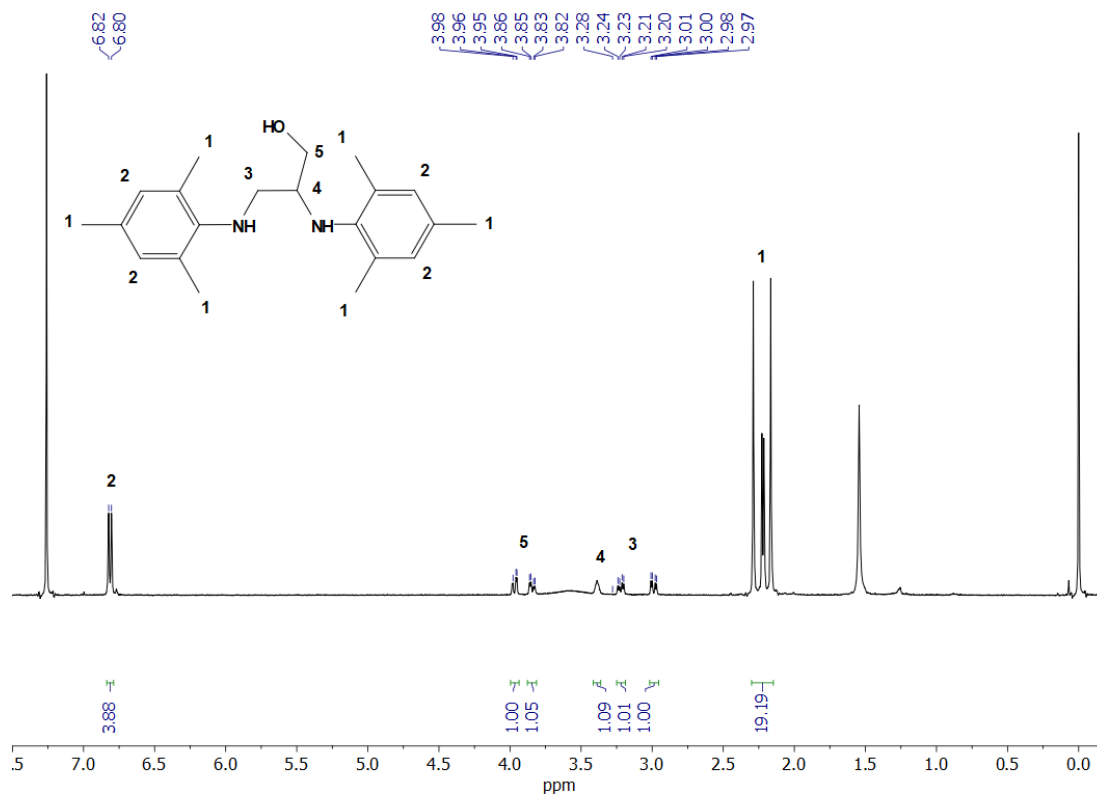
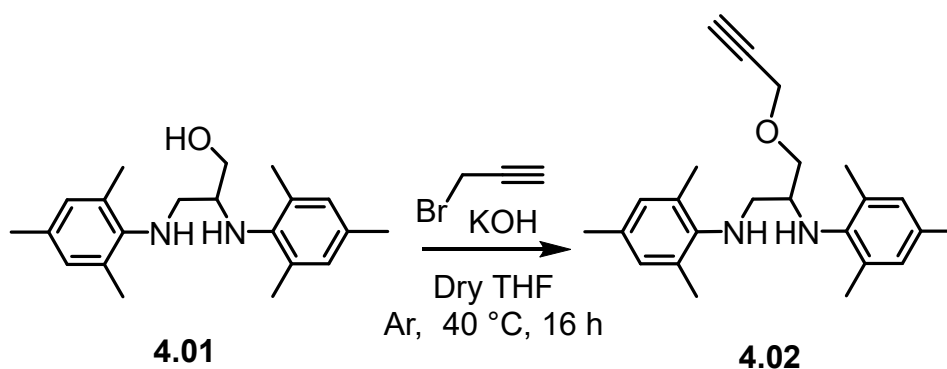


**Figure 4.20** <sup>1</sup>H NMR spectrum of **4.01** in CDCl<sub>3</sub> (400 MHz, 298K).

#### 4.5.4 Synthesis of 4.02



The small molecule was prepared based on modified version of a previously reported protocol.<sup>38</sup> *N,N'*-Dimesityl-2,3-diamino-1-propanol **4.02** (5 g, 15.3 mmol) and dry, degassed THF (65 mL) were placed in a schlenk tube and cooled to 0 °C. Sodium hydride (60% dispersion

in oil) (1.8 g, 45.9 mmol) was slowly added followed by propargyl bromide in toluene (3.4 mL, 30.6 mmol) and the mixture was allowed to slowly warm up to RT. The reaction was then stirred at 40 °C under argon. The reaction was monitored by TLC from 16 h and when the starting material had been consumed (19 h) the mixture was cooled to 0 °C and water (60 mL) was added slowly. The THF solvent was then evaporated under reduced pressure, and the water phase was extracted 3 times with CH<sub>2</sub>Cl<sub>2</sub> (80 mL). The organic phases were combined, dried with Na<sub>2</sub>SO<sub>4</sub> and evaporated. The crude product was solubilized in acetonitrile and then washed with hexane (40 mL, x4). The acetonitrile fraction was concentrated *in vacuo* to obtain a brown solid (4.1 g, 73%). <sup>1</sup>H NMR (400 MHz; 298K; CDCl<sub>3</sub>) δ = 6.81 (s, 4H, Arom-H), 4.17 (dd, 1H, <sup>2</sup>J<sub>H-H</sub> = 15.6 Hz, <sup>4</sup>J<sub>H-H</sub> = 2.2 Hz, CH<sub>A</sub>H<sub>B</sub>C≡CH), 4.09 (dd, 1H, <sup>2</sup>J<sub>H-H</sub> = 15.6, <sup>4</sup>J<sub>H-H</sub> = 2.2 Hz, CH<sub>A</sub>H<sub>B</sub>C≡CH), 3.48-3.65 (m, 5H, CH, CH<sub>2</sub>O, 2 x NH), 3.27 (dd, 1H, <sup>2</sup>J<sub>H-H</sub> = 11.9 Hz, <sup>3</sup>J<sub>H-H</sub> = 5.6 Hz, CH<sub>A</sub>H<sub>B</sub>,CH), 3.02 (dd, <sup>1</sup>H, <sup>2</sup>J<sub>H-H</sub> = 11.9 Hz, <sup>3</sup>J<sub>H-H</sub> = 5.8 Hz, CH<sub>A</sub>H<sub>B</sub>,CH), 2.40 (t, 1H, <sup>4</sup>J = 2.4 Hz, C≡CH), 2.23-2.30 (m, 18H, CH<sub>3</sub>). <sup>13</sup>C NMR (100 MHz; 298K; CDCl<sub>3</sub>) 143.6, 141.6, 131.2, 130.8, 129.9, 129.6, 129.4, 129.2 (Arom-C), 74.7 (C≡CH), 70.3 (OCH<sub>2</sub>CHCH<sub>2</sub>), 58.4 (CH<sub>2</sub>C≡H), 56.5 (OCH<sub>2</sub>CHCH<sub>2</sub>), 50.6 (OCH<sub>2</sub>CHCH<sub>2</sub>), 20.49, 18.78, 18.30 (CH<sub>3</sub>). IR (ν<sub>max</sub> / cm<sup>-1</sup>) 3268 (Alkyne C-H), 2114w (Alkyne C≡C). Characterization matches that reported in the literature.<sup>38</sup>

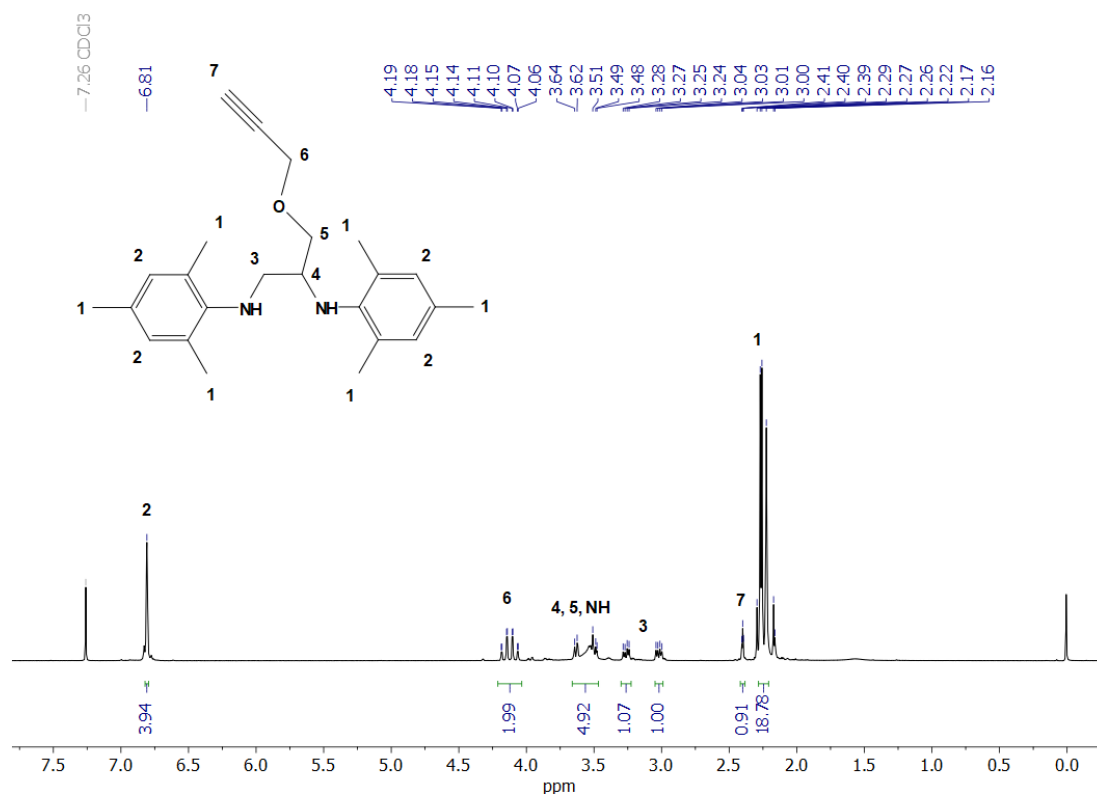
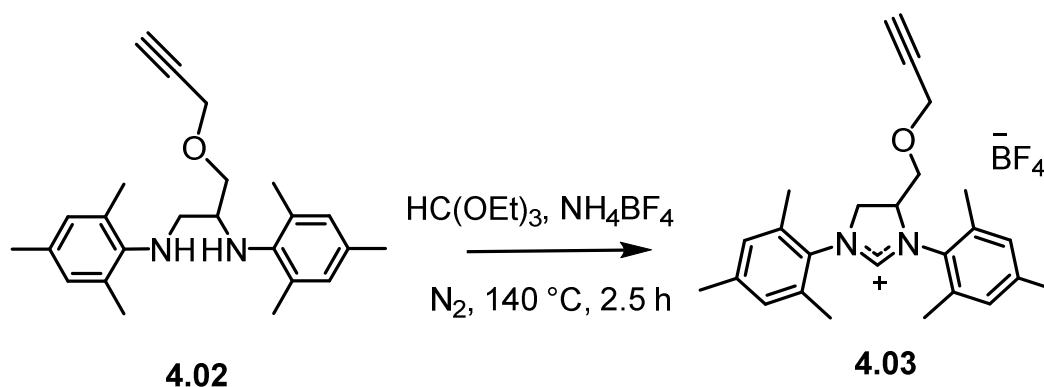


**Figure 4.21**  $^1\text{H}$  NMR spectrum of **4.02** in  $\text{CDCl}_3$  (400 MHz, 298K).

#### 4.5.5 Synthesis of 4.03



The ligand was prepared according to a previously reported protocol.<sup>38</sup> **4.02** (2 g, 5.49 mmol), triethyl orthoformate (1.83 mL, 11 mmol) and  $\text{NH}_4\text{BF}_4$  (0.576 g, 5.49 mmol) were placed in a schlenk tube and stirred at 140 °C for 2.5 h under Ar. At the end of the reaction the temperature was decreased to 50 °C and the liquid was evaporated under reduced pressure, to obtain a brown solid. The brown solid was collected and washed several times with pentane

and Et<sub>2</sub>O and then dried under reduced pressure to obtain a light brown solid (2.1 g, 82 %). <sup>1</sup>H NMR (400 MHz; 298K; CDCl<sub>3</sub>) δ = 7.75 (s, 1H, *H*-imidazolium), 6.98 (s, 2H, Arom-*H*), 6.98 (s, 2H, Arom-*H*), 5.25-5.30 (m, 1H, OCH<sub>2</sub>CHCH<sub>2</sub>), 4.77 (t, 1H, <sup>2</sup>J<sub>H-H</sub> = 12 Hz, OCH<sub>2</sub>CHCH<sub>A</sub>H<sub>B</sub>). 4.40 (dd, 1H, <sup>2</sup>J<sub>H-H</sub> = 12 Hz, <sup>3</sup>J<sub>H-H</sub> = 7.6 Hz, OCH<sub>2</sub>CHCH<sub>A</sub>H<sub>B</sub>), 4.23 (d, 2H, <sup>4</sup>J<sub>H-H</sub> = 2.0 Hz, CH<sub>2</sub>C≡CH), 3.59-3.75 (m, 2H, OCH<sub>2</sub>CHCH<sub>2</sub>), 2.44-2.45 (m, 1H, C≡CH), 2.3-2.42 (m, 18H, CH<sub>3</sub>). <sup>13</sup>C NMR (100 MHz; CDCl<sub>3</sub>; 298K) 157.6 (C-imidazolium), 140.8, 140.5, 136.7, 135.60, 135.3, 130.6, 130.2, 130.1, 128.1 (Arom-C), 75.9 (C≡CH), 66.2 (OCH<sub>2</sub>CHCH<sub>2</sub>), 63.8 (OCH<sub>2</sub>CHCH<sub>2</sub>), 58.5 (CH<sub>2</sub>C≡H), 52.8 (OCH<sub>2</sub>CHCH<sub>2</sub>), 21.0, 18.2, 17.6, (CH<sub>3</sub>). IR (ν<sub>max</sub> / cm<sup>-1</sup>) 3277 (Alkyne C-H), 1629s (C=N), 1033s (BF<sub>4</sub>). Characterization matches that reported in the literature.<sup>38</sup>

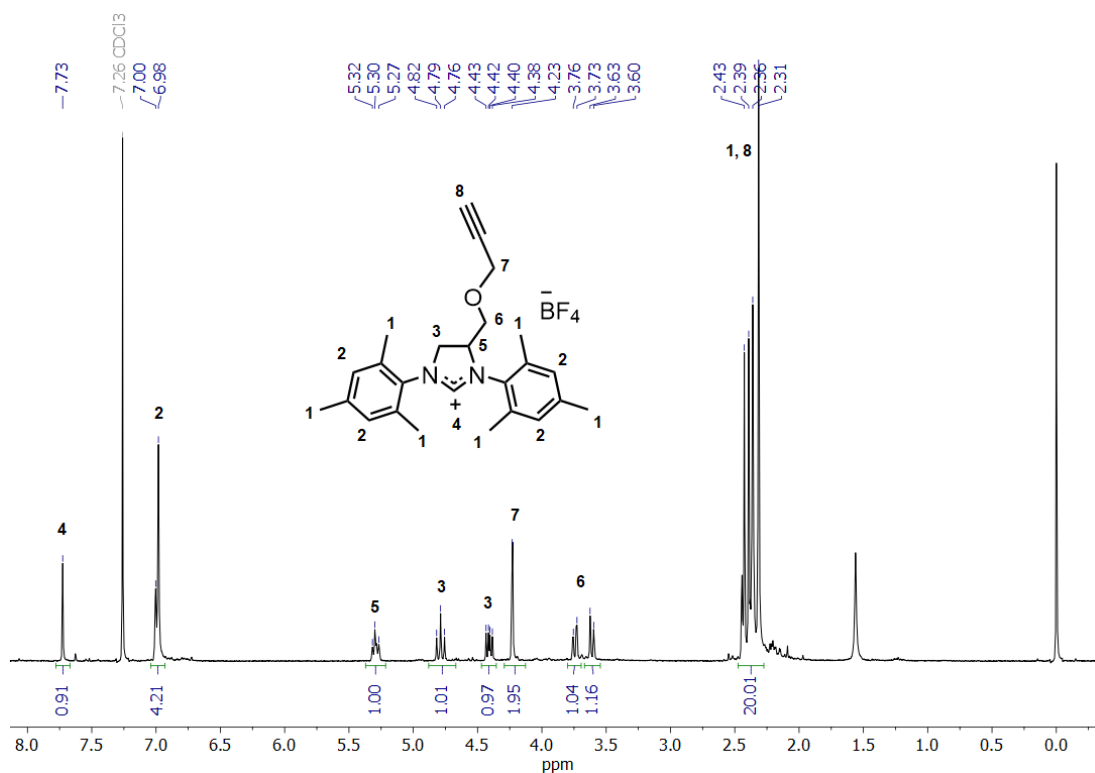
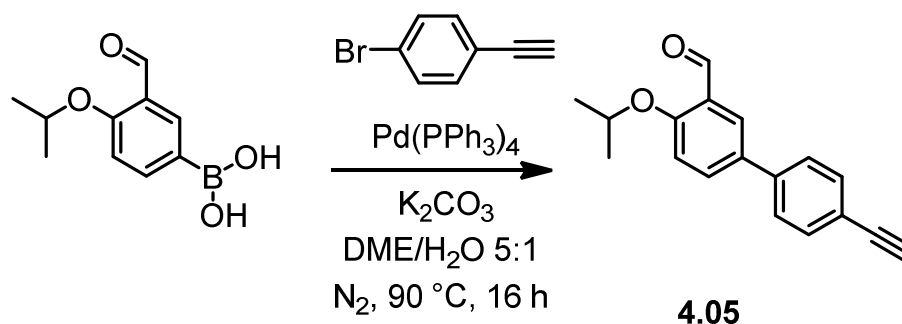


**Figure 4.22** <sup>1</sup>H NMR spectrum of **4.03** in CDCl<sub>3</sub> (400 MHz, 298K).

#### 4.5.6 Synthesis of 4.05



1-Bromo-4-ethynylbenzene (0.452 g, 2.5 mmol), 3-formyl-4-isopropoxyphenylboronic acid (0.520 g, 2.5 mmol) and potassium carbonate (0.864 g, 6.25 mmol) in DME/ $\text{H}_2\text{O}$  (5:1, 10 mL) were purged with  $\text{N}_2$  for 5 mins. Tetrakis(triphenylphosphine)palladium (0) (0.014 g, 0.012 mmol) was added, and the reaction mixture was heated to  $90\text{ }^\circ\text{C}$  and stirred for 16 h. The reaction mixture was cooled to room temperature, filtered through a pad of Celite and extracted in EtOAc. The organic layer was washed with 20 mL  $\text{H}_2\text{O}$  and then the aqueous layer was washed with 2 x 20 mL EtOAc. The organic layers were combined, dried over  $\text{MgSO}_4$  and then evaporated to yield a brown product. The crude product was purified by silica column chromatography eluting with 15 vol% EtOAc in hexane to yield a white solid (0.289 g, 44%).  $^1\text{H}$  NMR (400 MHz; 298K;  $\text{CDCl}_3$ )  $\delta$  = 10.53 (s, 1H, CHO), 8.07 (d, 1H,  $^4J_{\text{H-H}} = 2.4$  Hz, Arom-H), 7.76 (dd, 1H,  $^3J_{\text{H-H}} = 8.6$  Hz,  $^4J_{\text{H-H}} = 2.4$  Hz, Arom-H), 7.55 (s, 4H, 4 x Arom-H), 7.08 (d, 1H,  $^3J_{\text{H-H}} = 8.6$  Hz, Arom-H), 4.74 (sept, 1H,  $^3J_{\text{H-H}} = 6.2$  Hz,  $\text{OCH}(\text{CH}_3)_2$ ), 3.13 (s, 1H,  $\text{C}\equiv\text{CH}$ ), 1.44 (d, 6H,  $^3J_{\text{H-H}} = 6.2$  Hz,  $\text{OCH}(\text{CH}_3)_2$ ).  $^{13}\text{C}$  NMR (100 MHz; 298K;  $\text{CDCl}_3$ ) 190.2 (CHO) 160.5, 140.0, 134.2, 132.8, 132.6, 132.3, 132.2, 126.7, 126.6, 126.0, 121.0, 114.6 (Arom-C), 83.6, 78.0 ( $\text{C}\equiv\text{CH}$ ), 71.5 (CH), 22. ( $\text{CH}_3$ ). IR ( $\nu_{\text{max}} / \text{cm}^{-1}$ ) 3263 (C-H of alkyne), 1679s (C=O). HR-MS  $m/z$  calculated  $[\text{M} + \text{Na}]^+$   $m/z$  calculated 287.1043 found 287.1044.

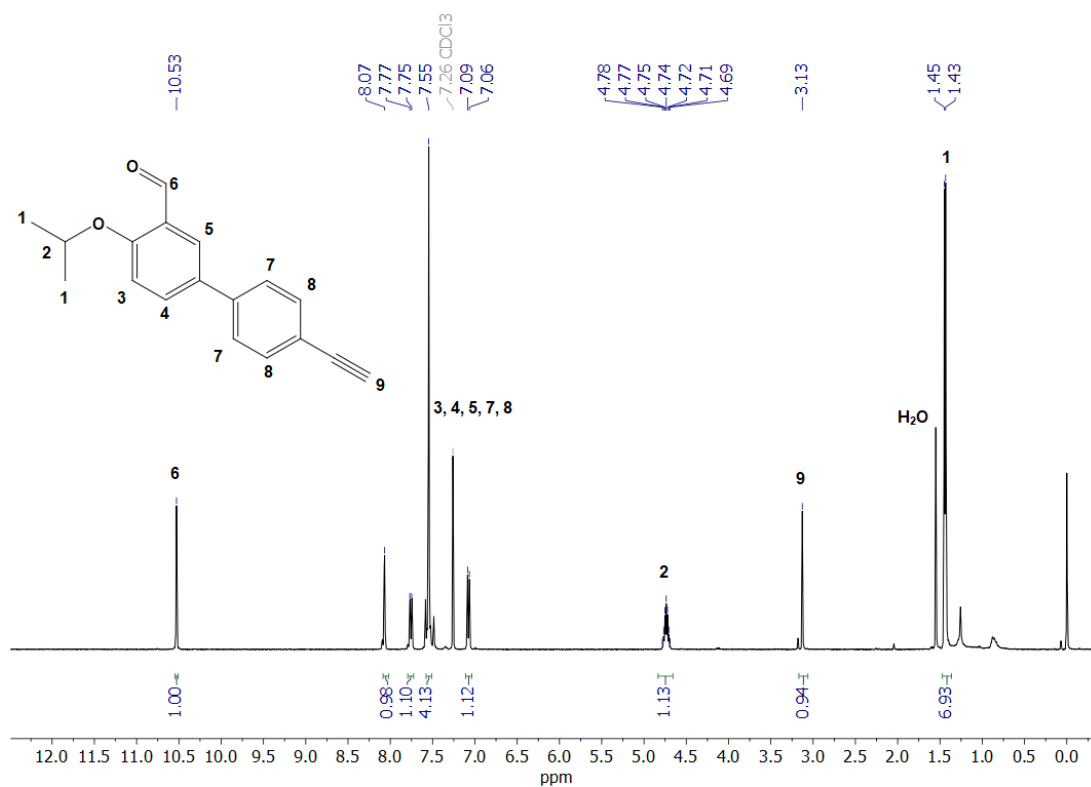


**Figure 4.23**  $^1\text{H}$  NMR spectrum of **4.05** in  $\text{CDCl}_3$  (400 MHz, 298K).

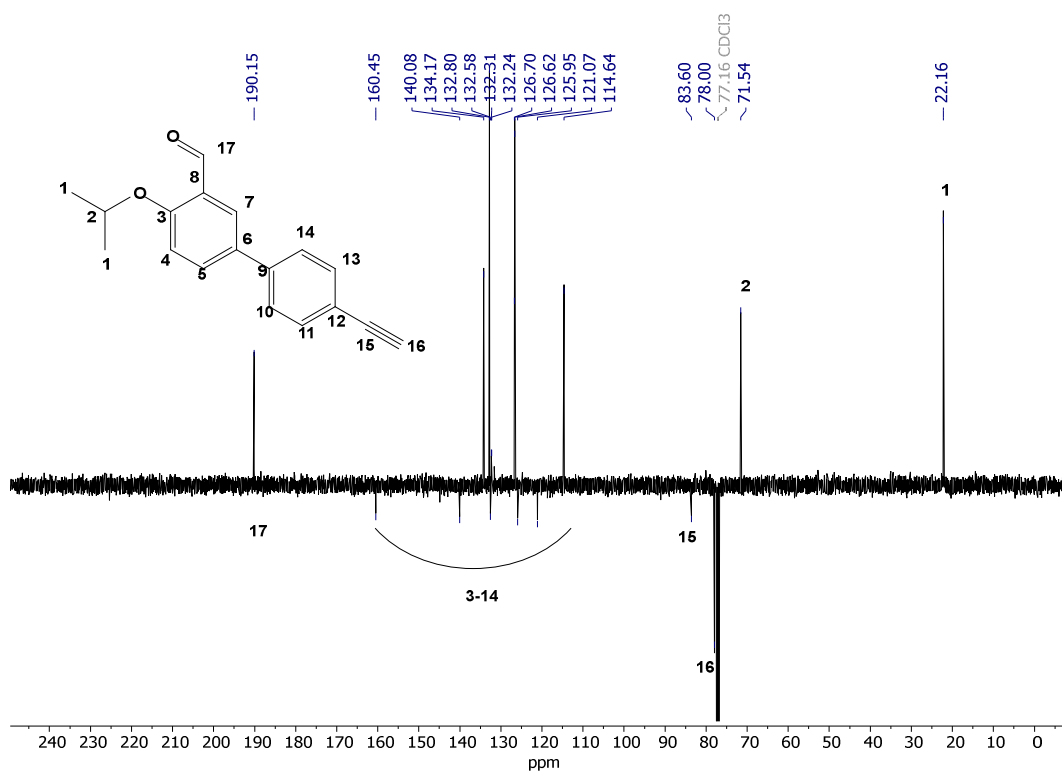
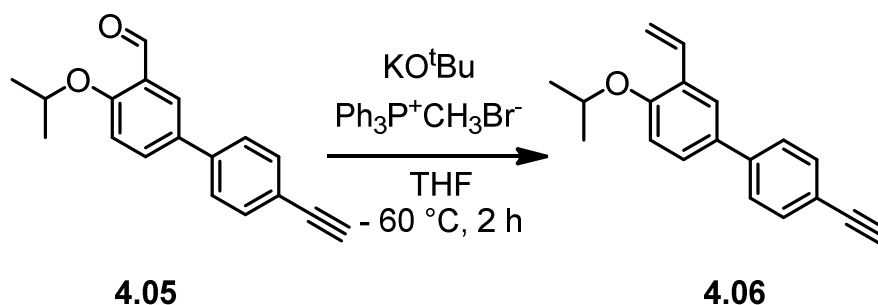


**Figure 4.24**  $^{13}\text{C}$ -JMOD NMR spectrum of **4.05** in  $\text{CDCl}_3$  (100 MHz, 298K).



#### 4.5.7 Synthesis of 4.06



An oven dried flask purged with N<sub>2</sub> was charged with BrCH<sub>3</sub>PPh<sub>3</sub> (0.401 g, 1.12 mmol, 1.2 equiv), dry and degassed THF (7.5 mL) and KO<sup>t</sup>Bu (0.157 g, 1.40 mmol, 1.5 equiv) in that order to give a bright yellow solution. The solution was allowed to stir at room temperature under a positive N<sub>2</sub> pressure for 2 h prior to cooling to approximately -60 °C with a dry-ice/acetone bath. **4.05** in 3 mL of dry and degassed THF was slowly added over a period of 20 minutes while maintaining a temperature of approximately -60 °C. The reaction was then allowed to continue under a positive nitrogen pressure whilst slowly warming to room temperature. After 2 h, the mixture was diluted with diethyl ether, transferred to a separatory funnel and rinsed (x2) with saturated NaHCO<sub>3</sub> and (x2) with brine. The organic layer was then dried over Na<sub>2</sub>SO<sub>4</sub> and evaporated to yield a yellow oil which was passed through a plug of neutral alumina with 5 vol% EtOAc in hexane. A clear, pale yellow oil was obtained (0.0648 g, 27%).

<sup>1</sup>H NMR (400 MHz; 298K; CDCl<sub>3</sub>) δ = 7.69 (d, 1H, <sup>4</sup>J<sub>H-H</sub> = 2 Hz, Arom-H), 7.54 (s, 4H, 4 x Arom-H), 7.43 (dd, 1H, <sup>3</sup>J<sub>H-H</sub> = 8.5 Hz, <sup>4</sup>J<sub>H-H</sub> = 2 Hz, Arom-H), 7.09 (dd, 1H, <sup>3</sup>J<sub>H-H</sub> = 17.2 Hz, <sup>3</sup>J<sub>H-H</sub> = 11.2 Hz, CH<sub>2</sub>=CH), 6.95 (d, 1H, <sup>3</sup>J<sub>H-H</sub> = 8.5 Hz, Arom-H), 5.81 (dd, 1H, <sup>2</sup>J<sub>H-H</sub> = 1.2 Hz, <sup>3</sup>J<sub>H-H</sub> = 17.2 Hz, CH<sub>A</sub>H<sub>B</sub>=CH), 5.30 (dd, 1H, <sup>2</sup>J<sub>H-H</sub> = 1.2 Hz, <sup>3</sup>J<sub>H-H</sub> = 11.2 Hz, CH<sub>A</sub>H<sub>B</sub>=CH), 4.60 (sept, 1H, <sup>3</sup>J<sub>H-H</sub> = 5.8 Hz, OCH(CH<sub>3</sub>)<sub>2</sub>), 3.12 (s, 1H, C≡H), 1.38 (d, 6H, <sup>3</sup>J<sub>H-H</sub> = 5.8 Hz) OCH(CH<sub>3</sub>)<sub>2</sub>). <sup>13</sup>C NMR (100 MHz; 298K; CDCl<sub>3</sub>) 155.1, 141.3, 132.5, 131.9, 128.1, 127.2, 126.5, 125.2, 120.3, 114.3 (Arom-C and

C=CH), 114.5 (C=CH<sub>2</sub>) 83.7, 77.5 (C≡CH), 70.9 (CH), 22.18 (CH<sub>3</sub>). IR ( $\nu_{\max}$  / cm<sup>-1</sup>) 3291 (C-H of alkyne), 2106w (C≡C of alkyne), 1624w (C=C of alkene), 1602m (C=C of aromatic). HR-MS [M + H]<sup>+</sup> m/z calculated 263.1430 found 263.1430.

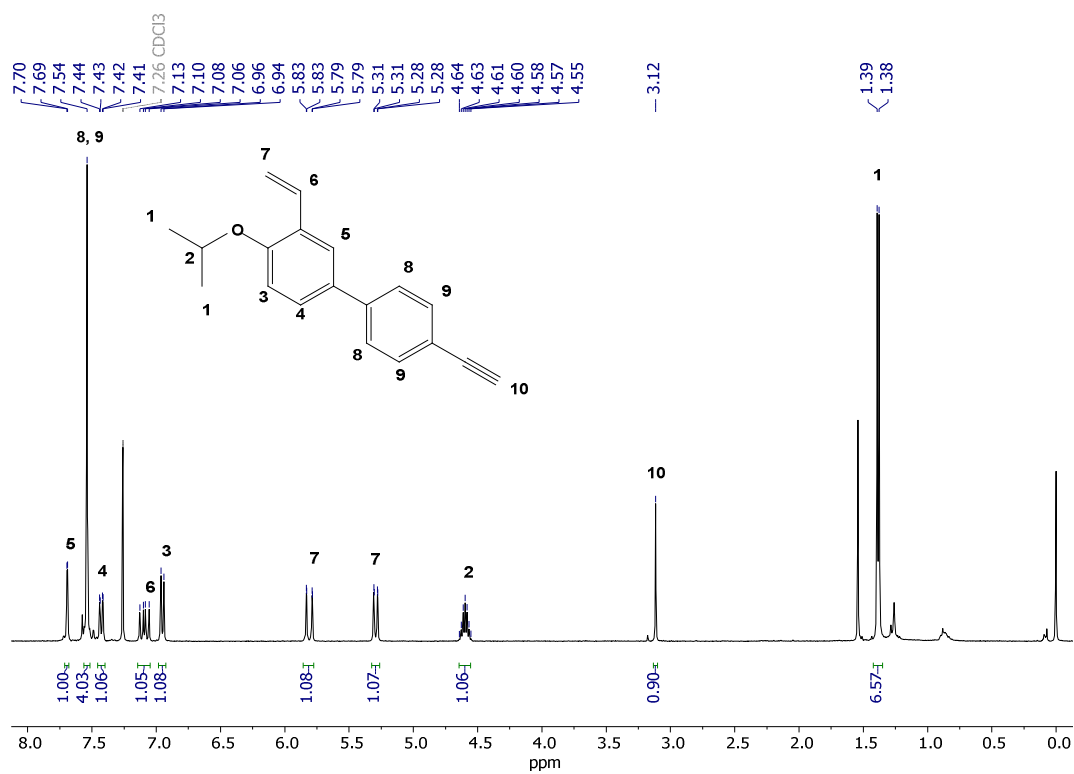


**Figure 4.25** <sup>1</sup>H NMR spectrum of **4.06** in CDCl<sub>3</sub> (400 MHz, 298K).

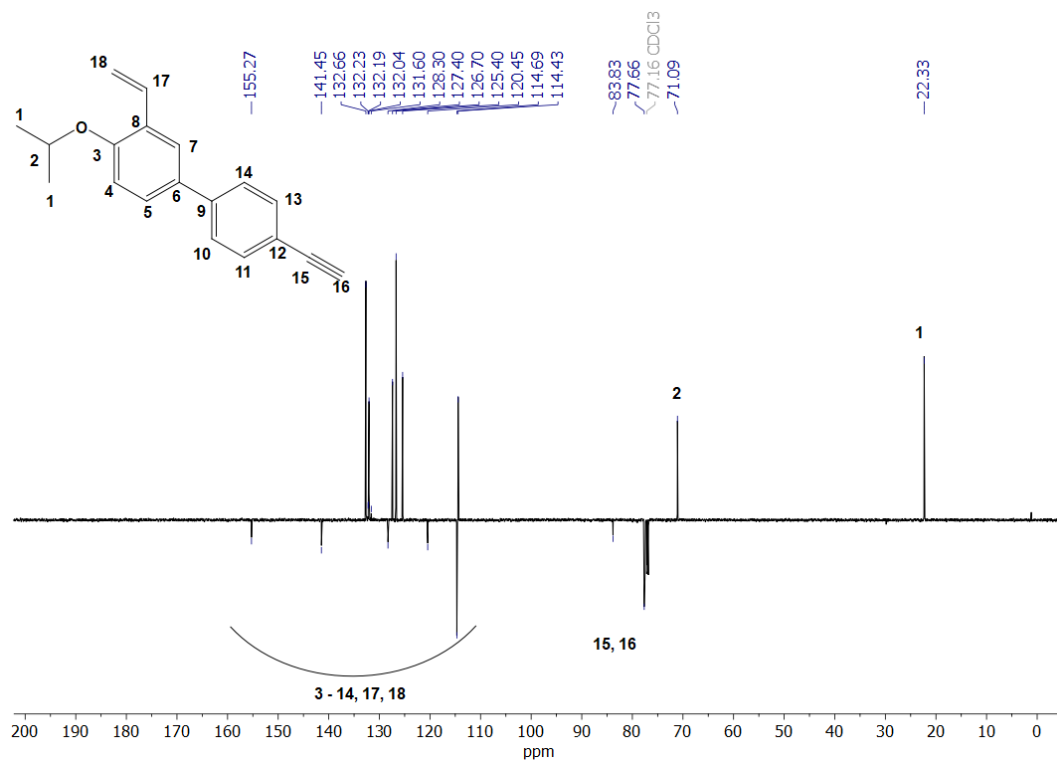
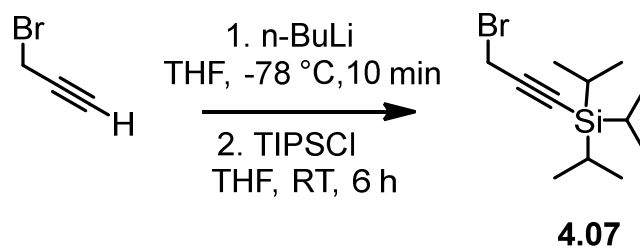


**Figure 4.26**  $^{13}\text{C}$  NMR spectrum of **4.06** in  $\text{CDCl}_3$  (100 MHz, 298K).

#### 4.5.8 Synthesis of 4.07



The small molecule was prepared based on a previous procedure.<sup>64</sup> A solution of 5 g of propargyl bromide (80 w% in toluene: 33.6 mmol) in 100 ml of THF was cooled to  $-78^\circ\text{C}$ , after which 21 ml (33.6 mmol) of *n*-BuLi (1.6 M in hexane) was added dropwise. After stirring for 10 minutes, 6.48 g (33.6 mmol) of TIPS-Cl was added dropwise. When the addition was complete, the mixture was slowly heated to room temperature and stirred for another 6 h. The mixture was quenched with ammonium chloride (20 mL), extracted with dichloromethane (2 x 50 mL) and dried over  $\text{MgSO}_4$ . The crude product was purified with column chromatography (5 v%

dichloromethane in hexane) to yield a colourless oil (3.7433 g, 41%).  $^1\text{H}$  NMR (400 MHz; 298 K;  $\text{CDCl}_3$ )  $\delta$  = 3.94 (s, 2H,  $\text{CH}_2\text{Br}$ ) 1.07 (s, 21H, 3 x  $\text{CH}(\text{CH}_3)_2$ ).  $^{13}\text{C}$  NMR (100 MHz; 298K;  $\text{CDCl}_3$ ) 101.9 ( $\text{CCH}_2\text{Br}$ ) 89.1 ( $\text{CSi}(\text{CH}(\text{CH}_3)_2)_3$ ) 18.5 ( $\text{CSi}(\text{CH}(\text{CH}_3)_2)_3$ ) 14.9 ( $\text{CCH}_2\text{Br}$ ) 11.1 ( $\text{CSi}(\text{CH}(\text{CH}_3)_2)_3$ ). Characterization matches that reported in the literature.<sup>65</sup>

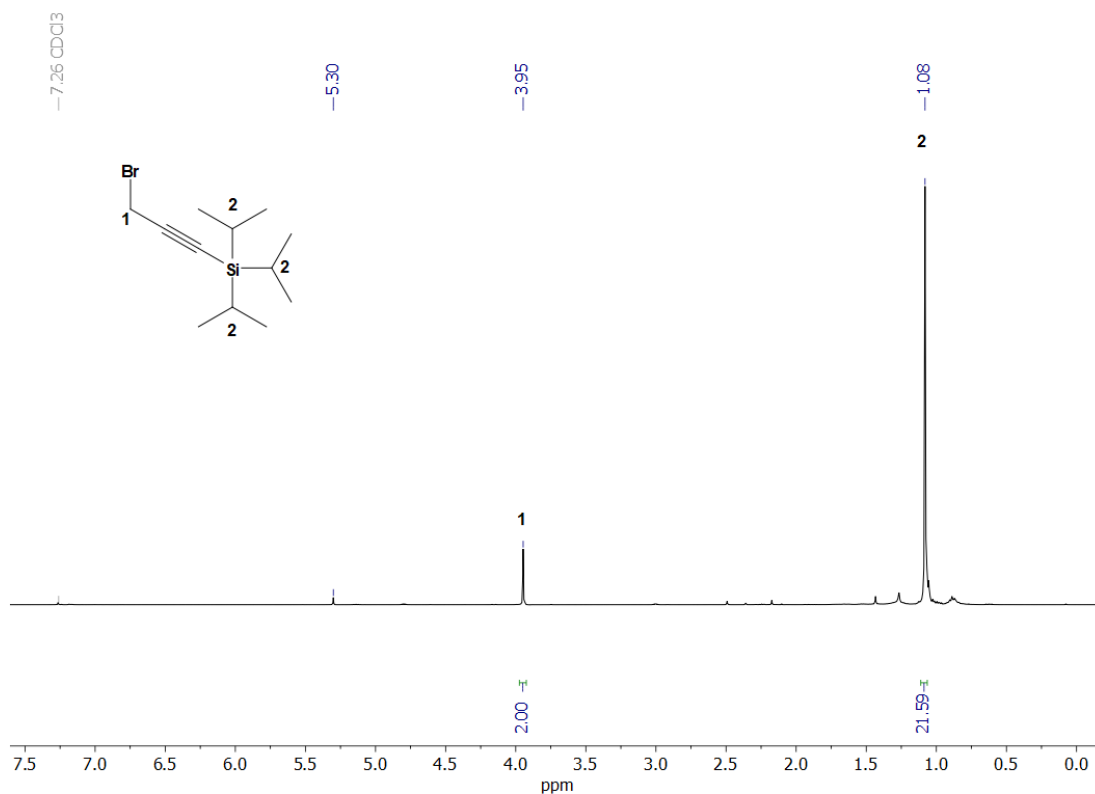
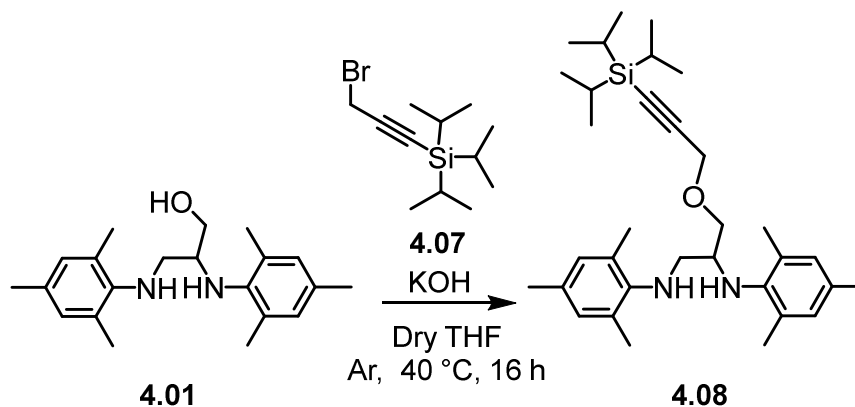


**Figure 4.27**  $^1\text{H}$  NMR spectrum of **4.07** in  $\text{CDCl}_3$  (400 MHz, 298K).

#### 4.5.9 Synthesis of 4.08



The synthesis was conducted as described for **4.02**. The crude product was then purified by column chromatography eluting with 10% Et<sub>2</sub>O in petroleum ether to yield a pale yellow oil, 0.7 g, 59%. <sup>1</sup>H NMR (400 MHz; 298K; CDCl<sub>3</sub>) δ = 6.81 (d, 4H, <sup>4</sup>J<sub>H-H</sub> = 7.0 Hz, CH), 4.25 – 4.09 (m, 2H, CH<sub>2</sub>), 3.65 (dd, 1H, <sup>2</sup>J<sub>H-H</sub> = 9.0, <sup>3</sup>J<sub>H-H</sub> = 2.4 Hz, CH<sub>2</sub>), 3.60 – 3.54 (m, 1H, CH), 3.48 (dd, 1H, <sup>2</sup>J<sub>H-H</sub> = 9.0 Hz, <sup>3</sup>J<sub>H-H</sub> = 4.2 Hz, CH<sub>2</sub>), 3.30 (dd, 1H, <sup>2</sup>J<sub>H-H</sub> = 11.9 Hz, <sup>3</sup>J<sub>H-H</sub> = 5.5 Hz, CH<sub>2</sub>), 3.03 (dd, 1H, <sup>2</sup>J<sub>H-H</sub> = 11.9 Hz, <sup>3</sup>J<sub>H-H</sub> = 6.2 Hz, CH<sub>2</sub>), 2.33 – 2.20 (m, 18H, CH<sub>3</sub>), 1.05 (s, 21H, CH(CH<sub>3</sub>)<sub>2</sub>). <sup>13</sup>C NMR (100 MHz; 298K; CDCl<sub>3</sub>) 141.6, 131.5, 131.0, 130.1, 129.7, 129.6, 129.4 (Arom-C), 102.9, 88.2 (CCSi), 70.1 (CH<sub>2</sub>), 59.2 (CH<sub>2</sub>), 56.3 (CH). 51.0 (CH<sub>2</sub>), 20.5, 18.8, 18.5, 18.3, 11.1 (CH<sub>3</sub>). HR-MS [M + H]<sup>+</sup> m/z calculated 521.3922 found 521.3924.

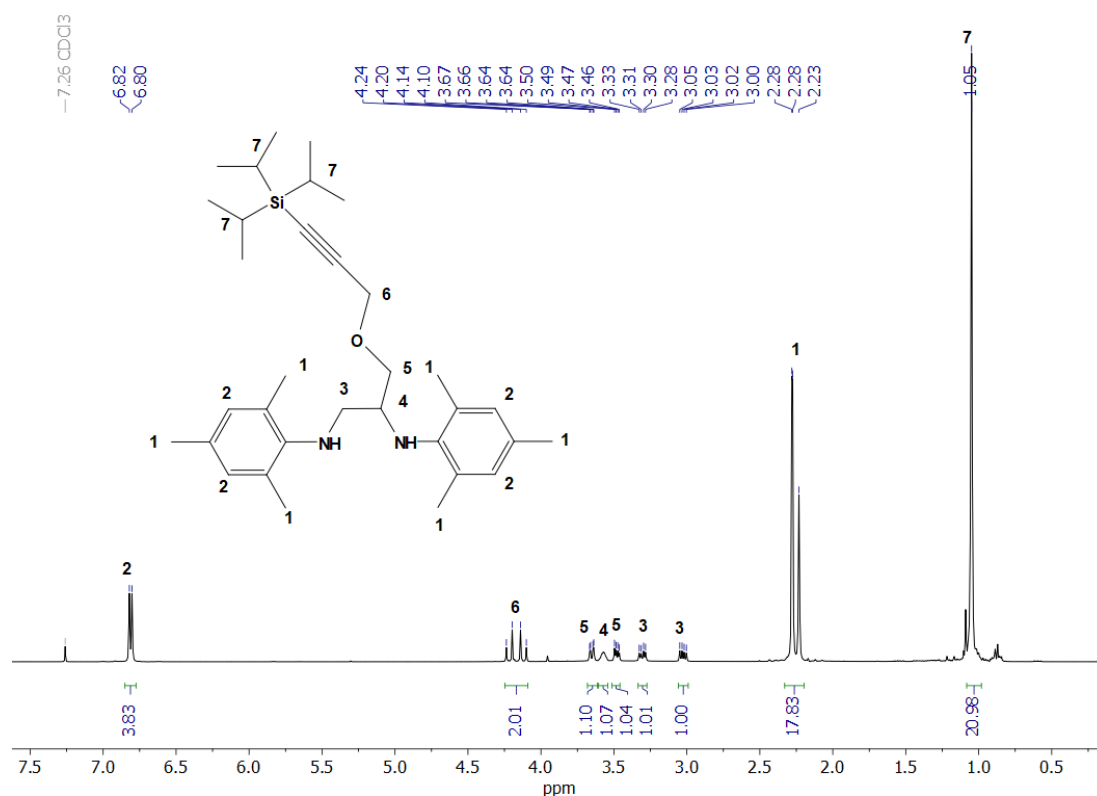


**Figure 4.28** <sup>1</sup>H NMR spectrum of **4.08** in CDCl<sub>3</sub> (400 MHz, 298K).

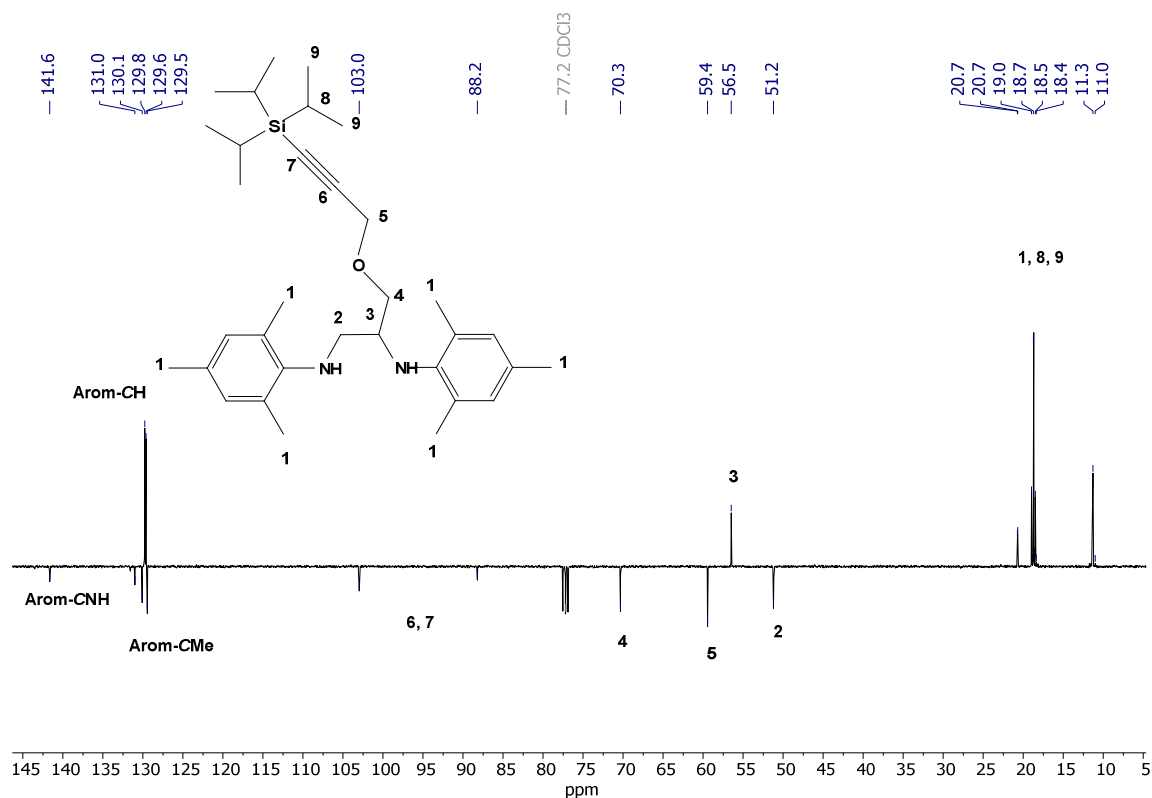
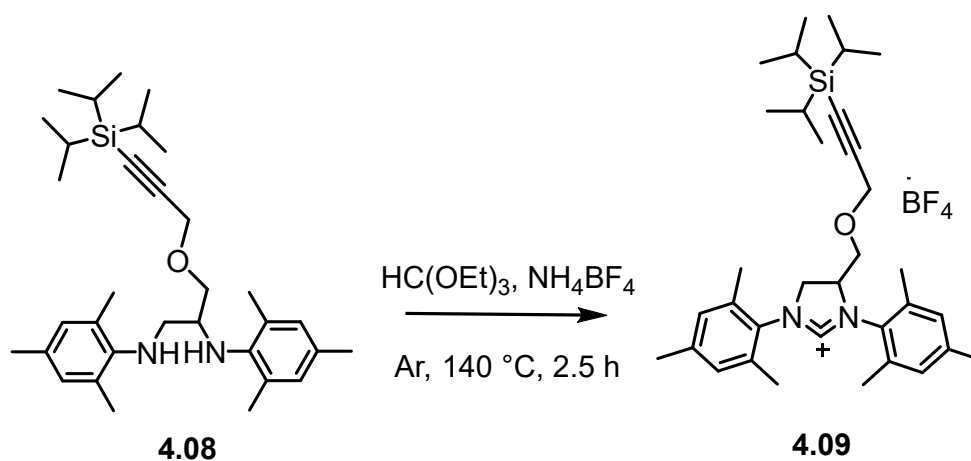


Figure 4.29  $^{13}\text{C}$ -JMOD NMR spectrum of **4.08** in  $\text{CDCl}_3$  (100 MHz, 298K).

#### 4.5.10 Synthesis of 4.09



The synthesis was conducted as described for **4.03**. The brown solid was collected recrystallized from hot ethanol and washed with pentane to yield an off-white solid, 0.13 g, 24%.  $^1\text{H}$  NMR (400 MHz; 298K;  $\text{CDCl}_3$ )  $\delta$  = 7.79 (s, 1H, CH), 6.97– 6.95 (m, 4H, CH), 5.28 – 5.24 (m, 1H, CH), 4.79-4.73 (m, 1H,  $\text{CH}_2$ ), 4.41-4.36 (m, 1H,  $\text{CH}_2$ ), 4.35 – 4.20 (m, 2H,  $\text{CH}_2$ ) 3.65 (s,

2H, CH<sub>2</sub>), 2.41 – 2.31 (m, 18H, CH<sub>3</sub>), 1.02 (s, 21H, CH(CH<sub>3</sub>)<sub>2</sub>). <sup>13</sup>C NMR (100 MHz; 298K; CDCl<sub>3</sub>) 158.1 (NCHN), 140.9, 140.6, 135.8, 135.7, 130.8, 130.4, 130.1, 128.3 (Arom-C), 101.1, 89.5 (CCSi), 66.2 (CH<sub>2</sub>), 63.9(CH), 59.6 (CH<sub>2</sub>), 53.0 (CH<sub>2</sub>), 21.2, 21.1, 18.6, 18.4, 17.8, 17.7, 11.2 (CH<sub>3</sub> and CH). HR-MS [M + H]<sup>+</sup> m/z calculated 531.3765 found 531.3767.

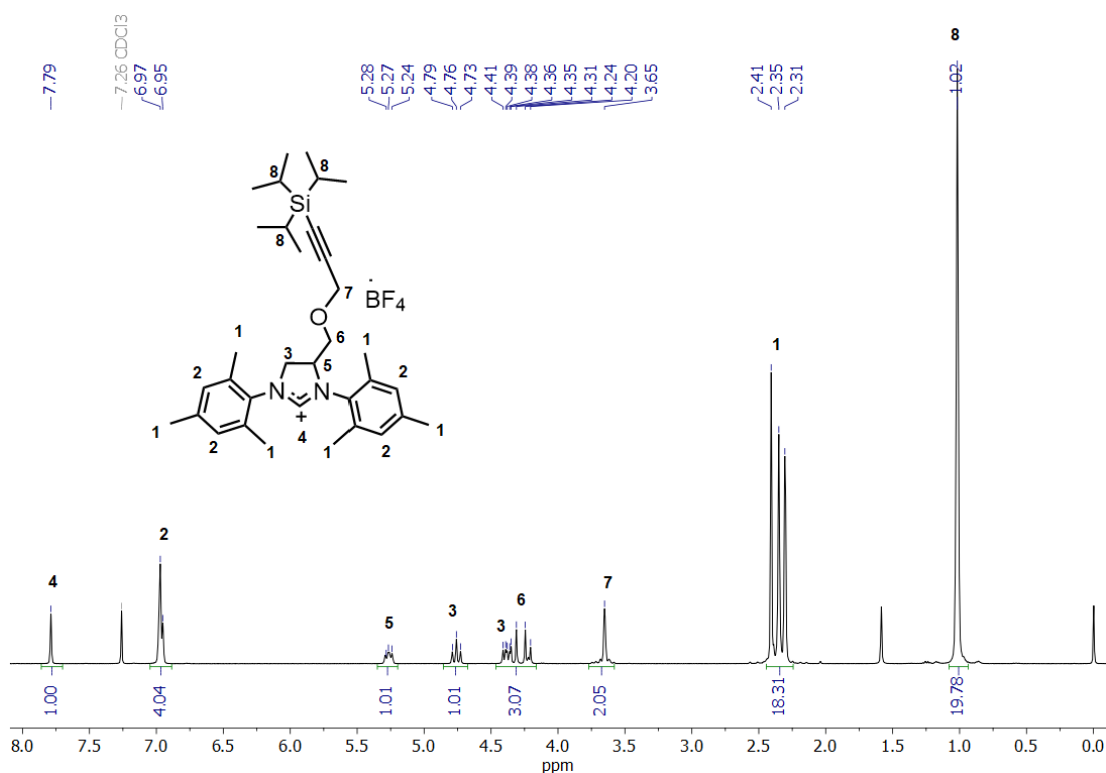


**Figure 4.30** <sup>1</sup>H NMR spectrum of **4.09** in CDCl<sub>3</sub> (400 MHz, 298K).

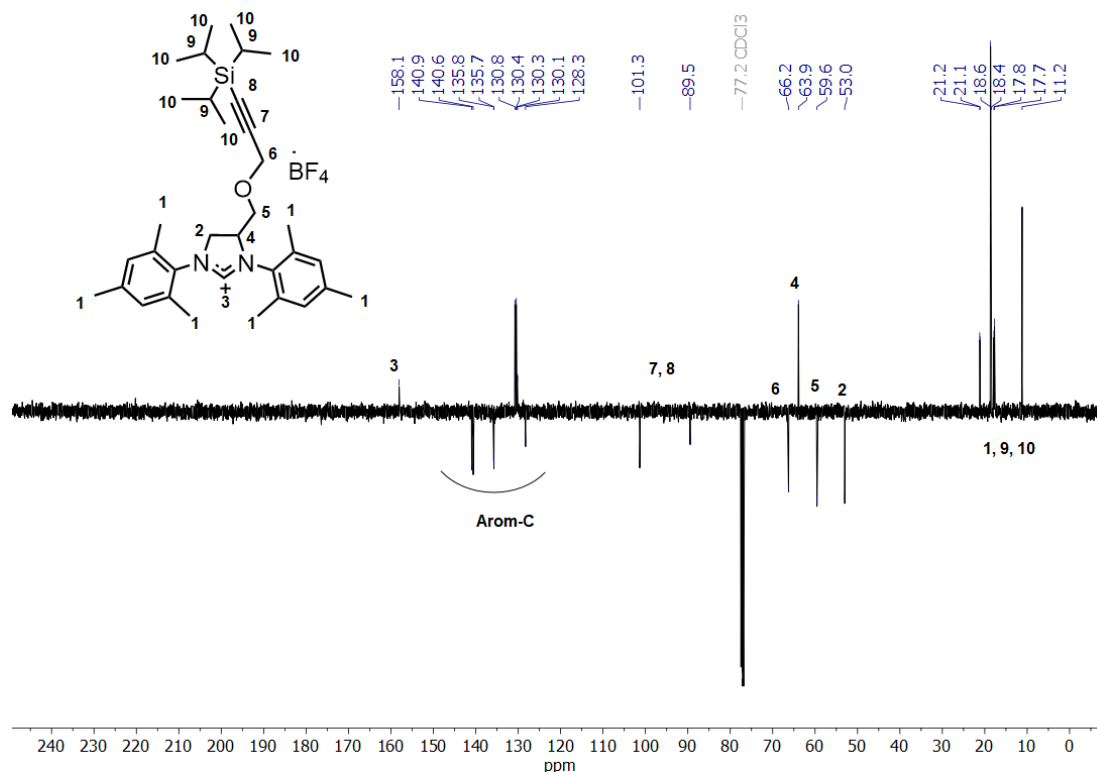
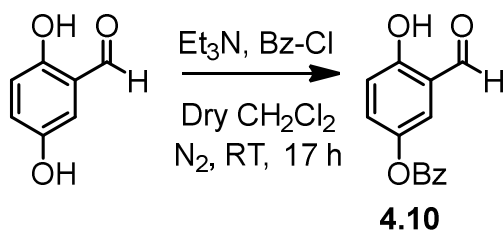


**Figure 4.31**  $^{13}\text{C}$  NMR spectrum of **4.09** in  $\text{CDCl}_3$  (100 MHz, 298K).

#### 4.5.11 Synthesis of 4.10



2,5-Dihydroxybenzaldehyde (10 g, 72.4 mmol) was dissolved in dry  $\text{CH}_2\text{Cl}_2$  in a schlenk and cooled to  $0\text{ }^\circ\text{C}$ . Triethylamine (22.2 mL, 159 mmol) was added to the schlenk followed by benzoyl chloride (9.25 mL, 79.6 mmol). The schlenk was allowed to warm to room temperature and the solution stirred for 17 h. Upon completion of the reaction the solution was diluted with  $\text{CH}_2\text{Cl}_2$  and washed three times with brine prior to drying over  $\text{Na}_2\text{SO}_4$  and concentration *in vacuo*. The crude product was purified by silica column chromatography eluting with  $\text{CH}_2\text{Cl}_2$  and then recrystallized in methanol to yield a white powder, 9.7 g, 55%.  $^1\text{H}$



NMR (300 MHz; 298 K; CDCl<sub>3</sub>) δ =10.95 (s, 1H, CHO), 9.89 (s, 1H, OH), 8.22-8.18 (m, 2H, CH), 7.69-7.64 (m, 1H, CH), 7.56-7.51 (m, 2H, CH), 7.47 (d, 3 Hz, 1H CH), 7.39 (dd, 9Hz, 3 Hz, 1H CH), 7.06 (d, 9 Hz, 1H, CH). Characterization matches that reported in the literature.<sup>66</sup>

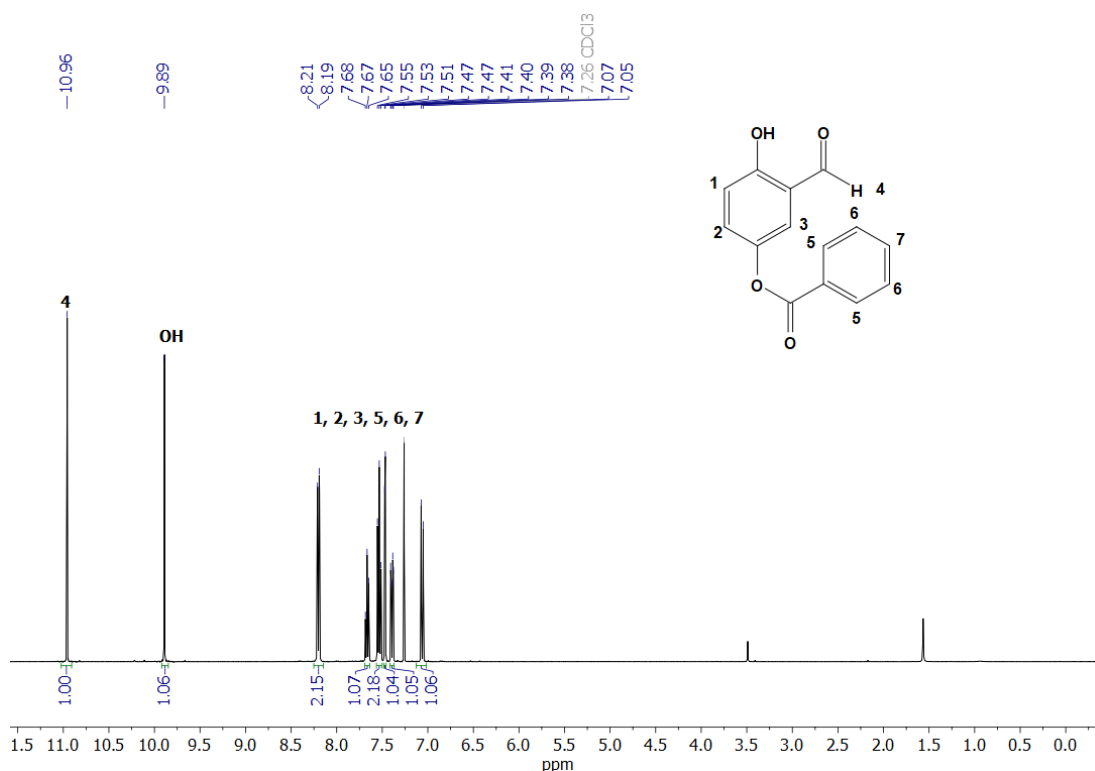
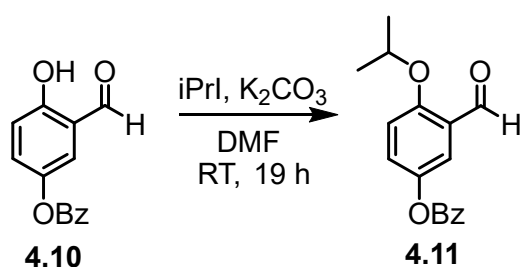


**Figure 4.32** <sup>1</sup>H NMR spectrum of **4.10** in CDCl<sub>3</sub> (300 MHz, 298K).

#### 4.5.12 Synthesis of 4.11



2-iodopropane (9.9 mL, 99 mmol), **4.10** (8 g, 33 mmol) and K<sub>2</sub>CO<sub>3</sub> (6.8g, 49.5 mmol) was combined in a round-bottom-flask and solubilised in DMF (260 mL). The solution was stirred at room temperature for 19 h and then the solvent was removed in vacuo. The crude product was solubilised in ethyl acetate and washed twice with brine prior to drying over Na<sub>2</sub>SO<sub>4</sub>. The

solvent was removed *in vacuo* to yield a light brown solid which was further purified by recrystallization from methanol to yield an off-white solid. 6.2 g, 63% which was used without further purification.  $^1\text{H NMR}$  (300 MHz; 298 K;  $\text{CDCl}_3$ )  $\delta$  = 10.47 (s, 1H, CHO), 8.22 – 8.15 (m, 2H, CH), 7.69 – 7.61 (m, 2H, CH), 7.55 – 7.48 (m, 2H, CH), 7.39 (dd,  $J$  = 9.0, 3.0 Hz, 1H, CH), 7.05 (d,  $J$  = 9.1 Hz, 1H, CH), 4.69 (sept,  $J$  = 6.1 Hz, 1H, CH), 1.43 (d,  $J$  = 6.0 Hz, 6H,  $\text{CH}_3$ ). Characterization matches that reported in the literature.<sup>56</sup>

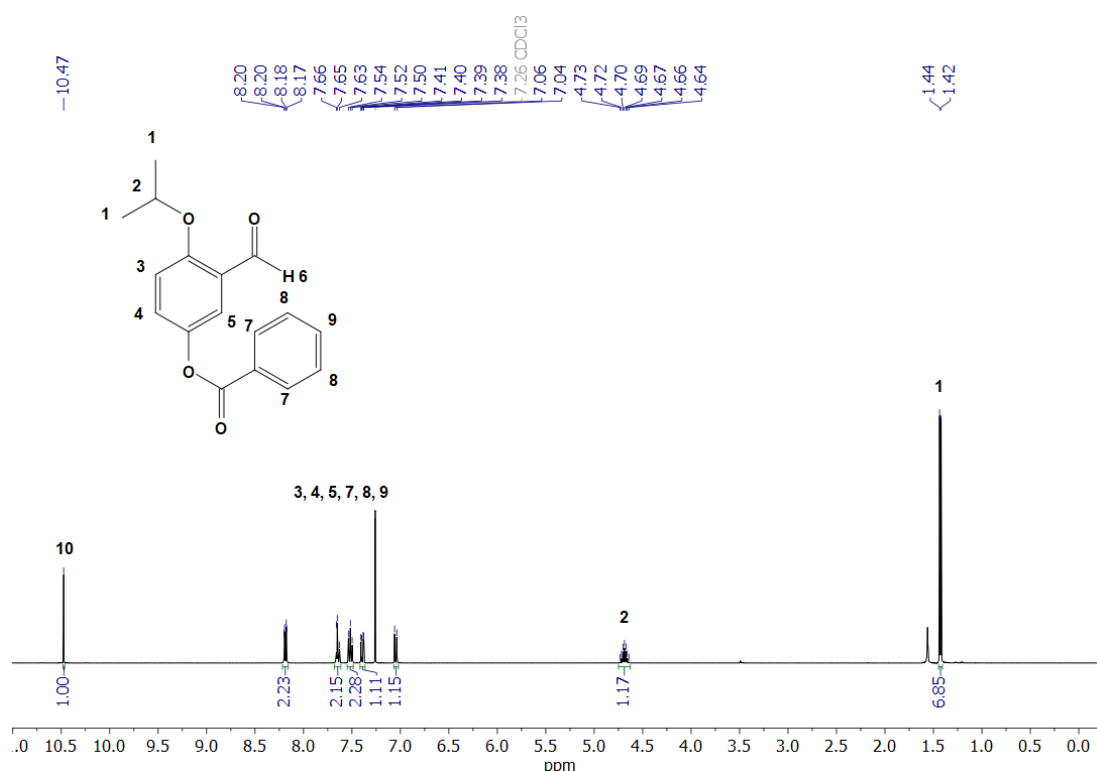
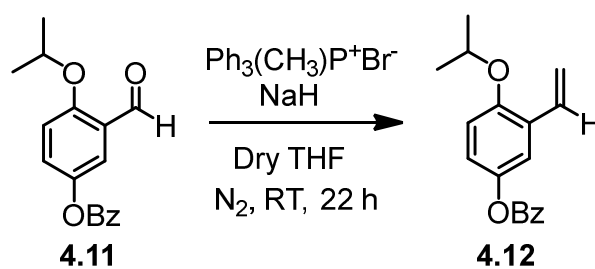


**Figure 4.33**  $^1\text{H NMR}$  spectrum of **4.11** in  $\text{CDCl}_3$  (300 MHz, 298K).

#### 4.5.13 Synthesis of 4.12



The small molecule was prepared based on a previous reported procedure.<sup>57</sup> To a stirred solution of  $\text{Ph}_3\text{P}^+\text{CH}_3\text{Br}^-$  (4.47 g, 12.5 mmol) in dry THF (50 mL) was added NaH (0.5 g, 12.5 mmol) at 0 °C. After stirring at 0 °C for 40 min, **4.11** (3 g, 10 mmol) in THF (20 mL) was added to the solution. The reaction mixture was then stirred at room temperature for 22 h before diluted with  $\text{Et}_2\text{O}$  (30 mL) and  $\text{H}_2\text{O}$  (2 mL). The crude product was washed with brine (2 x 50 mL), dried over  $\text{MgSO}_4$  and then the solvent was removed in vacuo. The product was purified by flash column chromatography on silica (petroleum ether:diethyl ether, 95:5 (v/v)) to yield a white solid (2.33 g, 83%).  $^1\text{H}$  NMR (300 MHz; 298K;  $\text{CDCl}_3$ )  $\delta$  8.26 – 8.17 (m, 2H, CH), 7.67 – 7.60 (m, 1H, CH), 7.51 (tt,  $J_{\text{H-H}} = 7.1, 1.5$  Hz, 2H, CH), 7.32 (d,  $J = 2.8$  Hz, 1H, CH), 7.12 – 6.99 (m, 2H, CH), 6.91 (d,  $J = 8.8$  Hz, 1H, CH), 5.72 (dd,  $^3J_{\text{H-H}} = 17.8, ^2J_{\text{H-H}} = 1.5$  Hz, 1H, CH), 5.3 (m, 1H, CH), 4.52 (Sept,  $^3J_{\text{H-H}} = 6.0$  Hz, 1H, CH), 1.37 (d,  $^3J_{\text{H-H}} = 6.0$  Hz, 6H,  $\text{CH}_3$ ). Characterization matches that reported in the literature.<sup>56</sup>

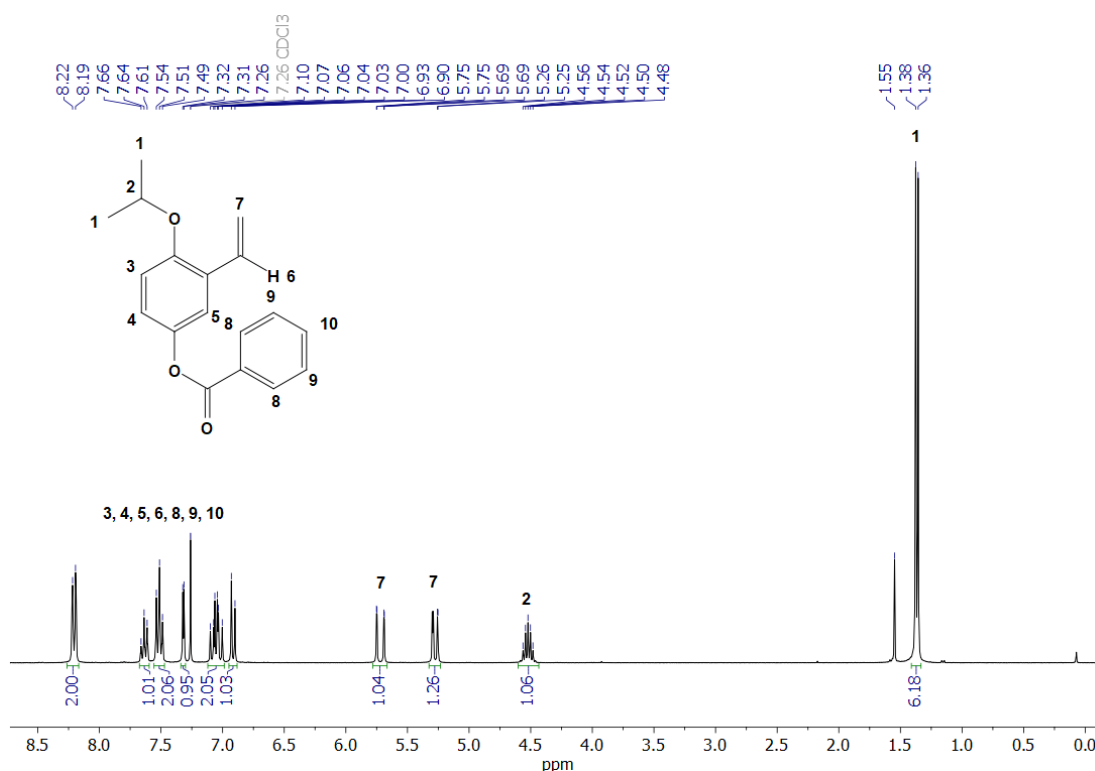
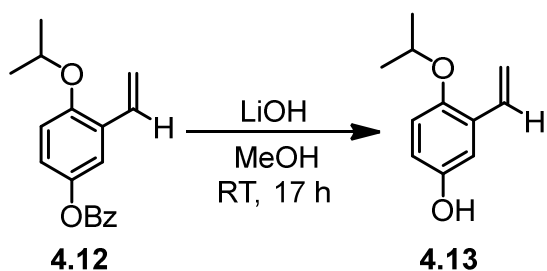


**Figure 4.34**  $^1\text{H}$  NMR spectrum of **4.12** in  $\text{CDCl}_3$  (300 MHz, 298K).

#### 4.5.14 Synthesis of 4.13



LiOH (0.38 g, 15.9 mmol), **4.12** (1.5 g, 5.3 mmol) and MeOH (40 mL) were combined in a round-bottom-flask over ice. The solution was allowed to warm to room temperature and stirred for 17 h prior to the addition of 100 mL sat.  $\text{NH}_4\text{Cl}$ . The product was extracted into ethyl acetate and washed with brine prior to purification by silica column chromatography using a 1:9 (v/v) ethyl acetate/petroleum ether eluent to obtain a pale-yellow oil (0.7 g, 74%).  $^1\text{H}$  NMR (400 MHz; 298K;  $\text{CDCl}_3$ )  $\delta$  = 7.01 (dd,  $^3J_{\text{H-H}} = 17.8, 11.1$  Hz, 1H, CH), 6.97 (s, 1H, CH), 6.79 (d,  $J_{\text{H-H}} = 8.8$  Hz, 1H, CH), 6.69 (dd,  $J_{\text{H-H}} = 8.8, 3.1$  Hz, 1H, CH), 5.68 (dd,  $^3J_{\text{H-H}} = 17.8, ^2J_{\text{H-H}} = 1.5$  Hz, 1H, CH), 5.24 (dd,  $^3J_{\text{H-H}} = 11.1, ^2J_{\text{H-H}} = 1.5$  Hz, 1H, CH), 4.48 – 4.43 (brs, 1H, OH), 4.36 (sept, 6.0 Hz, 1H, CH), 1.31 (d, 6.1 Hz, 6H,  $\text{CH}_3$ ). Characterization matches that reported in the literature.<sup>56</sup>

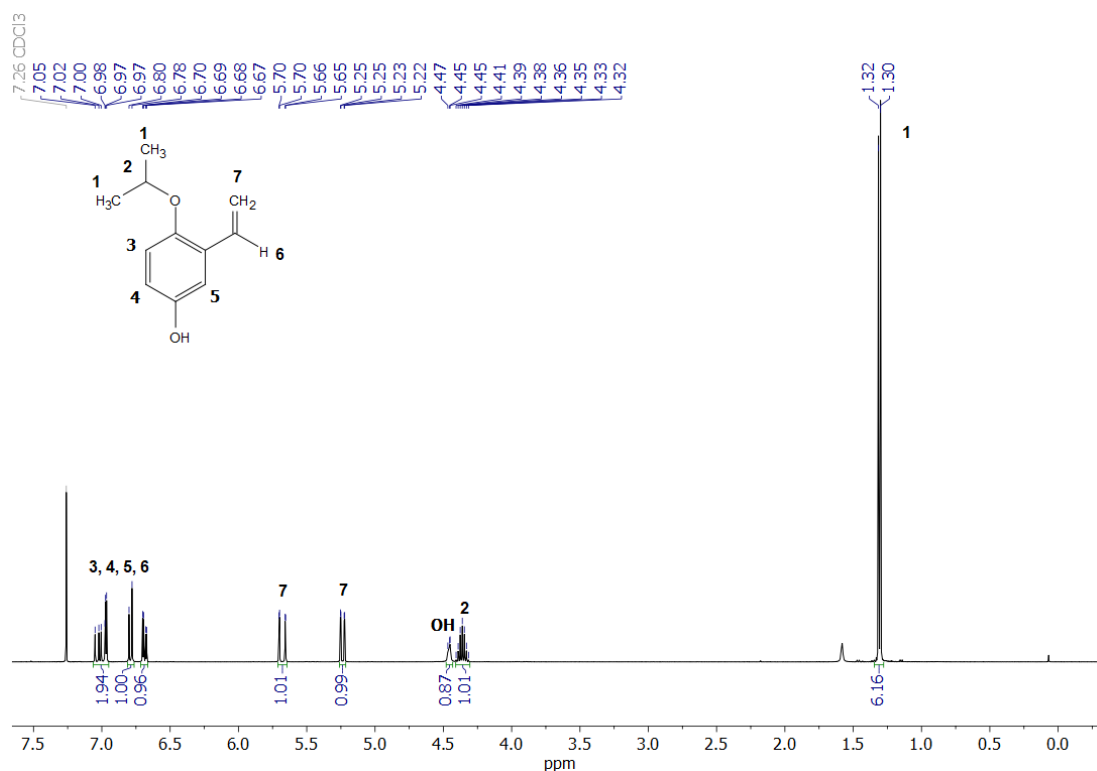
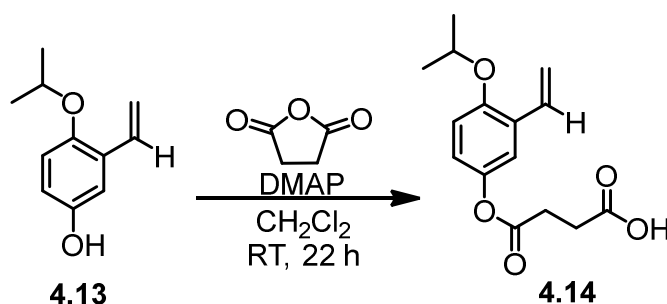


**Figure 4.35**  $^1\text{H}$  NMR spectrum of **4.13** in  $\text{CDCl}_3$  (400 MHz, 298K).

#### 4.5.15 Synthesis of 4.14



**4.13** (0.3 g, 1.68 mmol), succinic anhydride (0.2g, 1.2 mmol), 4-dimethylamino pyridine (0.1 g, 0.5 mmol) and  $\text{CH}_2\text{Cl}_2$  (5 mL) were combined in a round-bottom-flask and stirred for 22 h at room temperature. The solution was diluted with  $\text{CH}_2\text{Cl}_2$  (25 mL) and then washed with 1M HCl solution (2 x 25 mL) followed by brine (25 mL). The crude product was purified by silica column chromatography using a diethyl ether:petroleum ether eluent gradient to yield a white solid (0.28 g, 60%).  $^1\text{H}$  NMR (400 MHz; 298K;  $\text{CDCl}_3$ )  $\delta$  = 7.18 (d,  $J_{\text{H-H}}$  = 2.8 Hz, 1H, CH),

7.01 (dd,  $^3J_{\text{H-H}} = 17.8, 11.2$  Hz, 1H, CH), 6.92 (dd,  $J_{\text{H-H}} = 8.9, J_{\text{H-H}} = 2.8$  Hz, 1H, CH), 6.85 (d,  $J_{\text{H-H}} = 8.9$  Hz, 1H, CH), 5.69 (dd,  $^3J_{\text{H-H}} = 17.8, ^2J_{\text{H-H}} = 1.3$  Hz, 1H, CH), 5.26 (dd,  $^3J_{\text{H-H}} = 11.1, ^2J_{\text{H-H}} = 1.3$  Hz, 1H, CH), 4.48 (sept,  $^3J_{\text{H-H}} = 6.1$  Hz, 1H, CH), 2.92 – 2.76 (m, 4H, CH<sub>2</sub>), 1.34 (d,  $^3J_{\text{H-H}} = 6.1$  Hz, 6H, CH<sub>3</sub>). <sup>13</sup>C NMR (100 MHz; 298K; CDCl<sub>3</sub>) 177.4 (CO), 171.2 (CO), 153.0, 144.2, 131.3, 129.1, 121.4, 119.1, 115.2, 115.0 (Ar-C, CHCH<sub>2</sub> and CHCH<sub>2</sub>), 71.7 (CH(CH<sub>3</sub>)<sub>2</sub>), 29.1 (CH<sub>2</sub>), 28.9 (CH<sub>2</sub>), 22.3 (CH<sub>3</sub>). IR ( $\nu_{\text{max}}$  / cm<sup>-1</sup>) 2973 (COOH, OH stretch), 1750 (COOH, C=O stretch). HR-MS [M + Na]<sup>+</sup> m/z calculated 301.1046 found 301.1049.

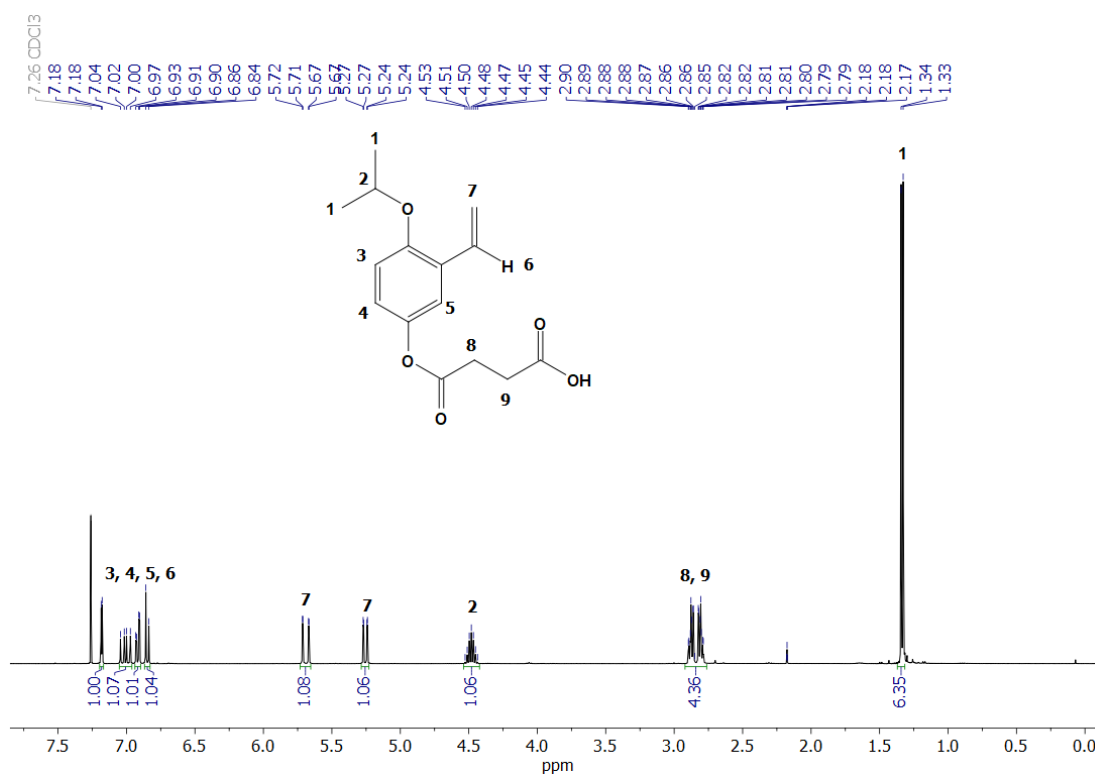


**Figure 4.36** <sup>1</sup>H NMR spectrum of 4.14 in CDCl<sub>3</sub> (400 MHz, 298K).

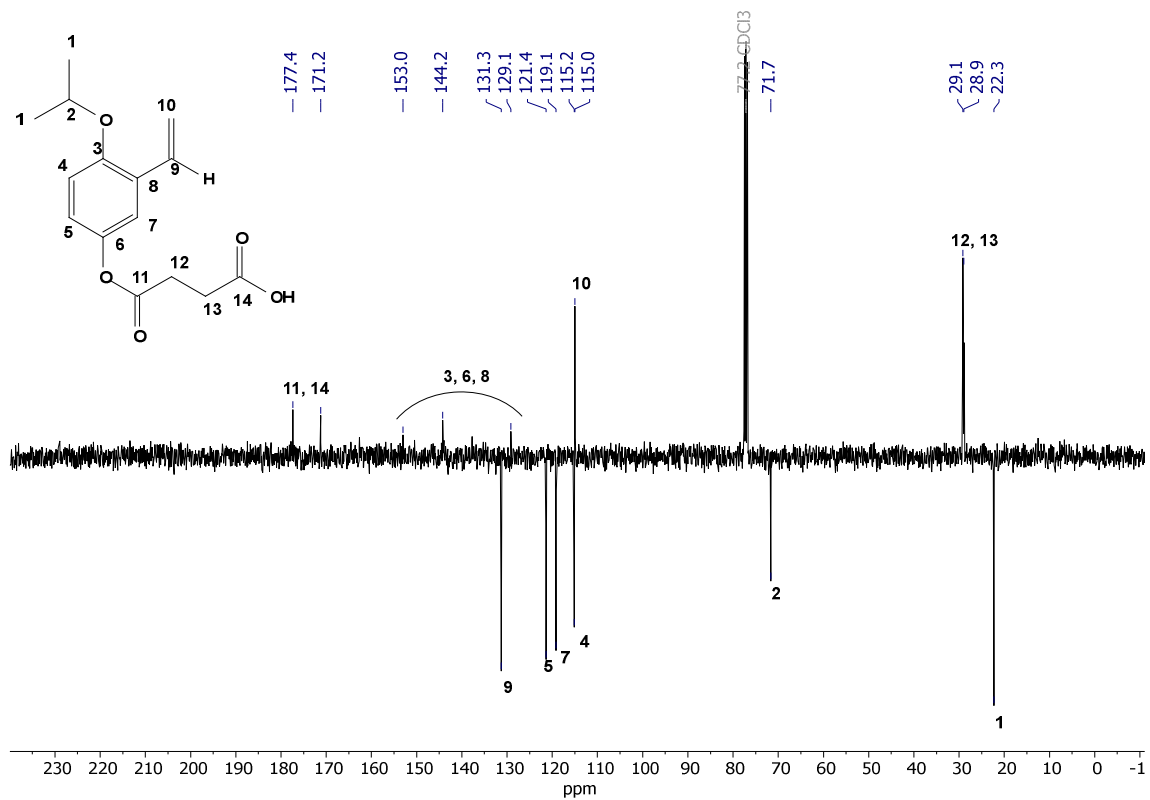
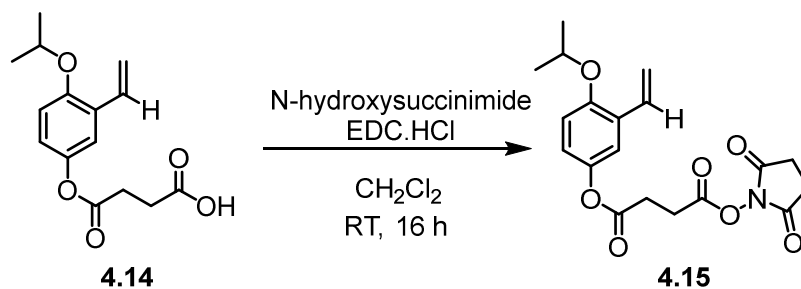


**Figure 4.37**  $^{13}\text{C}$  NMR spectrum of **4.14** in  $\text{CDCl}_3$  (100 MHz, 298K).

#### 4.5.16 Synthesis of 4.15



A round-bottom flask was charged with **4.14** (80 mg, 0.29 mmol), EDC.HCl (69 mg, 0.36 mmol), NHS (41 mg, 0.36 mmol) and CH<sub>2</sub>Cl<sub>2</sub> (5 mL). The solution was stirred at room temperature for 16 h and then washed with sat. NaHCO<sub>3</sub>, sat. NH<sub>4</sub>Cl and brine prior to drying over MgSO<sub>4</sub>. Following removal of the solvent *in vacuo* a white solid was yielded, 48 mg, 43%. <sup>1</sup>H NMR (400 MHz; 298K; CDCl<sub>3</sub>) δ = 7.20 (d, *J*<sub>H-H</sub> = 2.9 Hz, 1H, CH), 7.06 – 6.95 (m, 1H, CH), 6.93 (dd, *J*<sub>H-H</sub> = 8.9, *J*<sub>H-H</sub> = 2.9 Hz, 1H, CH), 6.85 (d, *J*<sub>H-H</sub> = 8.9 Hz, 1H, CH), 5.70 (dd, <sup>3</sup>*J*<sub>H-H</sub> = 17.8, <sup>2</sup>*J*<sub>H-H</sub> = 1.4 Hz, 1H, CH), 5.26 (dd, <sup>3</sup>*J*<sub>H-H</sub> = 11.1, <sup>2</sup>*J*<sub>H-H</sub> = 1.4 Hz, 1H, CH), 4.48 (sept, <sup>3</sup>*J*<sub>H-H</sub> = 6.1 Hz, 1H, CH), 3.12 – 3.04 (m, 2H, CH<sub>2</sub>), 2.98 (m, 2H, CH<sub>2</sub>), 2.84 (s, 4H, CH<sub>2</sub>), 1.33 (d, <sup>3</sup>*J*<sub>H-H</sub> = 6.1 Hz, 6H, CH<sub>3</sub>). <sup>13</sup>C NMR (100 MHz; 298K; CDCl<sub>3</sub>) 170.1 (CO), 169.0 (CO), 167.7 (CO), 153.1 (Arom-C), 144.1 (Arom-C), 131.3 (Arom-C), 129.1 (Arom-C), 121.3 (Arom-C), 119.1 (Arom-C), 115.1 (CHCH<sub>2</sub>), 114.94 (CHCH<sub>2</sub>), 71.7(CH(CH<sub>3</sub>)<sub>2</sub>), 29.0 (CH<sub>2</sub>), 26.5 (CH<sub>2</sub>), 25.7 (CH<sub>2</sub>), 22.17 (CH<sub>3</sub>). IR (ν<sub>max</sub> / cm<sup>-1</sup>) 1728 (C=O). HR-MS [M + H]<sup>+</sup> *m/z* calculated 376.1396 found 376.1397.



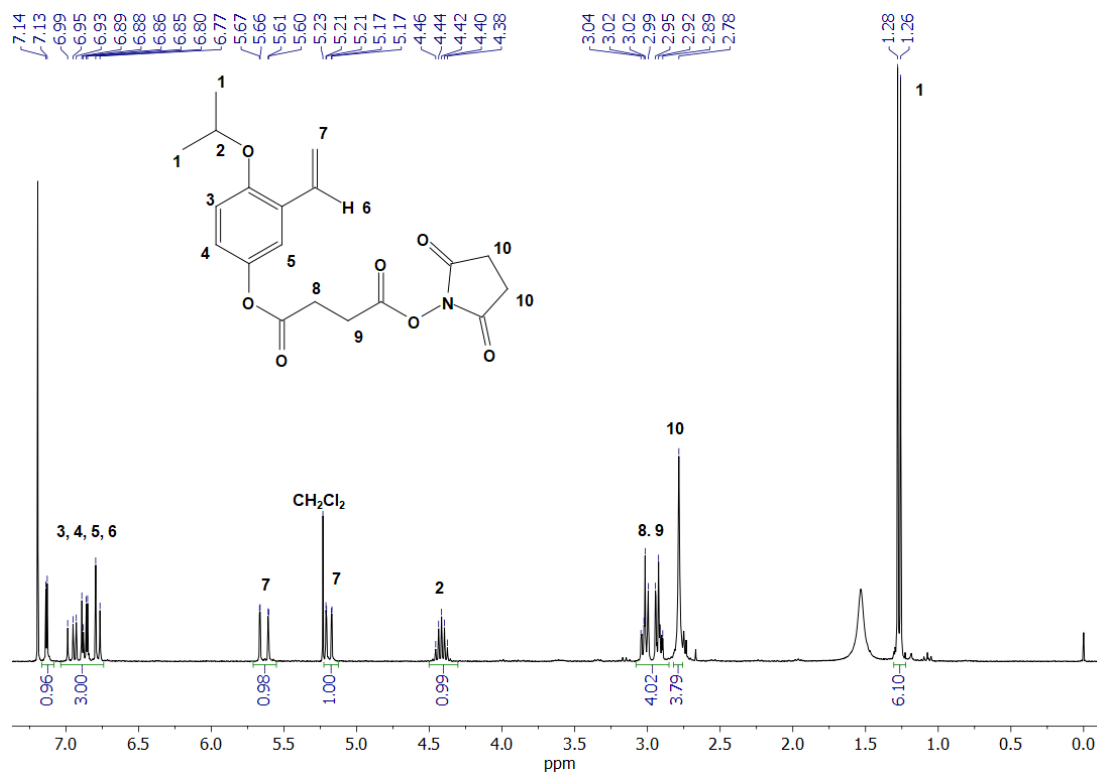


Figure 4.38 <sup>1</sup>H NMR spectrum of 4.15 in CDCl<sub>3</sub> (400 MHz, 298K).

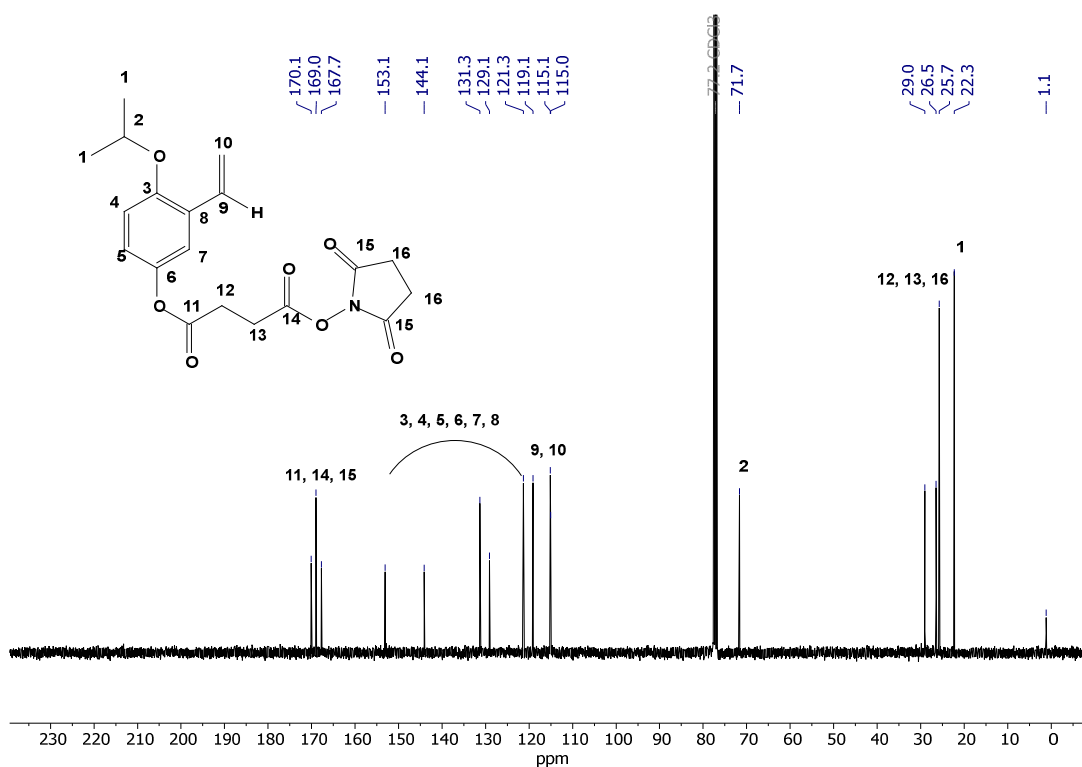
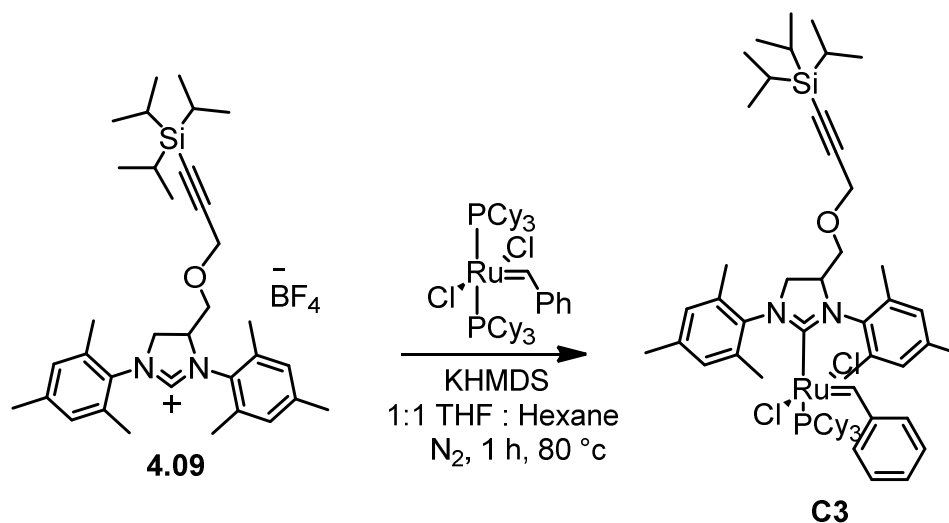


Figure 4.39 <sup>13</sup>C NMR spectrum of 4.15 in CDCl<sub>3</sub> (100 MHz, 298K).

#### 4.5.17 Preparation of C3



In a nitrogen-filled glovebox **4.09** (36 mg, 0.0582 mmol) was suspended in 0.5 mL THF and then added to a solution of KHMDS (11.6 mg, 0.0582 mmol) in 0.5 mL THF. This mixture was immediately transferred to a second vessel containing G1 (40 mg, 0.0486 mmol) in 1 mL hexane. The resulting mixture was heated at 80 °C for 1 h and then cooled. The solvent was removed under reduced pressure and then the crude product was purified by silica gel chromatography.  $^1\text{H NMR}$  (500 MHz; 298K;  $\text{CDCl}_3$ )  $\delta$  = 19.24-19.04 (m, 1H, Ru=CH), 7.35-6.74 (m, 9H, Arom-H), 5.85-5.76 (m, 1H, CH), 4.42-3.43 (m, 6H, 3 x  $\text{CH}_2$ ), 2.76-0.88 (m, 83H, 3 x  $\text{CH}(\text{CH}_3)_2$ , 6 x  $\text{CH}_3$ ,  $\text{P}(\text{C}_6\text{H}_{11})_3$ ). HR-MS  $[\text{M} - \text{Cl}]^+$   $m/z$  calculated 1031.5258 found 1031.5246

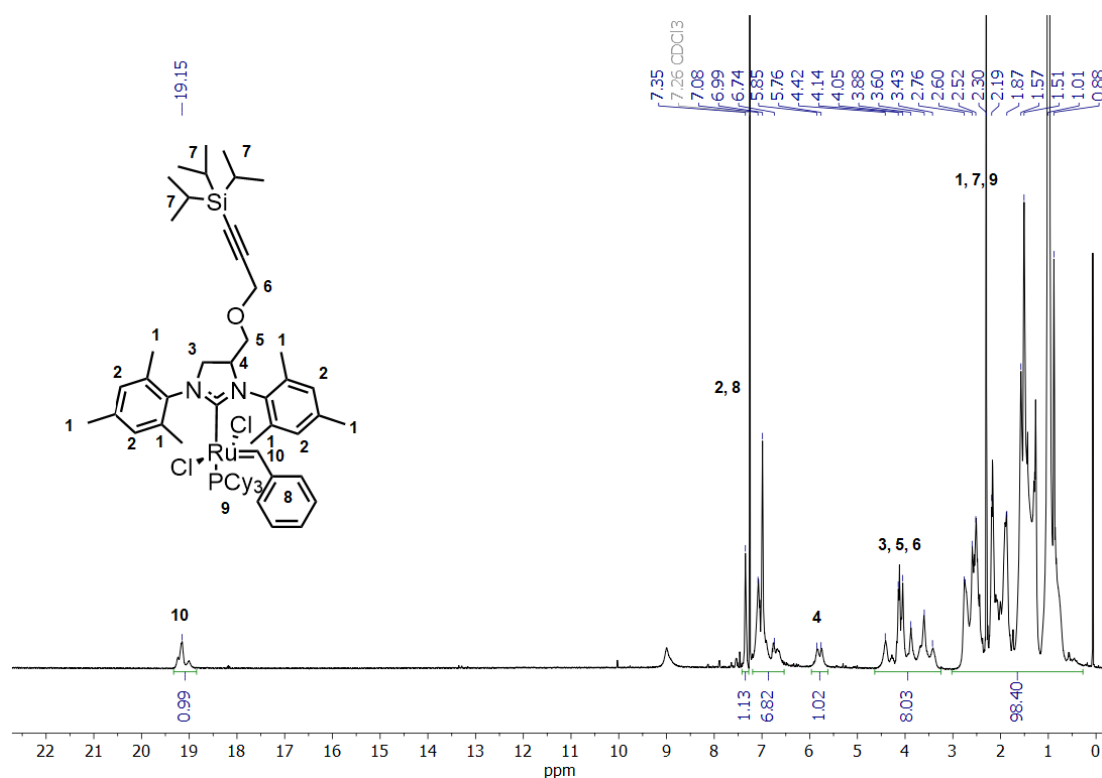
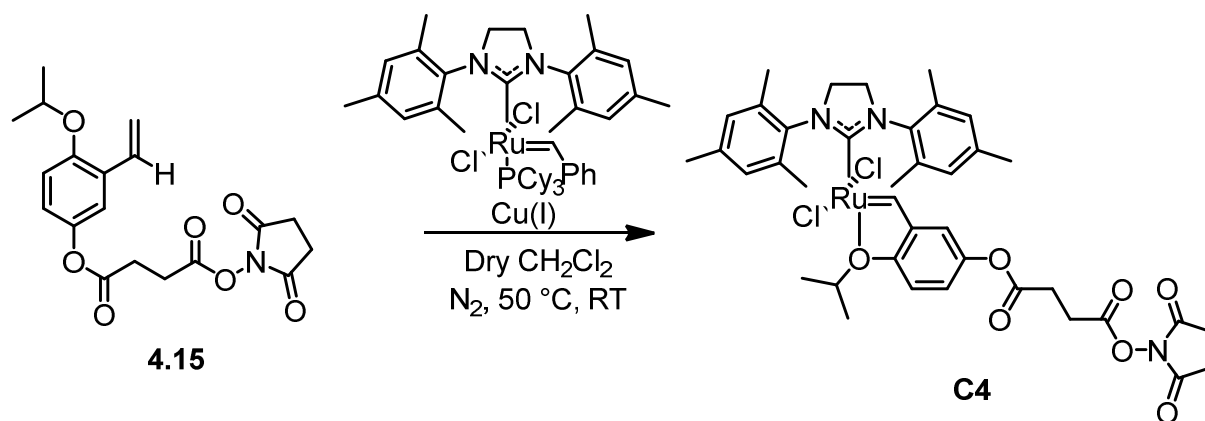


Figure 4.40  $^1\text{H}$  NMR spectrum of **C3** in  $\text{CDCl}_3$  (500 MHz, 298K).

#### 4.5.18 Preparation of **C4**



To a suspension of  $\text{CuCl}$  (23 mg, 0.1675 mmol) in dry  $\text{CH}_2\text{Cl}_2$  under dry  $\text{N}_2$  was added **4.11** (25mg, 0.067 mmol) followed by Grubbs 2nd generation catalyst (57 mg, 0.067 mmol). The mixture was heated at  $50\text{ }^\circ\text{C}$  for 2 h, then cooled and passed through a plug of celite. The solvent was removed *in vacuo* and then the solid was purified by silica column chromatography eluting with  $\text{CH}_2\text{Cl}_2$ , collecting a green band, 18.4 mg.  $^1\text{H}$  NMR (500 MHz;

298K; CDCl<sub>3</sub>)  $\delta$  = 16.45 (s, 1H, Ru=CH), 7.28 (dd, 1H,  $J_{H-H}$  = 8.9 Hz,  $J_{H-H}$  = 2.8 Hz, Arom-H), 7.07 (s, 4H, Arom-H), 6.76 (d, 1H,  $J_{H-H}$  = 8.9 Hz, Arom-H), 6.68 (d, 1H,  $J_{H-H}$  = 2.8 Hz, Arom-H), 4.85 (hept, 1H,  $^3J_{H-H}$  = 6.1 Hz, CH), 4.17 (s, 4H, CH<sub>2</sub>), 3.11-2.93 (m, 4H, 2 x CH<sub>2</sub>), 2.85 (s, 4H, CH<sub>2</sub>), 2.39-2.46 (m, 18H, CH<sub>3</sub>), 1.26 (d, 6H,  $^3J_{H-H}$  = 6.1 Hz, CH<sub>3</sub>). HR-MS [M - 2 x HCl]<sup>2+</sup> m/z calculated 384.6156 found 384.6154

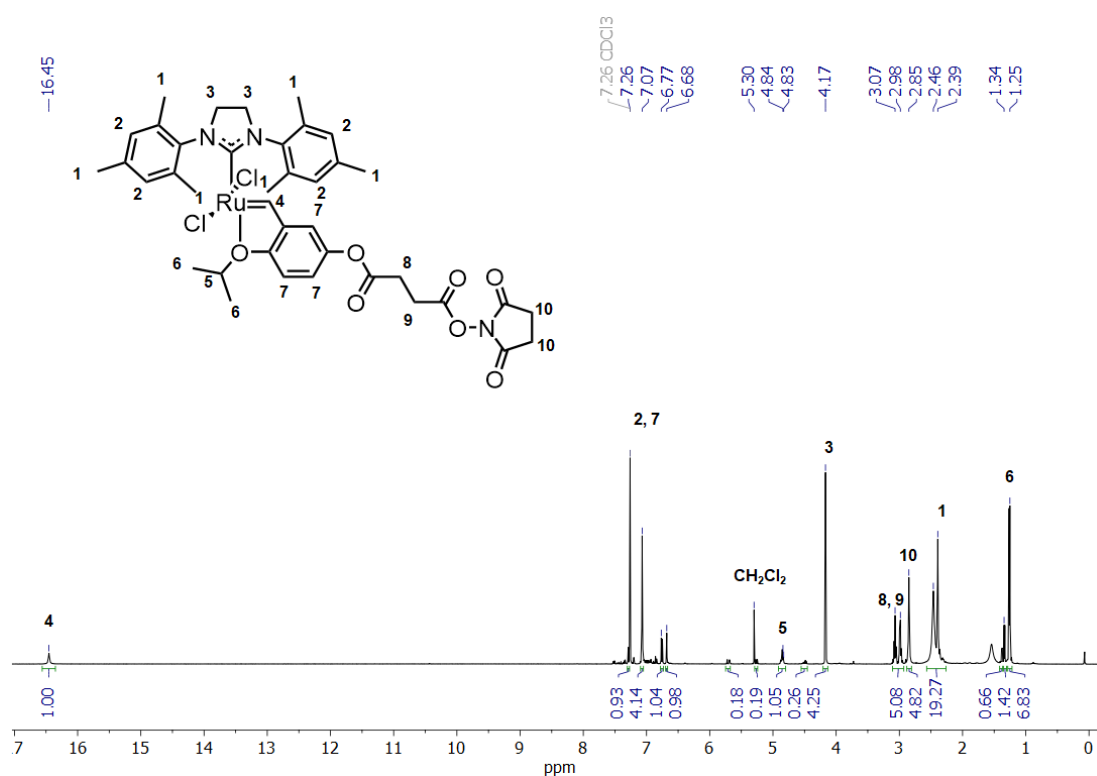


**Figure 4.41** <sup>1</sup>H NMR spectrum of **C4** in CDCl<sub>3</sub> (500 MHz, 298K).

#### 4.5.19 General procedure for the solution-phase coupling to DNA

A solution of **4.15** or **C4** in DMF was added to SO-NH<sub>2</sub> in DPBS adjusted to the desired pH. The mixture was placed in a thermomixer and shaken at 18 °C for the desired time. Solid precipitate was removed by centrifugation and then the supernatant was washed through a spin filter with 18 MΩ H<sub>2</sub>O prior to analysis. LCMS (ESI-) **4i** m/z calculated 5625.1 found 5625.2.

#### 4.5.20 General procedure for the solid-phase coupling to DNA

The immobilization and recovery of DNA from the DEAE Sepharose was carried out as previously reported by Harbury and co-workers.<sup>59</sup> **C4** in DMF (300 equivalents) and triethylamine (2 equivalents) was added to the column and the column was gently agitated for 60 minutes prior to recovery. The recovered product was washed through a spin filter with 18 MΩ H<sub>2</sub>O prior to analysis.

#### 4.5.21 General procedure for the solution-phase coupling to PNA

A solution of **4.15** or **C4** (500 equivalents) was added to **PSO** in DMF (0.5 mM). TEA (2 equivalents) was added and the mixture was placed in a thermomixer and shaken at 18 °C for the desired time. 80 μL of cold diethyl ether was added to the mixture and the solution was centrifuged at 4 °C to precipitate the PNA which was collected for LC-MS analysis. LCMS (ESI-) **4iii** m/z calculated 2985.2 m/z found 2985.3.

## 4.6 References

1. W. J. Meng, R. A. Muscat, M. L. McKee, P. J. Milnes, A. H. El-Sagheer, J. Bath, B. G. Davis, T. Brown, R. K. O'Reilly and A. J. Turberfield, *Nat. Chem.*, 2016, **8**, 542-548.
2. M. L. McKee, A. C. Evans, S. R. Gerrard, R. K. O'Reilly, A. J. Turberfield and E. Stulz, *Org. Biomol. Chem.*, 2011, **9**, 1661-1666.
3. M. L. McKee, P. J. Milnes, J. Bath, E. Stulz, A. J. Turberfield and R. K. O'Reilly, *Angew. Chem. Int. Ed.*, 2010, **49**, 7948-7951.
4. M. L. McKee, P. J. Milnes, J. Bath, E. Stulz, R. K. O'Reilly and A. J. Turberfield, *J. Am. Chem. Soc.*, 2012, **134**, 1446-1449.
5. P. J. Milnes, M. L. McKee, J. Bath, L. J. Song, E. Stulz, A. J. Turberfield and R. K. O'Reilly, *Chem. Commun.*, 2012, **48**, 5614-5616.
6. J. Tomasek and J. Schatz, *Green Chem.*, 2013, **15**, 2317-2338.
7. C. P. Casey, *J. Chem. Educ.*, 2006, **83**, 192.
8. R. R. Schrock, J. S. Murdzek, G. C. Bazan, J. Robbins, M. DiMare and M. O'Regan, *J. Am. Chem. Soc.*, 1990, **112**, 3875-3886.
9. P. Schwab, M. B. France, J. W. Ziller and R. H. Grubbs, *Angew. Chem. Int. Ed.*, 1995, **34**, 2039-2041.
10. J. Huang, H.-J. Schanz, E. D. Stevens and S. P. Nolan, *Organometallics*, 1999, **18**, 5375-5380.
11. J. Huang, E. D. Stevens, S. P. Nolan and J. L. Petersen, *J. Am. Chem. Soc.*, 1999, **121**, 2674-2678.
12. S. B. Garber, J. S. Kingsbury, B. L. Gray and A. H. Hoveyda, *J. Am. Chem. Soc.*, 2000, **122**, 8168-8179.
13. J. S. Kingsbury, J. P. A. Harrity, P. J. Bonitatebus and A. H. Hoveyda, *J. Am. Chem. Soc.*, 1999, **121**, 791-799.
14. P. H. Deshmukh and S. Blechert, *Dalton Trans.*, 2007, 2479-2491.
15. K. Skowerski, J. Białocki, S. J. Czarnocki, K. Żukowska and K. Grela, *Beilstein J. Org. Chem.*, 2016, **12**, 5-15.
16. H. Zhang, Y. Li, S. Shao, H. Wu and P. Wu, *J. Mol. Catal. A: Chem.*, 2013, **372**, 35-43.
17. K. Skowerski, G. Szczepaniak, C. Wierzbicka, Ł. Gułajski, M. Bieniek and K. Grela, *Catal. Sci. Technol.*, 2012, **2**, 2424-2427.
18. J. P. Gallivan, J. P. Jordan and R. H. Grubbs, *Tetrahedron Lett.*, 2005, **46**, 2577-2580.
19. A. Ben-Asuly, E. Tzur, C. E. Diesendruck, M. Sigalov, I. Goldberg and N. G. Lemcoff, *Organometallics*, 2008, **27**, 811-813.
20. P. Schwab, R. H. Grubbs and J. W. Ziller, *J. Am. Chem. Soc.*, 1996, **118**, 100-110.
21. A. K. Chatterjee and R. H. Grubbs, *Org. Lett.*, 1999, **1**, 1751-1753.
22. M. Scholl, T. M. Trnka, J. P. Morgan and R. H. Grubbs, *Tetrahedron Lett.*, 1999, **40**, 2247-2250.

23. M. Scholl, S. Ding, C. W. Lee and R. H. Grubbs, *Org. Lett.*, 1999, **1**, 953-956.
  24. I. Dragutan and V. Dragutan, *Platinum Met. Rev.*, 2008, **52**, 71-82.
  25. S. Gessler, S. Randl and S. Blechert, *Tetrahedron Lett.*, 2000, **41**, 9973-9976.
  26. J. M. Bates, J. A. M. Lummiss, G. A. Bailey and D. E. Fogg, *ACS Catalysis*, 2014, **4**, 2387-2394.
  27. S. J. Connon, A. M. Dunne and S. Blechert, *Angew. Chem. Int. Ed.*, 2002, **41**, 3835-3838.
  28. S. C. Schurer, S. Gessler, N. Buschmann and S. Blechert, *Angew. Chem. Int. Ed.*, 2000, **39**, 3898-3901.
  29. S. H. Hong and R. H. Grubbs, *J. Am. Chem. Soc.*, 2006, **128**, 3508-3509.
  30. J. P. Jordan and R. H. Grubbs, *Angew. Chem. Int. Ed.*, 2007, **46**, 5152-5155.
  31. C. Mayer, D. G. Gillingham, T. R. Ward and D. Hilvert, *Chem. Commun.*, 2011, **47**, 12068-12070.
  32. C. Lo, M. R. Ringenberg, D. Gnanadt, Y. Wilson and T. R. Ward, *Chem. Commun.*, 2011, **47**, 12065-12067.
  33. J. Zhao, A. Kajetanowicz and T. R. Ward, *Org. Biomol. Chem.*, 2015, **13**, 5652-5655.
  34. T. Matsuo, C. Imai, T. Yoshida, T. Saito, T. Hayashi and S. Hirota, *Chem. Commun.*, 2012, **48**, 1662-1664.
  35. F. Rosati and G. Roelfes, *ChemCatChem*, 2010, **2**, 916-927.
  36. T. R. Wilks, J. Bath, J. W. de Vries, J. E. Raymond, A. Herrmann, A. J. Turberfield and R. K. O'Reilly, *ACS Nano*, 2013, **7**, 8561-8572.
  37. S. N. Riduan and Y. Zhang, *Chem. Soc. Rev.*, 2013, **42**, 9055-9070.
  38. C. Deraedt, M. d'Halluin, S. Lesturgez, L. Salmon, G. Goglio, J. Ruiz and D. Astruc, *Eur. J. Inorg. Chem.*, 2015, 1345-1350.
  39. J. Lim, S. S. Lee and J. Y. Ying, *Chem. Commun.*, 2010, **46**, 806-808.
  40. S. S. Lee, S. N. Riduan, N. Erathodiyil, J. Lim, J. L. Cheong, J. H. Cha, Y. Han and J. Y. Ying, *Chem. - Eur. J.*, 2012, **18**, 7394-7403.
  41. J. E. Jee, J. L. Cheong, J. Lim, C. Chen, S. H. Hong and S. S. Lee, *J. Org. Chem.*, 2013, **78**, 3048-3056.
  42. D. G. Hall, in *Boronic Acids, Vol 2: Preparation and Applications in Organic Synthesis, Medicine and Materials, 2nd Edition*, ed. D. G. Hall, Wiley-V C H Verlag Gmbh, Weinheim, 2011, pp. 1-133.
  43. N. Miyaura, T. Ishiyama, M. Ishikawa and A. Suzuki, *Tetrahedron Lett.*, 1986, **27**, 6369-6372.
  44. Y. Wang, X. Li, Y. Li, Y. Pan, K. Cheng and H. Wang, *Chem. Res. Chin. Univ*, 2014, **30**, 614-618.
  45. US Pat., 2014/039039, 2014.
  46. C. Hobbs, Y.-C. Yang, J. Ling, S. Nicola, H.-L. Su, H. S. Bazzi and D. E. Bergbreiter, *Org. Lett.*, 2011, **13**, 3904-3907.
  47. V. Forcina, A. García-Domínguez and G. C. Lloyd-Jones, *Faraday Discuss.*, 2019, **220**, 179-195.
-

48. M. Jawiczuk, A. Marczyk and B. Trzaskowski, *Catalysts*, 2020, **10**, 887.
49. S. T. Diver and A. J. Giessert, *Chem. Rev.*, 2004, **104**, 1317-1382.
50. W. H. Binder and C. Kluger, *Macromolecules*, 2004, **37**, 9321-9330.
51. Z. M. Al-Badri and G. N. Tew, *Macromolecules*, 2008, **41**, 4173-4179.
52. S. A. Krovi, D. Smith and S. T. Nguyen, *Chem. Commun.*, 2010, **46**, 5277-5279.
53. M. Schaefer, N. Hanik and A. F. M. Kilbinger, *Macromolecules*, 2012, **45**, 6807-6818.
54. J. S. Davies, C. L. Higginbotham, E. J. Tremeer, C. Brown and R. C. Treadgold, *J. Chem. Soc., Perkin Trans. 1*, 1992, 3043-3048.
55. M. Bieniek, A. Michrowska, Ł. Gułajski and K. Grela, *Organometallics*, 2007, **26**, 1096-1099.
56. A. Keraani, C. Fischmeister, T. Renouard, M. Le Floch, A. Baudry, C. Bruneau and M. Rabiller-Baudry, *J. Mol. Catal. A: Chem.*, 2012, **357**, 73-80.
57. S.-W. Chen, J. H. Kim, C. E. Song and S.-g. Lee, *Org. Lett.*, 2007, **9**, 3845-3848.
58. Y. Jenkins and J. K. Barton, *J. Am. Chem. Soc.*, 1992, **114**, 8736-8738.
59. D. R. Halpin, J. A. Lee, S. J. Wrenn and P. B. Harbury, *PLOS Biology*, 2004, **2**, e175.
60. D. T. Flood, S. Asai, X. Zhang, J. Wang, L. Yoon, Z. C. Adams, B. C. Dillingham, B. B. Sanchez, J. C. Vantourout, M. E. Flanagan, D. W. Piotrowski, P. Richardson, S. A. Green, R. A. Shenvi, J. S. Chen, P. S. Baran and P. E. Dawson, *J. Am. Chem. Soc.*, 2019, **141**, 9998-10006.
61. A. Singhal, V. Bagnacani, R. Corradini and P. E. Nielsen, *ACS Chem. Biol.*, 2014, **9**, 2612-2620.
62. S. Nuñez-Pertiñez, PhD Thesis, University of Birmingham, 2020.
63. M. Mayr, M. R. Buchmeiser and K. Wurst, *Adv. Synth. Catal.*, 2002, **344**, 712-719.
64. J. Hoogboom and T. M. Swager, *J. Am. Chem. Soc.*, 2006, **128**, 15058-15059.
65. D. Göbel, N. Clamor and B. J. Nachtsheim, *Org. Biomol. Chem.*, 2018, **16**, 4071-4075.
66. M. L. Belyanin, E. V. Stepanova and V. D. Ogorodnikov, *Carbohydr. Res.*, 2012, **363**, 66-72.



# Chapter 5: Cross-Metathesis on Enyne-Functionalized DNA: An *in situ* Method

## 5.1 Abstract

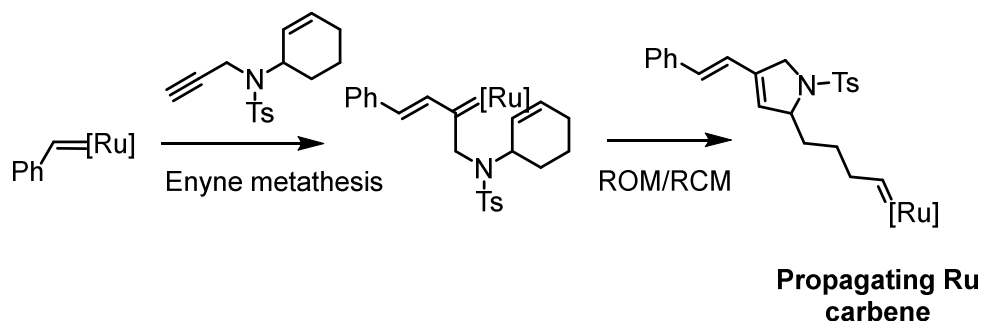
The use of enyne metathesis to prepare an *in situ* DNA metathesis catalyst has been explored. A range of aqueous metathesis conditions were screened and those conducted in H<sub>2</sub>O/organic solvent mixtures led to the successful CM 'on-DNA'. Electron rich, sterically unhindered alkenes were found to react with the *in situ* DNA-functionalized catalyst and the reaction products could be identified by LCMS. Additionally, a templated metathesis reaction was attempted using an *in situ* DNA-functionalized catalyst.

## 5.2 Introduction

In Chapter 4, attempts to isolate a metathesis functionalized catalyst were discussed with limited success. In this chapter, an *in situ* method to prepare an active DNA catalyst will be discussed utilizing enyne metathesis chemistry.

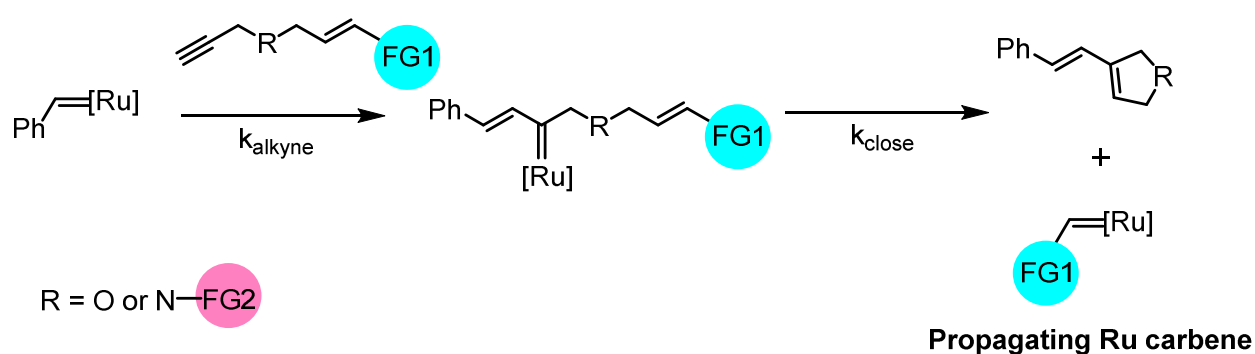
Enyne metathesis takes place between an alkene and an alkyne to produce a 1,3-diene; furthermore, intramolecular enyne metathesis leads to ring-formation.<sup>1</sup> In 2011, Tae-Lim Choi and co-workers utilized an enyne monomer consisting of a primary alkyne and typically unreactive low ring strain alkene, such as cyclohexene, to perform a tandem ring-opening/ring-closing metathesis (ROM/RCM) polymerization (Scheme 5.1).<sup>2, 3</sup> Mechanistic studies suggested that the reaction proceeded *via* reaction of the Ru-catalyst with the less sterically hindered alkyne, followed by a tandem ROM/RCM. Furthermore, alterations in the ring size

of the cycloalkane, the linker unit or the length of the alkyne moiety had a profound effect on the reaction which was attributed to the stability of the metallocyclobutane intermediate.<sup>3</sup>



**Scheme 5.1** Tandem ROM/RCM of a monomer containing two typically unreactive functional groups initially reported by Choi and co-workers.<sup>2,3</sup>

A key finding of this reaction was the formation of a new propagating Ru-carbene complex, and in 2018 the groups of Gutekunst and Kilbinger independently reported the utilization of enynes to prepare metathesis catalysts with a functional group of interest (Scheme 5.2).<sup>4,5</sup> The enyne monomer utilized was based on a similar construct to that designed by Choi and co-workers; however, the strained cycloalkene was replaced with a disubstituted alkene which can be further functionalized with groups of interest.

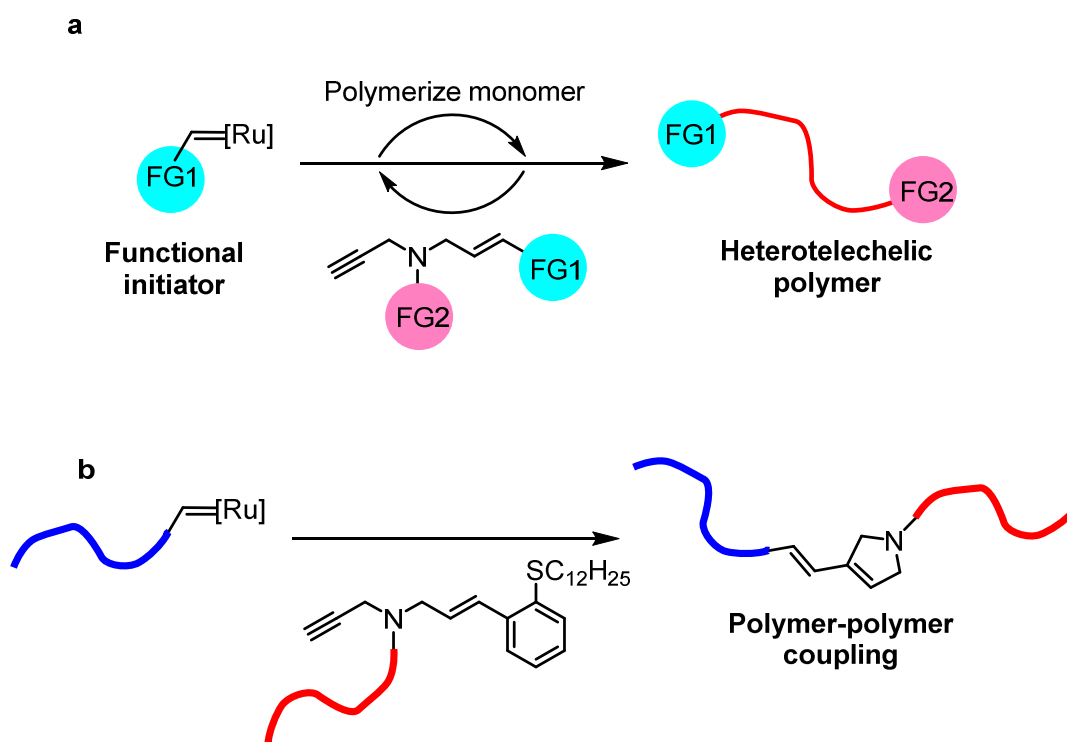


**Scheme 5.2** The synthesis of a functionalized metathesis catalyst using enynes, reported independently by the groups of Gutekunst<sup>4</sup> and Kilbinger<sup>5</sup>.

Following the reaction of **G3** with the alkyne, intramolecular RCM occurs leading to a new Ru-carbene complex with the functional group of interest and a 1,3-diene by-product. The

Kilbinger group studied an ether-linked enyne; however, the resulting diene led to rapid catalyst decomposition.<sup>5</sup> In contrast, the use of an amide or sulfonamide linkage was devoid of such side reactions and the resulting diene was unreactive to further metathesis.<sup>4</sup>

Gutekunst and co-workers demonstrated the potential of enyne metathesis to develop heterotelechelic polymers<sup>4, 6</sup> and for polymer-polymer coupling (Scheme 5.3).<sup>7, 8</sup>



**Scheme 5.3** The use of enyne metathesis to prepare (a) well-defined heterotelechelic polymers; or (b) polymer-polymer coupling.

In order to generate a well-controlled heterotelechelic polymer, complete conversion to the newly functionalized Ru-catalyst was required. As a consequence of this, the newly formed Ru-catalyst must not out-compete the reaction of the starting Ru-catalyst, in this case G3, with the enyne. Gutekunst and co-workers screened a number of enynes and identified an electron deficient carboxy-functionalized enyne led to near complete conversion when utilized in a slight excess (3 equivalents) and thus a range of carboxy derivatives were utilized,

demonstrating the versatility of this approach.<sup>4</sup> In contrast, to achieve polymer-polymer coupling, the resulting catalyst should be sequestered to prevent further reaction and thus, a thioester which chelates the Ru was utilized. Furthermore, a number of functional groups can be added through the linking amide or sulfonamide unit to successfully yield 1,4-dienes not susceptible to further metathesis, Figure 5.1 summarises the three main design features.

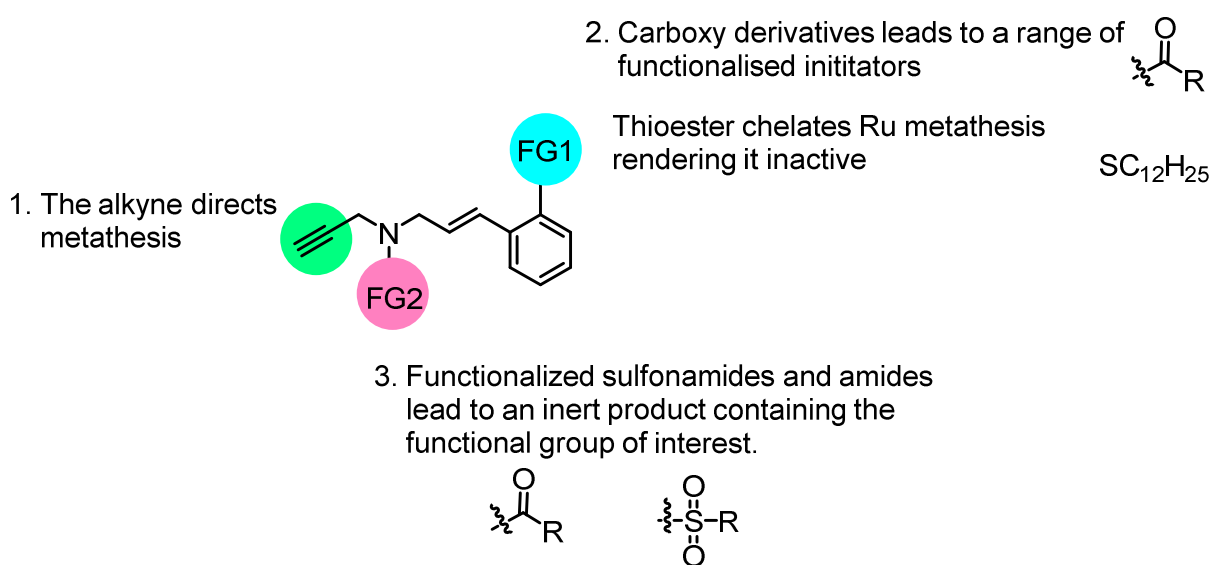
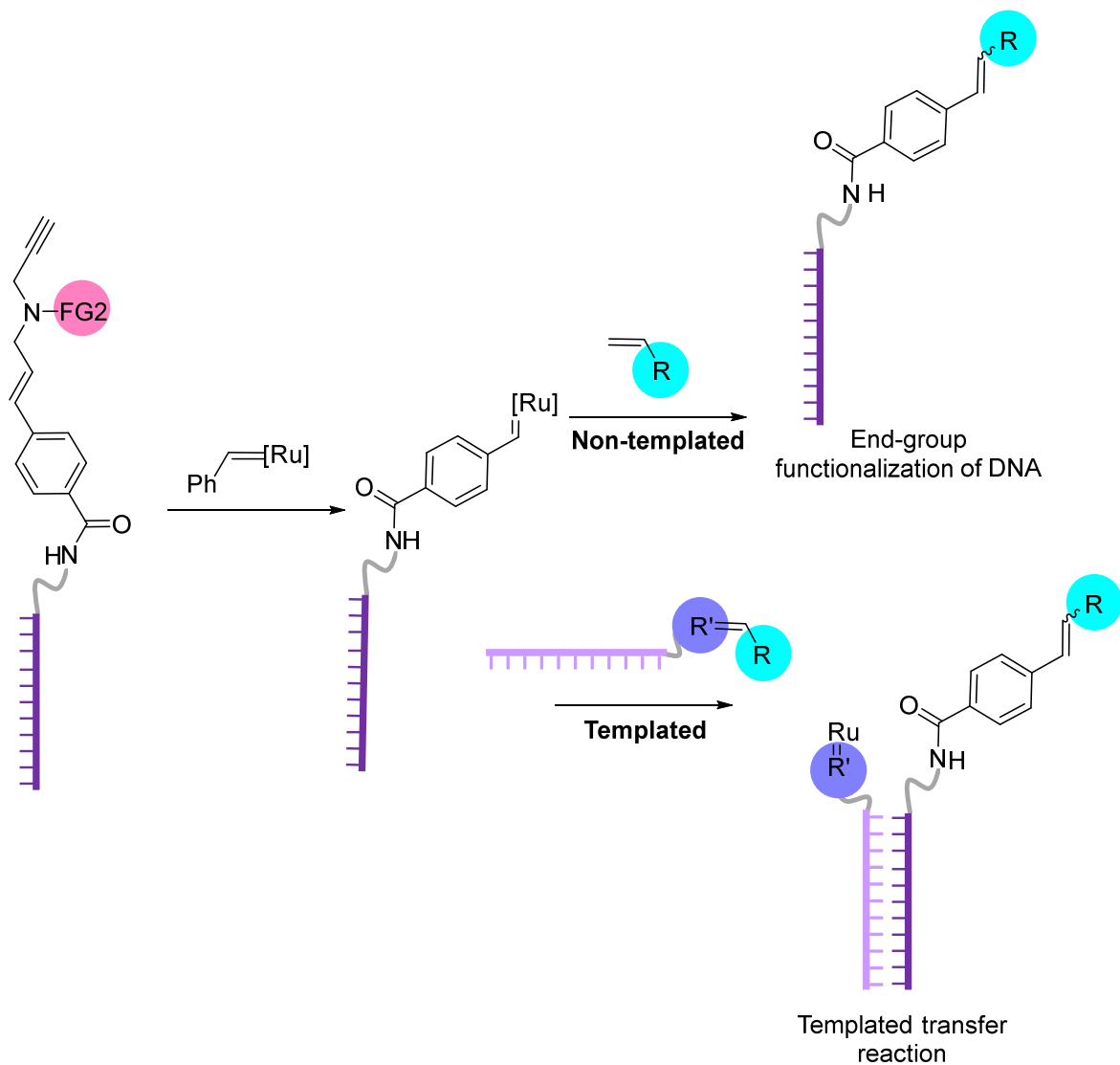


**Figure 5.1** The generic structure of the enyne scaffold designed by Gutekunst and co-workers.<sup>4, 6, 8</sup> The functional groups 1 and 2 can be varied to alter the reactivity accordingly.

Inspired by the apparent versatility of this approach, it was hypothesized that this enyne scaffold could be utilized to prepare an *in situ* DNA-functionalized Ru-catalyst, through reaction of enyne-functionalized DNA with a commercially available Ru-catalyst (Scheme 5.4). This approach was particularly attractive as it eliminated the need to isolate the DNA-functionalized Ru-catalyst which, as demonstrated in Chapter 4, is particularly challenging. Furthermore, subsequent CM with small molecule alkenes could yield DNA rendering an array of functional groups of interest for the preparation of DECLs. Finally, an exciting prospect of this mechanism is the controlled formation of a DNA-functionalized metathesis catalyst which

could subsequently go on to react with an alkene on a complementary DNA sequence, leading to the desired DNA-templated metathesis reaction, first introduced in Chapter 4.



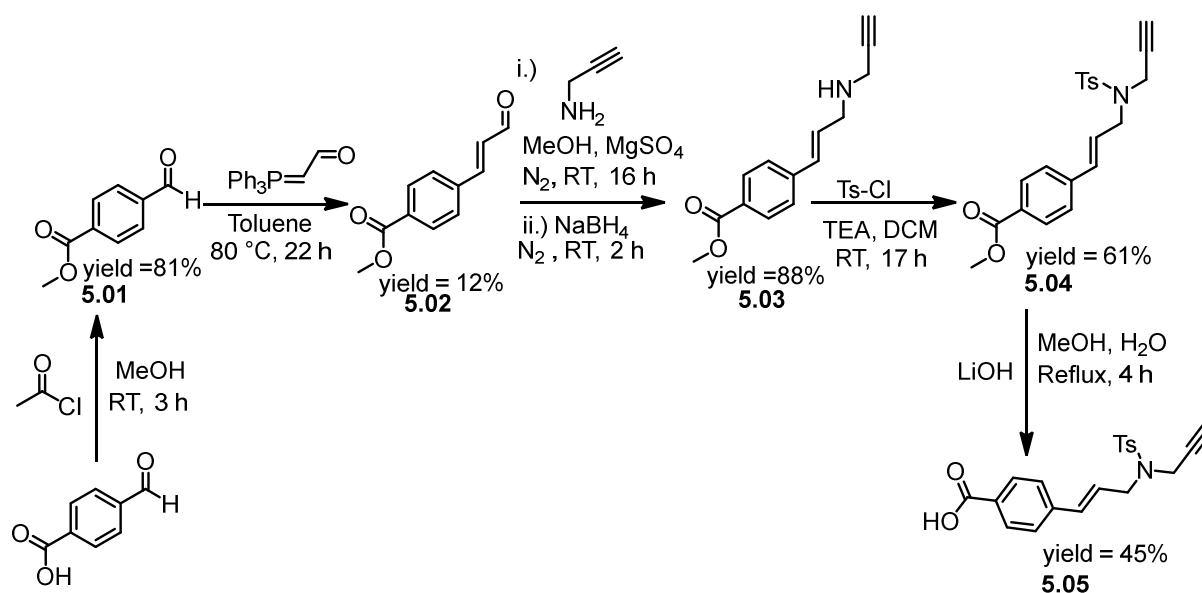
**Scheme 5.4** The potential of utilizing enyne functionalized DNA to prepare an *in situ* DNA-Ru catalyst which could subsequently go on to react with alkenes in both a templated and non-templated manner.

## 5.3 Results & Discussion

### 5.3.1 Synthesis of DNA-functionalized enyne

In order to utilize the enyne approach to prepare an *in situ* DNA-functionalized metathesis catalyst the preparation of an oligonucleotide-functionalized enyne was required. Towards

this end, an enyne was synthesized based on the aforementioned scaffold (Figure 5.1). An acid group was introduced at position 'FG1' for coupling to DNA and a tosylate group at position 'FG2' to render the resulting diene inactive. The enyne, **5.05**, was yielded in five steps from 4-formyl benzoic acid (Scheme 5.5, Figure 5.2).



**Scheme 5.5** The synthesis of **5.05** in five-steps from 4-formyl benzoic acid.

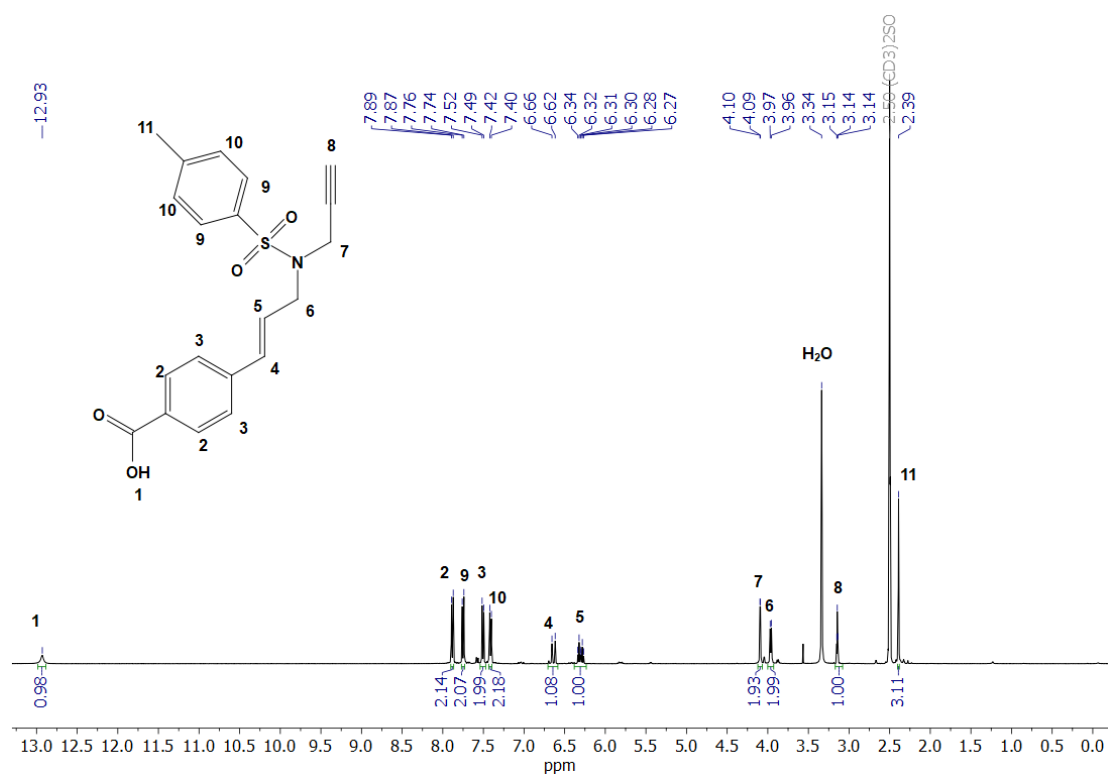


**Figure 5.2**  $^1\text{H}$  NMR spectrum of **5.05** in  $(\text{CD}_3)_2\text{SO}$  (400 MHz, 298 K).

It was anticipated that **5.05** could be conjugated to amino-DNA using activated-ester chemistry initially reported in Chapter 3. A 17-base oligonucleotide was purchased with an amine group at the 5' end (S0-NH<sub>2</sub>) and reacted with EDC.HCl and **5.05** for 2 h at room temperature. The desired oligonucleotide-functionalized enyne, **5i**, was obtained in near-quantitative yields and therefore, no further purification was required (Figure 5.3).

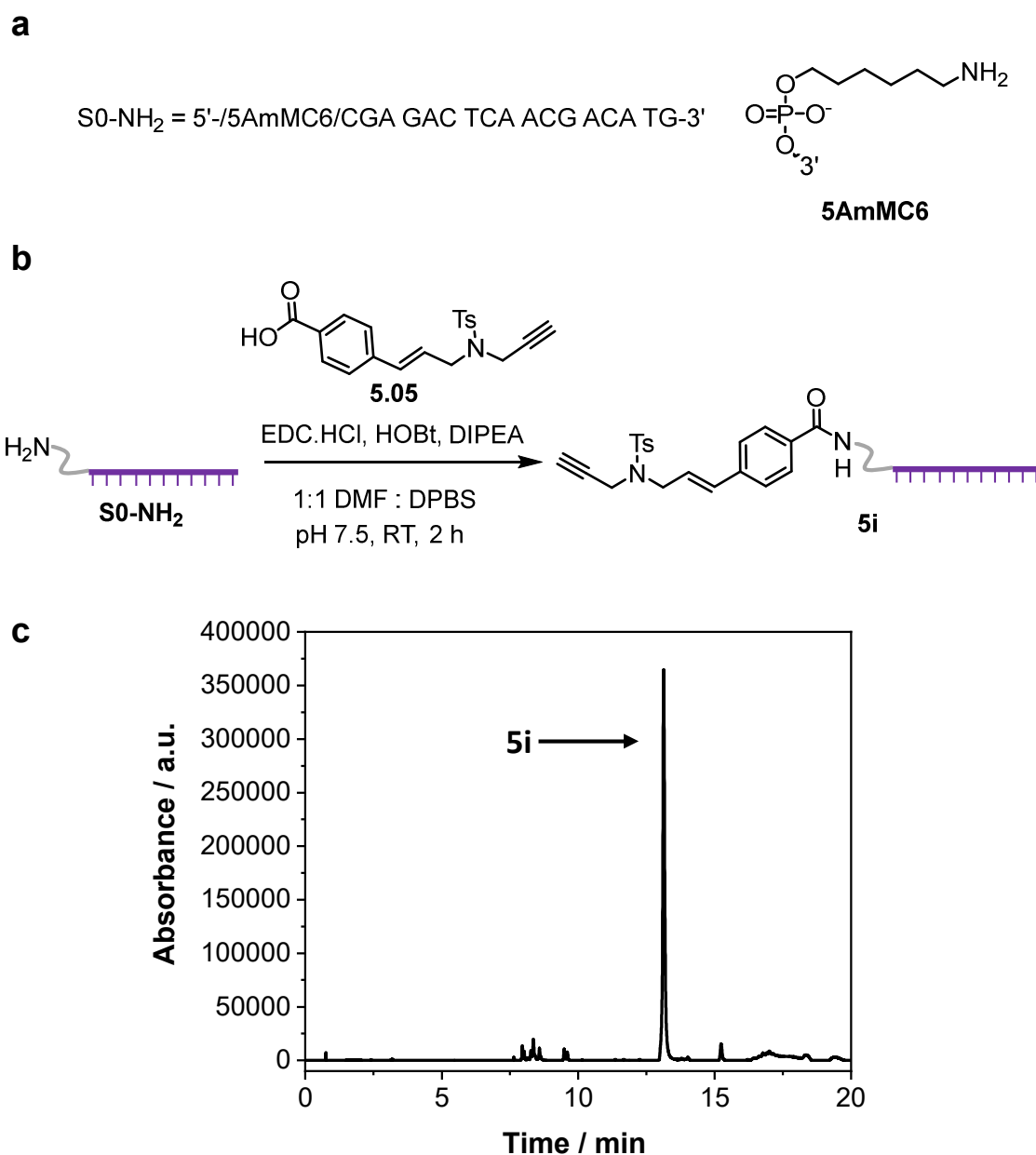
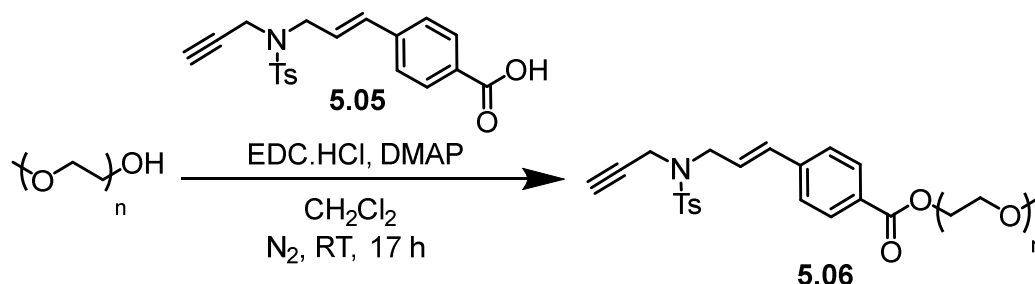


**Figure 5.3** (a) Sequence of S0-NH<sub>2</sub>; (b) Synthesis of **5i**; (c) LCMS-UV Chromatogram of **5i** at 260 nm eluted with a gradient of buffer A: 75 mM TEAA in H<sub>2</sub>O and buffer B: 75 mM TEAA in acetonitrile. Peaks assigned via mass spectrometry.

## 5.3.2 Off-templated DNA cross-metathesis

### 5.3.2.1 Proof-of-concept study using PEG-functionalized enyne

Before attempting a CM reaction on the oligonucleotide-functionalized enyne, **5i**, an initial proof-of-concept study was completed using PEG-functionalized enyne, to ensure the successful synthesis of a functionalized initiator. The PEGylated enyne (**5.06**) was prepared from **5.05** using activated-ester chemistry and methoxy-PEG (MW ca. 2000 g mol<sup>-1</sup>), Scheme 5.6. Note that, in order to encourage full conversion of **5.05** to **5.06**, a slight excess of methoxy-PEG was used (1.2 equivalents) and thus the product would contain a mixture of functionalized and unfunctionalized PEG. The polymer was precipitated into cold diethyl ether to remove residual small molecules and yield **5.06** as a white solid (Figure 5.4).



*Scheme 5.6 Synthesis of 5.06.*

Upon reaction of **5.06** with a Ru-metathesis catalyst and a fluorescent-disubstituted alkene (**5.07**) it was anticipated that fluorescent labelling of the PEG polymer could be observed as shown in Scheme 5.7. For this reaction, G2 was utilized and the dicoumarin based alkene, **5.07**, which absorbs light around 350 nm. Through analysis of the resultant polymer SEC, monitoring the UV absorbance at 350 nm, the success of the reaction was determined.



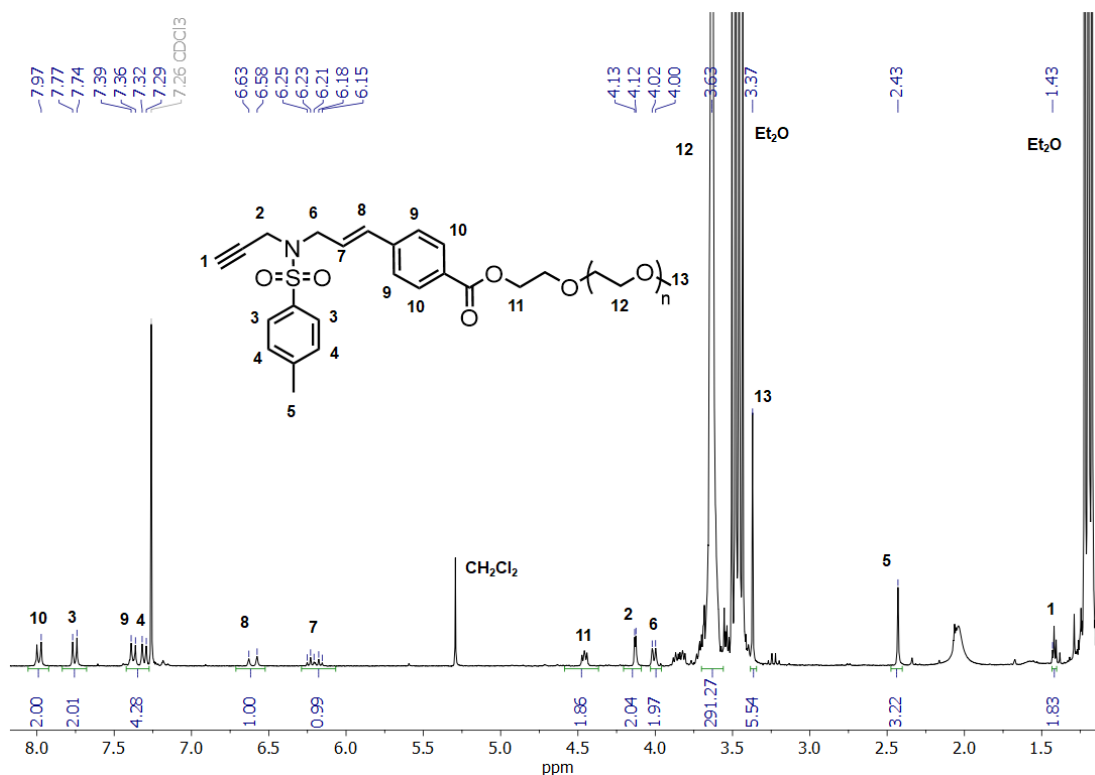
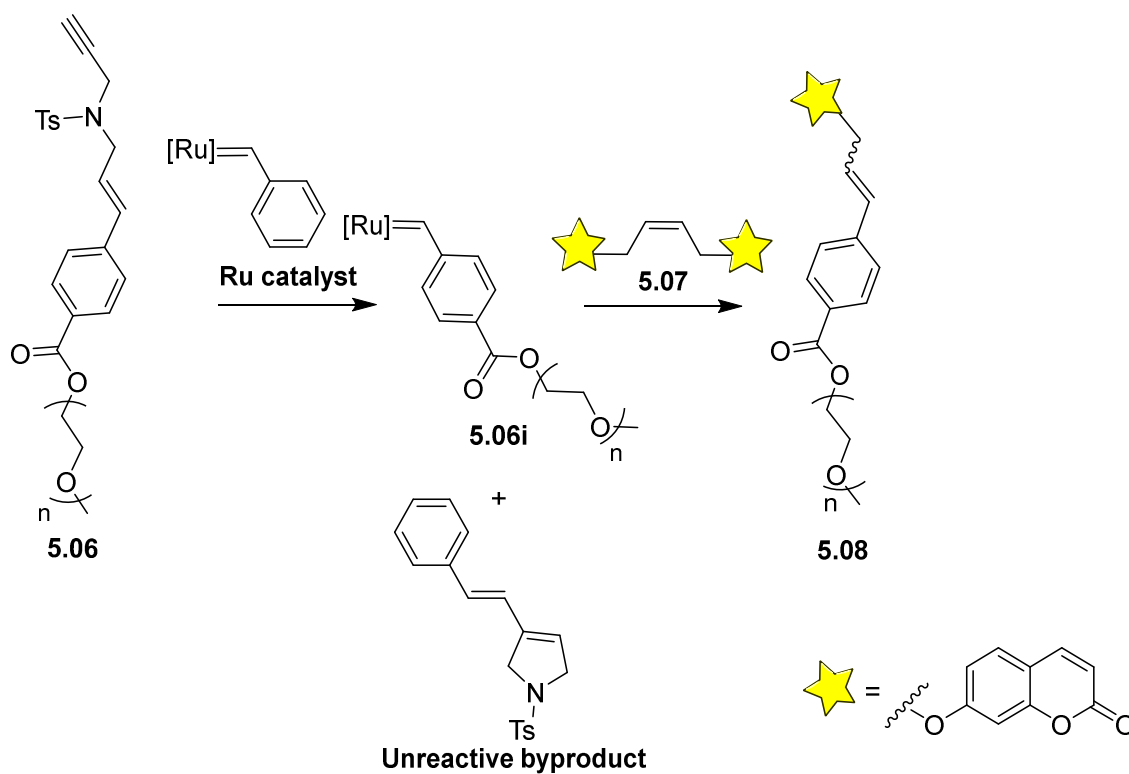
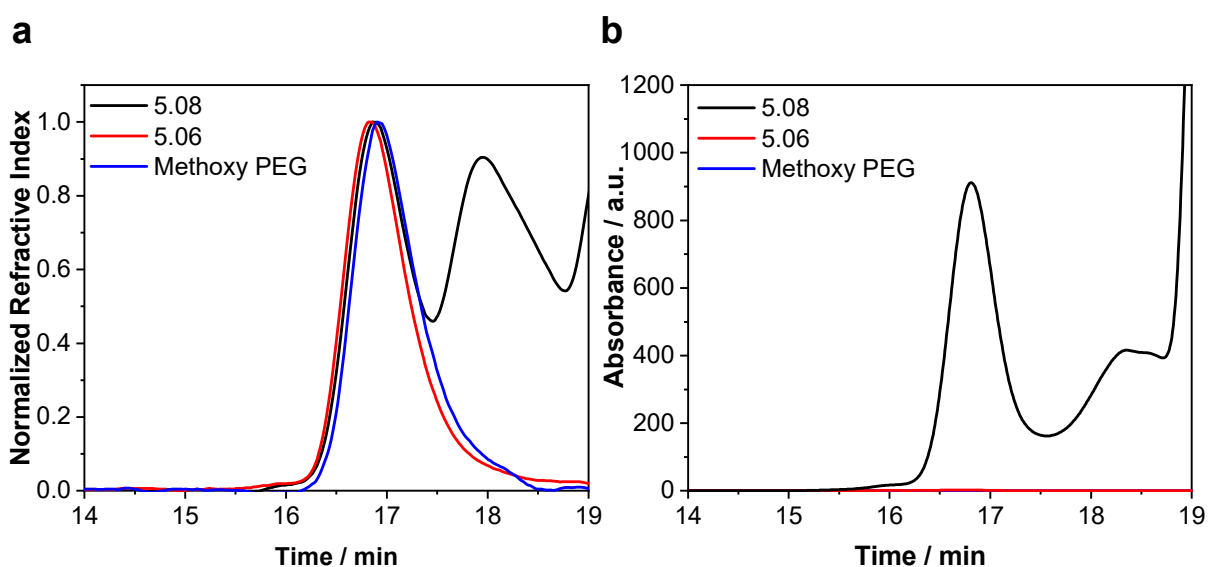


Figure 5.4 <sup>1</sup>H NMR spectrum of 5.06 in CDCl<sub>3</sub> (300 MHz, 298K).



Scheme 5.7 Enyne-metathesis reaction between 5.06 and 5.07 to prepare a fluorescently labelled PEG-polymer 5.08.

The resultant polymer (**5.08**) was analyzed by SEC and the traces compared to those for methoxy PEG and **5.06** (Figure 5.5). The 350 nm UV-chromatogram of the resultant polymer, **5.08**, contained a peak at 17 minutes which overlaid with the RI trace, indicating the successful transfer of the coumarin product to **5.06** (note that whilst the Ru-catalyst is also expected to absorb in this region it is unlikely to give such a large absorbance signal). Furthermore, the control polymers, **5.06** and methoxy-PEG did not absorb UV light at 350 nm.



**Figure 5.5** DMF SEC traces of **5.08**, **5.06** and methoxy PEG: (a) RI Chromatogram; (b) UV Chromatogram at 350 nm. Unreacted **5.07** remained in the sample during analysis and is therefore the cause of the bimodal distribution observed for **5.08**. Eluent: DMF + 5 mM  $\text{NH}_4\text{BF}_4$ .

### 5.3.2.2 Functionalization of DNA via enyne metathesis in $\text{H}_2\text{O}$

Following the successful demonstration of enyne-metathesis to prepare an *in situ* activated catalyst, the reaction was repeated using **5i**, in an attempt to prepare a coumarin-functionalized oligonucleotide (**5ii**) akin to the proof-of-concept study (Figure 5.6). However, due to the limited solubility of DNA in organic solvents, the reaction was conducted in aqueous media. The catalyst was therefore switched to AquaMet (AM), a commercially available, water-soluble catalyst first reported by Grela and co-workers.<sup>9</sup> Furthermore, a pH2 phosphate

solution (PB2) was utilized in order to prevent Ru-induced DNA degradation, as reported in Chapter 3. Note that **5.07** displayed limited solubility in PB2 and thus achieving a homogenous reaction mixture was not achieved. Despite this, the reaction was screened varying the equivalents of **5.07** and AM (between 10 and 1000 equivalents with respect to **5i**) (Figure 5.6b) and then analyzed by 15% native PAGE (Figures 5.6c and 5.6d). The DNA was compared to control lanes which were loaded with **5i** that had been subjected to **5.07** without the addition of AM.

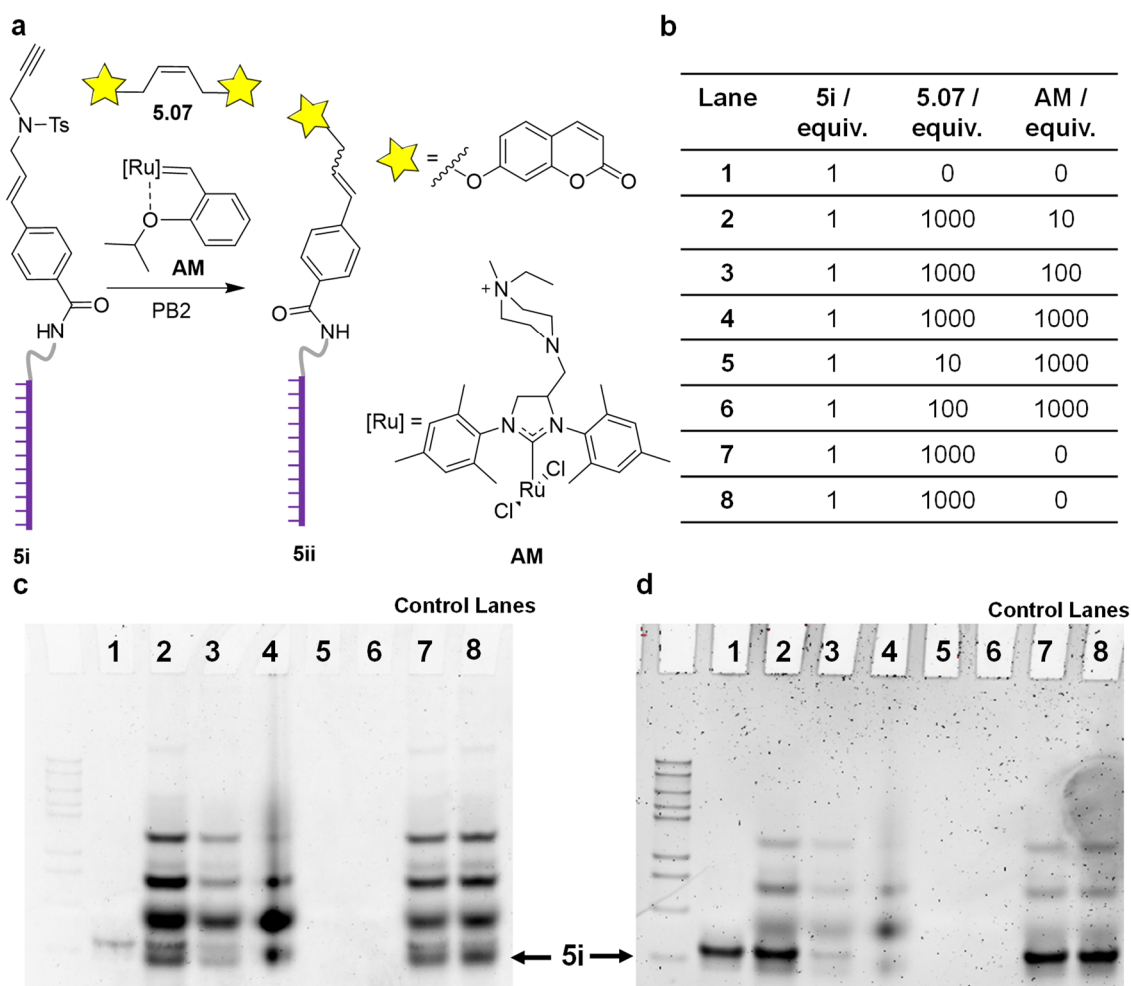


**Figure 5.6** (a) Enyne metathesis to prepare a fluorescently labelled oligonucleotide (**5ii**). (b) Reaction conditions explored varying the equivalents of **5.07** and AM. Note that lanes 1, 7 and 8 are control experiments in the absence of AM and/or **5.07**. (c) 15% Native PAGE gel visualized under UV light exciting coumarin fluorescence (d) 15% Native PAGE gel visualized under UV light exciting SYBR™ Gold fluorescence. Note that due to similar emission wavelengths of the two dyes and the light source (blue trans illumination) applied to visualize the gels, the coumarin absorbance is visible in the SYBR™ Gold stained gel and vice versa.

The PAGE gel was initially visualized whilst exciting the coumarin fluorescence (Figure 5.6c). It was anticipated that if enyne-metathesis had taken place a single fluorescent band overlapping with that of **5i** would be observed. Furthermore, any unreacted fluorescent small molecule, **5.07**, was expected to migrate very quickly through the gel thus not appear in the gel. However, unexpectedly, several fluorescent bands were observed in lanes 7 and 8 despite the absence of any catalyst to initiate metathesis. It was hypothesized that this could be due to the hydrophobicity of the coumarin dye leading to aggregation in the aqueous environment and the resultant slow migration of these aggregates through the gel. The presence of these fluorescent bands made interpretation of the gel extremely difficult as bands were appearing at the same height as the band due to **5i** was expected to appear. Of note, the samples exposed to a high catalyst loading (between 100 to 1000 equivalents AM) (lanes 3 to 6) resulted in either weak or no bands appearing in the PAGE gel when visualized under UV-light. This was suspected to be because of either Ru-induced DNA degradation or the Ru-induced fluorescence quenching which was discussed in depth in Chapter 2.

Due to the limited solubility of **5.07** in aqueous media, a range of commercially available small molecule alkenes which are known to be water-soluble were studied as alternative CM partners. However, due to the high cost of DNA, limited number of reports utilizing AM and unsuccessful first attempt, a small molecule study was first conducted to ensure that AM could remain catalytically active under the aqueous conditions required for DNA-metathesis. Thus far, the use of AM in the presence of biological materials is limited to just one report of the RCM of unprotected peptides.<sup>10</sup> In this study, published in late-2018, the authors reported the use of MgCl<sub>2</sub> and/or acidic conditions enabled the AM catalyzed RCM of peptides. The addition of acid, succinimide and/or MgCl<sub>2</sub> has previously been reported by us and others to minimize

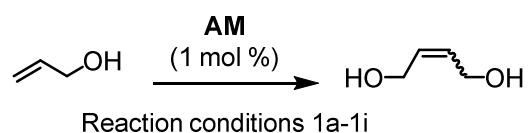
DNA-Ru interactions and thus the effect of these additives on the AM catalyzed CM was of interest.<sup>11, 12</sup> Towards this end, the AM catalyzed CM of allyl alcohol was studied under a range of conditions, shown in Table 5.1. After 2 h, the reaction mixture was diluted and monitored by gas chromatography-mass spectrometry (GCMS) (Figure 5.7). The conversion was reported by comparing the peak integration of the CM product, 2-Butene-1,4-diol, to allyl alcohol. Whilst this method allowed for a qualitative assessment of the impact of additives on cross-metathesis, the method does assume similar ionization capabilities of the two molecules. Therefore, whilst comparisons between different reaction conditions can be made the actual conversions reported may contain some inaccuracies.

In summary, over 50% conversion was achieved under all reaction conditions, suggesting that none of the additives had a detrimental effect on the catalyst. However, generally those reactions conducted in PB2 solution yielded higher conversions than those in neutral H<sub>2</sub>O despite the observed poorer solubility of AM in PB2. The enhancement of metathesis under acidic conditions has previously been reported on numerous occasions.<sup>13-15</sup> However, until recently the cause of this behavior was poorly understood and often assumed to be due to either (1) faster initiation through the promotion of ligand disassociation and/or (2) the prevention of catalyst degradation.

Two independent studies recently conducted in our group and the Pokorski group, identified that the metathesis activity is also very sensitive to the chloride ion concentration, with an increase in the free chloride ion concentration displacing the equilibrium away from Ru-(OH)<sub>n</sub> complexes which are metathesis inactive.<sup>16, 17</sup> The enhanced performance of CM in the presence of PB2 (Table 5.1, reactions **1a-1d**) was therefore attributed to the 10 mM chloride

ion concentration present. Consequently, it was surprising to see that the addition of  $\text{MgCl}_2$  in this experiment did not result in a conversion enhancement despite a 60-fold increase in free ion concentration. This is believed to be due to the high salt content (600 mM) causing AM to precipitate out of solution, as observed by Pokorski and co-workers.<sup>17</sup> Nevertheless, with the catalytic activity of AM confirmed under all tested conditions, a final study was conducted increasing the catalyst loading to 10 mol% AM and conditions **1a** and **1f** led to greater than 99% conversion as shown by GCMS (Experimental, Section 5.5.11).

**Table 5.1** Screening the CM of allyl-alcohol. <sup>‡</sup>Equivalents reported with respect to AM. <sup>‡</sup>Conversion reported based on the integration of product peak with respect to the starting material peak.



Reaction number	Solvent	$\text{MgCl}_2$ / equiv <sup>‡</sup>	Succinimide / equiv <sup>‡</sup>	Conversion <sup>‡</sup> / %
<b>1a</b>		0	0	80
<b>1b</b>		0	4	56
<b>1c</b>	PB2	4	0	71
<b>1d</b>		4	4	77
<b>1e</b>		0	0	57
<b>1f</b>		0	4	84
<b>1g</b>		4	0	51
<b>1h</b>	H <sub>2</sub> O	4	4	52
<b>1i*</b>		4	4	57

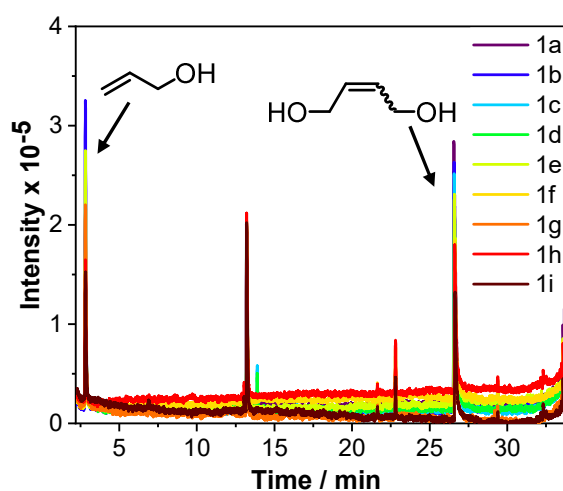


**Figure 5.7** GCMS chromatogram of reaction mixtures 1a-1i analysed at ca.  $0.5 \text{ mg mL}^{-1}$  in acetone. Allyl alcohol elutes at ca. 2.5 min and but-2-ene-diol elutes ca. 27 min. Note that the peak at 13 min. is due to the self-aldol condensation reaction of the eluent acetone.

As AM was identified to be particularly active in PB2 and the previous DNA-ROMP work (Chapter 3) had been conducted in this solvent, it was decided to investigate this solvent first.

In Chapter 3, the stability of S0-NH<sub>2</sub> in PB2 and the presence of 10 equivalents of **G3** was confirmed. However, a second study was conducted with DNA in PB2 in the presence of 0.01 and 0.1 equivalents of AM. Following, incubation of S0-NH<sub>2</sub> in the presence of AM the product was analyzed by 15% native PAGE, and only one band was observed representative of S0-NH<sub>2</sub> (Figure 5.8). This once again, confirmed the stability of DNA in PB2 and the presence of AM.

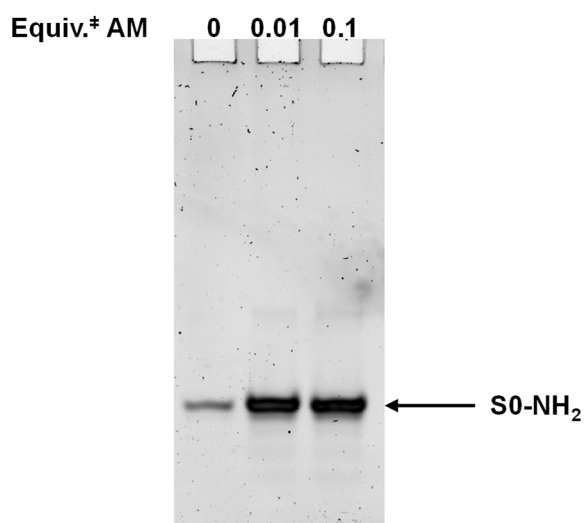


**Figure 5.8** 15% Native PAGE analysis of  $S0-NH_2$  subjected to varying equivalents of **AM**. Visualized under UV light following SYBR™ Gold staining.

With the stability of DNA, and the catalytic activity of **AM** confirmed in PB2, attention was once again turned to the CM of **5i**. However, to circumvent the aforementioned challenges with **5.07** a range of water-soluble commercially available alkenes were sought. The reactivity of alkenes towards metathesis has been classified into four distinct types: ‘type 1’ olefins can undergo rapid homodimerization and the homodimers can participate in cross-metathesis; ‘type 2’ olefins can undergo slow homodimerization and the resulting homodimers are sparingly consumable; ‘type 3’ olefins cannot undergo homodimerization but can react with type 1 and type 2 olefins; and ‘type 4’ olefins are inert to cross-metathesis. The alkenes chosen for this study were therefore carefully selected to ensure metathesis activity. ‘Type 1’ alkenes are the most reactive and typically consist of sterically unhindered, electron-rich alkenes; however, homodimerization will take place as a side reaction. In contrast, as alkenes become more sterically hindered or electron deficient the reactivity decreases (‘type 2’ through to ‘type 3’) and homodimerization is minimized. The classification of alkenes is unique to each

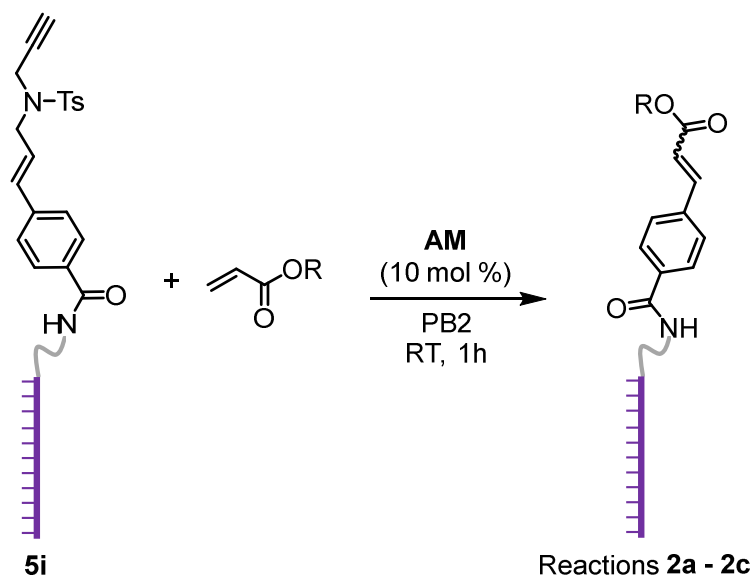


catalyst but classification tables for G1 and G2 catalysts have been published by Chatterjee *et al.*<sup>18</sup>

In this study, a series of acrylates ('type 2' olefins) were utilized (Table 5.2) which, as a consequence of the electron withdrawing character of the carbonyl group, are known to undergo slow homodimerization but are excellent CM partners with 'type 1' olefins such as styrene.<sup>18</sup> It was anticipated that this would minimize the chance of side reactions taking place as a result of homodimerization. The conditions used replicated those identified in the screening study. Therefore, 10 mol% AM was added to **5i** and the corresponding acrylate in PB2, and the samples were left to shake at 25 °C for 1 h. Following, the reaction, small molecules were removed *via* spin filtration through a molar mass cut-off filter and then the sample analyzed by LCMS. Upon analysis by LCMS, reactions **2a-2c** yielded no desired product and in all three cases **5i** was the major product detected.

As a consequence of this, the reaction was repeated with a more reactive 'type 1' olefin, allyl alcohol, used in the original small molecule screening. Whilst allyl alcohol is more reactive, it does increase the possibility of side reactions due to propensity of allyl alcohol to dimerize, forming 2-butene-1,4-diol. Therefore, an excess of allyl alcohol (100 equivalents) was used and the reaction was repeated at 10 mol% and 33 mol% AM (Figure 5.9), prior to analysis by LCMS.

**Table 5.2** Screening the CM of acrylate-esters.



Reaction number	R	% Conversion
<b>2a</b>	H	0
<b>2b</b>	(CH <sub>2</sub> ) <sub>2</sub> OH	0
<b>2c</b>	(CH <sub>2</sub> ) <sub>4</sub> OH	0

The latter conditions, were chosen to mimic the enyne:catalyst ratio optimized in the work of Gutekunst and co-workers.<sup>4</sup> However, once again both reactions yielded no conversion and the major product identified was **5i**. The lack of reactivity of both ‘type 1’ and ‘type 2’ olefins with **5i** in the presence of AM was unexpected as the enyne mechanism had been confirmed utilizing a PEG-functionalized enyne (Figure 5.5) and the activity of AM confirmed using a small molecule study (Table 5.1). However, our study and an independent study conducted by Monty *et al.* suggests that AM is not catalytically active in the presence of DNA and this was hypothesized to be due to a DNA-ammonium interaction rendering the catalyst inactive.<sup>19</sup> Furthermore, due to the limited scale of DNA, typically nanomoles, the reaction was carried

out at extremely low concentrations of AM (ca. 0.1 mM) which may be resulting in catalyst degradation outcompeting the metathesis reaction.

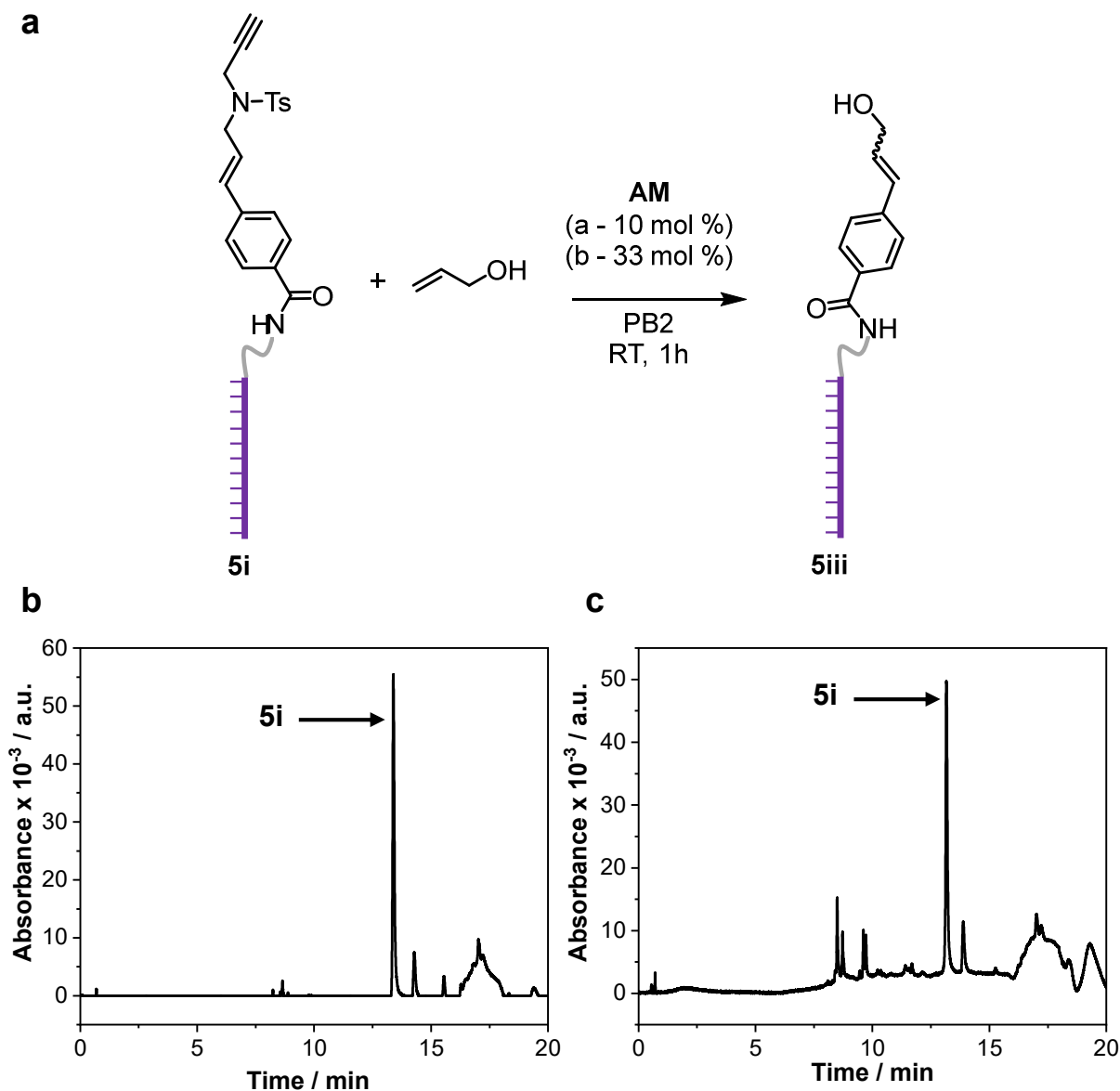


**Figure 5.9** (a) CM of allyl-alcohol; LCMS-UV chromatogram at 260 nm following the reaction of **5i** with (b) 10 mol% AM; and (c) 33 mol% AM eluted with a gradient of buffer A: 75 mM TEAA in H<sub>2</sub>O and buffer B: 75 mM TEAA in acetonitrile. Peaks assigned via mass spectrometry.

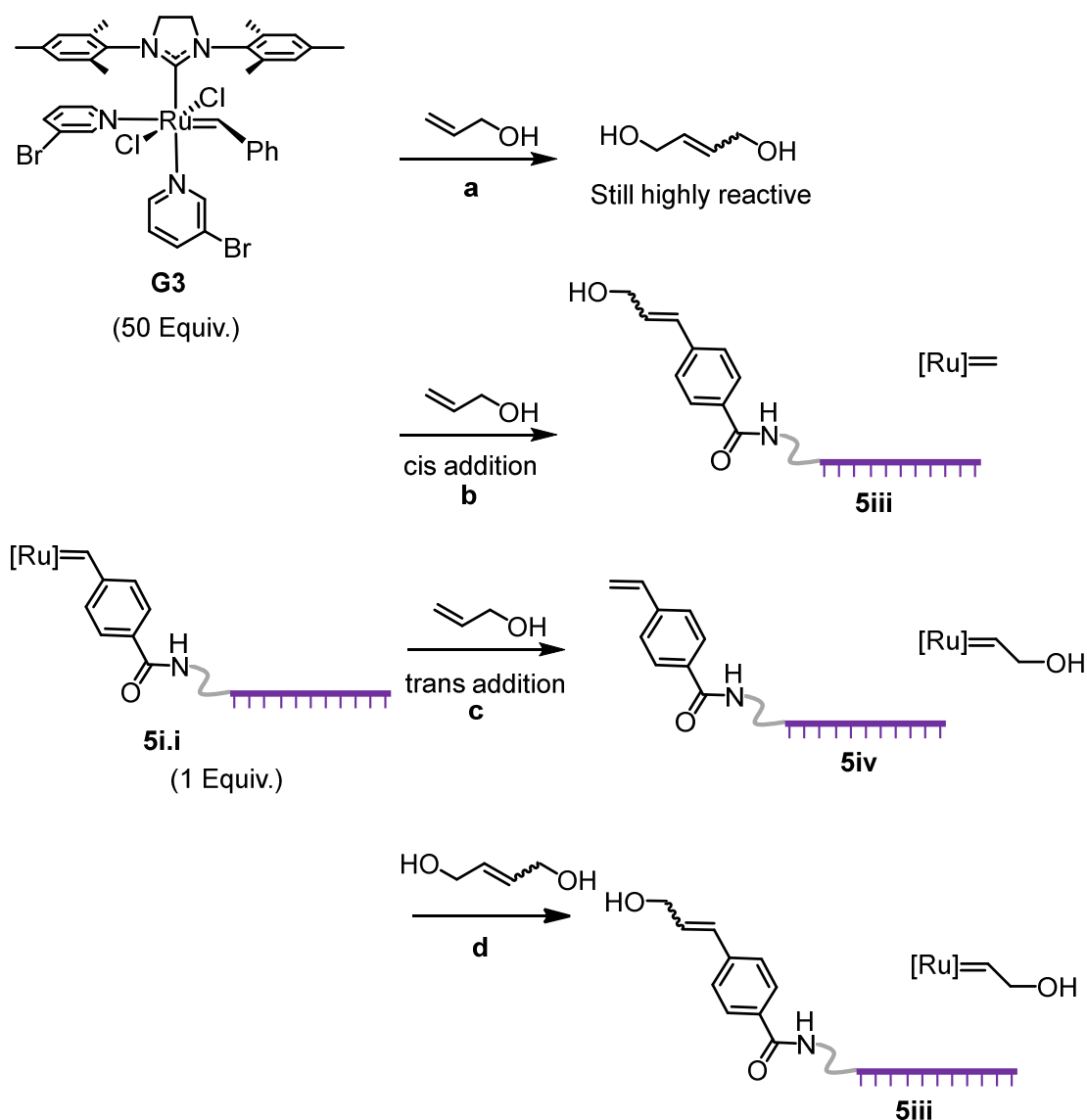
### 5.3.2.3 Functionalization of DNA *via* enyne metathesis in H<sub>2</sub>O/organic solvent mixtures

Despite the lack of activity of AM in the presence of DNA, in 2017 the RCM of unprotected DNA was reported by Lu *et al.*<sup>12</sup> The conditions were inspired by much of the early work on

peptide metathesis and utilized **G3** in a cosolvent system, H<sub>2</sub>O/tBuOH (3:2 v/v).<sup>20-22</sup> Furthermore, as discussed throughout this thesis, the addition of a large excess of MgCl<sub>2</sub> was utilized to prevent DNA degradation. This was particularly significant as 50 equivalents of **G3** were used which could lead to DNA degradation.

Keen to demonstrate the potential of enyne-metathesis on DNA, attempts to apply these reported conditions to our mechanism commenced. However, in contrast to our previous attempts which were conducted at ≤ 33 mol% catalyst, Lu *et al.* utilized an excess of **G3**.<sup>12</sup> This would mean that less than 1% of the active catalyst would be functionalized with DNA and therefore a high turn-over of 2-butene-1,4-diol would be expected. Nevertheless, 2-butene-1,4-diol is still metathesis active and can go on to react with the Ru-metathesis catalyst. The possible products formed following the reaction of **5i.i** (formed *in situ* from **5i**) with allyl alcohol and 2-butene-1,4-diol are shown in Scheme 5.8.

Due to the possibility of allyl alcohol adding *cis*- or *trans*- across the Ru-catalyst, two DNA-functionalized ligands can be produced **5iii** or **5iv**. In contrast, the addition of 1,4-butendiol leads to only one product **5iii**. The ratio of products is complex to predict and is expected to be dependent upon sterics and the propensity of the resulting alkenes, **5iii** and **5iv**, to react again. Note that the stereochemistry of the resulting olefins (**5iii** and **5iv**) is usually driven by thermodynamics and thus the (*E*)-isomer would be expected to be the major product; although, this was not investigated for this project.<sup>23</sup>



**Scheme 5.8** Possible reaction products formed following the reaction of **G3** with allyl alcohol in the presence of **5i**.

In the study conducted by Lu *et al.*, a dsDNA sequence covalently linked at one end *via* a uni-link™ amino modifier was used. However, with the goal of templating a metathesis reaction, the use of a standard duplex was required. In organic solvents the  $T_m$  of a duplex is often significantly reduced.<sup>24</sup> Therefore, the  $T_m$  of a short 17-base pair duplex in H<sub>2</sub>O/tBuOH was assessed *via* Förster-resonance energy transfer (FRET) and compared to that in aqueous conditions (Figure 5.10).

An oligonucleotide functionalized with a TAMRA fluorophore at the 3' end (S0-NH<sub>2</sub>-TAMRA) was mixed with a complementary sequence functionalized with a dark quencher at the 5' end (C0-Quencher). Whilst the duplex was intact the fluorescence was quenched; however, upon duplex melting a sharp increase in fluorescence was observed. The  $T_m$  is defined as the temperature at which 50% of the oligonucleotide is double-stranded and 50% free in solution. Therefore, the  $T_m$  was approximated from the temperature at which the normalized fluorescence intensity was 0.5. This was identified to be approximately 53 °C in H<sub>2</sub>O/tBuOH (3:2 v/v), 16 °C lower than that observed in tris-buffer. However, as the melting temperature was still above ambient temperature, this result confirmed that the conditions previously published by Lu *et al.* could be attempted with dsDNA.<sup>12</sup>

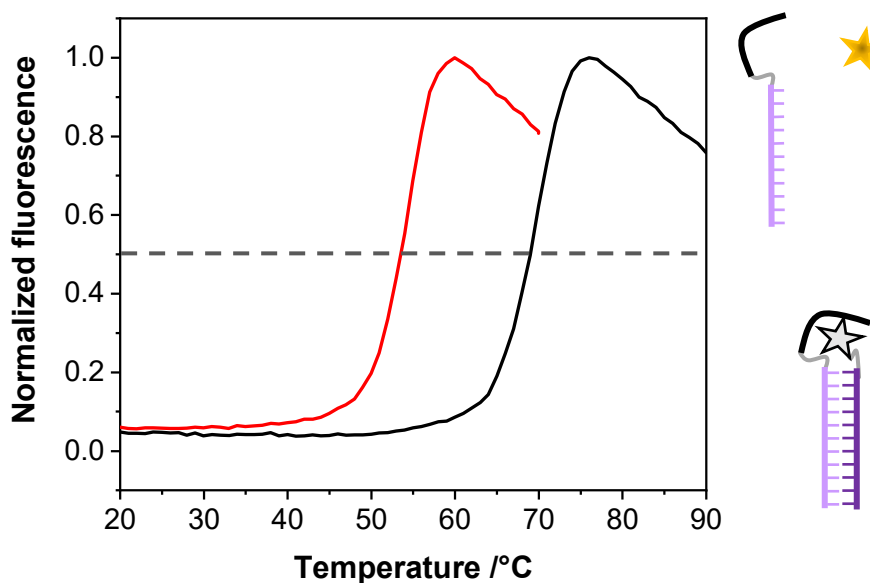


**Figure 5.10** Fluorescence melting profile of S0-NH<sub>2</sub>-TAMRA/C0-Quencher duplex in tris-buffer (black trace) and tBuOH/H<sub>2</sub>O (red trace). dsDNA was excited at 559 nm and the fluorescence emission monitored at 583 nm. Heating was conducted at 2 °C min<sup>-1</sup> and data collected from the second heating cycle.

Following on from the confirmation that dsDNA remains intact in H<sub>2</sub>O/tBuOH, the CM attempt on **5i** with a complementary oligonucleotide was attempted. The same 17-base pair duplex

formed from **5i** and C0 was mixed with **G3** and allyl alcohol in H<sub>2</sub>O/tBuOH (3:2 v/v) in the presence of 4000 equivalents of MgCl<sub>2</sub> for 1 h and then analyzed by LCMS (Figure 5.11). Under the LCMS conditions utilized, namely 75 mM TEAA in acetonitrile/H<sub>2</sub>O at 60 °C, the duplex melted and hence the complementary strand C0 could be identified in the LCMS-UV chromatogram at 8.5 min (Figure 5.11b). A peak at 9.5 min corresponded to two overlapping species, an unknown side product present in the starting material and **5iii**. The peak at 10 min corresponded to **5iv**, and a small amount of residual unreacted starting material was observed around 13.2 min. The ratio of the **5iii:5iv** was estimated to be 2:3. This result would suggest that the *trans*-addition, first introduced in Scheme 5.8, is favored over the *cis*-addition, likely due to the fewer steric interactions. Furthermore, the presence of a large amount of **5iv** would suggest that the DNA reduces the propensity of the terminal olefin to react again. It is also noted that, in this example the addition of the unknown side product would be contributing to the total integration of the peak at 9.5 minutes and therefore the true ratio is likely to lie even further towards the *trans*-product addition.

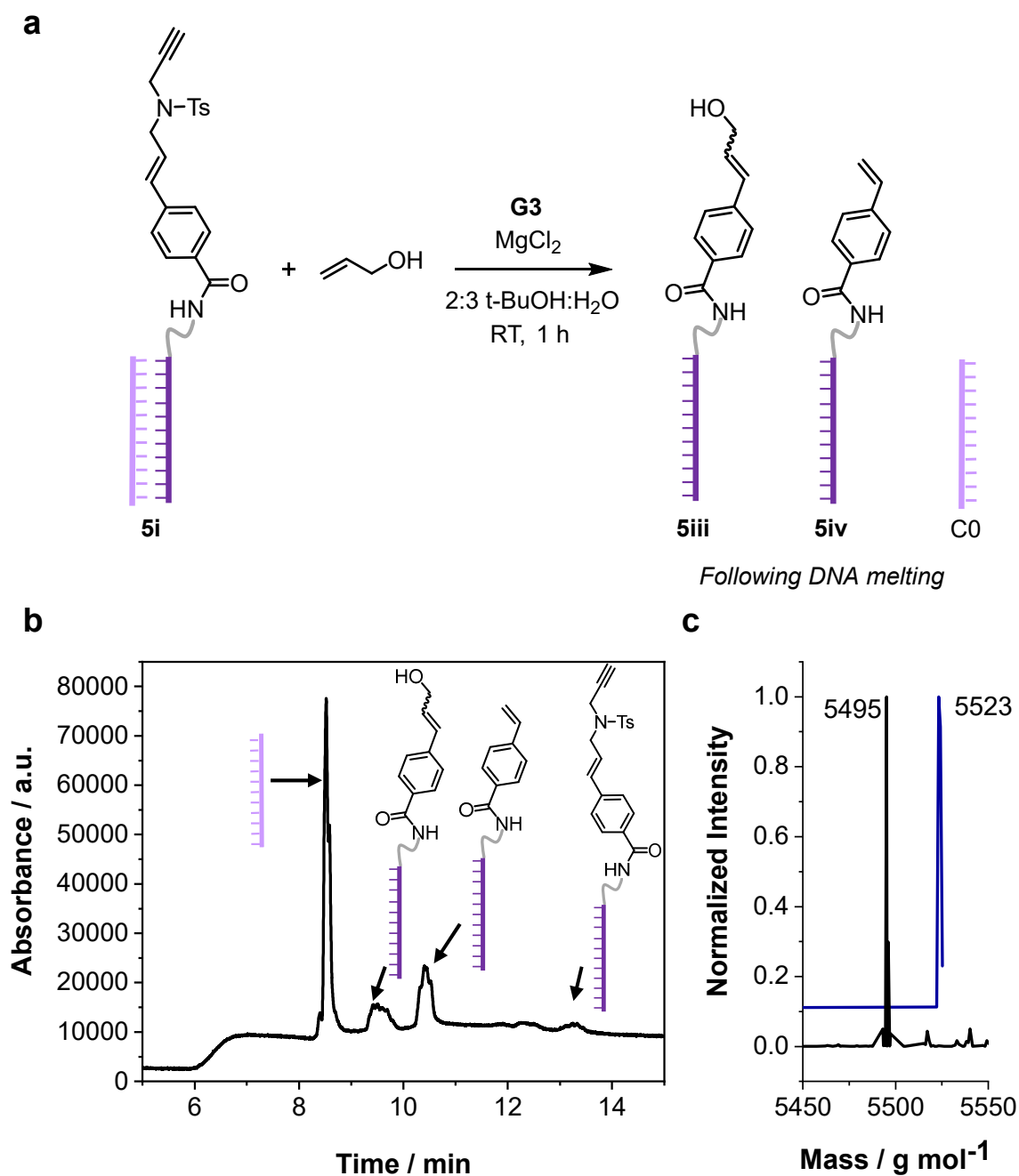


**Figure 5.11** (a) CM of **5i** with allyl alcohol. (b) LCMS-UV chromatogram at 260 nm of product mixture eluted with a gradient of buffer A: 75 mM TEAA in H<sub>2</sub>O and buffer B: 75 mM TEAA in acetonitrile. Peaks assigned via mass spectrometry. (c) Deconvoluted mass spectrum of the products eluted at 9.5 min (blue trace) and 10.5 min (black trace).

Despite this initial positive result, repeating the reaction with the symmetric alkene *cis*-2-butene-1,4-diol led to no DNA material observed *via* LCMS, highlighting the sensitivity of DNA to Ru-induced degradation. Keen to retain DNA integrity and maximize DNA recovery, the



catalyst loading was reduced to just 10 equivalents of Ru-catalyst and the CM reaction with *cis*-2-butene-1,4-diol was repeated in the presence of three commercially available catalysts: **G3**, HG2 and G2 to screen the influence of the catalyst on the reaction conversion (Figure 5.12a). As demonstrated in Scheme 5.8, the use of a symmetric alkene is expected to yield only one product **5iv** which elutes at 9.5 mins in the LCMS chromatogram. The conversion was estimated by comparing the peak area at 9.5 mins to the starting material at 13.3 mins (Figure 5.12b).

The lowest conversion was achieved when using G2, this may be explained by the presence of a labile phosphine ligand making the catalyst unstable in solution. This was also visualized by a rapid color change from purple to brown when the catalyst was solubilized in tBuOH. In contrast, HG2 typically possess much greater stability due to the replacement of a phosphine ligand with a benzylidene ligand and thus is typically the catalyst of choice for CM reactions. It was, therefore, not surprising to see the highest conversion was achieved when using HG2 (26%). However, the improvement over **G3** was only marginal and this was hypothesized to be as a consequence of the reduced solubility of HG2 in tBuOH compared to **G3**, reducing the effective catalyst loading.

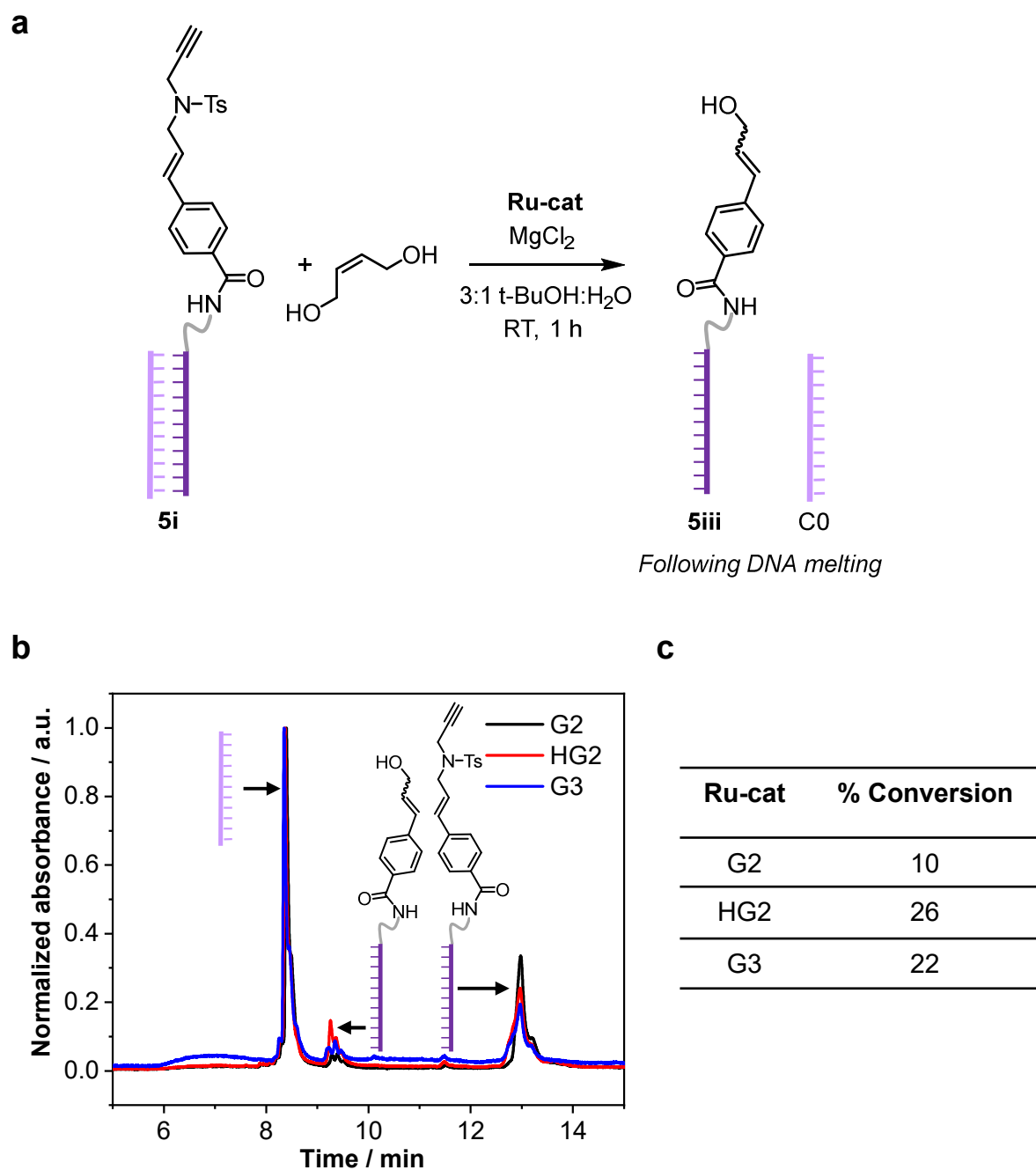


**Figure 5.12** (a) CM of **5i** with *cis*-2-butene-1,4-diol. (b) LCMS-UV chromatogram at 260 nm of product mixtures following the reactions with **G2** (black trace), **HG2** (red trace) and **G3** (blue trace), eluted with a gradient of buffer A: 75 mM TEAA in H<sub>2</sub>O and buffer B: 75 mM TEAA in acetonitrile. Peaks assigned via mass spectrometry. (c) Reaction conversions calculated from the integrations of the peak at 13 min compared to 9.5 min.

In early 2020, Simmons and co-workers published a follow-on paper to the study conducted by Lu *et al.*, in which they further optimized the conditions utilized above for the RCM of DNA-chemical conjugates. They addressed several limitations with the H<sub>2</sub>O/tBuOH system, namely

the limited solubility of the catalyst in tBuOH, the phase separation observed at high salt concentrations between tBuOH and H<sub>2</sub>O, and the absence of pH control. Their study identified three key findings: firstly, a solvent mixture consisting of H<sub>2</sub>O/EtOH/MeOAc resulted in homogenous conditions even at high ionic strength. Secondly, the addition of NH<sub>4</sub>Cl induced an acidic pH which the authors postulated enhanced the reaction conversion by preventing catalyst degradation at basic pH (although it is now acknowledged that the excess chloride ions may also play a role in the performance enhancement).<sup>16</sup> Finally, the addition of 2,2'-biphenyldiamine was found to further enhance the reaction conversion attributed to the formation of an *in situ* decomposition-resistant catalyst first identified by Fogg and co-workers.<sup>25</sup> When 2,2'-biphenyldiamine is added to the Ru-catalysts it acts as a hemilabile, bidentate ligand forming a new catalytic species in 40% equilibrium yield which is believed to retard decomposition.

Interested in how these new reaction conditions could improve the enyne metathesis reaction of **5i**, the melting temperature of the duplex (S0-NH<sub>2</sub>-TAMRA, C0) was first studied in H<sub>2</sub>O/EtOH/MeOAc (5:4:1 v/v/v) with added MgCl<sub>2</sub> (20,000 eq.) and NH<sub>4</sub>Cl (14,000 eq.) to ensure duplex formation at room temperature (Figure 5.13). The melting temperature was found to drop significantly from that in tris-buffer to approximately 38 °C. Nonetheless, as this was still significantly above room temperature, attempts commenced to perform the CM of *cis*-2-butene-1,4-diol under these new conditions.

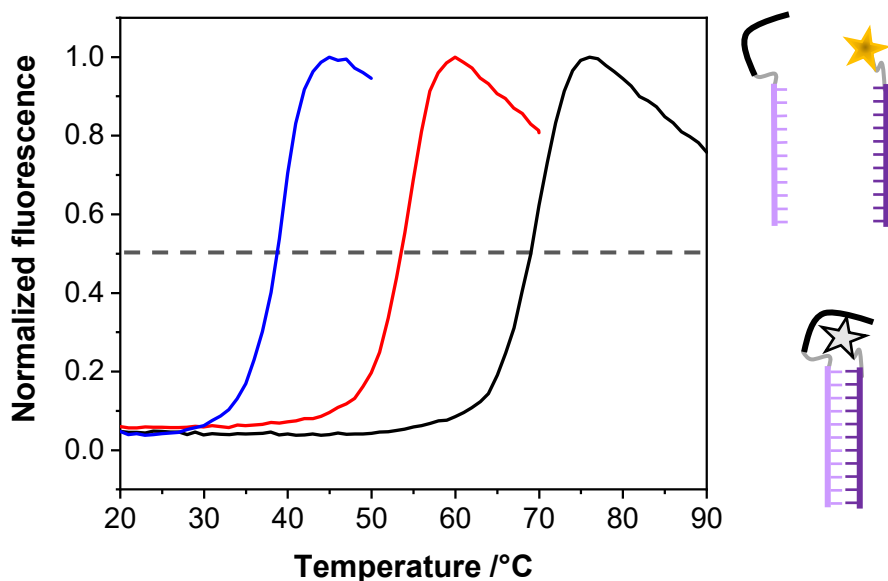


**Figure 5.13** Fluorescence melting profile of S0-NH<sub>2</sub>-TAMRA/CO-Quencher duplex in tris-buffer (black trace), tBuOH/H<sub>2</sub>O (red trace) and H<sub>2</sub>O/EtOH/MeOAc (blue trace). dsDNA was excited at 559 nm and the fluorescence emission monitored at 583 nm. Heating was conducted at 2 °C min<sup>-1</sup> and data collected from the second heating cycle.

Initially, the reaction of **5i** with *cis*-2-butene-1,4-diol was screened with three commercially available catalysts **G2**, **HG2** and **G3** under conditions similar to those reported by Simmons and co-workers (Figure 5.14a).<sup>19</sup> Furthermore, interested in how the presence of 2,2'-biphenyldiamine impacts the reaction conversion, two reactions were attempted with **G2** and **G3** in the presence of 10 equivalents of 2,2'-biphenyldiamine, **G2\*** and **G3\*** respectively (Figure 5.14a). Whilst the reaction catalyzed by **G3** succeeded the conversion obtained under the previous aforementioned reaction conditions (Figure 5.12a). Disappointingly, the reaction in the presence of **G2** and **HG2** obtained yields lower than those previously reported. However, the addition 2,2'-biphenyldiamine did indeed improve the reaction conversion with the reaction of **G3** in the presence of 2,2'-biphenyldiamine (**G3\***) achieving a conversion around 46%. The improvement was attributed to the retardation of catalyst degradation.

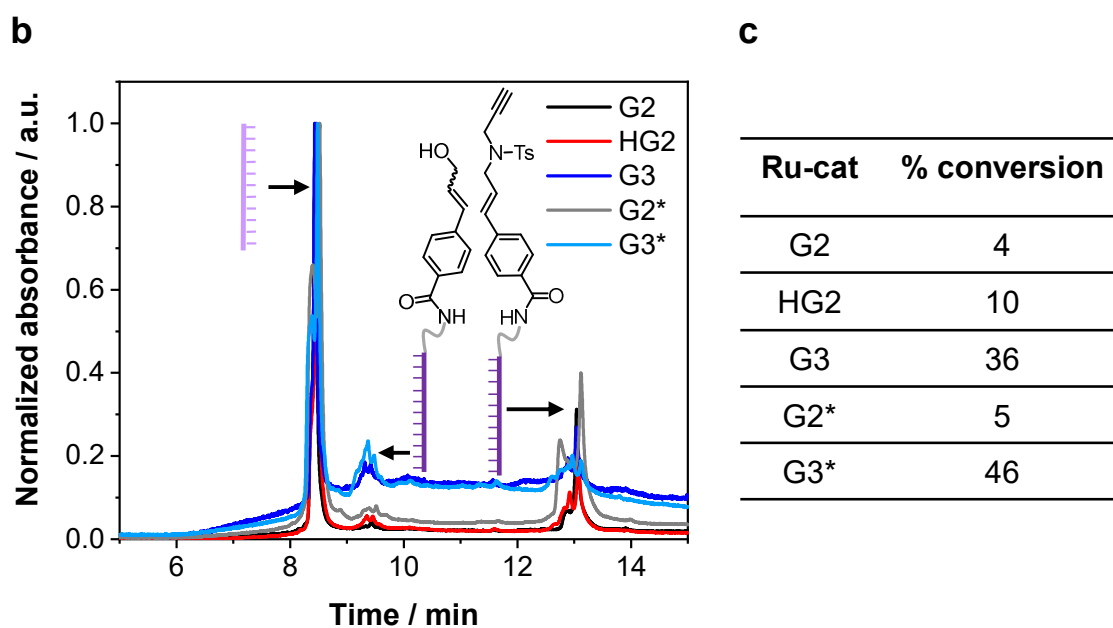
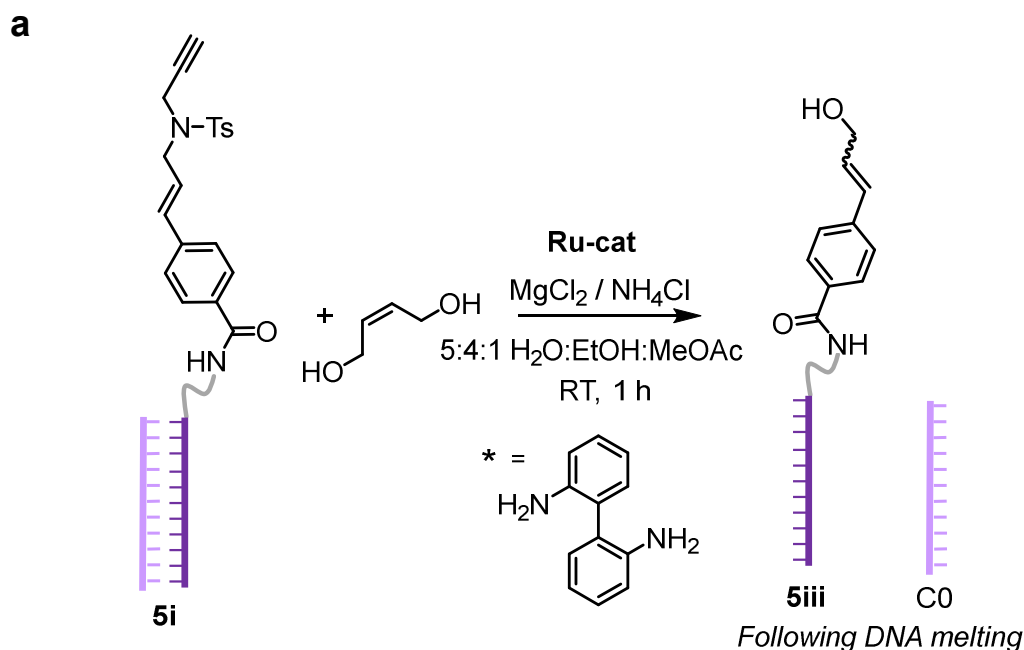


**Figure 5.14** (a) CM with *cis*-2-butene-1,4-diol. (b) LCMS-UV chromatogram at 260 nm of product mixtures following the reactions with **G2** (black trace), **HG2** (red trace), **G3** (blue trace), **G2** + 2,2'-biphenyldiamine (grey trace) and **G3** + 2,2'-biphenyldiamine (light blue trace), eluted with a gradient of buffer A: 75 mM TEAA in H<sub>2</sub>O and buffer B: 75 mM TEAA in acetonitrile. Peaks assigned via mass spectrometry. (c) Reaction conversions calculated from the integrations of the peak at 13 min compared to 9.5 min.

Finally, with the reaction conversions optimized using **G3** and 2,2-biphenyldiamine a number of asymmetric alkenes were screened (**3a-3d**, Figure 5.15). Of interest was the influence of sterics on the reaction conversion and product distribution.

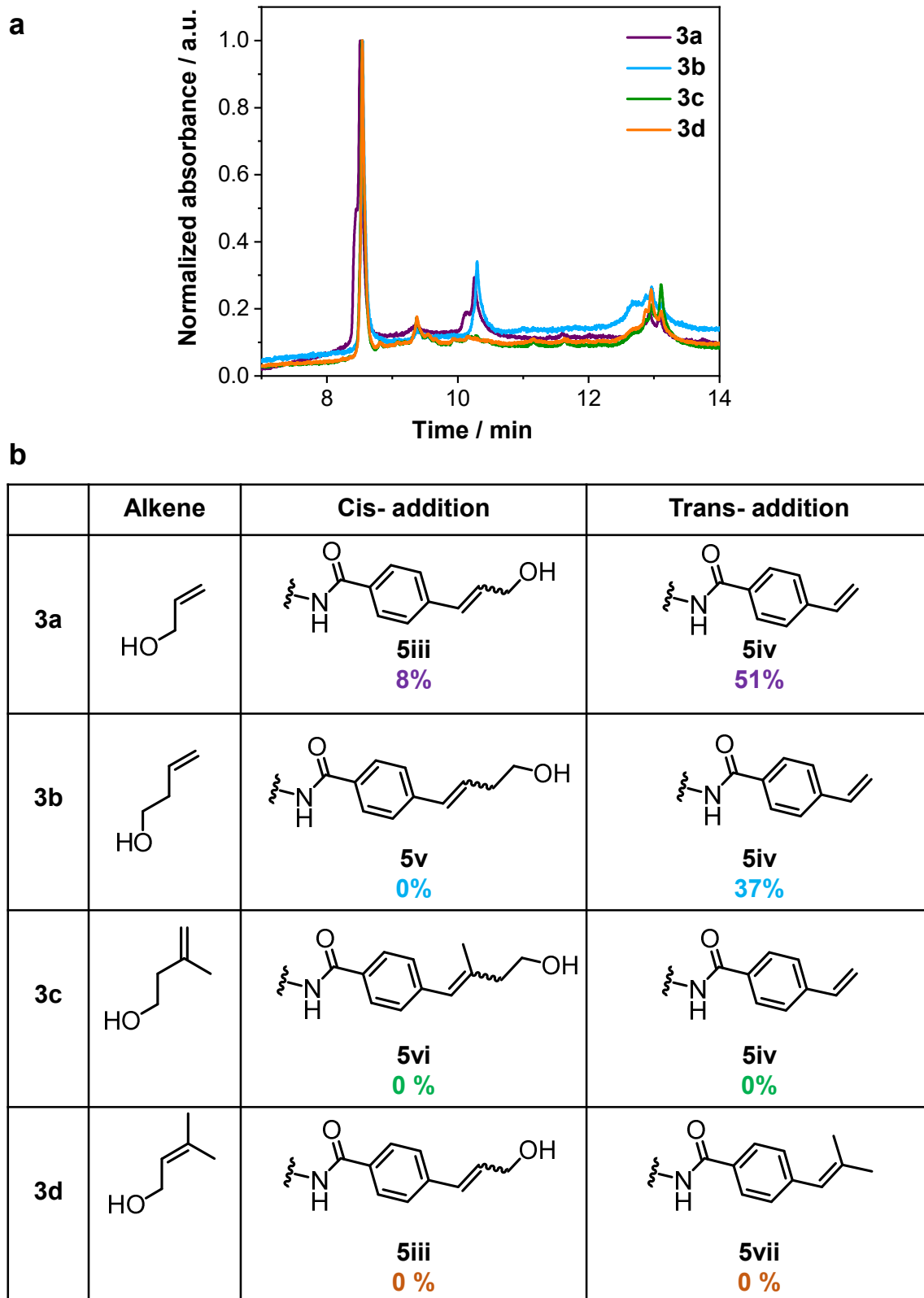


**Figure 5.15** (a) LCMS-UV chromatograms at 260 nm following the reaction of **5i** with **3a-3d**. Eluted with a gradient of buffer A: 75 mM TEAA in H<sub>2</sub>O and buffer B: 75 mM TEAA acetonitrile. (b) Reaction conversions calculated from the peak integrations.

The two monosubstituted alkenes **3a** and **3b** yielded reaction conversions around 50%, comparable to those with *cis*-2-butene-1,4-diol. Furthermore, the *trans*-addition product was heavily favoured over the *cis*-addition product which we once again attributed to sterics. Interestingly, the disubstituted terminal alkene **3c** and trisubstituted alkene **3d** yielded no reaction conversion. It was hypothesised that this was due to the steric hindrance slowing down the reaction such that catalyst decomposition occurred before any reaction could take place. Furthermore, the highly dilute reaction conditions (0.04M) are also known to allow catalyst decomposition to compete with metathesis. Unfortunately, further attempts to increase the reaction concentration failed due to the high salt content precipitating out of the mixture.

### 5.3.3 DNA-templated cross-metathesis

Following, the successful identification of conditions under which the CM on enyne-functionalized DNA, **5i** could be performed a templated reaction was attempted. A templated reaction was particularly interesting as not only would it provide the first step towards a multistep DNA-templated mechanism but it was also hypothesised that this may overcome the previous difficulties due to the low reaction concentration by increasing the local concentration.

Towards this end, a CM partner was first synthesized on an oligonucleotide complementary to **5i**. This was achieved using 3-butenic acid and activated-ester chemistry to yield the desired product, **5viii**, in 34% conversion (Figure 5.16). The desired product was isolated *via* HPLC prior to its use in the templating mechanism.

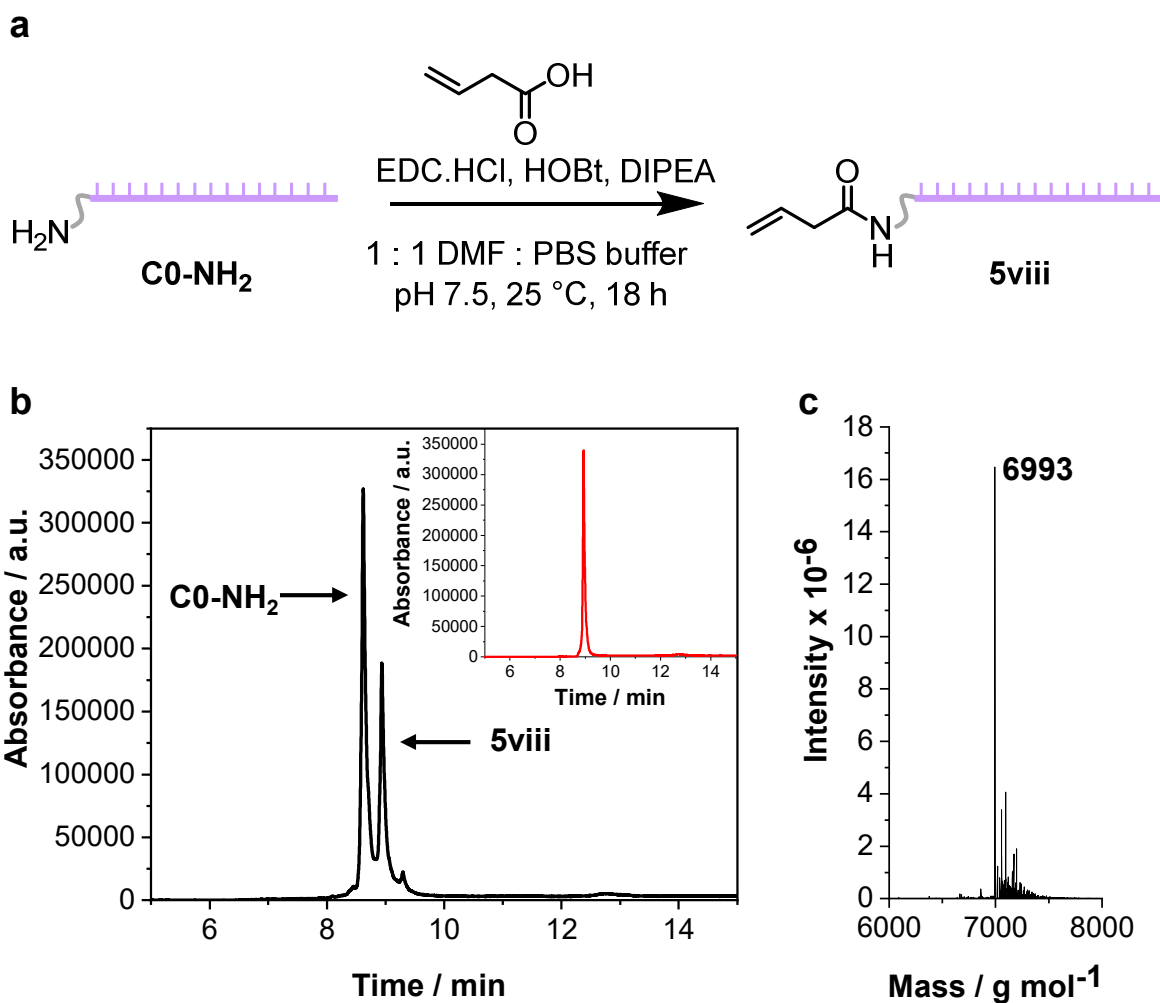


**Figure 5.16** (a) Synthesis of **5viii**. (b) LCMS UV chromatogram at 260 nm of **5viii**, eluted with a gradient of buffer A: 75 mM TEAA in H<sub>2</sub>O and buffer B: 75 mM TEAA in acetonitrile. Inset is LCMS chromatogram at 260 nm of **5viii** following purification, showing the presence of only one product. Peaks assigned via mass spectrometry. (c) Deconvoluted mass spectrum of the purified product obtained.

Following the synthesis and isolation of the CM partner a templating reaction was attempted (Figure 5.17a). In order to minimise the chances of any off-templating reactions occurring the reaction concentration was kept low (500 nM) but all other reaction conditions were kept the same as those optimized previously (Figure 5.14). **G3** was added to **5i** prior to the addition of **5viii** in order to encourage the enyne reaction to take place first to generate the *in situ* Ru-catalyst. Dependent upon whether the terminal alkene adds *cis*- or *trans*- to the catalyst two possible products were identified either a ligation reaction or the transfer of the Ru-catalyst



from **5i** to **5viii**. However, as the transfer reaction leads to a product which is still metathesis active, it was anticipated that this product could go on to react again leading to the ligated product. In order to determine if ligation had taken place the products were analyzed by denaturing PAGE (Figure 5.17b).

The addition of urea and formamide to the acrylamide gel successfully led to the melting of the DNA strands as confirmed by the presence of two bands in lane 3 when premixed samples of **5i** and **5viii** were added to the gel. It can therefore be assumed that any slower moving bands in the product lane (lane 4) are due to the chemical ligation of DNA. Promisingly, lane 4 does show a slower moving band which is higher up on the gel indicating that the ligation reaction may be taking place. However, as the distance between the bands is only modest, further analysis, such as mass spectrometry, would be required to confirm the successful ligation. Unfortunately, due to time constraints no further work was conducted on this, but initial results are appearing promising and would be of interest for the future.

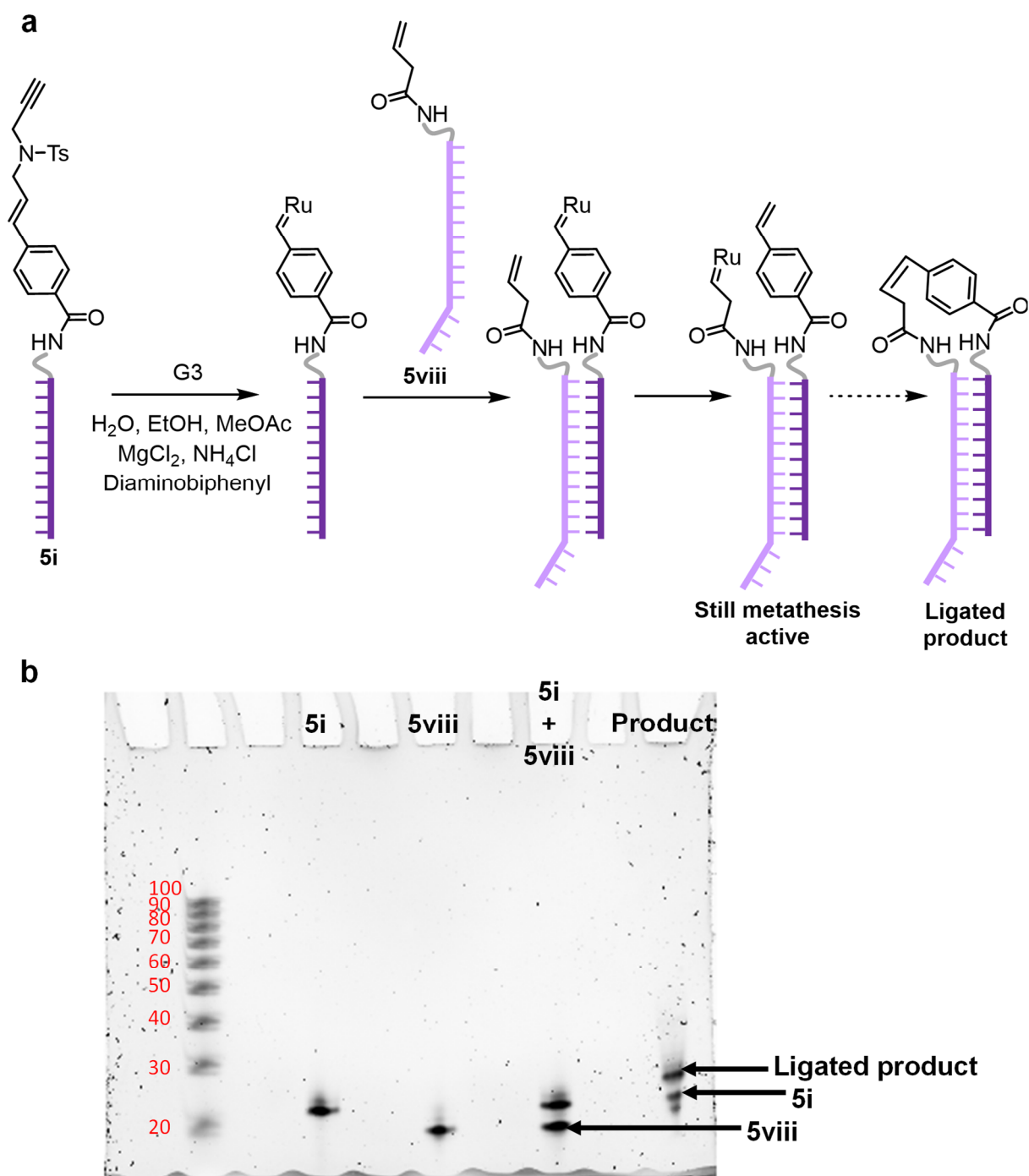


**Figure 5.17** (a) Templated metathesis mechanism between **5i** and **5viii**. (b) 15% denaturing PAGE analysis following the templated metathesis reaction visualized under UV light following SYBR™ Gold staining.

## 5.4 Conclusions

In this chapter, the use of an enyne scaffold to prepare an *in situ* DNA-functionalized metathesis catalyst was explored. The conjugation of the enyne scaffold to DNA was achieved efficiently in greater than 90 % conversion using activated-ester chemistry.

A number of conditions were then screened in order to attempt the enyne metathesis on DNA. Whilst attempts in a 100% aqueous environment, using the water-soluble catalyst AM, were unsuccessful attributed to an ammonium-DNA interaction, attempts were successful using an organosoluble catalyst in a H<sub>2</sub>O/organic solvent mixture. The reaction conditions were screened using **G3**, HG2 and G2. The use of G2 consistently led to poor conversions and this was attributed to the slow initiation of the catalyst and poor stability in the aqueous environment. In contrast, HG2 was anticipated to be the superior catalyst due to its greater stability compared to G2 and **G3**; however, despite out-competing G2, the catalyst often yielded lower conversions compared to **G3** and this was attributed to the poorer solubility of HG2 under the reaction conditions. The best performing catalyst was **G3** successfully yielding conversions up to 50% in a H<sub>2</sub>O/EtOH/MeOAc co-solvent mixture.

The versatility of the reaction was explored with a range of small-molecule alkenes and whilst the reaction performed successfully with electron rich, sterically unhindered alkenes, no conversion was observed when utilizing di- and tri-substituted alkenes. Therefore, further optimization of the reaction is required if it is to be widely utilized for the routine functionalization of DNA.

Finally, a templated CM reaction was attempted which will not only pave the way for the future use of metathesis in multistep DTS mechanisms but may also allow for the CM of more

challenging substrates due to the large increase in local concentration. Initial results appear promising and although it is acknowledged that further characterization data is required, the utilization of enyne-metathesis on DNA is an exciting future prospect.

## 5.5 Experimental Section

### 5.5.1 Materials

Oligonucleotides were purchased from Integrated DNA technologies, Inc. and resuspended in 18 MΩ.cm H<sub>2</sub>O to a concentration of 200 μM before use. Concentrations were calculated from the absorbance values at 260 nm using the reported extinction coefficients.

Name	Sequence (5' → 3')	Extinction coefficient/ L/(mole·cm)
S0-NH <sub>2</sub>	5AmMC6/CGA GAC TCA ACG ACA TG	169,300
C0	CAT GTC GTT GAG TCT CG	157,600
C0-NH <sub>2</sub>	ATC GCC ATG TCG TTG AGT CTC G/3AmMO	204,400
S0-NH <sub>2</sub> -TAMRA	5AmMC6/CGA GAC TCA ACG ACA TG/36-TAMSp	209,780
C0-Quencher	5IAbRQ/CAT GTC GTT GAG TCT CG	208,057

4-Dimethylamino pyridine (DMAP, ≥98 %), methoxy PEG (MW 2000 Da), *exo*-norbornene carboxylic acid (97%), N-(3-Dimethylaminopropyl)-N'-ethylcarbodiimide hydrochloride (EDC.HCl, BioXtra grade), HOBt hydrate (97%), DMF (Biological grade ≥99 %), allyl alcohol, Grubbs 2<sup>nd</sup> generation (G2) and Hoveyda-Grubbs 2<sup>nd</sup> generation catalyst (HG2) were purchased from Sigma-Aldrich. Allyl alcohol and *cis*-2-butene-1,4-diol were purchased from Acros. AquaMet (AM) was purchased from Strem Chemicals. Grubbs 3<sup>rd</sup> generation (G3) catalyst was synthesized as described in Chapter 2 – Section 2.5.4 and **5.07** was synthesized by Dr Jeffrey Foster and used as received.

DPBS buffer was prepared by dissolving 9.6 g of DPBS from Sigma-Aldrich into 1 L 18MΩ H<sub>2</sub>O. Phosphate solution, pH = 2 (PB2) was prepared using 100 mM sodium phosphate monobasic dihydrate (NaH<sub>2</sub>PO<sub>4</sub> · 2H<sub>2</sub>O) in 18MΩ H<sub>2</sub>O adjusted to pH 2 with HCl. Tris-buffer was prepared using 100 mM Tris, 50 mM NaCl and 1 mM EDTA in 18MΩ H<sub>2</sub>O adjusted to pH 8. 10 x Tris-acetate EDTA (TAE) buffer was purchased from Sigma-Aldrich and contains 0.4 M Tris acetate and 0.01 M EDTA. 10 x Tris-Borate EDTA (TBE) TBE buffer was purchased from Sigma-Aldrich and contains 0.89 M Tris and 0.02 M EDTA adjusted to pH 8.3 with boric acid.

Micro Bio-spin™ 6 columns were purchased from Bio-Rad laboratories. Amicon® Ultra-0.5 mL centrifugal filters (3000 MWCO) were purchased from Millipore.

### 5.5.2 Instrumentation

*NMR Spectroscopy.* <sup>1</sup>H and <sup>13</sup>C nuclear magnetic resonance (NMR) spectra were recorded on a Bruker AVIII-300 spectrometer, Bruker AVIII-400 spectrometer or a Bruker Avance-NEO-400 spectrometer in the solvents indicated at 298 K. Chemical shifts are reported on the δ scale in parts-per-million (ppm) and are referenced to the residual non-deuterated and deuterated solvent resonances respectively. (CDCl<sub>3</sub> - <sup>1</sup>H: δ = 7.26 ppm; <sup>13</sup>C: δ = 77.2 ppm or (CD<sub>3</sub>)<sub>2</sub>SO - <sup>1</sup>H: δ = 2.50 ppm; <sup>13</sup>C: δ = 39.5 ppm).

*High-Resolution Mass Spectrometry.* HRMS spectra were recorded by the MS Analytical Facility Service at the University of Birmingham on Waters Xevo G2-XS QToF Quadrupole Time-of-Flight mass spectrometer.

*Infrared Spectroscopy.* Infrared (IR) spectroscopy was completed on an Agilent Technologies Cary 630 FTIR spectrometer.

*High-Performance Liquid Chromatography.* High-performance liquid chromatography (HPLC) analysis of oligonucleotides was performed on a modular Shimadzu instrument with the following modules: CBM-20A system controller, LC-20AD solvent deliver module, SIL-20AC HT autosampler, CTO-20AC column oven, SPD-M20A photodiode array UV-Vis detector, RF-20A spectrofluorometric detector and a FRC-10 fraction collector. Chromatography was performed on a Waters XBridge™ OST C18 2.5  $\mu\text{M}$  column heated to 60 °C. Flow rate was set at 0.8 mL/min and a linear gradient of buffers A and B: buffer A, 0.1 M TEAA, in a 95:5 mixture of H<sub>2</sub>O and acetonitrile; buffer B, 0.1 M TEAA, 30:70 mixture of H<sub>2</sub>O and acetonitrile.

*Liquid Chromatography-Mass Spectrometry.* LCMS analysis was performed on a Waters ACQUITY UPLC system coupled to a Xevo GS2-XS qToF mass spectrometer in negative ion mode. The oligonucleotides were eluted through an AQUITY UPLC oligonucleotide BEH C18 column (130Å, 1.7  $\mu\text{m}$ , 2.1 x 50 mm) using a 75 mM TEAA, pH 7.0) solution in H<sub>2</sub>O (buffer A) and a 75 mM TEAA solution in MeCN (buffer B) at 60 °C and a 0.2 mL/min flow. The data was processed using Promass HR software.

*Size Exclusion Chromatography.* Size exclusion chromatography (SEC) in DMF was performed on an Agilent 1260 Infinity II LC system equipped with a Wyatt DAWN HELEOS II multi-angle laser light scattering (MALLS) detector, a Wyatt Optilab T-rEX differential refractive index detector, an Agilent 1260 Infinity II WR diode array detector, an Agilent guard column (PLGel 5  $\mu\text{M}$ , 50 x 7.5 mm) and two Agilent Mixed-C columns (PLGel 5  $\mu\text{M}$ , 300 x 7.5 mm). The mobile phase was DMF (HPLC grade) containing 5 mM NH<sub>4</sub>BF<sub>4</sub> at 50 °C at flow rate of 1.0 mL min<sup>-1</sup>. Number average molar mass ( $M_n$ ), mass average molar mass ( $M_w$ ) and dispersities ( $D_M =$

$M_w/M_n$ ) were determined using Wyatt ASTRA v7.1.3 software against poly(methyl methacrylate) (PMMA) standards.

*Gas chromatography-mass spectrometry.* Gas chromatography-mass spectrometry (GCMS) was performed Shimadzu GCMS QP2010 SE system with an Agilent CP-Chirasil Dex CB column (25 m, 0.25mm, 0.25  $\mu$ m). MS detection was used selective ion scanning  $m/z$  1.5-1000 amu.

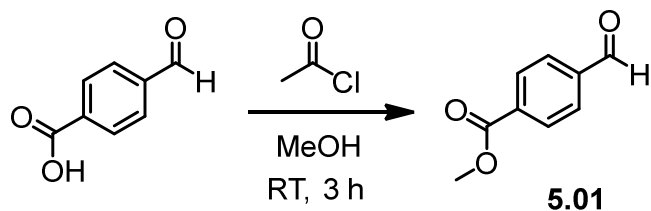
*Gel Electrophoresis.* Native polyacrylamide gels were run at 2 °C in 1 x TAE buffer at 180V – 200V using a vertical nucleic acid electrophoresis cell connected to a PowerPack basic power supply (BioRad). Samples were combined with 20% loading buffer (0.05% bromophenol blue, 25% glycerol, 1 x TAE) prior to running. Non-fluorescent DNA was stained using a 1:1000 aqueous SYBR® Gold nucleic acid gel stain (ThermoFisher) and visualized using a BioRad ChemiDoc™ MP Imaging system. The images were processed using ImageLab software. Denaturing polyacrylamide gels (15% acrylamide, 7M Urea, 25% formamide) were run at room temperature in 1 x TBE buffer at 14 amps using a vertical nucleic acid electrophoresis cell connected to a PowerPack basic power supply (BioRad). The samples were diluted with 1:1 v/v formamide solution (90 % formamide) and heated at 70 °C for 10 min prior to running. Non-fluorescent DNA was stained using a 1:1000 aqueous SYBR® Gold nucleic acid gel stain (ThermoFisher) and visualized using a BioRad ChemiDoc™ MP Imaging system. The images were processed using BioRad ImageLab software.

*Fluorescence Spectroscopy.* Fluorescence annealing studies were conducted on an Agilent Cary Eclipse Fluorescence spectrophotometer equipped with Photomultiplier tube (PMT) detector. Quartz cuvettes from with four polished sides were used for fluorescence. The



emission and excitation spectra were recorded using Cary Eclipse v.1.2.0.0 software. The sample were heated at 2 °C min.

### 5.5.3 Synthesis of 5.01



4-Formyl benzoic acid (3 g, 20 mmol) was solubilised in methanol (45 mL) and cooled over ice. Acetyl chloride (100 mmol) was added dropwise, and the solution was warmed to room temperature and allowed to stir for 3 h. The product was concentrated by rotary evaporation and then washed with 1M HCl solution, H<sub>2</sub>O and brine and dried over MgSO<sub>4</sub> prior to concentration *in vacuo*. Any acetal by-product was hydrolysed by stirring with a 1:1 vol. ratio of THF : 1M HCl solution for 30 minutes and then extracted twice with CH<sub>2</sub>Cl<sub>2</sub>. The organic layer was washed with brine and dried over MgSO<sub>4</sub>. The solvent was removed *in vacuo* to yield the desired product, 2.9 g, 88%. <sup>1</sup>H NMR (400 MHz; 298K; CDCl<sub>3</sub>) δ 10.10 (s, 1H, CHO), 8.20 (d, 2H, *J*<sub>H-H</sub> = 8.3 Hz, CH), 7.96 (d, 2H, *J*<sub>H-H</sub> = 8.3 Hz, CH), 3.96 (s, 3H, CH<sub>3</sub>).

Characterization matches that reported in the literature.<sup>26</sup>

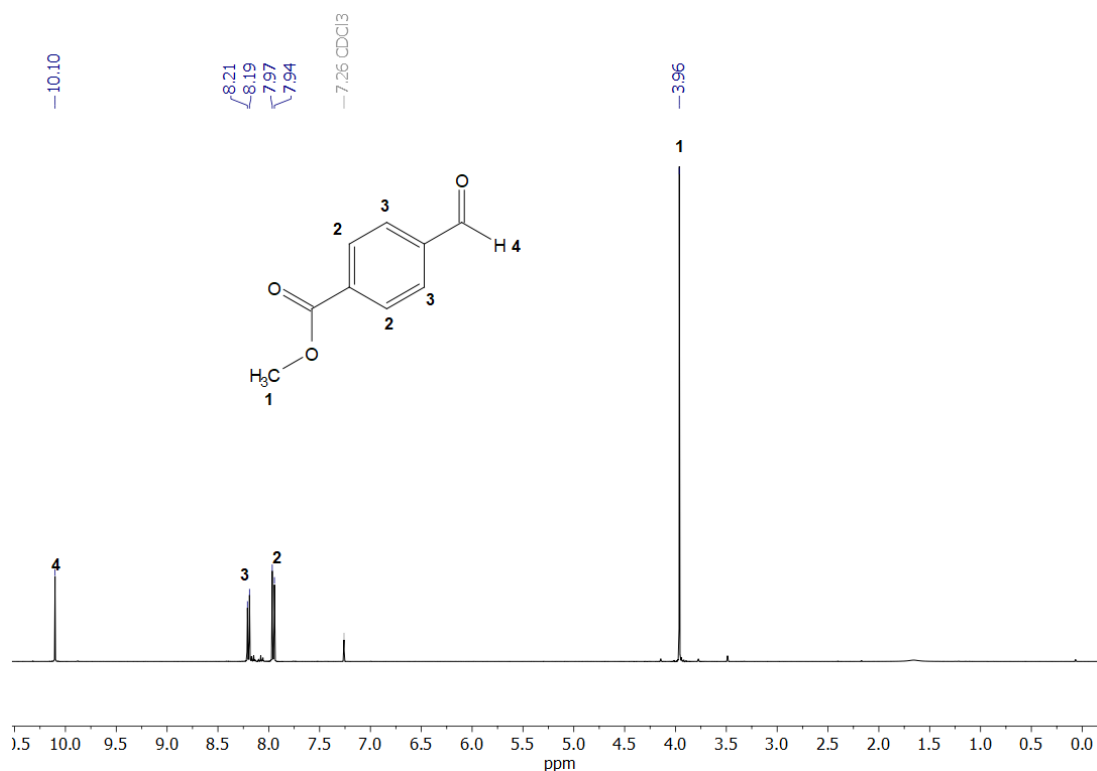
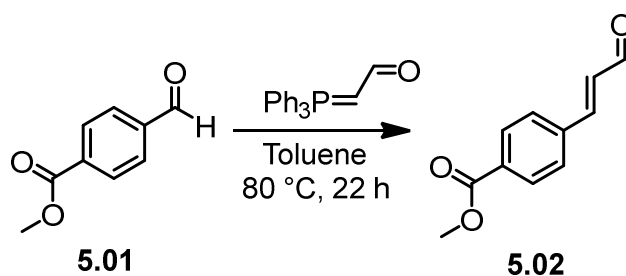


**Figure 5.18** <sup>1</sup>H NMR spectrum of **5.01** in CDCl<sub>3</sub> (400 MHz, 298K).

#### 5.5.4 Synthesis of 5.02



**5.01** (2 g, 12.2 mmol) and triphenylphosphoacrylydene (3.70 g, 12.2 mmol) was solubilised in 60 mL toluene and the solution was refluxed at 80 °C for 22 h. The solution was washed with H<sub>2</sub>O and extracted twice with ethyl acetate. The organic layers were combined and washed with sat. NaHCO<sub>3</sub> (aq.) followed by brine prior to drying over MgSO<sub>4</sub> and concentrated *in vacuo*. The crude product was purified by column chromatography 40:60 (vol%) EtOAc:Hexane and then recrystallized in hexane : EtOAc to yield an off-white solid, 286 mg, 12%. <sup>1</sup>H NMR

(400 MHz; 298K; CDCl<sub>3</sub>) δ 9.75 (d, <sup>3</sup>J<sub>H-H</sub> = 7.6 Hz, 1H, CHO), 8.10 (d, J<sub>H-H</sub> = 8.0 Hz, 2H, CH), 7.64 (d, J<sub>H-H</sub> = 8.3 Hz, 2H, CH), 7.51 (d, <sup>3</sup>J<sub>H-H</sub> = 16.0 Hz, 1H, CH), 6.78 (dd, <sup>3</sup>J<sub>H-H</sub> = 16.0, 8.0 Hz, 1H, CH), 3.95 (s, 3H, CH<sub>3</sub>).

Characterization matches that reported in the literature.<sup>26</sup>

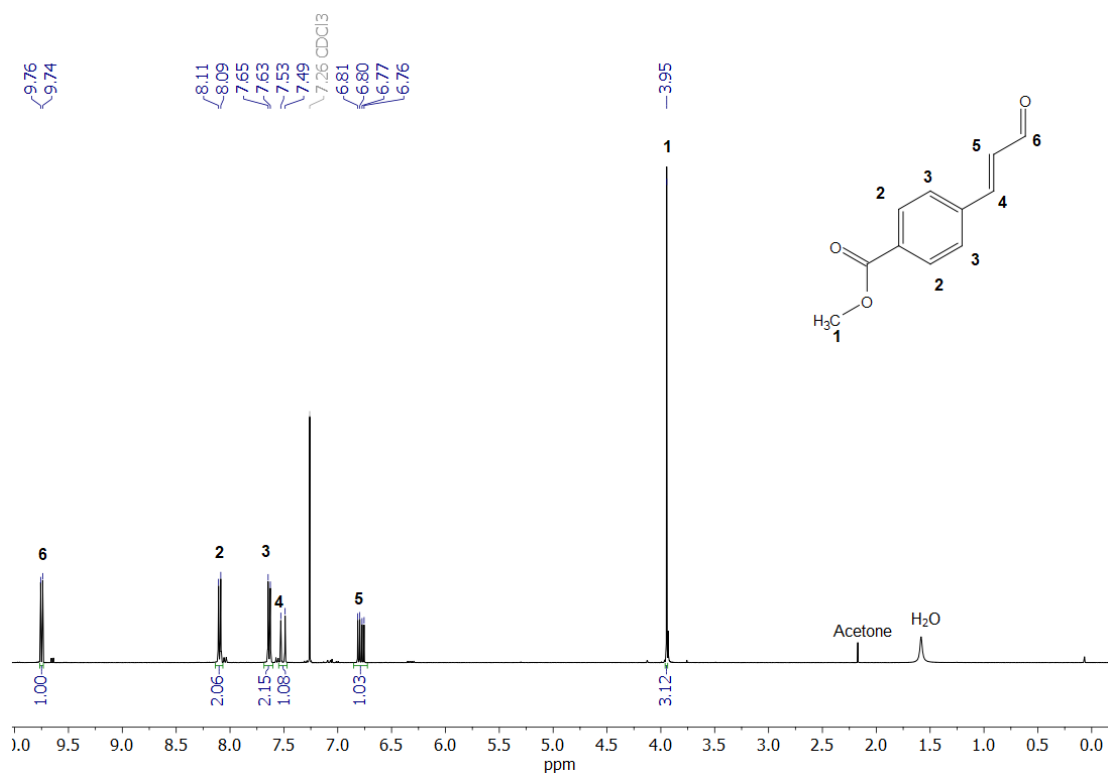
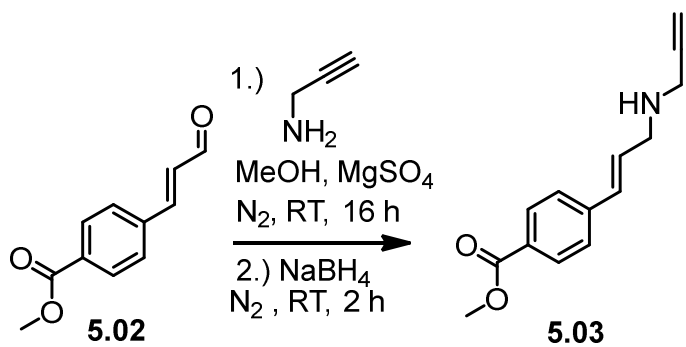


**Figure 5.19** <sup>1</sup>H NMR spectrum of **5.02** in CDCl<sub>3</sub> (400 MHz, 298K).

### 5.5.5 Synthesis of 5.03



**5.02** (250 mg, 1.3 mmol) and propargylamine (84  $\mu$ L, 1.3 mmol) were solubilised in methanol and anhydrous  $\text{MgSO}_4$  was added. The solution was allowed to stir overnight at room temperature under nitrogen.  $\text{NaBH}_4$  (0.059 g, 1.56 mmol) was then added and the solution was stirred at room temperature for a further 2 h prior to quenching with  $\text{H}_2\text{O}$ . The solution was extracted with ethyl acetate and then concentrated *in vacuo* to yield a yellow solid, 262 mg, 88%.  $^1\text{H}$  NMR (400 MHz; 298K;  $\text{CDCl}_3$ )  $\delta$  = 7.97 (d,  $J_{\text{H-H}}$  = 8.4 Hz, 2H, CH), 7.42 (d,  $J_{\text{H-H}}$  8.4 Hz, 2H, CH) 6.61 (d,  $^3J_{\text{H-H}}$  = 16.0, 1H, CH), 6.39 (dt,  $^3J_{\text{H-H}}$  = 16.0, 6.3 Hz, 1H, CH), 3.90 (s, 3H,  $\text{CH}_3$ ), 3.54 (dd,  $^3J_{\text{H-H}}$  = 6.3,  $^4J_{\text{H-H}}$  = 1.5 Hz, 2H,  $\text{CH}_2$ ), 3.48 (d,  $^4J_{\text{H-H}}$  = 2.4 Hz, 2H,  $\text{CH}_2$ ), 2.26 (t,  $^4J_{\text{H-H}}$  = 2.4 Hz, 1H, CH).  $^{13}\text{C}$  NMR (100 MHz,  $\text{CDCl}_3$ )  $\delta$  167.0, 141.6, 131.2, 130.4, 130.1, 129.0, 126.3 (Arom-C and CH), 71.95 (CCH), 52.21 ( $\text{CH}_3$ ), 50.24, 37.52 ( $\text{CH}_2$ ). IR ( $\nu_{\text{max}}$  /  $\text{cm}^{-1}$ ) 3300, 2088 ( $\text{C}\equiv\text{CH}$ ), 1694 ( $\text{C}=\text{O}$ ). HR-MS (+)  $m/z$  calcd.  $[\text{M} + \text{H}]^+$  calculated 230.1181 found 230.1184.

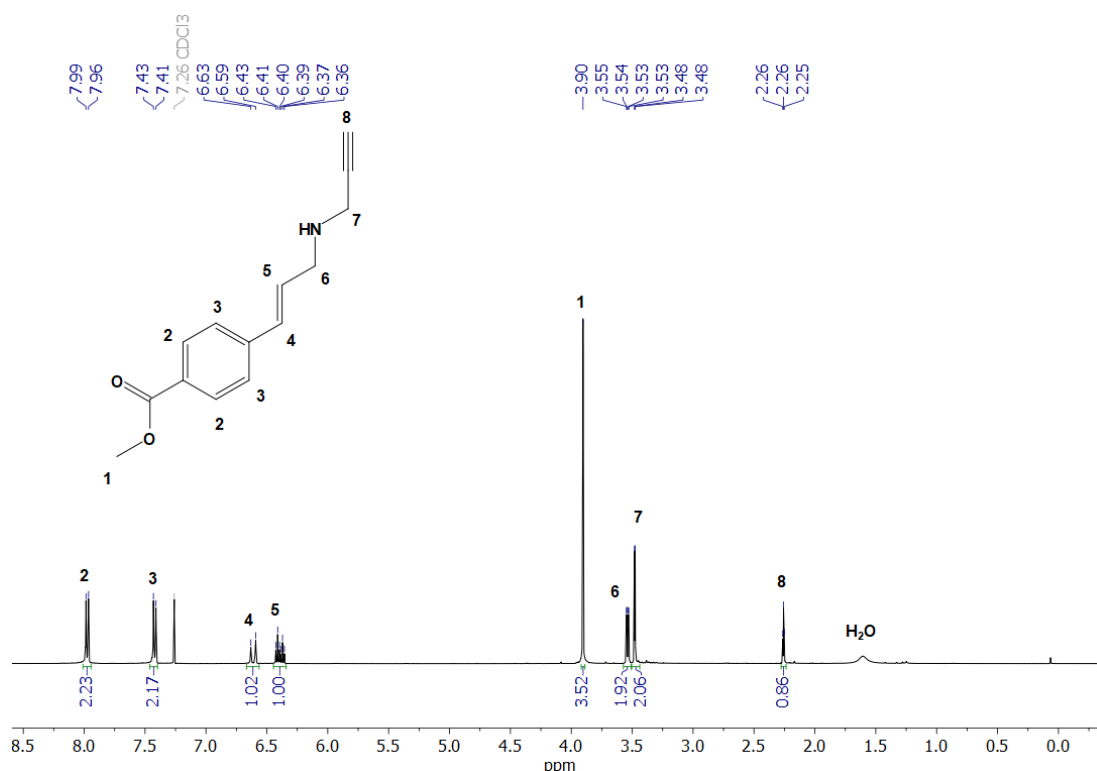


**Figure 5.20**  $^1\text{H}$  NMR spectrum of **5.03** in  $\text{CDCl}_3$  (400 MHz, 298K).

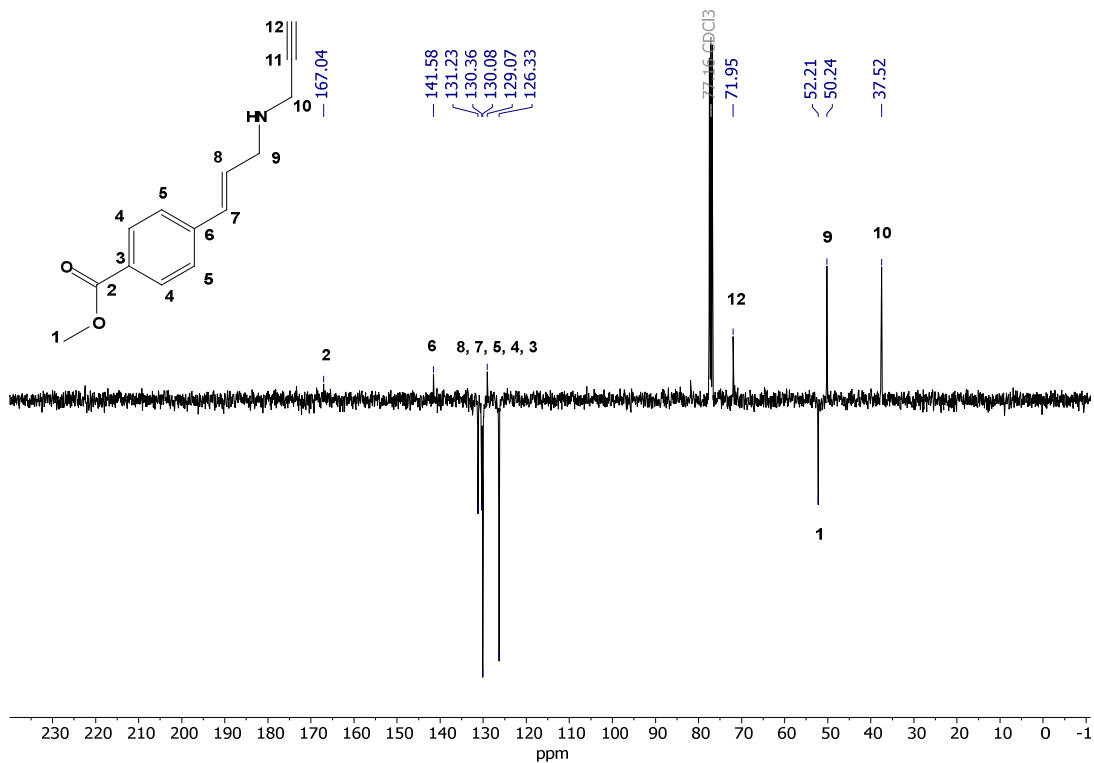
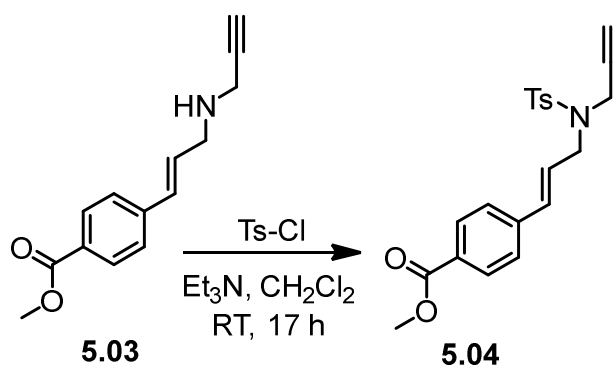


**Figure 5.21**  $^{13}\text{C}$  NMR spectrum of **5.03** in  $\text{CDCl}_3$  (100 MHz, 298K). Note - weak internal alkyne not detected.

### 5.5.6 Synthesis of 5.04



**5.03** (121.5 mg, 0.53 mmol), Tosyl-Cl (121 mg, 0.64 mmol) and triethylamine (148  $\mu\text{L}$ , 1.06 mmol) was combined in a round-bottomed-flask and solubilised in  $\text{CH}_2\text{Cl}_2$  (15 mL). The solution was allowed to stir overnight at room temperature prior to washing with Sat.  $\text{NaHCO}_3$

(aq.) followed by brine. The organic layer was dried over  $\text{MgSO}_4$  prior to concentration *in vacuo* to yield the crude product which was purified by silica column chromatography with hexane : ethyl acetate (7:3 v/v). An off-white solid was yielded, 124 mg, 61%.  $^1\text{H}$  NMR (400 MHz; 298K;  $\text{CDCl}_3$ )  $\delta$  7.98 (d,  $J_{\text{H-H}} = 8.4$  Hz, 2H, CH), 7.76 (d,  $J_{\text{H-H}} = 8.2$  Hz, 2H, CH), 7.39 (d,  $J_{\text{H-H}} = 8.4$  Hz, 2H, CH), 7.31 (d,  $J_{\text{H-H}} = 8.2$  Hz, 2H, CH), 6.61 (d,  $^3J_{\text{H-H}} = 15.9$  Hz, 1H, CH), 6.21 (dt,  $^3J_{\text{H-H}} = 15.9$ , 6.7 Hz, 1H, CH), 4.14 (d,  $^4J_{\text{H-H}} = 2.5$  Hz, 2H,  $\text{CH}_2$ ), 4.01 (d,  $^3J_{\text{H-H}} = 6.7$  Hz, 2H,  $\text{CH}_2$ ), 3.91 (s, 3H,  $\text{CH}_3$ ), 2.44 (m, 3H,  $\text{CH}_3$ ), 2.06 (t,  $^4J_{\text{H-H}} = 2.5$  Hz, 1H).  $^{13}\text{C}$  NMR (100 MHz; 298K;  $\text{CDCl}_3$ )  $\delta$  140.6, 133.8, 130.1, 129.7, 129.6, 127.9, 126.6, 126.0 (Arom-C and CH), 74.1 (CCH), 52.3 ( $\text{CH}_3$ ), 48.6, 36.3 ( $\text{CH}_2$ ), 21.7 ( $\text{CH}_3$ ). IR ( $\nu_{\text{max}} / \text{cm}^{-1}$ ) 3296 ( $\text{C}\equiv\text{CH}$ ), 1710 ( $\text{C}=\text{O}$ ). HR-MS (+)  $m/z$  calculated  $[\text{M} + \text{NH}_4]^+$  401.1535 found 401.1544.

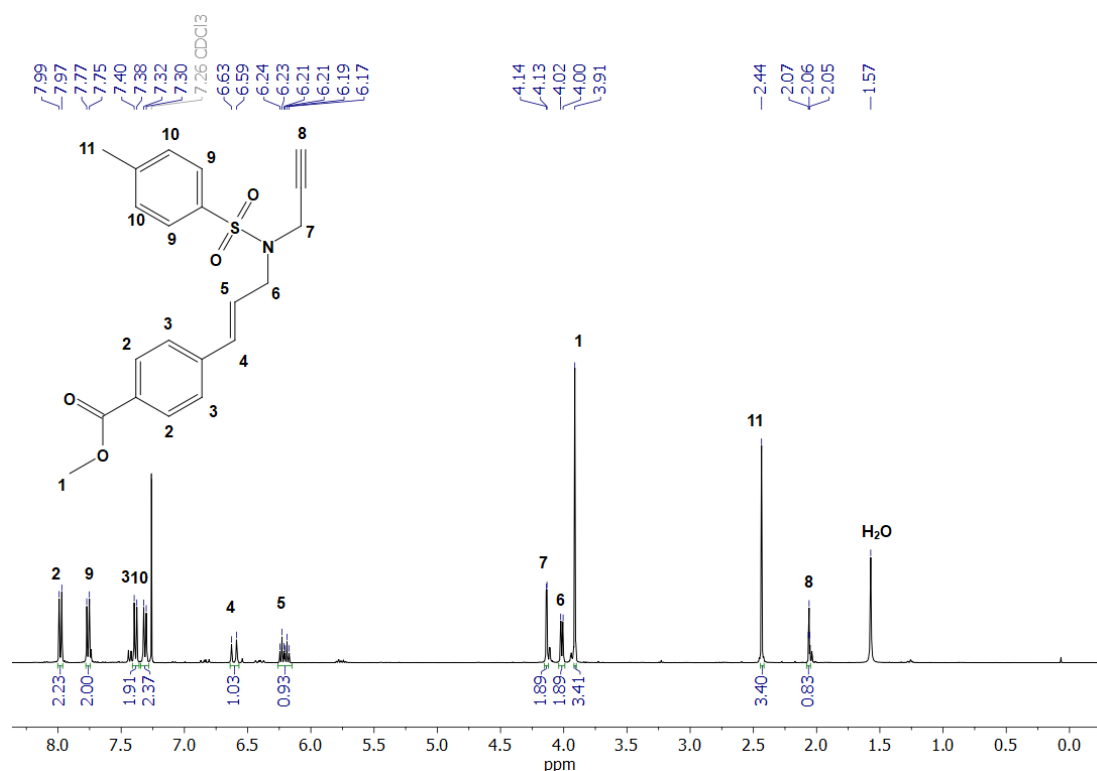


**Figure 5.22**  $^1\text{H}$  NMR spectrum of **5.04** in  $\text{CDCl}_3$  (400 MHz, 298K).

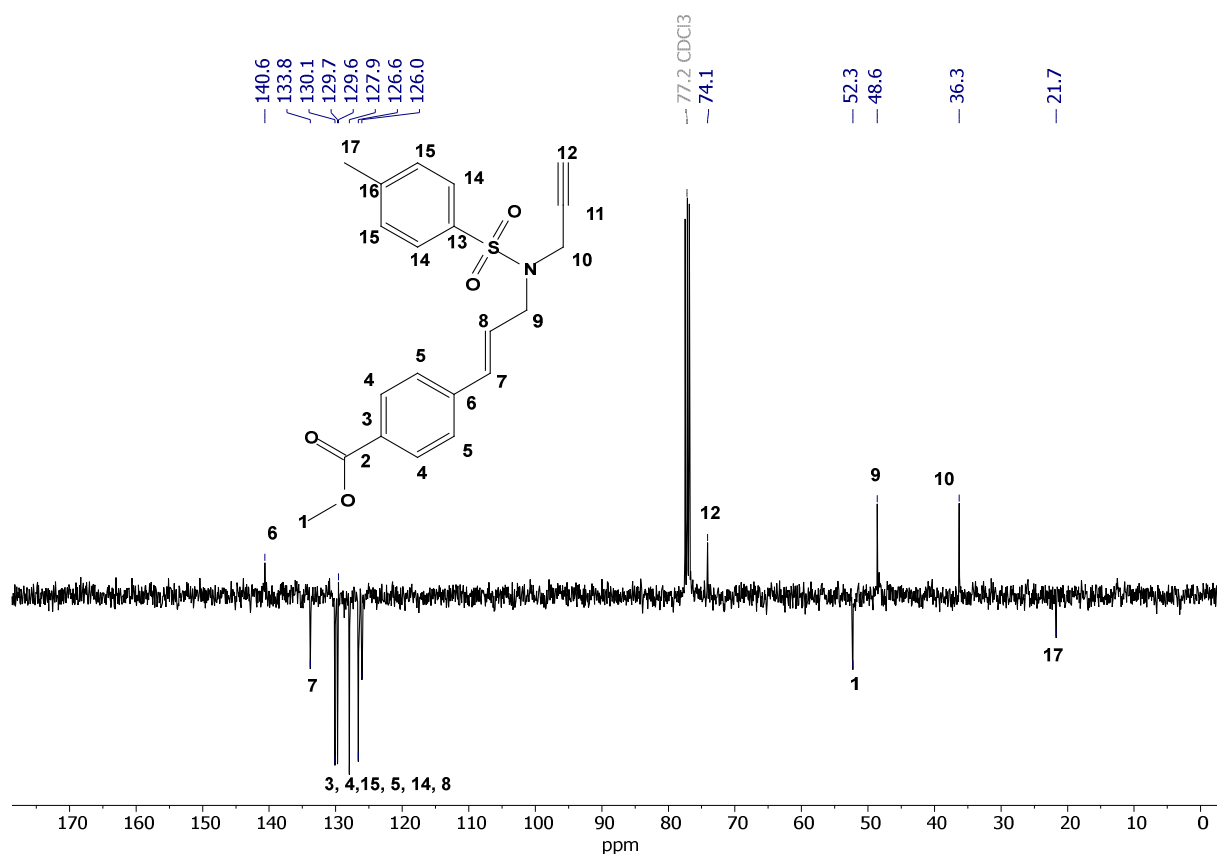
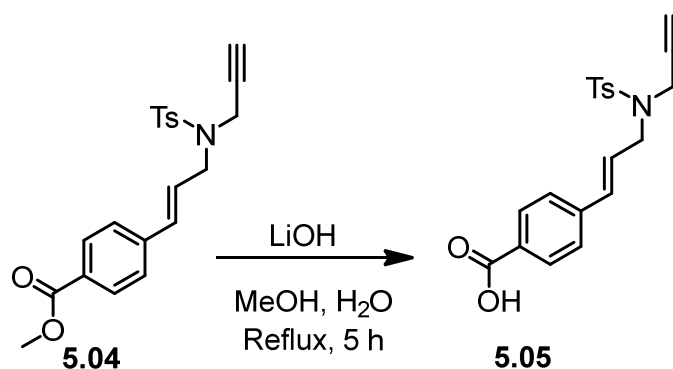


**Figure 5.23**  $^{13}\text{C}$  NMR spectrum of **5.04** in  $\text{CDCl}_3$  (100 MHz, 298K). Note - weak internal alkyne not detected.

### 5.5.7 Synthesis of 5.05



**5.04** (100 mg, 0.26 mmol) was solubilised in MeOH/ $\text{H}_2\text{O}$  (16 mL, 10:6 v/v). The solution was cooled over ice and LiOH (25 mg, 1.04 mmol) was added. The solution was heated to reflux and stirred for 5 h prior to cooling to room temperature. 1M HCl was added until the pH = ca. 2 and a white precipitate formed which was collected by filtration to yield an off-white solid,

43 mg, 45%.  $^1\text{H}$  NMR (400 MHz; 298K;  $(\text{CD}_3)_2\text{SO}$ )  $\delta$  12.93 (s, 1H, COOH), 7.88 (d,  $J_{\text{H-H}} = 8.4$  Hz, 2H, CH), 7.75 (d,  $J_{\text{H-H}} = 8.2$  Hz, 2H, CH), 7.51 (d,  $J_{\text{H-H}} = 8.4$  Hz, 2H, CH), 7.41 (d,  $J_{\text{H-H}} = 8.2$  Hz, 2H, CH), 6.64 (d,  $^3J_{\text{H-H}} = 15.9$  Hz, 1H, CH), 6.30 (dt,  $^3J_{\text{H-H}} = 15.9$ , 6.3 Hz, 1H, CH), 4.09 (d,  $^4J_{\text{H-H}} = 2.4$  Hz, 2H), 3.96 (d,  $^3J_{\text{H-H}} = 6.3$  Hz, 2H), 3.14 (t,  $^4J_{\text{H-H}} = 2.4$  Hz, 1H, CH), 2.39 (s, 3H,  $\text{CH}_3$ ).  $^{13}\text{C}$  (100 MHz; 298K;  $(\text{CD}_3)_2\text{SO}$ ) 167.0 (COOH) 143.6, 140.3, 135.6, 132.4, 129.8, 129.7, 129.7, 127.5, 126.5, 126.5 (Arom-C and CH), 76.5 (CCH), 48.6, 36.4 ( $\text{CH}_2$ ), 21.0 ( $\text{CH}_3$ ). IR ( $\nu_{\text{max}} / \text{cm}^{-1}$ ) 3290 ( $\text{C}\equiv\text{CH}$ ), 2900, 1671 (COOH). HR-MS (+)  $m/z$  calculated  $[\text{M} + \text{H}]^+$  370.1113 found 370.1104.

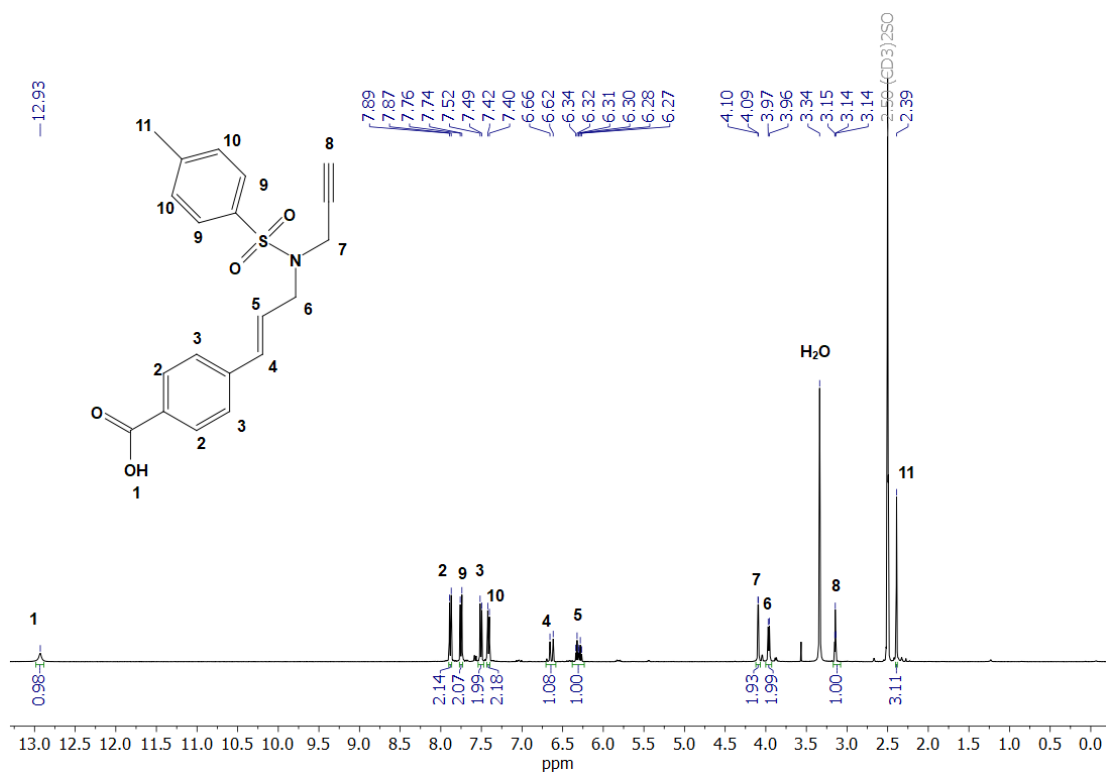
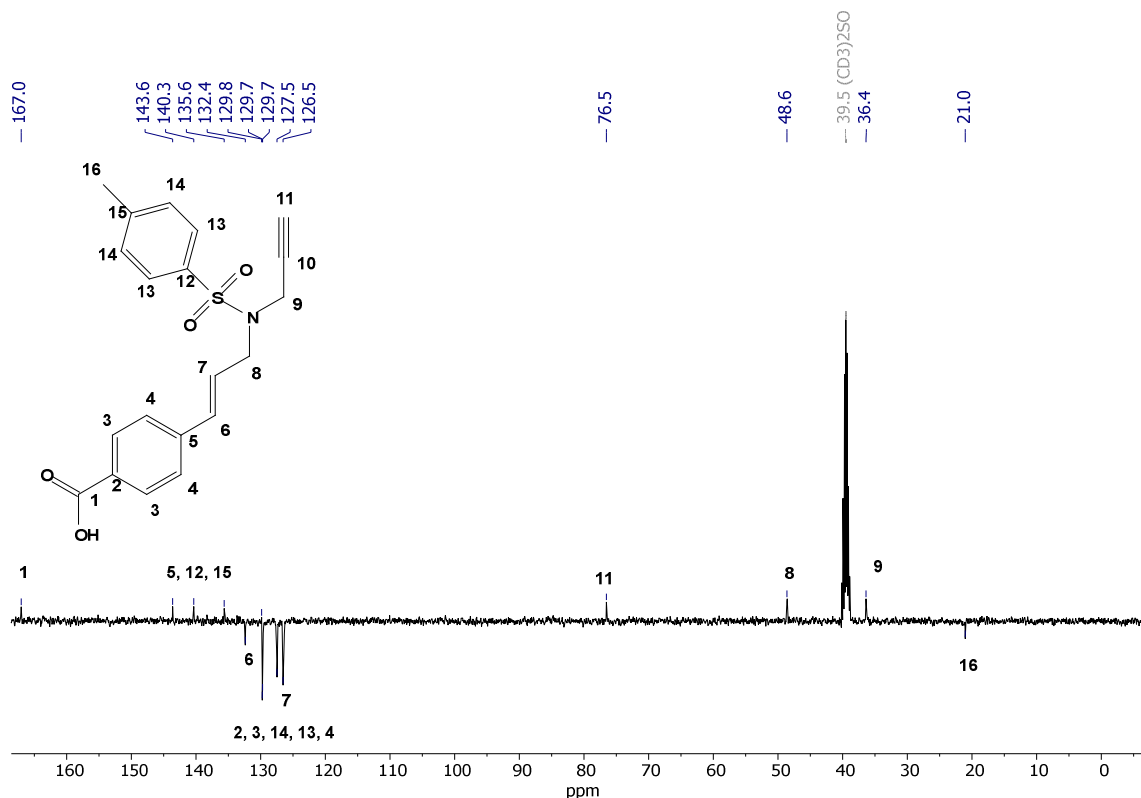


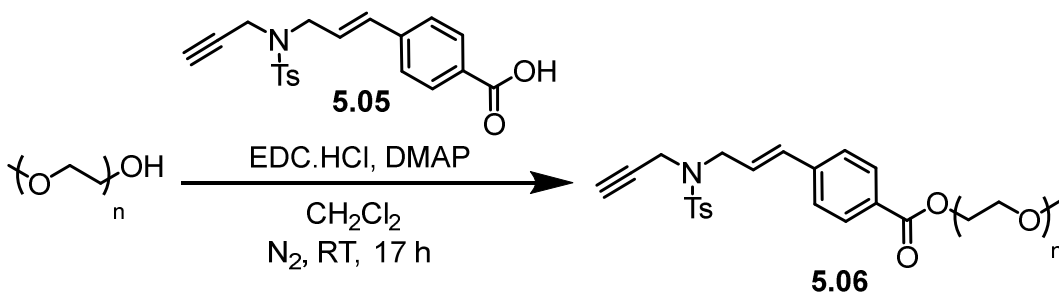
Figure 5.24  $^1\text{H}$  NMR spectrum of 5.05 in  $(\text{CD}_3)_2\text{SO}$  (400 MHz, 298 K).





**Figure 5.25**  $^{13}\text{C}$  NMR spectrum of **5.05** in  $(\text{CD}_3)_2\text{SO}$  (100 MHz, 298 K). Note - weak internal alkyne not detected.

### 5.5.8 Synthesis of 5.06



EDC.HCl (5.7 mg, 0.03 mmol), DMAP (1.7 mg, 0.014 mmol) and **5.05** (10 mg, 0.027 mmol) were added to a round-bottomed-flask and solubilised in 1 mL  $\text{CH}_2\text{Cl}_2$ . Methoxy PEG (MW = 2000) (64 mg, 0.032 mmol) was added and the solution was allowed to stir under  $\text{N}_2$  for 18 h. The reaction mixture was diluted with  $\text{CH}_2\text{Cl}_2$  and then washed twice with 1M HCl followed by brine. The organic layer was dried over  $\text{MgSO}_4$  and then concentrated in vacuo. The crude

polymer was precipitated from  $\text{CH}_2\text{Cl}_2$  in cold diethyl ether to yield a white solid (31 mg, 43%).  
 $^1\text{H}$  NMR (300 MHz; 298K;  $\text{CDCl}_3$ )  $\delta$  = 7.99 (d,  $J_{\text{H-H}}$  = 8.4 Hz, 2H, CH), 7.75 (d,  $J_{\text{H-H}}$  = 8.2 Hz, 2H, CH), 7.38 (d,  $J_{\text{H-H}}$  = 8.4 Hz, 2H, CH), 7.31 (d,  $J_{\text{H-H}}$  = 8.2 Hz, 2H, CH), 6.60 (d,  $^3J_{\text{H-H}}$  = 16.0 Hz, 1H, CH), 6.29 – 6.07 (m, 1H, CH), 4.46 (dd,  $^3J_{\text{H-H}}$  = 5.9, 3.8 Hz, 2H,  $\text{CH}_2$ ), 4.13 (d,  $^4J_{\text{H-H}}$  = 2.4 Hz, 2H,  $\text{CH}_2$ ), 4.01 (d,  $^3J_{\text{H-H}}$  = 6.6 Hz, 2H,  $\text{CH}_2$ ), 3.63 (s, 291H,  $\text{CH}_2$ ), 3.37 (s, 3H,  $\text{CH}_3$ ), 2.43 (s, 3H,  $\text{CH}_3$ ), 1.43 (s, 1H, CH). Product also contains unfunctionalized methoxy PEG.

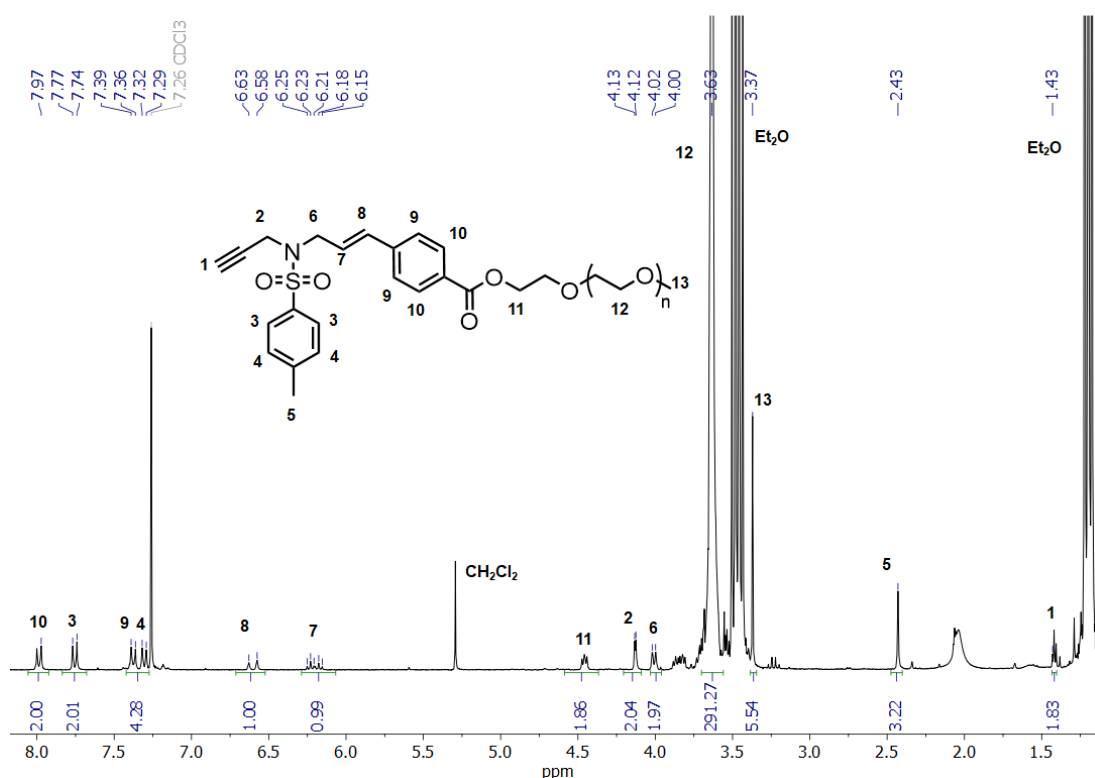


**Figure 5.26**  $^1\text{H}$  NMR spectrum of **5.06** in  $\text{CDCl}_3$  (300 MHz, 298K).

### 5.5.9 Synthesis of **5i**

EDC.HCl in DMF (300 mM, 67  $\mu\text{L}$ ), HOBT hydrate in DMF (300 mM, 67  $\mu\text{L}$ ) and **5.05** in DMF (300 mM, 67  $\mu\text{L}$ ) was mixed with 100  $\mu\text{L}$  DPBS. The solution was added to  $\text{SO-NH}_2$  (100  $\mu\text{L}$ , 200  $\mu\text{M}$ ) and DIPEA (3.6  $\mu\text{L}$ ) and mixed in a thermomixer at 25  $^\circ\text{C}$  for 2 h. 600  $\mu\text{L}$   $\text{H}_2\text{O}$  was added and the solution was centrifuged, the supernatant was taken and washed three times through an

amicon 3 kDa spin filter with 18 MΩ.cm H<sub>2</sub>O prior to LCMS analysis. LCMS (ESI-) m/z calculated 5716.1, found 5716.2.

#### 5.5.10 Synthesis of 5viii

EDC.HCl in DMF (300 mM, 100 μL), HOBt hydrate in DMF (300 mM, 100 μL) and 3-butenic acid in DMF (300 mM, 100 μL) was mixed with 150 μl DPBS. 300 μL of this solution was added to CO-NH<sub>2</sub> (100 μl, 200 μM) and DIPEA (3.6 μL) and mixed in a thermomixer at 25 °C for 18 h. 600 μL H<sub>2</sub>O was added and the solution was centrifuged, the supernatant was taken and washed three times through an amicon 3 kDa spin filter with 18 MΩ.cm H<sub>2</sub>O prior to LCMS analysis. **5viii** was isolated from unreacted CO-NH<sub>2</sub> by HPLC purification. LCMS (ESI-) m/z calculated 6993.2, found 6993.3.

### 5.5.11 Cross-metathesis small-molecule study

Allyl alcohol, AM, MgCl<sub>2</sub> and succinimide were dissolved in PB2 and stirred at room temperature for 2 h. Following the reaction, 9.5 mL acetone was added, and the samples were dried over MgSO<sub>4</sub>. The resulting solutions were filtered prior to analysis by GCMS.

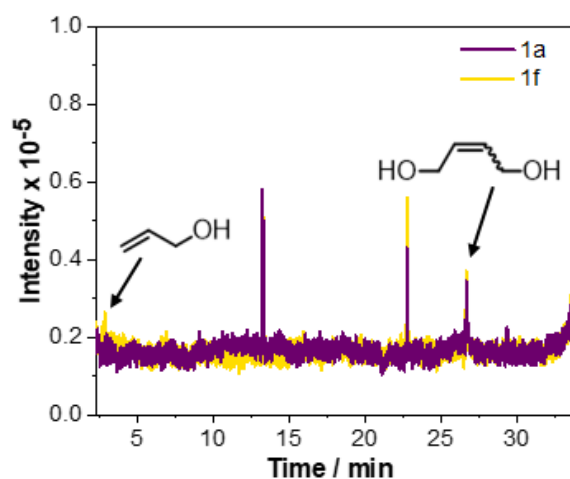


**Figure 5.27** GCMS chromatogram of reaction mixtures **1a** and **1f** (Figure 5.7) at 10 mol% catalyst loading. Samples were analysed at ca. 0.5 mg mL<sup>-1</sup> in acetone. Allyl alcohol elutes at ca. 2.5 min and but-2-ene-diol elutes ca. 27 min. Note that the peak at 13 min. is due to the self-aldol condensation reaction of the eluent acetone.

### 5.5.12 General protocols for the off-templated Cross-metathesis of **5i**

#### 5.5.12.1 Aquamet in PB2

To 1 equivalent of **5i** was added AM and the alkene in PB2 to a final DNA concentration of approximately 1 mM. The solution was mixed at room temperature for 1 h and then neutralized with sat. NaHCO<sub>3</sub>. The small molecules were removed by passing through a Micro Bio-spin™ 6 column equilibrated with 18 MΩ.cm H<sub>2</sub>O prior to LCMS analysis.

#### 5.5.12.2 Ru-Cat in tBuOH/H<sub>2</sub>O

The protocol was adjusted from a previously reported protocol by Donahue *et al.*<sup>12</sup>

To 1 equivalent of **5i** was added 1 equivalent of the complement DNA strand (C0) and 4000 equivalents of MgCl<sub>2</sub> in 18 MΩ.cm H<sub>2</sub>O. The solution was mixed in a thermomixer at room temperature for 5 min prior to the addition of the Ru-cat and alkene (150 equivalents) in tBuOH. The volume was adjusted to a final DNA concentration of 90 μM in 2:3 (v/v) tBuOH : H<sub>2</sub>O. The solution was mixed at room temperature for a further 1 h and then diluted with 1 mL H<sub>2</sub>O and centrifuged. The resulting supernatant was collected and washed three times through an amicon 3 kDa spin filter with 18 MΩ.cm H<sub>2</sub>O prior to LCMS analysis. **5iii** m/z calculated 5525.1, found 5525.2. **5iv** m/z calculated 5495.0, found 5495.2.

#### 5.5.12.3 Ru-Cat in MeOAc/EtOH/H<sub>2</sub>O

The protocol was adjusted from a previously reported protocol by Monty *et al.*<sup>19</sup>

To 1 equivalent of **5i** was added 1 equivalent of the complement DNA strand (C0), 20000 equivalents of MgCl<sub>2</sub> and 14000 equivalents of NH<sub>4</sub>Cl in 18 MΩ.cm H<sub>2</sub>O. The solution was mixed in a thermomixer at room temperature for 5 min prior to the addition of 2,2-biphenyldiamine (20 equivalents) and alkene (150 equivalents) in EtOH. The Ru-Cat (10 equivalents) in MeOAc was added and the volume adjusted to a final DNA concentration of 40 μM in 5:4:1 (v/v/v) H<sub>2</sub>O : EtOH : MeOAc. The solution was mixed at room temperature for a further 1 h and then diluted with 1 mL H<sub>2</sub>O and centrifuged. The resulting supernatant was collected and washed three times through an amicon 3 kDa spin filter with 18 MΩ.cm H<sub>2</sub>O prior to LCMS analysis. LC-MS (ESI-) **5iii** m/z calculated 5525.1, found 5525.1. **5iv** m/z calculated 5495.0, found 5495.1.

### 5.5.13 General protocol for the templated cross-metathesis

To 1 equivalent of **5i** was added 20000 equivalents of  $\text{MgCl}_2$  and 14000 equivalents of  $\text{NH}_4\text{Cl}$  in 18 M $\Omega$ .cm  $\text{H}_2\text{O}$ . 2,2-biphenyldiamine (20 equivalents) in EtOH was added followed by **G3** (10 equivalents) in MeOAc. **5viii** (1 equivalent) was added to achieve a final DNA concentration of 500 nM in 5:4:1 (v/v/v)  $\text{H}_2\text{O}$  : EtOH : MeOAc. The solution was mixed at room temperature for 1 h prior to analysis by 15% denaturing PAGE.

## 5.6 References

1. S. T. Diver and A. J. Giessert, *Chem. Rev.*, 2004, **104**, 1317-1382.
2. H. Park and T.-L. Choi, *J. Am. Chem. Soc.*, 2012, **134**, 7270-7273.
3. H. Park, H.-K. Lee and T.-L. Choi, *J. Am. Chem. Soc.*, 2013, **135**, 10769-10775.
4. T. Zhang, L. Fu and W. R. Gutekunst, *Macromolecules*, 2018, **51**, 6497-6503.
5. S. Pal, F. Lucarini, A. Ruggi and A. F. M. Kilbinger, *J. Am. Chem. Soc.*, 2018, **140**, 3181-3185.
6. T. Zhang and W. R. Gutekunst, *Polym. Chem.*, 2020, **11**, 259-264.
7. A. E. Levi, L. Fu, J. Lequieu, J. D. Horne, J. Blankenship, S. Mukherjee, T. Zhang, G. H. Fredrickson, W. R. Gutekunst and C. M. Bates, *Macromolecules*, 2020, **53**, 702-710.
8. L. Fu, T. Zhang, G. Fu and W. R. Gutekunst, *J. Am. Chem. Soc.*, 2018, **140**, 12181-12188.
9. K. Skowerski, G. Szczepaniak, C. Wierzbicka, Ł. Gułajski, M. Bieniek and K. Grela, *Catal. Sci. Technol.*, 2012, **2**, 2424-2427.
10. S. Masuda, S. Tsuda and T. Yoshiya, *Org. Biomol. Chem.*, 2018, **16**, 9364-9367.
11. H. S. Bazzi and H. F. Sleiman, *Macromolecules*, 2002, **35**, 9617-9620.
12. X. J. Lu, L. J. Fan, C. B. Phelps, C. P. Davie and C. P. Donahue, *Bioconjugate Chem.*, 2017, **28**, 1625-1629.
13. J. C. Foster, S. Varlas, L. D. Blackman, L. A. Arkinstall and R. K. O'Reilly, *Angew. Chem. Int. Ed.*, 2018, **57**, 10672-10676.
14. C. Mayer, D. G. Gillingham, T. R. Ward and D. Hilvert, *Chem. Commun.*, 2011, **47**, 12068-12070.
15. D. M. Lynn, B. Mohr and R. H. Grubbs, *J. Am. Chem. Soc.*, 1998, **120**, 1627-1628.
16. J. C. Foster, M. C. Grocott, L. A. Arkinstall, S. Varlas, M. J. Redding, S. M. Grayson and R. K. O'Reilly, *J. Am. Chem. Soc.*, 2020, **142**, 13878-13885.
17. D. C. Church, L. Takiguchi and J. K. Pokorski, *Polym. Chem.*, 2020, **11**, 4492-4499.
18. A. K. Chatterjee, T.-L. Choi, D. P. Sanders and R. H. Grubbs, *J. Am. Chem. Soc.*, 2003, **125**, 11360-11370.
19. O. B. C. Monty, P. Nyshadham, K. M. Bohren, M. Palaniappan, M. M. Matzuk, D. W. Young and N. Simmons, *ACS Comb. Sci.*, 2020, **22**, 80-88.
20. Y. A. Lin, J. M. Chalker, N. Floyd, G. J. L. Bernardes and B. G. Davis, *J. Am. Chem. Soc.*, 2008, **130**, 9642-9643.
21. Y. A. Lin, J. M. Chalker and B. G. Davis, *J. Am. Chem. Soc.*, 2010, **132**, 16805-16811.
22. Y. Y. A. Lin, O. Boutureira, L. Lercher, B. Bhushan, R. S. Paton and B. G. Davis, *J. Am. Chem. Soc.*, 2013, **135**, 12156-12159.
23. T. P. Montgomery, A. M. Johns and R. H. Grubbs, *Catalysts*, 2017, **7**, 87.
24. D. D. Albergo and D. H. Turner, *Biochemistry*, 1981, **20**, 1413-1418.

25. C. S. Higman, D. L. Nascimento, B. J. Ireland, S. Audörsch, G. A. Bailey, R. McDonald and D. E. Fogg, *J. Am. Chem. Soc.*, 2018, **140**, 1604-1607.
26. H. Huang, C. Yu, X. Li, Y. Zhang, Y. Zhang, X. Chen, P. S. Mariano, H. Xie and W. Wang, *Angew. Chem. Int. Ed.*, 2017, **56**, 8201-8205.



# Conclusions and Future work

This work set out to explore the potential of metathesis in DNA nanotechnology with an aim of expanding the chemical toolkit available for DNA transformations. This study demonstrates that the development of chemistries compatible with DNA is not a trivial problem and is particularly challenging due to the propensity of the multitude of functional groups on DNA to interact unproductively with small molecules.

The Ru-metathesis catalysts were shown to interact strongly with oligonucleotides and this was hypothesized to be due to an electrostatic interaction further strengthened by the interaction with PEG groups in the water-soluble derivative. This interaction was believed to facilitate the degradation of DNA; although, the mechanism of degradation was poorly understood and will certainly be a research priority in the future if metathesis is to be routinely used in DNA nanotechnology. Despite this setback, the addition of additives to disrupt the DNA-Ru interaction, namely  $\text{MgCl}_2$  and succinimide, were identified to minimize DNA degradation. Building upon this groundwork, the application of metathesis in two areas of DNA-nanotechnology was explored.

Firstly, the polymerization of DNA-macromonomers *via* ROMP was completed using a macroinitiator approach to prepare a water-soluble catalyst *in situ*. This was the first example of ROMP on native DNA and resulted in the preparation of DNA-PEG bottlebrush polymers. Interestingly, polymers prepared with short PEG sidechains appeared to collapse in aqueous solutions and thus future work will investigate the potential of these polymers to protect oligonucleotides against nucleases. If successful, this would offer a facile approach to the protection of oligonucleotides.

In addition, the investigation of metathesis in a templating mechanism was studied. The design of DNA-functionalized metathesis catalysts was originally targeted through the coupling of DNA to the NHC and benzylidene ligands on the metathesis catalysts. However, whilst such functionalizations have proven very successful for addition of water solubilising groups on to the catalysts, the addition of DNA was unsuccessful. The lack of success was attributed to the differing solubilities of the DNA and Ru-catalyst and the aforementioned DNA-Ru interaction. No further attempts were explored with DNA and investigations turned to PNA. Unfortunately, due to time restrictions, this approach was not comprehensively explored but it is predicted the neutral backbone and organosolubility of PNA is likely to avoid the previously found limitations with DNA and thus would be of interest in future studies.

Due to the difficulties isolating a DNA-functionalized metathesis catalyst an alternative approach inspired by enyne metathesis was studied. This approach utilized an enyne-functionalized DNA strand which when reacted with commercially available Ru-catalysts yielded an *in-situ* DNA-functionalized catalyst. Several off-templated cross-metathesis reactions were screened prior to attempting a templated cross-metathesis reaction. Initial results appear promising and indeed future work will focus on exploring the templated metathesis reaction further. Of particular interest would be how the templated reaction affects the stereochemistry of the metathesis reaction and whether the templating effect could be utilized to encourage CM of typically unreactive substrates.

To conclude, this study has demonstrated a number of limitations and challenges with performing metathesis in the presence native DNA and thus future work should focus on gaining a greater understanding of the interactions occurring between DNA and the Ru-

catalysts. Despite this, a number of examples utilizing metathesis 'on-DNA' were demonstrated and future work should now focus on further exploiting this chemistry.